Entwicklung von Radiofluorierungsmethoden zur Herstellung von Tracern für die Positronen-Emissions-Tomographie

Inaugural-Dissertation

zur

Erlangung des Doktorgrades

der Mathematisch-Naturwissenschaftlichen Fakultät

der Universität Köln

vorgelegt von

Benedikt Gröner

aus Adenau

Berichterstatter (Gutachter):	Prof. Dr. Boris D. Zlatopolskiy
	Prof. Dr. Bernd Goldfuß
Tag der mündlichen Prüfung:	19.04.2024

Kurzzusammenfassung

Die Positronen-Emissions-Tomographie (PET) ist für die moderne klinische Diagnostik von großer Bedeutung, da sie die nicht-invasive Visualisierung und Quantifizierung (patho)physiologischer Prozesse auf molekularer Ebene ermöglicht. Grundlage für die PET-Bildgebung sind mit β^+-Emittern markierte Sonden, sogenannte PET-Tracer, welche selektiv mit einem molekularen Target oder biochemischen Prozess interagieren. Angesichts des steigenden Bedarfs an bereits etablierten und neuen PET-Tracern ist die Entwicklung effizienter Radiomarkierungsmethoden, insbesondere mit dem weitverbreiteten PET-Nuklid ^{18}F, von besonderer Relevanz.

Das übergeordnete Ziel dieser Arbeit waren daher die Entwicklung und der Einsatz innovativer neuer Radiofluorierungsmethoden für die Herstellung etablierter und neuer PET-Tracer. So wurde in einem ersten Teilprojekt ein neuentwickeltes Protokoll zur kupfervermittelten Radiofluorierung für die Synthese von drei ^{18}F-markierten Phenylalanin-Derivaten aus den entsprechenden Boronsäure- und Boronsäurepinakolestern eingesetzt. Unter Verwendung eines neuen Kupfervermittlers konnten dabei radiochemische Umsätze (RCUs) von 69–91% erzielt, und die entsprechenden Tracer in radiochemischen Ausbeuten (RCAs) von 33–41% isoliert werden.

In einem weiteren Teilprojekt wurden zwei neue Analoga des etablierten Tracers O-[^{18}F]Fluorethyltyrosin ([^{18}F]FET), nämlich m-[^{18}F]FET und [^{18}F]FET-OMe, in RCAs von 56±6% bzw. 41±5% hergestellt. Ziel war es, ihre pharmakologischen Eigenschaften im Vergleich zur Leitverbindung sowohl in vitro als auch in vivo zu untersuchen.

Ein nächster Schwerpunkt der Arbeit lag in der Entwicklung von Azaisatosäureanhydrid-basierten prosthetischen Gruppen für die indirekte Radiofluorierung. Diese wurden anschließend für die Konjugation mit verschiedenen Aminen, Alkinen und Aziden mittels Acylierung oder kupferkatalysierter 1,3-dipolarer Cycloaddition eingesetzt. Auf diese Weise konnten unter anderem drei neue Tracer für das prostataspezifische Membranantigen (PSMA), ein neuer Tracer für das Fibroblasten-Aktivierungsprotein (FAP) sowie verschiedene radiomarkierte Insulinderivate herstellt werden.

Ein letztes Teilprojekt dieser Arbeit befasste sich schließlich mit der Radiofluorierung durch Bildung von Al[^{18}F]F-Komplexen. Unter Einsatz dieser Methode konnte ein zuvor mit einem

entsprechenden Chelator modifiziertes Insulin-Derivat mit einer radiochemischen Ausbeute von 25% radiomarkiert werden. Zudem wurde die Radiosynthese des bekannten Tracers Al[^{18}F]F-FAPI-42 optimiert, wodurch Aktivitätsausbeuten von 40% erreicht werden konnten. Abschließend wurde ein neuentwickelter Chelator mit einem RCU von 80% markiert und seine hydrolytische Stabilität sowie die Stabilität in Rattenserum evaluiert.

Abstract

The positron emission tomography (PET) plays an important role in modern clinical diagnostics, allowing for non-invasive visualization and quantification of (patho)physiological processes at the molecular level. PET imaging relies on probes labeled with β^+-emitters, known as PET tracers, which selectively interact with a molecular target or biochemical process. Given the increasing demand for established and new PET tracers, particularly those utilizing the widely used PET isotope ^{18}F, the development of efficient radiofluorination methods is of special significance.

The overarching goal of this work was the development and application of innovative new radiofluorination methods for the production of established and new PET tracers. In the first subproject, a newly developed protocol for copper-mediated radiofluorination was employed to synthesize three ^{18}F-labeled phenylalanine derivatives from corresponding boronic acid and boronic acid pinacol esters. Using novel copper mediators, radiochemical conversions (RCCs) of 69–91% were achieved, and the corresponding tracers were isolated in radiochemical yields (RCYs) of 33–41%.

In the next subproject, two new analogs of the established tracer *O*-[^{18}F]Fluoroethyltyrosine ([^{18}F]FET), namely *m*-[^{18}F]FET and [^{18}F]FET-OMe, were synthesized with RCYs of 56±6% and 41±5%, respectively, enabling preclinical study of these candidate probes as tumor imaging agents.

A further focus of the work was on the development of azaisatoic anhydride-based prosthetic groups for indirect radiofluorination. These were subsequently used for conjugation with various amines, alkynes, and azides through acylation or copper-catalyzed 1,3-dipolar cycloaddition. This approach resulted in the production of three new tracers for imaging of the prostate-specific membrane antigen (PSMA), a novel tracer for visualization of the fibroblast activation protein (FAP), as well as several ^{18}F-labeled insulin derivatives.

The final subproject of this work addressed radiofluorination through the formation of Al[^{18}F]F complexes. Using this method, an insulin derivative modified with a appropriate chelator was radiolabeled in a radiochemical yield of 25%. Additionally, the radiosynthesis of the known tracer Al[^{18}F]F-FAPI-42 was optimized to furnish activity yields of up to 40%. Finally, a newly

developed chelator was labeled in an RCC of up to 80%, and hydrolytic stability of the resulting radiolabeled conjugates as well as their stability in rat serum were evaluated.

Danksagung

An dieser Stelle möchte ich mich ganz herzlich bei Herrn Prof. Dr. Bernd Neumaier für die Möglichkeit diese Arbeit am INM-5: Nuklearchemie durchführen zu dürfen, für seine hilfreichen Anregungen, seine stetige Unterstützung sowie für das Interesse am Fortgang dieser Arbeit und die Bereitstellung optimaler Arbeitsbedingungen bedanken.

Besonders danke ich auch meinem Doktorvater Professor Dr. Boris Zlatopolskiy, dessen Betreuung und Ideen viel zu dieser Arbeit beigetragen haben.

Zudem danke ich Professor Dr. Bernd Goldfuß für die Übernahme des Zweitgutachtens und Professor Dr. Ines Neundorf für die Zweitbetreuung im Rahmen der Graduate School und den Prüfungsvorsitz.

Für die Durchführung der biologischen Evaluation der Tracer danke ich Professor Dr. Heike Endepols, Lukas Vieth, Dr. Felix Neumaier und Melanie Brugger.

Dr. Felix Neumaier danke ich zudem für seine umfangreiche Unterstützung bei der Konzeption, Verfassung und Korrektur von Texten.

Ich danke meinen Mitdoktoranden für den Zusammenhalt, Diskussionen über Probleme und Ideen, und Freundschaft auch abseits der Arbeit.

Ein großer Dank geht an alle Kollegen des IREMB und des INM-5 für die Unterstützung in so vielen Bereichen und das tolle Arbeitsklima.

Zuletzt Danke ich meiner Familie, die mich immer unterstützt und mir alles ermöglicht haben. Meiner Frau Marie, mit der ich schon so vieles durchgestanden habe.

Inhalt

1. Einleitung

1.1. Das Tracer Prinzip

Der sprunghafte Fortschritt in der klinischen Diagnostik der letzten Jahre ist nicht zuletzt der molekularen Bildgebung zu verdanken, welche es ermöglicht mittels sogenannter Tracer biologische Targets zu visualisieren. Die verwendeten Tracer bestehen typischerweise aus einem Pharmakophor, welches selektiv mit dem zu untersuchenden Target (Prozess, Struktur oder Biomolekül) interagiert, einem Label, welches die nicht-invasive Detektion des Tracers ermöglicht und einem Spacer, der beide verbindet. In der Nuklearmedizin werden als Label für die Bildgebung Radionuklide verwendet, die eine Detektion des Tracers im Rahmen der PET oder der Einzelphotonen-Emissions-Computertomographie (SPECT) möglich machen. Begründet wurde der Einsatz von radioaktiven Verbindungen zur Untersuchung von biologischen Prozessen 1923 durch George de Hevesy, als er das Radioisotop Blei-212 nutzte, um die Aufnahme und Verteilung von Blei in Pflanzen zu untersuchen. Wichtig ist, dass die untersuchten Prozesse durch die Gabe des Tracers nicht beeinflusst werden. Im Gegensatz zu anderen bildgebenden Verfahren wie dem Röntgen, der Computer-Tomographie (CT) oder der Magnet-Resonanz-Tomographie (MRT), welche primär die Struktur und Dichte von Geweben darstellen, sind PET und SPECT in der Lage, Prozesse auf molekularer Ebene darzustellen. So kann die Verteilung eines Tracers im Körper beispielsweise Aufschluss über die Verteilung von bestimmten Transportern oder Rezeptoren geben. Um diese auch morphologisch zuzuordnen, werden PET und SPECT in der Regel mit einem anderen Bildgebungsverfahren kombiniert, beispielsweise im Rahmen von PET/MRT oder SPECT/CT. Auf diese Weise können die beobachteten Prozesse genau lokalisiert werden.

1.2. PET-Bildgebung

Die Radionuklide, welche für die PET-Bildgebung eingesetzt werden, senden über einen β^+-Zerfall Positronen aus:

$$ {}^{1}_{1}p \rightarrow {}^{1}_{0}n + e^{+} + \nu_e $$

Während des β^+-Zerfalls wird ein Proton im Kern des Radionuklids in ein Neutron, ein Positron und ein Elektron-Neutrino umgewandelt. Während das Neutron im Kern verbleibt, verlässt das Positron diesen mit einer kinetischen Energie, die abhängig vom jeweiligen Mutternuklid ist. Das Positron durchläuft eine Reihe elastischer Stöße in seiner unmittelbaren Umgebung

(normalerweise wenige Millimeter, je nach Medium), welche seine kinetische Energie nach und nach reduzieren. Schließlich kommt es bei Kollision mit einem Elektron entweder zu einer direkten Vernichtungsreaktion (Annihilation) oder zur Bildung eines kurzlebigen Positroniums. Die Struktur des Positroniums ähnelt der eines Wasserstoffatoms, wobei das Positron formal den Kern ersetzt. Da das Positronium extrem instabil ist (Lebensdauer *para*-Positronium ca. 0,12 ns; *ortho*-Positronium 140 ns), kommt es kurz nach seiner Bildung ebenfalls zu einer Annihilation, wobei die Massen von Elektron und Positron in Energie umgewandelt werden. Dabei entstehen im Fall eines *para*-Positroniums zwei γ-Quanten mit einer Energie von jeweils 511 keV, welche sich annähernd antiparallel in einem Winkel von ungefähr 180° vom Ort der Annihilation ausbreiten (aufgrund der Impulserhaltung des Positrons wird der Winkel leicht von 180° abweichen). Beim Zerfall eines *ortho*-Positroniums, das mit wesentlich geringerer Wahrscheinlichkeit gebildet wird als das *para*-Positronium und nicht zur Generierung des PET-Bilds beiträgt, kommt es zur Emission von insgesamt drei γ-Quanten.

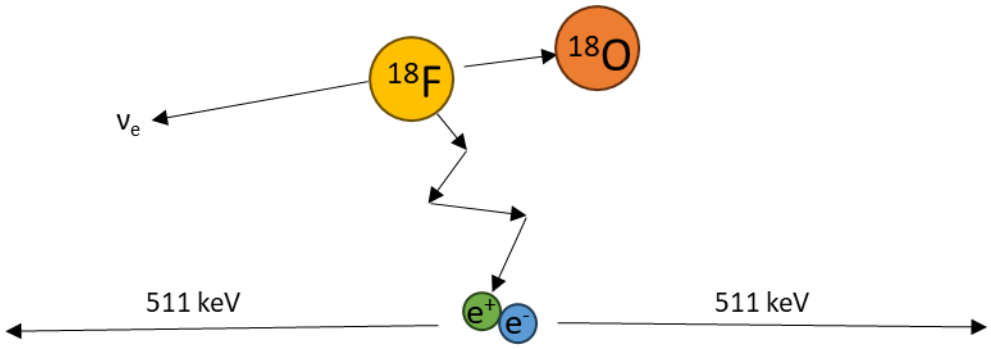

Abbildung 1: Schematische Darstellung des β^+-Zerfalls

Im Rahmen der PET-Bildgebung werden die bei der Annihilation freigesetzten γ-Quanten von ringförmig angeordneten Detektoren erfasst, welche um den liegenden Patienten angeordnet sind (siehe Abbildung 2). Dabei werden durch eine Koinzidenzschaltung nur γ-Quanten erfasst, die innerhalb eines kurzen Zeitfensters auf gegenüberliegende Detektoreinheiten treffen. Dies gewährleistet, dass ausschließlich Annihilationen auf der Verbindungslinie zwischen zwei Detektoren als Signal erfasst werden. Nach Registrierung einer ausreichenden Anzahl von Zerfällen kann aus diesen Signalen dann ein dreidimensionales Bild der Tracerverteilung rekonstruiert werden. Dessen Auflösung hängt von verschiedenen Faktoren, wie etwa den Dimensionen des Scanners und der Reichweite der Positronen im Gewebe, ab.

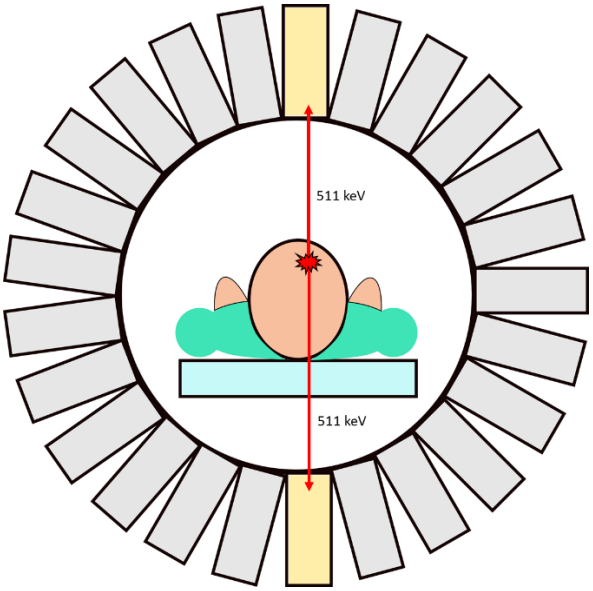

Abbildung 2: Schematische Darstellung eines Positronen-Emissions-Tomographen.

Neben ihrem Einsatz für wissenschaftliche und diagnostische Zwecke spielt die PET-Bildgebung eine zunehmende Rolle für theranostische Ansätze, bei denen es zu einer engen Verzahnung diagnostischer und therapeutischer Modalitäten kommt. In der nuklearmedizinischen Theranostik werden dafür verschiedene Radioisotope eines Elements oder chemisch verwandte Nuklide mit unterschiedlichen Zerfallseigenschaften in einer nahezu identischen chemischen Form eingesetzt. Bei diesen sogenannten theranostischen Paaren handelt es sich typischerweise um ein PET- oder SPECT-Radionuklid für die Bildgebung sowie ein therapeutisches Radionuklid für die Radionuklidtherapie. Ein Beispiel für ein solches theranostisches Paar sind die Iod-Isotope ^{123}I und ^{131}I.[1] Während [^{123}I]I$^-$ als γ-Emitter für die SPECT-Bildgebung von Schilddrüsenkrebs eingesetzt wird, kann [^{131}I]I$^-$ als β^--Emitter für die Krebstherapie verwendet werden. Da beide Isotope chemisch identisch sind, ist auch die Verteilung im Körper identisch, und die Bildgebung mit [^{123}I]I$^-$ kann vor und nach der Behandlung mit [^{131}I]$^-$ etwa zur Therapieplanung und Verlaufskontrolle eingesetzt werden. Ein Beispiel für ein theranostisches Paar von Nukliden unterschiedlicher Elemente sind ^{68}Ga und ^{177}Lu.[2] Beides sind Radiometalle, welche durch den Chelator DOTA komplexiert werden können. Wenn dieser Chelator, wie im Fall von PSMA I&T, mit einem Pharmakophor verbunden ist, kann der mit dem β^+-Strahler ^{86}Ga markierte Tracer [^{68}Ga]Ga-PSMA I&T zur PET-Bildgebung von Prostatakarzinomen im Rahmen der Diagnostik und Therapieplanung verwendet werden. Anschließend kann der mit dem β^--Emitter ^{177}Lu markiert analoge therapeutische Radioligand [^{177}Lu]Lu-PSMA I&T für die Radionuklidtherapie dieser Karzinome

eingesetzt werden. Die beiden radioaktiv markierten Verbindungen haben in diesem Fall aufgrund der unterschiedlichen Radiometalle zwar keine identische, aber eine sehr ähnliche Bioverteilung.

1.3. Radionuklide für die PET-Diagnostik

Die Auswahl des Radioisotops spielt eine entscheidende Rolle bei der Entwicklung neuer Radiotracer für die PET-Bildgebung, da seine chemischen Eigenschaften sowie die Halbwertszeit sich für den jeweiligen Tracer bzw. den zu beobachtenden Prozess eignen müssen. Die Zerfallseigenschaften, wie die Wahrscheinlichkeit der β^+-Emission und die maximale Energie der erzeugten Positronen, liefern grundlegende Informationen über die Leistungsfähigkeit des Radionuklids.

Einige der am häufigsten eingesetzten PET-Nuklide sind in Tabelle 1 aufgeführt.

Tabelle 1: Zerfallseigenschaften einer Auswahl von PET-Nukliden.[3, 4]

Radionuklid	**$t_{1/2}$ [min]**	**$E\beta^+_{max}$ [keV]**	**β^+-Anteil [%]**
^{11}C	20,4	960	99,8
^{13}N	10,0	1198	99,8
^{15}O	2,0	1732	99,9
^{18}F	109,8	634	96,7
^{68}Ga	67,6	1899	87,7

Grundsätzlich sollte die Markierung eines Pharmakophors mit einem Radionuklid die pharmakologischen Eigenschaften des resultierenden Tracers möglichst nicht oder nur geringfügig beeinflussen, um weiterhin Zielprozesse beobachten zu können. Da die meisten biologisch aktiven Moleküle Kohlenstoff-, Sauerstoff- und/oder Stickstoffatome enthalten, ermöglichen Radionuklide wie ^{11}C, ^{13}N und ^{15}O häufig eine Radiomarkierung ohne strukturelle Modifikation der Ausgangsverbindung. Aufgrund der kurzen Halbwertszeiten von ^{13}N ($t_{1/2}$=10 min) und ^{15}O ($t_{1/2}$=2 min) kommen diese jedoch hauptsächlich in Form sehr einfacher Moleküle wie $[^{13}N]NH_3$ oder $[^{15}O]H_2O$ zum Einsatz und eignen sich ausschließlich für die Beobachtung sehr schneller Prozesse, wie etwa der Durchblutung oder anderer

Verteilungsprozesse.[5, 6] Die etwas längere Halbwertszeit von ^{11}C ($t_{1/2}$=20,4 min) ermöglicht bereits die Herstellung komplexerer Tracer und einen Einsatz für Anwendungen wie die Rezeptorbildgebung, beispielsweise mit dem Dopamin-D_2-Rezeptorliganden [^{11}C]Racloprid (Abbildung 3).[7]

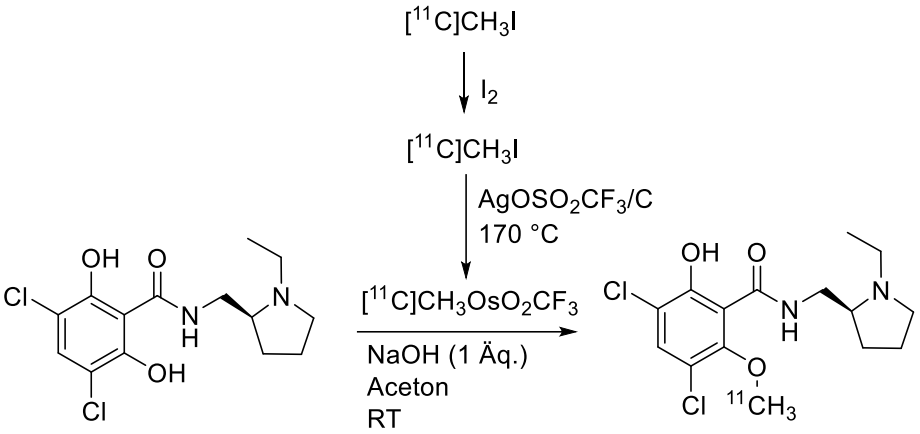

Abbildung 3: Radiosynthese von [^{11}C]Racloprid.[7]

Mit einer Halbwertszeit von 109,8 min ermöglicht ^{18}F dagegen selbst komplexe mehrstufige Tracersynthesen sowie die Bildgebung relativ langsamer biologischer Prozesse. Außerdem können radiofluorierte Tracer über eine gewisse Strecke vom Produktionsort zu entfernten Kliniken ohne eigene Produktionsmöglichkeiten transportiert werden, was eine Kommerzialisierung ermöglicht (Satellitenprinzip). Da Fluor und Wasserstoff ähnlich große Van-der-Waals-Radien (H: 1,20 Å, F: 1,35 Å) besitzen, beeinflusst die Substitution eines H- mit einem F-Atom die pharmakologischen Eigenschaften eines Moleküls in vielen Fällen nur geringfügig. Die deutlich höhere Elektronegativität von Fluor im Vergleich zu Wasserstoff verändert in diesem Fall jedoch die elektronischen Eigenschaften des markierten Moleküls, weshalb mögliche Auswirkungen auf pKs-Wert, Lipophilie und das Dipolmoment bei der Tracer-Entwicklung berücksichtigt werden müssen. Da der Einbau von Fluor in biologisch aktive Moleküle oft einen positiven Einfluss auf die metabolische Stabilität hat, ist die Zulassung fluorhaltiger Medikamente zudem in den letzten Jahrzehnten deutlich angestiegen. So enthielten 43% der von der FDA im Jahr 2019 zugelassenen "small molecules" ein Fluoratom, 2021 waren es 38%.[8, 9] Entsprechend stehen zunehmend auch Leitstrukturen zur Verfügung, bei denen eine ^{18}F-Markierung ohne strukturelle Veränderung möglich ist. Ein weiterer Vorteil von ^{18}F liegt in seiner geringen Positronenenergie, welche die Reichweite der

emittierten Positronen in Geweben begrenzt und somit PET-Messungen mit einer hohen Ortsauflösung ermöglicht.

Die verschiedenen zur Verfügung stehenden PET-Radionuklide unterscheiden sich auch hinsichtlich ihrer Produktionsmethoden. So erfolgt die Herstellung von ^{68}Ga in einem ^{68}Ge/^{68}Ga-Generator. Dieser enthält das an einem Ionentauscherharz gebundene Mutternuklid ^{68}Ge, welches mit einer Halbwertszeit von 270,8 Tagen zum Tochternuklid ^{68}Ga zerfällt. Letzteres kann über einen Zeitraum von 1 Jahr mehrmals täglich mit einer HCl-Lösung eluiert und für die Tracer-Herstellung verwendet werden. Die geringen Platzanforderungen und vergleichsweise niedrigen Kosten von ^{68}Ge/^{68}Ga-Generatoren ermöglichen ihren Einsatz auch in kleineren Kliniken. Im Gegensatz dazu werden Radionuklide wie ^{18}F, ^{11}C, ^{13}N und ^{15}O in speziellen Teilchenbeschleunigern, sogenannten Zyklotronen, hergestellt. Diese weisen zwar hohe Anschaffungs- und Betriebskosten auf, ermöglichen dafür jedoch die Produktion verschiedener Radionuklide in hohen Aktivitätsmengen. Im Fall von ^{18}F erfolgt die Herstellung im Zyklotron durch die Bombardierung von ^{18}O bzw. natürlichem Neon mit Protonen oder Deuteronen, wobei über die ^{18}O(p,n)^{18}F bzw. ^{20}Ne(d,α)^{18}F Kernreaktion ^{18}F entsteht.

1.4. ^{18}F-Radiomarkierung

Im Laufe der Zeit wurden verschiedene Radiofluorierungsmethoden entwickelt, wobei grundsätzlich zwischen den Strategien der direkten und indirekten Radiofluorierung unterschieden werden kann (Abbildung 4). Bei der direkten Radiofluorierung wird das Nuklid direkt in die Tracerstruktur eingeführt. Im Gegensatz dazu wird bei der indirekten Radiofluorierung zunächst eine prosthetische Gruppe mit dem Nuklid markiert, welche anschließend unter geeigneten Bedingungen mit dem Pharmakophor konjugiert wird. Die Wahl zwischen direkter oder indirekter Radiofluorierung als Markierungsstrategie hängt stark von dem zu synthetisierenden Radiotracer ab. Die direkte Radiofluorierung erfolgt oft in höchstens zwei Schritten – der Markierung selbst und ggf. der anschließenden Entfernung erforderlicher Schutzgruppen – und wird aufgrund höherer Ausbeuten und kürzerer Synthesezeiten grundsätzlich bevorzugt. Allerdings muss der Markierungsvorläufer unter den für die Radiofluorierung erforderlichen Bedingungen stabil und im Reaktionsmedium löslich sein. Zudem darf er keine reaktiven Gruppen enthalten, welche die Radiofluorierung negativ beeinflussen. Da viele Biomoleküle wie Peptide, Proteine und Antikörper diese Bedingungen

nicht erfüllen, muss bei ihnen häufig eine Methode zur indirekten Radiomarkierung verwendet werden.

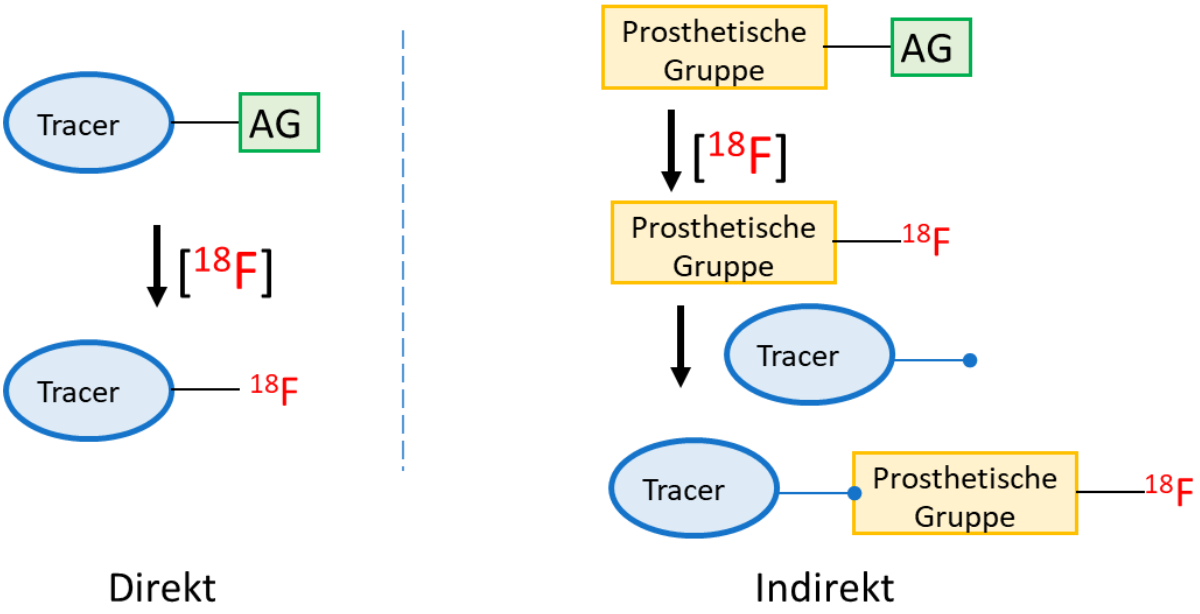

Abbildung 4: Direkte versus indirekte Radiofluorierung; AG = Abgangsgruppe.

1.4.1. Elektrophile Radiofluorierung

^{18}F kann in elektrophiler oder in nukleophiler Form hergestellt und entsprechend für die Synthese radiofluorierter Tracer über elektrophile oder nukleophile Reaktionen eingesetzt werden. Bei der elektrophilen Radiofluorierung wird elektrophiles [^{18}F]F_2 eingesetzt, welches bei der Herstellung von ^{18}F ausgehend von angereichertem [^{18}O]O_2 oder natürlichem Neon entsteht. Um eine Adsorption des produzierten atomaren ^{18}F an der Targetwand zu verhindern, wird dem Targetgas eine geringe Menge F_2 beigemischt, wodurch [^{18}F]F_2 entsteht. Dieses wird ausgeleitet und anschließend für die Radiofluorierung verwendet. Zu den ersten Radiotracern, die mithilfe der elektrophilen Radiofluorierung hergestellt wurden, gehört 2-[^{18}F]Fluor-2-desoxy-D-Glucose ([^{18}F]FDG).[10] Dabei wurde 3,4,6-tri-*O*-acetyl-D-glucal mit [^{18}F]F_2 markiert und anschließend mit HCl entschützt (Abbildung 5).

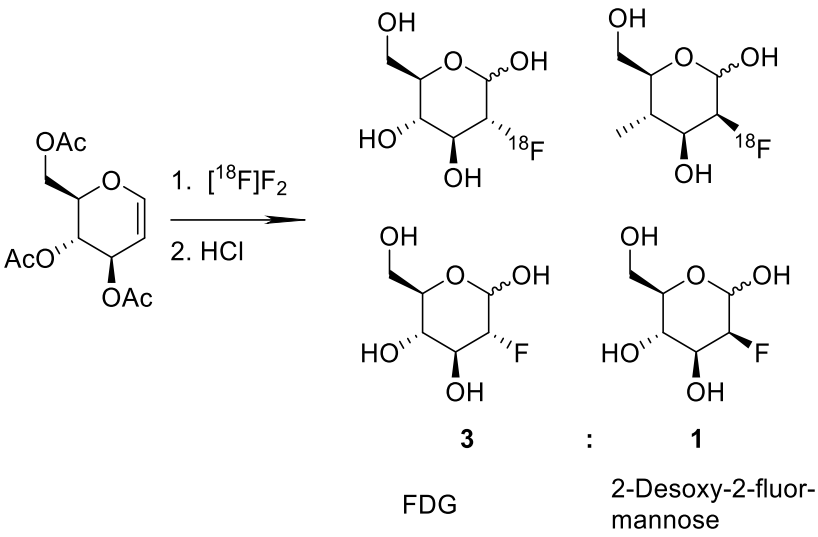

Abbildung 5: Radiosynthese von [^{18}F]FDG durch elektrophile Radiofluorierung nach Ido et al.[10]

Wie aus der Abbildung ersichtlich ist, weist diese Reaktion eine geringe Stereoselektivität auf, da etwa 25% 2-Desoxy-2-fluor-D-mannose entstehen. Zudem beträgt die maximale radiochemische Ausbeute (RCA) lediglich 50%, da statistisch betrachtet die Hälfte des [^{18}F]F_2 zu unreaktivem [^{18}F]Fluorid ([^{18}F]F^-) reagiert, und nur die andere Hälfte überhaupt zu der gewünschten Radiomarkierung führt. Die hohe Reaktivität von F_2 führt zudem zu einer Vielzahl unerwünschter Nebenreaktionen. Des Weiteren ist durch das während der Produktion als Träger zugesetzte F_2 die maximal erreichbare molare Aktivität (100–600 MBq/µmol) bei Verwendung von elektrophilem [^{18}F]F_2 gering.[11] Während sich die mit der hohen Reaktivität und geringen Regioselektivität verbundenen Probleme durch den Einsatz sekundärer elektrophiler Reagenzien wie Xe[^{18}F]F_2, Acetyl[^{18}F]hypofluorit oder [^{18}F]Selectfluor bzw. durch die Nutzung von metallorganischen Abgangsgruppen wie $Sn(Me)_3$ vermeiden lassen, bleibt die niedrige maximale molare Aktivität eine erhebliche Einschränkung. Aus diesem Grund findet die elektrophile Radiofluorierung heute kaum noch Anwendung.[12-15]

1.4.2. Nukleophile Radiofluorierung

Für die Herstellung von nukleophilem ^{18}F wird angereichertes [^{18}O]H_2O in einem Zyklotron durch Protonenbeschuss über die ^{18}O(p,n)^{18}F Kernreaktion zu [^{18}F]Fluor umgewandelt, welches als [^{18}F]F^- in wässriger Lösung erhalten wird. So können hohe Aktivitätsmengen und molare Aktivitäten von bis zu 4×10^4 GBq/µmol erreicht werden.[16] Allerdings weist das auf diese Weise hergestellte [^{18}F]F^- aufgrund der Hydratisierung eine stark verminderte

Nukleophilie auf und muss zur Erhöhung der Reaktivität zunächst aufbereitet werden. Dafür wird es üblicherweise auf einer Anionenaustauscherkartusche fixiert, um es von verbleibendem [^{18}O]H_2O abzutrennen. Dann wird es mit einer wässrigen oder organisch-wässrigen Lösung einer geeigneten Base oder Salz eluiert und das H_2O mittels mehrfacher azeotroper Trocknung vollständig entfernt. Typischerweise werden Phasentransferkatalysatoren wie Tetraalkylammoniumsalze oder Cäsium- bzw. Kaliumcarbonat als Basen in Verbindung mit Kryptofix oder Kronenethern verwendet, um die nukleophile Reaktivität des [^{18}F]F^- und seine Löslichkeit in aprotischen organischen Lösungsmitteln wie DMF oder MeCN zu erhöhen.

Als Alternative zu dieser relativ komplizierten Prozedur wurden zahlreiche vereinfachte Markierungsansätze wie, z.B., die „Minimalistische Methode“ entwickelt.[17] Bei dieser wird das [^{18}F]F^- ebenfalls auf einer Anionenaustauscherkartusche fixiert, die jedoch zunächst mit trockenem MeOH gespült wird, um Wasserreste zu entfernen. Anschließend erfolgt die Elution mit einer methanolischen Lösung eines Onium-Salz-Radiomarkierungsvorläufers. Nach Verdampfen des niedrigsiedenden MeOHs innerhalb weniger min wird ein für die Radiofluorierung geeignetes aprotisches Lösungsmittel zugesetzt. Diese Methode nimmt weniger Zeit in Anspruch und ist besonders vorteilhaft für die Markierung basenlabiler Moleküle. Sie kann in modifizierter Form auch für Vorläufer die keine Onium-Salze sind eingesetzt werden, indem das [^{18}F]F^- mit Phasentransferkatalysatoren in MeOH eluiert und nach Verdampfen des MeOHs der entsprechende Markierungsvorläufer im Reaktionsmedium zugesetzt wird.

Die eigentliche Radiomarkierung erfolgt dann durch Erhitzen der Reaktionsmischung aus getrocknetem [^{18}F]F^- und Markierungsvorläufer im Reaktionsmedium. Anschließend muss der hergestellte Radiotracer über HPLC oder Festphasenextraktion isoliert und für die Applikation in einer injektionsfähigen Lösung formuliert werden. Generell gilt aufgrund der hohen Basizität von [^{18}F]F^- in aprotischen Lösungsmitteln für die meisten nukleophilen Radiofluorierungsmethoden, dass nukleophile funktionelle Gruppen im Vorläufer die Markierung stören würden. Deshalb müssen sie mit geeigneten Schutzgruppen versehen werden (Abbildung 6). Dazu gehören, z.B., Methyl-, Ethyl- und *tert*-Butyl-Gruppen für Carbonsäuren, *tert*-Butyloxycarbonyl-Gruppen für primäre Amine und aromatische Alkohole,

Acetyl-Gruppen für aliphatische Alkohole oder Pivalyloxymethyl-Gruppen für sekundäre Amine.

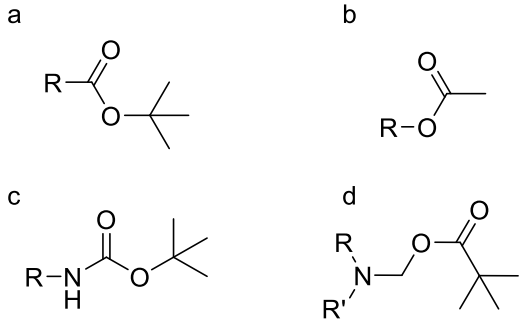

Abbildung 6: Verschiedene Schutzgruppen für funktionelle Gruppen. a: *tert*-Butyl-Gruppe; b: Acetyl-Gruppe; c: *tert*-Butyloxycarbonyl-Gruppe; d: Pivalyloxymethyl-Gruppe.

1.4.2.1. Markierung an Kohlenstoffatomen

Die nukleophile Radiofluorierung an Kohlenstoffatomen lässt sich grundsätzlich in zwei Reaktionstypen unterteilen: Markierungen an aliphatischen und aromatischen Positionen. Bei der Markierung an aliphatischen Positionen erfolgt die Reaktion über einen S_N-Mechanismus, wobei S_N2 Reaktionen bevorzugt werden. Die gewünschte Markierungsposition ist dabei durch eine Abgangsgruppe modifiziert, die unter Inversion des Stereozentrums (Walden-Umkehr) am Kohlenstoff ersetzt wird. Als Abgangsgruppen kommen Halogene wie Br oder I sowie Sulfonate wie Triflate, Nosylate, Tosylate oder Mesylate zum Einsatz. Ein gängiges Beispiel ist die moderne Radiosynthese von [^{18}F]FDG. Hierbei wird die Triflat-Gruppe in 1,3,4,6-Acetyl-mannosetriflat durch [^{18}F]F$^-$ ersetzt. Darauffolgende Abspaltung der Acetyl-Schutzgruppen führt zu dem gewünschten Tracer (Abbildung 7).[18]

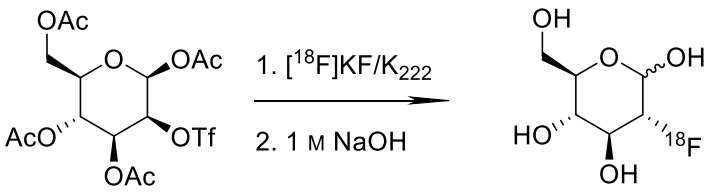

Abbildung 7: Radiosynthese von [^{18}F]FDG durch nukleophile Radiofluorierung.[18]

Der zweite Reaktionstyp ist die Markierung in (hetero)aromatischen Positionen und verläuft über einen S_NAr-Mechanismus. Als Abgangsgruppen werden typischerweise elektronenziehende Gruppen wie *N,N,N*-Trimethylamino- oder Nitro-Gruppen verwendet. Diese Methode funktioniert jedoch nur bei elektronenarmen Aromaten. Idealerweise werden diese durch elektronenziehende Gruppen in *ortho*- und/oder *para*-Position unterstützt, um

das während der Reaktion entstehende Carbanion (Meisenheimer-Komplex) zu stabilisieren (Abbildung 8).

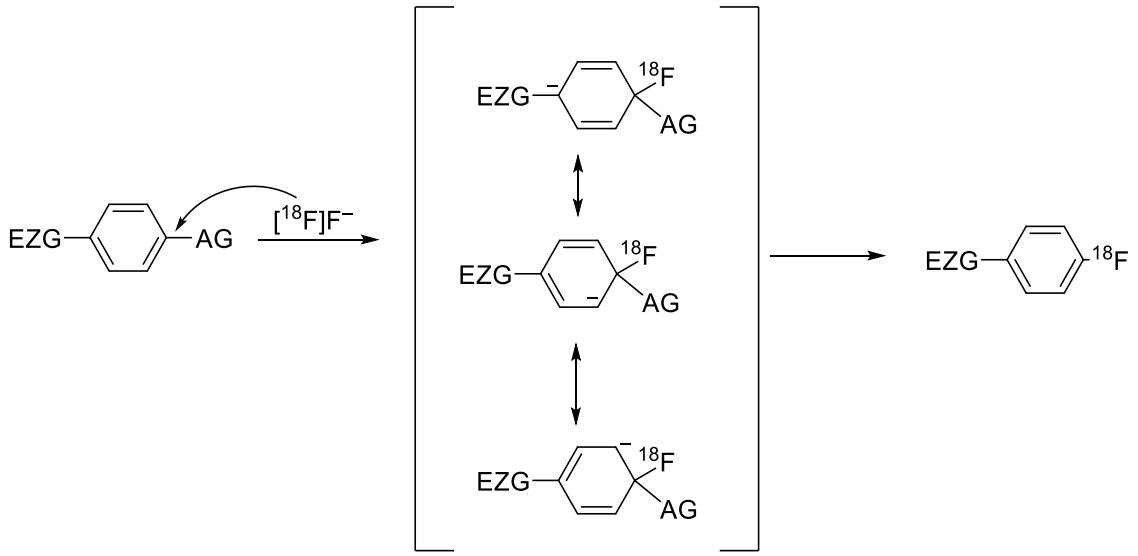

Abbildung 8: Mechanismus der nukleophilen aromatischen Radiofluorierung.

Dies beschränkt den Einsatz dieser Methode stark, da viele biologisch aktive Grundstrukturen eher elektronenreiche Aromaten aufweisen. Es ist zwar grundsätzlich möglich, elektronenziehende Gruppen in den Radiomarkierungsvorläufer einzuführen und sie nach der Reaktion wieder zu entfernen, dies erfordert jedoch mehrere Syntheseschritte und verlängert die Synthesezeit, was wiederrum zu niedrigeren Aktivitätsausbeuten führt. Ein Beispiel für diese Strategie ist die von Ermert et al. beschriebene Synthese radiofluorierter Noradrenalinderivate ausgehend von α-Aminopropiophenonen (Abbildung 9). Dabei wurde der elektronenarme Aromat radiofluoriert und anschließend das elektronenziehende Keton zum gewünschten Alkohol reduziert. Nach der Entschützung wurde das Produkt als Stereoisomerengemisch erhalten.[19]

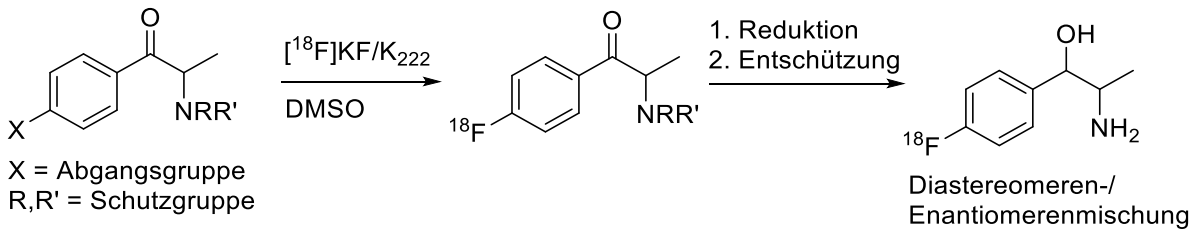

Abbildung 9: Radiosynthese von radiofluoriertem Noradrenalin über ein α-Aminopropiophenon.[19]

Schon 1953 zeigten Beringer et al., dass Diaryliodoniumsalze als Substrate für S_NAR-Reaktionen verwendet werden können.[20] Diese wurden von Pike et al. als erste genutzt, um

radiofluorierte Aromaten herzustellen (Abbildung 10a).[21] Als Alternative können auch spirozyklische Aryliodonium-Ylide verwendet werden (Abbildung 10b). Diese sind vergleichsweise leicht herzustellen und stabil. Die Substitution findet dabei regioselektiv am Aromaten statt.[22]

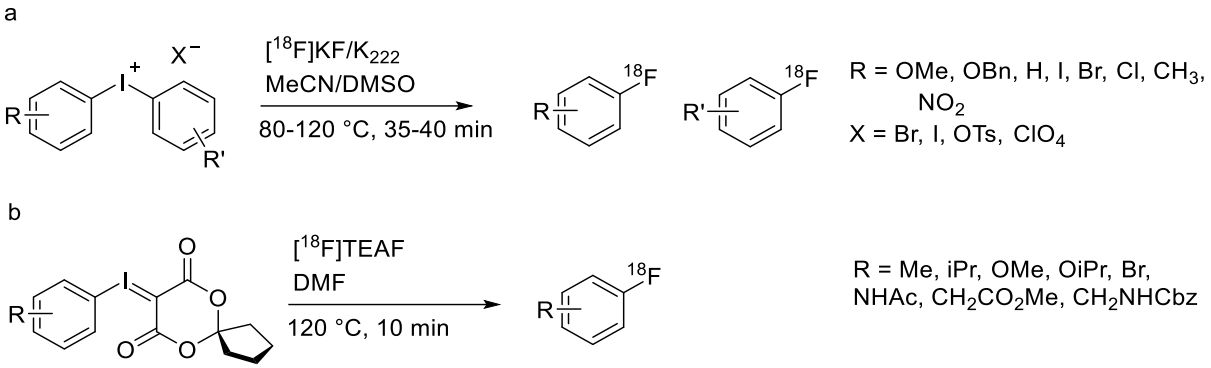

Abbildung 10: Radiofluorierungen von Iodonium-Vorläufern über nukleophile Substitution. a: Diaryliodoniumsalze,[21] b: Spirozyklische Iodonium-Ylide.[22]

Zusätzlich zu Aryliodonium-Salzen wurden auch Arylsulfonium-Vorläufer für die Radiofluorierung von Aromaten verwendet (Abbildung 11a). Mu et al. und Sander et al. nutzten diese für die Herstellung einer Reihe von Tracern und Modellverbindungen.[23, 24] Die Synthese der Triarylsulfonium-Salze ist allerdings aufwendig und benötigt Schutzgruppen um selektiv durchgeführt zu werden. Als Alternative entwickelten Gendron et al. eine Synthese von Dibenzothiophensulfonium-Salzen über die intramolekulare Zyklisierung von Biarylthioethern (Abbildung 11b). Diese sind über die Kupplung eines Biarylthiols mit dem entsprechenden Arylhalogenid zugänglich.[25] Im Jahr 2020 stellten Xu et al. eine weitere Methode für Synthese von Dibenzothiophensulfonium-Salzen vor (Abbildung 11c). Diese wurden durch selektive C-H Funktionalisierung von Aromaten mit verschiedenen

Dibenzothiophen-*S*-oxid-Derivaten erhalten. Durch die passende Auswahl des *S*-Oxids konnten so verschiedene Elektronenreiche und -arme Verbindungen markiert werden.[26]

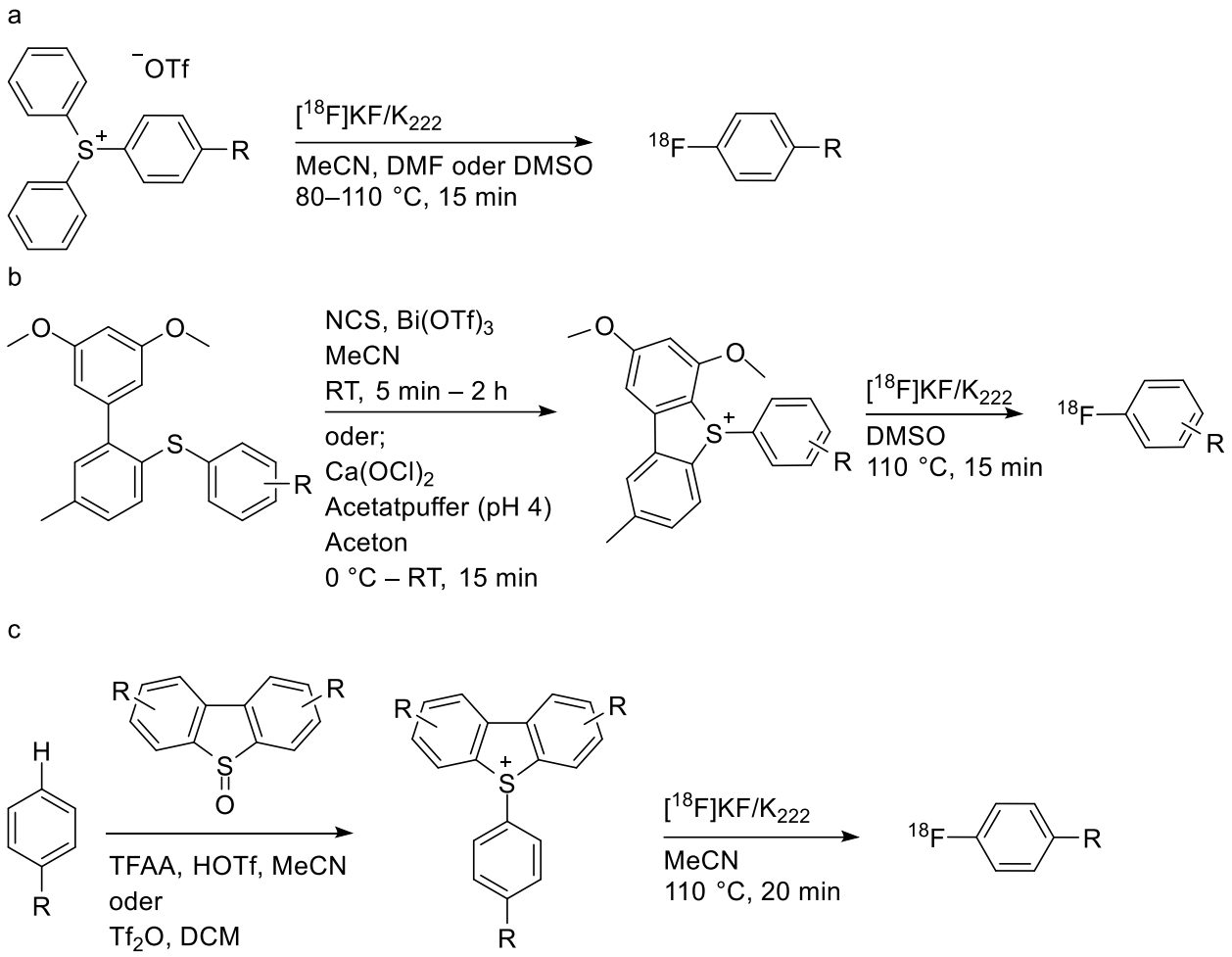

Abbildung 11:Radiofluorierungen an Aromaten über Arylsulfoniumsalze.[23-26]

Eine alternative zur Radiofluorierung über den S_NAr-Mechanismus stellt die photoredoxvermittelte [^{18}F]-Fluorierung dar (Abbildung 12). So beschrieben Chen et al. eine C-H-Radiofluorierung, bei der elektronenreiche oder -neutrale Aromaten über eine Einzelelektronenübertragung in Radikalkationen umgewandelt werden. Dadurch kann [^{18}F]F$^-$ an den nun elektronenarmen Aromaten binden. Die anschließende Oxidation mittels TEMPO stellt den Aromaten wieder her.[27] Wenn elektronenziehende Abgangsgruppen wie Halogenide verwendet werden, ersetzt das [^{18}F]F$^-$ diese.[28]

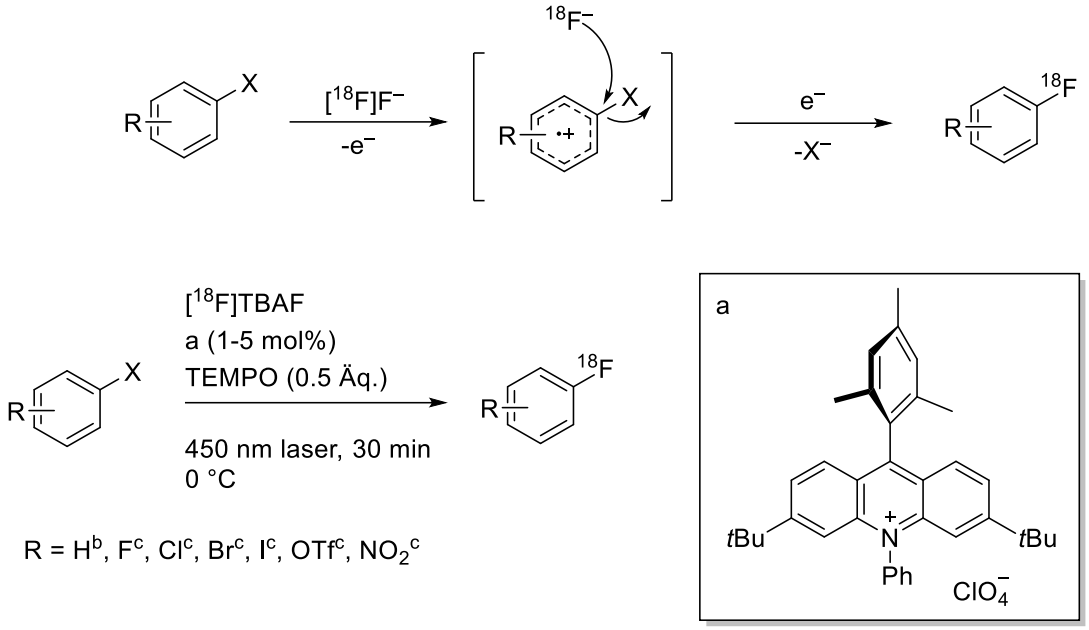

Abbildung 12: Aromatische Radiofluorierung mittels Photoredoxkatalyse. b: 0.5 Äq. TEMPO, O_2 (1 bar);[27] c: N_2 (1 bar).[28]

1.4.2.2. Markierung an Heteroatomen

In den vergangenen Jahrzehnten wurde auch eine Reihe von Methoden zur Radiofluorierung an Atomen von Heteroatomen wie B, Si, Al, Ga, Sc und S entwickelt. Diese zeichnen sich typischerweise durch eine hohe Stabilität der Fluorbindung aus, wobei in einigen Fällen die Dissoziationsenergie der X-F-Bindung sogar höher ist als die der C-F-Bindung.[29, 30]

[^{18}F]F-B-Markierung

Obwohl die ersten Beispiele der Radiofluorierungen über die Bildung einer B-F-Bindung schon in 60-gen Jahren publiziert wurden ,[31, 32] dauerte es fast 50 Jahre bis diese Radiomarkierungstechnik weiterentwickelt wurde. In 2005 zeigten Ting et al., dass Arylboronsäurepinakolester in wässriger Umgebung bei Raumtemperatur in [^{18}F]Aryltrifluoroborate umgewandelt werden können (Abbildung 13a).[33] Für die Synthese musste jedoch KHF_2 als Träger zugegeben werden, was zu niedrigerer molarer Aktivität führte. Ein weiterer Nachteil dieser Methode ist die geringe hydrolytische Stabilität von Aryltrifluoroboraten. Diese lässt sich bis zu einem bestimmten Grad durch die Verwendung stark elektronenziehender Substituenten verbessern, schränkt die Verwendung solcher radiofluorierter Verbindungen jedoch stark ein.[34] Um die niedrige molare Aktivität der so hergestellten Tracer zu umgehen, wurden Arylborimidine als Markierungsvorläufer eingesetzt (Abbildung 13b). Diese können ohne den Zusatz von Träger oder mit nur geringem

Trägerzusatz zu den entsprechenden [^{18}F]Trifluoroboraten umgesetzt werden. Dadurch steigt auch die molare Aktivität, da 3 Mol des Trägers in Form von F^- auf nur ein Mol des [^{18}F]Trifluoroborats übertragen werden. Auf diese Weise war es beispielsweise möglich, eine ^{18}F-markierte prosthetische Gruppe (Abbildung 13b) mit einer molaren Aktivität von über 555 GBq/µmol herzustellen.[35]

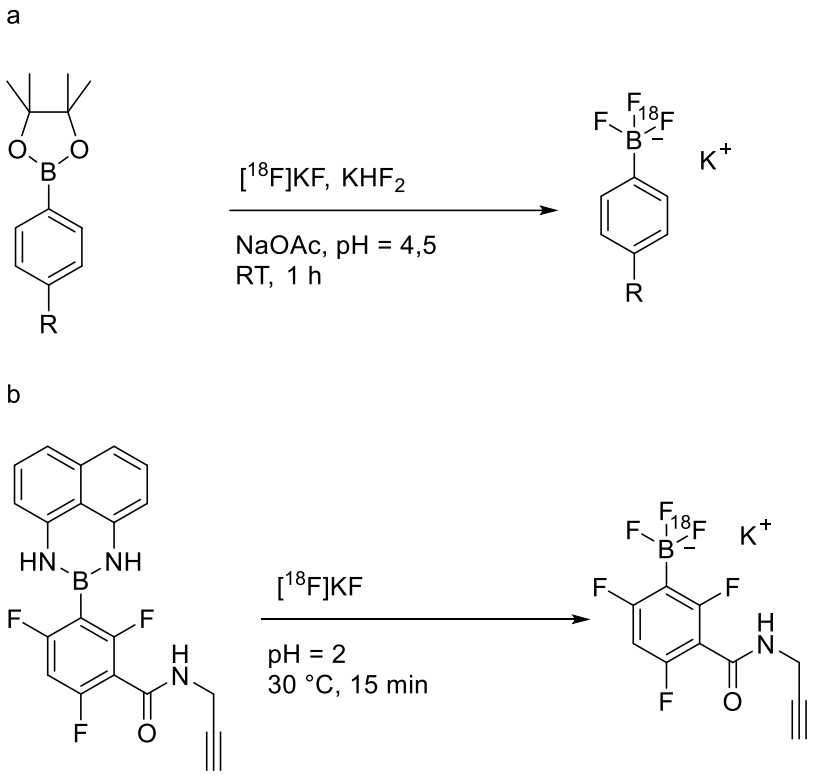

Abbildung 13: Synthese von [^{18}F]Aryltrifluoroboraten. a: ausgehend von Arylboronsäurepinakolestern;[33] b: ausgehend von Arylborimidinen.[35]

Weitere Untersuchungen von Li et al. zur Verbesserung der Stabilität von Aryltrifluoroboraten ergaben, dass die Anwesenheit von Oniumionen diese deutlich erhöht. Zusätzlich zeigten sie, dass diese zwitterionischen Verbindungen für einen ^{18}F/^{19}F-Isotopenaustausch geeignet sind (Abbildung 14a). Zwitterionische Aryltrifluoroborate konnten in H_2O bei Raumtemperatur innerhalb von 20 min mit einer RCA bis zu 87% radiofluoriert werden.[36] Ein aliphatisches Ammoniumtrifluoroborat mit einem Propargyl-Rest (Abbildung 14b) wurde ebenfalls durch ^{18}F/^{19}F-Isotopenaustausch markiert und konnte mittels kupfervermittelter 1,3-dipolarer Cycloaddition mit verschiedenen Peptiden verbunden werden. Die erhaltenen Peptidkonjugate zeigten zudem eine hohe in vivo Stabilität.[37] Einer der weiteren Klassen zwitterionischer Bor-Fluoridakzeptoren für den ^{18}F/^{19}F-Isotopenaustausch wurde 2020 von An et al. vorgestellt. Aus β-Diketonen, die in einigen Krebsmedikamenten vorhanden sind,

stellten sie in einem Schritt die entsprechenden Difluordioxaborinine her (Abbildung 14c). Diese ließen sich in Anwesenheit von Zinnchlorid in MeCN bei Raumtemperatur innerhalb von 10 min radiofluorieren. Einige der so erhaltenen [^{18}F]Difluordioxaborinine wiesen eine ausreichende in vivo Stabilität für PET-Messungen in gesunden Mäusen auf.[38]

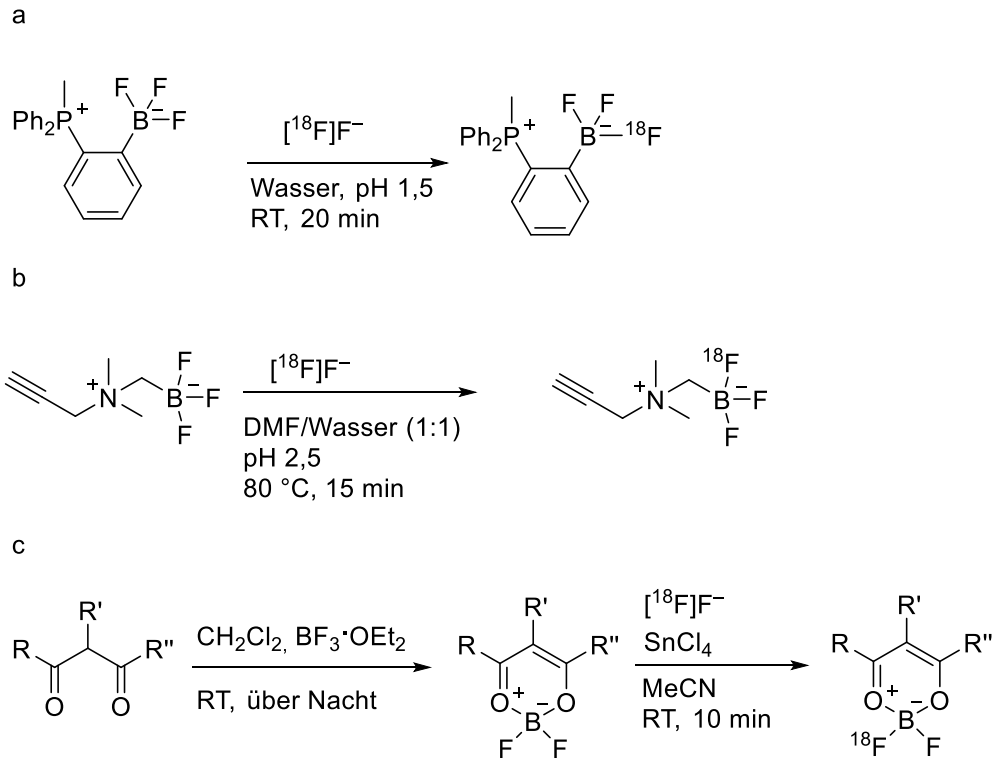

Abbildung 14: Radiofluorierung von Trifluoroboraten über ^{18}F/^{19}F-Isotopenaustausch. a: zwitterionische Aryltrifluoroborate; b: Ammoniumtrifluorborat; c: Difluordioxaborinine.[36-38]

[^{18}F]F-Si-Markierung

Im Jahr 1985 berichteten Rosenthal et al. von der ersten Radiofluorierung an einem Siliziumatom. [^{18}F]Fluortrimethylsilan wurde über einen Halogenaustausch ausgehend von Chlortrimethylsilan hergestellt (Abbildung 15a). Es stellte sich jedoch sowohl in vivo als auch bei Inkubation in H_2O als extrem instabil heraus. Analog zur Radiofluorierung von Boronsäurepinakolestern entwickelten Ting et al. auch eine Methode zur Radiofluorierung von Siliziumvorläufern (Abbildung 15b). Zwar war der radiochemische Umsatz (RCU) bei dieser Methode hoch, jedoch waren die Produkte in vivo nicht stabil genug für die Durchführung von PET-Messungen.[33, 39] Kurze Zeit später wurden di-*tert*-Butylphenylfluorsilane als starke Silikon-basierte Fluorakzeptoren (SiFAs) und Vorläufer für einen ^{18}F/^{19}F-Isotopenaustausch am Siliziumzentrum vorgestellt(Abbildung 15c). Mit dieser Methode markierte Tracer erwiesen sich in vivo als ausreichend stabil, was auf die sterische Abschirmung der di-*tert*-Butylgruppen

zurückgeführt werden konnte.[40, 41] Eine weitere Methode für die nukleophile ^{18}F-Fluorierung an einem Siliziumzentrum wurde 2008 von Mu et al. entwickelt (Abbildung 15d). Dabei wurden Aryldialkylsilane oder -dialkylsilanole als Radiomarkierungsvorläufer eingesetzt. Die Markierung fand unter Abgang von Hydrid beziehungsweise Hydroxid oder Alkoxiden statt, wobei die Ausbeuten im Fall von Radiomarkierungsvorläufern mit Hydroxy- oder Alkoxy-Abgangsgruppe durch Zusatz von Essigsäure verbessert werden konnten. Mit dieser Methode markierte Tetrapeptide erwiesen sich in vitro als ausreichend hydrolysestabil.[42] Kürzlich wurden zyklische Silikon-basierte Fluoridakzeptoren (CycloSiFA) vorgestellt (Abbildung 15e). Dabei wurden Azasilole unter Ringöffnung am Si-Atom Radiofluoriert. Die Reaktion läuft bei Raumtemperatur in MeCN unter Zugabe von Oxalsäure mit RCUs von bis zu 90% ab.[43]

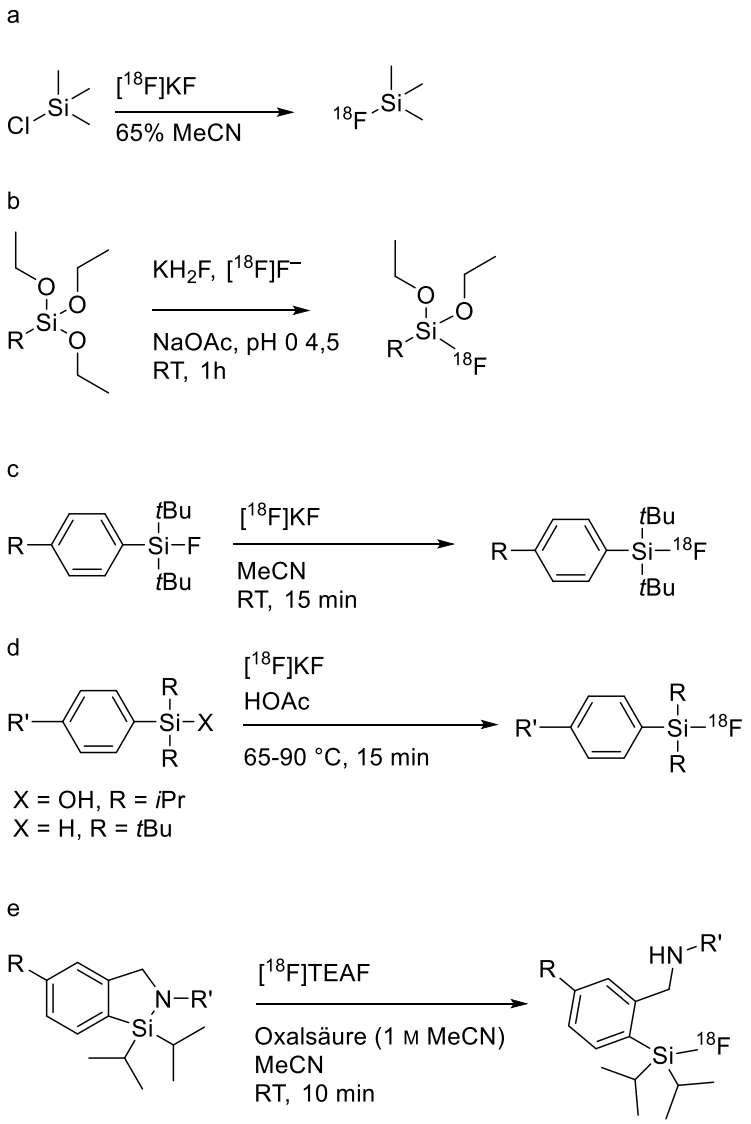

Abbildung 15: Radiofluorierung an Siliziumatomen. a: Chlortrimethylsilan; b: Tri-butoxy-silanole; c: ^{18}F/^{19}F-Isotopenaustausch an di-*tert*-Butylphenylfluorsilanen; d: Halogenaustausch an Dialkylsilanen oder Dialkylsilanolen; e: zyklische Silikon-basierte Fluoridakzeptoren.[33, 40, 42, 43]

[^{18}F]F-P-Markierung

Die erste Methode für den ^{18}F/^{19}F-Isotopenaustausch an einem Phosphoratom wurde 2019 von Hong et al. veröffentlicht (Abbildung 16a). Die sterisch abgeschirmten Organophosphinfluoride konnten bei Raumtemperatur in wässriger Lösung innerhalb von 15 min mit beinahe quantitativen RCUs markiert werden. In vivo wurde zudem über einen Zeitraum von 2 Stunden keine Defluorierung festgestellt.[44] Im Jahr 2021 entwickelten Wang et al. außerdem ein Verfahren zur nukleophilen Radiofluorierung von Phosphonaten (Abbildung 16b). Dabei wurden als Radiomarkierungsvorläufer Diphenoxyphosphonsäuren verwendet und zunächst unter wasserfreien Bedingungen eine der Phenoxy-Gruppen durch ^{18}F ersetzt. Anschließend wurde die zweite Phenoxy-Gruppe durch Zugabe von H_2O hydrolysiert. Diese Methode erwies sich als kompatibel mit vielen funktionellen Gruppen und ermöglichte die Radiofluorierung verschiedener empfindlicher Moleküle wie Peptide und Vitamine ohne den Einsatz von Schutzgruppen mit moderaten bis guten RCUs. Die erhaltenen [^{18}F]Fluorphosphonsäuren waren zudem über 2 Stunden in PBS-Puffer stabil.[45]

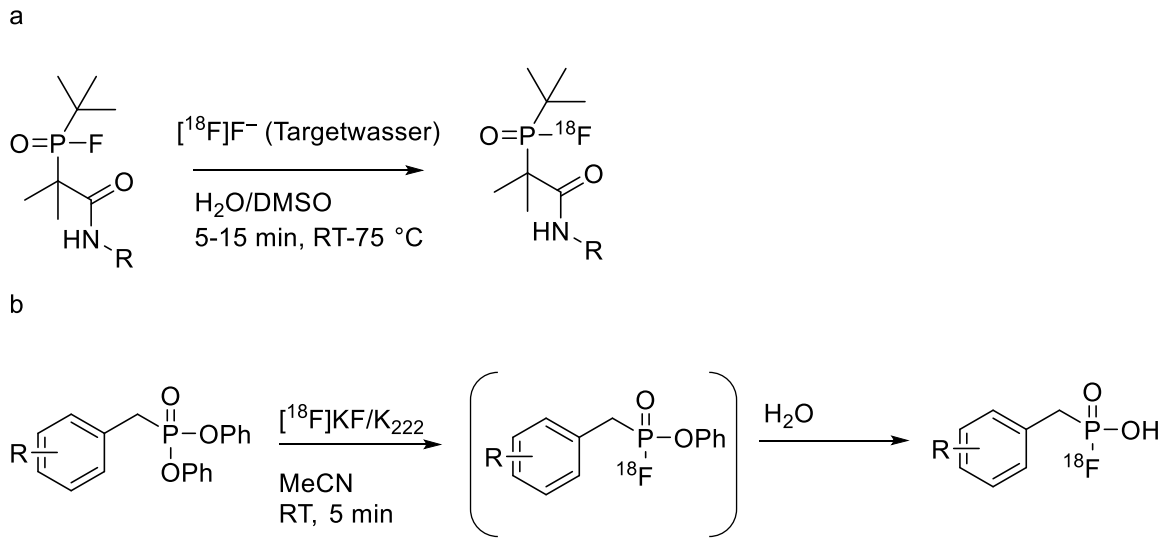

Abbildung 16: Synthese von [^{18}F]Organophosphinfluoriden[44] (a) und [^{18}F]Fluorphosphonsäuren (b).[45]

[^{18}F]F-S-Markierung

Inkster et al. präsentierten 2012 die Radiosynthese von [^{18}F]Arylsulfonylfluoriden durch die Substitution von Chlorid am Schwefelzentrum (Abbildung 17a). Die Reaktion verlief innerhalb von 15 min in Anwesenheit von H_2O mit RCUs von bis zu 80%.[46] Als großer Nachteil der [^{18}F]Sulfonylfluoride erwies sich jedoch ihre Anfälligkeit gegenüber Hydrolyse aufgrund der relativ schwachen S-F Bindung. Dieser Nachteil konnte weder durch die Markierung eines

vinylischen [^{18}F]Sulfonylfluorids mittels ^{18}F/^{19}F-Isotopenaustausch (Abbildung 17b),[47] noch durch die Herstellung verschiedener aliphatischer [^{18}F]Sulfonylfluoride oder eine sterische Abschirmung überwunden werden.[46-51] Auf Basis der höheren Stabilität von Arylfluorsulfaten im Vergleich zu Sulfonylfluoriden entwickelten Zheng et al. 2021 ein Verfahren für die Synthese von [^{18}F]Arylfluorsulfaten mittels ^{18}F/^{19}F-Isotopenaustausch (Abbildung 17c). Nach azeotroper Trocknung des [^{18}F]F$^-$ wurden die Fluorsulfonate in 30 Sekunden bei Raumtemperatur markiert.[52] Die über diese Methode produzierten Tracer wiesen eine relativ gute in vivo Stabilität auf. Eine weitere Optimierung von Walter et al. machte die zeitaufwendige azeotrope Trocknung überflüssig und ermöglichte die robuste Herstellung einer Reihe von neuen Tracern.[53]

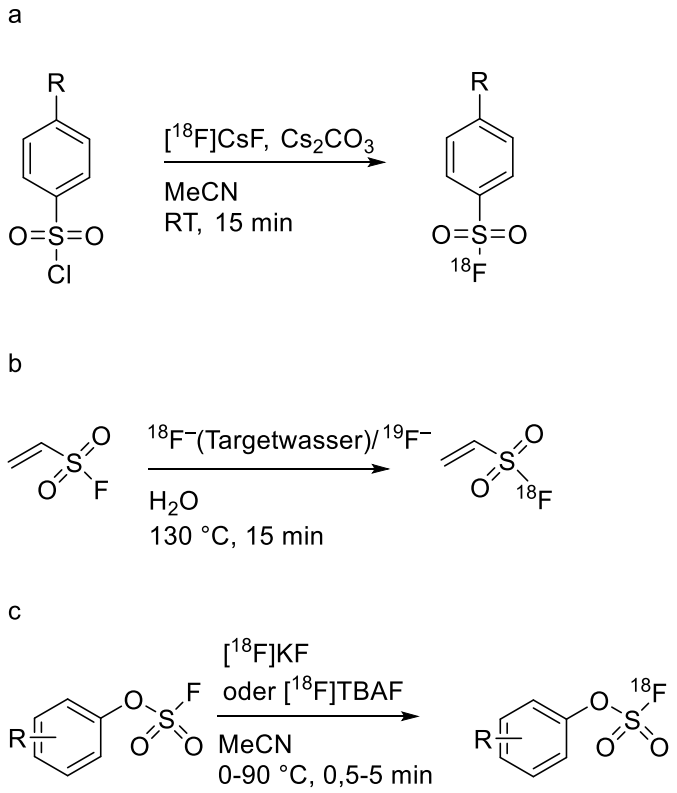

Abbildung 17: Synthese von [^{18}F]Sulfonylfluoriden und [^{18}F]Arylfluorsulfaten über nukleophile Substitution oder Isotopenaustausch. a: [^{18}F]Arylsulfonylfluoride, b: [^{18}F]Vinylsulfonylfluorid; c: [^{18}F]Arylfluorsulfate.[46, 47, 52, 53]

[^{18}F]F-M-Markierung

Einige Metalle bilden stabile M-F Bindungen. Zum Beispiel, sind die Dissoziationsenergien von Al-F (670 kJ/mol)[54] und Sc-F (586 kJ/mol)[55] sogar höher als die der C-F Bindung (485 kJ/mol).[56] McBride et al. nutzten diese Eigenschaft 2009, um ein Verfahren zur Herstellung ^{18}F-markierter PET-Tracer über Al[^{18}F]F-Komplexierung zu entwickeln.[57] Dafür werden Peptide

mit geeigneten Komplexbildnern konjugiert und nach Al[^{18}F]F-Markierung für die Bildgebung verwendet. Frühe Versuche zur Chelation von Al[^{18}F]F mit linearen Chelatoren wie DTPA (Abbildung 18a) gelangen zwar, jedoch erwiesen sich die erhaltenen Komplexe als instabil. Bei Verwendung des zyklischen Chelators NOTA waren zwar höhere Temperaturen zur Radiomarkierung erforderlich, dafür erwies sich in diesem Fall der radiomarkierte Komplex in vivo als stabil (Abbildung 18a).[29, 57-60] Bei der Markierung ist die Kontrolle des pH-Werts entscheidend, da Al^{3+} bei einem pH-Wert über 5 als Aluminiumhydroxid ausfällt, während das ^{18}F bei einem pH-Wert unter 4 als [^{18}F]HF vorliegt und deutlich weniger reaktiv gegenüber Al^{3+} ist. Da Al^{3+} eine Koordinationszahl von 6 und eine oktaedrische Komplexstruktur bevorzugt, sind zudem fünfzähnige Chelatoren mit einer sechsten Koordinationsstelle für das [^{18}F]Fluorid-Ion für die Al[^{18}F]F-Markierung besonders geeignet. Als Weiterentwicklung des N_3O_3-Chelators NOTA wurde daher der N_3O_2-Chelator NODA vorgeschlagen.[29, 60] Obwohl die Verwendung solcher zyklischen Chelatoren die Herstellung stabiler Komplexe in hohen Ausbeuten ermöglichte, erforderte die Markierung weiterhin Temperaturen von über 100 °C.[58] Ansätze, die Radiomarkierung bei niedrigeren Temperaturen durchzuführen waren nur bedingt erfolgreich und führten zu verringertem Umsatz.[61]

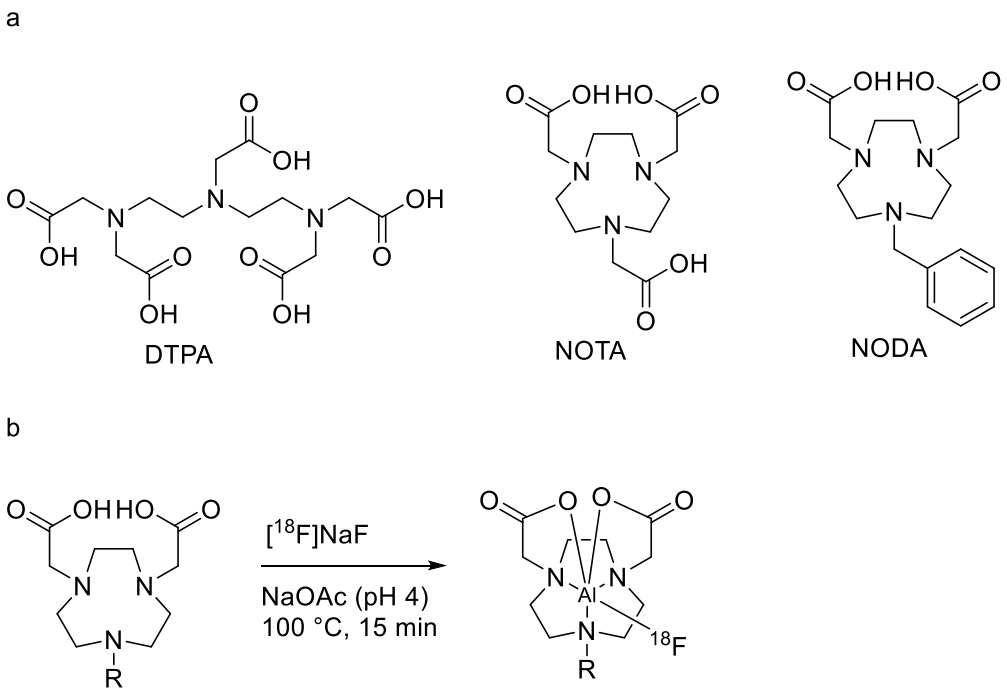

Abbildung 18: a: Verschiedene Chelatoren für die Al[^{18}F]F-Komplexierung; b: Radiosynthese von auf NOTA basierenden Al[^{18}F]F-Komplexen.[29, 57, 58, 60]

Um die hohen Komplexierungstemperaturen bei Verwendung zyklischer Chelatoren zu vermeiden, wurden Anstrengungen in die Entwicklung linearer Chelatoren mit ausreichender

Komplex-Stabilität investiert. 2015 berichteten Malik et al. von der Al[^{18}F]F-Markierung eines Liganden des Prostata-spezifischen Membranantigens (PSMA) unter Verwendung des linearen HBED-CC-Chelators (Abbildung 19).[62] Diese Markierung erfolgte mit hohen Umsätzen bereits bei 30 °C und konnte leicht automatisiert werden. Dennoch wurde eine erhebliche Defluorierung in vivo festgestellt.[63] Des Weiteren beschrieben Cleesen et al. H_3RESCA als einen alternativen Chelator für die Al[^{18}F]F-Markierung (Abbildung 19). H_3RESCA-Konjugate mit Peptiden, Proteinen und Antikörpern ließen sich bei Temperaturen unter 37 °C in wässrigem Puffer mit hohen Umsätzen markieren.[64] In vivo-Studien eines Al[^{18}F]F-markierten H_3RESCA-Peptidkonjugats zeigten im Vergleich zu einem entsprechenden NOTA-Konjugat eine ähnliche Clearance und eine leicht erhöhte Knochenaufnahme.[65] Russelli et al. berichteten 2020 über dem Chelator 2-AMPD-HB (Abbildung 19), der einen Piperidinring und einen Benzolring beinhaltet, um durch eine gewisse Starrheit des Chelators eine hohe kinetische Stabilität zu erzielen. Gleichzeitig ermöglichen die nicht-zyklische Struktur und zwei flexible Butansäurereste eine schnelle Komplexierung. Interessanterweise ließ sich dieser Chelator bei Raumtemperatur und einem pH-Wert von 6 mit guten RCUs markieren, was die Markierung säurelabiler Biomoleküle ermöglichen würde. In vivo Untersuchungen des reinen Al[^{18}F]F-Komplexes in gesunden Mäusen zeigten eine relativ geringe Anreicherung von Radioaktivität in den Knochen, was auf eine ausreichende Stabilität hindeutet.[66]

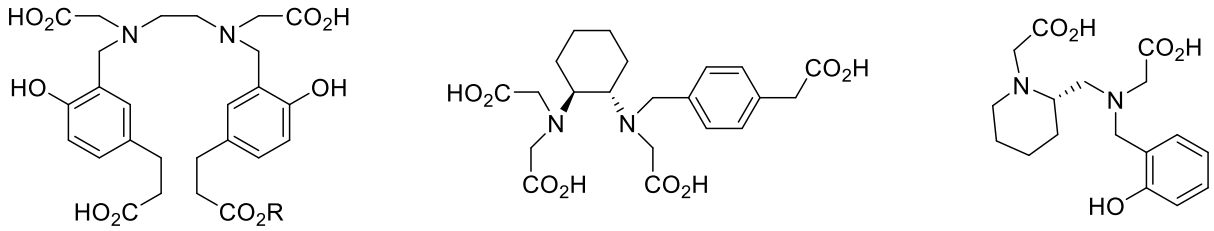

Abbildung 19: Lineare Chelatoren für die Al[^{18}F]F-Komplexierung.[62, 65, 66]

Als eine Alternative zur Al[^{18}F]F-Komplexierung wurde die Komplexierung von Ga[^{18}F]F vorgeschlagen. In diesem Fall konnte [GaF_3($BzMe_2$-tacn)] (Abbildung 20a) über einen ^{18}F/^{19}F-Isotopenaustausch mit einem RCU von 30% bei Raumtemperatur markiert werden.[67] Die Markierung des Komplexes [GaCl(Bz-NODA)] über Halogenaustausch mit trägerfreiem [^{18}F]F$^-$ (Abbildung 20b) ergab ebenfalls einen RCU von nur 30% bei Raumtemperatur, die Markierung bei 80 °C führte jedoch zu verbesserten Umsätzen von bis zu 70%.[68]

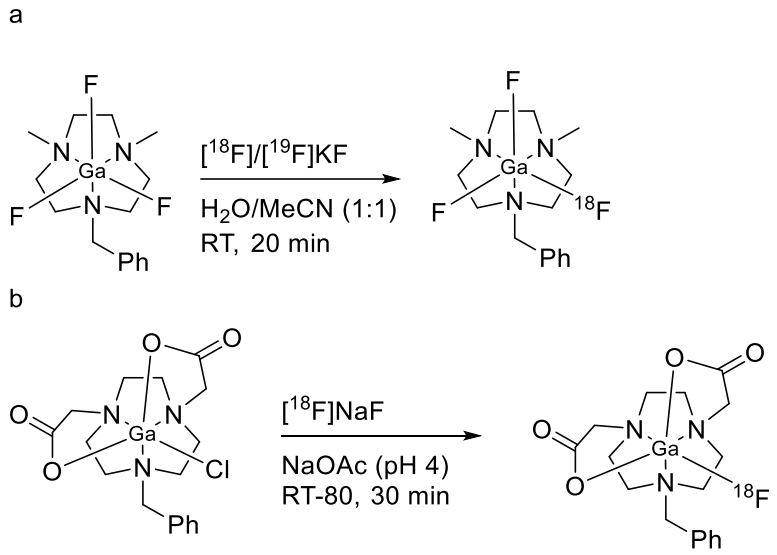

Abbildung 20: Radiofluorierung von Ga-Komplexen über Isotopenaustausch (a) und Halogenaustausch (b).[67, 68]

Im Jahr 2022 beschrieben Whetter et al. das erste Protokoll für die Sc[^{18}F]F-Markierung (Abbildung 21). Sie entdeckten, dass Scandium bei der Komplexierung mit dem von ihnen entwickelten sechszähnigen Chelator mpatcn eine freie Koordinationsstelle aufweist, die normalerweise von H_2O eingenommen wird. Diese kann alternativ mit einem [^{18}F]F^--Ligand besetzt werden, was eine Markierung des Chelators mit einem RCU von 89% ermöglichte. Die verwendeten Bedingungen waren weitgehend vergleichbar mit denen bei der Al[^{18}F]F-Markierung, allerdings waren keine organischen Lösungsmittel erforderlich. Ein mit dieser Methode radiomarkiertes AMPDA-PSMA-Konjugat zeigte eine hohe in vivo Stabilität und wies eine hohe Aufnahme im Tumor-Xenografen auf.[69]

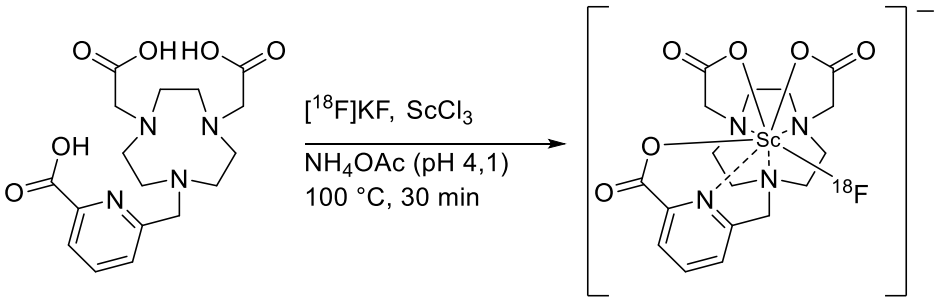

Abbildung 21: Synthese von Sc[^{18}F]F-mpatcn.[69]

1.4.3. Übergangsmetallvermittelte Radiofluorierung mit [^{18}F]Fluorid

In den letzten Jahren haben übergangsmetallvermittelte Radiofluorierungen stark an Bedeutung gewonnen. Sie ermöglichen die Radiofluorierung einer breiten Auswahl von Molekülen, insbesondere elektronenreicher (Hetero)Aromaten, deren Markierung zuvor

schwierig oder unmöglich war. Dabei wurden verschiedene Metalle wie Ni, Pd und Cu eingesetzt.[70-72] Ein zentraler Aspekt bei der metallvermittelten Radiomarkierung ist die Umpolung, die durch Umkehr der Polarität von $[^{18}F]F^-$ die Markierung von elektronenreichen (Hetero)Aromaten unter Verwendung von nukleophilem $[^{18}F]F^-$ ermöglicht.

Kupfervermittelte Radiofluorierung

Im Vergleich zu anderen metallvermittelten Radiofluorierungen zeichnet sich die kupfervermittelte Radiofluorierung durch ihre Robustheit gegenüber Feuchtigkeit und Sauerstoff aus. Die ersten Cu-vermittelten aromatischen Radiofluorierungen wurden von Ichiishi et al. und Tredwell et al. vorgestellt. Bei der von Ichiishi et al. entwickelten $Cu(Py)_4(OTf)_2$-vermittelte Markierung von (Aryl)(mesityl)-iodonium-Salzen konnte selektiv der weniger sterisch gehinderte Aromat unabhängig von dessen elektronischen Eigenschaften radiofluoriert werden.[73] Tredwell et al. nutzten hingegen Arylboronsäurepinakolester als Vorläufer, welche sich durch eine hohe Stabilität und gute Verfügbarkeit auszeichnen. Die Methode erzielte unter Vermittlung durch $Cu(Py)_4(OTf)_2$ hohe RCUs. Später wurden auch freie Boronsäuren[74], Trimethylstannane[75] und Arylhalogenide[76] als Vorläufer für die Cu-vermittelte Radiofluorierung vorgestellt (Abbildung 22c–e). Im Jahr 2019 stellten Lee et al. eine Methode zur direkten Radiofluorierung von C-H Bindungen am Aromaten vor (Abbildung 22f).[77]

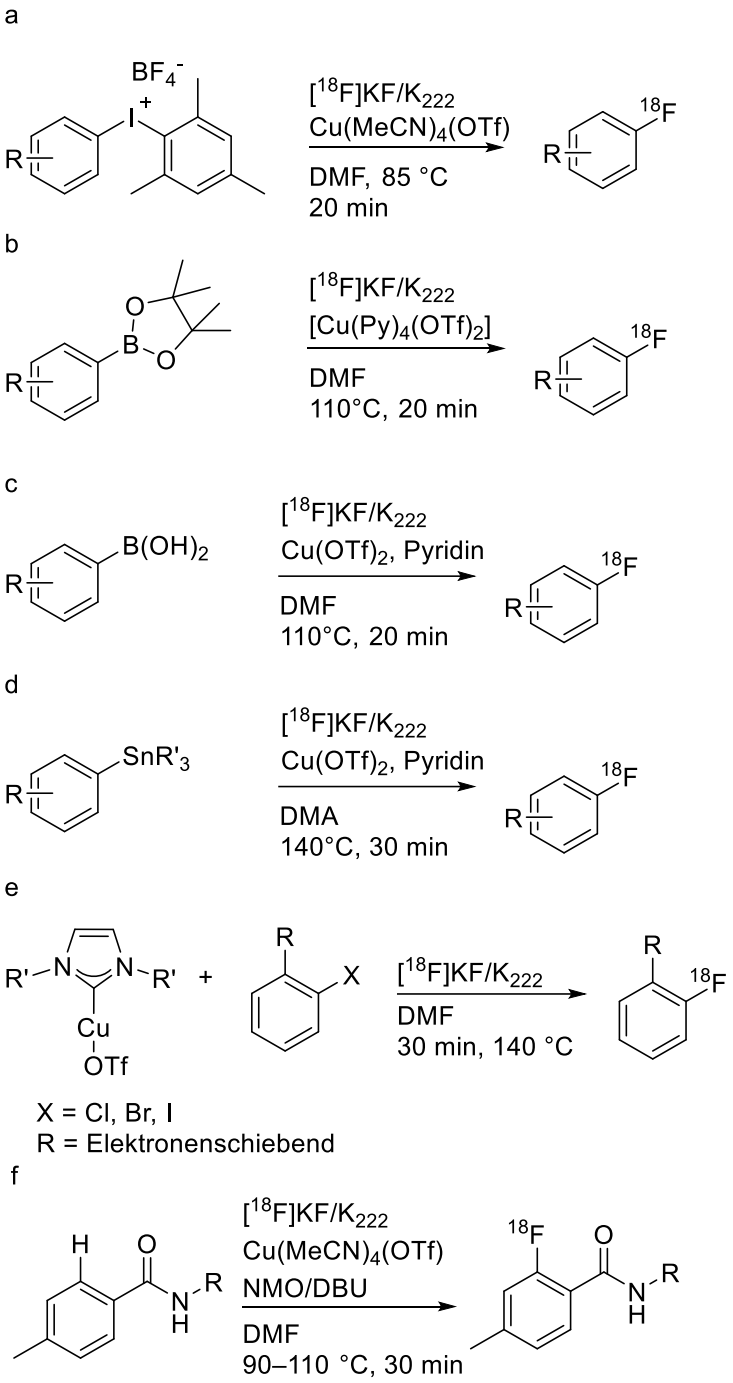

Abbildung 22: Cu-vermittelte Radiofluorierungen verschiedener Vorläufer. a: (Aryl)(mesityl)-iodonium-Salze; b: Arylboronsäurepinakolester; c: Boronsäuren; d: Trimethylstannane, e: Arylhalogenide; f: C-H Radiofluorierung.[73-78]

Ein Problem der ersten Prozeduren für die kupfervermittelten Radiosynthesen war die Übertragung auf Tracersynthesen im präparativen Maßstab. Dies lag hauptsächlich an der relativ großen Menge an Basen, die zur Elution des $[^{18}F]F^-$ verwendet wurden und eine sehr schnelle Zersetzung der verwendeten Kupfervermittlers verursachten. Zlatopolskiy et al. zeigten 2015, dass mit geringeren Basenmengen (Low-Base-Protokoll) wesentlich höhere RCUs erzielt werden können. Sie wendeten auch die "Minimalistische Methode" zur Elution

mit Aryliodoniumvorläufern an, um sowohl den Zusatz von Basen als auch die azeotrope Trocknung komplett zu vermeiden.[79] Zischler et al. berichteten 2017, dass die Zugabe von bestimmten Alkoholen zu den Reaktionsgemischen bei der Markierung von Boronsäuren, Boronsäurepinakolestern und Stannanen zu einer deutlichen Steigerung des RCUs führt. Zusätzlich konnten sie bei diesen nicht-ionischen Vorläufern durch Elution des $[^{18}F]F^-$ mit einer geringen Menge $TEAHCO_3$ im verwendeten Alkohol eine azeotrope Trocknung überflüssig machen.[80] Im Jahr 2023 beschrieben Hoffmann et al. eine Reihe neuer Kupferkomplexe, die zu erhöhten Umsätzen und oft einer Verringerung der erforderlichen Vorläufermenge bei einem breiten Spektrum von Boronsäurepinakolestern, Boronsäuren und Stannanen führten. Neben einer Reihe von Modellsubstraten wurden die neuen Kupferkomplexe erfolgreich für die Herstellung verschiedener PET-Tracer eingesetzt. Die effizientesten Kupfervermittler waren $[Cu(4\text{-}PhPy)_4(ClO_4)_2]$ und $[Cu(3,4\text{-}Me_2Py)_4(OTf)_2]$. Die Elution von $[^{18}F]F^-$ wurde mit Et_4NOTf durchgeführt, welches im Vergleich zu Hydrogencarbonat wesentlich weniger basisch ist, während sich DMI als optimales Lösungsmittel für die anschließende Radiofluorierung erwies (Abbildung 22).[81]

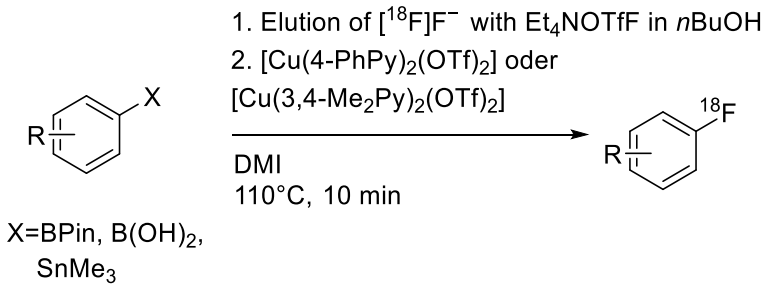

Abbildung 23: Cu-vermittelte Radiofluorierung mit neuen Kupferkomplexen.[81]

1.5. Indirekte Radiofluorierung

Wie schon eingangs erwähnt, sind zur Radiofluorierung von Biomolekülen oft indirekte Radiomarkierungsverfahren erforderlich, bei denen zunächst eine ^{18}F-markierte prosthetische Gruppe (PG) hergestellt und in einem zweiten Schritt mit dem Zielmolekül konjugiert wird.

Voraussetzung für diesen Ansatz ist die Verfügbarkeit geeigneter PGs, für deren Herstellung grundsätzlich alle der bisher vorgestellten Radiofluorierungstechniken genutzt werden können. Um sich für die indirekte Radiofluorierung praktisch einsetzen zu lassen, muss die PG zudem eine Reihe von Anforderungen erfüllen. Erstens sollte ihre Herstellung schnell und mit hohen Ausbeuten möglich sein, um die Zielverbindung trotz des zusätzlich erforderlichen

Konjugationsschritts ebenfalls in hohen Ausbeuten und mit möglichst geringer Synthesedauer zu erhalten. Außerdem sollten idealerweise keine zusätzlichen Reinigungsschritte erforderlich sein oder diese sollten schnell durchführbar sein. Für die Konjugation mit dem Zielmolekül muss die PG außerdem eine entsprechend reaktive funktionelle Gruppe enthalten, welche die Radiomarkierung nicht behindert und unter deren Bedingungen stabil sein sollte. Die anschließende Konjugation sollte zudem regioselektiv und unter möglichst milden Bedingungen durchführbar sein.

Ein Ansatz für die indirekte Radiofluorierung von nativen Peptiden und Proteinen ist es, die bereits in diesen Molekülen vorhandenen funktionellen Gruppen für die Konjugation mit einer PG zu nutzen. So können beispielsweise Lysin-haltige Biomoleküle durch Acylierung oder Alkylierung der Amino-Gruppe in der Lysin Seitenkette mit ^{18}F-markierten aktivierten Carbonsäureestern oder Anhydriden als PGs markiert werden. Ein bekanntes Beispiel für eine solche Amin-reaktive PG ist *N*-Succinimidyl-4-[^{18}F]fluorbenzoat ([^{18}F]SFB, Abbildung 22).[82]

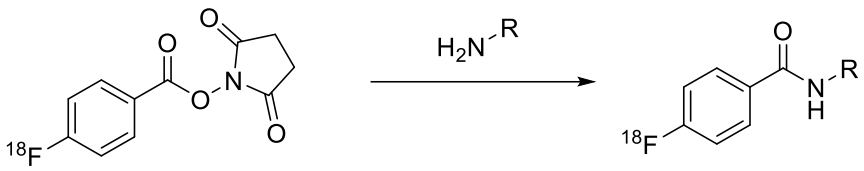

Abbildung 24: Indirekte Radiofluorierung durch Acylierung einer Aminogruppe mit [^{18}F]SFB.[82]

Die Thiolgruppe in der Seitenkette von Cystein stellt eine weitere funktionelle Gruppe dar, welche sich für die indirekte Radiofluorierung von Peptiden nutzen lässt. Thiole sind starke Nukleophile und können über eine Michael-Addition mit geeigneten Michael-Akzeptoren konjugiert werden. Häufig werden dafür Maleimide verwendet, die chemoselektiv mit den Thiolgruppen in Proteinen reagieren. Ein Beispiel für eine Thiol-reaktive PG mit Maleimid-Funktion ist [^{18}F]FBEM[83], welches sich in wässrigem Puffer (pH 7.4) bei Raumtemperatur innerhalb von 20 min mit Thiol-haltigen Peptiden konjugieren lässt (Abbildung 25 a).[84] Da die freie Thiol-Gruppe in Peptiden seltener vorkommt als Amino-Gruppen, kann mit Thiol-reaktiven PGs häufig eine höherer Selektivität als mit Amin-reaktiven PGs erreicht werden. Ein Nachteil vieler Maleimid-basierter PGs ist allerdings die aufwendige Radiosynthese mit geringen Ausbeuten sowie ihre Anfälligkeit für Hydrolyse über retro-Michael-Reaktionen.[85] Alternativ können ^{18}F-markierte Phenyloxadiazolmethylsulfon-Derivate als PGs eingesetzt werden (Abbildung 25 b). Mit einer solchen PG wurden bei niedrigen Temperaturen innerhalb von 15 min verschiedene radiofluorierte Peptide und Proteine hergestellt, welche sich in vivo

als stabil erwiesen.[86] Im Jahr 2021 stellten Ma et al. eine neue PG mit einer Vinylsulfonyl-Funktion als starkem Michael-Akzeptor vor (Abbildung 25 c). Diese konnte ohne azeotrope Trocknung (durch Elution von [^{18}F]F$^-$ mit kationischem Vorläufer wie in der Minimalist-Methode) in einem einzigen Schritt in einer moderaten RCA von 46% nach 41 min hergestellt werden. Durch Verwendung einer Festphasenextraktionskartusche zur Isolation war zudem keine HPLC-Reinigung erforderlich. Die Konjugation mit verschiedenen Peptiden erfolgte in hohen RCAs in wässrigem Puffer bei 35 °C innerhalb von 30 min. Ebenfalls im Jahr 2021 berichteten Humpert et al. über 5-Iod-2-[^{18}F]fluorpyridin, welches als PG für die indirekte Radiofluorierung mittels Pd-katalysierter *S*-Arylierung[87] eingesetzt werden kann (Abbildung 25 d). Dabei wurde das entsprechende DABCO-Triflat-Salz als Vorläufer verwendet und nach dem Minimalist-Protokoll ohne azeotrope Trocknung radiofluoriert. Die Reinigung erfolgte über Festphasenextraktion mit einer hohen RCA von 77% innerhalb von 30 min. Die Konjugation erfolgte Pd-vermittelt in einem Gemisch aus MeCN und wässrigem Puffer bei Raumtemperatur innerhalb von 1–6 min und lieferte verschiedene radiofluorierte Peptide und Proteine in guten isolierten Ausbeuten.[86]

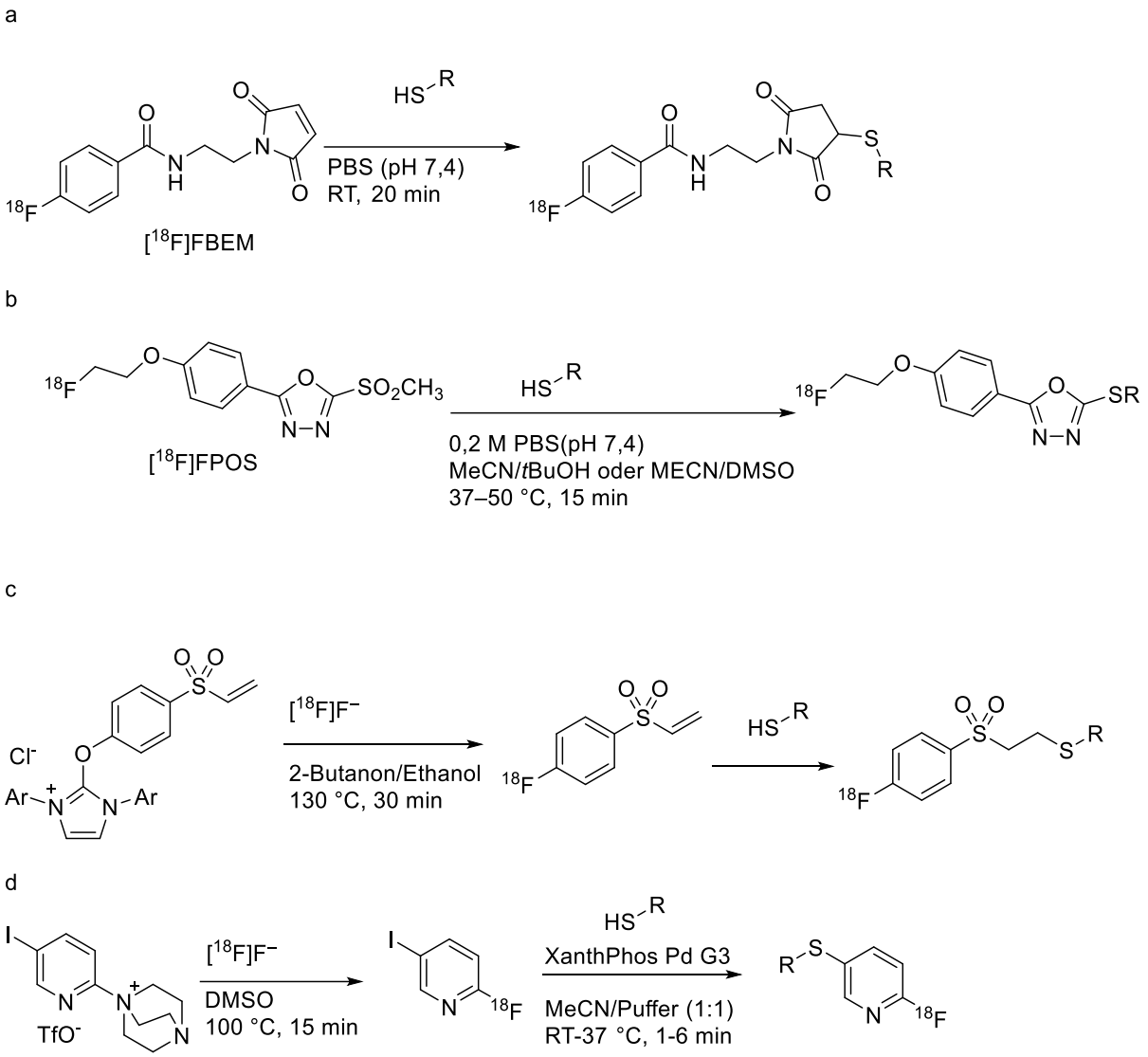

Abbildung 25: Indirekte Radiofluorierung durch Konjugation von verschiedenen PGs mit Thiolgruppen. a: [^{18}F]FBEM, b: [^{18}F]FPOS; c: 1-[^{18}F]Fluor-4-(vinylsulfonyl)benzol; d: 5-Iod-2-[^{18}F]fluorpyridin.[84, 86, 88, 89]

Eine Alternative zur indirekten Radiofluorierung mit Amin- oder Thiol-reaktiven PGs stellt die Konjugation von geeigneten PGs mit einer zuvor installierten funktionellen Gruppe im zu markierenden Biomolekül dar. Die dafür erforderlichen Funktionalisierungen können entweder am nativen Molekül oder, im Fall von Peptiden, während der Peptidsynthese über artifizielle Aminosäuren vorgenommen werden. Eine verbreitete Methode zur indirekten Radiofluorierung von funktionalisierten Biomolekülen ist etwa die Cu-katalysierte 1,3-dipolare Azid-Alkin Cycloaddition (Abbildung 26).[90] Dabei reagieren unter wässrigen Bedingungen und bei niedrigen Temperaturen ein Azid und ein Alkin zu einem 1,2,3-Triazol, welches eine hohe in vivo Stabilität aufweist. Für diesen Ansatz kann das Biomolekül entweder mit einem Azid oder einem Alkin Funktion funktionalisiert werden, während die PG die jeweils andere Funktion enthält. Die Konjugation erfolgt unter sehr milden Bedingungen und erreicht hohe

RCUs.[91] Kupferfreie Azid-Alkin 1,3-Dipolare Cycloadditionen können über den Einsatz von unter Ringspannung stehenden Alkinen erreicht werden. Ein Nachteil ist, dass die Reaktion in diesem Fall nicht regioselektiv ist und ein Gemisch der beiden möglichen Regioisomere erhalten wird.[90] In den letzten Jahren sind solche PGs, wie beispielsweise eine Alkin-funktionalisierte [^{18}F]Trifluorboronsäure[92], oder ein Azid- funktionalisiertes [^{18}F]SiFA Derivat[93], auch über moderne Radiofluorierungsmethoden hergestellt worden.

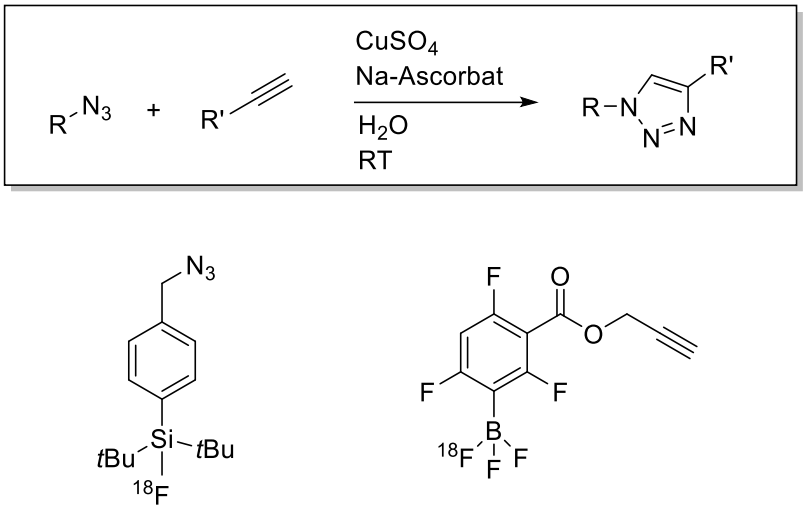

Abbildung 26: Indirekte Radiofluorierung über die Cu-katalysierte Azid-Alkin 1,3-dipolare Cycloaddition.[39, 92, 93]

Eine weitere bioorthogonale Cycloaddition welche für die indirekte Radiofluorierung eingesetzt wird, ist die Diels-Alder-Reaktion mit umgekehrtem Elektronenbedarf (inverse electron demand Diels-Alder, IEDDA). Dabei werden Tetrazine als elektronenarme Diene verwendet, die unter Elimination von N_2 mit einem unter Ringspannung stehenden *trans*-Cycloocten konjugiert werden. Die Reaktion verläuft sehr schnell bei Raumtemperatur und benötigt keine Metallkatalysatoren. Xu et al. beschrieben kürzlich eine neue hydrophile PG, die ein trans-Cycloocten enthält und in einem einzigen Schritt mit einer RCA von 52% hergestellt werden kann. Unter Verwendung dieser PG konnten verschiedene Tetrazin-modifizierte Proteine radiofluoriert werden (Abbildung 27).[94] Die IEDDA kann auch für Pretargeting-Ansätze genutzt werden, bei denen etwa ein Antikörper-*trans*-Cycloocten-Konjugat in vivo mit einem radiomarkierten Tetrazin konjugiert wird.[95]

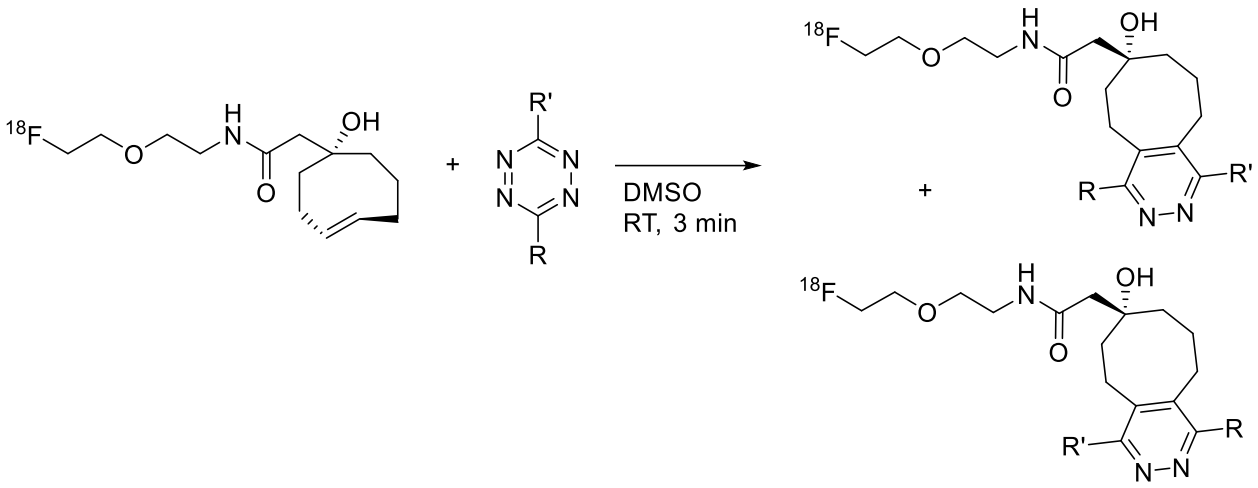

Abbildung 27: Indirekte Radiofluorierung eines Tetrazin-modifizierten Biomoleküls mit einer *trans*-Cycloocten-basierten PG über eine IEDDA.[94]

2. Zielsetzung

In den letzten Jahren wurden bedeutende Fortschritte bei der Entwicklung von Radiofluorierungsverfahren erzielt, welche die Synthese von zuvor nur schwer zugänglichen Tracern ermöglicht haben. Trotz dieser Entwicklungen besteht weiterhin Bedarf an der Erforschung und Optimierung neuer Markierungstechniken, um ihr volles Potenzial zu erschließen. Diese Arbeit sollte in mehreren Teilprojekten dazu beitragen.

Das erste Projekt konzentrierte sich auf die kupfervermittelte Radiofluorierung. Diese Methode hat in den letzten 10 Jahren die ^{18}F-Chemie stark beeinflusst und die Synthese vieler zuvor unzugänglichen radiomarkierten (Hetero)aromaten ermöglicht. Allerdings fehlten bis vor kurzem detaillierte Untersuchungen des verwendeten Kupfersystems und es wurden in der Regel Kupfertriflat und Pyridin oder $Cu(Py)_4(OTf)_2$ in MeCN oder *N,N*-Dimethylformamid (DMF) verwendet. Hoffmann et al. berichten jedoch kürzlich von einer neuen Generation von Kupferkomplexen für die kupfervermittelte Radiofluorierung und untersuchten deren Effizienz mit einer Auswahl an Modellsubstraten und insbesondere auch in Abhängigkeit des verwendeten Lösungsmittels.[81] Im Rahmen der vorliegenden Arbeit sollte einer der neuen Kupferkomplexe, $[Cu(3,4\text{-}Me_2Py)_4(OTf)_2]$, für die Radiosynthese von drei [^{18}F]Fluorphenylalaninen ([^{18}F]FPhes) verwendet werden (Abbildung 28). Die dazu benötigten Radiomarkierungsvorläufer sollten in Form von Nickelkomplexen hergestellt werden, um eine einfache und stereoselektive Synthese zu ermöglichen.[96] Dabei sollte auch ein Vergleich zwischen der Verwendung von $B(OH)_2$ und BPin als Abgangsgruppen durchgeführt werden. Um die Herstellung größerer Aktivitätsmengen für die präklinische Evaluation zu ermöglichen, sollte zudem die Automatisierung der Synthese von 3-[^{18}F]Fluorphenylalanin (3-[^{18}F]FPhe) in einem kommerziellen Synthesemodul demonstriert werden.

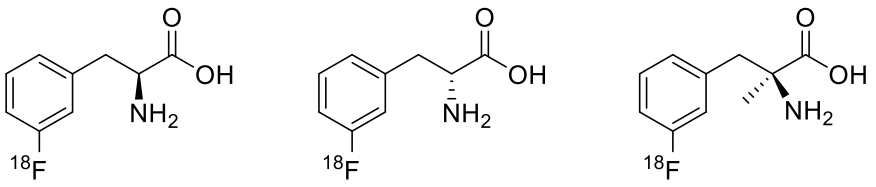

Abbildung 28: Strukturen von (*S*)- und (*R*)-3-[^{18}F]FPhe und (*S*)-αMe-3-[^{18}F]FPhe.

Ein wesentlicher Teil der Entwicklung neuer Radiotracer besteht darin, ihre Verteilung im Körper zu untersuchen und gegebenenfalls zu optimieren. So kann etwa durch strukturelle

Modifikation häufig die Penetration der Zellmembran oder Blut-Hirn-Schranke verbessert oder nachteilige Eigenschaften wie eine schnelle Metabolisierung reduziert werden. Im Rahmen des zweiten Projektes sollte der Methylester des Aminosäuretracers *O*-[^{18}F]Fluorethyltyrosin ([^{18}F]FET) hergestellt werden, um herauszufinden, ob der Ester ggf. bestimmte Vorteile in Hinblick auf die Tumoraufnahme haben könnte. (Abbildung 29). Zudem sollte *m*-[^{18}F]FET hergestellt werden, um seine Untersuchung als Alternative zu [^{18}F]FET zu ermöglichen.

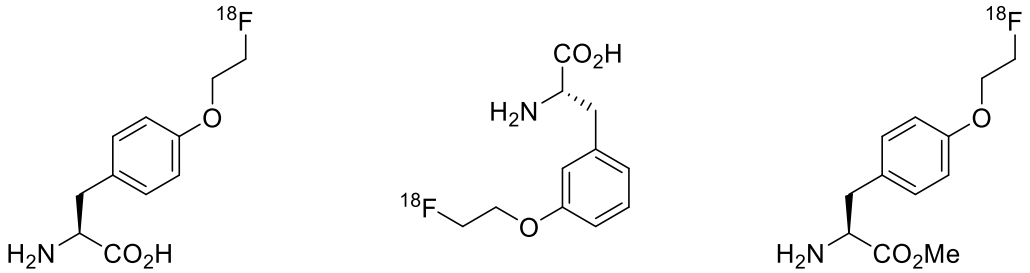

Abbildung 29: Strukturen von [^{18}F]FET, *m*-[^{18}F]FET und [^{18}F]FET-OMe.

Das dritte Projekt befasste sich mit der Entwicklung neuer PGs für die indirekte Radiofluorierung von emfindlichen (Bio)molekülen. Effektive PGs sollten in kurzer Zeit mit hoher Ausbeute herstellbar sein und eine Reaktivität aufweisen, die eine Konjugation mit dem Zielmolekül ermöglicht. Viele bisher verfügbare PGs erfüllen jedoch nicht alle dieser Anforderungen. Daher sollten im Rahmen dieser Arbeit neue Vertreter entwickelt und untersucht werden. Dafür wurden vier verschiedene *N*-substituierte 1-Amino-7-[^{18}F]fluor-8-azaisatosäureanhydride ([^{18}F]AFAs) beziehungsweise deren Hydrolyseprodukte, die entsprechende Aminosäuren, ausgewählt (Abbildung 30). Aufgrund der starken Aktivierung der Radiomarkierungsvorläufer zu SNAr Reaktionen sollte die Radiofluorierung „on-cartridge“ durchgeführt werden. Die anschließende Reinigung sollte über eine einfache Festphasenextraktion (FPE) erfolgen. Die so hergestellten PGs sollten dann mit verschiedenen Modellaminen, -alkinen und -aziden konjugiert werden.

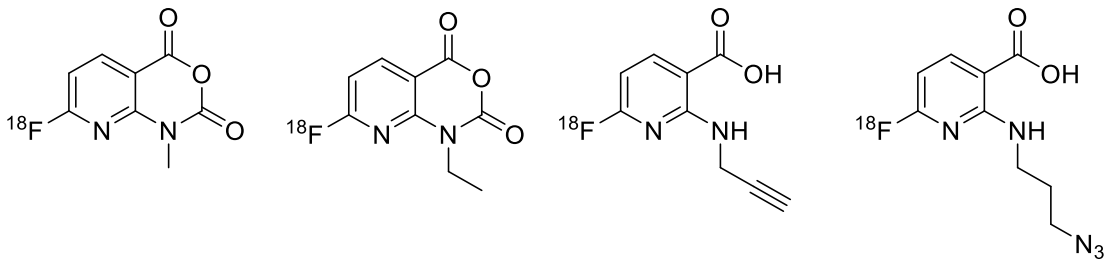

Abbildung 30: Strukturen der PGs basierend auf 1-Amino-7-fluor-8-azaisatosäureanhydrid.

Als Anwendungsbeispiel für die Methode sollten außerdem verschiedene Radiotracer hergestellt werden. Dafür wurden drei PSMA-Liganden und ein Inhibitor des Fibroblastenaktivierungsproteins (FAP) (Abbildung 31) ausgewählt. Schließlich sollte die Anwendbarkeit der neuen PGs für eine direkte Markierung von nativen Proteinen am Beispiel von Insulin untersucht werden.

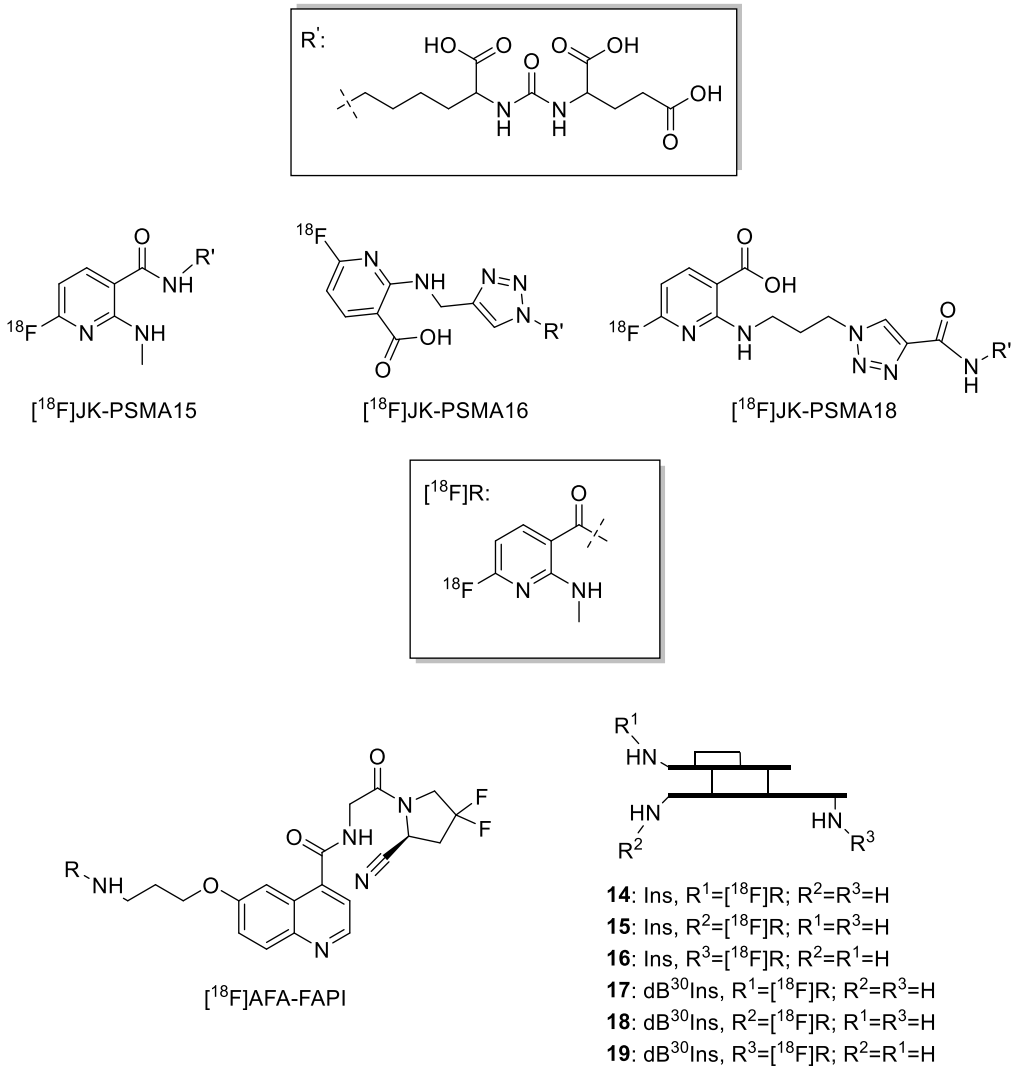

Abbildung 31: Strukturen der Radiotracer und Insulin- beziehungsweise desB^{30} Insulin-Konjugate, welche über indirekte Radiofluorierung mit *N*-substituierten 1-Amino-7-[^{18}F]fluor-8-azaisatosäureanhydriden hergestellt wurden.

Im letzten Projekt wurde schließlich die Radiofluorierung über die Al[^{18}F]F-Komplexierung behandelt. Die 2009 von McBride et al. vorgestellte Methode eröffnet einen völlig neuen Weg, mit geeigneten Komplexbildnern funktionalisierte Moleküle direkt mit ^{18}F zu markieren.[57] In dieser Arbeit sollte dies zur ersten direkten Radiofluorierung von humanem Insulin eigesetzt werden (Abbildung 32a). Zudem sollte die Synthese von Al[^{18}F]F-FAPI-42 optimiert werden (Abbildung32b). Zuletzt sollte die Al[^{18}F]F-Komplexierung mit einem neuen Chelator, basierend auf 2-AMPDA-HB,[66] untersucht werden (Abbildung32c).

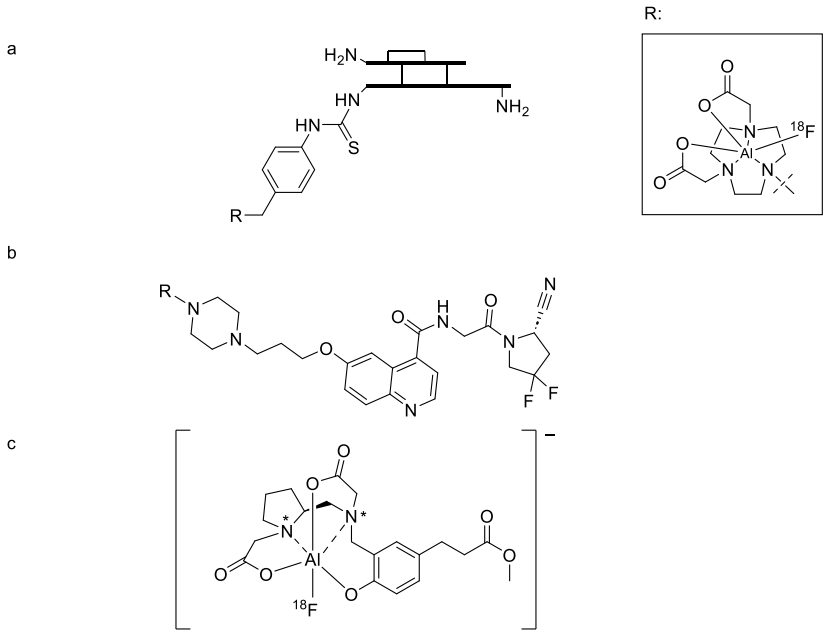

Abbildung 32: Synthese von Radiotracern über Al[^{18}F]F-Komplexierung. a: Radiofluorierung von B^{1}-NODA-Ins; b: Radiofluorierung von FAPI-42; c: Radiofluorierung eines neuen Chelators basierend auf 2-AMPDA-HB.

3. Ergebnisse

3.1. Synthese von ^{18}F-markierten Phe-Derivaten mittels kupfervermittelter Radiofluorierung

Radiomarkierte aromatische Aminosäuren werden seit Jahrzehnten routinemäßig für die Bildgebung von Gliomen eingesetzt. Ihr Einsatz beruht auf der Überexpression von Aminosäuretransportern wie dem "Large Amino Acid Transporter 1" (LAT1) in vielen Hirntumoren.[97, 98] Im Vergleich zu [^{18}F]FDG haben Aminosäuretracer den Vorteil, dass sie durch gesundes Hirngewebe kaum aufgenommen werden.[97] Entsprechend besteht ein hoher Bedarf an neuen Aminosäuretracern, die als Substrate für LAT1 oder ähnliche Transportsysteme fungieren. Aromatische Aminosäuren (AAS), die einen ^{18}F-Substituent direkt am Aromaten enthalten stellen vielversprechende Tracerkandidaten dar. Die Herstellung solcher radiomarkierter Verbindungen ist jedoch oft mit niedrigen RCAs und/oder aufwendigen mehrstufigen Radiosynthesen und Vorläufersynthesen verbunden. Daher wurde von Craig et al. eine neue Methode für die Produktion radiofluorierter AAS über kupfervermittelte ^{18}F-Fluorierung leicht zugänglicher Ni-BPX-AAS-Komplexe entwickelt (Abb. 33 und 35). [96,99] Dabei fungiert das Ni-BPX-Fragment gleichzeitig als eine Schutzgruppe für α-Amino- und α-Carboxyfunktionen. Die Markierung wurde durch $Cu(py)_4(OTf)_2$ in DMA als Mediator erreicht, wobei der arylische Boronsäurepinakolester durch [^{18}F]F^- substituiert wurde.

Im Rahmen dieser Arbeit wurde zunächst die von Craig et al. beschriebene Vorläufersynthese von (*S*,*S*)-Ni-BPB-3-(BPin)-Phe [(*S,S*)-**5**], (*R*,*R*)-Ni-BPB-3-(BPin)-Phe [(*R,R*)-**5**] und (*S*,*S*)-Ni-BPA-3-(BPin)-αMe-Phe [(*S,S*)-**6**] ausgehend von (*S*)-1-Benzophenyl-*N*-(2-formylphenyl)pyrrolidin-2-carboxamid [(*S*)-**1**)], (*R*)-1-Benzophenyl-*N*-(2-formylphenyl)pyrrolidin-2-carboxamid [(*R*)-**1**)] oder (*S*)-1-Benzyl-*N*-(2-formylphenyl)pyrrolidin-2-carboxamid [(*S*)-**2**)] und entweder Glycin oder Alanin in zwei Schritten nachvollzogen Abbildung 33).[96, 99] Nach der Bildung der Komplexe mit Nickel(II)acetat wurden diese mit 2-(3-Brommethyl)phenyl-4,4,5,5-tetramethyl-1,3,2-dioxaborolan zu den entsprechenden Radiomarkierungsvorläufern (*S,S*)-**5**, (*R,R*)-**5** und (*S,S*)-**6** umgesetzt.

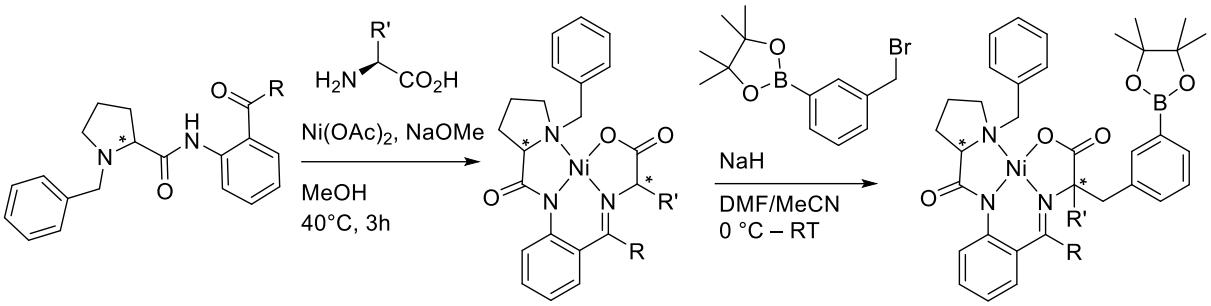

S-**1**: R=Ph
R-**1**: R=Ph
S-**2**: R=H

(*S,S*)-**3**: R=Ph, R'=H 78%
(*R,R*)-**3**[a]: R=Ph, R'=H
(*S,S*)-**4**[a]: R=H, R'=CH_3

(*S,S*)-**5**: R=Ph, R'=H 39%
(*R,R*)-**5**: R=Ph, R'=H 40%
(*S,S*)-**6**: R=H, R'=CH_3 40%

Abbildung 33: Synthese der Ni-BPX-BPin Vorläufer. a: Bereitgestellt von Dr. N. Kolks.

Die kupfervermittelte Radiofluorierung ist nicht nur für Boronsäurepinakolester bekannt, sondern auch für freie Boronsäuren.[74] Um einen direkten Vergleich an demselben Tracer durchzuführen, sollten sowohl Pinakolester als auch Boronsäuren als Radiomarkierungsvorläufer getestet und die jeweiligen Umsätze verglichen werden. Dazu wurden die Pinakolester mithilfe von Methylboronsäure in die entsprechenden Boronsäuren umgewandelt (Abbildung 34).[100]

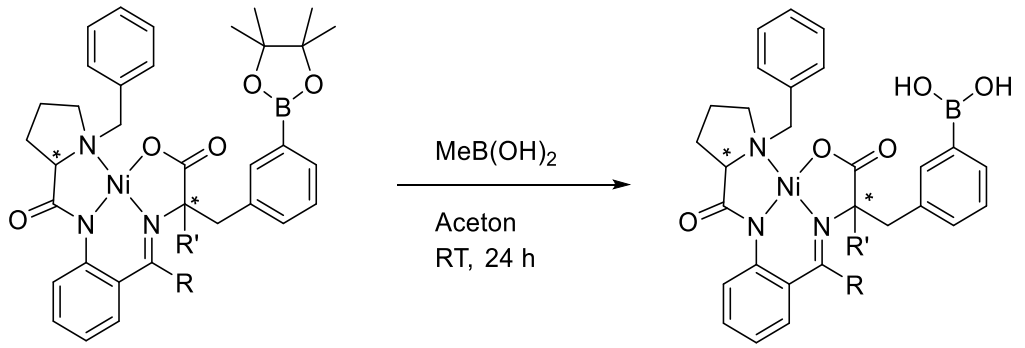

(*S,S*)-**5**: R=Ph, R'=H
(*R,R*)-**5**: R=Ph, R'=H
(*S,S*)-**6**: R=H, R'=Me

(*S,S*)-**7**: R=Ph, R'=H 85%
(*R,R*)-**7**: R=Ph, R'=H 98%
(*S,S*)-**8**: R=H, R'=Me 90%

Abbildung 34: Hydrolyse des Boronsäurepinakolesters zur Boronsäure.[100]

Die Radiofluorierung der Boronsäure- und Boronsäurepinakolestervorläufer wurde dann unter den von Hoffmann et al. optimierten Bedingungen durchgeführt (Abbildung 35).[81] Dabei wurde $[^{18}F]F^-$ auf einer Anionenaustauscherkartusche fixiert und mit wasserfreiem MeOH gespült, um Wasserreste zu entfernen. Nach der Trocknung im Luftstrom wurde das $[^{18}F]F^-$ mit einer Lösung von Et_4NOTf in *n*-Butanol direkt in eine Lösung des Radiomarkierungsvorläufers in 1,3-Dimethyl-2-imidazolidinon (DMI) eluiert. Das finale Verhältnis zwischen *n*-Butanol und DMI betrug dabei 1:2. Die Markierung wurde anschließend

bei 110 °C über 10 min durchgeführt. Die entsprechenden Umsätze sind in Abbildung 35 zusammengefasst und lagen zwischen 69 und 91%. Im Fall von (*S*)- und (*R*)-3-[^{18}F]FPhe waren die Umsätze höher, wenn die freien Boronsäuren als Vorläufer verwendet wurden, während sie im Fall von α-Me-[^{18}F]FPhe bei Verwendung des Boronsäurepinakolesters als Vorläufer höher waren. Allerdings waren in zwei von drei Fällen diese Unterschiede nicht signifikant, sodass kein allgemeingültiger Trend erkennbar ist. Ausgehend von den radiofluorierten Komplexen (*S,S*)-[^{18}F]**9** und (*R,R*)-[^{18}F]**9** wurden (*S*)- und (*R*)-3-[^{18}F]FPhe durch Hydrolyse mit 2 M HCl und anschließende HPLC-Isolierung in Aktivitätsausbeuten von 41±2% beziehungsweise 33±1% erhalten. Die molaren Aktivitäten erreichten dabei bis zu 538 GBq/µmol für 1,8 GBq (S)-3-[^{18}F]FPhe (ausgehend von 4,0 GBq Startaktivität).

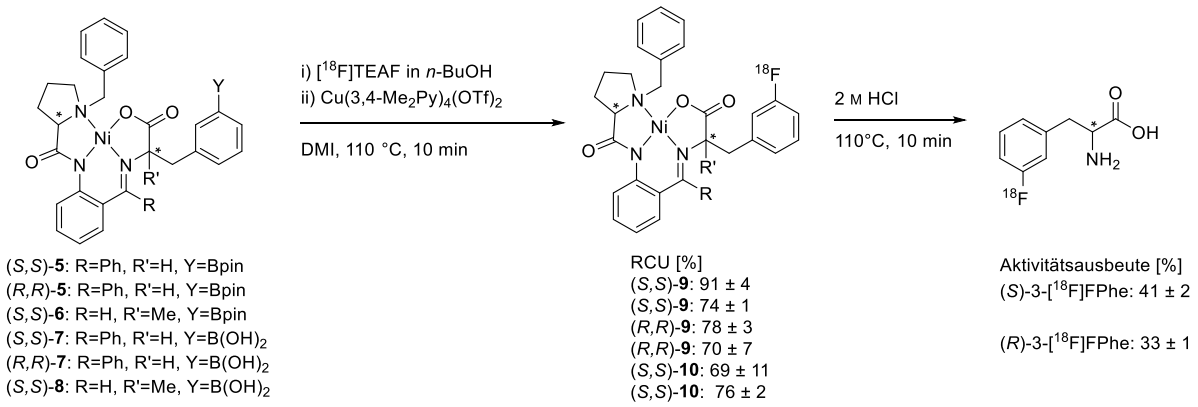

Abbildung 35: Synthese von 3-[^{18}F]FPhes und geschütztem α-Me-3-[^{18}F]FPhe.[81]

Eine Voraussetzung für die Routineanwendung eines Radiotracers ist die Möglichkeit, die Synthese in einem automatisierten Synthesemodul zu implementieren, da nur so die GMP-Konformität garantiert werden kann. Ein solches Synthesemodul ist das Trasis AllInOne, ein auf Einwegkasetten basierendes System. Die Herstellung von (*S*)-3-[^{18}F]FPhe wurde auf einem solchen System mit einer entsprechend gestalteten Kassette automatisiert (Abbildung 36). Dabei wurde das gewünschter PET-Tracer in einer Aktivitätsausbeute von 18±2% (n=3) innerhalb von 70 min erhalten.

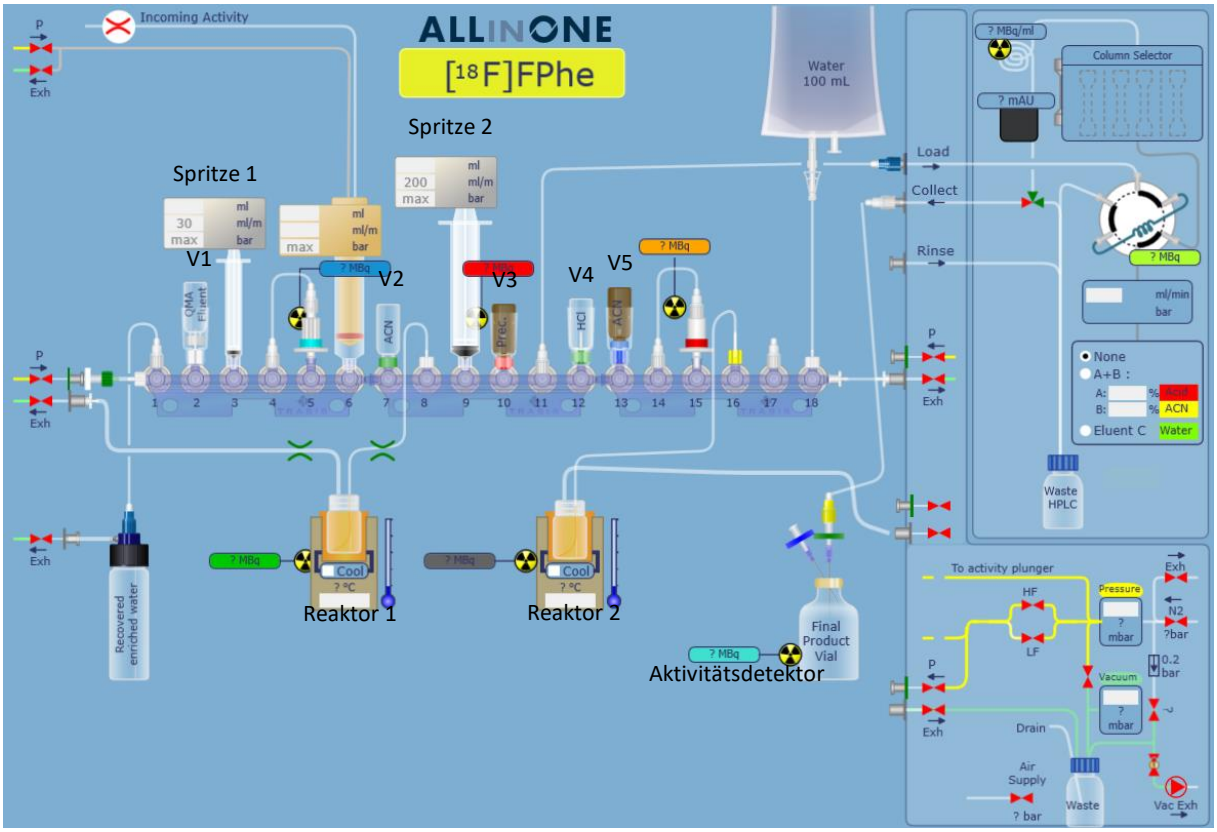

Abbildung 36: Schematische Darstellung des Trasis AllInOne Synthesemodulslayouts für die Synthese von (*S*)-3-[^{18}F]FPhe.

3.2. Radiosynthesis and preclinical evaluation of *m*-[^{18}F]FET and [^{18}F]FET-OMe as novel [^{18}F]FET analogs for brain tumor imaging

[^{18}F]FET wird als Aminosäuretracer für die Bildgebung von Hirntumoren eingesetzt, da es durch Aminosäuretransporter wie LAT1 über die Blut-Hirn-Schranke und in die Tumorzellen transportiert wird. Im Vergleich zu anderen Aminosäuren wie Phenylalanin weist [^{18}F]FET jedoch eine verringerte Affinität zu diesen Transportern auf[101, 102], was die Tumoraufnahme des Tracers in Gegenwart endogener Aminosäuren begrenzen könnte. Untersuchungen legen nahe, dass die Transportkapazitäten und/oder Affinitäten von *m*-substituierten Aminosäuren höher sein könnten als die von *para*-substituierten.[102-107] Es ist daher denkbar, dass ein [^{18}F]FET-Analogon mit dem [^{18}F]Fluorethoxy-Substituenten in *m*- statt *para*-Position eine verbesserte Tumoraufnahme aufweisen könnte. Des Weiteren ist der Einfluss von Modifizierungen der Amino- oder Carbonylfunktion von Aminosäuren auf den Transport durch LAT1 nicht gesichert. So deuten einige Arbeiten darauf hin, dass auch Carbonsäureester und Hydroxamsäureester von Aminosäuren durch LAT1 transportiert werden können.[105, 108] Im Rahmen dieser Arbeit wurden daher das *m*substituierte FET-Analogon *m*-[^{18}F]FET und das Methylesterderivat [^{18}F]FET-OMe hergestellt und biologisch bewertet. Die in vitro Zellaufnahme der Tracer wurde in U87 MG Glioblastomzellen unter Verwendung von Inhibitoren verschiedener Transportsysteme charakterisiert. Zusätzlich wurde der Proteineinbau beider Tracer untersucht. Anschließend erfolgten in vivo Untersuchungen in einem orthotopen Gliom-Modell in Ratten. Als Referenztracer wurde in diesen Experimenten [^{18}F]FET angesetzt.

Das Konzept der nachfolgenden Publikation wurde von Prof. Dr. B. D. Zlatopolskiy, B. Gröner und Prof. Dr. B. Neumaier entwickelt. Die organischen Vorläufer- und Referenzverbindungssynthesen wurden von E. A. Urusova und Prof. Dr. B. D. Zlatopolskiy durchgeführt. Optimierungen der Radiosynthesen wurden von B. Gröner durchgeführt. Präklinische biologische Untersuchungen wurden von Prof. Dr. H. Endepols und M. Brugger durchgeführt. Der Artikel wurde gemeinschaftlich von B. Gröner, Dr. F. Neumaier, Prof. Dr. B. D. Zlatopolskiy, Prof. Dr. H. Endepols und Prof. Dr. B. Neumaier verfasst.

Radiosynthesis and preclinical evaluation of *m*-[^{18}F]FET and [^{18}F]FET-OMe as novel [^{18}F]FET analogs for brain tumor imaging

Benedikt Gröner[1,2], Heike Endepols[1,2,3], Elizaveta A. Urusova[1,2], Melanie Brugger[1], Felix Neumaier[1,2], Marco Timmer[4], Bernd Neumaier[1,2]*, Boris D. Zlatopolskiy[1,2]

[1] *Forschungszentrum Jülich GmbH, Institute of Neuroscience and Medicine, Nuclear Chemistry (INM-5), Wilhelm-Johnen-Straße, 52428 Jülich, Germany.*

[2] *University of Cologne, Faculty of Medicine and University Hospital Cologne, Institute of Radiochemistry and Experimental Molecular Imaging, Kerpener Straße 62, 50937 Cologne, Germany.*

[3] *University of Cologne, Faculty of Medicine and University Hospital Cologne, Department of Nuclear Medicine, Kerpener Straße 62, 50937 Cologne, Germany.*

[4] *University of Cologne, Faculty of Medicine and University Hospital Cologne, Center for Neurosurgery, Department of General Neurosurgery, Kerpener Straße 62, 50937 Cologne, Germany.*

* *Corresponding author; e-mail: b.neumaier@fz-juelich.de*

Table of Contents/Abstract Graphic

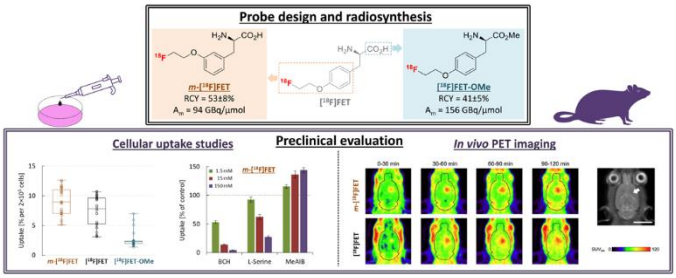

Abstract

O-([^{18}F]Fluoroethyl)-L-tyrosine ([^{18}F]FET) is actively transported into the brain and cancer cells by LAT1 and possibly other amino acid transporters, which enables brain tumor imaging by positron emission tomography (PET). However, tumor delivery of this probe in the presence of competing amino acids may be limited by a relatively low affinity for LAT1. The aim of the present work was to evaluate the *meta*-substituted [^{18}F]FET analog *m*-[^{18}F]FET, and the methyl ester [^{18}F]FET-OMe, which were designed to improve tumor delivery by altering the physicochemical, pharmacokinetic and/or transport properties. Both tracers could be prepared in acceptable to good radiochemical yields of 41–56% within 90 min. Preclinical evaluation with [^{18}F]FET as a reference tracer demonstrated reduced *in vitro* uptake of [^{18}F]FET-OMe by U87 glioblastoma cells and no advantage for *in vivo* tumor imaging. In contrast, *m*-[^{18}F]FET showed significantly improved *in vitro* uptake and accelerated *in vivo* tumor accumulation in an orthotopic glioblastoma model. As such, our work identifies *m*-[^{18}F]FET as a promising alternative to [^{18}F]FET for brain tumor imaging that deserves further evaluation with regard to its transport properties and *in vivo* biodistribution.

Keywords: *Fluorine-18, Positron emission tomography, radiopharmaceuticals, [^{18}F]FET, brain tumor imaging*

1 Introduction

Positron emission tomography (PET) imaging with probes capable to visualize tumor-associated proliferation markers is widely used in the diagnosis and treatment of neoplastic diseases. While detection of increased tumoral glucose metabolism with 2-[^{18}F]fluoro-2-deoxy-D-glucose ([^{18}F]FDG) has become the gold standard for PET imaging of peripheral tumors, high physiological uptake of [^{18}F]FDG by healthy brain tissue hampers the use of this tracer for visualizing brain tumors like gliomas[1,2]. In contrast, tracers derived from amino acids like *O*-([^{18}F]fluoroethyl)-L-tyrosine ([^{18}F]FET, **Fig. 1**) often exhibit high tumor accumulation but low uptake by normal brain tissue, enabling the detection and characterization of cerebral tumors with greater sensitivity than [^{18}F]FDG[1,2]. Although [^{18}F]FET does not significantly participate in specific metabolic pathways, it is actively transported across the blood-brain-barrier (BBB) and into cells by dedicated amino acid transport systems[3–6], which are upregulated in most cancer cells[7–9]. The majority of [^{18}F]FET transport is generally though to be mediated by LAT1 and possibly other members of system L[3–6,10,11], which possess a large maximal transport capacity (i.e. high V_{max}) and a relatively high affinity (i.e. low K_m) for large neutral amino acids like L-tyrosine and L-phenylalanine[12]. In addition to endogenous substrates, LAT1 has been demonstrated to transport a broad range of amino acid derivatives and prodrugs with an amino acid promoiety[13–15]. Although substitution of the aromatic ring in tyrosine and phenylalanine derivatives with small, moderately lipophilic groups is typically well tolerated by LAT1[16–19], [^{18}F]FET has been reported to be a substrate with relatively low affinity[10,20]. This could limit *in vivo* transport of the probe in the presence of competing neutral amino acids. Interestingly, *meta*-substituted amino acids have consistently been found to exhibit enhanced transport capacity and/or binding affinity relative to the corresponding *para*- or *ortho*-substituted derivatives[16–19,21], suggesting that [^{18}F]FET analogs containing the [^{18}F]fluoroethoxy group in *meta*- instead of *para* position could display improved transport properties. Other aspects of the structure-activity relationship (SAR) for substrates of LAT1, such as the role of amino and carboxylic acid function, remain controversial. Thus, while most previous studies concluded that the presence of both free amino and carboxyl groups is essential for substrate recognition[13,15,22,23], some recent findings indicate that carboxylic esters and hydroxamic acid derivatives of amino acids may also be transported by LAT1[21,24,25]. Accordingly, esterification or replacement of the carboxylic acid function in [^{18}F]FET could potentially be used to modify the physicochemical and pharmacokinetic profile of the probe while retaining tumor uptake via LAT1. Alternatively or in addition, [^{18}F]FET esters could serve as prodrugs that improve brain tumor delivery by altering factors not related to active transport across the BBB (e.g., passive

transfer across diffusion barriers like surrounding normal brain tissue) and are cleaved into unmodified [^{18}F]FET by brain esterases.

In the present work, we report the synthesis of *O*-([^{18}F]fluoroethyl)-L-*meta*-tyrosine (*m*-[^{18}F]FET) and *O*-([^{18}F]fluoroethyl)-L-tyrosine methyl ester ([^{18}F]FET-OMe) (**Fig. 1**), two novel analogs of [^{18}F]FET designed based on the SAR considerations summarized above. In addition, we describe the results of a preclinical evaluation of both probes *in vitro* and *in vivo*, using [^{18}F]FET as a reference tracer.

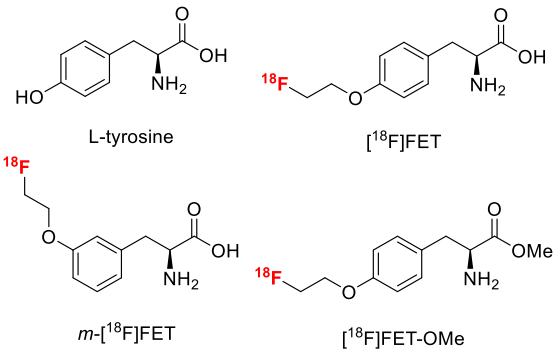

Figure 1: Structure of L-tyrosine and the established PET-tracer *O*-([^{18}F]fluoroethyl)-L-tyrosine ([^{18}F]FET) as well as of the two novel [^{18}F]FET analogs, *O*-([^{18}F]fluoroethyl)-L-*meta*-tyrosine (*m*-[^{18}F]FET) and *O*-([^{18}F]fluoroethyl)-L-tyrosine methyl ester ([^{18}F]FET-OMe), described in the present study.

2 Materials and Methods

2.1 Organic Chemistry

2.1.1 General

Unless noted otherwise, all reagents and solvents were purchased from Sigma-Aldrich (Steinheim, Germany), Acros (Fisher Scientific GmbH, Nidderrau, Germany), Alfa Aesar [Thermo Fisher (Kandel) GmbH, Kandel, Germany], BLDPharm (Kaiserslautern, Germany) or Key Organics (Camelford, UK), and used without further purification. Unless otherwise stated, all reactions were carried out with magnetic stirring and, if air or moisture sensitive substrates and/or reagents were used, in flame-dried glassware under argon. Organic extracts were dried over anhydrous Na_2SO_4 or $MgSO_4$. Solutions were concentrated under reduced pressure (1–900 mbar) at 40–50 °C using a rotary evaporator. **1** was prepared according to the literature[26]. Proton, carbon and fluorine nuclear magnetic resonance (^{1}H-, ^{13}C- and ^{19}F-NMR) spectra were recorded at ambient temperature in deuterochloroform ($CDCl_3$), or deuterodimethylsulfoxide [$(CD_3)_2SO$] (as indicated) using a Bruker Avance Neo (400 MHz) spectrometer. The measured chemical shifts are reported in parts per million (ppm) relative to residual peaks of deuterated

solvents. The observed signal multiplicities are characterized as follows: s = singlet, d = doublet, t = triplet, m = multiplet, br = broad, dd = doublet of doublets, ddd = doublet of doublets of doublets and qd = quartet of doublets. Coupling constants (*J*) are reported in hertz (Hz). Low resolution mass spectrometry (LRMS) was performed with an MSQ PlusTM mass spectrometer (Thermo Electron Corperation, San Jose, USA). High resolution mass spectrometry (HRMS) was performed with an LTQ Orbitrap XL spectrometer (Thermo Fischer Scintific Inc., Bremen, Germany).

2.1.2 Preparation of *Ni*-complex 2:

A solution of (*S*)-*N*-(2-benzoyl-4-chlorophenyl)-1-(3,4-dichlorobenzyl)pyrrolidine-2-carboxamide (**1**) (8.1 g, 16.6 mmol)**,** racemic *m*-Tyr (5.89 g, 32.5 mmol), $Ni(OAc)_2 \cdot 4\ H_2O$ (8.09 g, 32.5 mmol) and K_2CO_3 (20.4 g, 147.75 mmol) in anhydrous MeOH (400 mL) was stirred at 60 °C for 24 h and at ambient temperature for 72 h. The reaction mixture was poured into an ice-cold solution of AcOH (50 mL) in H_2O (3 L) and the resulting suspension was allowed to stand at ambient temperature for 24 h, after which a fine red precipitate had formed. The precipitate was collected by filtration, washed with H_2O (3×100 mL), air dried and dissolved in EtOAc (200 mL). The resulting solution was washed with H_2O (3×50 mL) and brine (2×50 mL), dried and concentrated under reduced pressure. The residue was triturated with Et_2O to give a red precipitate, which was recrystallized from EtOAc/hexane. The combined mother liquors (from trituration with Et_2O and recrystallization) were concentrated under reduced pressure and the residue was purified by column chromatography ($CHCl_3$:acetone = 5:1) followed by recrystallization from EtOAc/hexane to afford the title compound (10.35 g, 88%) as a red solid. R_f = 0.25 (broad spot; $CHCl_3$:acetone = 5:1). ^{1}H-NMR (400 MHz, $CDCl_3$) δ 8.90 (s, 1H), 8.30 (br, 1H), 8.09 (d, J = 8.9 Hz, 1H), 7.81 – 7.41 (m, 4H), 7.40 – 7.20 (m, 3H), 7.10 (d, J = 8.5 Hz, 1H), 6.91 (dd, J = 22.3, 6.9 Hz, 2H), 6.80 – 6.70 (m, 1H), 6.69 – 6.53 (m, 2H), 4.29 (s, 1H), 4.13 (d, J = 12.4 Hz, 1H), 3.33 – 3.16 (m, 1H), 3.09 (d, J = 11.6 Hz, 2H), 2.96 (d, J = 12.4 Hz, 1H), 2.67 (d, J = 8.8 Hz, 1H), 2.45 – 2.19 (m, 3H), 2.17 – 1.83 (m, 2H). ^{13}C-NMR (101 MHz, $CDCl_3$) δ 180.18, 179.11, 171.01, 157.69, 140.92, 136.76, 135.03, 133.81, 133.44, 133.36, 133.30, 132.59, 132.51, 131.06, 130.47, 130.17, 129.91, 129.61, 129.37, 127.82, 127.44, 127.23, 125.95, 123.95, 122.23, 117.65, 115.27, 71.66, 71.59, 63.46, 58.77, 39.17, 30.93, 23.12. *ortho*- and *meta*-Carbons of the phenyl substituent are not equivalent owing to hindered rotation. MS (ESI) m/z: $[M+H]^+$ calculated for $C_{34}H_{29}Cl_3N_3NiO_4^+$: 708.06; found: 707.98. MS (ESI) m/z: $[M–H]^–$ calculated for $C_{34}H_{27}Cl_3N_3NiO_4^–$: 706.04; found: 705.93. Correct isotopic pattern.

2.1.3 Preparation of tosylate 3:

Cs_2CO_3 (0.46 g, 1.41 mmol) was added to a solution of **2** (1 g, 1.41 mmol) in anhydrous MeCN (30 mL) and the reaction mixture was stirred at 70 °C for 1 h. After cooling to ambient temperature, $(CH_2)_2(OTos)_2$ (0.7 g, 1.89 mmol) was added and the mixture was stirred at 50 °C for another 48 h. The resulting suspension was allowed to cool to ambient temperature, the precipitate was removed by filtration and the filtrate was concentrated under reduced pressure. The residue was purified by column chromatography ($CHCl_3$:acetone = 5:1) to afford the title compound (0.6 g, 47%) as a red foam. ^{1}H-NMR (400 MHz, $CDCl_3$) δ 8.91 (s, 1H), 8.13 (d, J = 9.3 Hz, 1H), 7.79 (d, J = 7.9 Hz, 2H), 7.63 (d, J = 7.6 Hz, 1H), 7.60 – 7.51 (m, 2H), 7.45 – 7.40 (m, 1H), 7.34 (d, J = 7.9 Hz, 2H), 7.32 – 7.28 (m, 2H), 7.26 (d, J = 4.2 Hz, 1H), 7.08 (d, J = 7.3 Hz, 1H), 6.86 (d, J = 7.3 Hz, 1H), 6.72 (t, J = 7.3 Hz, 2H), 6.62 – 6.54 (m, 2H), 5.29 (s, 1H), 4.35 – 4.20 (m, 3H), 4.16 (d, J = 12.4 Hz, 1H), 4.06 – 3.90 (m, 2H), 3.29 – 3.13 (m, 2H), 3.09 (d, J = 12.8 Hz, 2H), 2.78 (dd, J = 13.6, 5.1 Hz, 1H), 2.44 (s, 3H), 2.30–2.21 (m, 1H), 2.02 – 1.88 (m, 1H), 1.87 – 1.64 (m, 2H). ^{13}C-NMR (101 MHz, $CDCl_3$) δ 179.94, 178.27, 170.85, 158.70, 145.10, 141.07, 137.20, 135.07, 133.81, 133.44, 133.37, 133.26, 132.92, 132.65, 132.52, 131.07, 130.40, 130.03 (×2), 129.84, 129.54, 129.30, 128.14, 127.80, 127.33, 127.16, 125.79, 123.87, 123.66, 115.64, 114.82, 71.71, 71.55, 68.30, 65.54, 63.42, 58.69, 40.01, 30.95, 23.19, 21.78. *ortho*- and *meta*-Carbons of the phenyl substituent are not equivalent owing to hindered rotation. MS (ESI) m/z: $[M+H]^+$ calculated for $C_{43}H_{39}Cl_3N_3NiO_7S^+$: 906.09; found: 906.44. Correct isotopic pattern.

2.1.4 Preparation of *Ni*-complex 4:

4 (1.0 g, 94%, red solid) was prepared from **2** (1 g, 1.41 mmol), 1-bromo-2-fluoroethane (0.32 mL, 0.55 g, 4.30 mmol) and Cs_2CO_3 (0.92 g, 2.82 mmol) in anhydrous MeCN (30 mL) using the same procedure as described for preparation of **3**, except that the reaction time at 50 °C after addition of the alkylating agent was reduced to 5 h. The crude product was purified by trituration with Et_2O. ^{1}H-NMR (400 MHz, $CDCl_3$) δ 8.91 (d, J = 2.0 Hz, 1H), 8.15 (d, J = 9.3 Hz, 1H), 7.64 (dd, J = 8.2, 2.1 Hz, 1H), 7.60 – 7.50 (m, 2H), 7.45 – 7.39 (m, 1H), 7.34 – 7.27 (m, 3H), 7.10 (dd, J = 9.3, 2.6 Hz, 1H), 7.02 – 6.95 (m, 1H), 6.77 – 6.73 (m, 1H), 6.72 – 6.70 (m, 1H), 6.70 – 6.67 (m, 1H), 6.59 (d, J = 2.6 Hz, 1H), 4.80 – 4.53 (m, 2H), 4.26 (t, J = 5.1 Hz, 1H), 4.17 (d, J = 12.5 Hz, 1H), 4.13 – 3.94 (m, 2H), 3.25 – 3.08 (m, 4H), 2.80 (dd, J = 13.8, 5.4 Hz, 1H), 2.56 – 2.26 (m, 3H), 1.98 – 1.89 (m, 1H), 1.86 – 1.76 (m, 1H). ^{13}C-NMR (101 MHz, $CDCl_3$) δ 179.90, 178.30, 170.84, 159.03, 141.10, 137.18, 135.04, 133.81, 133.45, 133.39, 133.29, 132.65, 132.52, 131.07, 130.36, 130.10, 129.83, 129.52, 129.28, 127.81, 127.34, 127.17,

125.78, 123.87, 123.53, 115.60, 115.03, 81.97 (d, J = 170.8 Hz), 71.75, 71.57, 67.12 (d, J = 20.2 Hz), 63.41, 58.66, 40.07, 30.95, 23.17. *ortho*- and *meta*-Carbons of the phenyl substituent are not equivalent owing to hindered rotation. ^{19}F-NMR (376 MHz, $CDCl_3$) δ -223.51. MS (ESI) m/z: $[M+H]^+$ calculated for $C_{36}H_{32}Cl_3FN_3NiO_4^+$: 754.08; found: 754.40. Correct isotopic pattern.

2.1.5 Preparation of (*S*)-2-amino-3-(3-(2-fluoroethoxy)phenyl)propanoic acid (*m*-FET):

6 N HCl (10 mL) was added dropwise at 65 °C to a stirred solution of **4** (0.5 g, 0.66 mmol) in MeOH (30 mL) and the reaction mixture was stirred at 65 °C until the color had changed from red to a light green (approximately 40 min). The mixture was allowed to cool to ambient temperature and concentrated under reduced pressure. The residue was taken up into H_2O (30 mL) and the pH value was adjusted with 30% NH_3 to approximately 9. The resulting suspension was washed with CH_2Cl_2 (3×20 mL), which was dried and concentrated under reduced pressure to recycle ligand **1**. The remaining aqueous fraction was concentrated under reduced pressure and the residue was triturated with H_2O. The resulting precipitate was collected by filtration, washed with acetone and Et_2O, and dried to afford the title compound (0.14 g, 93%) as a colorless solid. ^{1}H-NMR [400 MHz, 10% TFA in $(CD_3)_2SO$] δ 8.30 (d, J = 16.9 Hz, 1H), 7.19 (t, J = 6.8 Hz, 1H), 6.87 – 6.80 (m, J = 10.8 Hz, 2H), 4.68 (d, J = 47.7 Hz, 2H), 4.20 (s, 1H), 4.15 (d, J = 15.2 Hz, 2H), 3.12 – 2.93 (m, 2H). ^{13}C-NMR [101 MHz, 10% TFA in $(CD_3)_2SO$] δ 170.54, 158.54, 136.54, 129.98, 122.32, 116.02, 113.57, 82.31 (d, J = 166.8 Hz), 67.14 (d, J = 19.0 Hz), 53.19, 35.92. ^{19}F-NMR [376 MHz, 10% TFA in $(CD_3)_2SO$] δ -222.51. MS (ESI) m/z: $[M+H]^+$ calculated for $C_{11}H_{15}FNO_3^+$: 228.11; found: 228.24. HR-MS (ESI) m/z: $[M+H]^+$ calculated for $C_{11}H_{15}FNO_3^+$: 228.10305; found: 228.10328.

2.1.6 Preparation of (*S*)-2-amino-3-(3-hydroxyphenyl)propanoic acid (*m*-Tyr):

6 N HCl (30 mL) was added dropwise at 65 °C to a stirred solution of **2** (5 g, 7.07 mmol) in MeOH (60 mL) and the reaction mixture was stirred at 65 °C until the color had changed from red to a light green (approximately 40 min). The mixture was allowed to cool to ambient temperature and concentrated under reduced pressure. The residue was taken up into H_2O (30 mL) and the pH value was adjusted with 30% NH_3 to approximately 9. The resulting suspension was washed with CH_2Cl_2 (3×20 mL), which was dried and concentrated under reduced pressure to recycle ligand **1**. The remaining aqueous fraction was concentrated under reduced pressure and the residue was taken up into aqueous MeOH (300 mL). Preswollen Amberlite IR-120 in the H^+ form (150 mL) was then added and the mixture was stirred for 16 h. The ion-exchange resin was recovered by filtration, washed with H_2O until the pH of the filtrate reached 5 and

treated with 30% NH_3:MeOH 2:1 (3×300 mL). The combined filtrates were concentrated under reduced pressure, the residue was triturated with acetone and Et_2O, and the resulting precipitate was collected by filtration to afford the title compound (0.59 g, 46%) as a colorless solid. The spectral data of *m*-Tyr were in accordance with the literature[27].

2.1.7 Preparation of *tert*-butyl (*S*)-2-[(*tert*-butoxycarbonyl)amino]-3-(3-hydroxyphenyl)propanoate (Boc-*m*-Tyr-O*t*Bu, 6):

a) (S)-2-[(tert-Butoxycarbonyl)amino]-3-(3-hydroxyphenyl)propanoic acid (Boc-m-Tyr-OH)[28]*:*

Boc_2O (3.1 g, 14.20 mmol) was added to a vigorously stirred solution of *m*-Tyr (2 g, 11.04 mmol) in 1 N NaOH (11 mL) and 10% $NaHCO_3$ (20 mL). MeOH (and, if necessary, H_2O) was added until a homogenous solution was obtained and the reaction mixture was stirred at ambient temperature for 16 h. The MeOH was removed under reduced pressure and the resulting solution was diluted with H_2O (50 mL) and washed with pentane (3×30 mL). The aqueous fraction was acidified with solid $NaHSO_4$ to pH 2 and extracted with Et_2O (2×50 mL). The combined ethereal fractions were washed with H_2O (3×30 mL) and brine (2×30 mL), dried and concentrated under reduced pressure to afford the title compound (2.82 g, 91%) as a colorless oil. The spectral data of Boc-*m*-Tyr-OH were in accordance with the literature.

*b) Boc-m-Tyr-OtBu (**6**)*[29]*:*

N,*N*-Dimethylformamide dineopentylacetal (8.4 mL, 6.96 g, 30.08 mmol) was added dropwise under reflux to a stirred solution of Boc-*m*-Tyr-OH (2.82 g, 10.03 mmol) and anhydrous *tert*-BuOH (13 mL, 10.14 g, 136.81 mmol) in anhydrous toluene (100 mL) and the mixture was stirred under reflux for 16 h. After cooling to ambient temperature, the reaction mixture was washed with 10% $NaHCO_3$ (3×30 mL), H_2O (3×30 mL) and brine (2×30 mL), dried and concentrated under reduced pressure. The resulting crude product was purified by column chromatography (EtOAc:hexane 1:3) to afford the title compound (2.16 g, 64%, 58% over two steps) as a colorless solid. NMR spectra showed the presence of two rotamers in approximately 4:1 ratio. Only data for the major rotamer are reported. ^{1}H-NMR (400 MHz, $CDCl_3$) δ 7.13 (t, J = 7.9 Hz, 1H), 6.76 – 6.72 (m, J = 2.6 Hz, 1H), 6.70 (d, J = 7.3 Hz, 2H), 6.22 (s, 1H), 5.07 (d, J = 8.1 Hz, 1H), 4.43 (dd, J = 14.1, 6.5 Hz, 1H), 3.07 – 2.91 (m, 2H), 1.42 (s, 9H), 1.40 (s, 9H). ^{13}C-NMR (101 MHz, $CDCl_3$) δ 171.29, 156.22, 155.51, 138.06, 129.63, 121.66, 116.58, 114.11, 82.38, 80.15, 54.97, 38.55, 28.45, 28.06. MS (ESI) m/z: $[M+H]^+$ calculated for $C_{18}H_{28}NO_5^+$: 338.20; found: 338.25. HR-MS (EI) m/z: $[M]^{\cdot+}$ calculated for $C_{18}H_{27}NO_5^{\cdot+}$: 337.1884; found: 337.1881.

2.1.8 Preparation of *tert*-butyl (*S*)-2-[(*tert*-butoxycarbonyl)amino]-3-{3-[2-(tosyloxy)ethoxy]phenyl}propanoate (5):

6 (0.9 g, 56%, colorless oil that contained 15 mol.% *n*-pentane according to the ^{1}H-NMR spectrum) was prepared from **6** (1.0 g, 2.96 mmol), $(CH_2)_2(OTos)_2$ (1.43 g, 3.85 mmol) and Cs_2CO_3 (0.97 g, 2.96 mmol) in anhydrous MeCN (20 mL) using the same procedure as described for preparation **5**, except that the reaction time at 50 °C after addition of the alkylating agent amounted to 24 h. The crude product was purified by column chromatography (EtOAc:hexane = 1:3). ^{1}H-NMR (400 MHz, $CDCl_3$) δ 7.82 (d, J = 8.3 Hz, 2H), 7.35 (d, J = 8.3 Hz, 2H), 7.16 (t, J = 7.8 Hz, 1H), 6.77 (d, J = 7.8 Hz, 1H), 6.65 (dd, J = 7.8, 1.8 Hz, 1H), 6.62 – 6.59 (m, 1H), 4.97 (d, J = 7.2 Hz, 1H), 4.41 (dd, J = 11.9, 7.2 Hz, 1H), 4.37 – 4.31 (m, 2H), 4.15 – 4.09 (m, 2H), 3.00 (t, J = 11.9 Hz, 2H), 2.45 (s, 3H), 1.41 (s, 9H), 1.39 (s, 9H). ^{13}C-NMR (101 MHz, $CDCl_3$) δ 171.00, 158.13, 155.20, 145.07, 138.22, 133.05, 130.00, 129.47, 128.16, 122.75, 116.03, 112.95, 82.22, 79.85, 68.21, 65.47, 54.87, 38.60, 28.45, 28.08, 21.79. MS (ESI) m/z: $[M+H]^+$ calculated for $C_{27}H_{38}NO_8S^+$: 536.23; found: 536.22.

2.1.9 Preparation of methyl (*S*)-2-[(*tert*-butoxycarbonyl)amino]-3-{4-[2-(tosyloxy)ethoxy]phenyl}propanoate (7):

Cs_2CO_3 (1.21 g, 3.71 mmol) was added to a solution of Boc-Tyr-OMe (1 g, 3.37 mmol) in anhydrous MeCN (100 mL) and the reaction mixture was stirred at 80 °C for 30 min. After cooling to ambient temperature, $(CH_2)_2(OTos)_2$ (2.0 g, 5.40 mmol) was added and the mixture was stirred at 80 °C for another 30 min. The resulting suspension was allowed to cool to ambient temperature and the precipitate was removed by filtration. The filtrate was concentrated under reduced pressure and the residue was purified by column chromatography (EtOAc:hexane = 1:2.1; dry loading) followed by RP chromatography with a C_{18} phase (40% MeCN, 2 L, followed by 45% MeCN, 2 L, 100 mL fractions; dry loading) to afford the title compound (1.03 g, 55%; contained 28 mol.% Et_2O according to the ^{1}H-NMR spectrum) as a yellow oil. ^{1}H-NMR (400 MHz, $CDCl_3$) δ 7.81 (d, J = 8.2 Hz, 2H), 7.34 (d, J = 8.2 Hz, 2H), 7.00 (d, J = 8.6 Hz, 2H), 6.75 – 6.65 (m, 2H), 4.95 (d, J = 7.8 Hz, 1H), 4.59 – 4.46 (m, 1H), 4.34 (dd, J = 13.7, 6.3 Hz, 2H), 4.11 (dd, J = 6.3, 4.0 Hz, 2H), 3.70 (s, 3H), 3.00 (qd, J = 13.9, 5.9 Hz, 2H), 2.45 (s, 3H), 1.41 (s, 9H). ^{13}C-NMR (101 MHz, $CDCl_3$) δ 172.47, 157.24, 155.20, 145.08, 133.03, 130.45, 129.99, 128.95, 128.15, 114.77, 80.05, 68.23, 65.58, 54.63, 52.32, 37.60, 28.42, 21.78. MS (ESI) m/z: $[M+H]^+$ calculated for $C_{24}H_{32}NO_8S^+$: 494.18; found: 494.28.

2.1.10 Preparation of methyl (*S*)-2-amino-3-[4-(2-fluoroethoxy)phenyl]propanoate hydrochloride (HCl·FET-OMe):

a) *Methyl (S)-2-[(tert-butoxycarbonyl)amino]-3-[4-(2-fluoroethoxy)phenyl]propanoate (**9**):*

9 was prepared from Boc-Tyr-OMe (1 g, 3.37 mmol), 1-bromo-2-fluoroethane (1.0 mL, 1.82 g, 14.41 mmol) and Cs_2CO_3 (1.9 g, 5.83 mmol) in anhydrous MeCN (20 mL) using the same procedure as described for preparation **3**, except that the reaction time at 50 °C after addition of the alkylating agent amounted to 16 h. The crude product was purified by recrystallization from EtOAc/hexane to afford a first crop of the title compound (0.64 g, 56%) as a colorless solid. The mother liquor was concentrated under reduced pressure and the residue was purified by column chromatography (EtOAc.hexane = 1:2.1) to afford a second crop of the title compound (0.3 g, total 82%). ^{1}H-NMR (400 MHz, $CDCl_3$) δ 7.08 – 6.99 (m, J = 8.5 Hz, 2H), 6.89 – 6.80 (m, 2H), 4.96 (d, J = 6.8 Hz, 1H), 4.83 – 4.76 (m, 1H), 4.72 – 4.65 (m, 1H), 4.54 (dd, J = 13.6, 6.8 Hz, 1H), 4.26 – 4.19 (m, 1H), 4.18 – 4.12 (m, 1H), 3.70 (s, 3H), 3.02 (qd, J = 13.6, 5.9 Hz, 2H), 1.41 (s, 9H). ^{13}C-NMR (101 MHz, $CDCl_3$) δ 172.52, 157.65, 155.21, 130.51, 128.80, 114.85, 82.05 (d, J = 170.7 Hz), 80.03, 67.24 (d, J = 20.7 Hz), 54.65, 52.31, 37.62, 28.42. ^{19}F-NMR (376 MHz, $CDCl_3$) δ -223.87. MS (ESI) m/z: $[M+H]^+$ calculated for $C_{17}H_{25}FNO_5^+$: 342.17; found: 342.27.

b) *HCl·FET-OMe:*

9 (0.54 g, 1.58 mmol) was taken up into 4.8 M HCl in EtOAc (20 mL, prepared according to Nudelman et al.[30,31]) and the mixture was incubated at ambient temperature for 1 h. All volatiles were then removed under reduced pressure, the residue was triturated with Et_2O and the solid was collected by filtration to afford the title compound (0.45 g, 100%; 82% over two steps) as a colorless solid. ^{1}H-NMR [400 MHz, $(CD_3)_2SO$] δ 8.76 (s, 3H), 7.22 – 7.11 (m, 2H), 6.96 – 6.84 (m, 2H), 4.82 – 4.75 (m, 1H), 4.66 (dt, J = 15.9, 7.3 Hz, 1H), 4.26 – 4.22 (m, 1H), 4.20 – 4.12 (m, 2H), 3.66 (s, 3H), 3.11 (ddd, J = 21.4, 14.1, 6.5 Hz, 2H). ^{13}C-NMR [101 MHz, $(CD_3)_2SO$] δ 169.37, 157.39, 130.60, 126.86, 114.59, 82.16 (d, J = 166.5 Hz), 67.01 (d, J = 18.9 Hz), 53.35, 52.51, 34.93. ^{19}F NMR [376 MHz, $(CD_3)_2SO$] δ -222.07. MS (ESI) m/z: $[M+H]^+$ calculated for $C_{12}H_{17}ClFNO_3^+$: 242.12; found: 242.24.

2.2 Radiochemistry

2.2.1 General

No-carrier-added aqueous [^{18}F]fluoride ([^{18}F]F^-) was produced via the $^{18}O(p,n)^{18}F$ nuclear reaction by bombardment of enriched [^{18}O]H_2O with 16.5 MeV protons using a BC1710 cyclotron (The Japan Steel Works Ltd., Shinagawa, Japan) at the INM-5 (Forschungszentrum

Jülich). All radiosyntheses were carried out in 5 mL Wheaton V-Vials equipped with PTFE-coated wing stir bars. Anhydrous solvents (MeCN) were purchased from Sigma-Aldrich (Steinheim, Germany). Anion exchange cartridges (Sep-Pak Accell Plus QMA carbonate plus light cartridges with 40 mg sorbent per cartridge) were obtained from Waters GmbH (Eschborn, Germany). [^{18}F]FET was prepared according to a known procedure[32].

HPLC analyses were carried out on a Dionex Ultimate® 3000 HPLC system equipped with a Multokrom C18 AQ 100-5, 250×4.6 mm column (CS-Chromatographie Service GmbH, Langerwehe, Germany) and a DAD UV-detector coupled in series with a Berthold NaI detector, giving a time delay of 0.1–0.3 min between the corresponding responses (depending on the flow rate). The identity of radiolabeled products was confirmed by co-injection of the corresponding non-radiolabeled reference compounds. Isolated yields of the purified radiolabeled products are reported in terms of decay-corrected radiochemical yields (RCYs) and/or non-decay-corrected activity yields (AY), as determined by comparing the initial activity on the QMA cartridge and the activity of the radiolabeled product. The system used for purification of crude products by semi-preparative HPLC consisted of a Merck Hitachi L-6000 pump, a Knauer K-2500 UV detector, a Rheodyne 6-port injection valve, a custom-made Geiger-Müller counter and a Hydro-RP, 250×10 mm, 80 Å, 10 µm column (Synergi; Phenomenex LTD, Aschaffenburg, Germany).

2.2.2 Preparation of *m*-[^{18}F]FET

a) From precursor **3**

Aqueous [^{18}F]F$^-$ was loaded onto a QMA cartridge, the cartridge was washed with dry MeCN (1 mL) and the [^{18}F]F$^-$ was eluted with a solution of TBAOTos (4 mg, 9.7 µmol) in MeOH (0.5 mL). The solvent was removed at 85 °C for 5 min under reduced pressure in a stream of argon and a solution of radiolabeling precursor **3** (2 mg, 2.2 µmol) in dry MeCN (0.5 mL) was added. The reaction mixture was stirred at 100 °C for 5 min and the solvent was removed at 100 °C for 5 min under reduced pressure in a stream of argon. 2 M HCl (0.5 mL) and EtOH (0.1 mL) were then added and the resulting mixture was stirred at 125 °C for 10 min to decompose the radiolabeled intermediate [^{18}F]**4**. Following addition of 2 M NaOH (0.4 mL) and EtOH (0.2 mL), the product was purified by semi-preparative HPLC [eluent: 10% EtOH (300 mg/mL NH_4OAc); flow rate: 4.5 mL/min; t_R = 8–9 min]. The RCY of *m*-[^{18}F]FET thus obtained amounted to 29±6% (n=3) after 94 min. The radiochemical purity amounted to 97%.

b) From precursor **5**

Aqueous [^{18}F]F$^-$ was loaded onto a QMA cartridge, the cartridge was washed with dry MeCN (1 mL) and the [^{18}F]F$^-$ was eluted with a solution of TBAOH·30 H_2O (25 mg, 31.3 µmol) in

MeCN (0.5 mL). The solvent was removed at 85 °C for 5 min under reduced pressure in a stream of argon and a solution of radiolabeling precursor **5** (5 mg, 9.34 µmol) in dry MeCN (0.5 mL) was added. The reaction mixture was stirred at 85 °C for 5 min and the solvent was removed at 85 °C for 5 min under reduced pressure in a stream of argon. 2 M HCl (0.5 mL) and EtOH (0.1 mL) were then added and the resulting mixture was stirred at 100 °C for 10 min to deprotect the radiolabeled intermediate [^{18}F]**8**. Following addition of 2 M NaOH (0.4 mL) and EtOH (0.2 mL), the product was purified by semi-preparative HPLC [eluent: 10% EtOH (300 mg/mL NH_4OAc); flow rate: 4.5 mL/min; t_R = 8–9 min] and formulated by dilution of the eluate with 0.9% NaCl. The RCY of *m*-[^{18}F]FET thus obtained amounted to 53±8% (n=8) after 90 min. The radiochemical purity amounted to >98% and the molar activity to 94 GBq/µmol (for 200 MBq *m*-[^{18}F]FET).

2.2.3 Preparation of [^{18}F]FET-OMe

Aqueous [^{18}F]F^- was loaded onto a QMA cartridge and eluted with a solution of TBAOH·30 H_2O (25 mg, 31.3 µmol) in MeCN (0.5 mL). The solvent was removed at 85 °C for 5 min under reduced pressure in a stream of argon and a solution of radiolabeling precursor **7** (4.9 mg, 9.93 µmol) in dry MeCN (0.5 mL) was added. The reaction mixture was stirred at 85 °C for 10 min and the solvent was removed at 85 °C for 5 min under reduced pressure in a stream of argon. Trifluoroacetic acid (TFA, 50 µL) was then added and the resulting mixture was incubated at room temperature for 1 min to deprotect the radiolabeled intermediate [^{18}F]**9**. Following addition of MeCN (100 µL) and H_2O (1 mL), the product was purified by semi-preparative HPLC [eluent: 15% MeCN (0.1% TFA); flow rate: 4.5 mL/min; t_R = 7–8 min]. The product fraction was diluted with saturated $NaHCO_3$ (9 fold volume) and loaded onto a SPE cartridge (Strata-X RP, 30 mg). The cartridge was washed with H_2O (10 mL) and the product was eluted with EtOH (1 mL). The solvent was removed under reduced pressure in a stream of argon at 85 °C and the product was dissolved in 0.9% NaCl (500 µL). The RCY of [^{18}F]FET-OMe thus obtained amounted to 41±5% (n=8) after 90 min. The radiochemical purity amounted to > 98% and the molar activity to 156 GBq/µmol (for 710 MBq [^{18}F]FET-OMe).

2.3 Biological Evaluation

2.3.1 Cell culture

Human U87 MG glioblastoma cells were purchased from the American Type Culture Collection (ATCC) and cultured under normal growth conditions (37 °C and 5% CO_2) in minimum essential medium GlutaMAX (MEM, Gibco 41090028, Fisher Scientific GmbH,

Schwerte, Germany) supplemented with 10% fetal bovine serum (FBS, Sigma- Aldrich F2442, Merck KGaA, Darmstadt, Germany), 1% penicillin/streptomycin (Gibco 115140122), 1% non-essential amino acids (NEAA, Gibco 11140050), 1% human recombinant insulin (Sigma-Aldrich 91077C), and 1% sodium pyruvate (ThermoFisher 11360070, Fisher Scientific GmbH, Schwerte, Germany). The cells were grown in cell-culture dishes (ThermoFisher 150350, F 100 mm) with 9 mL culture medium and routinely passaged every 4–5 days when they had reached 80–90% confluency. For the cellular uptake and inhibition studies, cells were seeded into 12-well plates (2×10^5 cells in 1 mL medium / well) 48 h before the start of the experiments.

2.3.2 Cellular Uptake Experiments

Two hours before the start of the experiments, the culture medium was carefully aspirated, the cells were washed with phosphate-buffered saline (PBS, 1 mL, Gibco 10010023), and a dye exclusion test with trypan blue (Sigma-Aldrich T 8154) was performed to determine cell viability and the exact cell count (cell viability was always >95%). The tracer solutions were prepared in FBS- and amino acid-free Earle's balanced salt solution (EBSS) at a concentration of 150 kBq/mL. PBS was removed from the wells and the tracer solution was added (1 mL/well). The cells were then incubated at 37 °C for 60 min, washed twice with ice-cold PBS (1 mL), trypsinized and harvested. The accumulated radioactivity was measured in an automatic gamma counter (Hidex AMG version 1.4.4, Turku, Finland). Each experiment was conducted at least in triplicate.

2.3.3 Protein incorporation studies

To determine the degree of protein incorporation, U87 MG cells were incubated with *m*-[^{18}F]FET at 37 °C for 60 min, the tracer solution was removed and the cells were trypsinized and harvested as described in section 2.3.2. After centrifugation for 5 min at 2500 × g and 4 °C, the cell pellet was resuspended in 1 mL TRIS-EDTA buffer (Sigma-Aldrich 93302) and homogenized with a disperser (Ultra-Turrax®, Proxxon, Wecker, Luxembourg) at the highest level for 1 min at 4 °C. The resulting homogenate was centrifuged for 30 min at 18400 × g and 4 °C, and the supernatant was loaded onto a PD 10 cartridge (VWR International GmbH, Darmstadt, Germany; pre-conditioned with 25 mL EBSS). The cartridge was then eluted with 20 mL EBSS and consecutive 1 mL fractions were collected and measured with a gamma counter to determine the amount of radioactivity in the high- and low-molecular-weight fractions.

2.3.4 Cellular inhibition experiments

For the inhibition experiments, U87 MG cells were used and cultured as described above. The following inhibitors, obtained from Sigma Aldrich, were used: 2-(methylamino)-2-methylpropionic acid (MeAIB) for system A, L-serine for system ASC and 2-aminobicyclo [2,2,1]heptane-2-carboxylic acid (BCH) for system L. The inhibitors were diluted with EBSS to give the desired final concentrations (1.5 mM, 15 mM or 150 mM) and added together with the tracer. After incubation for 60 min at 37 °C, the cells were processed and uptake of radioactivity measured as described in section 2.3.2.

2.3.5 Experimental Animals

All animal studies were conducted in accordance with the EU directive 2010/63/EU for animal experiments and the German Animal Welfare Act (TierSchG, 2006) and were approved by the regional authorities (LANUV, NRW; 84-02.04.2017.A288). In total, 6 immunodeficient male Rowett Nude Rats (Crl:NIH-Foxn1rnu, Charles River; 197–359 g body weight) were used for the orthotopic glioblastoma model. The animals were housed in groups of up to 5 animals in individually ventilated cages (NexGen Ecoflo, cages Rat1800 or Mouse500; Allentown Inc., Allentown, NJ, USA) under controlled ambient conditions (22 ± 1 °C and 55 ± 5% relative humidity) and on a 12 h light/dark schedule (lights on from 9:00 p.m. to 9:00 a.m.). Food and water were provided *ad libitum*. The health status of the animals was monitored daily and showed no changes throughout the experiments.

2.3.6 Orthotopic U87 MG glioblastoma xenograft rat model

For induction of the orthotopic glioblastoma model, rats were anesthetized with isoflurane (5% for induction and 3–4% for maintenance) in O_2/air (3:7) and 10^5 U87 MG cells in 3 µL Matrigel^{TM} were stereotactically implanted into the brain. The stereotactic coordinates were 0.5 mm anterior, 2.5 mm lateral, and 4.5 mm ventral from Bregma. MRI scans were performed 1, 2, and 3 weeks after tumor cell implantation to determine the size of the intracranial tumor. The measurements were performed under inhalation anesthesia with isoflurane as described above using a 3T Achieva® MRI scanner (Philips Healthcare, Best, The Netherlands) in combination with an 8 Channel Volumetric Rat Array (Rapid Biomedical GmbH, Rimpar, Germany). Three-dimensional T_2-weighted MR images were acquired using a turbo-spin echo sequence with repetition time = 14 s, echo time = 30 ms, field of view = 60 × 60 × 60 mm^3, and voxel size = 0.5 × 0.5 × 0.5 mm^3.

2.3.7 PET measurements

Prior to the PET measurements, rats were anesthetized with isoflurane (5% for induction and 3-4% for maintenance) in O_2/air (3:7), placed in an animal holder (Minerve, Esternay, France) and fixed with a tooth bar in a respiratory mask. Respiratory rate was monitored with a pressure sensor placed under the animals and maintained at around 40–60 breaths per minute by adjusting the isoflurane concentration. Core body temperature was maintained at about 37 °C by warm water flow through the animal bed. Dynamic PET scans in list mode were performed with a Focus 220 micro-PET scanner (CTI-Siemens, Knoxville, TN, USA) with a resolution at the center of field of view of 1.4 mm. Data acquisition started with tracer injection (49–65 MBq in 0.5 mL i.v.), proceeded for 120 min and was followed by a 10 min transmission scan with a ^{57}Co point source. After full 3D rebinning, data were reconstructed using an iterative OSEM3D/MAP procedure with attenuation and decay correction[33] in two different ways: (1) 28 frames (2 × 1 min, 2 × 2 min, 6 × 4 min, 18 × 5 min) for the compilation of regional time activity curves (TACs), and (2) 4 frames (4 × 30 min) for visual display. The resulting voxel sizes were 0.38 mm × 0.38 mm × 0.80 mm. Data analysis was performed using the software VINCI[34]. Standardized uptake values normalized by body weight (SUV_{bw}) were determined by dividing each image by the injected dose and multiplying the result by body weight times 100. To obtain TACs, an elliptical volume of interest (VOI) was placed over the tumor, the mean SUV_{bw} values were extracted from each of the 28 frames and then plotted over time.

3 Results

3.1 Synthesis of radiolabeling precursors and non-radioactive reference compounds

Initially, we intended to produce *m*-[^{18}F]FET by application of a radiolabeling precursor with Ni-BPB-moiety as double protecting group (for selected examples of this strategy, see[35–38]). To this end, racemic *m*-Tyr was used for preparation of the enantiomerically and diastereomerically pure Ni-complex **2** according to the protocol of Nian et al.[26] (**Scheme 1**). **2** was then alkylated with $(CH_2)_2(OTos)_2$ using Cs_2CO_3 as a base to afford the desired radiolabeling precursor **3** in 41% yield over two steps. In order to prepare the reference compound *m*-FET, **2** was alkylated with 1-bromo-2-fluoroethane and the resulting intermediate **4** was decomposed using HCl in aqueous MeOH, which furnished *m*-FET in 87% yield over two steps.

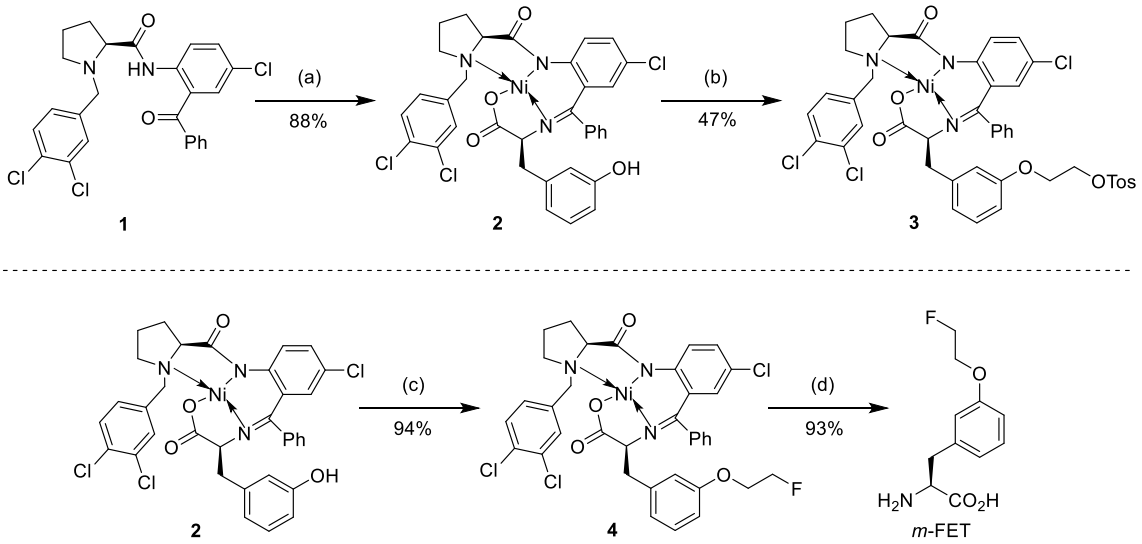

Scheme 1: Preparation of radiolabeling precursor **3** for *m*-[^{18}F]FET (top) and reference compound *m*-FET (bottom). Conditions: (a) (*RS*)-*m*-Tyr, $Ni(OAc)_2 \cdot 4H_2O$, K_2CO_3, MeOH, 60 °C, 72 h; (b) i) Cs_2CO_3, MeCN, 70 °C, 1 h; ii) $(CH_2)_2(OTos)_2$, 50 °C, 48 h; (c) i) Cs_2CO_3, MeCN, 70 °C, 1 h; ii) 1-bromo-2-fluoroethane, 50 °C, 5 h; (d) HCl, aq. MeOH, 65 °C, 40 min.

Due to limited stability of precursor **3** (see below), the alternative radiolabeling precursor **5** for *m*-[^{18}F]FET was also prepared from **2** as follows (**Scheme 2**). Acidolytic decomposition of **2** into *m*-Tyr was followed by *N*-Boc and CO_2-*t*Bu protection to give Boc-*m*-Tyr-O*t*Bu (**6**). The latter was then alkylated with $(CH_2)_2(OTos)_2$ to afford radiolabeling precursor **5** in 14% yield over four steps.

The radiolabeling precursor **7** for [^{18}F]FET-OMe was prepared by alkylation of commercially available Boc-Tyr-OMe with ethylene ditosylate, which afforded the desired tosylate **7** in 55% yield (**Scheme 2**). For preparation of the corresponding reference compound, Boc-Tyr-OMe was instead alkylated with 1-bromo-2-fluoroethane followed by deprotection of the resulting intermediate with HCl in EtOAc to obtain HCl·FET-OMe[39] in 82% yield over two steps (**Scheme 2**).

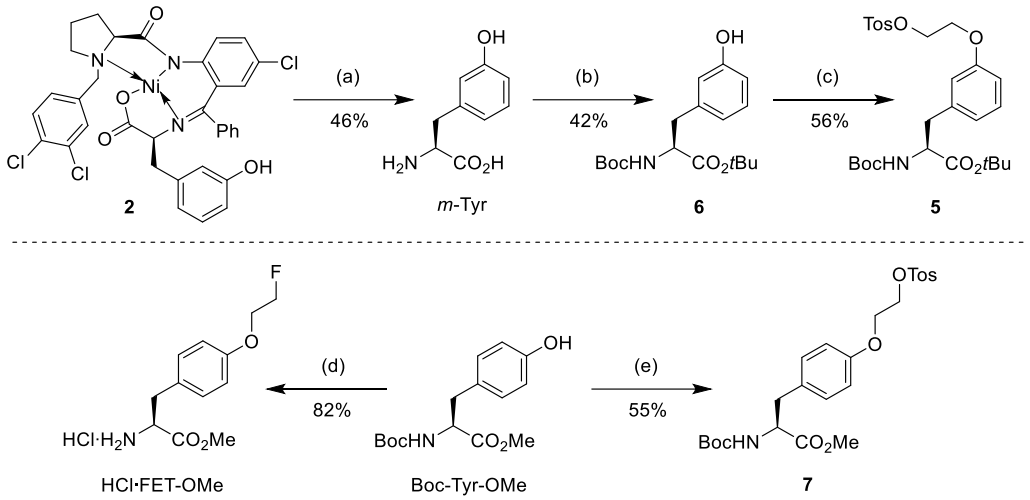

Scheme 2: Preparation of radiolabeling precursor **5** for *m*-[^{18}F]FET (top), radiolabeling precursor **7** for [^{18}F]FET-OMe (bottom right) and reference compound HCl·FET-OMe (bottom left). Conditions: (a) i) HCl, aq. MeOH, 65 °C, 40 min; ii) IRA-120; (b) i) Boc_2O, $NaHCO_3$, MeOH, 12 h; ii) *N*,*N*-dimethyl-1,1-bis(neopentyloxy)methanamine, *t*BuOH, toluene, 110 °C, 16 h; (c) i) Cs_2CO_3, MeCN, 70 °C, 1 h; ii) $(CH_2)_2(OTos)_2$, 50 °C, 48 h; (d) i) Cs_2CO_3, MeCN, 70 °C, 1 h; ii) 1-bromo-2-fluoroethane, 50 °C, 16 h; iii) HCl in EtOAc; (e) i) Cs_2CO_3, MeCN, 80 °C, 30 min; ii) $(CH_2)_2(OTos)_2$, 80 °C, 30 min.

3.2 Radiotracer production

3.2.1 Radiosynthesis of *m*-[^{18}F]FET

The radiosynthesis of *m*-[^{18}F]FET was initially accomplished by a one-pot, 2-step procedure using precursor **3** (**Scheme 3**). To this end, aqueous [^{18}F]fluoride ([^{18}F]F^-) was trapped on a QMA anion exchange cartridge and eluted with Bu_4NOTos (4 mg, 9.6 µmol) in MeOH. MeOH was removed under reduced pressure in a stream of argon and a solution of **3** (2 mg, 2.2 µmol) in MeCN was added to the residue. The reaction mixture was then heated at 100 °C for 10 min to afford the radiolabeled complex [^{18}F]**4**, which was decomposed with 0.5 M HCl at 125 °C for 10 min. After HPLC purification and formulation, this protocol afforded *m*-[^{18}F]FET in radiochemical yields (RCYs) of 29±6% (n=3) and with a radiochemical purity (RCP) of 97% within 94 min. Unfortunately, the stability of **3** under ambient conditions proved to be limited and the decomposition products formed during storage negatively influenced ^{18}F-incorporation. Accordingly, *m*-[^{18}F]FET was also prepared from the more stable radiolabeling precursor **5** as follows. Aqueous [^{18}F]F^- was trapped on an anion exchange cartridge and eluted with a solution of TBAOH·30 H_2O (24 mg, 30 µmol) in MeCN (0.5 mL) (**Scheme 3**). The solvent was removed at 85 °C under reduced pressure in a stream of argon and the residue was taken up in a solution of **5** (10 µmol) in anhydrous MeCN. The reaction mixture was then heated at 85 °C for 10 min to afford the radiolabeled intermediate [^{18}F]**8**, which was deprotected with 0.83 M HCl in 20%

EtOH. Subsequent purification by semi-preparative HPLC and formulation by dilution of the eluate with isotonic saline afforded *m*-[^{18}F]FET in RCYs of 53±8% (n=8) and an RCP of >98% within 80–90 min. The molar activity amounted to 94 GBq/µmol (for 200 MBq *m*-[^{18}F]FET).

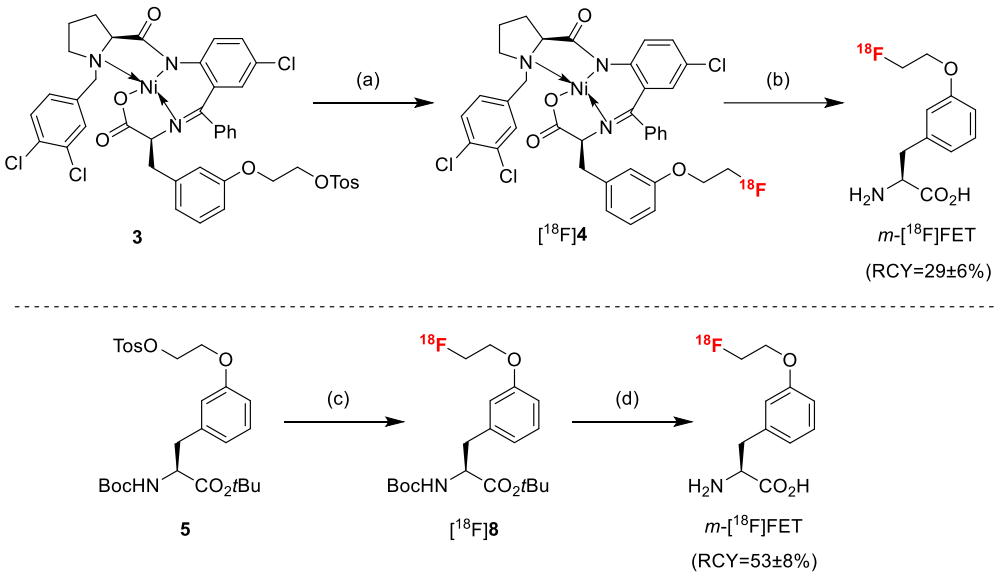

Scheme 3: Radiosynthesis of *m*-[^{18}F]FET from Ni-BPB complex **3** (top) or precursor **5** (bottom). Conditions: (a) TBAOTos, [^{18}F]F^{-}, MeCN, 100 °C, 10 min; (b) 0.5 M HCl, 125 °C, 10 min; (c) TBAOH, [^{18}F]F^{-}, MeCN, 85 °C, 10 min; (d) HCl in aq. EtOH, 100 °C, 10 min.

3.2.2 Radiosynthesis of [^{18}F]FET-OMe

For preparation of [^{18}F]FET-OMe, **7** was radiofluorinated using the same procedure as described above for **5** and the resulting intermediate Boc-[^{18}F]FET-OMe ([^{18}F]**9**) was deprotected with trifluoroacetic acid (TFA) for 1 min at ambient temperature (**Scheme 4**). The crude product was purified by semi-preparative HPLC and subsequent solid phase extraction with a Strata-X reversed phase cartridge. After elution of the product with EtOH, the solvent was removed and the residue was formulated in isotonic saline to afford [^{18}F]FET-OMe in RCYs of 41±5% (n=8) and an RCP of 98% within 90±5 min. The molar activity amounted to 156 GBq/µmol (for 710 MBq [^{18}F]FET-OMe).

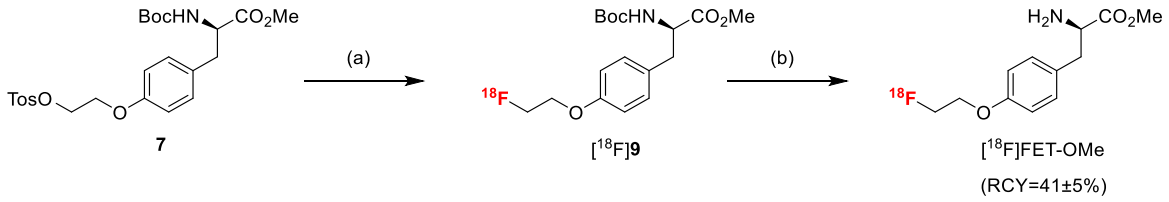

Scheme 4: Radiosynthesis of [^{18}F]FET-OMe from precursor **7**. Conditions: (a) TBAOH, [^{18}F]F^{-}, MeCN, 85 °C, 10 min; (b) TFA, 1 min.

3.3 Biological evaluation

3.3.1 Cellular uptake and protein incorporation studies

To assess cellular uptake of the two novel radiolabeled probes, their accumulation in human U87 MG glioblastoma cells was compared with that of the established tracer [^{18}F]FET (**Fig. 2**). After incubation for 1 h, cellular uptake of *m*-[^{18}F]FET amounted to 9.1±2.2% of the applied activity per 2×10^5 cells and was significantly higher than that of the reference tracer [^{18}F]FET (7.4±2.6% per 2×10^5 cells, p=0.034). Conversely, cellular uptake of [^{18}F]FET-OMe amounted to only 2.6±1.3% of the applied activity per 2×10^5 cells and was significantly lower than that of both [^{18}F]FET (p<0.001) and *m*-[^{18}F]FET (p<0.001). To exclude that the higher cellular uptake of *m*-[^{18}F]FET compared to [^{18}F]FET was related to increased protein incorporation, the soluble fractions obtained by lysis of U87 MG cells incubated with *m*-[^{18}F]FET were separated with PD10 columns, which demonstrated complete elution of radioactivity in the low-molecular-weight fraction and no coelution with the protein fraction (see **Fig. S3**).

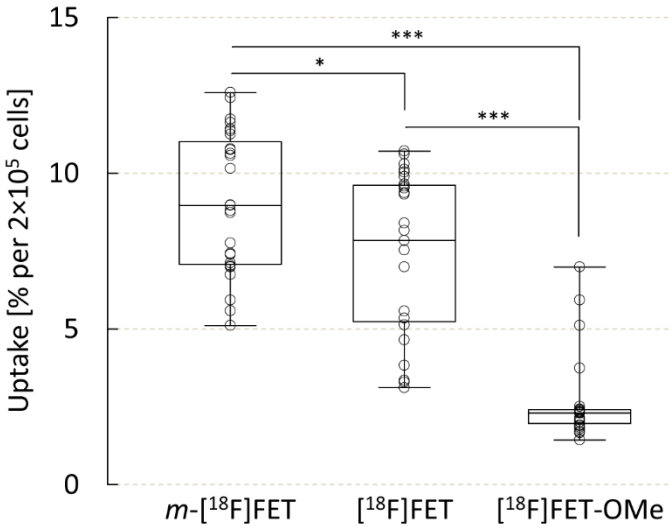

Figure 2: Uptake of *m*-[^{18}F]FET, [^{18}F]FET and [^{18}F]FET-OMe by human U87 MG glioblastoma cells. Uptake was quantified after incubation of the cells with 150 kBq of the different probes for 1 h and is expressed as the percentage of total activity added per 2×10^5 cells. Boxplots indicate median, 25th and 75th percentile (box), minimum and maximum values (whiskers) and individual data points (circles). Statistically significant differences between cellular uptake of the probes were identified by Welch's ANOVA with Games-Howell post-hoc test and are indicated by asterisks (*, p<0.05, ***, p<0.001).

3.3.2 Competitive inhibition studies

To obtain insight into the amino acid transporters involved in uptake of the different probes, their accumulation in U87 MG cells was also measured in the presence of competitive inhibitors of the main transport systems for neutral amino acids (**Fig. 3**). Inhibition of system L with 2-

aminobicyclo[2,2,1]heptane-2-carboxylic acid (BCH) significantly reduced cellular accumulation of [^{18}F]FET and *m*-[^{18}F]FET in a concentration-dependent manner, with almost complete suppression of *m*-[^{18}F]FET uptake at the highest concentration examined (**Fig. 3A** & **B**). BCH addition also significantly reduced cellular uptake of [^{18}F]FET-OMe, but the inhibition showed no evident concentration-dependence and did not exceed 60% (**Fig. 3C**). Conversely, inhibition of system ASC with L-serine reduced cellular accumulation of all three probes in a concentration-dependent manner, although the effects of this inhibitor on uptake of [^{18}F]FET and *m*-[^{18}F]FET were less pronounced than those of BCH and only reached statistical significance at higher inhibitor concentrations. Finally, inhibition of system A with α-(methylamino)isobutyric acid (MeAIB) had no significant effects on the accumulation of [^{18}F]FET (**Fig. 3A**) or [^{18}F]FET-OMe (**Fig. 3C**), but actually increased cellular uptake of *m*-[^{18}F]FET in a concentration-dependent manner (**Fig. 3B**).

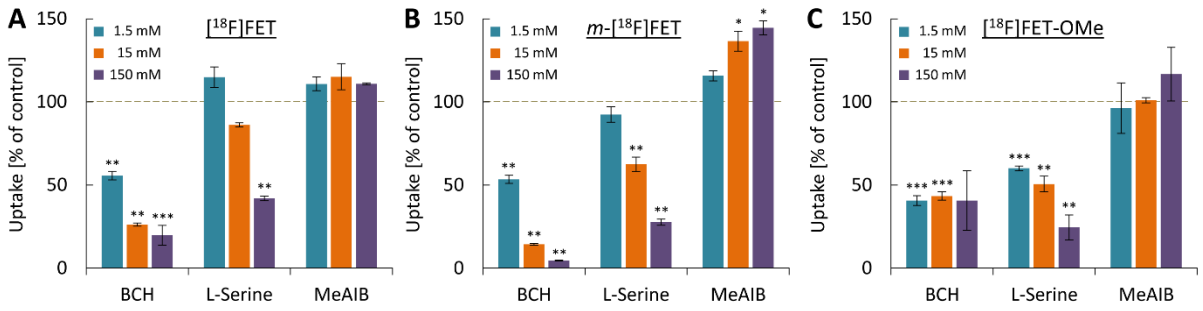

Figure 3: Effect of different amino acid transport inhibitors on uptake of (**A**) [^{18}F]FET, (**B**) *m*-[^{18}F]FET and (**C**) [^{18}F]FET-OMe by U87 MG glioblastoma cells. Uptake was quantified after incubation of the cells with 150 kBq of the probes for 1 h in the presence of the indicated inhibitor concentrations and is expressed as the percentage of uptake observed in control experiments without inhibitor. The inhibitors used were 2-aminobicyclo[2,2,1]heptane-2-carboxylic acid (BCH) for system L, L-serine for system ASC and α-(methylamino)isobutyric acid (MeAIB) for system A. Statistically significant differences in uptake compared to control experiments without inhibitor were identified (before normalization) by Welch's ANOVA with Games-Howell post-hoc test and are indicated by asterisks (*, $p<0.05$, **, $p<0.01$, ***, $p<0.001$).

3.3.3 *In vivo* biodistribution studies

Next, the *in vivo* imaging properties of the two novel analogs and [^{18}F]FET were compared in immunodeficient Rowett Nude Rats xenotransplanted with intracerebral U87 MG tumors. While maximal tumor uptake of *m*-[^{18}F]FET was similar to that of the reference tracer [^{18}F]FET, the *meta*-substituted probe exhibited faster brain and tumor uptake kinetics, which resulted in higher tumoral SUV_{bw} values during the first 30 min p.i. (**Fig. 4**). [^{18}F]FET-OMe showed faster brain uptake as well, but the time course of tumoral radioactivity accumulation with this probe was similar to that with [^{18}F]FET (**Fig. 5**). In addition, the maximum tumor uptake of

radioactivity in measurements with [^{18}F]FET-OMe tended to be lower than that in the measurements with [^{18}F]FET (**Fig. 5**), although this difference did not reach statistical significance.

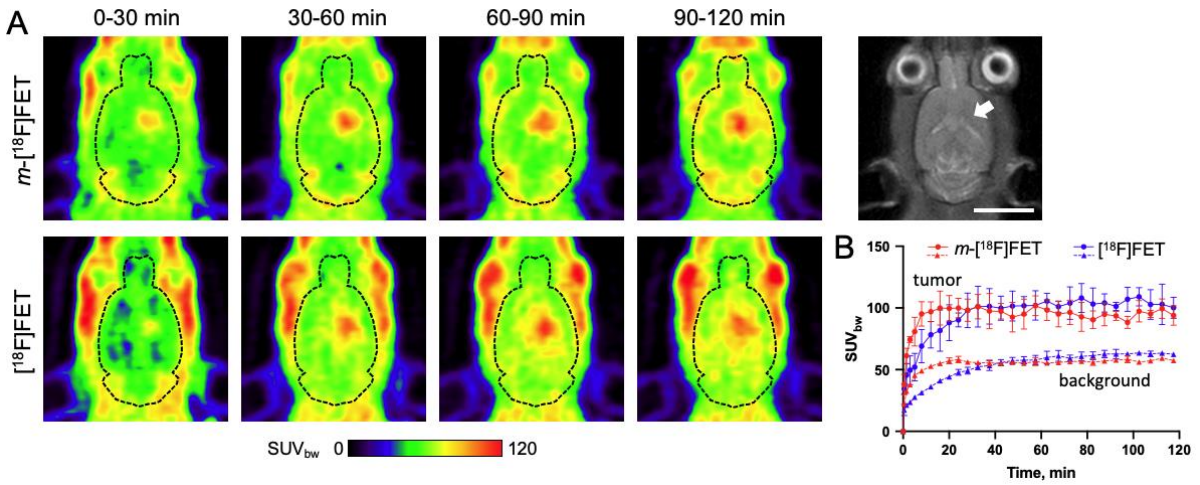

Figure 4: Comparison of *in vivo* tumor uptake of *m*-[^{18}F]FET and [^{18}F]FET in an orthotopic U87 MG glioblastoma rat model. (**A**) Representative horizontal PET images (summed over the indicated 30 minute time frames) of the same tumor-bearing rat measured (on different days) with *m*-[^{18}F]FET (top) or [^{18}F]FET (bottom). The outline of the brain is indicated by dashed lines. Also shown is a T_2-weigthed MRI of the animal, with the location of the intracerebral tumor indicated by an arrow. Scale bar: 10 mm. (**B**) Comparison of the mean time-activity curves (n=3) for tumoral and brain (background) accumulation of radioactivity in measurements with *m*-[^{18}F]FET (red) and [^{18}F]FET (blue).

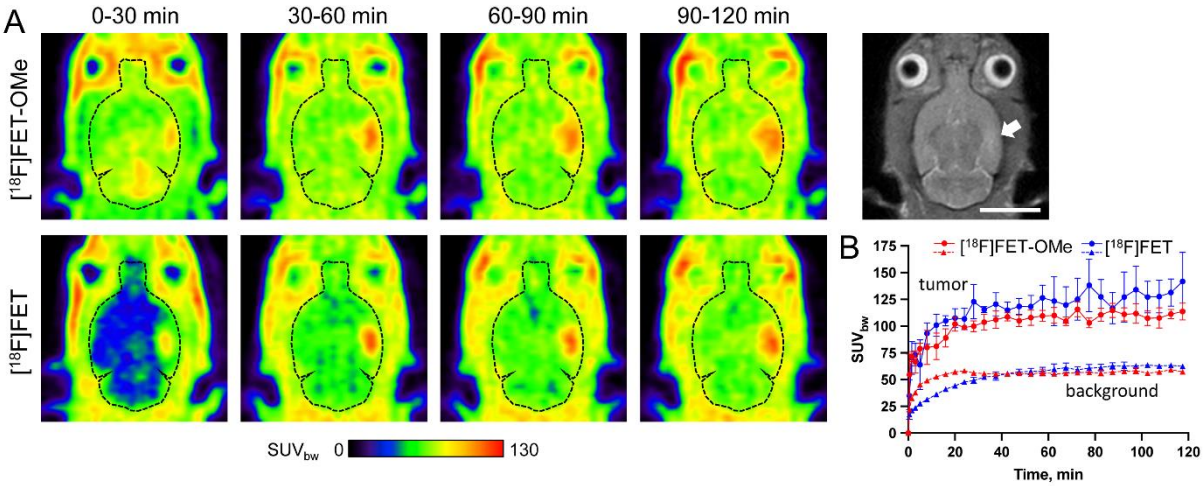

Figure 5: Comparison of *in vivo* tumor uptake of [^{18}F]FET-OMe and [^{18}F]FET in an orthotopic U87 MG glioblastoma rat model. (**A**) Representative horizontal PET images (summed over the indicated 30 minute time frames) of the same tumor-bearing rat measured (on different days) with [^{18}F]FET-OMe (top) or [^{18}F]FET (bottom). The outline of the brain is indicated by dashed lines. Also shown is a T_2-weigthed MRI of the animal, with the location of the intracerebral tumor indicated by an arrow. Scale bar: 10 mm. (**B**) Comparison of the mean time-activity curves (n=3) for tumoral and brain (background) accumulation of radioactivity in measurements with [^{18}F]FET-OMe (red) and [^{18}F]FET (blue).

4 Discussion

In the present work, two novel analogs of the established radiotracer [^{18}F]FET were prepared and compared with the parent compound using *in vitro* cellular uptake studies and *in vivo* PET imaging. Both tracers could be prepared in good radiochemical yields (41–56%) within 80–90 min, which is comparable to the radiosynthesis of [^{18}F]FET[40]. In addition, i*n vitro* studies with human U87 MG glioblastoma cells revealed significantly higher cellular uptake of *m*-[^{18}F]FET compared to [^{18}F]FET. While our data provide no direct insight into the exact transporters involved in the accumulation of *m*-[^{18}F]FET, uptake of large neutral amino acids by U87 MG cells has been shown to be mainly mediated by LAT1[41]. Moreover, inhibition of system L with BCH significantly reduced cellular uptake of both *m*-[^{18}F]FET and (to a lesser extent) [^{18}F]FET, which is in line with previous studies demonstrating reduced accumulation of [^{18}F]FET after inhibition of system L or knock-down of LAT1[4,6,10]. As such, it seems reasonable to assume that the higher cellular uptake of *m*-[^{18}F]FET compared to [^{18}F]FET observed in the present study can at least in part be attributed to the fact that *meta*-substituted amino acids are typically better substrates of LAT1 than the corresponding *para*-substituted derivatives[16–19,21]. However, apart from LAT1, several other amino acid transporters belonging to the systems L, B^0, $B^{0,+}$ and ASC have been shown or proposed to be (directly or indirectly) involved in tumoral [^{18}F]FET uptake[3–6,10,11] and many of them are also present in U87 MG cells[41]. Indeed, our finding that cellular uptake of both, *m*-[^{18}F]FET and [^{18}F]FET, was also sensitive to L-serine points to an involvement of system ASC, which is primarily responsible for transport of small neutral amino acids. While a direct transport of the probes by members of this system cannot be excluded, it is also possible that their inhibition indirectly reduced cellular uptake by other systems. Thus, transport of small neutral amino acids by systems like ASC and A has been shown to contribute to the counter-gradients required for uptake of large neutral amino acids by system L, thereby increasing the net accumulation of substrates by transporters like LAT1[42–44]. Interestingly, co-expression of transporters from system L and A has been shown to increase the net accumulation of amino acids that are specific system L substrates while decreasing the net accumulation of amino acids that are substrates for both transport systems[42]. With this in mind, the paradoxical stimulation of *m*-[^{18}F]FET uptake observed after inhibition of system A with MeAIB could indicate that this probe is also a substrate for transport by members of system A.

Another finding of the present study that deserves further investigation is that maximum tumor uptake of *m*-[^{18}F]FET in the orthotopic glioblastoma model was comparable to that of [^{18}F]FET, which is in apparent contrast to the higher cellular uptake observed *in vitro*. One possible

explanation for this finding could be that LAT1 and other members of system L operate through an exchange mechanism that utilizes the intracellular pool of small neutral amino acids for exchange with large neutral amino acids from the extracellular space. As a consequence, their ability to directly concentrate substrates strongly depends on the counter-gradients of various amino acids across the plasma membrane[44,45], which are likely to differ between *in vitro* and *in vivo* conditions. For example, it seems conceivable that the exact concentration gradients present *in vivo* could simply impose an upper limit on the net accumulation of tracers by the tumor cells, resulting in similar tumoral accumulation of [^{18}F]FET and *m*-[^{18}F]FET despite differences in the transport capacity of both probes. In line with this assumption, tumoral tracer accumulation of *m*-[^{18}F]FET during the first 30 min p.i. was indeed faster and more pronounced, suggesting an improved capacity of this analog for transport across the BBB and into the tumor cells. Regardless of the underlying mechanisms, the faster *in vivo* tumor accumulation of *m*-[^{18}F]FET compared to [^{18}F]FET could have certain practical advantages for clinical PET imaging by, e.g., shortening the necessary scan times in brain tumor patients. In addition, given that kinetic analysis of tumoral [^{18}F]FET uptake has been shown to provide valuable information for the differential diagnosis and grading of gliomas[46–49], it remains to be evaluated whether the uptake kinetics of *m*-[^{18}F]FET are also affected by the exact tumor type or grade.

While the effects of aromatic substituents on amino acid transport by LAT1 are relatively well established, the consequences of modification of the carboxyl group remain controversial, with some[13,15,22,23] but not all studies[21,24,25] reporting a loss of substrate activity. Our present findings indicate that esterification of the carboxyl group in [^{18}F]FET does not completely prevent but significantly reduces cellular uptake via the main amino acid transport systems in U87 MG cells *in vitro*. In addition, our results suggest that the contribution of individual amino acid transport systems to *in vitro* uptake of [^{18}F]FET-OMe may differ from their contribution to the accumulation of [^{18}F]FET. Thus, while the present and previous studies demonstrate that high concentrations of BCH almost completely abolish cellular uptake of [^{18}F]FET[4,6], uptake of [^{18}F]FET-OMe was less sensitive to inhibition of system L with BCH. Nevertheless, the reduced but still significant BCH-sensitivity of [^{18}F]FET-OMe uptake indicates that LAT1 or other members of system L are still capable of transporting this probe, albeit possibly with a reduced transport capacity. Additionally, the partial sensitivity to L-serine suggests that members of system ASC contribute to uptake of [^{18}F]FET-OMe, either by direct transport or through a functional coupling with other transport systems as discussed above. In any case, the fact that none of the inhibitors examined completely prevented *in vitro* accumulation of [^{18}F]FET-OMe suggests that cellular uptake of this probe either involves multiple transport

systems or additional mechanisms, such as passive transfer across the cell membrane. Interestingly, and in contrast to the rather low cellular uptake observed *in vitro*, tumoral uptake of [^{18}F]FET-OMe in the orthotopic glioma model was only slightly lower that of [^{18}F]FET. The most likely explanation for this observation is that [^{18}F]FET-OMe was rapidly demethylated into [^{18}F]FET by endogenous carboxylesterases, which have been shown to catalyze the *in vivo* biotransformation of numerous ester-containing drugs and prodrugs[50]. However, even though the faster overall brain uptake of radioactivity observed with [^{18}F]FET-OMe compared to [^{18}F]FET indicates that esterification accelerated brain entry (possibly by enabling rapid passive transfer of the intact tracer across the BBB), there was no beneficial effect on the time-course or magnitude of tumor accumulation. Considering the poor cellular uptake of intact [^{18}F]FET-OMe by U87 MG cells *in vitro*, the latter might reflect the low activity of brain esterases, which typically results in much slower ester hydrolysis than in peripheral tissues[51,52]. Accordingly, most of the tumor-specific radioactivity uptake might be attributable to [^{18}F]FET formed by rapid peripheral cleavage of [^{18}F]FET-OMe and subsequent transport across the BBB and into the tumor, while a small fraction of intact [^{18}F]FET-OMe quickly reaches the brain but is only slowly hydrolyzed into [^{18}F]FET and mainly contributes to non-specific binding. If this was the case, faster hydrolysable esters could possibly be used to increase brain cleavage and subsequent transporter-mediated tumor uptake, although this might also accelerate peripheral cleavage and thus reduce delivery of intact tracer to the brain. Lacking detailed radiometabolite analyses, an alternative albeit much less likely assumption is that a significant fraction of the tumoral radioactivity accumulation was indeed attributable to intact [^{18}F]FET-OMe. However, in this case, the fact that maximum tumor accumulation of radioactivity was very similar to that observed with [^{18}F]FET and *m*-[^{18}F]FET could only be explained if, e.g., the upper limit of cellular uptake by the relevant tumoral transporters *in vivo* is considerably lower than that in the *in vitro* assays. In addition, given that our inhibition studies point to differences in the exact transport systems involved in uptake of [^{18}F]FET-OMe and [^{18}F]FET by U87 MG cells, it seems unlikely that both probes would exhibit essentially identical tumoral uptake kinetics. In any case, while firm conclusions regarding the underlying mechanisms would require further studies, our findings indicate that modification of the aromatic side-chain is a more promising strategy for development of [^{18}F]FET analogs with improved transport properties than modification of the carboxylic acid function.

5 Conclusion

In summary, two novel [^{18}F]FET analogs were prepared in acceptable to good radiochemical yields and subjected to a preclinical evaluation. While esterification of the carboxyl group in [^{18}F]FET reduced cellular uptake *in vitro* and provided no advantage for *in vivo* tumor imaging, placement of the [^{18}F]fluoroethoxy group in *meta*- instead of *para*-position significantly improved *in vitro* uptake and accelerated tumor accumulation in an orthotopic glioblastoma model. As such, *m*-[^{18}F]FET represents a promising alternative to [^{18}F]FET for brain tumor imaging and deserves further evaluation with regard to its transport properties and *in vivo* biodistribution.

6 Abbreviations

[^{18}F]F^-, [^{18}F]fluoride; [^{18}F]FDG, 2-[^{18}F]fluoro-2-deoxy-D-glucose; [^{18}F]FET, *O*-([^{18}F]fluoroethyl)-L-tyrosine; [^{18}F]FET-OMe, *O*-([^{18}F]fluoroethyl)-L-tyrosine methyl ester; AY, activity yield; BBB, blood-brain-barrier; BCH, 2-aminobicyclo[2,2,1]heptane-2-carboxylic acid; $(CD_3)_2SO$, deuterodimethylsulfoxide; $CDCl_3$, deuterochloroform; EBSS, Earle's balanced salt solution; HRMS, high resolution mass spectrometry; LRMS, low resolution mass spectrometry; *m*-[^{18}F]FET, *O*-([^{18}F]fluoroethyl)-L-meta-tyrosine; MeAIB, α-(methylamino)isobutyric acid; PBS, phosphate-buffered saline; PET, positron emission tomography; RCP, radiochemical purity; RCY, radiochemical yield; SAR, structure-activity relationship; SUV_{bw}, standardized uptake value normalized by body weight; TFA, trifluoroacetic acid; VOI, volume of interest.

7 Supporting information

^{1}H-, ^{13}C- and ^{19}F-NMR spectra for all prepared compounds; HPLC chromatograms for *m*-[^{18}F]FET and [^{18}F]FET-OMe; details on the determination of carrier amount and molar activity of the probes; results of the protein incorporation studies with *m*-[^{18}F]FET (PDF).

8 Acknowledgements

Funding: This work was supported, in part, by Deutsche Forschungsgemeinschaft (DFG) grants ZL 65/1-1, ZL 65/3-1 and ZL 65/4-1.

9 References

(1) Verger, A.; Kas, A.; Darcourt, J.; Guedj, E. PET Imaging in Neuro-Oncology: An Update and Overview of a Rapidly Growing Area. *Cancers (Basel)*. **2022**, *14* (5), 1103.

https://doi.org/10.3390/cancers14051103.

(2) Parent, E. E.; Sharma, A.; Jain, M. Amino Acid PET Imaging of Glioma. *Curr. Radiol. Rep.* **2019**, *7* (5), 14. https://doi.org/10.1007/s40134-019-0324-x.

(3) Heiss, P.; Mayer, S.; Herz, M.; Wester, H. J.; Schwaiger, M.; Senekowitsch-Schmidtke, R. Investigation of Transport Mechanism and Uptake Kinetics of O-(2-[18F]Fluoroethyl)-L-Tyrosine in Vitro and in Vivo. *J. Nucl. Med.* **1999**, *40* (8), 1367–1373.

(4) Langen, K.-J.; Jarosch, M.; Mühlensiepen, H.; Hamacher, K.; Bröer, S.; Jansen, P.; Zilles, K.; Coenen, H. H. Comparison of Fluorotyrosines and Methionine Uptake in F98 Rat Gliomas. *Nucl. Med. Biol.* **2003**, *30* (5), 501–508. https://doi.org/10.1016/S0969-8051(03)00023-4.

(5) Langen, K.-J.; Hamacher, K.; Weckesser, M.; Floeth, F.; Stoffels, G.; Bauer, D.; Coenen, H. H.; Pauleit, D. O-(2-[18F]Fluoroethyl)-l-Tyrosine: Uptake Mechanisms and Clinical Applications. *Nucl. Med. Biol.* **2006**, *33* (3), 287–294. https://doi.org/10.1016/j.nucmedbio.2006.01.002.

(6) Krämer, F.; Gröner, B.; Hoffmann, C.; Craig, A.; Brugger, M.; Drzezga, A.; Timmer, M.; Neumaier, F.; Zlatopolskiy, B. D.; Endepols, H.; Neumaier, B. Evaluation of 3-l- and 3-d-[18F]Fluorophenylalanines as PET Tracers for Tumor Imaging. *Cancers (Basel).* **2021**, *13* (23), 6030. https://doi.org/10.3390/cancers13236030.

(7) Nawashiro, H.; Otani, N.; Shinomiya, N.; Fukui, S.; Ooigawa, H.; Shima, K.; Matsuo, H.; Kanai, Y.; Endou, H. L-type Amino Acid Transporter 1 as a Potential Molecular Target in Human Astrocytic Tumors. *Int. J. Cancer* **2006**, *119* (3), 484–492. https://doi.org/10.1002/ijc.21866.

(8) Bröer, S. Amino Acid Transporters as Targets for Cancer Therapy: Why, Where, When, and How. *Int. J. Mol. Sci.* **2020**, *21* (17), 6156. https://doi.org/10.3390/ijms21176156.

(9) Saito, Y.; Soga, T. Amino Acid Transporters as Emerging Therapeutic Targets in Cancer. *Cancer Sci.* **2021**, *112* (8), 2958–2965. https://doi.org/10.1111/cas.15006.

(10) Habermeier, A.; Graf, J.; Sandhöfer, B. F.; Boissel, J.-P.; Roesch, F.; Closs, E. I. System L Amino Acid Transporter LAT1 Accumulates O-(2-Fluoroethyl)-l-Tyrosine (FET). *Amino Acids* **2015**, *47* (2), 335–344. https://doi.org/10.1007/s00726-014-1863-3.

(11) Langen, K.-J.; Stoffels, G.; Filss, C.; Heinzel, A.; Stegmayr, C.; Lohmann, P.; Willuweit, A.; Neumaier, B.; Mottaghy, F. M.; Galldiks, N. Imaging of Amino Acid Transport in Brain Tumours: Positron Emission Tomography with O-(2-[18F]Fluoroethyl)-L-Tyrosine (FET). *Methods* **2017**, *130*, 124–134.

https://doi.org/10.1016/j.ymeth.2017.05.019.

(12) Smith, Q. R. Transport of Glutamate and Other Amino Acids at the Blood-Brain Barrier. *J. Nutr.* **2000**, *130* (4), 1016S-1022S. https://doi.org/10.1093/jn/130.4.1016S.

(13) Uchino, H.; Kanai, Y.; Kim, D. K.; Wempe, M. F.; Chairoungdua, A.; Morimoto, E.; Anders, M. W.; Endou, H. Transport of Amino Acid-Related Compounds Mediated by L-Type Amino Acid Transporter 1 (LAT1): Insights Into the Mechanisms of Substrate Recognition. *Mol. Pharmacol.* **2002**, *61* (4), 729–737. https://doi.org/10.1124/mol.61.4.729.

(14) Ylikangas, H.; Malmioja, K.; Peura, L.; Gynther, M.; Nwachukwu, E. O.; Leppänen, J.; Laine, K.; Rautio, J.; Lahtela-Kakkonen, M.; Huttunen, K. M.; Poso, A. Quantitative Insight into the Design of Compounds Recognized by the L-Type Amino Acid Transporter 1 (LAT1). *ChemMedChem* **2014**, *9* (12), 2699–2707. https://doi.org/10.1002/cmdc.201402281.

(15) Gynther, M.; Laine, K.; Ropponen, J.; Leppänen, J.; Mannila, A.; Nevalainen, T.; Savolainen, J.; Järvinen, T.; Rautio, J. Large Neutral Amino Acid Transporter Enables Brain Drug Delivery via Prodrugs. *J. Med. Chem.* **2008**, *51* (4), 932–936. https://doi.org/10.1021/jm701175d.

(16) Peura, L.; Malmioja, K.; Laine, K.; Leppänen, J.; Gynther, M.; Isotalo, A.; Rautio, J. Large Amino Acid Transporter 1 (LAT1) Prodrugs of Valproic Acid: New Prodrug Design Ideas for Central Nervous System Delivery. *Mol. Pharm.* **2011**, *8* (5), 1857–1866. https://doi.org/10.1021/mp2001878.

(17) Venteicher, B.; Merklin, K.; Ngo, H. X.; Chien, H.; Hutchinson, K.; Campbell, J.; Way, H.; Griffith, J.; Alvarado, C.; Chandra, S.; Hill, E.; Schlessinger, A.; Thomas, A. A. The Effects of Prodrug Size and a Carbonyl Linker on L-Type Amino Acid Transporter 1-Targeted Cellular and Brain Uptake. *ChemMedChem* **2021**, *16* (5), 869–880. https://doi.org/10.1002/cmdc.202000824.

(18) Augustyn, E.; Finke, K.; Zur, A. A.; Hansen, L.; Heeren, N.; Chien, H.-C.; Lin, L.; Giacomini, K. M.; Colas, C.; Schlessinger, A.; Thomas, A. A. LAT-1 Activity of Meta-Substituted Phenylalanine and Tyrosine Analogs. *Bioorg. Med. Chem. Lett.* **2016**, *26* (11), 2616–2621. https://doi.org/10.1016/j.bmcl.2016.04.023.

(19) Ylikangas, H.; Peura, L.; Malmioja, K.; Leppänen, J.; Laine, K.; Poso, A.; Lahtela-Kakkonen, M.; Rautio, J. Structure–Activity Relationship Study of Compounds Binding to Large Amino Acid Transporter 1 (LAT1) Based on Pharmacophore Modeling and in Situ Rat Brain Perfusion. *Eur. J. Pharm. Sci.* **2013**, *48* (3), 523–531.

https://doi.org/10.1016/j.ejps.2012.11.014.

(20) Verhoeven, J.; Hulpia, F.; Kersemans, K.; Bolcaen, J.; De Lombaerde, S.; Goeman, J.; Descamps, B.; Hallaert, G.; Van den Broecke, C.; Deblaere, K.; Vanhove, C.; Van der Eycken, J.; Van Calenbergh, S.; Goethals, I.; De Vos, F. New Fluoroethyl Phenylalanine Analogues as Potential LAT1-Targeting PET Tracers for Glioblastoma. *Sci. Rep.* **2019**, *9* (1), 2878. https://doi.org/10.1038/s41598-019-40013-x.

(21) Kärkkäinen, J.; Gynther, M.; Kokkola, T.; Petsalo, A.; Auriola, S.; Lahtela-Kakkonen, M.; Laine, K.; Rautio, J.; Huttunen, K. M. Structural Properties for Selective and Efficient L-Type Amino Acid Transporter 1 (LAT1) Mediated Cellular Uptake. *Int. J. Pharm.* **2018**, *544* (1), 91–99. https://doi.org/10.1016/j.ijpharm.2018.04.025.

(22) Smith, Q. R. Carrier-Mediated Transport to Enhance Drug Delivery to Brain. *Int. Congr. Ser.* **2005**, *1277*, 63–74. https://doi.org/10.1016/j.ics.2005.02.012.

(23) Rautio, J.; Kärkkäinen, J.; Huttunen, K. M.; Gynther, M. Amino Acid Ester Prodrugs Conjugated to the α-Carboxylic Acid Group Do Not Display Affinity for the L-Type Amino Acid Transporter 1 (LAT1). *Eur. J. Pharm. Sci.* **2015**, *66*, 36–40. https://doi.org/10.1016/j.ejps.2014.09.025.

(24) Zur, A. A.; Chien, H.-C.; Augustyn, E.; Flint, A.; Heeren, N.; Finke, K.; Hernandez, C.; Hansen, L.; Miller, S.; Lin, L.; Giacomini, K. M.; Colas, C.; Schlessinger, A.; Thomas, A. A. LAT1 Activity of Carboxylic Acid Bioisosteres: Evaluation of Hydroxamic Acids as Substrates. *Bioorg. Med. Chem. Lett.* **2016**, *26* (20), 5000–5006. https://doi.org/10.1016/j.bmcl.2016.09.001.

(25) Nagamori, S.; Wiriyasermkul, P.; Okuda, S.; Kojima, N.; Hari, Y.; Kiyonaka, S.; Mori, Y.; Tominaga, H.; Ohgaki, R.; Kanai, Y. Structure–Activity Relations of Leucine Derivatives Reveal Critical Moieties for Cellular Uptake and Activation of MTORC1-Mediated Signaling. *Amino Acids* **2016**, *48* (4), 1045–1058. https://doi.org/10.1007/s00726-015-2158-z.

(26) Nian, Y.; Wang, J.; Zhou, S.; Wang, S.; Moriwaki, H.; Kawashima, A.; Soloshonok, V. A.; Liu, H. Recyclable Ligands for the Non-Enzymatic Dynamic Kinetic Resolution of Challenging A-Amino Acids. *Angew. Chemie Int. Ed.* **2015**, *54* (44), 12918–12922. https://doi.org/10.1002/anie.201507273.

(27) Humphrey, C. E.; Furegati, M.; Laumen, K.; La Vecchia, L.; Leutert, T.; Müller-Hartwieg, J. C. D.; Vögtle, M. Optimized Synthesis of L-m-Tyrosine Suitable for Chemical Scale-Up. *Org. Process Res. Dev.* **2007**, *11* (6), 1069–1075. https://doi.org/10.1021/op700093y.

(28) Terasawa, Y.; Sataka, C.; Sato, T.; Yamamoto, K.; Fukushima, Y.; Nakajima, C.; Suzuki, Y.; Katsuyama, A.; Matsumaru, T.; Yakushiji, F.; Yokota, S.; Ichikawa, S. Elucidating the Structural Requirement of Uridylpeptide Antibiotics for Antibacterial Activity. *J. Med. Chem.* **2020**, *63* (17), 9803–9827. https://doi.org/10.1021/acs.jmedchem.0c00973.

(29) Nakao, H.; Hoshino, J.; Ogata, T.; Miyashita, N.; Yamamoto, Y. Tyrosine Derivative and Method for Producing Tyrosine Derivative. US 2014/0187814 A1, 2014. https://lens.org/112-464-238-220-270.

(30) Nudelman, A.; Bechor, Y.; Falb, E.; Fischer, B.; Wexler, B. A.; Nudelman, A. Acetyl Chloride-Methanol as a Convenient Reagent for: A) Quantitative Formation of Amine Hydrochlorides B) Carboxylate Ester Formation C) Mild Removal of N-t-Boc-Protective Group. *Synth. Commun.* **1998**, *28* (3), 471–474. https://doi.org/10.1080/00397919808005101.

(31) Kolks, N.; Neumaier, F.; Neumaier, B.; Zlatopolskiy, B. D. Preparation of NIn-Methyl-6-[18F]Fluoro- and 5-Hydroxy-7-[18F]Fluorotryptophans as Candidate PET-Tracers for Pathway-Specific Visualization of Tryptophan Metabolism. *Int. J. Mol. Sci.* **2023**, *24* (20), 15251. https://doi.org/10.3390/ijms242015251.

(32) Hamacher, K.; Coenen, H. H. Efficient Routine Production of the 18F-Labelled Amino Acid O-(2-[18F]Fluoroethyl)-l-Tyrosine. *Appl. Radiat. Isot.* **2002**, *57* (6), 853–856. https://doi.org/10.1016/S0969-8043(02)00225-7.

(33) Qi, J.; Leahy, R. M.; Cherry, S. R.; Chatziioannou, A.; Farquhar, T. H. High-Resolution 3D Bayesian Image Reconstruction Using the MicroPET Small-Animal Scanner. *Phys Med Biol* **1998**, *43* (4), 1001–1013.

(34) Vollmar, S.; Hampl, J. A.; Kracht, L.; Herholz, K. Integration of Functional Data (PET) into Brain Surgery Planning and Neuronavigation. In *Advances in Medical Engineering*; Buzug, T. M., Holz, D., Bongartz, J., Kohl-Bareis, M., Hartmann, U., S., W., Eds.; Springer Berlin Heidelberg: Berlin, Heidelberg, 2007; pp 98–103. https://doi.org/10.1007/978-3-540-68764-1_16.

(35) Hoffmann, C.; Kolks, N.; Smets, D.; Haseloer, A.; Gröner, B.; Urusova, E. A.; Endepols, H.; Neumaier, F.; Ruschewitz, U.; Klein, A.; Neumaier, B.; Zlatopolskiy, B. D. Next Generation Copper Mediators for the Efficient Production of 18F-Labeled Aromatics. *Chem. – A Eur. J.* **2022**. https://doi.org/10.1002/chem.202202965.

(36) Craig, A.; Kolks, N.; Urusova, E. A.; Zischler, J.; Brugger, M.; Endepols, H.; Neumaier, B.; Zlatopolskiy, B. D. Preparation of Labeled Aromatic Amino Acids via Late-Stage 18 F-Fluorination of Chiral Nickel and Copper Complexes. *Chem. Commun.* **2020**, *56* (66),

9505–9508. https://doi.org/10.1039/D0CC02223C.

(37) Orlovskaya, V.; Fedorova, O.; Nadporojskii, M.; Krasikova, R. A Fully Automated Azeotropic Drying Free Synthesis of O-(2-[18F]Fluoroethyl)-L-Tyrosine ([18F]FET) Using Tetrabutylammonium Tosylate. *Appl. Radiat. Isot.* **2019**, *152*, 135–139. https://doi.org/10.1016/j.apradiso.2019.07.006.

(38) Krasikova, R. N.; Kuznetsova, O. F.; Fedorova, O. S.; Maleev, V. I.; Saveleva, T. F.; Belokon, Y. N. No Carrier Added Synthesis of O-(2′-[18F]Fluoroethyl)-l-Tyrosine via a Novel Type of Chiral Enantiomerically Pure Precursor, NiII Complex of a (S)-Tyrosine Schiff Base. *Bioorg. Med. Chem.* **2008**, *16* (9), 4994–5003. https://doi.org/10.1016/j.bmc.2008.03.040.

(39) Kolb, H. C.; Walsh, J. C.; Kasi, D.; Mocharla, V.; Wang, B.; Gangadharmath, U. B.; Duclos, B. A.; Chen, K.; Zhang, W.; Chen, G.; Padgett, H. C.; Karimi, F.; Scott, P. J. H.; Gao, Z.; Liang, Q.; Collier, T. L.; Zhao, T.; Xia, C. Development of Molecular Imaging Probes for Carbonic Anhydrase-Ix Using Click Chemistry. WO 2008/124703 A2, 2008. https://lens.org/065-486-829-122-79X.

(40) Wester, H. J.; Herz, M.; Weber, W.; Heiss, P.; Senekowitsch-Schmidtke, R.; Schwaiger, M.; Stöcklin, G. Synthesis and Radiopharmacology of O-(2-[18F]Fluoroethyl)-L-Tyrosine for Tumor Imaging. *J. Nucl. Med.* **1999**, *40* (1), 205–212.

(41) Gauthier-Coles, G.; Vennitti, J.; Zhang, Z.; Comb, W. C.; Xing, S.; Javed, K.; Bröer, A.; Bröer, S. Quantitative Modelling of Amino Acid Transport and Homeostasis in Mammalian Cells. *Nat. Commun.* **2021**, *12* (1), 5282. https://doi.org/10.1038/s41467-021-25563-x.

(42) Baird, F. E.; Bett, K. J.; MacLean, C.; Tee, A. R.; Hundal, H. S.; Taylor, P. M. Tertiary Active Transport of Amino Acids Reconstituted by Coexpression of System A and L Transporters in Xenopus Oocytes. *Am. J. Physiol. Metab.* **2009**, *297* (3), E822–E829. https://doi.org/10.1152/ajpendo.00330.2009.

(43) Nicklin, P.; Bergman, P.; Zhang, B.; Triantafellow, E.; Wang, H.; Nyfeler, B.; Yang, H.; Hild, M.; Kung, C.; Wilson, C.; Myer, V. E.; MacKeigan, J. P.; Porter, J. A.; Wang, Y. K.; Cantley, L. C.; Finan, P. M.; Murphy, L. O. Bidirectional Transport of Amino Acids Regulates MTOR and Autophagy. *Cell* **2009**, *136* (3), 521–534. https://doi.org/10.1016/j.cell.2008.11.044.

(44) Verrey, F. System L: Heteromeric Exchangers of Large, Neutral Amino Acids Involved in Directional Transport. *Pflügers Arch. - Eur. J. Physiol.* **2003**, *445* (5), 529–533. https://doi.org/10.1007/s00424-002-0973-z.

(45) Scalise, M.; Console, L.; Rovella, F.; Galluccio, M.; Pochini, L.; Indiveri, C. Membrane Transporters for Amino Acids as Players of Cancer Metabolic Rewiring. *Cells* **2020**, *9* (9), 2028. https://doi.org/10.3390/cells9092028.

(46) Pöpperl, G.; Kreth, F. W.; Herms, J.; Koch, W.; Mehrkens, J. H.; Gildehaus, F. J.; Kretzschmar, H. A.; Tonn, J. C.; Tatsch, K. Analysis of 18F-FET PET for Grading of Recurrent Gliomas: Is Evaluation of Uptake Kinetics Superior to Standard Methods? *J. Nucl. Med.* **2006**, *47* (3), 393–403.

(47) Weckesser, M.; Langen, K. J.; Rickert, C. H.; Kloska, S.; Straeter, R.; Hamacher, K.; Kurlemann, G.; Wassmann, H.; Coenen, H. H.; Schober, O. O-(2-[18F]Fluorethyl)-L-Tyrosine PET in the Clinical Evaluation of Primary Brain Tumours. *Eur. J. Nucl. Med. Mol. Imaging* **2005**, *32* (4), 422–429. https://doi.org/10.1007/s00259-004-1705-8.

(48) Pöpperl, G.; Kreth, F. W.; Mehrkens, J. H.; Herms, J.; Seelos, K.; Koch, W.; Gildehaus, F. J.; Kretzschmar, H. A.; Tonn, J. C.; Tatsch, K. FET PET for the Evaluation of Untreated Gliomas: Correlation of FET Uptake and Uptake Kinetics with Tumour Grading. *Eur. J. Nucl. Med. Mol. Imaging* **2007**, *34* (12), 1933–1942. https://doi.org/10.1007/s00259-007-0534-y.

(49) Debus, C.; Afshar-Oromieh, A.; Floca, R.; Ingrisch, M.; Knoll, M.; Debus, J.; Haberkorn, U.; Abdollahi, A. Feasibility and Robustness of Dynamic 18F-FET PET Based Tracer Kinetic Models Applied to Patients with Recurrent High-Grade Glioma Prior to Carbon Ion Irradiation. *Sci. Rep.* **2018**, *8* (1), 14760. https://doi.org/10.1038/s41598-018-33034-5.

(50) Yang, Y.; Aloysius, H.; Inoyama, D.; Chen, Y.; Hu, L. Enzyme-Mediated Hydrolytic Activation of Prodrugs. *Acta Pharm. Sin. B* **2011**, *1* (3), 143–159. https://doi.org/10.1016/j.apsb.2011.08.001.

(51) Durrer, A.; Walther, B.; Racciatti, A.; Boss, G.; Testa, B. Structure-Metabolism Relationships in the Hydrolysis of Nicotinate Esters by Rat Liver and Brain Subcellular Fractions. *Pharm. Res.* **1991**, *8* (7), 832–839. https://doi.org/10.1023/a:1015839109449.

(52) Anderson, B. D.; Galinsky, R. E.; Baker, D. C.; Chi, S.-C.; Hoesterey, B. L.; Morgan, M. E.; Murakami, K.; Mitsuya, H. Approaches toward the Optimization of CNS Uptake of Anti-AIDS Agents. *J. Control. Release* **1992**, *19* (1–3), 219–229. https://doi.org/10.1016/0168-3659(92)90078-6.

3.3. 7-[^{18}F]Fluoro-8-azaisatoic Anhydrides: Versatile Prosthetic Groups for the Preparation of PET-Tracers

Die direkte Radiofluorierung ist aufgrund der oft harschen Bedingungen und der Notwendigkeit von Schutzgruppen nicht für alle potenziellen Radiotracer geeignet. Insbesondere bei größeren Biomolekülen wie Peptiden, Proteinen und Antikörpern wird daher häufig auf die indirekte Radiofluorierung mittels PGs zurückgegriffen. Diese PGs sollten einfach und schnell synthetisiert und gereinigt werden können, und sie müssen eine hohe Reaktivität gegenüber den potenziellen Konjugationsstellen aufweisen. In diesem Projekt wurden vier neue PGs entwickelt, die aus leicht erhältlichen Ausgangsstoffen in wenigen Schritten hergestellt werden können. Innerhalb von 15 bis 20 min konnten diese Gruppen radiofluoriert und isoliert werden. Zwei dieser Gruppen reagieren mit Aminen, welche in Peptiden und Proteinen primär in den Seitenketten von Lysin-Resten vorkommen, während die anderen beiden für die kupfervermittelte 1,3-dipolare Cycloaddition mit Alkinen bzw. Aziden geeignet sind.

Mit diesen PGs wurden drei neue Tracer für das PSMA synthetisiert und biologisch untersucht. Dieses Protein wird in Prostatakrebszellen 100–1000 Mal stärker exprimiert als in gesunden Prostatazellen.[109] Aufgrund der Häufigkeit von Prostatakrebs bei Männern und seiner Bedeutung als eine der Hauptursachen für krebsbedingte Todesfälle ist die Bildgebung von Prostatakarzinomen von großem Wert.[110] Bisher wurden mehrere verschiedene PSMA-spezifische Radiotracer für die PET Diagnostik entwickelt.[111] Die im folgenden verwendeten Tracer haben als Grundmotiv das Harnstoffderivat Glu-C(O)-Lys, welches zuerst von Chen et al. beschrieben wurde und über die Seitenkette des Lysin Rests konjugiert oder funktionalisiert wurde.[112] Die Tracer wurden anhand ihrer Aufnahme in die PSMA-positiven Spinalganglien von gesunden Ratten evaluiert, welche aufgrund ihrer symmetrischen Anordnung eine genaue Bestimmung der Performance von PSMA-gerichteten bildgebenden Sonden ermöglichen.[113]

Das Konzept der nachfolgenden Publikation wurde von Prof. Dr. B. D. Zlatopolskiy, Dr. M. Willmann, B. Gröner und Prof. Dr. B. Neumaier entwickelt. Die organischen Vorläufer- und Referenzverbindungssynthesen wurden von L. Donnerstag, M. Willmann, B. Gröner, Dr. S. Humpert, E. A. Urusova und Prof. Dr. B. D. Zlatopolskiy durchgeführt. Optimierungen der Radiosynthesen wurden von L. Donnerstag, M. Willmann und B. Gröner durchgeführt. Präklinische biologische Untersuchungen wurden von Prof. Dr. H. Endepols und M. Brugger

durchgeführt. Der Artikel wurde gemeinschaftlich von B. Gröner, M. Willmann, Dr. F. Neumaier, Prof. Dr. B. D. Zlatopolskiy, Prof. Dr. H. Endepols und Prof. Dr. B. Neumaier verfasst.

Journal of Medicinal Chemistry

pubs.acs.org/jmc

Article

Open Access

This article is licensed under CC-BY 4.0

7-[^{18}F]Fluoro-8-azaisatoic Anhydrides: Versatile Prosthetic Groups for the Preparation of PET Tracers

Benedikt Gröner,[⊥] Michael Willmann,[⊥] Lisa Donnerstag, Elizaveta A. Urusova, Felix Neumaier, Swen Humpert, Heike Endepols, Bernd Neumaier,* and Boris D. Zlatopolskiy

Cite This: *J. Med. Chem.* 2023, 66, 12629−12644

Read Online

ACCESS | Metrics & More | Article Recommendations | Supporting Information

ABSTRACT: ^{18}F-Fluorination of sensitive molecules is often challenging, but can be accomplished under suitably mild conditions using radiofluorinated prosthetic groups (PGs). Herein, 1-alkylamino-7-[^{18}F]fluoro-8-azaisatoic anhydrides ([^{18}F]AFAs) are introduced as versatile ^{18}F-labeled building blocks that can be used as amine-reactive or "click chemistry" PGs. [^{18}F]AFAs were efficiently prepared within 15 min by "on cartridge" radiolabeling of readily accessible trimethylammonium precursors. Conjugation with a range of amines afforded the corresponding 2-alkylamino-6-[^{18}F]fluoronicotinamides in radiochemical conversions (RCCs) of 15−98%. In addition, radiolabeling of alkyne- or azide-functionalized precursors with azidopropyl- or propargyl-substituted [^{18}F]AFAs using Cu-catalyzed click cycloaddition afforded the corresponding conjugates in RCCs of 44−88%. The practical utility of the PGs was confirmed by the preparation of three ^{18}F-labeled PSMA ligands in radiochemical yields of 28−42%. Biological evaluation in rats demonstrated excellent *in vivo* stability of all three conjugates. In addition, one conjugate ([^{18}F]JK-PSMA-15) showed favorable imaging properties for high-contrast visualization of small PSMA-positive lesions.

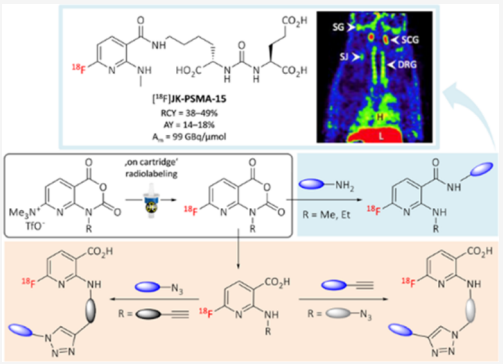

INTRODUCTION

Positron emission tomography (PET) is a noninvasive imaging technique that enables *in vivo* visualization and quantification of physiological processes by tracking the biodistribution of pharmaceuticals labeled with positron-emitting radionuclides. Unlike conventional imaging techniques such as computed tomography or magnetic resonance imaging, which primarily provide anatomical information, PET can be used for functional imaging on the cellular or molecular level.[1] For example, PET imaging with ^{68}Ga-labeled probes targeting prostate-specific membrane antigen (PSMA), a transmembrane glycoprotein that is highly overexpressed on malignant prostate cells,[2−7] has proven instrumental for the detection and staging of prostate cancer (PCa).[2,3,7,8] However, ^{68}Ga-labeled PSMA radioligands are increasingly replaced by ligands labeled with fluorine-18 (like [^{18}F]DCFPyL,[9] [^{18}F]JK-PSMA-7,[10] or [^{18}F]PSMA-1007[11]), which is the most frequently used radionuclide for PET imaging. Important advantages of fluorine-18 over gallium-68 include the accessibility of [^{18}F]fluoride ([^{18}F]F$^-$) in >100 GBq quantities via the ^{18}O-(p,n)^{18}F nuclear reaction and a longer half-life ($t_{1/2}$ = 110 vs 68 min), which enable large-scale, centralized production and distribution of ^{18}F-labeled radioligands.[1,12] In addition, due to the lower positron energy of fluorine-18 compared to gallium-68 (E_{max} = 0.63 vs 1.9 MeV), imaging with ^{18}F-labeled probes offers an improved spatial resolution. While a few direct ^{18}F-labeling methods described in the literature are sufficiently mild to be applied to sensitive substrates (e.g., SiFA, boron-^{18}F, or [^{18}F]AlF-based approaches), most of them require harsh and/or strictly anhydrous reaction conditions that are incompatible with sensitive compounds or biomolecules.[1,12−14] As a consequence, such substrates are often labeled by indirect radiofluorination using ^{18}F-labeled prosthetic groups (PGs), which can be conjugated to the target molecule under mild conditions.[12,15] Among the most common traditional PGs are radiolabeled active esters like *N*-succinimidyl 4-[^{18}F]-fluorobenzoate ([^{18}F]SFB)[13,16−19] or 2,3,5,6-tetrafluorophenyl 6-[^{18}F]fluoronicotinate ([^{18}F]FPy-TFP),[6,20] which readily react with primary amine groups present in peptides or proteins. However, their preparation often involves time-consuming multistep procedures[21−23] or is complicated by the formation of reactive side products that cannot be easily separated from the radiolabeled active ester.[6,20,24] In addition, biomolecules like peptides or proteins typically contain more than one reactive amino group, which can lead to the formation of isomeric side products during conjugation reactions. An alternative approach for indirect radiolabeling

Received: July 20, 2023
Published: August 25, 2023

© 2023 The Authors. Published by American Chemical Society

Scheme 1. Preparation of 2-Alkylamino-6-halonicotinic Acids[a]

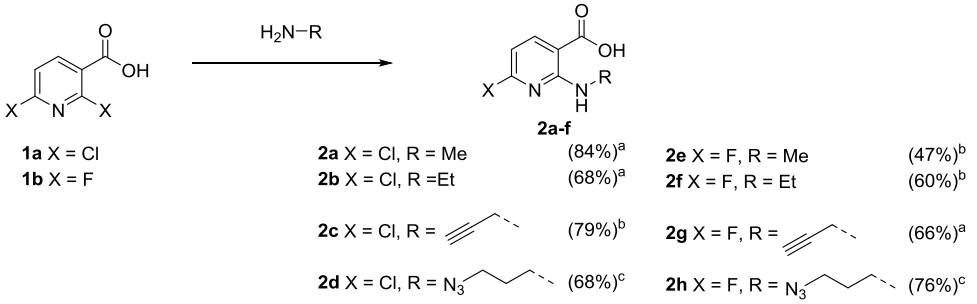

[a]Reaction conditions: (a) THF, 80 °C, 3 d; (b) THF, 55 °C, 4 d; (c) THF, 45 °C, 7 d.

Scheme 2. Synthesis of Radiolabeling Precursors and Reference Compounds[a]

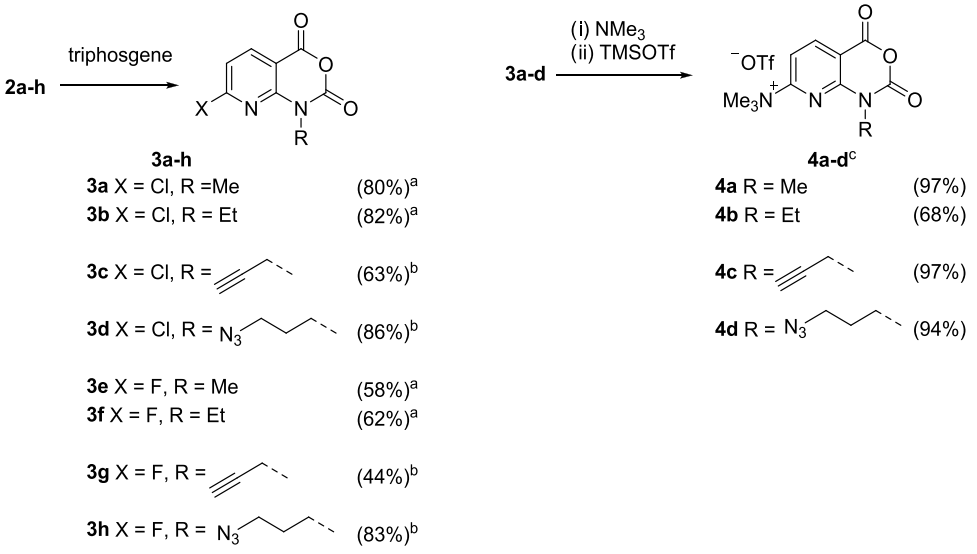

[a]Reaction conditions: (a) 1,4-dioxane, reflux, 3 d; (b) 1,4-dioxane, 60 °C, 3 d; (c) (i) THF, r.t., 1 h; (ii) CH_2Cl_2, r.t., 40 min.

is based on ^{18}F-labeled "click chemistry" PGs with an alkyne or azide moiety, which can be conjugated to suitably functionalized precursors using the copper-catalyzed alkyne-azide cycloaddition (CuAAC).

Herein, we describe 1-alkylamino-7-[^{18}F]fluoro-8-azaisatoic anhydrides ([^{18}F]AFAs) as easily accessible ^{18}F-labeled building blocks that can be utilized for radiolabeling via acylation or "click chemistry". We also show that amine-reactive [^{18}F]AFAs can preferentially acylate the more reactive or sterically accessible amine present in a mixture of amines. Finally, we exemplify the application of [^{18}F]AFAs for the radiofluorination of different PSMA ligands and provide preliminary results of *in vivo* evaluation of the resulting radiotracers by small animal PET imaging.

RESULTS AND DISCUSSION

Synthesis of Radiolabeling Precursors 4a−d and Reference Compounds 3e−h. *N,N,N*-Trimethylammonium triflate radiolabeling precursors[25] **4a−d** and reference compounds **3e−h** were prepared starting from 2,6-dichloronicotinic (**1a**) or 2,6-difluoronicotinic acid (**1b**), respectively (Schemes 1 and 2).

To this end, 2,6-dihalonicotinic acids were regioselectively aminated at the second position by heating them with a 3- to 20-fold molar excess of the respective amine over 2−7 days, which afforded the corresponding 2-alkylamino-6-halo-nicotinic acid intermediates (**2a−h**) in 47−84% yields (Scheme 1).[26] Subsequent cyclization of **2a−h** with triphosgene in boiling 1,4-dioxane gave the 1-alkylamino-7-halo-8-azaisatoic anhydrides **3a−h** in 44−83% yields (Scheme 2).

N,N,N-Trimethylammonium triflate precursors **4a−d** were prepared by treatment of **3a−d** with an excess of trimethylamine in THF followed by anion metathesis with trimethylsilyl triflate. All four precursors were stable at −20 °C under argon for at least 6 months. Single crystals of **4c** for X-ray crystallography were obtained by slow evaporation of a solution of the compound in MeCN/*t*BuOH (1:4) at ambient temperature. Crystallographic data are provided in Figure 1.

Radiosynthesis of ^{18}F-Labeled AFAs [^{18}F]3e−f and Model Compounds [^{18}F]5a−m. We first attempted to radiolabel the azaisatoic anhydrides **4a** and **4b** according to the "minimalist protocol"[27] as follows. [^{18}F]F$^-$ was loaded onto an anion exchange resin and eluted with a solution of the corresponding radiolabeling precursor in MeOH. Following the evaporation of MeOH, DMSO or MeCN were added and the resulting solution was briefly heated. This approach afforded the desired radiolabeled building blocks, albeit in highly variable radiochemical conversions (RCCs) of 10−60%, as determined by radio-HPLC analysis with post-column injection (for details, see ref 28 and Experimental Section). Based on significant contamination of the products by the corresponding acids and methyl esters, we reasoned that these

https://doi.org/10.1021/acs.jmedchem.3c01310
J. Med. Chem. 2023, 66, 12629−12644

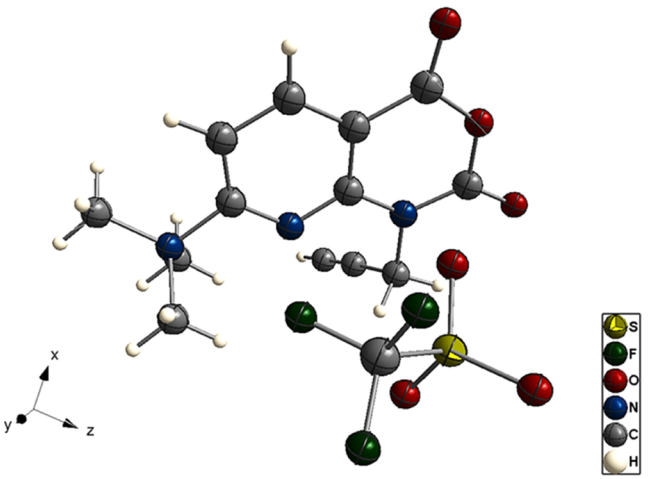

Figure 1. X-ray crystal structure of alkyne-substituted azaisatoic anhydride **4c**. View along *y*-axis.

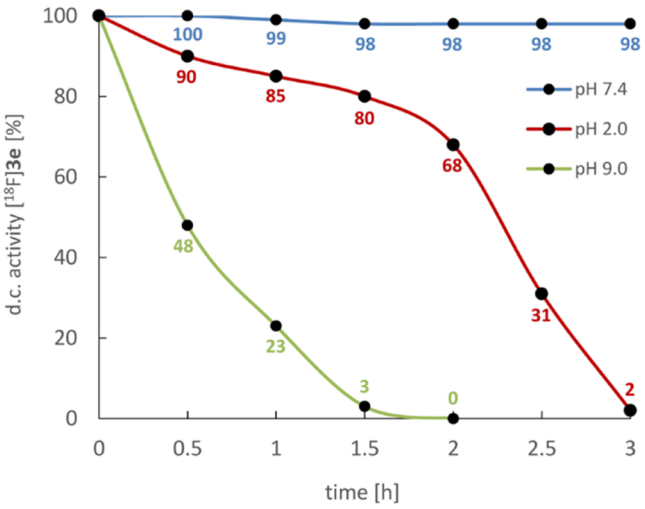

Figure 2. Stability of [^{18}F]**3e** at pH 2.0 (30 mM citric acid, 8 mM HCl, 61 mM NaCl; red), pH 7.4 (50 mM TRIS·HCl; blue), and pH 9.0 (50 mM Na_2CO_3/Na_2HCO_3; green) at 20 °C. The percentage of intact [^{18}F]**3e** at the different time points was determined by radio-HPLC and corrected for decay.

results could be explained by the insufficient thermal/solvolytic stability of 8-azaisatoic anhydrides. Therefore, we next tested a protocol for "on cartridge" radiofluorination of highly activated precursors, which enabled ^{18}F-labeling at ambient temperature and obviated the need for evaporation steps.[29] To this end, [^{18}F]F^- trapped on an anion exchange cartridge (PS-HCO_3^-) was slowly eluted with a solution of the respective precursor (**4a** or **4b**) in MeCN/*t*BuOH (1:4), furnishing the labeled products [^{18}F]**3e** or [^{18}F]**3f** in RCCs of 70−80% and radiochemical purities (RCPs) of >99% (n > 50).

Unreacted *N,N,N*-trimethylammonium triflate precursors were effectively removed by solid-phase extraction (SPE) using polymer reversed-phase cartridges (like Oasis HLB Plus Short), affording analytically pure [^{18}F]**3e** and [^{18}F]**3f** in activity yields (AYs) of 65 ± 5% (n = 8 for each) within only 15 min (Scheme 3).

The hydrolytic stability of [^{18}F]**3e** was investigated at different pH values (Figure 2). [^{18}F]**3e** proved to be stable for several hours at a physiological pH value (98% intact after 3 h at pH 7.4), while it rapidly decomposed in basic solution (half-life <30 min at pH 9.0) and showed moderate stability in acidic medium (half-life <2.5 h at pH 2.0).

The suitability of [^{18}F]**3e** and [^{18}F]**3f** as amine-reactive PGs was first assessed using *n*-butylamine and several other primary and secondary amines as model substrates (Scheme 4). Given the structural similarity and comparable base strength, *n*-butylamine (pK_a = 10.6[30,31]) can be considered as a surrogate for the lysine side chain (pK_a around 10.5[30,31]) present in typical PSMA-binding motifs (like Glu-ureido-Lys) and other biomolecules. The reaction between [^{18}F]**3e** or [^{18}F]**3f** and *n*-butylamine (10 μmol) in MeCN proceeded within 10 min at 40 °C and afforded [^{18}F]**5a** or [^{18}F]**5b** in RCCs of >85%. Various other amines could also be acylated with [^{18}F]**3e** or [^{18}F]**3f** at 40−110 °C for 10−20 min in MeCN or DMF, affording the radiofluorinated 2-(alkylamino)nicotinamides [^{18}F]**5c−m** in RCCs of 11−96% (Scheme 4).

Based on the results obtained for the different model compounds, conjugation with long-chained terminal amines gave good to excellent RCCs ([^{18}F]**5a−d**, [^{18}F]**5l,m**), whereas the RCCs for α-branched amines were lower ([^{18}F]**5g−j**). Conjugation with piperidine as a model secondary amine yielded the corresponding radiolabeled amide [^{18}F]**5k** in moderate RCCs of 19 ± 1%.

Biomolecules like peptides and proteins are usually insoluble in pure organic solvents. To determine the suitability of [^{18}F]AFAs for bioconjugation in aqueous medium, we also acylated *n*-butylamine with [^{18}F]**3e** using 20% MeCN in borate buffer (pH 7.4), which afforded the desired product [^{18}F]**5a** in 65% RCC. RCCs of >90% were obtained with 20% MeCN in borate buffer (pH 8.7) as reaction solvent (Scheme 4).

In general, [^{18}F]AFAs [^{18}F]**3e** and [^{18}F]**3f** appeared to be less reactive acylating agents than the radiofluorinated OSu or OTfp active esters conventionally applied for indirect radiolabeling. Accordingly, their application could enable regiose-

Scheme 3. "On Cartridge" Radiolabeling of Azaisatoic Anhydrides 4a and 4b[a]

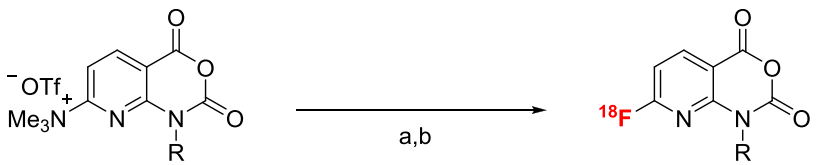

4a, R = Me
4b, R = Et

AY = 65±5% (n = 8)

[^{18}F]**3e**, R = Me
[^{18}F]**3f**, R = Et

[a]Reaction conditions: (a) [^{18}F]F^--elution (from PS-HCO_3^- cartridge) with a solution of the respective precursor in MeCN/*t*BuOH (1:4) over 2 min; (b) removal of unreacted precursor and [^{18}F]F^- by solid-phase extraction (SPE). AY—activity yield.

https://doi.org/10.1021/acs.jmedchem.3c01310
J. Med. Chem. 2023, 66, 12629−12644

Scheme 4. Preparation of [^{18}F]5a–m by Conjugation of [^{18}F]3e and [^{18}F]3f with Various Amines (10 μmol)[a]

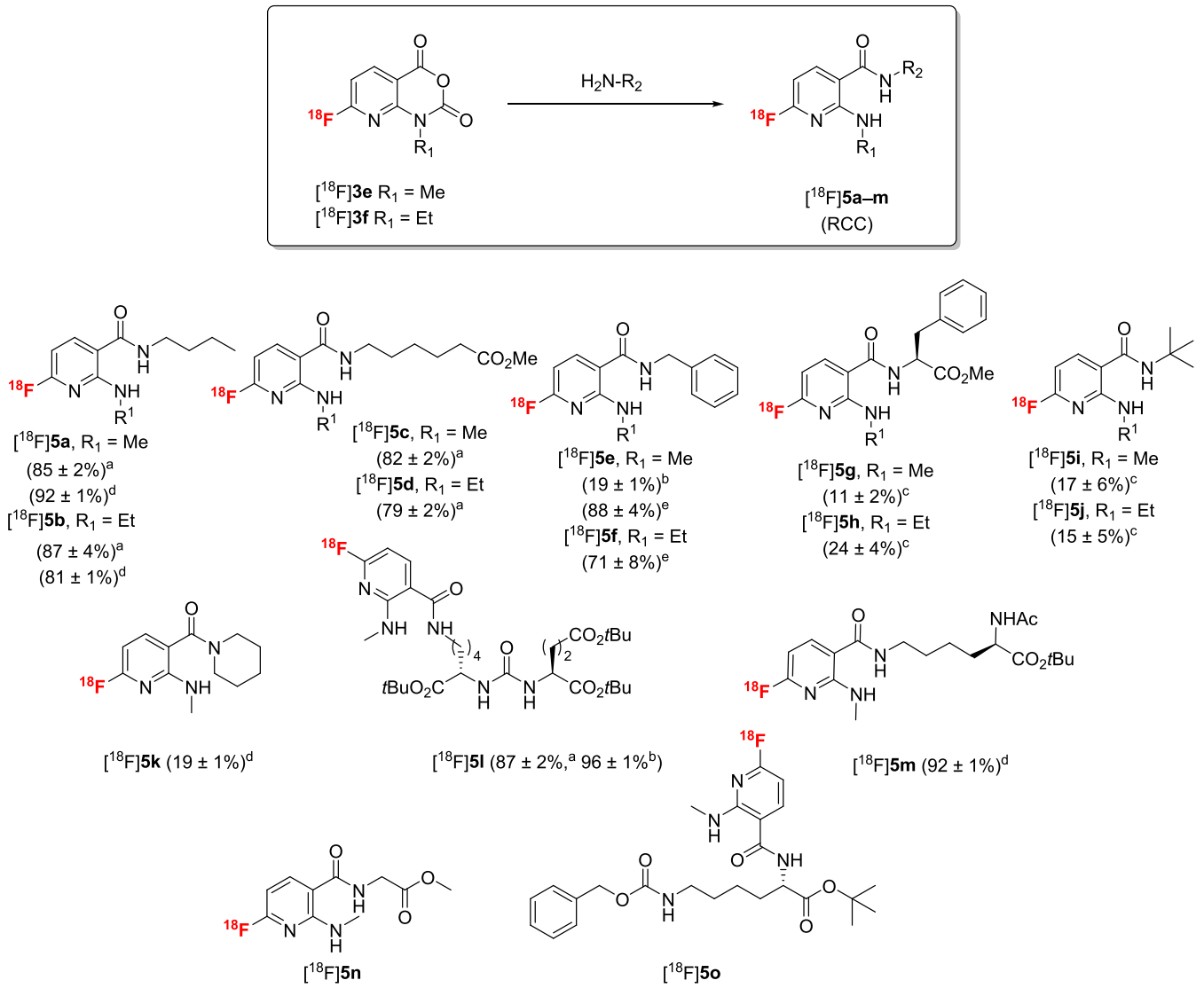

[a]Reaction conditions: (a) 40 °C, 10 min, MeCN, (b) 60 °C, 15 min, MeCN, (c) 110 °C, 20 min, DMF, (d) 35 °C, 10 min, 20% MeCN in 0.2 M borate buffer (pH 8.7), (e) 80 °C, 10 min, 20% MeCN in 0.2 M borate buffer (pH 8.7). Following radiolabeling, H_2O (1 mL) was added to the reaction mixture and radiochemical conversions (RCCs) were determined by radio-HPLC with post-column injection. Compounds [^{18}F]**5n** and [^{18}F]**5o** were obtained as side products in competition experiments with different amino acid derivatives (see text and Tables 1 and 2).

lective conjugation to the less sterically hindered/more nucleophilic amino group like the ε-amino group in lysine-containing biomolecules.

In order to test this assumption, we performed competition experiments with *n*-butylamine and different amino acid esters in 0.2 M sodium borate buffer (pH 8.7) at 35 °C for 10 min using the *N*-methyl-substituted AFA [^{18}F]**3e** as acylating agent (Table 1). Under these conditions, 1:1 mixtures of *n*-butylamine and amino acid esters afforded *n*-butyl amide [^{18}F]**5a** as a single product. The only exception was H-Gly-OMe, the addition of which led to the concurrent formation of 2–3% of the radiolabeled Gly derivative [^{18}F]**5n** (for structure, see Scheme 4).

Similarly, acylation of 1:1 mixtures of the *N*-ε- or *N*-α-protected lysine esters H-Lys(Z)-O*t*Bu and Ac-Lys(H)-O*t*Bu with [^{18}F]**3e** furnished side-chain-radiolabeled [^{18}F]**5m** (for structure, see Scheme 4) as a single product (Table 2).

Table 1. Competition between *n*BuNH$_2$ and Different Amino Acid Esters for Conjugation with [^{18}F]3e[a]

	RCC [%, *n* = 3]	
added amino acid derivative	[^{18}F]**5a**	other products
none	92 ± 1	
H-Phe-OH	35 ± 1	0
H-Gly-OMe	81 ± 2	3 ± 1[b]
H-Phe-OMe	88 ± 1	0
H-Pro-OMe	81 ± 1	0
H-Lys(Z)-O*t*Bu	84 ± 1	0
H-Ala-OMe	89 ± 1	0
Ac-Lys(H)-O*t*Bu	83 ± 1	0

[a]Experiments were performed with 10 μmol of *n*BuNH$_2$ and equimolar amounts of the indicated amino acid esters. Reaction conditions: 10 min at 35 °C with 20% MeCN in 0.2 M borate buffer (pH 8.7, 0.5 mL) as the reaction solvent. [b]Acylated Gly-OMe ([^{18}F]**5n**).

https://doi.org/10.1021/acs.jmedchem.3c01310
J. Med. Chem. 2023, 66, 12629–12644

Table 2. Competition between H-Lys(Z)-O*t*Bu and Ac-Lys(H)-O*t*Bu for the Conjugation with [^{18}F]3e[a]

ratio [H-Lys(Z)-O*t*Bu : Ac-Lys(H)-O*t*Bu]	RCC [%; n = 3]	
	[^{18}F]**5m**	[^{18}F]**5o**
1:1	85 ± 1	0 ± 0
2:1	79 ± 2	2 ± 2
4:1	71 ± 1	11 ± 1
8:1	28 ± 3	24 ± 2
10:1	22 ± 2	25 ± 1

[a]Experiments were performed with 10 μmol of Ac-Lys(H)-O*t*Bu and variable amounts of H-Lys(Z)-O*t*Bu as indicated. Reaction conditions: 10 min at 35 °C with 20% MeCN in 0.2 M borate buffer (pH 8.7, 0.5 mL) as the reaction solvent.

Additionally, the robustness of the observed selectivity was evaluated using different ratios of H-Lys(Z)-O*t*Bu to Ac-Lys(H)-O*t*Bu (Table 2). At ratios below 4:1, acylation of H-Lys(Z)-O*t*Bu was insignificant and the side-chain-acylated lysine derivative [^{18}F]**5m** was obtained in >79% RCCs. At a ratio of 4:1, acylation of the α-amino group in H-Lys(Z)-O*t*Bu became more prominent and 11% of the lysine derivative [^{18}F]**5o** (for structure, see Scheme 4) was observed in the reaction mixture. At a ratio of 10:1, [^{18}F]**5o** became the major product and was produced in RCCs of 25%. Based on these observations, [^{18}F]AFAs could potentially be applied for selective radiolabeling of the ε-amino group (or other sterically less hindered amino groups) in peptides and proteins. In order to evaluate this assumption, we are currently investigating the acylation of insulins by [^{18}F]**3e**. The preliminary results confirm that, under suitable conditions, [^{18}F]AFAs can indeed be applied for site-selective radiolabeling of polypeptides at the more sterically accessible amino group. Once these investigations are concluded, a comprehensive report will be published as a separate article.

Radiosynthesis of [^{18}F]JK-PSMA-15 ([^{18}F]5p). Having established efficient protocols for the preparation and conjugation of [^{18}F]AFAs, we next evaluated their applicability for the preparation of PET tracers. Being interested in the development of novel PET tracers for PCa imaging,[10,32,33] we applied [^{18}F]**3e** as amine-reactive PG to prepare the novel PSMA radioligand [^{18}F]JK-PSMA-15 (Scheme 5).

To this end, [^{18}F]**3e** was allowed to react with *t*BuO-Glu(O*t*Bu)-CO-Lys(H)-O*t*Bu in MeCN for 15 min at 60 °C, furnishing the *t*Bu-protected intermediate [^{18}F]**5l** in >95% RCC. Deprotection of [^{18}F]**5l** was achieved by adding an equal volume of 37% HCl directly to the reaction mixture and heating for an additional 15 min at 60 °C. Finally, isolation of [^{18}F]JK-PSMA-15 ([^{18}F]**5p**) by semipreparative HPLC and formulation afforded the desired candidate PET tracer in AYs of 14−18% (n = 5) over three steps within a total synthesis time of 70−90 min at end of synthesis (EOS). Molar activity (EOS) of the probe amounted to 99 GBq/μmol (for 365 MBq [^{18}F]JK-PSMA-15).

Application of [^{18}F]AFAs for Radiolabeling Using CuAAC. The operational simplicity of [^{18}F]AFA production raised the question whether they might also be useful building blocks for indirect radiofluorination via Cu-catalyzed click conjugation. Therefore, we produced ^{18}F-labeled *N*-propargyl- and *N*-3-azidopropyl-substituted azaisatoic anhydrides [^{18}F]**3g** and [^{18}F]**3h** using the "on cartridge" protocol in AYs of 52 ± 3 and 59 ± 4%, respectively.

Before conjugation with different azides or alkynes, both [^{18}F]AFAs were hydrolyzed into the corresponding 2-alkylamino-6-[^{18}F]fluoronicotinic acids ([^{18}F]**2g** and [^{18}F]**2h**) using 10 mM NaOH at 60 °C for 5 min (note that almost complete hydrolysis of the *N*-propargyl-substituted [^{18}F]**3g** to [^{18}F]**2g** was observed already during SPE purification) (Scheme 6). The resulting solutions were directly used for Cu-mediated click cycloadditions under the reaction conditions described by Krapf et al.[34] To this end, alkyne-substituted [^{18}F]**2g** was treated with $CuSO_4$ (20 μmol), L-histidine (50 μmol), sodium ascorbate (100 μmol), and benzyl azide (20 μmol) for 15 min at 60 °C to yield the desired radiolabeled triazole [^{18}F]**6a** in RCCs of 77 ± 2% (n = 3) (Scheme 7). Under the same conditions, azido-substituted [^{18}F]**2h** was reacted with phenylacetylene as a model alkyne to give [^{18}F]**6c** in RCCs of 88 ± 6% (n = 3) (Scheme 8).

Scheme 5. Preparation of [^{18}F]5p ([^{18}F]JK-PSMA-15)[a]

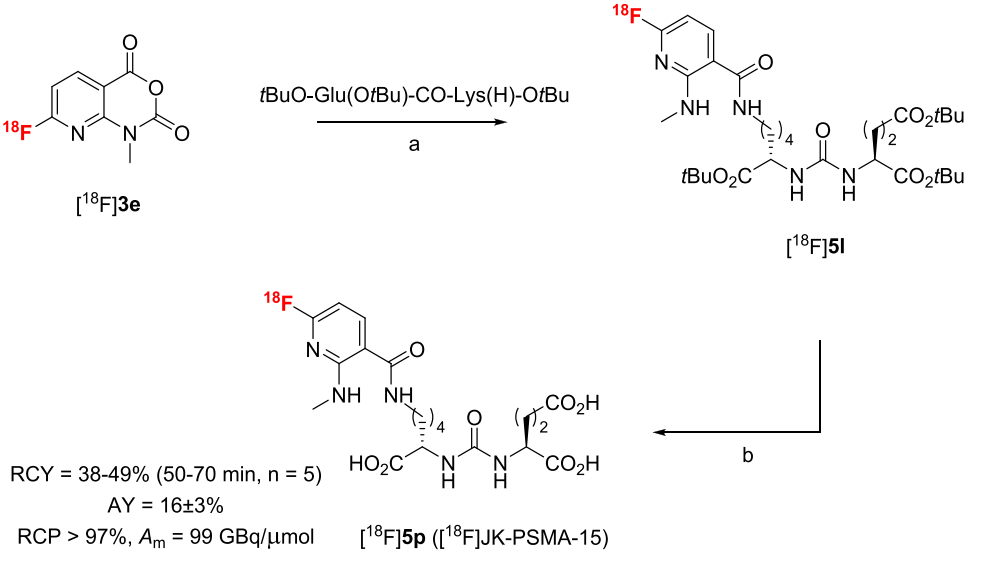

[a]Reaction conditions: (a) 60 °C, 15 min, MeCN; (b) 60 °C, 15 min, 6 M HCl.

https://doi.org/10.1021/acs.jmedchem.3c01310
J. Med. Chem. 2023, 66, 12629−12644

Scheme 6. Preparation of Radiolabeled Nicotinic Acids [^{18}F]2g and [^{18}F]2h[a]

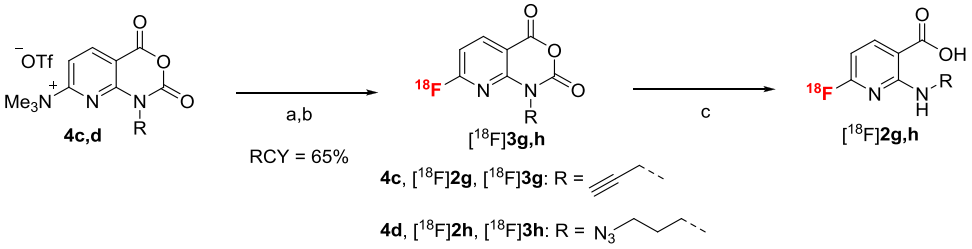

[a]Reaction conditions: (a) [^{18}F]F$^-$-elution (from PS-HCO$_3^-$ cartridge) with a solution of the respective precursor in MeCN:*t*BuOH (1:4) over 2 min; (b) removal of unreacted precursor and [^{18}F]F$^-$ by solid-phase extraction (SPE); (c) 60 °C, 5 min, 10 mmol NaOH.

Scheme 7. Copper(I)-Catalyzed Azide Alkyne Cycloaddition (*CuAAC*) of [^{18}F]2g with Different Azides[a]

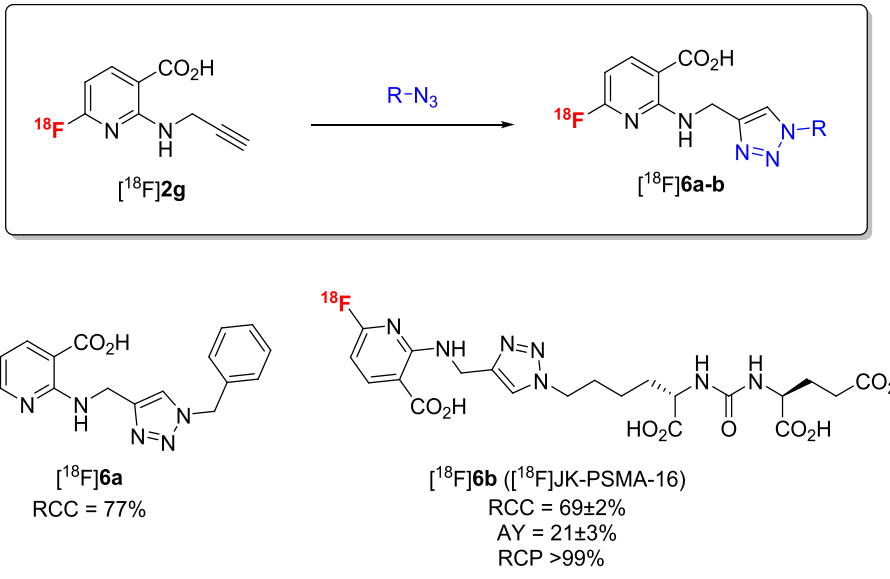

[a]Reaction conditions: [^{18}F]**2g** in MeCN (100 μL), 0.2 M CuSO$_4$·5H$_2$O (100 μL), 0.5 M L-histidine (100 μL), 1 M sodium ascorbate (100 μL), R-N$_3$ (5 μmol) in MeCN (100 μL; [^{18}F]**6a**) or 50% aq. MeCN (100 μL; [^{18}F]**6b**), 60 °C, 15 min.

Scheme 8. Copper(I)-Catalyzed Azide Alkyne Cycloaddition (*CuAAC*) of [^{18}F]2h with Different Alkynes[a]

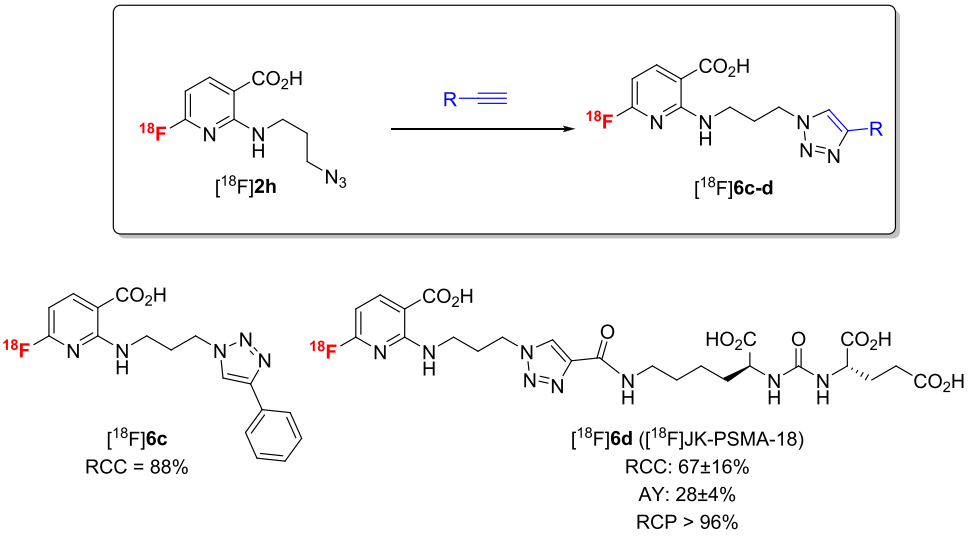

[a]Reaction conditions: [^{18}F]**2h** in MeCN (25 μL), 0.2 M CuSO$_4$·5H$_2$O (25 μL), L-histidine (2 mg, 13 μmol) in H$_2$O (25 μL), sodium ascorbate (5 mg, 25 μmol) in H$_2$O (25 μL), alkyne (5 μmol) in MeCN (100 μL; [^{18}F]**6c**) or in 50% aq. MeCN (100 μL; [^{18}F]**6d**), 60 °C, 15 min.

Both building blocks were also applied for the preparation of novel PSMA radioligands as candidate PET probes. For this purpose, propargyl-substituted [^{18}F]**2g** was allowed to react with HO-Glu(OH)-CO-6-N$_3$-Nle-OH (**7**),[34] which furnished

https://doi.org/10.1021/acs.jmedchem.3c01310
J. Med. Chem. 2023, 66, 12629−12644

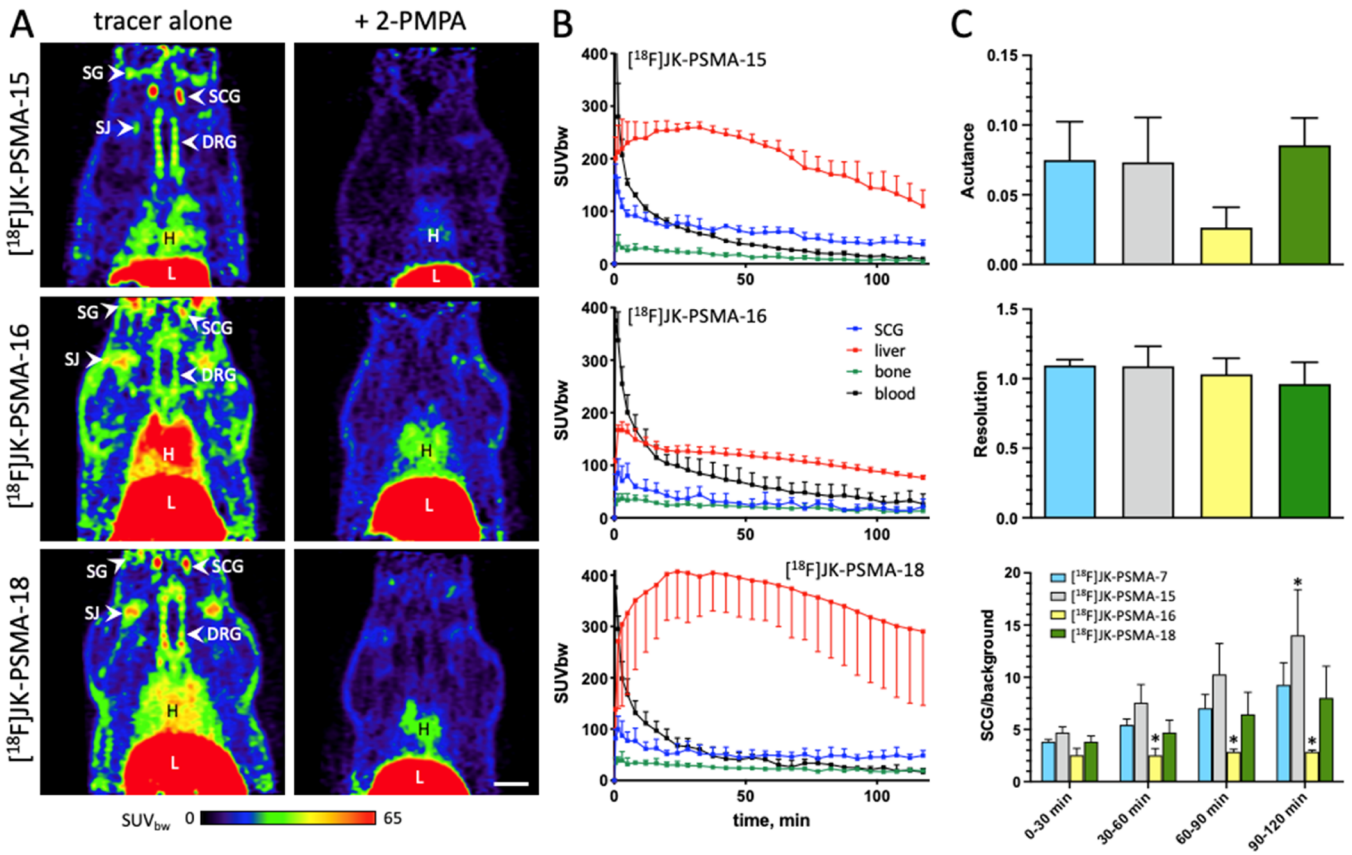

Figure 3. Biodistribution of [^{18}F]AFA-conjugated PSMA ligands in healthy rats. (A) Horizontal PET images of the neck and thorax region with the sympathetic and dorsal root ganglia, which have a high endogenous PSMA expression. Shown are summed images (60−120 min post injection) of representative experiments. Blocking experiments (right column) were performed by co-injection of 23 mg/kg 2-PMPA. (B) Time-activity curves, calculated as mean (± standard deviation) SUV_{bw} (n = 3 each). (C) Image properties quantified in terms of acutance (=edge contrast, top) and resolution (=ability to distinguish two neighboring ganglia, middle) during the uptake period 60−120 min p.i., as well as the signal-to-background ratios ("signal" extracted from the biggest ganglion SCG) during four consecutive 30 min uptake periods (bottom). * Significant differences compared to the established tracer [^{18}F]JK-PSMA-7 (data from ref 10). For full statistics and details on the analysis, see Section 7 in the Supporting Information. Abbreviations: DRG: cervical dorsal root ganglia; H: heart; L: liver; SCG: superior cervical ganglion; SG: salivary gland; SJ: shoulder joint. Scale bar: 1 cm.

(after HPLC purification) [^{18}F]JK-PSMA-16 in AYs of 21 ± 3% (EOS) over two steps (Scheme 7).

The "click" conjugation of [^{18}F]**2h** with HO-Glu(OH)-CO-Lys(propiolyl)-OH (**8**) in turn afforded the desired radioligand [^{18}F]JK-PSMA-18 in RCCs of 67 ± 16%. Semipreparative HPLC purification and formulation furnished [^{18}F]JK-PSMA-18 in AYs of 28 ± 4% (EOS) over two steps with RCP >96% and a molar activity (EOS) of 75 GBq/μmol (for 630 MBq tracer) (Scheme 8).

***In Vivo* Evaluation of the Conjugates for PSMA-Specific PET Imaging.** The PET probes (60.3 ± 5.6 MBq) were evaluated by μPET imaging in healthy rats, using the PSMA-expressing sympathetic and dorsal root ganglia as surrogates for small PSMA-positive lesions (for details, see refs 4, 10 and Section 7 in the Supporting Information). This approach is particularly useful for the initial screening of new PSMA radioligands, as the lower inter- and intra-individual variance of tracer uptake compared to tumor models enables a more reliable comparison of multiple tracers.[4,10] All tracers accumulated in PSMA-expressing structures, and uptake was strongly reduced by co-injection of the PSMA-inhibitor 2-PMPA (23 mg/kg) (Figure 3; for time-activity curves with 2-PMPA, see Section 7.2 in the Supporting Information). In comparison to the established tracer [^{18}F]JK-PSMA-7,[10,35] [^{18}F]JK-PSMA-15 showed a significantly higher signal-to-background ratio during the uptake period of 90−120 min p.i. (Figure 3C, bottom). All other parameters for the two tracers, such as the acutance (a measure for the perceived sharpness of the image and the ability to measure the size of small PSMA-positive tissues) and the resolution (a measure for the ability to delineate two small PSMA-positive tissues located close to each other), were similar (for details on the quantification and significance of the parameters, see Section 7.1 in Supporting Information). In contrast, the signal-to-background ratio for [^{18}F]JK-PSMA-16 was significantly lower when compared to [^{18}F]JK-PSMA-7, which was mainly attributable to low uptake into PSMA-expressing structures and high retention in blood (see Figure 3B, middle). The acutance of [^{18}F]JK-PSMA-16 was also considerably lower than that of the other tracers, although this difference did not reach statistical significance. The imaging properties of [^{18}F]JK-PSMA-18 were comparable to those of [^{18}F]JK-PSMA-7, although it is noteworthy that this tracer showed a high and more variable liver uptake (Figure 3B, bottom, red curve).

https://doi.org/10.1021/acs.jmedchem.3c01310
J. Med. Chem. 2023, 66, 12629−12644

CONCLUSIONS

[^{18}F]AFAs are novel, easily accessible radiolabeled building blocks that enable the efficient and fast production of metabolically stable radiolabeled conjugates. Their applicability for PET tracer syntheses was confirmed by the preparation of novel PSMA radioligands via acylation or click conjugation. One of the new probes, [^{18}F]JK-PSMA-15, showed promising results in the preclinical *in vivo* μPET studies and could be suitable for high-quality visualization of small PSMA-positive lesions, although further studies in appropriate tumor models may be required to corroborate these findings. Additionally, amine-reactive [^{18}F]AFAs demonstrated a remarkable preference for acylation of the sterically more accessible amino group, which could be exploited for the regioselective radiolabeling of peptides and proteins.

EXPERIMENTAL SECTION

General Procedures. All chemicals and solvents were purchased from Aldrich (Taufkirchen, Germany), BLDPharm (Kaiserslautern, Germany), Fluorochem (Hadfield, United Kingdom), or Merck (Darmstadt, Germany) and used without further purification. Thin-layer chromatography (TLC) was performed on precoated plates of silica gel 60 F254 (Merck, Darmstadt, Germany), and the compounds were detected by UV at 254 nm and/or phosphomolybdic acid. All reactions were carried out with magnetic stirring and, if sensitive to moisture, under argon and in reaction flasks dried overnight at 140 °C prior to use. Unless noted otherwise, organic extracts were dried over anhydrous $MgSO_4$. Nuclear magnetic resonance (NMR) spectra were recorded in 5% solutions at 25 °C using a Bruker Avance Neo 400 (^{1}H: 400 MHz; ^{13}C: 101 MHz; ^{19}F: 376 MHz) or a Bruker DPX Avance 200 (^{1}H: 200 MHz; ^{13}C: 50 MHz). The measured chemical shifts (δ) are reported in parts per million (ppm) relative to the residual peaks of deuterated solvents. The observed signal multiplicities are characterized as follows: s = singlet, d = doublet, t = triplet, m = multiplet, dd = doublet of doublets, ddd = doublet of doublets of doublets, dt = doublet of triplets, td = triplet of doublets, dq = doublet of quartets, ddq = doublet of doublets of quartets, q = quartet, p = pentet. Coupling constants J are reported in hertz (Hz). High-resolution mass spectrometry (HRMS) analyses were performed using a hybrid linear ion trap FTICR mass spectrometer LTQ-FT (Thermo Fisher Scientific, Bremen, Germany) equipped with a 7 T superconducting magnet by infusion. The mass spectrometer was tuned and calibrated in the positive mode following the standard optimization procedure for all voltages and settings. Mass spectra were recorded in full scan from 200 to 1000 Da with a resolution of 100,000 at m/z 400. All data were processed using the Xcalibur software. Elemental analyses were carried out on a TCH 600 Nitrogen/Oxygen/Hydrogen and a CS 600 Carbon/Sulfur Determinator (Leco Corporation, St. Joseph, MI). Unless noted otherwise, all synthesized compounds had a purity of >95%, as determined by analytical HPLC with a Multokrom 100-5 C18 AQ column (250 mm × 4.6 mm, CS Chromatographie, Langerwehe, Germany) using a gradient from 0 to 100% MeCN over 20 min with or without addition of 0.1% TFA.

Materials. 3-Azidopropylamine,[36] benzyl azide,[37] Ac-Lys(H)-O*t*Bu,[38] di-*tert*-butyl {[(*S*)-6-amino-1-(*tert*-butoxy)-1-oxohexan-2-yl]-carbamoyl}-(*S*)-glutamate (*t*BuO-Glu(O*t*Bu)-CO-Lys(H)-O*t*Bu),[39] (*S*)-2-({[(*S*)-5-azido-1-carboxypentyl]carbamoyl}amino)pentanedioic acid (**7**),[34] 1,5-di-*tert*-butyl (*S*)-2-({[(*S*)-6-azido-1-(*tert*-butoxy)-1-oxohexan-2-yl]carbamoyl}amino)pentanedioate (**9**),[34] and pentafluorophenyl propiolate[40] were prepared according to known procedures. "Click" reactions were performed based on a published procedure.[41]

*6-Chloro-2-(methylamino)nicotinic Acid (**2a**).*[26] Methylamine (22.7 mL 33% solution in EtOH, 553 mmol, 27.0 equiv) was added to a solution of 2,6-dichloronicotinic acid (**1a**) (3.99 g, 20.8 mmol, 1.00 equiv) in anhydrous THF (5 mL) in a thick-walled glass reactor. The reactor was closed, and the reaction mixture was stirred at 80 °C for 3 days. The mixture was then concentrated under reduced pressure and the residue was taken up in MeOH (40 mL) and EtOAc (160 mL). The extract was successively washed with 1 M HCl (4 × 50 mL) and brine (100 mL), dried, and concentrated under reduced pressure to afford **2a** (3.25 g, 84% yield) as a colorless solid. ^{1}H-NMR [400 MHz, $(CD_3)_2SO$]: δ 2.91 (s, 3H), 6.57 (d, J = 8.0 Hz, 1H), 8.02 (d, J = 8.0 Hz, 1H). ^{13}C-NMR [101 MHz, $(CD_3)_2SO$]: δ 27.8, 106.0, 109.7, 142.8, 153.0, 158.8, 168.3. HRMS (ESI): m/z calcd for $C_7H_6ClN_2O_2^-$: 185.01233, found, 185.01199 [M − H$^+$].

*6-Chloro-2-(ethylamino)nicotinic Acid (**2b**).*[42] **2b** (68% yield, colorless solid) was prepared according to the same procedure as described for **2a** using 2 M $EtNH_2$ in THF. ^{1}H-NMR [400 MHz, $(CD_3)_2SO$]: δ 1.16 (t, J = 7.2 HZ, 3H), 3.42 (q, J = 7.1 Hz, 2H), 6.59 (d, J = 8.0 Hz, 1H), 8.03 (d, J = 8.0 Hz, 1H). ^{13}C-NMR [101 MHz, $(CD_3)_2SO$]: δ 15.0, 35.7, 105.3, 110.4, 143.5, 153.9, 158.5, 168.7. HRMS (ESI): m/z calcd for $C_8H_8ClN_2O_2^-$: 199.02798, found, 199.02794 [M − H$^+$].

*6-Chloro-2-(prop-2-yn-1-ylamino)nicotinic Acid (**2c**).* Propargylamine (3.22 mL, 2.77 g, 50.22 mmol) was added to a solution of **1a** (2.3 g, 11.16 mmol) in anhydrous THF (5 mL) in a thick-walled glass reactor. The reactor was closed, and the reaction mixture was stirred at 50−55 °C for 4 days. The semisolid mixture was allowed to cool to ambient temperature and transferred into 1 M HCl (60 mL). The resulting precipitate was isolated by filtration, washed with H_2O until the pH of the washings was neutral, and dried (first in air for 16 h and then at 2 mbar for 3 h). Thereafter, the precipitate was thoroughly washed with CH_2Cl_2:MeOH (12:1) followed by CH_2Cl_2 and dried, which furnished **2c** (1.6 g, 68%) as a colorless solid. The mother liquor was concentrated under reduced pressure, and the residue was purified as above to obtain a second crop of the product (0.25 g, 79% total yield). ^{1}H-NMR (400 MHz, $CDCl_3$): δ 11.80 (s, 1H), 8.21 (s, 1H), 7.94 (d, J = 8.0 Hz, 1H), 6.43 (d, J = 8.0 Hz, 1H), 4.16 (dd, J = 5.2, 2.2 Hz, 2H), 2.23−1.94 (m, 1H). ^{13}C-NMR (101 MHz, $CDCl_3$): δ 168.71, 157.51, 154.12, 142.59, 111.19, 105.53, 80.39, 70.81, 30.34. HRMS (ESI) calcd for $C_9H_8ClN_2O_2^+$ ([M + H$^+$]): 210.01906, found, 210.01889.

*2-[(3-Azidopropyl)amino]-6-chloronicotinic Acid (**2d**).* 3-Azidopropylamine[36] (6.2 g, 61.88 mmol) was added to a solution of **1a** (2 g, 10.42 mmol) in THF (10 mL). The resulting mixture was stirred at 45 °C for 7 days under argon and protection from light, and then concentrated under reduced pressure. The residue was taken up in EtOAc and 1 M HCl (70 mL of each), and the organic fraction was separated, washed with brine (2 × 10 mL), dried, and concentrated under reduced pressure. The residue was recrystallized from Et_2O/pentane to afford **2d** (1.7 g, 68%) as an off-white solid. **2d** is light-sensitive and should be stored under argon and protected from light in the fridge. ^{1}H-NMR (400 MHz, $CDCl_3$): δ 8.13 (d, J = 8.1 Hz, 1H), 8.03 (t, J = 5.1 Hz, 1H), 6.60 (d, J = 8.1 Hz, 1H), 3.67 (dd, J = 12.5, 6.6 Hz, 2H), 3.45 (t, J = 6.6 Hz, 2H), 1.98 (p, J = 6.7 Hz, 2H). ^{13}C-NMR (101 MHz, $CDCl_3$): δ 172.29, 158.66, 156.54, 143.37, 111.33, 102.99, 49.36, 38.58, 28.61. Elemental Anal.: Calcd for $C_9H_{10}ClN_5O_2$: C, 42.3; H, 3.94; N, 27.4. Found: C, 42.6; H, 3.96; N, 27.0.

*6-Fluoro-2-(methylamino)nicotinic Acid (**2e**).* A solution of 2,6-difluoronicotinic acid (**1b**) (2 g, 12.57 mmol) in 2 M $MeNH_2$ in THF (30 mL) was heated in a thick-walled glass reactor at 55−60 °C for 4 days and then concentrated under reduced pressure. The residue was taken up in H_2O (100 mL) and filtered. The filter cake was washed with 0.5 M NaOH (2 × 10 mL), and the combined filtrate and washings were acidified to pH 2 using 0.2 M HCl in H_2O. The resulting precipitate was isolated by filtration, washed with H_2O until the pH of the washings was neutral, dried, and recrystallized from Et_2O/pentane to afford **2e** (1 g, 47% yield) as an off-white solid. ^{1}H-NMR [400 MHz, $(CD_3)_2SO$]: δ 2.90 (d, J = 4.4 Hz, 3H), 6.21 (dd, J = 8.3 Hz, 1H), 8.18 (d, J = 8.4 Hz, 1H). ^{13}C-NMR [101 MHz, $(CD_3)_2SO$]: δ 168.4, 165.2 (d, J = 240.1 Hz), 159.4 (d, J = 19.4 Hz), 146.3 (d, J = 10.8 Hz), 104.4 (d, J = 3.7 Hz), 94.5 (d, J = 38.5 Hz), 28.16. ^{19}F-NMR [376 MHz, $(CD_3)_2SO$]: δ -61.00. HRMS (ESI): m/z calcd for $C_7H_6FN_2O_2^-$: 169.04188, found, 169.04154 [M − H$^+$].

https://doi.org/10.1021/acs.jmedchem.3c01310
J. Med. Chem. 2023, 66, 12629−12644

*6-Fluoro-2-(ethylamino)nicotinic Acid (**2f**).* **2f** (60% yield, off-white solid) was prepared according to the same procedure as described for **2e** but using 2 M $EtNH_2$ in THF. ^{1}H-NMR [400 MHz, $(CD_3)_2SO$]: δ 1.16 (t, J = 7.2 Hz, 3H), 3.39 (q, J = 7.1 Hz, 2H), 6.21 (dd, J = 8.3, 2.8 Hz, 1H), 8.19 (t, J = 8.5 Hz, 1H). ^{13}C-NMR [101 MHz, $(CD_3)_2SO$]: δ 168.5, 165.2 (d, J = 239 Hz) 158.7 (d, J = 19.2 Hz), 146.4 (d, J = 10.1 Hz), 104.1 (d, J = 4.0 Hz), 94.7 (d, J = 39.4 Hz), 35.7, 15.0. ^{19}F-NMR [376 MHz, $(CD_3)_2SO$]: δ -60.92. HRMS (ESI): m/z calcd for $C_8H_8FN_2O_2^-$: 183.05753, found, 183.05753 [M − H^+].

*6-Fluoro-2-(prop-2-yn-1-ylamino)nicotinic Acid (**2g**).* Propargylamine (2.4 mL, 2.09 g, 37.9 mmol) was added to a solution of **1b** (1 g, 6.29 mmol) in anhydrous THF (5 mL). The resulting mixture was stirred at 45 °C for 3 days and then concentrated under reduced pressure. The residue was taken up in EtOAc and 1 M HCl (70 mL of each), and the organic fraction was separated, washed with brine (2 × 10 mL), and dried. After concentration under reduced pressure, the crude product was purified by column chromatography (CH_2Cl_2/MeOH 10:1) to afford **2g** (0.8 g, 66% yield) as an off-white solid. ^{1}H-NMR (400 MHz, CD_3CN): δ 8.28 (dd, J = 25.0, 16.7 Hz, 2H), 6.24 (dd, J = 8.4, 2.7 Hz, 1H), 4.20 (dd, J = 5.7, 2.5 Hz, 2H), 2.44 (t, J = 2.5 Hz, 1H). ^{13}C-NMR (101 MHz, CD_3CN): δ 168.4, 166.3 (d, J = 242.1 Hz), 159.2 (d, J = 19.4 Hz), 147.2 (d, J = 10.8 Hz), 104.6 (d, J = 3.9 Hz), 96.7 (d, J = 38.5 Hz), 71.6, 31.0. ^{19}F-NMR (376 MHz, CD_3CN): δ -61.99 (s). ESI-MS: m/z 195.20 [M + H^+]. HRMS (ESI): m/z calcd for $C_9H_8FN_2O_2^+$: 195.05643, found, 195.05671 [M + H^+].

*2-[(3-Azidopropyl)amino]-6-fluoronicotinic Acid (**2h**).* 3-Azidopropylamine[36] (3.77 g, 37.26 mmol) was added to a solution of **1b** (1 g, 6.29 mmol) in THF (10 mL). The resulting mixture was stirred at 45 °C for 7 days while under argon and protected from light, and then concentrated under reduced pressure. The residue was taken up in EtOAc and 1 M HCl (70 mL of each), and the organic fraction was separated, washed with brine (2 × 10 mL), dried, and concentrated under reduced pressure. The residue was purified by column chromatography (CH_2Cl_2/MeOH 10:1 with 0.1% AcOH) to afford **2h** (1.2 g, 95% pure according to the ^{1}H-NMR spectrum, 76% yield) as a gray solid. **2h** is light-sensitive and should be stored under argon and protected from light in the fridge. ^{1}H-NMR (400 MHz, $CDCl_3$): δ 8.30 (t, J = 8.3 Hz, 1H), 8.14 (s, 1H), 6.18 (dd, J = 8.4, 2.8 Hz, 1H), 3.76−3.62 (m, 2H), 3.45 (t, J = 6.6 Hz, 2H), 1.97 (p, J = 6.7 Hz, 2H). ^{13}C-NMR (101 MHz, $CDCl_3$): δ 172.0, 165.5 (d, J = 241.2 Hz), 159.2 (d, J = 19.6 Hz), 146.1 (d, J = 11.0 Hz), 102.9 (d, J = 3.8 Hz), 94.7 (d, J = 39.1 Hz), 77.4, 77.0, 76.7, 49.3, 38.5, 28.6. 63. ^{19}F-NMR (376 MHz, $CDCl_3$): δ -57.12. ESI-MS: m/z 240.14 [M + H^+]. HRMS (ESI): m/z calcd for $C_9H_{11}FN_5O_2^+$: 240.08913, found, 240.08945 [M + H^+].

*7-Chloro-1-methyl-2H-pyrido[2,3-d][1,3]oxazine-2,4(1H)-dione (**3a**).* Triphosgene (160 mg, 0.53 mmol, 0.6 equiv) was added in a stream of argon to a solution of 6-chloro-2-(methylamino)nicotinic acid (**2a**) (170 mg, 0.91 mmol, 1.0 equiv) in anhydrous dioxane (30 mL). The reaction mixture was refluxed for 3 days and concentrated under reduced pressure. The residue was purified by flash column chromatography (silica, petrol ether/EtOAc) to afford **3a** (155 mg, 80% yield) as a colorless solid. ^{1}H-NMR (400 MHz, $CDCl_3$): δ 3.46 (s, 3H), 7.46 (d, J = 8.1 Hz, 1H), 8.40 (d, J = 8.1 Hz, 1H). ^{13}C-NMR (101 MHz, $CDCl_3$): δ 30.3, 107.2, 119.6, 141.6, 147.5, 152.8, 157.5, 168.0. Elemental Anal.: Calcd for $C_8H_5ClN_2O_3$: C, 45.2; H, 2.37; N, 13.2. Found: C, 45.4; H, 2.09; N, 12.9. MS (ESI): m/z calcd for $C_8H_6ClN_2O_3^+$: 213.59, found, 213.11 [M + H^+].

*7-Chloro-1-ethyl-2H-pyrido[2,3-d][1,3]oxazine-2,4(1H)-dione (**3b**).*[43] **3b** (82% yield, colorless solid) was prepared from 6-chloro-2-(ethylamino)nicotinic acid (**2b**) according to the same procedure as described for **3a**. ^{1}H-NMR [400 MHz, $(CD_3)_2SO$]: δ 1.24 (t, J = 7.1, 3H, H-1), 4.11 (q, J = 7.1 Hz, 2H), 7.46 (d, J = 8.1 Hz, 1H), 8.40 (d, J = 8.1 Hz, 1H). ^{13}C-NMR [101 MHz, $(CD_3)_2SO$]: δ 12.6, 39.2, 107.9, 120.1, 142.2, 147.5,152.6, 155.9, 158.1. Elemental Anal.: Calcd for $C_9H_7ClN_2O_3$: C, 47.7; H, 3.11; N, 12.4. Found: C, 47.6; H, 3.33; N, 12.0. MS(ESI): m/z calcd for $C_9H_8ClN_2O_3^+$: 227.02, found, 227.15 [M + H^+].

*7-Chloro-1-(prop-2-yn-1-yl)-2H-benzo[d][1,3]oxazine-2,4(1H)-dione (**3c**).* Triphosgene (1.37 g, 4.6 mmol) was added to a suspension of **2c** (1 g, 5.15 mmol) in anhydrous dioxane (10 mL), and the resulting mixture was stirred at 60 °C for 3 days. The mixture was concentrated under reduced pressure, and the residue was triturated with H_2O, after which the resulting precipitate was isolated by filtration and thoroughly dried. The solid was taken up in boiling EtOAc, filtered while still hot, and the filtrate was diluted with boiling hexane. The resulting solution was allowed to cool to ambient temperature and then cooled further in a water/ice bath. The resulting precipitate was isolated by filtration to afford **3c** (1.15 g, 63% yield, >95% HPLC purity) as an off-white solid. ^{1}H-NMR (400 MHz, CD_3CN): δ 8.4 (d, J = 8.1 Hz, 1H), 7.4 (d, J = 8.1 Hz, 1H), 4.9 (d, J = 2.5 Hz, 2H), 2.6 (t, J = 2.5 Hz, 1H). ^{13}C-NMR [101 MHz, $(CD_3)_2SO$]: δ 157.1, 155.3, 151.3, 146.8, 141.8, 120.3, 107.6, 77.8, 74.7, 33.0. Elemental Anal.: Calcd for $C_{10}H_5ClN_2O_3$: C, 50.8; H, 2.13; N, 11.8. Found: C, 50.5; H, 1.98; N, 11.6.

*1-(3-Azidopropyl)-7-chloro-2H-pyrido[2,3-d][1,3]oxazine-2,4(1H)-dione (**3d**).* Triphosgene (148 mg, 0.5 mmol) was added to a solution of 2-[(3-azidopropyl)amino]-6-chloronicotinic acid (**2d**) (255 g, 0.1 mmol) in anhydrous dioxane (3 mL), and the resulting mixture was stirred at 60 °C for 3 days while protected from light. The mixture was concentrated under reduced pressure, and the residue was recrystallized from EtOAc/hexane to afford **3d** (241 mg, 86% yield) as an off-white solid. ^{1}H-NMR (400 MHz, $CDCl_3$): δ 8.36 (d, J = 8.1 Hz, 1H), 7.46−7.14 (m, 1H), 4.38 (t, J = 6.9 Hz, 2H), 3.49 (t, J = 6.4 Hz, 2H), 2.09 (t, J = 6.7 Hz, 2H). ^{13}C-NMR (101 MHz, $CDCl_3$): δ 158.40, 156.68, 152.27, 147.06, 141.69, 120.63, 105.73, 49.04, 41.93, 26.82. Elemental Anal.: Calcd for $C_{10}H_8ClN_5O_3$: C, 42.6; H, 2.86; N, 24.9. Found: C, 42.6; H, 2.88; N, 24.8. MS(ESI): m/z calcd for $C_{10}H_9ClN_5O_3^+$: 282.03, found, 282.10 [M + H^+].

*7-Fluoro-1-methyl-2H-pyrido[2,3-d][1,3]oxazine-2,4(1H)-dione (**3e**).* **3e** (58% yield, colorless solid) was prepared from **2e** according to the same procedure as described for **3a**. ^{1}H-NMR [400 MHz, $(CD_3)_2SO$]: δ 3.45 (s, 3H), 7.14 (dd, J = 8.4, 2.2 Hz, 1H), 8.58 (dd, J = 8.3, 7.7 Hz, 1H). ^{13}C-NMR [101 MHz, $(CD_3)_2SO$]: δ 165.4 (d, J = 248.5 Hz), 164.2, 157.2, 152.9 (d, J = 18.2 Hz), 147.7, 145.0 (d, J = 11.1 Hz) 106.0 (d, J = 4.0 Hz), 104.9 (d, J = 37.4 Hz), 30.3. ^{19}F-NMR [376 MHz, $(CD_3)_2SO$]: δ −56.82. HRMS (ESI): m/z calcd for $C_8H_5FN_2O_3^+$: 196.02787, found, 196.02770 [M + H^+].

*1-Ethyl-7-fluoro-2H-pyrido[2,3-d][1,3]oxazine-2,4(1H)-dione (**3f**).* **3f** (62% yield, colorless solid) was prepared from **2f** according to the same procedure as described for **3b**. ^{1}H-NMR [400 MHz, $(CD_3)_2SO$]: δ 1.24 (t, J = 7.1 Hz, 3H), 4.08 (q, J = 7.1 Hz, 2H), 7.13 (dd, J = 8.4, 2.1 Hz, 1H), 8.57 (t, J = 8.0 Hz, 1H). ^{13}C-NMR [101 MHz, $(CD_3)_2SO$]: δ 166.0 (d, J = 248.4 Hz), 157.7, 152.8 (d, J = 18.2 Hz), 147. 7, 145.5 (d, J = 11.1 Hz), 106.7 (d, J = 3.8 Hz), 105.4 (d, J = 37.1 Hz), 49.1, 40.6, 40.4, 40.2, 39.9, 39.8, 39.6, 39.4, 39.3, 12.6. HRMS (ESI): m/z calcd for $C_9H_7FN_2O_3^+$: 210.04352, found, 210.04337 [M + H^+].

*7-Fluoro-1-(prop-2-yn-1-yl)-2H-pyrido[2,3-d][1,3]oxazine-2,4(1H)-dione (**3g**).* Triphosgene (0.75 g, 2.53 mmol) was added to a solution of 6-fluoro-2-(prop-2-yn-1-ylamino)nicotinic acid (**2g**) (1.5 g, 7.67 mmol) in anhydrous dioxane (10 mL), and the resulting mixture was stirred at 60 °C for 3 days. The mixture was concentrated under reduced pressure, and the residue was purified by column chromatography (EtOAc:hexane 1:1.8) to afford **3g** (0.74 g, 44% yield) as an off-white solid. ^{1}H-NMR (400 MHz, $CDCl_3$): δ 8.53 (dd, J = 8.4, 7.2 Hz, 1H), 6.91 (dd, J = 8.4, 2.4 Hz, 1H), 4.96 (d, J = 2.5 Hz, 2H), 2.27 (t, J = 2.5 Hz, 1H). ^{13}C-NMR (101 MHz, $CDCl_3$): δ 166.7 (d, J = 256.5 Hz), 155.9, 151.8 (d, J = 18.2 Hz), 146.51, 145.3 (d, J = 10.1 Hz), 106.4 (d, J = 37.4 Hz), 104.9 (d, J = 3.8 Hz), 72.7, 33.4. ^{19}F-NMR (376 MHz, $CDCl_3$): δ −52.35. Elemental Anal.: Calcd for $C_{10}H_5FN_2O_3$: C, 54.56, H, 2.29; N, 12.72. Found: C, 53.97; H, 2.46; N, 12.47. HRMS (ESI): m/z calcd for $C_{10}H_5FN_2O_3^+$: 220.02787, found, 220.02779 [M + H^+].

*1-(3-Azidopropyl)-7-fluoro-2H-pyrido[2,3-d][1,3]oxazine-2,4(1H)-dione (**3h**).* **3h** (83% yield, off-white solid) was prepared from **2h** according to the same procedure as described for **3d**. ^{1}H-NMR (400 MHz, $CDCl_3$): δ 8.53 (dd, J = 8.4, 7.3 Hz, 1H), 6.90 (dd, J =

https://doi.org/10.1021/acs.jmedchem.3c01310
J. Med. Chem. 2023, 66, 12629−12644

8.4, 2.4 Hz, 1H), 4.51−4.28 (m, 2H), 3.48 (t, J = 6.6 Hz, 2H), 2.23−1.89 (m, 2H). ^{13}C-NMR (101 MHz, $CDCl_3$): δ 166.7 (d, J = 254.5 Hz), 156.3, 152.7 (d, J = 17.9 Hz), 147.2, 145.2 (d, J = 11.0 Hz), 106.0 (d, J = 36.5 Hz), 104.9 (d, J = 4.1 Hz), 49.0, 42.0, 26.8. ^{19}F-NMR (376 MHz, $CDCl_3$): δ -52.44. Elemental Anal.: Calcd for $C_{10}H_8FN_5O_3$: C, 45.29; H, 3.04; N, 26.41. Found: C, 45.15; H, 3.09; S, 7.66; N, 26.12. MS(ESI): m/z calcd for $C_{10}H_9FN_5O_3^+$: 265.06, found, 266.12 [M + H$^+$].

*N,N,N,1-Tetramethyl-2,4-dioxo-1,4-dihydro-2H-pyrido[2,3-d][1,3]oxazin-7-aminium Triflate (**4a**).* 2 M Me_3N in THF (14.8 mL, 29.63 mmol, dried with CaH_2 for at least 24 h and stored under argon) was added to a solution of **3a** (2.1 g, 9.88 mmol) in anhydrous THF (20 mL), and the resulting white suspension was stirred for 1 h. All volatiles were removed under partial vacuum in a stream of argon, and the residue (chloride salt) was dried at 2 mbar and ambient temperature for 10 min. TMSOTf (3.31 ml, 4.06 g, 18.27 mmol) from a freshly opened glass ampule (Cat. Nr. 225649, Sigma-Aldrich/Merck, Darmstadt, Germany) was added to a suspension of the dried crude chloride salt in anhydrous CH_2Cl_2 (30 mL), and the reaction mixture was stirred for 40 min. That followed, all volatiles were removed under partial vacuum in a stream of argon, the residue was dried at 2 mbar and ambient temperature for 10 min and then triturated with Et_2O. The resulting precipitate was isolated by filtration, washed with Et_2O, and taken up in EtOAc (50 mL). The suspension was stirred under reflux for 10 min, cooled to 4 °C, and filtered. The filter cake was washed with EtOAc followed by Et_2O and dried to afford **4a** (3.69 g, 97% yield) as a colorless solid. ^{1}H-NMR [400 MHz, $(CD_3)_2SO$]: δ 3,56 (s, 3H), 3.66 (s, 9H), 7.93 (d, J = 8.4 Hz, 1H), 8.80 (d, J = 8.4 Hz, 1H). ^{13}C-NMR [101 MHz, $(CD_3)_2SO$]: δ 30.9, 55.1, 110.6, 110.7, 144.2, 147.9, 152.2, 157.4, 160.0. ^{19}F-NMR [376 MHz, $(CD_3)_2SO$]: δ -77.76. HRMS (ESI): m/z calcd for $C_{10}H_{11}F_3N_3O_3^+$: 221.07926, found, 221.07949 [M − CH_3] (in HRMS, loss of CH_3 was observed for several anhydrides). ESI-MS: m/z calcd for $C_{11}H_{14}N_3O_3^+$: 236.10, found, 236.20 [M$^+$].

*1-Ethyl-N,N,N-trimethyl-2,4-dioxo-1,4-dihydro-2H-pyrido[2,3-d][1,3]oxazin-7-aminium Triflate (**4b**).* **3b** (0.67 g, 2.96 mmol) was added to 2 M Me_3N in THF (12.6 mL, 25.2 mmol), and the resulting suspension was stirred for 1 h. The mixture was concentrated under reduced pressure, the residue was suspended in CH_2Cl_2 (5 mL), filtered, and washed successively with Et_2O and n-pentane (20 mL of each). Drying at 2 mbar and ambient temperature afforded 0.8 g (94%) of the moisture-sensitive chloride salt, which was directly converted into the triflate by treatment with TMSOTf (1.10 mL, 6.30 mmol) in anhydrous CH_2Cl_2 (12 mL) for 40 min under stirring at ambient temperature. After removal of volatiles under reduced pressure, the residue was washed successively with Et_2O and EtOAc and dried at 2 mbar and ambient temperature, which afforded **4b** (0.8 g, 68% yield) as a colorless solid. ^{1}H-NMR [400 MHz, $(CD_3)_2SO$]: δ 1.28 (t, J = 7.0 Hz, 3H), 3.66 (s, 9H), 4.21 (q, J = 7.0, 2H), 7.93 (d, J = 8.4, 1H), 8.79 (d, J = 8.4, 1H). ^{13}C-NMR [101 MHz, $(CD_3)_2SO$]: δ 12.6, 39.5, 55.07 (C-10), 110.6, 110.8, 144.2, 147.4, 152.3, 157.4, 160.1. ^{19}F-NMR [376 MHz, $(CD_3)_2SO$]: δ -77.76. HRMS (ESI): m/z calcd for $C_{11}H_{13}F_3N_3O_3^+$: 235.09514, found, 235.09500 [M − CH_3] (in HRMS, loss of CH_3 was observed for several anhydrides). ESI-MS: m/z calcd for $C_{12}H_{16}N_3O_3^+$: 250.12, found, 250.22 [M$^+$].

*N,N,N-Trimethyl-2,4-dioxo-1-(prop-2-yn-1-yl)-1,4-dihydro-2H-pyrido[2,3-d][1,3]oxazin-7-aminium Triflate (**4c**).* **4c** (97% yield, colorless solid) was prepared from **3c** according to the same procedure as described for **4a**. ^{1}H-NMR (400 MHz, CD_3CN): δ 8.7 (d, J = 8.4 Hz, 1H), 7.8 (d, J = 8.4 Hz, 1H), 5.0 (d, J = 2.5 Hz, 2H), 3.6 (s, 9H), 2.6 (t, J = 2.5 Hz, 1H). ^{13}C-NMR (101 MHz, CD_3CN): δ 160.6, 157.1, 152.0, 147.6, 145.6, 111.6, 111.5, 77.8, 73.9, 56.2, 34.7. ^{19}F-NMR (376 MHz, CD_3CN): δ -79.3. Elemental Anal.: Calcd for $C_{14}H_{14}F_3N_3O_6S$: C, 41.08; H, 3.45; N, 10.27; S, 7.83. Found: C, 40.77; H, 3.59; N, 9.88; S, 7.66.

*N,N,N-Trimethyl-2,4-dioxo-1-(3-azidopropyl)-1,4-dihydro-2H-pyrido[2,3-d][1,3]oxazin-7-aminium Triflate (**4d**).* **4d** (94% yield, colorless solid) was prepared from **3d** according to the same procedure as described for **4a**. ^{1}H-NMR [400 MHz, $(CD_3)_2SO$]: δ 8.81 (d, J = 8.4 Hz, 1H), 7.94 (d, J = 8.4 Hz, 1H), 4.25 (t, J = 6.8 Hz, 2H), 3.66 (s, 9H), 3.50 (t, J = 6.9 Hz, 2H), 1.96 (p, J = 6.9 Hz, 2H). ^{13}C-NMR [101 MHz, $(CD_3)_2SO$]: δ 160.03, 157.38, 151.72, 147.65, 144.24, 144.24, 110.85, 110.78, 55.09, 48.64, 41.63, 26.70. ^{19}F-NMR [376 MHz, $(CD_3)_2SO$]: δ -77.0. HRMS (ESI): m/z calcd for $C_{13}H_{17}N_6O_6^+$: 477.07746, found; 477.07704 [M$^+$].

*N-Butyl-6-fluoro-2-(methylamino)nicotinamide (**5a**).* A solution of n-butylamine (0.2 mmol, 2 equiv) in MeCN (500 μL) was added to **3e** (0.1 mmol), and the reaction mixture was stirred at 50 °C for 30 min. The product was isolated by flash column chromatography (silica, CH_2Cl_2/MeOH) to afford **5a** (18.6 mg, 82% yield) as a colorless solid. ^{1}H-NMR (400 MHz, $CDCl_3$): δ 8.41 (s, 1H), 7.64 (t, J = 8.1 Hz, 1H), 6.02 (dd, J = 8.2, 2.9 Hz, 1H), 3.39 (td, J = 7.2, 5.7 Hz, 2H), 2.99 (d, J = 4.9 Hz, 3H), 1.69−1.48 (m, 2H), 1.47−1.28 (m, 3H), 1.05−0.82 (m, 5H). ^{13}C-NMR (101 MHz, $CDCl_3$): δ 167.6, 164.7 (d, J = 241.2 Hz), 158.9 (d, J = 19.3 Hz), 139.7 (d, J = 10.2 Hz), 107.0 (d, J = 4.2 Hz), 93.3 (d, J = 38.7 Hz), 39.6, 31.7, 27.9, 20.2, 13.8. ^{19}F-NMR (376 MHz, $CDCl_3$): δ -62.83. HRMS (ESI): m/z calcd for $C_{11}H_{17}FN_3O^+$: 226.13502, found, 226.13524 [M + H$^+$].

*N-Butyl-2-(ethylamino)-6-fluoronicotinamide (**5b**).* **5b** (71% yield, colorless solid) was prepared from **3f** and n-butylamine according to the same procedure as described for **5a**. ^{1}H-NMR (400 MHz, $CDCl_3$): δ 7.63 (t, J = 8.1 Hz, 1H), 6.02 (dd, J = 8.2, 3.0 Hz, 1H), 5.91 (s, 1H), 3.60−3.17 (m, 4H), 1.84−1.53 (m, 2H), 1.53−1.15 (m, 5H), 1.08−0.92 (m, 3H). ^{13}C-NMR (101 MHz, $CDCl_3$): δ 167.7, 164.8 (d, J = 240.1 Hz), 158.2 (d, J = 19.1 Hz), 139.8 (d, J = 10.2 Hz), 106.7 (d, J = 3.9 Hz), 93.5 (d, J = 38.9 Hz), 39.7, 35.9, 31.8, 29.8, 20.3, 14.8, 13.9. ^{19}F-NMR (376 MHz, $CDCl_3$): δ -62.62. HRMS (ESI): m/z calcd for $C_{12}H_{19}FN_3O^+$: 240.15068, found, 240.15085 [M + H$^+$].

*Methyl 6-[6-fluoro-2-(methylamino)nicotinamido]hexanoate (**5c**).* A solution of 6-fluoro-2-(methylamino)nicotinic acid (**2e**) (0.6 g, 3.53 mmol) in $SOCl_2$ (0.64 mL, 1.05 g, 14.08 mmol) was stirred for 1 h and then concentrated under reduced pressure. The residue was taken up in anhydrous toluene (20 mL), and the resulting solution was concentrated under reduced pressure (×3) to afford the corresponding chloroanhydride, which was dissolved in anhydrous CH_2Cl_2 (10 mL). Methyl 6-aminohexanoate hydrochloride (1.9 g, 10.45 mmol) followed by DIEA (1.6 mL, 1.19 g, 9.19 mmol) were added to the solution and the reaction mixture was stirred for 3 h, and then concentrated under reduced pressure. The residue was taken up in Et_2O and 1 M HCl (50 mL of each). The organic fraction was separated; successively washed with 1 M HCl (3 × 10 mL), H_2O (3 × 10 mL), 5% $NaHCO_3$ (3 × 10 mL), and brine (2 × 10 mL); dried; and concentrated under reduced pressure. The residue was recrystallized from pentane (low-temperature recrystallization) to afford **5c** (0.67 g, 64% yield) as a colorless solid. ^{1}H-NMR (400 MHz, $CDCl_3$): δ 8.42 (s, 1H), 7.68 (t, J = 8.1 Hz, 1H), 6.16 (s, 1H), 6.02 (dd, J = 8.2, 2.9 Hz, 1H), 3.68 (s, 3H), 3.40 (td, J = 7.1, 5.6 Hz, 2H), 2.99 (s, 3H), 2.35 (t, J = 7.3 Hz, 2H), 1.74−1.54 (m, 4H), 1.45−1.35 (m, 2H). ^{13}C-NMR (101 MHz, $CDCl_3$): δ 174.1, 167.6, 164.7 (d, J = 241.1 Hz), 159.0 (d, J = 19.2 Hz), 139.8 (d, J = 10.2 Hz), 106.9 (d, J = 4.2 Hz), 93.3 (d, J = 38.8 Hz), 51.6, 39.4, 33.7, 29.1, 27.8, 26.3, 24.2. ^{19}F-NMR (376 MHz, $CDCl_3$): δ -62.80. ESI-MS: m/z 298.32 [M + H$^+$], 320.31 [M + Na$^+$], 336.28 [M + K$^+$]. HRMS (ESI): m/z calcd for $C_{14}H_{22}FN_3O_3Na^+$: 320.1386, found, 320.1386 [M + Na$^+$].

*Methyl 6-[6-fluoro-2-(ethylamino)nicotinamido]hexanoate (**5d**).* **5d** (72% yield; colorless solid) was prepared from **2f** and methyl 6-aminohexanoate hydrochloride according to the same procedure as described for **5c**. ^{1}H-NMR (400 MHz, $CDCl_3$): δ 8.42 (s, 1H), 7.68 (t, J = 8.1 Hz, 1H), 6.15 (s, 1H), 6.01 (dd, J = 8.2, 3.0 Hz, 1H), 3.68 (s, 3H), 3.49−3.31 (m, 4H), 2.35 (t, J = 7.3 Hz, 2H), 1.79−1.53 (m, 4H), 1.50−1.36 (m, 2H), 1.25 (t, J = 7.3 Hz, 3H). ^{13}C-NMR (101 MHz, $CDCl_3$): δ 174.1, 167.6, 164.6 (d, J = 241.0 Hz), 158.2 (d, J = 19.0 Hz), 139.9 (d, J = 10.2 Hz), 106.6 (d, J = 4.4 Hz), 93.3 (d, J = 38.8 Hz), 51.6, 39.4, 35.8, 33.8, 29.1, 26.3, 24.2, 14.7. ^{19}F-NMR (376 MHz, $CDCl_3$): δ -62.66. ESI-MS: m/z 312.35 [M + H$^+$], 334.31 [M + Na$^+$], 350.27 [M + K$^+$]. HRMS (ESI): m/z calcd for $C_{15}H_{24}FN_3O_3Na^+$: 334. 1543, found, 334.1544 [M + Na$^+$].

*N-Benzyl-6-fluoro-2-(methylamino)nicotinamide (**5e**).* A solution of benzylamine (0.2 mmol, 2 equiv) in MeCN (500 μL) was added to

https://doi.org/10.1021/acs.jmedchem.3c01310
J. Med. Chem. 2023, 66, 12629−12644

3e (0.1 mmol), and the reaction mixture was stirred at 80 °C for 30 min. The product was isolated by flash column chromatography (silica, CH_2Cl_2/MeOH) to afford **5e** (25.2 mg, 92% yield) as a colorless solid. ^{1}H-NMR (400 MHz, $CDCl_3$): δ 8.47 (s, 1H, NH), 7.50−7.18 (m, 5H), 6.24 (s, 1H, NH), 6.02 (dd, J = 8.2, 2.9 Hz, 1H), 4.59 (d, J = 5.6 Hz, 2H), 3.02 (s, 3H). ^{13}C-NMR (101 MHz, $CDCl_3$): δ 167.4, 164.8 (d, J = 241.6 Hz), 158.9 (d, J = 10.2 Hz), 139.9 (d, J = 10.2 Hz), 137.9, 128.9, 127.9, 127.8, 106.5 (d, J = 6.2 Hz), 103.6, 93.5 (d, J = 38.9 Hz), 43.89, 27.89. ^{19}F-NMR (376 MHz, $CDCl_3$): δ -62.17. HRMS (ESI): m/z calcd for $C_{14}H_{14}FN_3O^+$: 260.119367, found, 260.11940 [M + H$^+$].

*N-Benzyl-2-(ethylamino)-6-fluoronicotinamide (**5f**).* **5f** (74% yield, colorless solid) was prepared from **3f** and benzylamine according to the same procedure as described for **5e**. ^{1}H-NMR (400 MHz, $CDCl_3$): δ 8.49 (s, 1H), 7.67 (t, J = 8.1 Hz, 1H), 7.44−7.26 (m, 5H), 6.33 (s, 1H), 6.00 (dd, J = 8.2, 3.0 Hz, 1H), 4.58 (d, J = 5.5 Hz, 2H), 3.50 (q, J = 7.2 Hz, 2H), 1.26 (t, J = 7.2 Hz, 3H). ^{13}C-NMR (101 MHz, $CDCl_3$): δ 167.4, 164.7 (d, J = 241.4 Hz), 158.3 (d, J = 19.2 Hz), 140.0 (d, J = 10.4 Hz), 137.9, 128.9, 127.8, 127.7, 106.1 (d, J = 4.3 Hz), 93.5 (d, J = 39.0 Hz), 43.8, 35.9, 14.7. ^{19}F-NMR (376 MHz, $CDCl_3$): δ -62.11. HRMS (ESI): m/z calcd for $C_{15}H_{17}FN_3O^+$: 274.13502, found, 274.13508 [M + H$^+$].

*Methyl [6-fluoro-2-(methylamino)nicotinoyl]phenylalaninate (**5g**).* **5g** (41% yield, colorless solid) was prepared from **3e** and HCl·H-Phe-OMe according to the same procedure as described for **5a**. ^{1}H-NMR [400 MHz, $(CD_3)_2SO$]: δ 8.80 (d, J = 7.6 Hz, 1H), 8.44 (q, J = 5.0 Hz, 1H), 8.12 (t, J = 8.2 Hz, 1H), 7.28 (d, J = 4.3 Hz, 4H), 7.21 (q, J = 4.3 Hz, 1H), 6.24 (dd, J = 8.2, 2.7 Hz, 1H), 4.60 (ddd, J = 10.0, 7.4, 5.3 Hz, 1H), 3.64 (s, 3H), 3.20−3.00 (m, 2H), 2.82 (d, J = 4.7 Hz, 3H). ^{13}C-NMR [101 MHz, $(CD_3)_2SO$]: δ 172.6, 167.4, 164.3 (d, J = 238.5 Hz), 158.7 (d, J = 19.1 Hz), 142.8 (d, J = 10.2 Hz), 138.1, 129.5, 128.7, 127.0, 106.7 (d, J = 4.0 Hz), 93.5 (d, J = 38.5 Hz), 54.6, 52.5, 36.6, 28.1. ^{19}F-NMR [376 MHz, $(CD_3)_2SO$]: δ -63.13. HRMS (ESI): m/z calcd for $C_{17}H_{19}FN_3O_3^+$: 332.14050, found, 332.14084 [M + H$^+$].

*Methyl [2-(ethylamino)-6-fluoronicotinoyl]phenylalaninate (**5h**).* **5h** (27% yield, colorless solid) was prepared from **3f** and HCl·H-Phe-OMe according to the same procedure as described for **5a**. ^{1}H-NMR (400 MHz, $CDCl_3$): δ 8.34 (s, 1H), 7.57 (t, J = 8.1 Hz, 1H), 7.35−7.24 (m, 3H), 7.20−7.08 (m, 2H), 6.38 (d, J = 7.4 Hz, 1H), 6.01 (dd, J = 8.2, 3.0 Hz, 1H), 5.00 (dt, J = 7.4, 5.7 Hz, 1H), 3.80 (s, 3H), 3.47 (q, J = 7.2 Hz, 2H), 3.23 (qd, J = 13.9, 5.8 Hz, 2H), 1.26 (t, J = 7.3 Hz, 3H). ^{13}C-NMR (101 MHz, $CDCl_3$): δ 172.1, 166.9, 164.8 (d, J = 241.8 Hz), 158.2 (d, J = 19.3 Hz), 140.4 (d, J = 10.5 Hz), 135.7, 129.3, 128.7, 127.3, 105.7 (d, J = 4.2 Hz), 93.8 (d, J = 39.0 Hz), 53.3, 52.6, 37.9, 35.8, 14.7. ^{19}F-NMR (376 MHz, $CDCl_3$): δ -61.58. HRMS (ESI): m/z calcd for $C_{18}H_{21}FN_3O_3^+$: 346.15614, found, 346.15654 [M + H$^+$].

*N-tert-Butyl-6-fluoro-2-(methylamino)nicotinamide (**5i**).* **5i** (57% yield, colorless solid) was prepared from **3e** and *N-tert*-butylamine according to the same procedure as described for **5e**. ^{1}H-NMR (400 MHz, $CDCl_3$): δ 8.24 (s, 1H, NH), 7.46 (td, J = 8.1, 1.2 Hz, 1H), 5.94−5.85 (m, 1H), 5.61 (s, 1H, NH), 2.87 (s, 3H), 1.34 (d, J = 1.3 Hz, 9H). ^{13}C-NMR (101 MHz, $CDCl_3$): δ 167.4, 163.8 (d, J = 237.3 Hz), 157.9 (d, J = 18.8 Hz), 143.0 (d, J = 9.8 Hz), 108.5 (d, J = 4.2 Hz), 93.1 (d, J = 38.1 Hz), 51.5, 35.6, 29.0, 15.1. ^{19}F-NMR (376 MHz, $CDCl_3$): δ -63.42. HRMS (ESI): m/z calcd for $C_{11}H_{17}FN_3O^+$: 226.1344, found, 226.1346 [M + H$^+$].

*N-tert-Butyl-2-(ethylamino)-6-fluoronicotinamide (**5j**).* **5j** (82% yield, colorless solid) was prepared from **3f** and *N-tert*-butylamine according to the same procedure as described for **5e**. ^{1}H-NMR [400 MHz, $(CD_3)_2SO$]: δ 8.56 (d, J = 5.6 Hz, 1H), 8.08 (t, J = 8.3 Hz, 1H), 7.70 (s, 1H), 6.16 (dd, J = 8.2, 2.9 Hz, 1H), 3.38−3.17 (m, 6H), 1.36 (s, 9H), 1.14 (t, J = 7.2 Hz, 3H). ^{13}C-NMR (101 MHz, $(CD_3)_2SO$) δ 166.2 (d, J = 244.8 Hz), 162.6, 158.0 (d, J = 18.8 Hz), 143.0 (d, J = 9.8 Hz), 108.5 (d, J = 4.2 Hz), 93.1 (d, J = 38.1 Hz), 51.5, 35.6, 29.0, 15.1. ^{19}F-NMR [376 MHz, $(CD_3)_2SO$]: δ -64.65. HRMS (ESI): m/z calcd for $C_{12}H_{19}FN_3O^+$: 240.15068, found, 240.15069 [M + H$^+$].

*[6-Fluoro-2-(methylamino)pyridin-3-yl](piperidin-1-yl)-methanone (**5k**).* **5k** (92% yield, colorless solid) was prepared from **3e** and piperidine according to the same procedure as described for **5e**. ^{1}H-NMR (400 MHz, $CDCl_3$): δ 7.39 (t, J = 8.1 Hz, 1H), 6.24 (s, 1H, NH), 6.09 (dd, J = 8.0, 2.7 Hz, 1H), 3.56 (t, J = 5.5 Hz, 4H), 2.96 (d, J = 4.8 Hz, 3H), 1.74−1.58 (m, 7H). ^{13}C-NMR (101 MHz, $CDCl_3$): δ 168.7, 163.8 (d, J = 240.4 Hz), 157.9 (d, J = 18.2 Hz), 140.7 (d, J = 9.1 Hz), 109.5 (d, J = 5.1 Hz), 93.5 (d, J = 38.4 Hz), 29.7, 28.2, 26.2, 24.6. ^{19}F-NMR (376 MHz, $CDCl_3$): δ -65.86. HRMS (ESI): m/z calcd for $C_{12}H_{17}FN_3O^+$: 238.13502, found, 238.13506 [M + H$^+$].

*Di-tert-butyl [(S)-{1-(tert-butoxy)-6-[6-fluoro-2-(methylamino)-nicotinamido]-1-oxohexan-2-yl}-carbamoyl]-(S)-glutamate (**5l**).* **5l** (47% yield, colorless solid) was prepared from **3e** and *t*BuO-Glu(O*t*Bu)-CO-Lys(H)-O*t*Bu[39] according to the same procedure as described for **5a**. ^{1}H-NMR (400 MHz, $CDCl_3$) δ 8.56 (s, 1H), 7.97 (t, J = 8.0 Hz, 1H), 6.02 (dd, J = 8.2, 2.7 Hz, 1H), 5.59 (s, 1H), 5.32 (s, 1H), 4.30−4.16 (m, 2H), 3.42 (dd, J = 8.5, 4.1 Hz, 1H), 3.31 (d, J = 4.8 Hz, 1H), 2.97 (d, J = 4.7 Hz, 3H), 2.37−2.17 (m, 2H), 2.03 (s, 1H), 1.71 (m, 7H), 1.43 (2×s, 18H), 1.40 (s, 9H). ^{13}C-NMR (101 MHz, $CDCl_3$): δ 173.4, 173.5, 172.5, 172.5, 172.3, 168.1, 164.7 (d, J = 241.4 Hz), 159.2 (d, J = 19.2 Hz), 157.44, 141.2 (d, J = 10.1 Hz), 107.2 (d, J = 4.2 Hz), 93.3 (d, J = 38.4 Hz), 82.8, 81.9, 80.9, 76.8, 53.6, 53.3, 39.8, 32.9, 31.7, 28.7, 28.2, 28.1, 28.1, 28.0, 27.9, 23.4. ^{19}F-NMR (376 MHz, $CDCl_3$): δ -63.45. HRMS (ESI): m/z calcd for $C_{31}H_{50}FN_5O_8Na^+$: 662.35356, found, 662.35404 [M + H$^+$].

*tert-Butyl N^2-acetyl-N^6-[6-fluoro-2-(methylamino)nicotinoyl]-lysinate (**5m**).* **5m** (78% yield, colorless solid) was prepared from **3e** and Ac-Lys(H·HCl)-O*t*Bu according to the same procedure as described for **5a**. ^{1}H-NMR (400 MHz, $CDCl_3$) δ 8.52 (s, 1H), 7.86 (t, J = 8.1 Hz, 1H), 6.44 (s, 1H), 6.16 (d, J = 7.9 Hz, 1H), 6.03 (dd, J = 8.2, 2.9 Hz, 1H), 4.53 (td, J = 8.6, 4.4 Hz, 1H), 3.40 (dt, J = 6.7, 3.6 Hz, 2H), 3.00 (s, 3H), 2.01 (s, 3H), 1.76 (m, 2H), 1.71−1.60 (m, 2H), 1.48 (s, 9H), 1.45−1.38 (m, 2H). ^{13}C-NMR (101 MHz, $CDCl_3$) δ 171.79 (s), 170.2, 167.8, 164.6 (d, J = 240.9 Hz), 159.0 (d, J = 18.8 Hz), 140.3 (d, J = 10.1 Hz), 106.8 (d, J = 4.2 Hz), 93.3 (d, J = 38.7 Hz), 82.5, 52.0, 39.4, 32.9, 28.1, 27.8, 22.4. ^{19}F-NMR (376 MHz, $CDCl_3$) δ -63.00. ESI-MS: m/z 397.53 [M + H$^+$], 419.12 [M + Na$^+$]. HRMS (ESI): m/z calcd for $C_{19}H_{30}FN_4O_4^+$: 397.22456, found, 397.22494 [M + H$^+$].

*Methyl [6-fluoro-2-(methylamino)nicotinoyl]glycinate (**5n**).* **5n** (94% yield, colorless solid) was prepared from **2e** and HCl·H-Gly-OMe according to the same procedure as described for **5c**. ^{1}H-NMR (400 MHz, $CDCl_3$) δ 8.37 (s, 1H), 7.75 (t, J = 8.1 Hz, 1H), 6.51 (s, 1H), 6.06 (dd, J = 8.2, 2.9 Hz, 1H), 4.18 (d, J = 5.1 Hz, 2H), 3.83 (s, 3H), 3.00 (s, 3H). ^{13}C-NMR (101 MHz, $CDCl_3$) δ 170.6, 167.5, 164.9 (d, J = 242.3 Hz), 159.0 (d, J = 19.0 Hz), 140.4 (d, J = 10.4 Hz), 105.8 (d, J = 4.2 Hz), 93.8 (d, J = 39.0 Hz), 52.6, 41.5, 27.9. ^{19}F-NMR (376 MHz, $CDCl_3$) δ -61.51. ESI-MS: m/z 242.23 [M + H$^+$], 264.21 [M + Na$^+$]. HRMS (ESI): m/z calcd for $C_{12}H_{25}FN_2O_3^+$: 242.09354, found,242.09369 [M + H$^+$].

*tert-Butyl N^6-[(benzyloxy)carbonyl]-N^2-[6-fluoro-2-(methylamino)nicotinoyl]lysinate (**5o**).* **5o** (91% yield, colorless solid) was prepared from **2e** and HCl·H-Lys(Z)-O*t*Bu according to the same procedure as described for **5c**. ^{1}H-NMR (400 MHz, $CDCl_3$): δ 8.39 (s, 1H), 7.82 (t, J = 8.0 Hz, 1H), 7.46−7.31 (m, 5H), 6.67 (d, J = 7.0 Hz, 1H), 6.04 (dd, J = 8.2, 2.8 Hz, 1H), 5.17−4.94 (m, 2H), 4.83 (s, 1H), 4.56 (dd, J = 12.0, 7.2 Hz, 1H), 3.29−3.14 (m, 2H), 2.99 (s, 3H), 1.99−1.72 (m, 2H), 1.68−1.33 (m, 4H), 1.51 (s, 9H). ^{13}C-NMR (101 MHz, $CDCl_3$): δ 171.8, 167.3, 166.6 (d, J = 122.6 Hz), 159.0 (d, J = 19.0 Hz), 156.7, 140.5 (d, J = 10.2 Hz), 136.5, 128.6, 128.2, 128.0, 106.3 (d, J = 3.9 Hz), 93.6 (d, J = 38.8 Hz), 82.50, 66.69, 52.77, 40.37, 32.01, 29.65, 28.04, 27.85, 22.26. ^{19}F-NMR (376 MHz, $CDCl_3$): δ -62.14. ESI-MS: m/z 489.31 [M + H$^+$], 511.07 [M + Na$^+$]. HRMS (ESI): m/z calcd for $C_{19}H_{30}FN_4O_4^+$: 489.25132, found, 489.25106, [M + H$^+$].

*((S)-{1-Carboxy-5-[6-fluoro-2-(methylamino)nicotinamido]-pentyl}carbamoyl)-(S)-glutamic Acid (**5p**, JK-PSMA-15).* **5l** (65 mg, 0.10 mmol) was treated with 95% TFA (1 mL) for 3 h at ambient temperature. TFA was removed *in vacuo* and another portion of TFA

https://doi.org/10.1021/acs.jmedchem.3c01310
J. Med. Chem. 2023, 66, 12629−12644

(1 mL) was added. This was concentrated slowly over the course of 1 h on the rotary evaporator. The residue was dissolved in a small amount of MeOH and precipitated with Et_2O. The mixture was sonicated, and the precipitate was isolated by filtration to afford JK-PSMA-15 (30 mg, 63% yield) as a colorless solid. ^{1}H-NMR (400 MHz, CD_3OD) δ7.77 (td, J = 8.1, 2.9 Hz, 1H), 5.92 (dd, J = 8.2, 2.2 Hz, 1H), 4.16−4.01 (m, 1H), 3.27−3.00 (m, 1H), 2.74 (s, 3H), 2.54−2.35 (m, 1H), 2.30−2.16 (m, 2H), 2.00−1.88 (m, 1H), 1.83 (d, J = 7.1 Hz, 1H), 1.82−1.55 (m, 2H), 1.56−1.36 (m, 3H), 1.36−1.18 (m, 3H). ^{19}F-NMR (376 MHz, CD_3OD) δ -62.93, -77.06. ^{13}C-NMR (101 MHz, CD_3OD) δ 174.7, 174.5, 174.2, 168.4, 165.3 (d, J = 237.7 Hz), 159.3 (s, J = 2.2 Hz), 142.1 (d, J = 10.2 Hz), 108.4 (d, J = 4.4 Hz), 93.9 (d, J = 41.6 Hz), 39.8, 32.1, 30.5, 29.5, 27.9, 23.5. HRMS (ESI): m/z calcd for $C_{16}H_{14}FN_5O_2Na^+$: 350.10237, found, 350.10228 [M + H$^+$].

*2-{[(1-Benzyl-1H-1,2,3-triazol-4-yl)methyl]amino}-6-fluoronicotinic Acid (**6a**).* Sodium ascorbate (0.7 equiv) was added to a 1.8 M solution of **2g** (423 mg, 2.18 mmol, 1 equiv) and benzyl azide (290 mg, 2.18 mmol, 1 equiv) in 75% MeOH, and the mixture was briefly sonicated. 1 M $CuSO_4{\cdot}5H_2O$ (0.2 equiv) was added, which induced a color change to yellow-green. The reaction mixture was briefly sonicated again, kept in a water bath at ambient temperature for 2 h, and then concentrated under reduced pressure. The remaining oil was taken up in CH_2Cl_2 or EtOAc and washed with a saturated aqueous solution of EDTA until the aqueous phase was colorless. The organic fraction was dried over Na_2SO_4, and the solvent was removed under reduced pressure to afford **6a** (524 mg, 74% yield) as a colorless solid. ^{1}H-NMR [400 MHz, $(CD_3)_2SO$]: δ 8.6 (t, J = 5.9 Hz, 1H), 8.1 (td, J = 8.3, 1.9 Hz, 1H), 7.7−7.5 (m, 1H), 7.4−7.1 (m, 5H), 6.2−5.9 (m, 1H), 5.4 (s, 2H), 4.6 (d, J = 5.6 Hz, 2H). ^{13}C-NMR [101 MHz, $(CD_3)_2SO$]: δ 167.7, 164.2 (d, J = 242.7 Hz), 157.5 (d, J = 19.6 Hz), 145.0 (d, J = 10.5 Hz), 144.6, 134.3, 128.1, 127.6, 127.1, 121.6, 111.4, 103.4 (d, J = 4.4 Hz), 94.3 (d, J = 38.1 Hz), 52.9, 35.6. ^{19}F-NMR [376 MHz, $(CD_3)_2SO$]: δ -60.8. HRMS (ESI): m/z calcd for $C_{16}H_{14}FN_5O_2Na^+$: 350.10237, found, 350.10228 [M + H$^+$].

*2-({[(S,S)-1-{6-(tert-Butoxy)-5-[3-(1,5-di-tert-butoxy-1,5-dioxopentan-2-yl)ureido]-6-oxohexyl}-1H-1,2,3-triazol-4-yl]methyl}amino)-6-fluoronicotinic Acid (**10**).* **10** (87% yield, colorless solid) was prepared from **2g** and 1,5-di-*tert*-butyl (*S*)-2-({[(*S*)-6-azido-1-(*tert*-butoxy)-1-oxohexan-2-yl]carbamoyl}amino)pentanedioate (**9**; for preparation, see Scheme S1 in the Supporting Information) according to the same procedure as described for **6a**. ^{1}H-NMR (400 MHz, $CDCl_3$): δ 9.04 (s, 1H), 8.27 (t, J = 8.2 Hz, 1H), 7.71 (s, 1H), 6.12 (dd, J = 8.3, 2.5 Hz, 1H), 5.46 (d, J = 8.1 Hz, 1H), 5.39 (d, J = 7.9 Hz, 1H), 4.82 (t, J = 4.6 Hz, 2H), 4.33 (d, J = 6.1 Hz, 4H), 2.32 (dq, J = 16.4, 9.8 Hz, 2H), 2.13−2.00 (m, 1H), 1.99−1.70 (m, 4H), 1.69−1.56 (m, 1H), 1.45 (s, 9H). 1.44 (s, 9H), 1.43 (s, 9H). ^{13}C-NMR (101 MHz, $CDCl_3$): δ 172.67, 172.20, 166.57, 164.15, 158.48, 158.29, 157.13, 146.00, 145.19, 123.16, 104.17, 95.30, 94.92, 82.20, 80.75, 53.20, 53.16, 53.16, 50.20, 35.58, 32.30, 31.65, 29.60, 28.19, 28.06, 27.99, 27.96, 21.92. ^{19}F-NMR (376 MHz, $CDCl_3$): δ -60.40. HRMS (ESI): m/z calcd for $C_{313}H_{51}FN_7O_9Na^+$: 708.37268, found, 708.37272 [M + Na$^+$].

*({1-Carboxy-5-[(S)-4-{[(3-carboxy-6-fluoropyridin-2-yl)amino]methyl}-1H-1,2,3-triazol-1-yl]pentyl}carbamoyl)-(S)-glutamic Acid (**6b**, JK-PSMA-16).* **6b** (20% yield, colorless solid) was prepared from **10** according to the same procedure as described for JK-PSMA-15. ^{1}H-NMR (400 MHz, CD_3OD): δ 8.29 (t, J = 8.3 Hz, 1H), 7.95 (s, 1H), 6.20 (dd, J = 8.3, 2.6 Hz, 1H), 4.74 (s, 2H), 4.40 (t, J = 7.1 Hz, 2H), 4.31 (ddd, J = 15.4, 8.4, 5.0 Hz, 2H), 3.33 (dt, J = 3.2, 1.6 Hz, 1H), 2.54−2.34 (m, 2H), 2.26−2.10 (m, 1H), 2.06−1.79 (m, 4H), 1.70 (dq, J = 14.8, 8.1 Hz, 1H), 1.44 (dd, J = 14.6, 6.9 Hz, 2H). ^{13}C-NMR (101 MHz, CD_3OD): δ 177.4, 175.2, 174.9, 173.6, 168.5, 166.3 (d, J = 243.4 Hz), 158.5 (d, J = 41.4 Hz), 152.5, 145.8 (d, J = 10.1 Hz), 104.1 (d, J = 5.1 Hz), 94.8 (d, J = 38.4 Hz), 52.56, 49.68, 35.64, 31.43, 31.21, 29.66, 29.37, 22.10. ^{19}F-NMR (376 MHz, CD_3OD): δ -60.88. MS (ESI): m/z calcd for $C_{21}H_{25}FN_7O_9^-$: 538.17, found, 538.26 [M − H$^+$]. HRMS (ESI): m/z calcd for $C_{21}H_{27}FN_7O_9^+$: 540.18488, found, 540.18491 [M + H$^+$].

*6-Fluoro-2-{[3-(4-phenyl-1H-1,2,3-triazol-1-yl)propyl]amino}-nicotinic Acid (**6c**).* **6c** (85% yield, colorless solid) was prepared from **2h** and phenylacetylene according to the same procedure as described for **6a**. ^{1}H-NMR (400 MHz, $CDCl_3$) δ 8.30 (td, J = 8.4, 3.3 Hz, 2H), 8.02 (s, 1H), 7.87 (d, J = 7.2 Hz, 2H), 7.45 (t, J = 7.2 Hz, 2H), 7.36 (t, J = 7.3 Hz, 1H), 6.17 (td, J = 8.4, 2.8 Hz, 1H), 4.56 (t, J = 6.6 Hz, 2H), 3.63 (q, J = 5.9 Hz, 2H), 2.44−2.26 (m, 2H). ^{13}C-NMR (101 MHz, CD_3OD): δ 168.6, 165.4 (d, J = 242.0 Hz), 158.9 (d, J = 19.1 Hz), 147.4, 145.8 (d, J = 10.6 Hz), 130.4, 128.5, 127.9, 125.3, 121.0, 104.2 (d, J = 6.2 Hz), 94.2 (d, J = 38.4 Hz), 47.9, 37.4, 29.6. ^{19}F-NMR (376 MHz, CD_3OD): δ -63.23. HRMS (ESI): m/z calcd for $C_{17}H_{15}FN_5O_2^-$: 340.12153, found, 340.12171 [M − H$^+$].

*Di-tert-butyl {[(S)-1-(tert-butoxy)-1-oxo-6-propiolamidohexan-2-yl]carbamoyl}-(S)-glutamate (**11**).* A solution of pentafluorophenyl propiolate[40] (1.28 g, 5.50 mmol) in DMF (1.5 mL) was rapidly added to a stirred solution of *t*BuO-Glu(O*t*Bu)-CO-Lys(H)-O*t*Bu (2.44 g, 5.00 mmol) and DIEA (1.15 mL, 0.85 g, 6.57 mmol) in DMF (10 mL) at −10 °C (see Scheme S2 in the Supporting Information). Stirring was continued at −10 °C for 30 min, after which the reaction mixture was allowed to reach ambient temperature and stirring was continued for another 2 h. The solution was then concentrated under reduced pressure, taken up in 0.25 M HCl (20 mL), and extracted three times with ether. The combined organic fractions were washed with water and brine, dried over sodium sulfate, and purified by flash chromatography (EtOAc/petrol ether 1:1). After lyophilization from MeCN, **11** (2.35 g, 87% yield) was obtained as a white amorphous powder. R_f: 0.29 (EtOAc/petrol ether 1:1) ^{1}H-NMR (200 MHz, CD_3OD): δ 6.41 (1H), 6.37 (1H), 4.22 (m, 2H) 3.58 (s, 1H), 3.25 (t, J = 6.7 Hz, 2H), 2.35 (m, 2H), 2.18-1.52 (m, 8H), 1.51 (s, 9H). 1.50 (s, 9H), 1.48 (s, 9H). ^{13}C-NMR (50 MHz, CD_3OD): δ 173.83, 173.71, 173.43, 159.89, 154.64, 82.77, 82.58, 81.70, 78.30, 75.64, 54.74, 54.14, 40.36, 33.16, 32.46, 29.60, 28.96, 28.36, 28.32, 28.29, 23.85. HRMS (ESI) calcd for $C_{27}H_{46}N_3O_8$: 540.32794, found, 540.32819 [M + H$^+$].

*{[(S)-1-Carboxy-5-propiolamidopentyl]carbamoyl}-(S)-glutamic Acid (**8**).* **11** (1.00 g, 1.85 mmol) was dissolved in TFA/water/TIPS (20 mL; 95:2.5:2.5) and stirred at ambient temperature for 1 h (see Scheme S2 in the Supporting Information). The solution was concentrated under reduced pressure, and the resulting oil was dissolved in MeCN (20 mL) and concentrated again under reduced pressure three times. Lyophilization from water gave **8** (0.68 g, 99% yield) as a hygroscopic white powder. ^{1}H-NMR (200 MHz, D_2O): δ 4.15 (m, 2H), 3.36 (s, 1H), 3.15 (t, J = 6.5 Hz, 2H), 2.42 (t, J = 7.2 Hz, 2H), 2.18−1.15 (m, 8H). ^{13}C-NMR (50 MHz, D_2O): δ 177.19, 177.00, 176.17, 159.27, 154.32, 76.37, 75.93, 53.13, 52.52, 39.43, 30.55, 30.03, 27.44, 26.26, 22.28. HRMS (ESI) calcd for $C_{15}H_{22}N_3O_8$: 372.14014, found, 372.14031 [M + H$^+$].

*{[1-Carboxy-5-(1-{3-[(S)-(3-carboxy-6-fluoropyridin-2-yl)amino]propyl}-1H-1,2,3-triazole-4-carboxamido)pentyl]carbamoyl}-(S)-glutamic Acid (**6d**, JK-PSMA-18).* JK-PSMA-18 (44% yield, colorless solid) was prepared from **2h** and **8** according to the same procedure as described for **6a**. ^{1}H-NMR (400 MHz, CD_3CN): δ 8.58−8.39 (m, 1H), 8.31 (t, J = 8.4 Hz, 1H), 8.06−7.83 (m, 1H), 6.29 (t, J = 11.7 Hz, 1H), 6.26−6.16 (m, 1H), 4.68 (dt, J = 55.4, 6.9 Hz, 1H), 4.50−4.39 (m, 1H), 4.36 (td, J = 8.0, 4.8 Hz, 1H), 3.66−3.53 (m, 1H), 3.45 (ddq, J = 20.3, 13.3, 6.9 Hz, 1H), 2.56−2.39 (m, 1H), 2.33 (p, J = 6.8 Hz, 1H), 2.27−2.12 (m, 1H), 2.02−1.85 (m, 1H), 1.85−1.58 (m, 2H), 1.58−1.44 (m, 1H). ^{13}C-NMR (101 MHz, CD_3CN): δ 173.7, 173.5, 173.4, 167.8, 165.4 (d, J = 242.4 Hz), 160.27, 159.1 (d, J = 30.3 Hz), 158.2, 146.0 (d, J = 11.1 Hz), 143.2, 126.0, 103.3 (d, J = 4.9 Hz), 94.7 (d, J = 39.4 Hz), 52.9, 52.3, 48.0, 38.3, 37.8, 31.6, 29.7, 29.2, 27.8, 22.5. ^{19}F-NMR (376 MHz, CD_3CN): δ -61.48. HRMS (ESI): m/z calcd for $C_{24}H_{28}FN_8O_{10}^{3-}$: 202.39726, found, 202.39763 [M − 3H$^+$].

Radiochemistry. All radiosyntheses were carried out using anhydrous solvents (Aldrich). Anion exchange resins (PS-HCO_3^-, 45 mg sorbent) were obtained from Synthra GmbH (Hamburg, Germany) and preconditioned with 1 mL of H_2O directly before use. Solid-phase extraction (SPE) cartridges (Oasis HLB Plus Short and HLB PriME Light) were obtained from Waters GmbH (Eschborn,

https://doi.org/10.1021/acs.jmedchem.3c01310
J. Med. Chem. 2023, 66, 12629−12644

Germany) and used without preconditioning. [^{18}F]Fluoride ([^{18}F]F$^-$) was produced via the ^{18}O(p,n)^{18}F reaction by bombardment of enriched [^{18}O]water with 16.5 MeV protons using a BC1710 cyclotron (The Japan Steel Works Ltd., Shinagawa, Japan) at the INM-5 (Forschungszentrum Jülich, Germany). All radiolabeling experiments were carried out under ambient atmosphere. Before radiosynthesis, [^{18}F]F$^-$ was processed as follows. Aqueous [^{18}F]F$^-$ was loaded onto the anion exchange resin from the male side, whereas flushing, washing, and [^{18}F]F$^-$-elution were carried out from the female side. To determine radiochemical conversions (RCCs) as a measure of the efficiency of a specific labeling reaction,[44] reaction mixtures were diluted with an equal volume of H_2O (to dissolve any [^{18}F]F$^-$ adsorbed onto the reaction vessel walls) and analyzed by radio-HPLC. The RCCs were then calculated by dividing the integrated peak area of the radiolabeled product by the integrated area of a post-column injection peak.[28] Isolated yields of ^{18}F-labeled compounds were determined for the radiochemically and chemically pure products and are reported in terms of decay-corrected radiochemical yields (RCYs) and/or non-decay-corrected activity yields (AYs), respectively, as recommended in the consensus nomenclature rules for radiopharmaceutical chemistry.[45] HPLC analyses were carried out on a Dionex Ultimate 3000 HPLC system and a DAD UV-detector coupled in series with a Berthold NaI detector. A Multokrom C18 AQ 100-5, 250 mm × 4.6 mm column (CS-Chromatographie Service GmbH, Langerwehe, Germany) was used. UV and radioactivity detectors were connected in series, giving a time delay of 0.1−0.6 min depending on the flow rate, exact peak shapes, and the length of the capillary between both detectors. ^{18}F-Labeled compounds were identified by co-injection of the non-radioactive reference compounds using HPLC. General methods for HPLC can be found in the Supporting information. The HPLC system used for the purification of crude products consisted of a Merck Hitachi L-6000 pump, a Knauer K-2500 detector, a Rheodyne 6-way valve, a Geiger-Müller counter, and a Hydro-RP, 250 mm × 10 mm, 80 Å, 10 μm column (Synergi; Phenomenex LTD, Aschaffenburg, Germany).

*Production of [^{18}F]AFAs ([^{18}F]**3e-h**)—General Procedure 1 (GP 1).* [^{18}F]F$^-$ was loaded onto an anion exchange-cartridge (PS-HCO_3^-, 45 mg sorbent). The cartridge was washed with anhydrous MeCN (4 mL), and [^{18}F]F$^-$ was eluted dropwise with a solution of the respective *N,N,N*-trimethylammonium triflate precursor (12 mg of **4a**/**4b** or 15 mg of **4c**/**4d**) in 1 mL of MeCN/*t*BuOH (1:4) into a vial containing H_2O (35 mL). The cartridge was additionally flushed with MeCN (1 mL), which was collected into the same vial. The resulting solution was passed through an SPE cartridge (Oasis HLB Plus Short), the cartridge was washed with H_2O (5 mL), briefly dried in a steam of argon (1 min), and the labeled product was eluted with MeCN (1 mL).

*Production of [^{18}F]**5a-m**—General Procedure 2 (GP 2).* To [^{18}F]**3e-f** in MeCN (50 μL) was added the respective amine (10 μmol) in MeCN, DMF, or 20% MeCN in 0.2 M borate buffer at pH 8.7 (450 μL). The mixture was stirred at 40−110 °C for 10−20 min as indicated (see Scheme 4), and RCCs were determined by HPLC as described in the general radiochemical section.

*Preparation of [^{18}F]**5p** ([^{18}F]JK-PSMA-15).* [^{18}F]**3e** was synthesized from [^{18}F]F$^-$ (6.9 GBq) according to GP1 and loaded onto an Oasis HLB Plus Short cartridge. The cartridge was washed with 5% acetone (6 mL) and briefly dried in a stream of argon. [^{18}F]**3e** was eluted from the cartridge with MeCN (1.5 mL). The solvent was removed under reduced pressure at 100 °C before a solution of *t*BuO-Glu(O*t*Bu)-CO-Lys(H)-O*t*Bu (10 μmol) in MeCN (500 μL) was added. The vial was equipped with a septum cap and heated under stirring at 60 °C for 15 min. Thereafter, 38% HCl (500 μL) was added and the mixture was stirred for another 15 min at 60 °C. The resulting crude product was purified by semipreparative HPLC [eluent: 20% MeCN (0.1% TFA); flow rate: 8 mL/min; t_R = 8−9 min]. The product fraction was diluted with H_2O to 35 mL and loaded onto an SPE cartridge (Oasis HLB Plus Short). The cartridge was washed with H_2O (10 mL) and [^{18}F]JK-PSMA-15 was eluted with MeOH (1.5 mL). MeOH was removed under reduced pressure in a stream of argon at 60 °C and [^{18}F]JK-PSMA-15 was dissolved in 0.9% NaCl (450 μL) containing sodium ascorbate (4.5 mg) to afford the desired tracer as a solution ready for injection. The average isolated AYs amounted to 16 ± 3% (n = 5), within a total synthesis time of 90 min. The radiochemical purity amounted to >97% and the molar activity to 99 GBq/μmol (for 980 MBq [^{18}F]**5p**).

*Radiosynthesis of [^{18}F]**6a-d** via the Azide Alkyne "Click" Cycloaddition—General Procedure 3 (GP 3).* A solution of [^{18}F]**3g** or [^{18}F]**3h** in MeCN prepared according to GP1 was concentrated under reduced pressure in a stream of argon for 5 min at 80 °C. 10 mM NaOH (0.5 mL) was added to the residue, and the reaction mixture was stirred at 60 °C for 5 min. Then, 100 μL stock solutions of the following reagents were added (in the indicated order). For [^{18}F]**3g**: 0.2 M $CuSO_4$, 0.5 M L-histidine, 1 M sodium ascorbate, and a 0.2 M solution of the respective azide in MeCN or MeOH. For [^{18}F]**3h**: 0.2 M $CuSO_4$, 0.5 M L-histidine, and 1 M sodium ascorbate were added to a 0.2 M solution of the respective alkyne in MeCN or MeOH, and the resulting mixture was added to the solution of the radiolabeled building block. The reaction mixture was stirred at 60 °C for 15 min, cooled to ambient temperature, diluted with H_2O, and analyzed by HPLC as described above.

*Preparation of [^{18}F]**6a**.* [^{18}F]**6a** was synthesized in RCCs of 77 ± 2% (n = 3) according to GP3 by the reaction of [^{18}F]**2g** with benzyl azide (20 μmol in MeCN).

*Preparation of [^{18}F]**6b** ([^{18}F]JK-PSMA-16).* [^{18}F]**3g** was synthesized from [^{18}F]F$^-$ (4.5 GBq) and **4c** (15 mg, 33 μmol) in 1 mL of MeCN/*t*BuOH (1:4) according to GP1. A solution of the crude prosthetic group was diluted with H_2O (35 mL) and loaded onto an SPE cartridge (Oasis HLB Plus Short). The cartridge was washed with 5% acetone (6 mL) and briefly dried in a steam of argon. [^{18}F]**3g** was eluted from the cartridge with MeCN (1.5 mL). The solvent was removed under reduced pressure at 100 °C, and the title radiolabeled compound was prepared according to GP 3 using azide **7** (1.9 mg; 0.2 M in MeOH; for preparation, see Scheme S1 in the Supporting Information). The crude product was purified by semipreparative HPLC [column: Hydro-RP, 250 mm × 10 mm; eluent: 30% MeCN (0.1% TFA); flow rate: 4.7 mL/min; t_R = 9 min]. The product fraction was diluted with H_2O to 35 mL and loaded onto an SPE cartridge (Oasis HLB Plus Short), which was washed with H_2O (10 mL). [^{18}F]JK-PSMA-16 was eluted into a vial with MeOH (1.5 mL), the solvent was removed under reduced pressure in a stream of argon at 60 °C, and the tracer was formulated as described for [^{18}F]JK-PSMA-15. [^{18}F]JK-PSMA-16 was obtained in AYs of 21 ± 3% (n = 3) within a total synthesis time of 90 min. Radiochemical purity was >99%.

*Preparation of [^{18}F]**6c**.* [^{18}F]**6c** was synthesized in RCCs of 88 ± 6% (n = 3) according to GP3 by the reaction of [^{18}F]**2h** with phenylacetylene (1.0 mg, 10 μmol as a 0.2 M solution in MeCN).

*Preparation of [^{18}F]**6d** ([^{18}F]JK-PSMA-18).* [^{18}F]**3h** produced according to GP1 was hydrolyzed to [^{18}F]**2h** according to GP3. The latter was conjugated with **8** (1.9 mg, 5 μmol; as a 0.2 M solution in MeOH). The reaction mixture was cooled to ambient temperature, TFA (10 μL) was added, and the radiolabeled product was isolated by semipreparative HPLC [eluent: 30% MeCN (0.1% TFA); flow rate: 4.7 mL/min; t_R = 8.7 min]. The product fraction was diluted with H_2O (35 mL), and the resulting solution was loaded onto an SPE cartridge (Oasis HLB Plus Short), which was washed with H_2O (10 mL). The purified tracer was eluted with MeOH (1.5 mL), the solvent was removed under reduced pressure in a stream of argon at 60 °C and [^{18}F]JK-PSMA-18 was formulated as described for [^{18}F]JK-PSMA-15. [^{18}F]JK-PSMA-18 was obtained in AYs of 28 ± 4% (n = 3) within a total synthesis time of 90 min. Radiochemical purity was >96%, and the molar activity was determined to be 75 GBq/μmol (for 89 MBq tracer).

Determination of Carrier Content. The amount of non-radioactive carrier was calculated from the peak area in UV−HPLC chromatograms using a UV absorbance/concentration calibration curve. To this end, solutions of the radiolabeled products obtained after HPLC purification were allowed to stand at ambient temperature for at least 24 h, concentrated under reduced pressure, and the

https://doi.org/10.1021/acs.jmedchem.3c01310
J. Med. Chem. 2023, 66, 12629−12644

residues were redissolved in the appropriate HPLC eluents (200 μL). 100 μL of the resulting solution was injected into the HPLC system (20 μL loop, equals 10% of total carrier content). The peak area was determined, and the amount of carrier was calculated according to a calibration curve.

Crystal Data for Compound 4c. Formula: $C_{14}H_{14}F_3N_3O_6S$; formula weight: 409.34 g/mol; crystal system: monoclinic; space group: $P2_1$; unit cell parameters: a = 8.2196(2) Å, b = 13.1737(4) Å, c = 8.8585(2) Å, α = 90°, β = 115.1110(10)°, γ = 90°; temperature of data collection: 100(2) K; value of Z: 2; final values of R_1, wR_2 [$I > 2\sigma(I)$]: 0.0211, 0.0543; goodness-of-fit on F^2: 1.063.

Experimental Animals. Animal experiments were carried out in accordance with the EU directive 2010/63/EU and the German Animal Welfare Act (TierSchG, 2006) and were approved by the regional authorities (Ministry for Environment, Agriculture, Conservation and Consumer Protection of the State of North Rhine-Westphalia, license number 84-02.04.2015.A240). Nine healthy Long Evans rats (females; 237−370 g; three of them were measured twice) were used for this study. Rats were housed in groups of 2−3 in individually ventilated cages (NexGen Ecoflo, Allentown, Inc., Allentown, NJ) under controlled ambient conditions (22 ± 1 °C and 55 ± 5% relative humidity). Food and water were available *ad libitum*.

***In Vivo* PET Experiments.** Prior to PET measurements, animals were anesthetized with isoflurane in O_2/air (3:7) [5% for induction, 1.5−2.5% for maintenance], and a catheter for tracer injection was inserted into the lateral tail vein. Rats were placed on an animal holder (Equipment Vétérinaire Minerve, Esternay, France) and fixed with a tooth bar in a respiratory mask. PET scans in list mode were performed using a Focus 220 micro PET scanner (CTI-Siemens, Germany) with a resolution at the center of field of view of 1.4 mm. Data acquisition started with the injection of the tracer (60.3 ± 5.6 MBq in 500 μL i.v.; for details, see Table S1 in the Supporting Information), continued for 120 min, and followed by a 10 min transmission scan using a ^{57}Co point source. For each tracer (i.e., [^{18}F]JK-PSMA-15, [^{18}F]JK-PSMA-16, and [^{18}F]JK-PSMA-18), three rats were measured. For PSMA blocking, 2-(phosphonomethyl)-pentanedioic acid (2-PMPA; 23 mg/kg; n = 1 per tracer) was added directly to the radiotracer solution. The breathing rate was monitored and maintained at around 60/min by adjusting the isoflurane concentration (1.5−2.5%). Body temperature was maintained at 37 °C by a feedback-controlled system. After the scan, the rat was returned to its home cage.

The emission scans were histogrammed into time frames (2 × 1 min, 2 × 2 min, 6 × 4 min, 18 × 5 min for time-activity curves, 4 × 30 min for signal-to-background ratio, and 2 min × 60 min for display) and fully 3D rebinned (span 3, ring difference 47), followed by OSEM3D/MAP reconstruction with attenuation and decay correction.[46] The resulting voxel sizes were 0.47 × 0.47 × 0.80 mm^3. Postprocessing and image analysis was performed with VINCI 5.21 (Max-Planck-Institute for Metabolism Research, Cologne, Germany). Images were intensity-normalized to injected dose and corrected for body weight (SUV_{bw}). To this end, every frame was divided by injected dose and multiplied by body weight times 100. Time-activity curves were determined for volumes of interest (VOIs) placed in the superior cervical ganglion (SCG), blood (lumen of the left ventricle), liver, and bone (sternum). Tracer accumulation in the same VOIs and background (neck muscles) was also measured for the 60−120 min frame and compared between tracers using one-way ANOVA followed by Dunnett's multiple comparisons test. For SCGs, the signal-to-background ratio and edge contrast were determined, while the resolution was calculated for the first pair of DRGs (described in detail by Zlatopolskiy et al.[10] and in the Supporting information). Data of [^{18}F]JK-PSMA-7 from a previous publication[10] were included for comparison.

■ ASSOCIATED CONTENT

Supporting Information

The Supporting Information is available free of charge at https://pubs.acs.org/doi/10.1021/acs.jmedchem.3c01310.

Synthesis schemes for compounds **7**−**9** and **11**, NMR spectra and HPLC traces of synthesized compounds, calibration curves for determination of carrier content, supplementary methods, and additional results of the *in vivo* experiments (PDF)

Molecular formula strings (CSV)

Accession Codes

The single-crystal structure information of compound **4c** is deposited at the Cambridge Crystallographic Data Centre (CCDC, deposition number: 2205488). The authors will release the atomic coordinates and experimental data upon article publication.

■ AUTHOR INFORMATION

Corresponding Author

Bernd Neumaier − *Forschungszentrum Jülich GmbH, Institute of Neuroscience and Medicine, Nuclear Chemistry (INM-5), 52428 Jülich, Germany; Faculty of Medicine and University Hospital Cologne, Institute of Radiochemistry and Experimental Molecular Imaging, University of Cologne, 50937 Cologne, Germany; Max Planck Institute for Metabolism Research, 50931 Cologne, Germany;* orcid.org/0000-0001-5425-3116; Email: b.neumaier@fz-juelich.de

Authors

Benedikt Gröner − *Forschungszentrum Jülich GmbH, Institute of Neuroscience and Medicine, Nuclear Chemistry (INM-5), 52428 Jülich, Germany; Faculty of Medicine and University Hospital Cologne, Institute of Radiochemistry and Experimental Molecular Imaging, University of Cologne, 50937 Cologne, Germany;* orcid.org/0000-0002-2355-3017

Michael Willmann − *Forschungszentrum Jülich GmbH, Institute of Neuroscience and Medicine, Nuclear Chemistry (INM-5), 52428 Jülich, Germany*

Lisa Donnerstag − *Forschungszentrum Jülich GmbH, Institute of Neuroscience and Medicine, Nuclear Chemistry (INM-5), 52428 Jülich, Germany; Faculty of Medicine and University Hospital Cologne, Institute of Radiochemistry and Experimental Molecular Imaging, University of Cologne, 50937 Cologne, Germany*

Elizaveta A. Urusova − *Forschungszentrum Jülich GmbH, Institute of Neuroscience and Medicine, Nuclear Chemistry (INM-5), 52428 Jülich, Germany; Faculty of Medicine and University Hospital Cologne, Institute of Radiochemistry and Experimental Molecular Imaging, University of Cologne, 50937 Cologne, Germany*

Felix Neumaier − *Forschungszentrum Jülich GmbH, Institute of Neuroscience and Medicine, Nuclear Chemistry (INM-5), 52428 Jülich, Germany; Faculty of Medicine and University Hospital Cologne, Institute of Radiochemistry and Experimental Molecular Imaging, University of Cologne, 50937 Cologne, Germany;* orcid.org/0000-0002-6376-6391

Swen Humpert − *Forschungszentrum Jülich GmbH, Institute of Neuroscience and Medicine, Nuclear Chemistry (INM-5), 52428 Jülich, Germany*

Heike Endepols − *Forschungszentrum Jülich GmbH, Institute of Neuroscience and Medicine, Nuclear Chemistry (INM-5), 52428 Jülich, Germany; Faculty of Medicine and University Hospital Cologne, Institute of Radiochemistry and Experimental Molecular Imaging, University of Cologne, 50937 Cologne, Germany; Faculty of Medicine and University Hospital Cologne, Department of Nuclear Medicine, University of Cologne, 50937 Cologne, Germany*

Boris D. Zlatopolskiy − *Forschungszentrum Jülich GmbH, Institute of Neuroscience and Medicine, Nuclear Chemistry (INM-5), 52428 Jülich, Germany; Faculty of Medicine and University Hospital Cologne, Institute of Radiochemistry and Experimental Molecular Imaging, University of Cologne, 50937 Cologne, Germany; Max Planck Institute for Metabolism Research, 50931 Cologne, Germany;* orcid.org/0000-0001-5818-1260

Complete contact information is available at: https://pubs.acs.org/10.1021/acs.jmedchem.3c01310

Author Contributions

$^{\perp}$B.G. and M.W. contributed equally to this work. The manuscript was written through contributions of all authors. All authors have approved the final version of the manuscript.

Notes

The authors declare no competing financial interest.

■ ACKNOWLEDGMENTS

This work was supported by Deutsche Forschungsgemeinschaft (DFG), grant number ZL 65/4-1.

■ ABBREVIATIONS USED

[^{18}F]AFA, 1-alkylamino-7-[^{18}F]fluoro-8-azaisatoic anhydride; AY, activity yield; [^{18}F]F^{-}, [^{18}F]fluoride; [^{18}F]SFB, *N*-succinimidyl 4-[^{18}F]fluorobenzoate; [^{18}F]FPy-TFP, 2,3,5,6-tetrafluorophenyl 6-[^{18}F]fluoronicotinate; 2-PMPA, 2-(phosphonomethyl)pentanedioic acid; CuAAC, copper-catalyzed alkyne-azide cycloaddition; DRG, cervical dorsal root ganglia; E_{max}, maximum positron energy; EOS, end of synthesis; H, heart; L, liver; PCa, prostate cancer; PET, positron emission tomography; PG, prosthetic group; PSMA, prostate-specific membrane antigen; RCC, radiochemical conversion; RCY, radiochemical yield; SCG, superior cervical ganglion; SG, salivary gland; SJ, shoulder joint; SPE, solid-phase extraction; SUV_{bw}, standardized uptake value (normalized to body weight); *t*BuO-Glu(O*t*Bu)-CO-Lys(H)-O*t*Bu, di-*tert*-butyl {[(*S*)-6-amino-1-(*tert*-butoxy)-1-oxohexan-2-yl]-carbamoyl}-(*S*)-glutamate; VOI, volume of interest

■ REFERENCES

(1) Ametamey, S. M.; Honer, M.; Schubiger, P. A. Molecular Imaging with PET. *Chem. Rev.* **2008**, *108*, 1501−1516.

(2) Afshar-Oromieh, A.; Zechmann, C. M.; Malcher, A.; Eder, M.; Eisenhut, M.; Linhart, H. G.; Holland-Letz, T.; Hadaschik, B. A.; Giesel, F. L.; Debus, J.; Haberkorn, U. Comparison of PET Imaging with a ^{68}Ga-Labelled PSMA Ligand and ^{18}F-Choline-Based PET/CT for the Diagnosis of Recurrent Prostate Cancer. *Eur. J. Nucl. Med. Mol. Imaging* **2014**, *41*, 11−20.

(3) Donswijk, M. L.; van Leeuwen, P. J.; Vegt, E.; Cheung, Z.; Heijmink, S. W. T. P. J.; van der Poel, H. G.; Stokkel, M. P. M. Clinical Impact of PSMA PET/CT in Primary Prostate Cancer Compared to Conventional Nodal and Distant Staging: A Retrospective Single Center Study. *BMC Cancer* **2020**, *20*, No. 723.

(4) Endepols, H.; Morgenroth, A.; Zlatopolskiy, B. D.; Krapf, P.; Zischler, J.; Richarz, R.; Muñoz Vásquez, S.; Neumaier, B.; Mottaghy, F. M. Peripheral Ganglia in Healthy Rats as Target Structures for the Evaluation of PSMA Imaging Agents. *BMC Cancer* **2019**, *19*, No. 633.

(5) Ghosh, A.; Heston, W. D. W. Tumor Target Prostate Specific Membrane Antigen (PSMA) and Its Regulation in Prostate Cancer. *J. Cell. Biochem.* **2004**, *91*, 528−539.

(6) Malik, N.; Machulla, H.-J.; Solbach, C.; Winter, G.; Reske, S. N.; Zlatopolskiy, B. Radiosynthesis of a New PSMA Targeting Ligand ([^{18}F]FPy-DUPA-Pep). *Appl. Radiat. Isot.* **2011**, *69*, 1014−1018.

(7) van der Sar, E. C. A.; van Kalmthout, L. M.; Lam, M. G. E. H. PSMA PET/CT in Primary Prostate Cancer Diagnostics: An Overview of the Literature. *Tijdschr. voor Urol.* **2020**, *10*, 101−108.

(8) Afshar-Oromieh, A.; Haberkorn, U.; Eder, M.; Eisenhut, M.; Zechmann, C. [^{68}Ga]Gallium-Labelled PSMA Ligand as Superior PET Tracer for the Diagnosis of Prostate Cancer: Comparison with ^{18}F-FECH. *Eur. J. Nucl. Med. Mol. Imaging* **2012**, *39*, 1085−1086.

(9) Chen, Y.; Pullambhatla, M.; Foss, C. A.; Byun, Y.; Nimmagadda, S.; Senthamizhchelvan, S.; Sgouros, G.; Mease, R. C.; Pomper, M. G. 2-(3-{1-Carboxy-5-[(6-[^{18}F]Fluoro-Pyridine-3-Carbonyl)- Amino]-Pentyl}-Ureido)-Pentanedioic Acid, [^{18}F]DCFPyL, a PSMA-Based PET Imaging Agent for Prostate Cancer. *Clin. Cancer Res.* **2011**, *17*, 7645−7653.

(10) Zlatopolskiy, B. D.; Endepols, H.; Krapf, P.; Guliyev, M.; Urusova, E. A.; Richarz, R.; Hohberg, M.; Dietlein, M.; Drzezga, A.; Neumaier, B. Discovery of ^{18}F-JK-PSMA-7, a PET Probe for the Detection of Small PSMA-Positive Lesions. *J. Nucl. Med.* **2019**, *60*, 817−823.

(11) Giesel, F. L.; Hadaschik, B.; Cardinale, J.; Radtke, J.; Vinsensia, M.; Lehnert, W.; Kesch, C.; Tolstov, Y.; Singer, S.; Grabe, N.; Duensing, S.; Schäfer, M.; Neels, O. C.; Mier, W.; Haberkorn, U.; Kopka, K.; Kratochwil, C. F-18 Labelled PSMA-1007: Biodistribution, Radiation Dosimetry and Histopathological Validation of Tumor Lesions in Prostate Cancer Patients. *Eur. J. Nucl. Med. Mol. Imaging* **2017**, *44*, 678−688.

(12) Jacobson, O.; Kiesewetter, D. O.; Chen, X. Fluorine-18 Radiochemistry, Labeling Strategies and Synthetic Routes. *Bioconjugate. Chem.* **2015**, *26*, 1−18.

(13) van der Born, D.; Pees, A.; Poot, A. J.; Orru, R. V. A.; Windhorst, A. D.; Vugts, D. J. Fluorine-18 Labelled Building Blocks for PET Tracer Synthesis. *Chem. Soc. Rev.* **2017**, *46*, 4709−4773.

(14) Scroggie, K. R.; Perkins, M. V.; Chalker, J. M. Reaction of [^{18}F]Fluoride at Heteroatoms and Metals for Imaging of Peptides and Proteins by Positron Emission Tomography. *Front. Chem.* **2021**, *9*, No. 687678.

(15) Krishnan, H. S.; Ma, L.; Vasdev, N.; Liang, S. H. ^{18}F-Labeling of Sensitive Biomolecules for Positron Emission Tomography. *Chem. − Eur. J.* **2017**, *23*, 15553−15577.

(16) Vaidyanathan, G.; Bigner, D. D.; Zalutsky, M. R. Fluorine-18-Labeled Monoclonal Antibody Fragments: A Potential Approach for Combining Radioimmunoscintigraphy and Positron Emission Tomography. *J. Nucl. Med.* **1992**, *33*, 1535−1541.

(17) Vaidyanathan, G.; Zalutsky, M. R. Fluorine-18 Labeled Chemotactic Peptides: A Potential Approach for the PET Imaging of Bacterial Infection. *Nucl. Med. Biol.* **1995**, *22*, 759−764.

(18) Vaidyanathan, G.; Zalutsky, M. R. Fluorine-18-Labeled [Nle4,d-Phe7]-α-MSH, an α-Melanocyte Stimulating Hormone Analogue. *Nucl. Med. Biol.* **1997**, *24*, 171−178.

(19) Vaidyanathan, G.; Zalutsky, M. R. Synthesis of N-Succinimidyl 4-[^{18}F]Fluorobenzoate, an Agent for Labeling Proteins and Peptides with ^{18}F. *Nat. Protoc.* **2006**, *1*, 1655−1661.

(20) Olberg, D. E.; Arukwe, J. M.; Grace, D.; Hjelstuen, O. K.; Solbakken, M.; Kindberg, G. M.; Cuthbertson, A. One Step Radiosynthesis of 6-[^{18}F]Fluoronicotinic Acid 2,3,5,6-Tetrafluorophenyl Ester ([^{18}F]F-Py-TFP): A New Prosthetic Group for Efficient Labeling of Biomolecules with Fluorine-18. *J. Med. Chem.* **2010**, *53*, 1732−1740.

(21) Ackermann, U.; Yeoh, S. D.; Sachinidis, J. I.; Poniger, S. S.; Scott, A. M.; Tochon-Danguy, H. J. A Simplified Protocol for the

Automated Production of Succinimidyl 4-[^{18}F]Fluorobenzoate on an IBA Synthera Module. *J. Label. Compd. Radiopharm.* **2011**, *54*, 671−673.
(22) Glaser, M.; Årstad, E.; Luthra, S. K.; Robins, E. G. Two-Step Radiosynthesis of [^{18}F]N-Succinimidyl-4-Fluorobenzoate ([^{18}F]SFB). *J. Label. Compd. Radiopharm.* **2009**, *52*, 327−330.
(23) Kim, H.-K.; Javed, M. R.; Chen, S.; Zettlitz, K. A.; Collins, J.; Wu, A. M.; Kim, C.-J. "C. J.; Michael van Dam, R.; Keng, P. Y. On-Demand Radiosynthesis of N-Succinimidyl-4-[^{18}F]Fluorobenzoate ([^{18}F]SFB) on an Electrowetting-on-Dielectric Microfluidic Chip for ^{18}F-Labeling of Protein. *RSC Adv.* **2019**, *9*, 32175−32183.
(24) Basuli, F.; Zhang, X.; Jagoda, E. M.; Choyke, P. L.; Swenson, R. E. Facile Room Temperature Synthesis of Fluorine-18 Labeled Fluoronicotinic Acid-2,3,5,6-Tetrafluorophenyl Ester without Azeotropic Drying of Fluorine-18. *Nucl. Med. Biol.* **2016**, *43*, 770−772.
(25) Haka, M. S.; Kilbourn, M. R.; Leonard Watkins, G.; Toorongian, S. A. Aryltrimethylammonium Trifluoromethanesulfonates as Precursors to Aryl [^{18}F]Fluorides: Improved Synthesis of [^{18}F]GBR-13119. *J. Label. Compd. Radiopharm.* **1989**, *27*, 823−833.
(26) Didiuk, M. T.; Dow, R. L.; Griffith, D. A. N1-Pyrazolospiroketone Acetyl-CoA Carboxylase Inhibitors. WO2012/042433/A1, 2012.
(27) Richarz, R.; Krapf, P.; Zarrad, F.; Urusova, E. A.; Neumaier, B.; Zlatopolskiy, B. D. Neither Azeotropic Drying, nor Base nor Other Additives: A Minimalist Approach to ^{18}F-Labeling. *Org. Biomol. Chem.* **2014**, *12*, 8094−8099.
(28) Humpert, S.; Hoffmann, C.; Neumaier, F.; Zlatopolskiy, B. D.; Neumaier, B. Validation of Analytical HPLC with Post-Column Injection as a Method for Rapid and Precise Quantification of Radiochemical Yields. *J. Chromatogr. B* **2023**, No. 123847.
(29) Basuli, F.; Zhang, X.; Jagoda, E. M.; Choyke, P. L.; Swenson, R. E. Rapid Synthesis of Maleimide Functionalized Fluorine-18 Labeled Prosthetic Group Using "Radio-Fluorination on the Sep-Pak" Method. *J. Label. Compd. Radiopharm.* **2018**, *61*, 599−605.
(30) Hall, H. K. Correlation of the Base Strengths of Amines1. *J. Am. Chem. Soc.* **1957**, *79*, 5441−5444.
(31) Oregioni, A.; Stieglitz, B.; Kelly, G.; Rittinger, K.; Frenkiel, T. Determination of the PK_a of the N-Terminal Amino Group of Ubiquitin by NMR. *Sci. Rep.* **2017**, *7*, No. 43748.
(32) Morgenroth, A.; Urusova, E. A.; Dinger, C.; Al-Momani, E.; Kull, T.; Glatting, G.; Frauendorf, H.; Jahn, O.; Mottaghy, F. M.; Reske, S. N.; Zlatopolskiy, B. D. New Molecular Markers for Prostate Tumor Imaging: A Study on 2-Methylene Substituted Fatty Acids as New AMACR Inhibitors. *Chem. − Eur. J.* **2011**, *17*, 10144−10150.
(33) Humpert, S.; Omrane, M. A.; Urusova, E. A.; Gremer, L.; Willbold, D.; Endepols, H.; Krasikova, R. N.; Neumaier, B.; Zlatopolskiy, B. D. Rapid ^{18}F-Labeling via Pd-Catalyzed S-Arylation in Aqueous Medium. *Chem. Commun.* **2021**, *57*, 3547−3550.
(34) Krapf, P.; Richarz, R.; Urusova, E. A.; Neumaier, B.; Zlatopolskiy, B. D. Seyferth-Gilbert Homologation as a Route to ^{18}F-Labeled Building Blocks: Preparation of Radiofluorinated Phenylacetylenes and Their Application in PET Chemistry. *Eur. J. Org. Chem.* **2016**, *2016*, 430−433.
(35) Hohberg, M.; Kobe, C.; Krapf, P.; Täger, P.; Hammes, J.; Dietlein, F.; Zlatopolskiy, B. D.; Endepols, H.; Wild, M.; Neubauer, S.; Heidenreich, A.; Neumaier, B.; Drzezga, A.; Dietlein, M. Biodistribution and Radiation Dosimetry of [^{18}F]-JK-PSMA-7 as a Novel Prostate-Specific Membrane Antigen-Specific Ligand for PET/CT Imaging of Prostate Cancer. *EJNMMI Res.* **2019**, *9*, 66.
(36) Carboni, B.; Benalil, A.; Vaultier, M. Aliphatic Amino Azides as Key Building Blocks for Efficient Polyamine Syntheses. *J. Org. Chem.* **1993**, *58*, 3736−3741.
(37) Amyes, T. L.; Jencks, W. P. Concerted Bimolecular Substitution Reactions of Acetal Derivatives of Propionaldehyde and Benzaldehyde. *J. Am. Chem. Soc.* **1989**, *111*, 7900−7909.
(38) Di Carlo, D.; Wester, H.-J. Silicon-Fluoride Acceptor Substituted Radiopharmaceuticals and Precursors Thereof. WO2020/157128/A1, 2020.
(39) Maresca, K. P.; Hillier, S. M.; Femia, F. J.; Keith, D.; Barone, C.; Joyal, J. L.; Zimmerman, C. N.; Kozikowski, A. P.; Barrett, J. A.; Eckelman, W. C.; Babich, J. W. A Series of Halogenated Heterodimeric Inhibitors of Prostate Specific Membrane Antigen (PSMA) as Radiolabeled Probes for Targeting Prostate Cancer. *J. Med. Chem.* **2009**, *52*, 347−357.
(40) Brooke, G. M.; Matthews, R. S.; Harman, M. E.; Hursthouse, M. B. Polyfluorinated Heterocyclic Compounds. Part 29[1]. The Synthesis of 4,5,6,7,8-Pentafluoro-2H-Cyclohepta[b]Furan-2-One and Its Reaction with Sodium Methoxide. *J. Fluorine Chem.* **1991**, *53*, 339−354.
(41) Presolski, S. I.; Hong, V.; Cho, S.-H.; Finn, M. G. Tailored Ligand Acceleration of the Cu-Catalyzed Azide−Alkyne Cycloaddition Reaction: Practical and Mechanistic Implications. *J. Am. Chem. Soc.* **2010**, *132*, 14570−14576.
(42) Bernhart, C.; Bouaboula, M.; Casellas, P.; Jegham, S.; Arigon, J.; Combet, R.; Hilairet, S.; Fraisse, P. Nicotinamide Derivatives, Preparation Thereof And Therapeutic Use Thereof. U.S. Patent US2010/0222319/A1, 2010.
(43) Commercon, A.; Gauzy-Lazo, L.; Hubert, P. Anticancer Derivatives, Preparation Thereof, and Therapeutic Use Thereof. WO2012/014147/A1, 2012.
(44) Herth, M. M.; Ametamey, S.; Antuganov, D.; Bauman, A.; Berndt, M.; Brooks, A. F.; Bormans, G.; Choe, Y. S.; Gillings, N.; Häfeli, U. O.; James, M. L.; Kopka, K.; Kramer, V.; Krasikova, R.; Madsen, J.; Mu, L.; Neumaier, B.; Piel, M.; Rösch, F.; Ross, T.; Schibli, R.; Scott, P. J. H.; Shalgunov, V.; Vasdev, N.; Wadsak, W.; Zeglis, B. M. On the Consensus Nomenclature Rules for Radiopharmaceutical Chemistry − Reconsideration of Radiochemical Conversion. *Nucl. Med. Biol.* **2021**, *93*, 19−21.
(45) Coenen, H. H.; Gee, A. D.; Adam, M.; Antoni, G.; Cutler, C. S.; Fujibayashi, Y.; Jeong, J. M.; Mach, R. H.; Mindt, T. L.; Pike, V. W.; Windhorst, A. D. Consensus Nomenclature Rules for Radiopharmaceutical Chemistry — Setting the Record Straight. *Nucl. Med. Biol.* **2017**, *55*, v−xi.
(46) Qi, J.; Leahy, R. M.; Cherry, S. R.; Chatziioannou, A.; Farquhar, T. H. High-Resolution 3D Bayesian Image Reconstruction Using the MicroPET Small-Animal Scanner. *Phys. Med. Biol.* **1998**, *43*, 1001−1013.

https://doi.org/10.1021/acs.jmedchem.3c01310
J. Med. Chem. 2023, 66, 12629−12644

3.4. Preclinical comparison of known and novel radiofluorinated FAP ligands prepared using different 18F-labeling methods

FAP wird beinahe ausschließlich von Krebs-Assoziierten-Fibroblasten gebildet und ist in etwa 90% der endothelialen Tumore nachweisbar.[114, 115] Aufgrund dieser Eigenschaft eignen sich spezifische FAP-Inhibitoren sehr gut als Leitstrukturen für die Entwicklung von Radioliganden für die PET-Diagnostik. Basierend auf dem FAP-Inhibitor UAMC1110[116, 117] wurden daher verschiedene neue FAP Tracer entwickelt und ihre biologischen Eigenschaften in vitro und in vivo mit den bekannten Tracern Al[^{18}F]F-FAPI-42[118] und 6-[^{18}F]F-FAPI[119] verglichen. 6-[^{18}F]F-FAPI wurde dabei direkt mittels der kupfervermittelten Radiofluorierung mit dem verbesserten Protokoll von Hoffmann et. al. hergestellt,[81] während der neue FAP-Radioligand [^{18}F]AFA-FAPI mittels indirekter Radiofluorierung über die Reaktion mit 1-Methylamino-7-[^{18}F]fluor-8-azaisatosäureanhydrid synthetisiert wurde.[120]

Das Konzept der nachfolgenden Publikation wurde von Prof. Dr. B. D. Zlatopolskiy, C. Hoffmann, B. Gröner und Prof. Dr. B. Neumaier entwickelt. Die organischen Vorläufer- und Referenzverbindungssynthesen wurden von C. Hoffmann, B. Gröner ([^{18}F]AFA-FAPI) und Prof. Dr. B. D. Zlatopolskiy durchgeführt. Optimierungen der Radiosynthesen wurden von C. Hoffmann und B. Gröner (Al[^{18}F]F-FAPI-42, [^{18}F]AFA-FAPI) durchgeführt. Präklinische biologische Untersuchungen wurden von Prof. Dr. H. Endepols, M. Brugger, O. Gokhadze, H. Grüll, und M. Timmer durchgeführt. Der Artikel wurde gemeinschaftlich von C. Hoffmann, B. Gröner, Dr. F. Neumaier, Prof. Dr. B. D. Zlatopolskiy, Prof. Dr. H. Endepols und Prof. Dr. B. Neumaier verfasst.

Preclinical comparison of known and novel radiofluorinated FAP ligands prepared using different ^{18}F-labeling methods

Benedikt Gröner[1,2], Chris Hoffmann[1,2], Heike Endepols[1,2,3], Johannes Lindemeyer[4], Marco Timmer[5], Otari Gokhadze[2], Melanie Brugger[2], Felix Neumaier[1,2], Bernd Neumaier*[1,2], Boris D. Zlatopolskiy[1,2]

[1] *University of Cologne, Faculty of Medicine and University Hospital Cologne, Institute of Radiochemistry and Experimental Molecular Imaging, Kerpener Straße 62, 50937 Cologne, Germany.*

[2] *Forschungszentrum Jülich GmbH, Institute of Neuroscience and Medicine, Nuclear Chemistry (INM-5), Wilhelm-Johnen-Straße, 52428 Jülich, Germany.*

[3] *University of Cologne, Faculty of Medicine and University Hospital Cologne, Department of Nuclear Medicine, Kerpener Straße 62, 50937 Cologne, Germany.*

[4] *University of Cologne, Faculty of Medicine and University Hospital Cologne, Department of Radiology, Kerpener Straße 62, 50937 Cologne, Germany.*

[5] *University of Cologne, Faculty of Medicine and University Hospital Cologne, Center for Neurosurgery, Kerpener Straße 62, 50937 Cologne, Germany.*

* *Corresponding author; e-mail: b.neumaier@fz-juelich.de*

Abstract

Fibroblast activation protein (FAP) is almost exclusively expressed by cancer-associated stromal cells, making it a promising target for positron emission tomography (PET) imaging. While chelator-conjugated FAP inhibitors (FAPIs) labeled with ^{68}Ga or [^{18}F]AlF have been characterized in detail, only a few FAPIs containing a covalent radiolabel have been described to date and their potential advantages are still mostly unknown. To close this gap, the aim of the present work was to compare known and novel radiofluorinated FAPIs prepared using different ^{18}F-labeling methods.

^{18}F-labeled UAMC1110 derivatives were either prepared by direct (6-[^{18}F]F-FAPI) or indirect ([^{18}F]AZA-FAPI) radiofluorination of suitable precursors, or using the [^{18}F]AlF chelation method ([^{18}F]AlF-FAPI-42). The *in vitro* FAP-selectivity of all three probes was compared by cellular uptake assays with WT- and FAP-transfected HT1080 fibrosarcoma cells. In addition, PET imaging in mice inoculated with the two cell lines and rats bearing subcutaneous DSL-6A/C1 or intracerebral U87 tumors was used to identify the most promising candidates for *in vivo* imaging of different tumors.

All radiotracers were prepared in activity yields of 25–57% and with molar activities of 5–170 GBq/µmol. Cellular uptake experiments revealed significantly higher uptake of all three compounds into HT1080-FAP compared to HT1080-WT cells, but [^{18}F]AFA-FAPI suffered from a loss of FAP-selectivity *in vivo*. 6-[^{18}F]F-FAPI and [^{18}F]AlF-FAPI-42 showed comparable FAP-selectivity and tumor uptake in the subcutaneous tumor models, but the latter

tracer exhibited lower hepatobiliary excretion and achieved higher TBRs due to faster clearance from FAP-negative tissues. In contrast, 6-[^{18}F]F-FAPI showed higher tumor uptake, better tumor retention and TBRs comparable to [^{18}F]AlF-FAPI-42 in the intracerebral tumor model.

In conclusion, the chelator-based radioligand [^{18}F]AlF-FAPI-42 was the most suitable tracer for imaging of peripheral tumors, while 6-[^{18}F]F-FAPI showed more favorable properties for brain tumor imaging.

Keywords: FAP, fluorine-18, positron emission tomography, brain tumor imaging, radiopharmaceuticals, FAPI-PET

1 Introduction

Fibroblast activation protein (FAP) is a membrane-bound type II glycoprotein from the S9B oligopeptidase subfamily that acts as proline-selective serine protease[1]. Expression of FAP in most normal adult tissues is low or undetectable and knockout studies suggest that it may be non-essential under physiological conditions[1,2]. However, FAP is strongly overexpressed on cancer-associated fibroblasts (CAFs) or other cellular components of the tumor microenvironment in the vast majority of solid tumors[1,2]. As such, radiolabeled FAP inhibitors (FAPIs) have emerged as a promising new class of pantumoral positron emission tomography (PET) tracers that could be of particular value for cancers unsuitable for [^{18}F]fluorodeoxyglucose ([^{18}F]FDG) imaging[3–5]. Thus, while tumor uptake of these tracers is usually similar to that of [^{18}F]FDG, lower accumulation of radiolabeled FAPIs in non-target tissues results in significantly higher tumor-to-background ratios (TBRs), especially in locations with high physiological [^{18}F]FDG uptake like brain or liver[6,7].

Most radioligands for FAPI-PET imaging have been derived from small molecule inhibitors with a 4-quinolinyl-glycyl-2-cyanopyrrolidine scaffold like UAMC1110, which inhibit FAP with low nanomolar IC_{50} values and very high selectivity over related peptidases[8,9]. For example, ^{68}Ga-labeled FAPIs like [^{68}Ga]FAPI-02[10], [^{68}Ga]FAPI-04[11] and [^{68}Ga]FAPI-46[12] have been developed by coupling the quinoline group in UAMC1110 or its analogs with the radiometal chelator DOTA (**Fig. 1**). These tracers show promising properties, such as rapid and almost complete internalization, very low accumulation in normal tissues and fast clearance from circulation[3,10–12]. However, their practical application is complicated by the relatively short half-live of gallium-68 (68 min), which prevents large-scale batch production and distribution of ^{68}Ga-labeled FAPIs via satellite concepts. In this regard, ^{18}F-labeled FAPIs provide an attractive alternative for FAPI-PET imaging, as the longer half-life of fluorine-18

(110 min) enables their centralized production and distribution to remote imaging centers. In addition to eliminating the need for on-site radiochemistry, the superior decay properties of fluorine-18 compared to gallium-68 (e.g., higher positron yield, lower positron energy) should result in an improved spatial resolution[13]. Accordingly, several ^{18}F-labeled FAP-radioligands like [^{18}F]AlF-FAPI-42[14] or [^{18}F]AlF-FAPI-74[15] have been developed by replacement of the DOTA chelator in existing FAPIs with NOTA for radiolabeling with aluminum [^{18}F]fluoride ([^{18}F]AlF) (**Fig. 1**). Preclinical and clinical studies with these tracers indicate that they exhibit equal or superior imaging properties when compared to ^{68}Ga-labeled radioligands with the same pharmacophore[14–17].

An alternative to chelator-based ^{18}F-labeling methods is the covalent incorporation of ^{18}F, either by direct radiofluorination or through the use of ^{18}F-labeled prosthetic groups (PGs). For example, conjugation of an alkyne-bearing derivative of FAPI-04 with an ^{18}F-labeled glycosyl moiety has been used to prepare the ^{18}F-fluoroglycosylated candidate tracer [^{18F}]FGlc-FAPI[18] (**Fig. 1**). While small-animal PET studies showed higher specific tumor uptake and retention of [^{18}F]FGlc-FAPI compared to [^{68}Ga]FAPI-04, significant hepatobiliary excretion and bone uptake of this tracer have prevented its use for tumor imaging. Likewise, FAP ligands containing a 6-[^{18}F]fluoronicotineamide moiety, such as [^{18}F]FAPI-72 and [^{18}F]FAPI-73 (**Fig. 1**), showed unfavorable biodistribution in preclinical studies[15]. Since factors like molecular size, polar surface area and lipophilicity can strongly affect tissue penetration and passive transfer across the blood-brain barrier (BBB), we and others have also investigated FAPI-PET tracers obtained by direct radiofluorination of UAMC-1110 derivatives to identify promising candidates for, e.g., brain tumor imaging. For example, SuFEx click chemistry was used to prepare the [^{18}F]fluorosulfurylated UAMC-1110 analog [^{18}F]FS-FAPI (**Fig. 1**), but this probe showed insufficient *in vivo* stability for tumor imaging[19]. More recently, a FAPI-PET tracer obtained by introduction of fluorine-18 at the 6-position of the quinoline ring in UAMC-1110 (6-[^{18}F]F-FAPI, **Fig. 1**) has been evaluated in cellular assays and different preclinical tumor models[20,21]. The results demonstrated a promising FAP-selectivity of 6-[^{18}F]F-FAPI and improved tumor uptake and retention compared to [^{68}Ga]FAPI-04 in a subcutaneous tumor model[20,21]. In addition, 6-[^{18}F]F-FAPI proved to be suitable for the visualization of intracranial tumors[21], supporting clinical evidence that FAPI-PET could be applied for the detection of FAP-positive primary or metastatic cerebral lesions[22–28]. However, a direct comparison of 6-[^{18}F]F-FAPI with other ^{18}F-labeled FAPIs or non-FDG radioligands for brain tumor imaging is still lacking.

In the present work, we therefore prepared 6-[^{18}F]F-FAPI by Cu-mediated radiofluorination of the corresponding trimethylstannyl precursor and compared it with the chelator-based probe [^{18}F]AlF-FAPI-42 using cellular uptake studies and PET imaging in different subcutaneous and intracerebral tumor models. In addition, brain tumor accumulation of both FAP-radioligands was compared with that of the established glioma tracer *O*-([^{18}F]fluoroethyl)-L-tyrosine ([^{18}F]FET) and the *in vivo* FAP-specificity of 6-[^{18}F]F-FAPI was studied by blocking and displacement studies. Finally, the hitherto unknown FAP-radioligand 6-([^{18}F]fluoro-2-(methylamino)nicotinamido)propoxy-UAMC1110 ([^{18}F]AFA-FAPI, **Fig. 1**) was prepared by indirect radiofluorination of appropriately modified UAMC1110 with an amine-reactive PG and also evaluated with regard to its *in vitro* and *in vivo* FAP-selectivity.

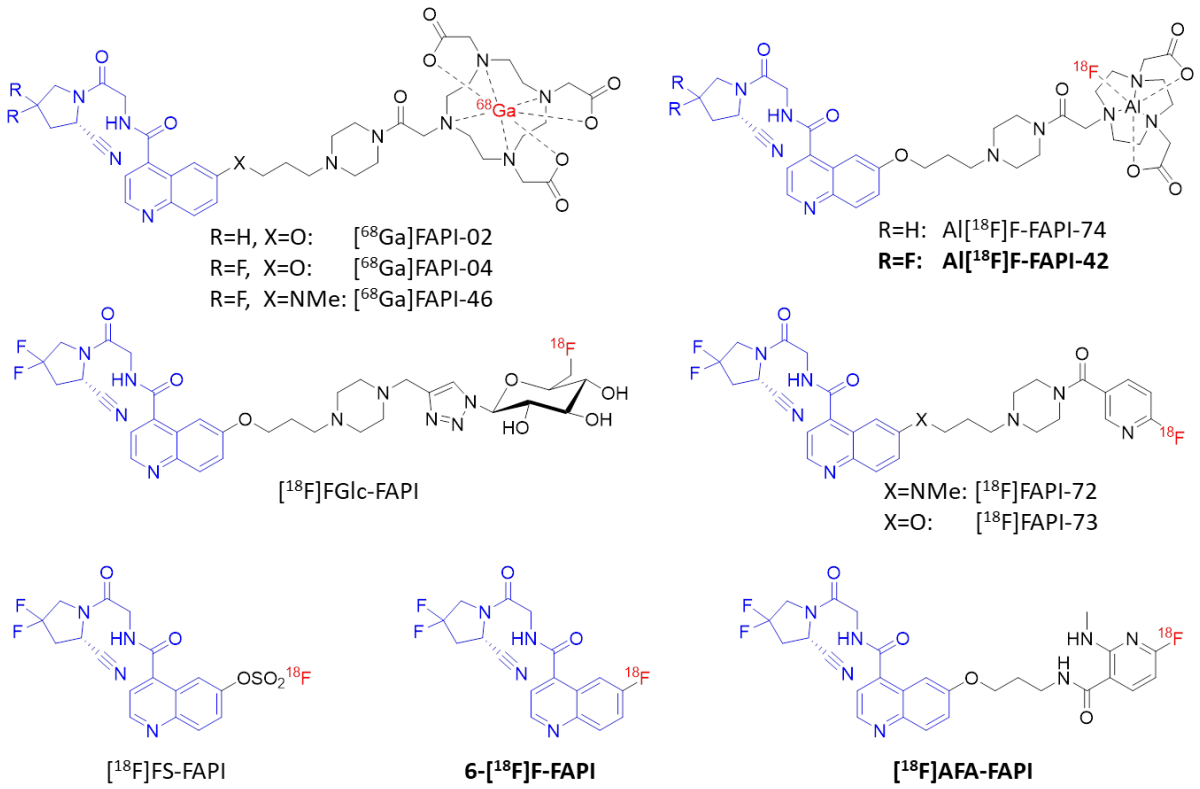

Figure 1: Structure of ^{68}Ga- or ^{18}F-labeled FAP inhibitors (FAPIs) for FAPI-PET imaging, with the common 4-quinolinyl-glycyl-2-cyanopyrrolidine pharmacophore highlighted in blue. Bold names indicate compounds prepared and evaluated in the present study.

2 Results

2.1 Precursor and non-radioactive reference compound preparations

2.1.1 Preparation of the trimethylstannyl precursor for radiosynthesis of 6-[^{18}F]F-FAPI by (alcohol-enhanced) Cu-mediated radiofluorination

The trimethylstannyl precursor for preparation of 6-[^{18}F]F-FAPI by Cu-mediated radiofluorination was obtained as follows (Scheme 1). First, the active ester 6-bromoquinoline-4-carboxylic acid 2,3,5,6-tetrafluorophenyl ester (**2**) was prepared by esterification of the corresponding carboxylic acid (**1**) with 2,3,5,6-tetrafluorophenol, which was followed by Miyaura stannylation with hexamethyl ditin to afford 6-(trimethylstannyl)-quinoline-4-carboxylic acid 2,3,5,6-tetrafluorophenyl ester (**3**). Subsequent coupling of **3** with (*S*)-(2-(2-cyano-4,4-difluoropyrrolidin-1-yl)-2-oxoethyl) ammonium trifluoroacetate (**4**) gave 6-(trimethylstannyl)-quinoline-4-carboxylic acid (*S*)-[2-(2-cyano-4,4-difluoro-pyrrolidin-1-yl-2-oxoethyl]-amide (**5**) in a total yield of 21% over the three steps. The corresponding boronic acid precursor (**6**) was prepared according to the literature[19].

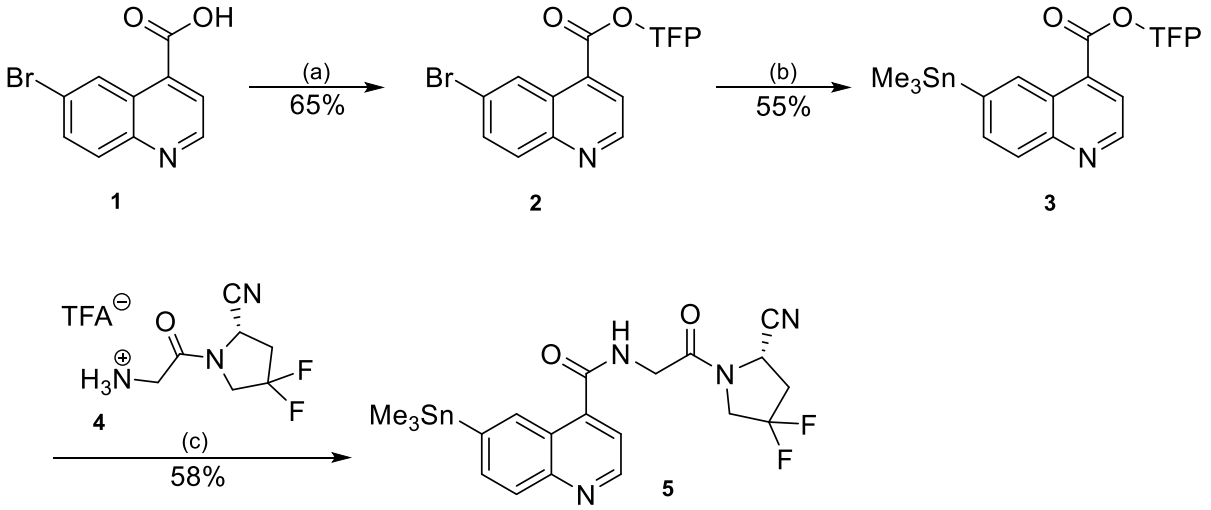

Scheme 1: Preparation of trimethylstannyl radiolabeling precursor **5**. Conditions: (a) $SOCl_2$, rt, 16 h; 2,3,5,6-tetrafluorophenol, Et_3N, DCM, rt, 1.5 h. (b) $Pd(Ph_3P)_4$, LiCl, Sn_2Me_6, toluene, 120 °C, 2.5 h. (c) Et_3N, DCM, rt, 3.5 h. Abbreviations: TFA – trifluoroacetate, TFP – 2,3,5,6-tetrafluorophenyl.

2.1.2 Preparation of aminopropyl-functionalized UAMC1110 for radiosynthesis of [^{18}F]AFA-FAPI by indirect radiofluorination

Aminopropyl-functionalized UAMC1110 for the radiosynthesis of [^{18}F]AFA-FAPI by conjugation with an amine-reactive 1-alkylamino-7-[^{18}F]fluoro-8-azaisatoic anhydride ([^{18}F]AFA) PG was prepared from 6-(3-chloropropoxy)quinoline-4-carboxylic acid (**7**) (Scheme 2). To this end, **7** was converted to the corresponding azide **8**, which was then

esterified with 2,3,4,5-tetrafluorophenol to obtain the active ester 2,3,5,6-tetrafluorophenyl 6-(3-azidopropoxy)quinoline-4-carboxylate (**9**). Subsequent coupling of **9** with (*S*)-(2-(2-cyano-4,4-difluoropyrrolidin-1-yl)-2-oxoethyl) ammonium tosylate (**10**) followed by reduction and Boc-protection of the resulting intermediate **11** gave *tert*-butyl (3-((4-((2-(2-cyano-4,4-difluoropyrrolidin-1-yl)-2-oxoethyl)carbamoyl)quinolin-6-yl)oxy)propyl)carbamate (**12**). Finally, acidic deprotection of **12** afforded the desired aminopropyl-functionalized UAMC1110 derivative **13** in a total yield of 32% over the five steps.

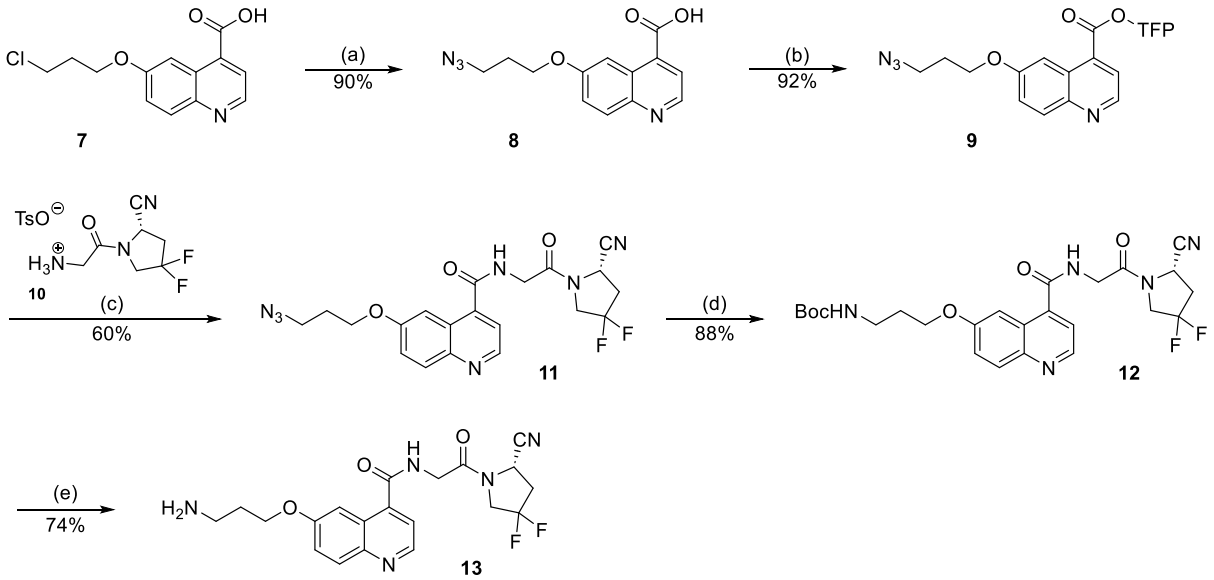

Scheme 2: Synthesis of the aminopropyl-functionalized UAMC1110 derivative **13**. Conditions: (a) NaN_3, NaI, DMF, 2,6-lutidine, 60 °C, 12 h. (b) 2,3,5,6-tetrafluorophenol, EDC, DCM, rt, 2 h. (c) Et_3N, DCM, rt, 14 h. (d) H_2, Pd/C (10%), EtOAc, Boc_2O, MeCN, rt, 80 min. (e) TFA, TIPS, H_2O (95:2.5:2.5), rt, 2h. Abbreviations: TsO – tosylate, TFP – 2,3,5,6-tetrafluorophenyl.

2.1.3 Preparation of (*S*)-*N*-[2-(2-Cyanopyrrolidin-1-yl)-2-oxoethyl]-6-fluoroquinoline-4-carboxamide

The non-radioactive reference compound (*S*)-*N*-[2-(2-cyanopyrrolidin-1-yl)-2-oxoethyl]-6-fluoroquinoline-4-carboxamide (6-F-FAPI) was obtained starting from 6-fluoroquinoline-2,4-dicarboxylic acid (**14**), which was prepared according to the literature[8] (Scheme 3). After decarboxylation of **14**, the resulting monocarboxylic acid **15** was esterified with 2,3,5,6-tetrafluorphenol to give the bench-stable active ester 6-fluoroquinoline-4-2,3,5,6-tetrafluorphenyl carboxylic ester (**16**). Subsequent amidation of **16** with **10** afforded 6-F-FAPI in a yield of 87% over three steps.

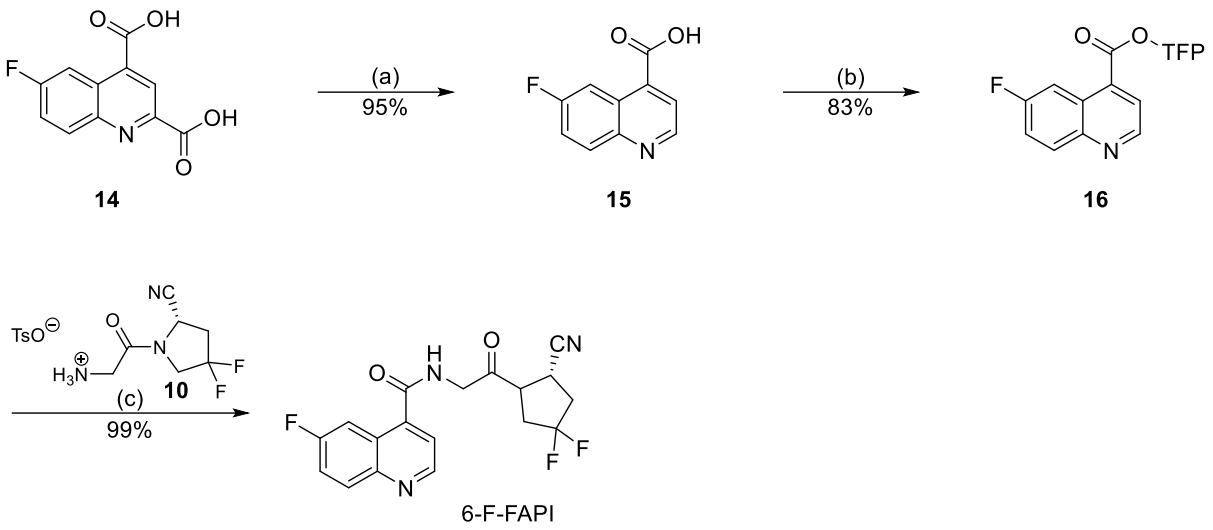

Scheme 3: Synthesis of non-radioactive reference compound 6-F-FAPI. Conditions: (a) $PhNO_2$, 210 °C, 50 min. (b) 2,3,5,6-tetrafluorophenol, EDC, CH_2Cl_2, rt, 16 h. (c) 2,6-lutidine, MeCN, rt, 16 h. Abbreviations: TsO – tosylate, TFP – 2,3,5,6-tetrafluorophenyl.

2.1.4 AFA-FAPI

The reference compound [^{19}F]AFA-FAPI was synthesized), as previously described in literature (Scheme 4).[31] 6-Fluoro-2-(methylamino)nicotinic acid was transformed to the respective acid chloride **17** in thionyl chloride and was directly conjugated with the amine **13** to give AFA-FAPI in 48% yield over two steps.

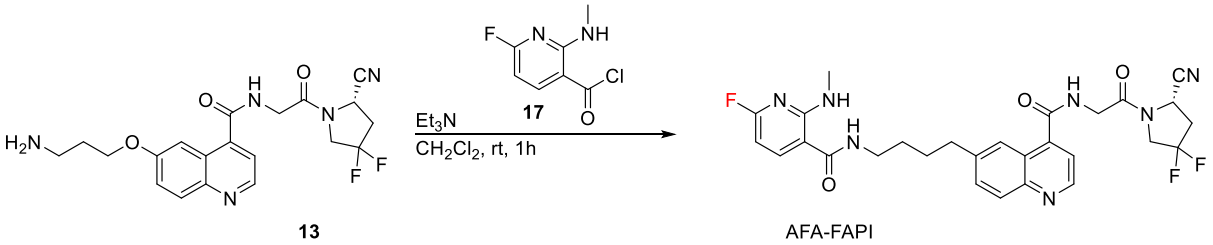

Scheme 4: Synthesis of non-radioactive reference compound AFA-FAPI. Conditions: i. thionyl chloride, 80 °C, 2 h, ii. 13, Et_3N, CH_2Cl_2, rt, 1 h.

2.2 Radiotracer syntheses

Radiosynthesis of [^{18}F]AlF-FAPI-42

The radiosynthesis of [^{18}F]AlF-FAPI-42 was carried out according to literature.[44]

Radiosynthesis of 6-[^{18}F]F-FAPI by Cu-mediated radiofluorination

The radiosynthesis of 6-[^{18}F]F-FAPI was initially attempted using an optimized protocol for "alcohol-enhanced" Cu-mediated radiofluorination of the boronic acid precursor **6**. To this end, aqueous [^{18}F]fluoride ([^{18}F]F$^-$) was trapped on an anion exchange cartridge, which was washed with anhydrous MeOH and dried with air. The [^{18}F]F$^-$ was then eluted with a solution of

Et_4NOTf (1 mg, 4 µmol) in *n*BuOH directly into a solution of the copper(II) mediator and precursor **6** (10 µmol of each) in DMI (800 µL). The reaction mixture was heated at 110 °C for 10 min to afford crude 6-[^{18}F]F-FAPI and the radiochemical conversions (RCCs) were determined by HPLC with post-column injection[29]. However, radiofluorination of the boronic acid precursor with either $Cu(4\text{-}PhPy)_4(ClO_4)_2$ or $Cu(3,4\text{-}Me_2Py)_4(OTf)_2$ as Cu mediators gave unsatisfactory RCCs of 15±1% or 17±3% (n=3), respectively (data not shown). As this indicated that the boronic acid leaving group is not suitable for efficient radiolabeling of the quinoline motif with this protocol, we switched to a precursor with $SnMe_3$ leaving group and used the optimized protocol for radiofluorination of stannyl precursors from our previous work[30] (Scheme 5).

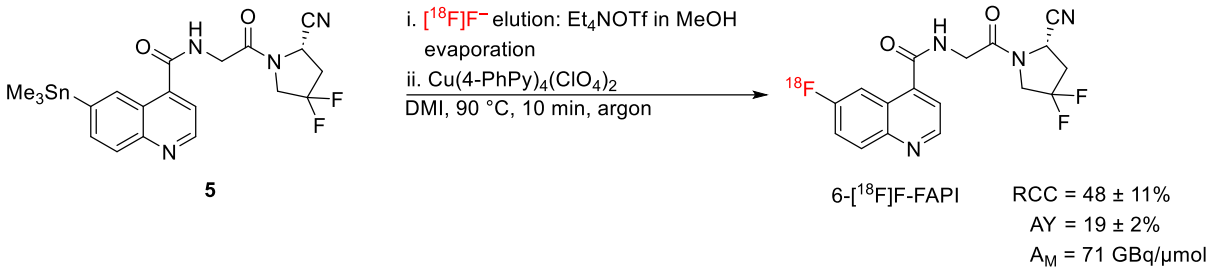

Scheme 5: Radiosynthesis of 6-[^{18}F]F-FAPI by an optimized protocol for Cu-mediated radiofluorination. Conditions: Elution of [^{18}F]F$^-$ with Et_4NOTf (1 mg, 4 µmol) in MeOH (500 µL) followed by evaporation at 80 °C under reduced pressure in a stream of argon within 3 min; the residue was taken up into a solution of $Cu(4\text{-}PhPy)_4(ClO_4)_2$ and **5** (10 µmol of each) in DMI (800 µL) and the mixture was heated at 90 °C for 10 min under argon.

Accordingly, after elution of [^{18}F]F$^-$ from the QMA cartridge with a solution of Et_4NOTf (1 mg, 4 µmol) in MeOH (500 µL), the MeOH was evaporated at 60 °C under reduced pressure in a stream of argon. The residue was taken up into a solution of $Cu(4\text{-}PhPy)_4(ClO_4)_2$ and precursor **5** (10 µmol of each) in DMI (800 µL), and the reaction mixture was heated at 90 °C for 10 min to afford crude 6-[^{18}F]F-FAPI with an RCC of 48±11% (n=6). The reaction mixture was diluted with H_2O (15 mL) and the crude product was trapped on a reversed phase cartridge, washed with H_2O (5 mL) and eluted with MeCN (500 µL). Following dilution with H_2O (1 mL) and purification by preparative HPLC, 6-[^{18}F]F-FAPI was obtained in activity yields (AYs) of 19±2% and radiochemical purities (RCPs) of ≥99%. The molar activity (A_m) amounted to 71 GBq/µmol for 1.1 GBq 6-[^{18}F]F-FAPI (from 5.9 GBq [^{18}F]F$^-$).

2.2.1 Radiosynthesis of [^{18}F]AFA-FAPI by indirect radiofluorination

The radiosynthesis of [^{18}F]AFA-FAPI was performed according to a protocol for indirect radiofluorination with amine-reactive [^{18}F]AFAs recently introduced by our group[31] (Scheme 6). After evaporation of the solvent at 60 °C under reduced pressure in a stream of argon, the

aminopropyl-functionalized UAMC1110 derivative **13** (10 µmol) in DMF (500 µL) was added and the mixture was heated at 110 °C for 15 minutes. The crude [^{18}F]AFA-FAPI thus obtained was purified by preparative HPLC, trapped on an SPE cartridge and eluted with EtOH. After removal of the solvent at 80 °C in a stream of argon, the product was formulated in isotonic saline solution. [^{18}F]AFA-FAPI was obtained in AYs of 22±5 % and RCPs of >97% after 70 minutes. The A_m amounted to 170 GBq/µmol for 770 MBq [^{18}F]AFA-FAPI (from 3.5 GBq [^{18}F]F$^-$).

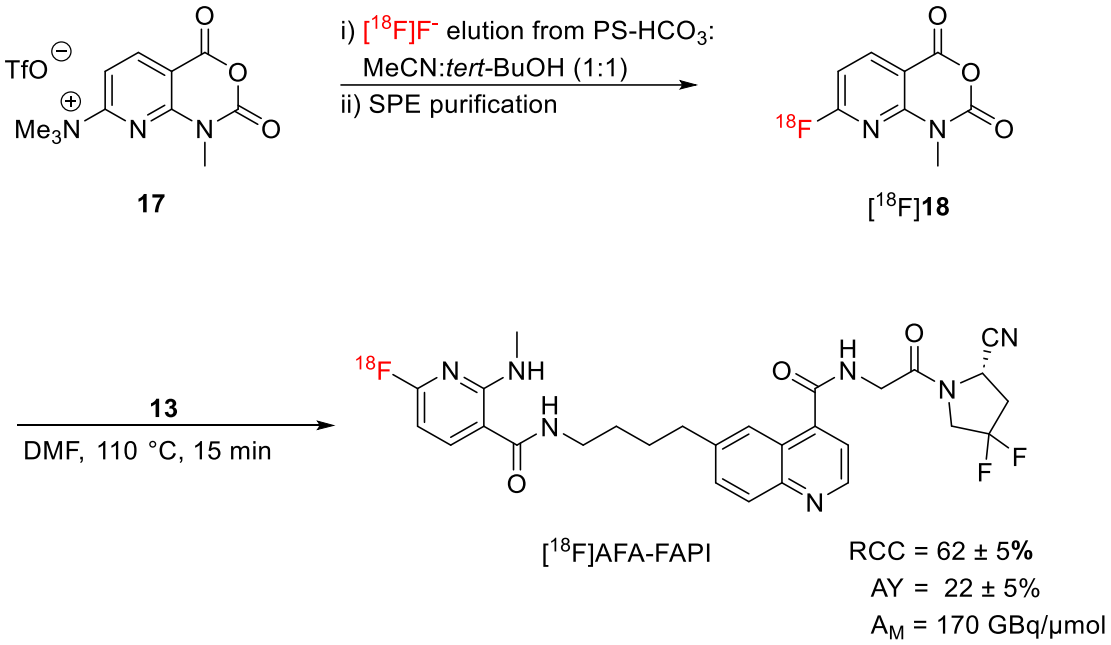

Scheme 6: Radiosynthesis of [^{18}F]AFA-FAPI by indirect radiofluorination of **13** with 1-methylamino-7-[^{18}F]fluoro-8-azaisatoic anhydride ([^{18}F]**18**) as amine-reactive prosthetic group. Conditions: Elution of [^{18}F]F$^-$ with **17** (12 mg, 31 µmol) in MeCN/*t*BuOH (1:1, 1 mL) followed by SPE extraction and evaporation at 60 °C under reduced pressure in a stream of argon within 3 min; the residue was taken up into a solution of **12** (10 µmol) in DMF (500 µL) and the mixture was heated at 110 °C for 15 min. Abbreviations: TfO – trifluoromethylsulfonate, SPE – solid phase extraction.

2.3 Biological evaluation

2.3.1 Cell uptake studies

To compare the FAP-selectivity of 6-[^{18}F]F-FAPI, [^{18}F]AFA-FAPI and [^{18}F]AlF-FAPI-42, cellular uptake studies were performed by incubating FAP-transfected (HT1080-FAP) and non-transfected (HT1080-WT) human fibrosarcoma cells with the different radiotracers for 1 h. As summarized in Figure 2, all three tracers showed significantly higher uptake by HT1080-FAP compared to HT1080-WT cells, although absolute cellular uptake as well as the degree of FAP-selectivity were variable. Thus, when compared to the other tracers, [^{18}F]AFA-FAPI exhibited the highest uptake by HT1080-WT cells (0.64±0.30%) and the lowest uptake by HT1080-FAP

cells (3.54±1.26%) (Fig. 2A), which resulted in a relatively low FAP/WT ratio of 5±2 (Fig. 2B). 6-[^{18}F]F-FAPI showed roughly two-fold lower uptake by HT1080-WT cells (0.3±0.2%) and three-fold higher uptake by HT1080-FAP cells (9.4±3.3%), as reflected in a six-fold higher FAP/WT ratio of 29±10 (Fig. 2B). Finally, [^{18}F]AlF-FAPI-42 showed almost no uptake by HT1080-WT cells (0.03±0.01%) and the highest uptake by HT1080-FAP cells (12.34±0.25%), so that the FAP/WT ratio for this probe amounted to 414±8 and was significantly higher than that for the two other probes (Fig. 2B). Separation of the membrane-bound and cytoplasmic fractions after incubation of cells with 6-[^{18}F]F-FAPI demonstrated that approximately half of the cell-associated radioactivity in HT1080-FAP cells was internalized, while most of the cell-associated radioactivity in HT1080-WT cells (>85%) was membrane-bound (Fig. 2C).

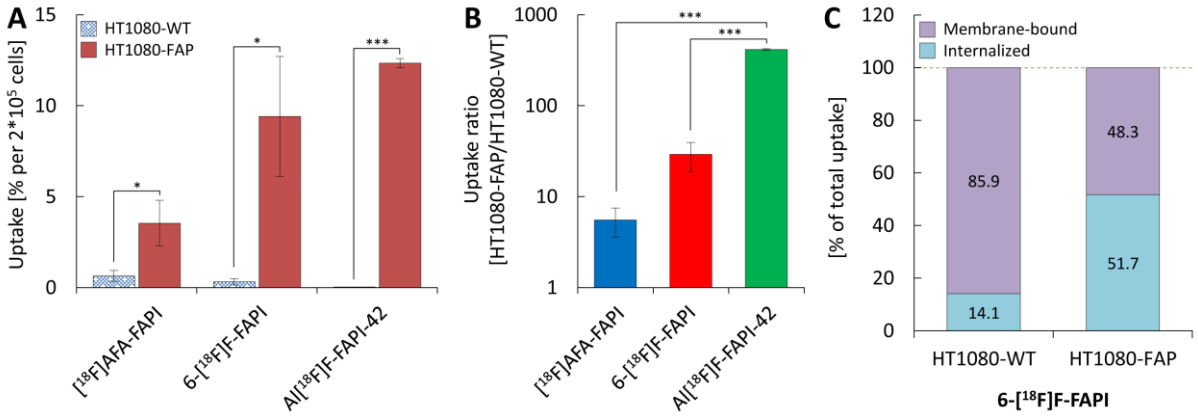

Figure 2: *In vitro* uptake of FAP-radioligands by wildtype (HT1080-WT) and FAP-transfected (HT1080-FAP) human fibrosarcoma cells. (A) Comparison of absolute cellular uptake by HT1080-WT and HT1080-FAP cells quantified after incubation with the different probes for 60 min and expressed as the percentage of total activity added per 2×10^5 cells (n=3-4 per tracer). (B) FAP-selectivity of the probes determined as the ratio between cellular uptake by HT1080-FAP and HT1080-WT cells after 60 min (same data as in A). Note that the y-axis is shown on a log scale to facilitate comparison of the uptake ratios for the different probes. (C) Comparison of membrane-bound and internalized radioactivity after incubation of cells with 6-[^{18}F]F-FAPI for 60 min (n=1). Statistically significant differences between the groups in A and B were identified by two-tailed t-tests (A) or Welch's ANOVA with Games-Howell post-hoc test (B), respectively, and are indicated by asterisks (*, $p<0.05$, ***, $p<0.001$).

2.3.2 Subcutaneous HT1080-WT and HT1080-FAP xenograft mouse model

Next, the biodistribution of the three FAP-radioligands was evaluated in HT1080-FAP or HT1080-WT tumor-bearing mice. As illustrated in Figure 3A & B, both [^{18}F]AlF-FAPI-42 and 6-[^{18}F]F-FAPI showed pronounced accumulation in the FAP-positive HT1080-FAP tumors and very little washout. The uptake of [^{18}F]AlF-FAPI-42 peaked at 20 min p.i. (SUV_{bw} of 61), while 6-[^{18}F]F-FAPI reached a plateau of high mean uptake values between 32 and 68 min p.i. (SUV_{bw} values of 76–78). For both tracers, uptake into HT1080-FAP tumors after the initial 30 min was significantly higher than uptake into FAP-negative HT1080-WT tumors. The uptake ratio

(HT1080-FAP/HT1080-WT) was higher for 6-[^{18}F]F-FAPI during the first hour p.i., and higher for [^{18}F]AlF-FAPI-42 during the second hour p.i. (Table 1).

Table 1: Comparison of tracer uptake between subcutaneous FAP-positive (HT1080-FAP) and FAP-negative (HT1080-WT) tumors in mice.

Tracer	**SUV_{bw}**	**SUV_{bw}**	**Ratio**	**Significance[a]**
	HT1080-FAP	**HT1080-WT**		
[^{18}F]AlF-FAPI-42	n=4	n=5		F(1,7)=11.2; p=0.0123
0-30 min	47.6 ± 18.6	40.2 ± 14.0	1.2	p=0.8758
30-60 min	56.9 ± 19.0	28.2 ± 8.1	2.0	p=0.0108
60-90 min	52.7 ± 18.0	17.9 ± 5.3	3.0	p=0.0017
90-120 min	48.6 ± 16.6	12.5 ± 4.7	3.9	p=0.0011
6-[^{18}F]F-FAPI	n=5	n=3		F(1,6)=25.8; p=0.0023
0-30 min	50.9 ± 12.8	28.3 ± 6.4	1.8	p=0.0776
30-60 min	77.0 ± 15.3	33.7 ± 6.0	2.3	p=0.0003
60-90 min	73.7 ± 16.9	27.6 ± 3.1	2.7	p=0.0001
90-120 min	66.8 ± 16.0	23.4 ± 3.0	3.0	p=0.0003
[^{18}F]AFA-FAPI	n=4	n=4		F(1,6)=0.27; p=0.6198
0-30 min	50.1 ± 10.2	57.0 ± 7.8	0.9	n.s.
30-60 min	40.1 ± 15.4	39.3 ± 3.6	1.0	n.s.
60-90 min	24.4 ± 11.6	24.8 ± 4.0	1.0	n.s.
90-120 min	13.2 ± 9.1	16.8 ± 4.8	0.8	n.s.

[a] Shown are results of two-way ANOVA, factor "tumor type".

Although 6-[^{18}F]F-FAPI showed a higher mean uptake into HT1080-FAP tumors than [^{18}F]AlF-FAPI-42, the TBR of the former tracer was lower. Thus, due to fast washout from FAP-negative tissues (Suppl. Fig. XX [backgroud] B), very high TBRs of 12–14 were achieved with [^{18}F]AlF-FAPI-42 during the second hour p.i. Since washout of 6-[^{18}F]F-FAPI from FAP-negative tissues was slower, the TBRs for this tracer did not exceed 5, although they showed a steady increase during the 120 min uptake period as well. For [^{18}F]AFA-FAPI, there was no difference in tracer uptake between FAP-positive and FAP-negative tumors and the time-activity curves (TACs) for both tumors (Figure 3B) closely resembled the background TAC for 6-[^{18}F]F-FAPI (i.e. high initial uptake followed by washout).

All tested tracers were eliminated by renal and hepatobiliary excretion. Accumulation in the gall bladder and intestine was highest for 6-[^{18}F]F-FAPI followed by [^{18}F]AlF-FAPI-42 (Figure 3C). [^{18}F]AFA-FAPI showed the lowest biliary excretion. Retention in the liver was highest for 6-[^{18}F]F-FAPI (Figure 3C).

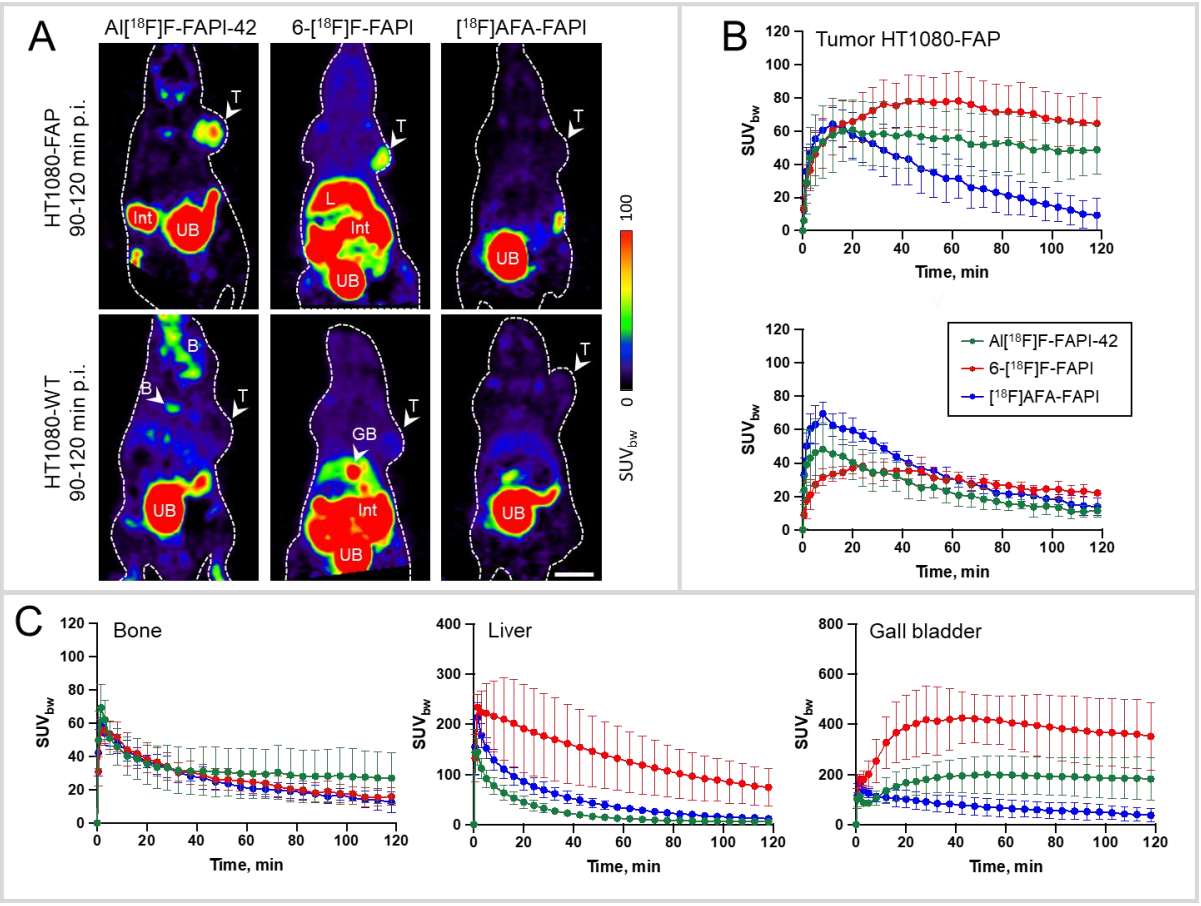

Figure 3: Comparison of FAP ligands in the subcutaneous HT1080 tumor mouse model. (A) Representative summed PET images (horizontal sections) of mice implanted with FAP-positive HT1080-FAP (top row) or FAP-negative HT1080-WT (bottom row) tumors for the uptake period 90-120 min p.i. The dashed line indicates the mouse outline, while the arrows indicate the location of the subcutaneous tumors. (B) Time-activity-curves (mean ± standard deviation) for the different tracers in HT1080-FAP (top row) or HT1080-WT (bottom row) tumors. (C) Time-activity-curves for the different tracers in bone, liver and gall-bladder. n=3–5 per tracer, see Tab. 1. Scale bar in A: 10 mm. Abbreviations: B – bone, GB – gall bladder, Int – intestine, L – liver, T – tumor, UB – urinary bladder.

Subcutaneous DSL allograft rat model

The performance of 6-[^{18}F]F-FAPI as the more promising FAP radioligand with a covalent radiolabel was further compared with that of [^{18}F]AlF-FAPI-42 in rats bearing subcutaneous DSL-6A/C1 tumors, a model with physiological FAP expression in stromal CAFs[32,33]. Compared to the HT1080-FAP tumors in the mouse model, both tracers showed more than two-fold higher absolute tumor uptake in this rat model (Figure 4A). However, as already observed in the mouse model, the tumoral TACs for both tracers were almost identical and washout of 6-[^{18}F]F-FAPI from FAP-negative tissues was slower, leading to considerably higher tumor-to-background ratios for [^{18}F]AlF-FAPI-42 (Figure 4B).

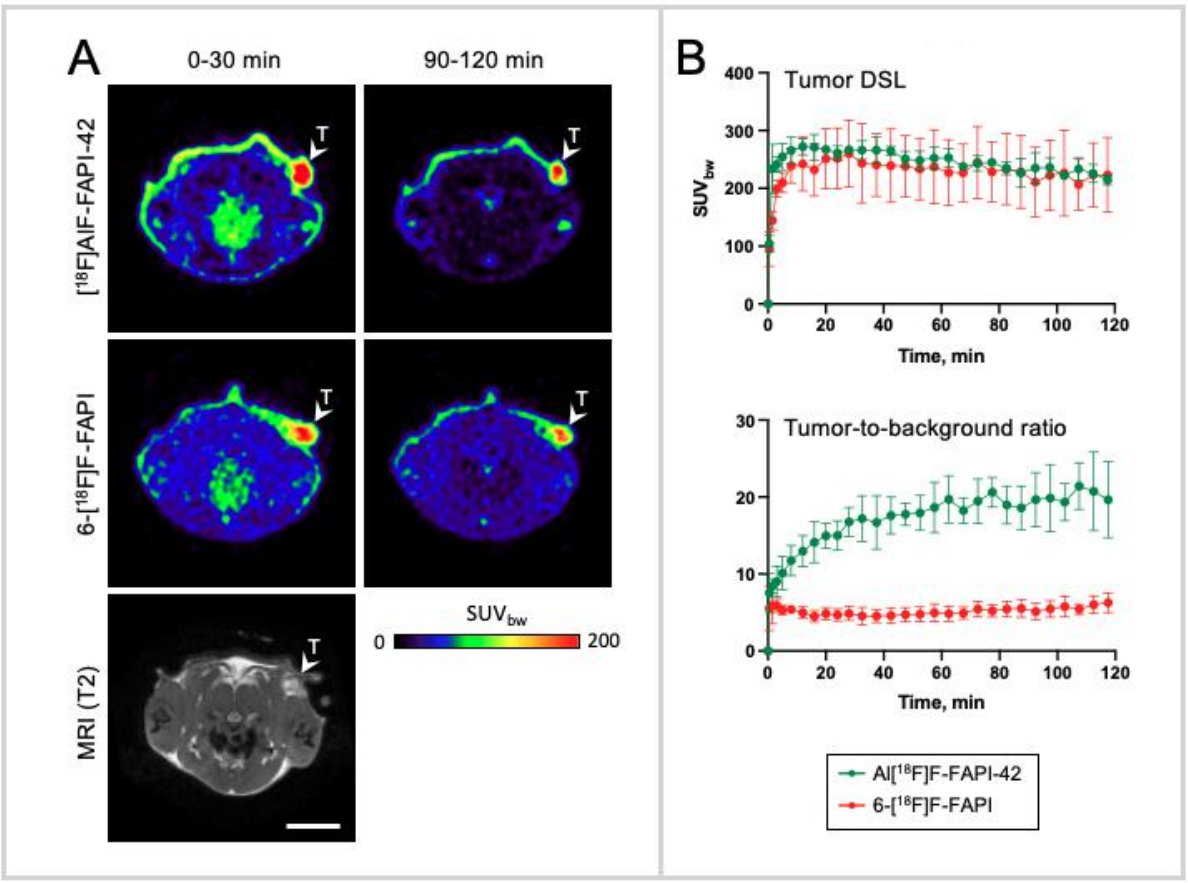

Figure 4: Comparison of [^{18}F]AlF-FAPI-42 and 6-[^{18}F]F-FAPI in the subcutaneous DSL-6A/C1 tumor rat model. (A) Representative summed PET images (transverse sections) obtained with the two tracers in the same rat (measured on different days) for the uptake periods 0–30 min p.i. and 90–1l0 min p.i. (B) Time-activity-curves for the tumor (top) and changes in the tumor-to-background ratio over time (bottom). n=4 per tracer. Scale bar in A: 15 mm. Abbreviation: T - tumor.

Orthotopic U87 glioma xenograft rat model

As previous pilot studies with [^{68}Ga]FAPI-02 and -04 have yielded promising results in glioblastoma patients[22,23], we also compared 6-[^{18}F]F-FAPI and [^{18}F]AlF-FAPI-42 with the established glioma tracer [^{18}F]FET in an orthotopic glioma rat model (Figure 5). Although [^{18}F]FET showed a higher absolute tumor uptake, the two FAP-targeting tracers exhibited much lower background uptake in healthy brain tissue (Figure 5A), which resulted in higher TBRs for both 6-[^{18}F]F-FAPI and [^{18}F]AlF-FAPI-42 compared to [^{18}F]FET (Figure 5B). In addition, while accumulation of 6-[^{18}F]F-FAPI and [^{18}F]AlF-FAPI-42 was restricted to the T2-delineated lesion and most pronounced in the core of the tumor, [^{18}F]FET showed a more diffuse accumulation pattern that appeared to partly extended into the peritumoral brain zone (Figure 5A). When comparing the two FAP-targeting tracers, absolute tumor uptake was higher and more persistent for 6-[^{18}F]F-FAPI. Moreover, and in contrast to the results in the subcutaneous DSL model, there was no significant difference between the TBRs for 6-[^{18}F]F-FAPI and [^{18}F]AlF-FAPI-42 (Figure 5B).

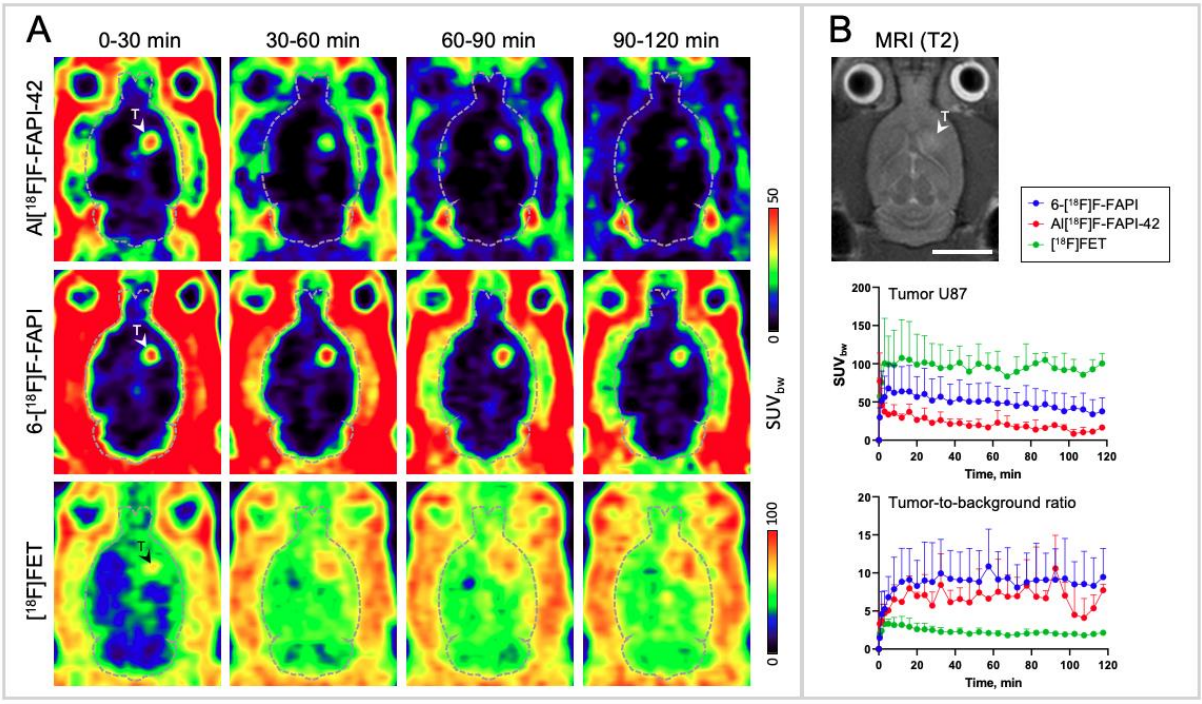

Figure 5: Comparison of [^{18}F]AlF-FAPI-42, 6-[^{18}F]F-FAPI and [^{18}F]FET in the orthotopic U87 glioma rat model. (A) Representative summed PET images (horizontal sections) for the indicated uptake periods obtained in the same rat with the three tracers. (B) T2-weighted MRI of the same rat, showing the location of the intracerebral tumor (top). Also shown are time-activity-curves (n=3 per tracer) for the tumor (middle) and changes in the tumor-to-background ratio (n=3) over time (bottom). Scale bar in B: 10 mm. Abbreviation: T - tumor.

Finally, since contrast-enhanced MRI (Figure 6A, T1+CA) indicated extensive BBB disruption within the T2-delineated lesion (Fig. 6A, T2), we performed blocking and displacement experiments to confirm that accumulation of 6-[^{18}F]F-FAPI in the intracerebral tumors was due to FAP-specific binding. As illustrated in Figure 6A, co-injection of 6-[^{18}F]F-FAPI with an excess of the FAP-selective ligand UAMC1110 (5 mg/kg) reduced tumoral tracer uptake by approximately 70%. Likewise, administration of UAMC1110 (5 mg/kg) 60 min after tracer injection produced a rapid decrease of tumoral tracer accumulation by approximately 50% within 20 min and 68% within 60 min (Fig. 6B).

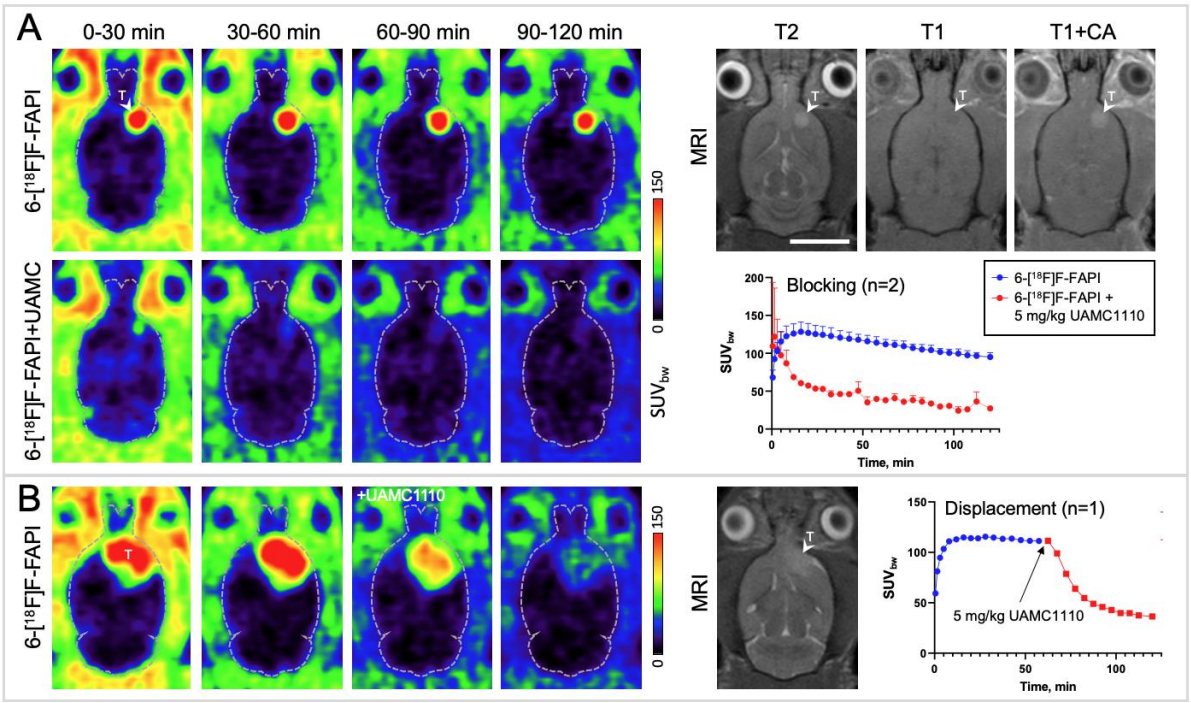

Figure 6: Blocking and displacement of 6-[^{18}F]F-FAPI accumulation in the orthotopic U87 glioma rat model. (A) Representative summed PET images (horizontal sections) for the indicated uptake periods obtained in the same rat without (upper row) and with co-injection of 5 mg/kg UAMC1110 (lower row). Also shown on the right are T2-weighted (left), T1-weighted (middle) and contrast-enhanced T1-weigthed MRI images of the same rat and mean time-activity-curves for the tumor (n=2). (B) Summed PET images and corresponding T2-weigthed MRI of a rat injected with UAMC1110 (5 mg/kg) 60 min after tracer injection. Also shown is the time-activity-curve for the tumor (n=1). Scale bar in A: 10 mm. Abbreviations: CA - contrast agent, T - tumor.

3 Discussion

Although a number of chelator-based ^{68}Ga- or [^{18}F]AlF-labeled FAP-radioligands derived from UAMC1110 or related compounds have been described and evaluated in detail, there is still a lack of data on tracer candidates bearing a covalent ^{18}F-label. Since such compounds could have pharmacokinetic advantages and a more favorable biodistribution profile for certain applications (e.g., brain tumor imaging), the present study focused on two ^{18}F-labeled UAMC1110 derivatives prepared by direct or indirect radiofluorination and their comparison with [^{18}F]AlF-FAPI-42 as chelator-based reference tracer. Under optimized conditions, the two covalently labeled radiotracer candidates could be prepared in AYs of 22–57% and with molar activities of 5–170 GBq/µmol using either Cu-mediated radiofluorination of the corresponding trimethylstannyl precursor (6-[^{18}F]F-FAPI), or indirect radiofluorination of aminopropyl-functionalized UAMC1110 with an amine-reactive [^{18}F]AFA PG ([^{18}F]AFA-FAPI), respectively.

A first analysis of the *in vitro* properties with human fibrosarcoma cells revealed significantly higher uptake of all three radiotracers into FAP-transfected (HT1080-FAP) compared to wildtype (HT1080-WT) cells. However, absolute uptake of the probes by HT1080-FAP cells as well as their exact FAP-selectivity showed considerable differences, with [^{18}F]AFA-FAPI exhibiting the worst and [^{18}F]AlF-FAPI-42 the best *in vitro* performance.

In addition, *in vivo* PET imaging in mice bearing subcutaneous HT1080-FAP or HT1080-WT tumors demonstrated a lack of FAP-specific tumor accumulation for [^{18}F]AFA-FAPI. Comparable results have previously been reported for structurally similar FAP-radioligands labeled with a 6-[^{18}F]fluoronicotineamide moiety[15], suggesting that indirect radiofluorination of UAMC1110 derivatives with ^{18}F-labeled heteroaromatic building blocks may not be an optimal strategy for development of FAPI-PET tracers.

In contrast, 6-[^{18}F]F-FAPI exhibited a promising *in vivo* FAP-specificity in the subcutaneous HT1080 tumor model, as reflected in significantly higher uptake into FAP-expressing compared to WT tumors. In addition, 6-[^{18}F]F-FAPI showed good tumor retention and low uptake into FAP-negative background tissues, resulting in TBRs of around 5 in both, mice bearing subcutaneous HT1080-FAP tumors and rats bearing subcutaneous DSL-6A/C1 tumors. However, while absolute tumor uptake of 6-[^{18}F]F-FAPI in the subcutaneous tumor models was comparable to or even somewhat higher than that of [^{18}F]AlF-FAPI-42, the latter showed faster clearance from FAP-negative background tissues, so that much higher TBRs (up to 20) were achieved with this radioligand. Additionally, 6-[^{18}F]F-FAPI exhibited more pronounced hepatobiliary excretion, which could hamper its use for detection of abdominal tumors. Taken together, these findings confirm and extent the results of previous studies with 6-[^{18}F]F-FAPI, which observed tumor-to-muscle ratios of 4-8 in different subcutaneous tumor models and predominant hepatobiliary excretion of the radiotracer[20,21]. In addition, the direct comparison of 6-[^{18}F]F-FAPI with [^{18}F]AlF-FAPI-42 performed in the present work demonstrates that the latter tracer is superior for high-contrast visualization of peripheral tumors in preclinical models. Nevertheless, given its comparable or even higher absolute tumor uptake, 6-[^{18}F]F-FAPI could represent a promising starting point for development of candidates with improved pharmacokinetic properties. For example, even though difluoro substitution of the cyanopyrrolidine ring has been shown to slightly improve the FAP-affinity of inhibitors with a 4-quinolinyl-glycyl-2-cyanopyrrolidine scaffold[9], previous studies with chelator-based FAP-radioligands indicate that it can also increase hepatobiliary excretion as well as uptake and retention by FAP-negative tissues[11,15]. Accordingly, 6-[^{18}F]F-FAPI analogs lacking the

difluoro-substituents could potentially show accelerated clearance from non-target tissues and a more favorable excretion profile for imaging of abdominal tumors.

Apart from its usefulness for imaging peripheral tumors, FAPI-PET represents a promising approach for detection and staging of brain tumors like gliomas. Thus, brain tumor imaging with the standard-of-care radiotracer [^{18}F]FDG is often hampered by high physiological tracer uptake in the brain, and several recent case reports and pilot studies indicate that FAPI-PET imaging may be superior in detecting small primary or metastatic cerebral lesions[22–28]. In addition, 6-[^{18}F]F-FAPI has been demonstrated to visualize intracranial tumors in an orthotopic tumor model[21], but a direct comparison with other ^{18}F-labeled FAPIs or non-FDG radioligands for brain tumor imaging was so far still lacking. As such, the present study also compared the performance of 6-[^{18}F]F-FAPI and [^{18}F]AlF-FAPI-42 with that of the established brain tumor tracer [^{18}F]FET in an orthotopic U87 glioma model. The fact that both FAP-radioligands showed tumor-specific accumulation in this model is consistent with previous results demonstrating that U87 cells recruit a large number of FAP-positive murine stromal cells and/or exhibit upregulated FAP-expression *in vivo*[22,34]. Moreover, even though absolute tumor uptake of the FAP-radioligands was lower than that of [^{18}F]FET, they exhibited more than two-fold higher TBRs due to much lower uptake by healthy brain tissue. Interestingly, while the TBRs for [^{18}F]AlF-FAPI-42 in the orthotopic glioma model were roughly half of those achieved in the subcutaneous models, the TBRs for 6-[^{18}F]F-FAPI in the orthotopic model were two-fold higher, which resulted in comparable TBRs for both tracers in this model. In addition, 6-[^{18}F]F-FAPI showed higher absolute tumor uptake and a better tumor retention than [^{18}F]AlF-FAPI-42, suggesting that it may be a superior candidate for brain tumor imaging. This could at least in part be related to the lack of a chelator, which should improve tissue- and brain-penetration through increased lipophilicity and reduced molecular size of the probe. Although brain tumors often compromise the integrity of the BBB, there can be significant regional heterogeneity and interindividual differences in the degree of BBB-disruption[35,36]. Accordingly, FAP-radioligands capable of penetrating into tumors or tumor regions with intact BBB would be preferable, but the hydrophilic nature of the chelators in ^{68}Ga- or [^{18}F]AlF-labeled tracers and their considerable molecular size are expected to result in negligible passive transfer across the BBB[37]. Indeed, tumoral tracer accumulation in previous studies with ^{68}Ga-labeled FAP-radioligands was exclusively observed in contrast-enhancing gliomas[22,38] suggesting that brain uptake of chelator-based radioligands in patients with an intact BBB may be insufficient. Moreover, and in line with our present findings, a recent preclinical study showed that uptake of [^{68}Ga]FAPI-04 into intracerebral U87 tumors is much lower than that of the ^{11}C-labeled

probe [^{11}C]RJ1102, which closely resembles 6-[^{18}F]F-FAPI but contains an [^{11}C]methoxy- instead of the [^{18}F]fluoro-group[39]. In this regard, it is important to note that the orthotopic U87 model is well known to be characterized by extensive BBB-disruption[40,41], as confirmed by the strong contrast-enhancement observed in the present study. As such, increased permeability of the BBB presumably contributed to tumor uptake of [^{68}Ga]FAPI-04, [^{18}F]AlF-FAPI-42 and, at least to some extent, also 6-[^{18}F]F-FAPI and [^{11}C]RJ1102 in this preclinical model. In line with this assumption, the most pronounced accumulation of both FAP-radioligands in the present study was observed in the contrast-enhancing core region of the intracerebral U87 tumors, while [^{18}F]FET showed a much more diffuse accumulation pattern that appeared to extent beyond the T2-defined tumor border. Importantly however, blocking or displacement with UAMC1110 strongly reduced uptake of 6-[^{18}F]F-FAPI by the intracerebral tumors, indicating that it reflects FAP-specific binding rather than, e.g., passive tracer extravasation due to local BBB impairment. Altogether, these results support to the notion that FAPI-PET can be used to detect FAP-positive cerebral lesion and indicate that it may provide complementary information to amino acid tracers like [^{18}F]FET. However, further preclinical and clinical studies will clearly be required to reliably assess the role of BBB-disruption for FAPI-PET imaging of brain tumors and to identify the most suitable radioligands for different applications (e.g. tumor detection and staging vs. tumor delineation) and/or patient populations (e.g. patients with contrast-enhancing vs. non-enhancing lesions).

4 Materials and Methods

4.1 Organic Chemistry

4.1.1 General

Unless otherwise stated, all reagents and solvents were purchased from Sigma-Aldrich (Steinheim, Germany), Acros (Fisher Scientific GmbH, Nidderrau, Germany), Alfa Aesar [Thermo Fisher (Kandel) GmbH, Kandel, Germany], BLDPharm (Kaiserslautern, Germany) or Key Organics (Camelford, UK), and used without further purification. Unless otherwise stated, all reactions were carried out with magnetic stirring and, if air or moisture sensitive substrates and/or reagents were used, in flame-dried glassware under argon. Organic extracts were dried over anhydrous Na_2SO_4 or $MgSO_4$. Solutions were concentrated under reduced pressure (1–900 mbar) at 40–50 °C using a rotary evaporator. (*S*)-(2-(2-cyano-4,4-difluoropyrrolidin-1-yl)-2-oxoethyl) ammonium trifluoroacetate (**4**)[42], 6-(3-chloropropoxy)quinoline-4-carboxylic acid

(**7**)[43], (*S*)-4,4-difluoro-1-glycylpyrrolidine-2-carbonitrile 4-methylbenzenesulfonate (**10**)[9], *N*,*N*,*N*,1-tetramethyl-2,4-dioxo-1,4-dihydro-2*H*-pyrido[2,3-d][1,3]oxazin-7-aminium trifluoromethanesulfonate (**17**)[31], 7-fluoro-1-methyl-2*H*-pyrido[2,3-d][1,3]oxazine-2,4(1*H*)-dione (**18**)[31] and 6-fluoro-2-(methylamino)nicotinic acid (**19**)[31] were prepared according to the literature.

Proton, carbon and fluorine nuclear magnetic resonance (^{1}H-, ^{13}C- and ^{19}F-NMR) spectra were recorded on a Bruker Avance Neo (400 MHz) spectrometer. Chemical shifts are reported in parts per million (ppm) relative to residual peaks of deuterated solvents. The observed signal multiplicities are characterized as follows: s = singlet, d = doublet, t = triplet, q = quartet, p = pentet, m = multiplet, dd = doublet of doublets, dt = doublet of triplets, tt = triplet of triplets, qd = quartet of doublets and br = broad. Coupling constants (*J*) are reported in hertz (Hz). Low resolution mass spectra (LRMS) were measured with an MSQ PlusTM mass spectrometer (Thermo Electron Corperation, San Jose, USA). High resolution mass spectra (HRMS) were measured with an LTQ Orbitrap XL (Thermo Fischer Scintific Inc., Bremen, Germany).

4.1.2 Preparation of precursor for [^{18}F]AlF-FAPI-42

The radiolabeling precursor for preparation of [^{18}F]AlF-FAPI-42 was prepared according to the literature[44].

4.1.3 Preparation of precursor for 6-[^{18}F]F-FAPI

Synthesis of 6-bromoquinoline-4-carboxylic acid 2,3,5,6-tetrafluorophenyl ester (2)

A suspension of 6-bromoquinoline-4-carboxylic acid **1** (185 mg, 0.73 mmol, 1 eq.) in thionyl chloride (1 mL) was heated until all solids had dissolved and the resulting solution was stirred at room temperature for 16 h. All volatiles were then removed under reduced pressure and the residue was taken up with a solution of 2,3,5,6-tetrafluorophenol (134 mg, 0.81 mmol, 1.1 eq.) in anhydrous CH_2Cl_2 (5 mL). After addition of NEt_3 (0.11 mL, 82 mg, 0.81 mmol, 1.1 eq.), the reaction mixture was stirred at room temperature for 1.5 h and the solvent was removed under reduced pressure. The residue was suspended in toluene/ethyl acetate and treated with 20% citric acid. The solid was recovered by filtration and purified by flash chromatography (PE/CH_2Cl_2, 1:1) to afford the title compound **2** as brown solid (190 mg, 0.48 mmol, 65%). ^{1}H NMR (400 MHz, $CDCl_3$): δ = 9.15 (d, *J* = 4.53 Hz, 1H), 9.06 (d, *J* = 2.11 Hz, 1H), 8.28 (d, *J* = 4.49, 1H), 8.15 (d, *J* = 9.03 Hz, 1H), 7.94 (d, *J* = 11.12, 2.09 Hz, 1H), 7.13 (m, 1H). ^{13}C-NMR (101 MHz, $CDCl_3$): δ = 161.34, 149.86, 147.51, 145.10, 142.15, 139.67, 136.55 134.43, 131.52, 130.79, 127.78, 126.24, 124.47, 124.31, 104.20. ^{19}F-NMR (376 MHz, $CDCl_3$): δ = -

138.06, -152.32. HR-MS-ESI: m/z $[M+H]^+$ calculated for $[C_{16}H_7BrF_2NO_2]^+$ = 399.95908, found: 399.95907.

Synthesis of 6-(trimethylstannyl)-quinoline-4-carboxylic acid 2,3,5,6-tetrafluorophenyl ester (3)

Sn_2Me_6 (0.80 mL, 2.0 g, 6.1 mmol, 1.5 eq.) was added to a suspension of **2** (1.4 g, 3.5 mmol, 1 eq.), $Pd(Ph_3P)_4$ (901 mg, 0.78 mmol, 0.2 eq.) and LiCl (835 mg, 20 mmol, 4.8 eq.) in anhydrous 1,4-dioxane (49 mL) and the reaction mixture was refluxed for 2.5 h. After the mixture had returned to ambient temperature, the solid was removed by filtration through a plug of Celite® and the filter cake was washed with Et_2O. The organic phase was washed with brine (2 × 30 mL), dried over $MgSO_4$ and concentrated under reduced pressure. The residue was purified by flash chromatography (SiO_2, cHex/EA, 19:1) to afford the title compound **3** as a colorless solid (751 mg, 1.9 mmol, 55%).

^{1}H-NMR (400 MHz, $CDCl_3$): δ = 9.13 (d, *J* = 4.44 Hz, 1H), 8.95 (s, 1H), 8.22 (m, *J* = 4.10 Hz, 3H), 7.99 (dd, *J* = 0.96, 8.24 Hz, 1H), 7.14 (m, *J* = 4.24 Hz, 1H), 0.42 (s, 9H).

^{13}C-NMR (101 MHz, $CDCl_3$): δ = 161.94, 149.19, 148.55, 147.56, 146.20, 145.13, 137.53, 132.76, 131.93, 128.24, 124.64, 123.31, 104.07 (t, *J* = 22.7 Hz), 95.91 (t, *J* = 23.2 Hz), 77.16, -9.23. ^{19}F-NMR (376 MHz, $CDCl_3$): δ = -162.50 (q, *J* = 9.16 Hz, 1F), -152.37 (q, *J* = 10.19 Hz, 1F), -140.83 (q, *J* = 9.71 Hz, 1F), -138.17 (q, *J* = 10.22 Hz, 1F). HR-MS-ESI: m/z $[M+H]^+$ calculated for $[C_{19}H_{16}F_4NO_2Sn]^+$ = 486.01337, found: 486.01336.

Synthesis of 6-(trimethylstannyl)-quinoline-4-carboxylic acid [2-(2-cyano-4,4-difluoro-pyrrolidin-1-yl-2-oxoethyl]-amide (5)

TFA (1.4 mL) was added to a solution of **4** (200 mg, 0.70 mmol, 1.04 eq.) in CH_2Cl_2 (7 mL), and the reaction mixture was stirred at ambient temperature for 1 h. All volatiles were removed under reduced pressure and the residue was taken up in anhydrous CH_2Cl_2 (5 mL) and NEt_3 (200 µL). A solution of **3** (264 mg, 0.67 mmol, 1 eq.) in CH_2Cl_2 was then slowly added at 0 °C and the reaction mixture was allowed to warm up to ambient temperature. After stirring for 1 h, all volatiles were removed under reduced pressure and the residue was purified by flash chromatography (cHex/acetone, 2:1, R_f = 0.09) to afford the title compound **5** as yellowish solid (200 mg, 0.39 mmol, 58%). ^{1}H-NMR (400 MHz, $CDCl_3$): δ = 8.85 (d, *J* = 4.3 Hz, 1H), 8.48 – 8.27 (m, 1H), 8.15 – 8.00 (m, 1H), 7.97 – 7.77 (m, 1H), 7.45 (d, *J* = 4.3 Hz, 1H), 7.16 (t, *J* = 4.6 Hz, 1H), 4.95 (t, *J* = 6.5 Hz, 1H), 4.41 (dd, *J* = 17.5, 5.5 Hz, 1H), 4.17 (dd, *J* = 17.5, 4.3 Hz, 1H), 4.09 – 3.86 (m, 2H), 2.98 – 2.68 (m, 2H), 0.36 (s, 9H). ^{13}C-NMR (101 MHz, $CDCl_3$):

δ = 167.64 (d, J = 41.3 Hz), 149.80, 148.78, 143.75, 140.23, 136.91, 132.87, 128.83, 125.30, 123.96, 118.88, 116.14, 77.16, 52.18 (t, J = 32.1 Hz), 44.42, 44.38, 42.38, 37.50 (t, J = 25.5 Hz), 28.71, -9.18. ^{19}F-NMR (376 MHz, $CDCl_3$): δ = -96.46 (t, *J* = 235.8 Hz), -99.30 (dd, *J* = 1366.4, 238.1 Hz), -102.66 (d, *J* = 232.9 Hz), -104.33 (d, *J* = 240.2 Hz).
HR-MS-ESI: m/z $[M+H]^+$ calculated for $[C_{20}H_{23}F_2N_4O_2Sn]^+$ = 509.08056, found: 509.08026.

4.1.4 Preparation of precursor for [^{18}F]AFA-FAPI

Synthesis of 6-(3-azidopropoxy)quinoline-4-carboxylic acid (8)

7 (397 mg, 1.53 mmol, 1 eq), sodium azide (293 mg, 4.51 mmol, 3 eq.) and sodium iodide (460 mg, 3.07 mmol, 2 eq.) were dissolved in DMF (5 mL) at 60 °C. 2,6-Lutidine (348 µL, 3.00 mmol, 2 eq.) was added and the reaction mixture was stirred at 60 °C for 12 h. The mixture was then diluted with H_2O (100 mL), acidified with AcOH (260 µL), and the resulting precipitate was isolated by centrifugation. The solid was dried at 70 °C under reduced pressure to afford the title compound **8** as a colorless solid (367 mg, 1.35 mmol, 90% yield). ^{1}H-NMR (400 MHz, $[CD_3]_2SO$) δ = 8.87 (t, *J* = 4.5 Hz, 1H), 8.19 (d, *J* = 2.8 Hz, 1H), 8.06 – 7.98 (m, 1H), 7.94 (d, *J* = 4.4 Hz, 1H), 7.66 – 7.31 (m, 1H), 4.19 (t, *J* = 6.1 Hz, 2H), 3.71 – 3.49 (m, 2H), 2.08 (p, *J* = 6.4 Hz, 2H). ^{13}C-NMR (101 MHz, $[CD_3]_2SO$) δ = 168.08, 157.96, 148.09, 145.33, 134.31, 131.71, 126.39, 123.17, 122.63, 104.94, 65.53, 48.20, 28.53. HR-MS-ESI: m/z $[M+H]^+$ calculated for $[C_{13}H_{13}N_4O_3]^+$ = 273.09822, found: 273.09844.

Synthesis of 2,3,5,6-tetrafluorophenyl 6-(3-azidopropoxy)quinoline-4-carboxylate (9)

8 (493 mg, 1.81 mmol, 1 eq.) and 2,3,5,6-tetrafluorophenol (320 mg, 1.93 mmol, 1.05 eq.) were treated with a solution of EDC (373 mg, 1.95 mmol, 1.05 eq.) in CH_2Cl_2 (9 mL) and the mixture was stirred for 72 h. The solvent was removed under reduced pressure and the residue was taken up in a mixture of 10% aq. citric acid (10 mL) and EtOAc (20 mL). The crude product was extracted with EtOAc (3 × 10 mL) and the combined organic phases were washed with H_2O (3 × 10 mL) followed by brine (3 × 10 mL). The organic phase was dried over $NaSO_4$ and the solvent was removed under reduced pressure to afford the title compound **9** as a colorless solid (696 mg, 1.66 mmol, 92%). ^{1}H-NMR (400 MHz, $CDCl_3$) δ = 9.00 (t, *J* = 3.8 Hz, 1H), 8.25 (dd, *J* = 5.6, 3.7 Hz, 2H), 8.16 (d, *J* = 9.3 Hz, 1H), 7.55 – 7.47 (m, 1H), 7.14 (tt, *J* = 9.9, 7.1 Hz, 1H), 4.25 (t, *J* = 5.9 Hz, 2H), 3.59 (t, *J* = 6.6 Hz, 2H), 2.16 (p, *J* = 6.4 Hz, 2H). ^{13}C-NMR (101 MHz, $CDCl_3$) δ = 162.03, 159.09, 147.41, 146.76, 145.56, 144.93, 141.86, 139.41, 131.51, 129.27, 126.80, 123.87, 123.61, 103.84 (t), 103.42, 64.97, 49.36 (p), 48.13, 28.51. ^{19}F-NMR (376 MHz, $CDCl_3$) δ = -138.39, -138.42, -152.58, -152.61. HR-MS-ESI: m/z $[M+H]^+$ calculated for $[C_{19}H_{13}F_4N_4O_3]^+$ = 421.09183, found: 421.09184.

Synthesis of 6-(3-azidopropoxy)-*N*-(2-(2-cyano-4,4-difluoropyrrolidin-1-yl)-2-oxoethyl)quinoline-4-carboxamide (11)

NEt_3 (263 µL, 1.89 mmol, 2 eq.) was added to a pre-cooled (0 °C) solution of **10** (341 mg, 0.94 mmol, 1 eq.) and **9** (398 mg, 0.96 mmol, 1.02 eq.) in CH_2Cl_2 (10 mL). The reaction mixture was allowed to warm up to ambient temperature and stirred for 12 h. All volatiles were removed under reduced pressure at 30 °C and the residue was taken up in a mixture of H_2O (30 mL) and EtOAc (50 mL). The crude product was extracted with EtOAc (3 × 30 mL) and the combined organic phases were washed with H_2O (3 × 30 mL). The organic phase was dried over $NaSO_4$ and the solvent was removed under reduced pressure to afford the title compound **11** as a colorless solid (162 mg, 371 mmol, 40%) . ^{1}H-NMR (400 MHz, CD_3OD) δ = 8.77 (d, *J* = 4.4 Hz, 1H), 8.05 – 7.90 (m, 2H), 7.59 (d, *J* = 4.4 Hz, 1H), 7.50 (dd, *J* = 9.2, 2.8 Hz, 1H), 5.16 (dd, *J* = 9.3, 3.2 Hz, 1H), 4.43 – 4.04 (m, 5H), 3.58 (t, *J* = 6.7 Hz, 2H), 3.03 – 2.70 (m, 2H), 2.15 (p, *J* = 6.5 Hz, 2H). ^{13}C-NMR (101 MHz, CD_3OD) δ = 169.34, 168.10, 157.95, 146.70, 143.96, 141.41, 129.50, 125.95, 123.48, 118.98, 116.75, 103.91, 65.41, 51.86, 51.54, 51.21, 50.73, 44.45, 44.40, 41.48, 36.95, 36.70, 36.45, 28.21. ^{19}F-NMR (376 MHz, CD_3OD) δ = -98.60 (d, *J* = 236.8 Hz), -105.38 (d, *J* = 236.0 Hz). HR-MS-ESI: m/z $[M+H]^+$ calculated for $[C_{20}H_{20}F_2N_7O_3]^+$ = 444.15902, found: 444.15918.

Synthesis of *tert*-butyl (3-((4-((2-(2-cyano-4,4-difluoropyrrolidin-1-yl)-2-oxoethyl)carbamoyl)quinolin-6-yl)oxy)propyl)carbamate (12)

MeCN in EtOAc (0.8 mL, 1 M, 10 eq.) was added to a suspension of **11** (35 mg, 0.08 mmol, 1 eq.), Boc_2O (21 mg, 0.10 mmol, 1.2 eq.) and Pd/C (8 mg) in anhydrous EtOAc (2.5 mL). The reaction vessel was flushed with H_2 and the mixture was stirred at ambient temperature for 80 min. The reaction mixture was then passed over a SiO_2 column and the product was eluted with EtOAc/MeOH (20:1). The solvent was removed under reduced pressure to afford the title compound **12** as a colorless solid (36.6 mg, 0.07 mmol, 88%).

^{1}H-NMR (400 MHz, CD_3OD) δ = 8.76 (d, *J* = 4.4 Hz, 1H), 7.99 (d, *J* = 9.3 Hz, 1H), 7.91 (d, *J* = 2.8 Hz, 1H), 7.59 (d, *J* = 4.5 Hz, 1H), 7.49 (dd, *J* = 9.3, 2.7 Hz, 1H), 5.17 (dd, *J* = 9.3, 3.2 Hz, 1H), 4.43 – 4.02 (m, 6H), 3.30 (s, 1H), 3.16 – 2.76 (m, 2H), 2.18 – 1.95 (m, 3H), 1.44 (s, 9H). ^{13}C-NMR (101 MHz, CD_3OD) δ = 169.32, 168.12, 158.13, 157.13, 146.60, 143.93, 141.27, 129.44, 128.66, 126.20, 125.96, 123.71, 123.56, 119.02, 116.73, 103.82, 78.57, 65.99, 60.14, 51.90, 51.58, 51.25, 44.46, 44.40, 41.48, 37.09, 36.98, 36.73, 36.48, 29.09, 27.38, 19.45,

13.06. ^{19}F-NMR (376 MHz, CD_3OD) δ = -98.52 (d, *J* = 236.4 Hz), -105.33 (d, *J* = 237.6 Hz). HR-MS-ESI: m/z $[M+H]^+$ calculated for $[C_{25}H_{30}F_2N_5O_5]^+$ = 518.22095, found: 518.22080.

Synthesis of 6-(3-aminopropoxy)-N-(2-(2-cyano-4,4-difluoropyrrolidin-1-yl)-2-oxoethyl)quinoline-4-carboxamide (13)

12 (39 mg, 0.08 mmol, 1 eq.) was treated with triisopropylsilane (31 µL) and TFA (200 µL), and the resulting suspension was stirred at ambient temperature for 30 min. The reaction mixture was diluted with H_2O (1 mL) and MeCN (3 mL) and all volatiles were removed under reduced pressure at 40 °C. This procedure was repeated with MeCN (3 mL) before the residue was taken up in Et_2O, basified with saturated $NaCO_3$ and extracted with EtOAc. The combined organic phases were dried over $NaSO_4$ and the solvent was removed under reduced pressure to afford the title compound **13** as a colorless oil (21.9 mg, 0.05 mmol, 74%). ^{1}H-NMR (400 MHz, CD_3OD) δ = 8.77 (d, *J* = 4.5 Hz, 1H), 8.03 – 7.91 (m, 2H), 7.58 (d, *J* = 4.4 Hz, 1H), 7.48 (dd, *J* = 9.3, 2.8 Hz, 1H), 5.15 (dd, *J* = 9.3, 3.2 Hz, 1H), 4.43 – 4.08 (m, 6H), 3.03 – 2.77 (m, 3H), 2.06 (p, *J* = 6.6 Hz, 2H). ^{13}C-NMR (101 MHz, CD_3OD) δ = 168.04, 166.75, 159.61, 149.15, 141.98, 135.54, 128.27, 127.79, 122.75, 119.65, 116.85, 114.23, 105.11, 66.43, 51.48, 44.54, 44.48, 41.63, 36.98, 36.56, 27.43, 27.40, 26.60, 22.15. ^{19}F-NMR (376 MHz, CD_3OD) δ = -98.59 (d, *J* = 235.8 Hz), -105.41 (d, *J* = 236.4 Hz). HR-MS-ESI: m/z $[M+H]^+$ calculated for $[C_{20}H_{22}F_2N_5O_3]^+$ = 418.16852, found: 418.16863.

4.1.5 Preparation of reference compound 6-F-FAPI

Synthesis of 6-fluoroquinoline-4-carboxylic acid (15)

A suspension of 6-fluoroquinoline-2,4-dicarboxylic acid **14** (1.01 g, 4.29 mmol, 1 eq.) in nitrobenzene (8.5 mL) was refluxed for 50 min. The reaction mixture was allowed to cool to ambient temperature and diluted with toluene (8.5 mL). The solid was recovered by filtration, washed with toluene and pentane, and dried under reduced pressure to afford the title compound **15** (782 mg, 4.09 mmol, 95%), which was used without further purification. ^{1}H NMR [400 MHz, $(CD_3)_2SO$]: δ = 9.04 (d, *J* = 4.4 Hz, 1H), 8.50 (dd, *J* = 11.2, 2.9 Hz, 1H), 8.20 (dd, *J* = 9.3, 5.9 Hz, 1H), 8.03 (d, *J* = 4.3 Hz, 1H), 7.77 (ddd, *J* = 9.2, 8.3, 2.9 Hz, 1H). ^{13}C NMR [101 MHz, $(CD_3)_2SO$]: δ = 167.15, 161.90, 159.45, 149.99 (d, *J* = 2.6 Hz), 145.90, 134.84 (d, *J* = 5.8 Hz), 132.65 (d, *J* = 9.8 Hz), 125.48 (d, *J* = 11.0 Hz), 123.31, 119.98 (d, *J* = 25.9 Hz), 109.24 (d, *J* = 24.8 Hz). ^{19}F NMR [376 MHz, $(CD_3)_2SO$]: δ = -110.65.

Synthesis of 6-fluoroquinoline-4-2,3,5,6-tetrafluorophenyl carboxylic acid ester (16)

EDC (529 mg, 3.41 mmol, 1.3 eq.) was added to an pre-cooled (0 °C, ice bath) suspension of **15** (500 mg, 2.62 mmol, 1 eq.) and 2,3,5,6-tetrafluorophenol (870 mg, 5.24 mmol, 2 eq.) in anhydrous CH_2Cl_2 (26 mL) and the reaction mixture was stirred at 0 °C for 10 min. The ice bath was removed and the reaction mixture stirred at ambient temperature for 16 h before it was diluted was CH_2Cl_2 (25 mL) and washed with 0.05 M NaOH (3 × 25 mL) and brine (3 × 25 mL). The organic phase was dried over Na_2SO_4 and concentrated under reduced pressure. The crude product was purified by flash chromatography (SiO_2, cHex/EtOAc, 9:1, R_f = 0.17) to afford the title compound **16** as a colorless solid (739 mg, 2.18 mmol, 83%). ^{1}H NMR [400 MHz, $CDCl_3$]: δ = 9.11 (d, *J* = 4.4 Hz, 1H), 8.53 (dd, *J* = 10.6, 2.8 Hz, 1H), 8.33 – 8.19 (m, 2H), 7.62 (ddd, *J* = 9.3, 7.8, 2.8 Hz, 1H), 7.12 (tt, *J* = 9.9, 7.1 Hz, 1H). ^{13}C NMR [101 MHz, $(CD_3)_2SO$]: δ = 163.59, 161.61, 161.10, 149.13 (d, *J* = 2.9 Hz), 146.74, 133.12 (d, *J* = 9.5 Hz), 130.65, 130.59, 126.27, 126.16, 124.33, 120.91 (d, *J* = 26.1 Hz), 109.42 (d, *J* = 25.4 Hz), 104.09 (t, *J* = 22.8 Hz). ^{19}F NMR [376 MHz, $(CD_3)_2SO$]: δ = -107.80, -138.20 (dd, *J* = 21.4, 9.5 Hz), -152.42 (dd, *J* = 21.4, 9.5 Hz).

4.1.6 Preparation of the reference compound AFA-FAPI

Synthesis of *N*-(2-(2-cyano-4,4-difluoropyrrolidin-1-yl)-2-oxoethyl)-6-(3-(6-fluoro-2-(methylamino)nicotinamido)propoxy)quinoline-4-carboxamide (AFA-FAPI)

Thionyl chloride (1 mL) was added dropwise at ambient temperature to 6-Fluoro-2-(methylamino)nicotinic acid (5 mg, 29 µmol) and the mixture was stirred at 80 °C for 2 h. The solvent was removed under reduced pressure, toluene (10 mL) was added and removed again under reduced pressure. **13** (12 mg, 29 µmol) and a solution of NEt_3 (0.3 µL) in CH_2Cl_2 (1 mL) were then added and the reaction mixture was stirred at room temperature for 1 h. The mixture was diluted with H_2O (10 mL) and extracted with CH_2Cl_2 (3 × 10 mL). The combined organic phases were dried over Na_2SO_4 and the solvent was removed under reduced pressure. The product was purified by flash chromatography (5% MeOH in DCM) to afford the title compound as a colorless solid (8 mg, 48%). ^{1}H-NMR (400 MHz, CD_3CN) δ 8.78 (d, *J* = 4.4 Hz, 1H), 8.48 (s, 1H), 7.98 (d, *J* = 9.2 Hz, 1H), 7.85 (t, *J* = 8.2 Hz, 1H), 7.81 (d, *J* = 2.8 Hz, 1H), 7.49 (d, *J* = 4.3 Hz, 1H), 7.41 (dd, *J* = 9.2, 2.8 Hz, 1H), 7.08 (s, 1H), 6.08 (dd, *J* = 8.2, 2.8 Hz, 1H), 4.99 (dd, *J* = 8.9, 3.4 Hz, 1H), 4.33 – 4.14 (m, 3H), 3.53 (qd, *J* = 6.7, 2.4 Hz, 2H), 2.88 (d, *J* = 4.9 Hz, 3H), 2.15 (s, 16H), 2.12 – 2.04 (m, 2H), 1.94 (dt, *J* = 5.0, 2.5 Hz, 17H). ^{13}C-NMR (101 MHz, CD_3CN) δ 167.93, 167.85, 165.56, 163.20, 157.71, 147.50, 144.76, 141.18, 141.08, 140.30, 131.06, 125.62, 122.66, 119.26, 117.32, 104.25, 93.08, 92.70, 66.27, 52.07, 51.75, 51.43, 44.49, 44.43, 41.71, 37.04, 36.80, 36.55, 36.42, 28.74, 27.11. ^{19}F-NMR

(376 MHz, CD_3CN) δ -65.81 (s), -97.46 (d, *J* = 235.8 Hz), -104.99 (d, *J* = 235.8 Hz). HRMS (ESI): m/z calculated for $C_{27}H_{26}F_3N_7O_4^+$: 569.19929, found 569.19881.

4.2 Radiochemistry

4.2.1 General

[^{18}F]Fluoride ([^{18}F]F^-) was produced via the $^{18}O(p,n)^{18}F$ nuclear reaction by bombardment of enriched [^{18}O]H_2O with 16.5 MeV protons using a BC1710 cyclotron (The Japan Steel Works Ltd., Shinagawa, Japan) at the INM-5 (Forschungszentrum Jülich). All radiosyntheses were carried out in 5 mL Wheaton V-Vials equipped with PTFE-coated wing stir bars. Anhydrous solvents (DMI, *n*BuOH and MeOH, dried over molecular sieves) were purchased from Sigma-Aldrich (Steinheim, Germany). Anion exchange resins (Sep-Pak Accell Plus QMA carbonate plus light cartridges, 40 mg sorbent per cartridge) and solid phase extraction Sep-Pak C18 and HLB short cartridges (360 mg sorbent per cartridge) were obtained from Waters GmbH (Eschborn, Germany). The polymeric-based StrataX cartridge (60 mg) was obtained from Phenomenex (Aschaffenburg, Deutschland).

Analytical radio-HPLC was performed on a HPLC system (Knauer Wissenschaftliche Geräte GmbH, Berlin, Germany) with Azura P 6.1L pump and Azura UVD 2.1S UV/Vis detector. For monitoring absorbance at 254 nm and radioactivity, the UV/Vis detector was coupled in series with a Berthold NaI detector, giving a time of delay of 0.1–0.3 min between the corresponding responses (depending on the flow rate). For determination of radiochemical conversions (RCCs), the reaction mixtures were diluted with H_2O (2 mL) or 20% MeCN (2 mL) and analyzed by radio-HPLC with a post-column injection of the reaction mixture. The RCCs were then calculated by comparison of the peak areas of the radiolabeled product and the post-column injection, respectively.[19] The identity of radiolabeled products was confirmed by co-injection of the corresponding non-radiolabeled reference compound. Activity yields (AY) were determined by comparing the initial activity on the QMA cartridge and the activity of the radiolabeled product.

Semipreparative HPLC for purification of crude 6-[^{18}F]F-FAPI was performed in a dedicated semipreparative system consisting of a Merck Hitachi L-6000 pump, a Knauer K-2500 detector, a Rheodyne 6-way valve and a Geiger-Müller counter.

High-Performance Liquid Chromatography (HPLC)

Analytical HPLC

Column: MultoKrom® 100-5, 5 µm, 250 × 4.6 mm (CS-Chromatography, Langerwehe, Germany); eluent: 30% MeCN; flow rate: 1.5 mL/min; t_R = 14.1 min.
Column: Kinetex EVO C18, 5 µm, 250 × 4.6 mm (Phenomenex, Aschaffenburg, Germany); eluent: 20% MeCN, flow rate: 1.5 mL, t_R = 8.41 min.

Preparative HPLC

Column: Gemini C18 110A, 5 µm, 250 × 10 mm (Phenomenex, Aschaffenburg, Germany); eluent: 30% MeCN; flow rate: 7.1 mL/min; t_R = 12.5 – 14.5 min.

4.2.2 Preparation of [^{18}F]AlF-FAPI-42

The preparation of [^{18}F]AlF-FAPI-42 was performed based on the [^{18}F]AlF chelation method described by McBride et al.[45] as follows: Aqueous [^{18}F]F^- was loaded onto a Sep-Pak Accell Plus QMA carbonate plus light cartridge (preconditioned with 5 mL 0.5 M sodium acetate and 10 mL H_2O). The cartridge was washed with H_2O (5 mL) and the [^{18}F]F^- was eluted with 0.05 M sodium acetate buffer (350 µL, pH 4) into a reaction vessel. DMSO (1.4 mL), a solution of FAPI-42 (3.2 mM, 64 nmol) in 0.05 M sodium acetate (20 µL) and a solution of $AlCl_3 \cdot 6H_2O$ (0.01 M, 29 nmol) in 0.05 M sodium acetate (0.3 µL) were then added and the reaction mixture was incubated at 110 °C for 10 min. The crude product solution thus obtained was diluted with H_2O (50 mL) and saturated $NaHCO_3$ (1 mL), and loaded onto a polymer RP cartridge (HLB). The cartridge was washed with H_2O (5 mL) and dried with air (10 mL) before the product was eluted with EtOH (1 mL). The solvent was removed at 600 mbar in a stream of argon, and the residue was taken up in isotonic saline solution.

4.2.3 Preparation of 6-[^{18}F]F-FAPI

Aqueous [^{18}F]F^- (0.1–5 GBq) was loaded (from the male side) onto a QMA cartridge (preconditioned with 1 mL H_2O from the female side). The cartridge was washed (from the male side) with anhydrous MeOH (1 mL) to remove residual H_2O and dried (from the female side) with air (2×10 mL). [^{18}F]F^- was then eluted with a solution of Et_4NOTf (1 mg, 4 µmol) in anhydrous MeOH (500 µL) into a V-Vial and the MeOH was evaporated at 60 °C under reduced pressure in a stream of argon. The V-Vial was filled with argon, sealed with a silicon septum and a solution of **5** (5.1 mg, 10 µmol) and $Cu(4\text{-}PhPy)_4(ClO_4)_2$ (8.7 mg, 10 µmol) in DMI (800 µL) was added via a cannula through the septum. The reaction mixture was heated at 90 °C for 10 min, diluted with H_2O (15 mL) and loaded onto a StrataX cartridge. The cartridge was washed with H_2O (5 mL) and the crude radiolabeled product was eluted with MeCN (500 µL). The eluent was diluted with H_2O (1 mL) and purified by preparative HPLC.

The product fraction was collected at 12.5 – 14.5 min. For formulation, the collected fraction was diluted with H_2O (15 mL) and loaded onto a StrataX. The cartridge was washed with H_2O (5 mL) and air dried, before the radiotracer was eluted with EtOH (500 µL). EtOH was removed at 40 °C under reduced pressure in a stream of arganon, and the residue was taken up in 1% Tween80 to afford 6-[^{18}F]F-FAPI as ready-to-inject solution.

4.2.4 Preparation of [^{18}F]AFA-FAPI

The prosthetic group for radiosynthesis of [^{18}F]AFA-FAPI was prepared by direct elution of [^{18}F]F^- (3.5 GBq) from an anion exchange resin (PS-HCO_3-45 mg) with a solution of **17** (12 mg) in MeCN/*t*BuOH (1:4, 1 mL) into a vial, followed by flushing of the cartridge with MeCN (1 mL). The solution was diluted with H_2O (35 mL) and passed through a SPE cartridge (Oasis® HLB Plus Short), which was washed with 5% acetone in H_2O (6 mL) and briefly dried in a steam of argon. The prosthetic group [^{18}F]**18** was then eluted with 1.5 mL MeCN (1.5 mL) and the solvent was removed under reduced pressure at 100 °C before a solution of **13** (10 µmol) in DMF (500 µL) was added. The vial was equipped with a septum cap and heated under stirring at 110 °C for 15 min. After addition of H_2O (1 mL), the resulting solution was purified by semi-preparative HPLC (MeCN/H_2O/TFA = 50% MeCN, 0.1% TFA; 8 mL/min; t_R = 6.5–7.8 min). The product fraction (2 mL) was diluted with H_2O (10 mL) and loaded onto an SPE cartridge (Oasis® HLB Plus Short), which was washed with H_2O (10 mL) before the product was eluted with MeOH (1 mL). Subsequent removal of the solvent under reduced pressure in a stream of argon at 60 °C for 3 min followed by addition of isotonic saline solution afforded [^{18}F]AFA-FAPI (872 MBq) as injectable solution. The isolated radiochemical yield was 34 ± 10% (n=3) in a synthesis time of 70 min. The radiochemical purity was >97%, with molar activities of up to 170 GBq/µmol (for 3.5 GBq starting activity).

4.3 Biological Evaluation

4.4 Cell cultures

HT1080-WT (ATCC: CCL 121) and HT1080-FAP cells, were cultured under normal growth conditions (37 °C and 5% CO_2) in minimum essential medium GlutaMAX (MEM, Gibco 41090028, Fisher Scientific GmbH, Schwerte, Germany) supplemented with 10% fetal bovine serum (FBS, Sigma-Aldrich F2442, Merck KGaA, Darmstadt, Germany), 1% penicillin/streptomycin (Gibco 115140122), 1% non-essential amino acids (NEAA, Gibco 11140050), 1% human recombinant insulin (Sigma Aldrich 91077C), and 1% sodium pyruvate (ThermoFisher 11360070, Fisher Scientific GmbH, Schwerte, Germany). The cells were grown

in cell-culture dishes (ThermoFisher 150350, F 100 mm) with 9 mL culture medium for 4–5 days until they reached 80–90% confluency. For the cellular uptake studies, cells were seeded into 12-well plates (2×10^5 cells in 1 mL medium / well) 48 h before the start of the experiments.

4.5 Cellular Uptake Experiments

Two hours prior to the start of experiments, the culture medium was carefully aspirated, the cells were washed with phosphate-buffered saline (PBS, 1 mL, Gibco 10010023), and a dye exclusion test with trypan blue (Sigma Aldrich T 8154) was performed to determine cell viability and the exact cell count (cell viability was always >95%). The tracer solutions were prepared in FBS- and amino acid-free Earle's balanced salt solution (EBSS) at a concentration of 150 kBq/mL. PBS was removed from the wells and the tracer solution was added (1 mL/well). The cells were then incubated at 37 °C for 60 min, washed twice with ice-cold PBS (1 mL), trypsinized and harvested. The accumulated radioactivity was measured in an automatic gamma counter (Hidex AMG version 1.4.4, Turku, Finland). Each experiment was conducted at least in triplicate.

4.6 Experimental Animals

All experiments were carried out in accordance with the EU directive 2010/63/EU for animal experiments and the German Animal Welfare Act (TierSchG, 2006) and were approved by regional authorities (LANUV NRW; 81-02.04.2020.A348). Twenty-three CB17-SCID mice (11 male, 12 female; Janvier Labs, Le Genest-Saint-Isle, France) and three male Lewis rats (Charles River Laboratories, Sulzfeld, Germany) were used for the *in vivo* experiments. They were housed in groups in individually ventilated cages (Allentown LLC, Allentown, NJ, USA) in a temperature- and humidity-controlled room (20 ± 2°C, 50 – 60% humidity) on a 12:12 h light-dark cycle. Throughout the experiments the animals had *ad libitum* access to water and food.

4.7 Subcutaneous HT1080-WT and HT1080-FAP xenograft mouse model

In this model, tracer uptake was compared between tumor xenografts induced by subcutaneous implantation of HT1080-FAP or HT1080-WT cells in T-cell-deficient SCID mice. Mice were between 7 and 8 weeks old and weighed 20–23 g (males) or 16–19 g (females) at the start of the experiments. To promote tumor cell survival and growth, natural killer cell activity was reduced by intraperitoneal injection of 20 µl anti-asialo GM1 rabbit (Fujifilm Wako Chemicals Europe GmbH, Neuss, Germany) diluted with 80 µl 0.9% NaCl 24 h before tumor inoculation. For tumor inoculation, 2×10^6 tumor cells were resuspended in 75 µl culture medium, mixed

with 75 µl Corning Matrigel (Merck, Darmstadt, Germany), and injected subcutaneously in the right shoulder region. Twelve mice (6 males, 6 females) were inoculated with HT1080-WT cells, and 11 mice (5 males, 6 females) were inoculated with HT1080-FAP cells. PET measurements took place 10–15 days after tumor implantation.

4.8 Subcutaneous DSL allograft rat model

This model in immunocompetent rats was chosen for further evaluation of the most promising tracer candidate identified in the mouse xenograft experiments, as it should more closely recapitulate clinically relevant conditions. Thus, similar to the situation in most human cancers, tumors induced by implantation of DSL-6A/C1 cells are characterized by a pronounced tumor stroma with a high density of FAP-positive CAFs, while the tumor cells themselves should be FAP-negative[32,33]. Rats were between 10 and 14 weeks old and weighed 277–330 g at the start of the experiments. 1×10^7 DSL-6A/C1 rat pancreatic carcinoma cells (CLS Cell Lines Service GmbH, Eppelheim, Germany) were resuspended in 100 µl cell culture medium and injected subcutaneously in the shoulder or hip region. As tumor growth in this model was extremely slow, PET measurements took place 79–121 days after tumor implantation.

4.8 Orthotopic U87 glioma xenograft rat model

For this model, immunodeficient male Rowett Nude Rats (Charles River, Sulzfeld, Germany) weighting 235–304 g were anesthetized with isoflurane (5% for induction, 3–4% for maintenance) in O_2/air (3:7) and 10^5 U87 MG glioma cells in 1 µL were stereotactically implanted into the brain. The stereotactic coordinates were 0.5 mm anterior, 2.5 mm lateral and 3 mm ventral from Bregma. MRI scans were performed one week after tumor cell implantation to determine the size of the intracranial tumors, and PET measurements followed during the next three days. The MRI measurements were performed under isoflurane anesthesia (5% for induction, 2.0–2.5% for maintenance) in an MRI scanner (3T Achieva®, Philips Healthcare, Best, The Netherlands) in combination with an 8 Channel Volumetric Rat Array (Rapid Biomedical GmbH, Rimpar, Germany). The MRI protocol included horizontal and transverse T_2-weighted sliced spin echo sequences to localize the tumor and a coronal T_1-weighted sliced gradient echo sequence for contrast-enhanced measurements. The spin echo acquisition included the following parameters: TR = 14540 ms , TE = 30 ms, FA = 90°, FOV = 60 x 60 x 60 mm³ at 0.3 x 0.3 mm² acquired and 0.19 x 0.19 mm² reconstructed in-plane resolution, slice thickness 1 mm, TSE factor 19, halfscan 0.6, 2 averages. The T_1-weighted scans were acquired prior to and after i.v. contrast agent administration (Clariscan, GE Healthcare, 0.5 mmol/ml, 0.2

ml/kg body weight) with: TR = 230 ms, TE = 4.7 ms, FA = 60°, FOV = 60 x 60 x 22 mm³ at 0.3 x 0.3 mm² acquired and 0.27 x 0.27 mm² reconstructed in-plane resolution, slice thickness 1 mm, slice gap: 0.1 mm, CS-SENSE factor 2, 4 averages.

4.9 PET measurements

Table XX: Number of PET-measurements

Tracer	HT1080-FAP male mice	HT1080-FAP female mice	HT1080-WT male mice	HT1080-WT female mice	DSL-6A/C1 male rats	U87 MG male rats
[^{18}F]AlF-FAPI-42	n=2	n=2	n=2	n=3	n=3	n=3
6-[^{18}F]F-FAPI	n=2	n=3	n=1	n=2	n=4	n=6
[^{18}F]AFA-FAPI	n=1	n=3	n=2	n=2	-	-
[^{18}F]FS-FAPI	n=1	n=1	n=1	n=1	-	-
[^{18}F]FET	-	-	-	-	-	n=2

Mice and rats were anesthetized with isoflurane (5% for induction, 2% for maintenance) in O_2/air (3:7), and a catheter for tracer injection was inserted into the lateral tail vein. They were placed on an animal holder (mice: double mouse holder from Medres, Cologne, Germany; rats: single rat holder from Minerve, Esternay, France) and fixed with a tooth bar in a respiratory mask. Body temperature was maintained at 37 °C by warming the animal bed. Eyes were protected from drying with Bepanthen eye and nose ointment (Bayer, Leverkusen, Germany). Respiratory rate was monitored and maintained at around 40–60 breaths per minute by adjusting the isoflurane concentration. PET scans were conducted in list mode using a Focus 220 micro PET scanner (CTI-Siemens, Erlangen, Germany) with a resolution at the center of field of view of 1.4 mm. Data acquisition started with intravenous tracer injection and ended after 120 min. For blocking experiments (n=2) in the U87 glioma model, 5 mg/kg UAMC1110 were injected together with 6-[^{18}F]F-FAPI. For displacement (n=1), 5 mg/kg UAMC1110 was injected i.v. 60 min after 6-[^{18}F]F-FAPI injection. Emission scans were followed by a 10 min transmission scan using a ^{57}Co point source for attenuation correction. After the scan, the catheter was removed and the animals were allowed to recover in their home cages. Data were histogrammed in two ways: 4 × 30 min frames for visual display and 28 frames (2 × 1 min, 2 × 2 min, 6 × 4 min, 18 × 5 min) for time-activity curves. Full 3D rebinning was followed by an iterative OSEM3D/MAP reconstruction algorithm with attenuation and decay correction. The resulting voxel sizes were 0.47 mm x 0.47 mm x 0.80 mm. All further analysis was performed with the software VINCI 5.21 (Max Planck Institute for Metabolism Research, Cologne, Germany).

Standardized uptake values based on body weight (SUV_{bw}) were determined according to the following equation: SUV_{bw}= radioactivity [Bq/g] × body weight [g] / injected dose [Bq].

5 Conclusion

In conclusion, our preclinical comparison of three FAP-radioligands prepared by different ^{18}F-labeling methods indicates that [^{18}F]AlF-FAPI-42 is the most suitable tracer for delineation of FAP-positive peripheral tumors, while 6-[^{18}F]F-FAPI is a more promising candidate for brain tumor imaging. In addition, structural modification of 6-[^{18}F]F-FAPI could potentially be used to develop tracers with improved pharmacokinetic properties (e.g. faster clearance from FAP-negative tissues, reduced hepatobiliary excretion) for imaging of peripheral tumors.

6 References

1. Fitzgerald, A. A. & Weiner, L. M. The role of fibroblast activation protein in health and malignancy. *Cancer Metastasis Rev.* **39**, 783–803 (2020).
2. Hamson, E. J., Keane, F. M., Tholen, S., Schilling, O. & Gorrell, M. D. Understanding fibroblast activation protein (FAP): Substrates, activities, expression and targeting for cancer therapy. *PROTEOMICS - Clin. Appl.* **8**, 454–463 (2014).
3. Sollini, M. *et al.* State-of-the-art of FAPI-PET imaging: a systematic review and meta-analysis. *Eur. J. Nucl. Med. Mol. Imaging* **48**, 4396–4414 (2021).
4. Huang, R. *et al.* FAPI-PET/CT in Cancer Imaging: A Potential Novel Molecule of the Century. *Front. Oncol.* **12**, (2022).
5. Lindner, T., Giesel, F. L., Kratochwil, C. & Serfling, S. E. Radioligands Targeting Fibroblast Activation Protein (FAP). *Cancers (Basel).* **13**, 5744 (2021).
6. Giesel, F. L. *et al.* Head-to-head intra-individual comparison of biodistribution and tumor uptake of 68Ga-FAPI and 18F-FDG PET/CT in cancer patients. *Eur. J. Nucl. Med. Mol. Imaging* **48**, 4377–4385 (2021).
7. Ballal, S. *et al.* Biodistribution, pharmacokinetics, dosimetry of [68Ga]Ga-DOTA.SA.FAPi, and the head-to-head comparison with [18F]F-FDG PET/CT in patients with various cancers. *Eur. J. Nucl. Med. Mol. Imaging* **48**, 1915–1931 (2021).
8. Jansen, K. *et al.* Selective Inhibitors of Fibroblast Activation Protein (FAP) with a (4-Quinolinoyl)-glycyl-2-cyanopyrrolidine Scaffold. *ACS Med. Chem. Lett.* **4**, 491–496 (2013).
9. Jansen, K. *et al.* Extended Structure–Activity Relationship and Pharmacokinetic

Investigation of (4-Quinolinoyl)glycyl-2-cyanopyrrolidine Inhibitors of Fibroblast Activation Protein (FAP). *J. Med. Chem.* **57**, 3053–3074 (2014).

10. Loktev, A. *et al.* A Tumor-Imaging Method Targeting Cancer-Associated Fibroblasts. *J. Nucl. Med.* **59**, 1423–1429 (2018).
11. Lindner, T. *et al.* Development of Quinoline-Based Theranostic Ligands for the Targeting of Fibroblast Activation Protein. *J. Nucl. Med.* **59**, 1415–1422 (2018).
12. Loktev, A. *et al.* Development of Fibroblast Activation Protein–Targeted Radiotracers with Improved Tumor Retention. *J. Nucl. Med.* **60**, 1421–1429 (2019).
13. Sanchez-Crespo, A. Comparison of Gallium-68 and Fluorine-18 imaging characteristics in positron emission tomography. *Appl. Radiat. Isot.* **76**, 55–62 (2013).
14. Hu, K. *et al.* Preclinical evaluation and pilot clinical study of [18F]AlF-labeled FAPI-tracer for PET imaging of cancer associated fibroblasts. *Acta Pharm. Sin. B* **12**, 867–875 (2022).
15. Lindner, T. *et al.* 18F-labeled tracers targeting fibroblast activation protein. *EJNMMI Radiopharm. Chem.* **6**, 26 (2021).
16. Giesel, F. L. *et al.* FAPI-74 PET/CT Using Either 18F-AlF or Cold-Kit 68Ga Labeling: Biodistribution, Radiation Dosimetry, and Tumor Delineation in Lung Cancer Patients. *J. Nucl. Med.* **62**, 201–207 (2021).
17. Hu, K. *et al.* [18F]FAPI-42 PET imaging in cancer patients: optimal acquisition time, biodistribution, and comparison with [68Ga]Ga-FAPI-04. *Eur. J. Nucl. Med. Mol. Imaging* **49**, 2833–2843 (2022).
18. Toms, J. *et al.* Targeting Fibroblast Activation Protein: Radiosynthesis and Preclinical Evaluation of an 18 F-Labeled FAP Inhibitor. *J. Nucl. Med.* **61**, 1806–1813 (2020).
19. Walter, N. *et al.* Convenient PET-tracer production via SuFEx 18F-fluorination of nanomolar precursor amounts. *Eur. J. Med. Chem.* **237**, 114383 (2022).
20. Zhang, N. *et al.* Synthesis, radiolabeling, and evaluation of a (4-quinolinoyl)glycyl-2-cyanopyrrolidine analogue for fibroblast activation protein (FAP) PET imaging. *Front. Bioeng. Biotechnol.* **11**, (2023).
21. Yu, Z. *et al.* Design, Synthesis, and Evaluation of 18F-Labeled Tracers Targeting Fibroblast Activation Protein for Brain Imaging. *ACS Pharmacol. Transl. Sci.* **6**, 1745–1757 (2023).
22. Röhrich, M. *et al.* IDH-wildtype glioblastomas and grade III/IV IDH-mutant gliomas show elevated tracer uptake in fibroblast activation protein–specific PET/CT. *Eur. J. Nucl. Med. Mol. Imaging* **46**, 2569–2580 (2019).

23. Windisch, P. *et al.* Fibroblast Activation Protein (FAP) specific PET for advanced target volume delineation in glioblastoma. *Radiother. Oncol.* **150**, 159–163 (2020).
24. Giesel, F. L. *et al.* FAPI-PET/CT improves staging in a lung cancer patient with cerebral metastasis. *Eur. J. Nucl. Med. Mol. Imaging* **46**, 1754–1755 (2019).
25. Fu, W., Liu, L., Liu, H., Zhou, Z. & Chen, Y. Increased FAPI Uptake in Brain Metastasis From Lung Cancer on 68Ga-FAPI PET/CT. *Clin. Nucl. Med.* **46**, e1–e2 (2021).
26. Kömek, H. *et al.* 68Ga-FAPI-04 PET/CT, a new step in breast cancer imaging: a comparative pilot study with the 18F-FDG PET/CT. *Ann. Nucl. Med.* **35**, 744–752 (2021).
27. Wei, Y. *et al.* [18F]AlF-NOTA-FAPI-04: FAP-targeting specificity, biodistribution, and PET/CT imaging of various cancers. *Eur. J. Nucl. Med. Mol. Imaging* **49**, 2761–2773 (2022).
28. Yao, Y. *et al.* Performance of 18F-FAPI PET/CT in assessing glioblastoma before radiotherapy: a pilot study. *BMC Med. Imaging* **22**, 226 (2022).
29. Humpert, S., Hoffmann, C., Neumaier, F., Zlatopolskiy, B. D. & Neumaier, B. Validation of analytical HPLC with post-column injection as a method for rapid and precise quantification of radiochemical yields. *J. Chromatogr. B* 123847 (2023) doi:10.1016/j.jchromb.2023.123847.
30. Hoffmann, C. *et al.* Next Generation Copper Mediators for the Efficient Production of 18F-Labeled Aromatics. *Chem. – A Eur. J.* (2022) doi:10.1002/chem.202202965.
31. Gröner, B. *et al.* 7-[18F]Fluoro-8-azaisatoic Anhydrides: Versatile Prosthetic Groups for the Preparation of PET Tracers. *J. Med. Chem.* (2023) doi:10.1021/acs.jmedchem.3c01310.
32. Pettengill, O. S., Faris, R. A., Bell, R. H., Kuhlmann, E. T. & Longnecker, D. S. Derivation of ductlike cell lines from a transplantable acinar cell carcinoma of the rat pancreas. *Am. J. Pathol.* **143**, 292–303 (1993).
33. Hotz, H. G. *et al.* An Improved Clinical Model of Orthotopic Pancreatic Cancer in Immunocompetent Lewis Rats. *Pancreas* **22**, 113–121 (2001).
34. Busek, P. *et al.* Fibroblast activation protein alpha is expressed by transformed and stromal cells and is associated with mesenchymal features in glioblastoma. *Tumor Biol.* **37**, 13961–13971 (2016).
35. Arvanitis, C. D., Ferraro, G. B. & Jain, R. K. The blood–brain barrier and blood–tumour barrier in brain tumours and metastases. *Nat. Rev. Cancer* **20**, 26–41 (2020).
36. Sarkaria, J. N. *et al.* Is the blood–brain barrier really disrupted in all glioblastomas? A

critical assessment of existing clinical data. *Neuro. Oncol.* **20**, 184–191 (2018).

37. Djekidel, M., Alsadi, R., Abi Akl, M., Bouhali, O. & O'Doherty, J. Tumor microenvironment and fibroblast activation protein inhibitor (FAPI) PET: developments toward brain imaging. *Front. Nucl. Med.* **3**, (2023).
38. Röhrich, M. *et al.* FAP-specific PET signaling shows a moderately positive correlation with relative CBV and no correlation with ADC in 13 IDH wildtype glioblastomas. *Eur. J. Radiol.* **127**, 109021 (2020).
39. Wang, C. *et al.* Radiosynthesis and First Preclinical Evaluation of the Novel 11C-Labeled FAP Inhibitor 11C-FAPI: A Comparative Study of 11C-FAPIs and (68Ga) Ga-DOTA-FAPI-04 in a High–FAP-Expression Mouse Model. *Front. Chem.* **10**, (2022).
40. Brighi, C. *et al.* Comparative study of preclinical mouse models of high-grade glioma for nanomedicine research: the importance of reproducing blood-brain barrier heterogeneity. *Theranostics* **10**, 6361–6371 (2020).
41. Schulz, J. A., Rodgers, L. T., Kryscio, R. J., Hartz, A. M. S. & Bauer, B. Characterization and comparison of human glioblastoma models. *BMC Cancer* **22**, 844 (2022).
42. Jansen, K. *et al.* Novel FAP inhibitors. (2013).
43. Haberkorn, U. *et al.* FAP Inhibitor. (2019).
44. Haberkorn, U. *et al.* FAP Inhibitor. (2019).
45. McBride, W. J. *et al.* A Novel Method of 18F Radiolabeling for PET. *J. Nucl. Med.* **50**, 991–998 (2009).

3.5. Radiofluorierung von humanem Insulin

Die Radiofluorierung von großen Biomolekülen wie Peptiden, Proteinen oder Antikörpern stellt eine Herausforderung dar, da in diesen meist zahlreiche funktionelle Gruppen unterschiedlicher Reaktivität vorhanden sind. Dies erfordert entweder die Einführung geeigneter Schutzgruppen, was nicht immer möglich ist und die Tertiärstruktur irreversibel beeinträchtigen kann, oder eine vorherige Funktionalisierung des Moleküls, um eine bioorthogonale Markierung zu ermöglichen. Ein Beispiel für ein solches Biomolekül ist das Peptidhormon Insulin, welches aus 51 Aminosäuren besteht, die in zwei über Disulfidbrücken verbundenen Ketten angeordnet sind (Abb. 10). Insulin reguliert nicht nur den Blutzuckerspiegel und Stoffwechselprozesse in peripheren Organen, sondern beeinflusst auch Vorgänge im zentralen Nervensystem.[121] Eine Störung des Insulinsignalwegs ist er Auslöser von Diabetes mellitus.[122]

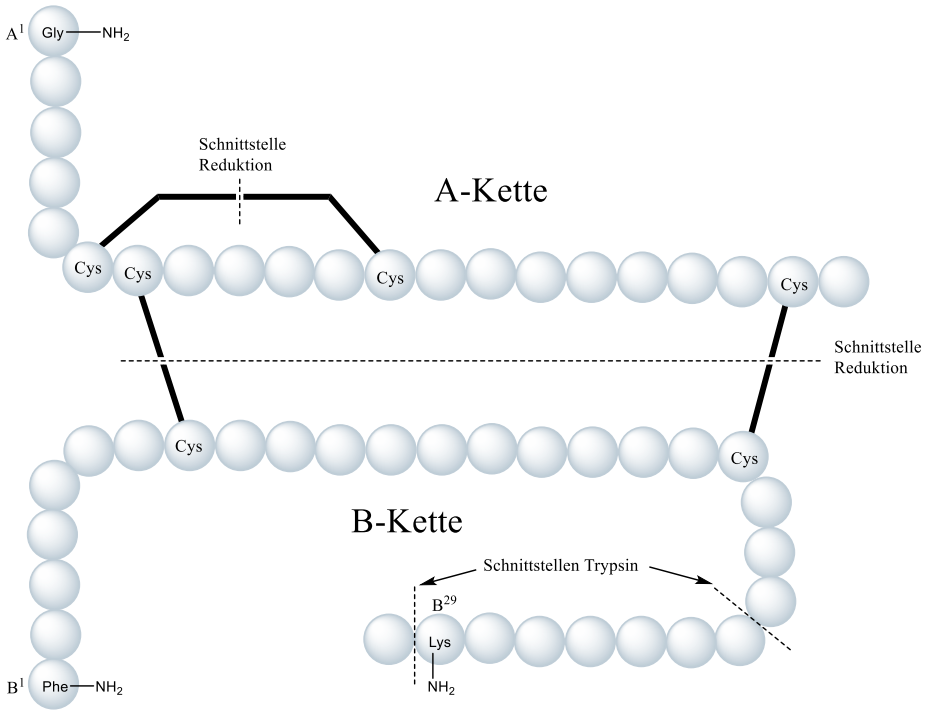

Abbildung 37: Struktur von Humanem Insulin nach Kim et al.[123]

Die erste Synthese eines radiofluorierten Insulin-Konjugates wurde durch Shai et al. 1989 veröffentlicht (Abb. 11). Dabei wurde eine PG verwendet, um ein in Position B^1 modifiziertes und an den Aminfunktionen an Position A^1 und B^{29} Boc-geschütztes Insulin indirekt zu markieren. Nach der Entschützung wurde das in B^1 Position markierte Insulin-Konjugat erhalten, jedoch betrug die Synthesezeit vier Stunden und die Gesamtausbeute lag bei <5%.[124]

Eine weitere Synthese von Guenther et al. von 2006 nutzte Succinimidyl-[^{18}F]-4-fluorbenzoat ([^{18}F]SFB) als prosthetische Gruppe um ein A^{1}- und B^{29}-Boc-geschütztes und in B^{1} Position mit einem Aminohexansäurelinker versehenes Insulin mit einer radiochemischen Ausbeute von 9% innerhalb von 200 min indirekt zu markieren.[125] Kim et al. erzielten mit derselben Methode eine radiochemische Ausbeute von 6% über 240 min durch Konjugation von [^{18}F]SFB mit A^{1},B^{29}-Di-Boc-Insulin ohne den Einsatz eines zusätzlichen Linkers.[123] In allen Fällen betrug allein die Synthesedauer für die Herstellung der PG etwa 80–100 min (keine detaillierten Informationen für die Prozedere von Guenther et al.) bei einer RCA von 45–56%, was einen erheblichen Verlust von ^{18}F vor der eigentlichen Konjugation bedeutet. Eine direkte Radiofluorierung von Insulin wurde bisher nicht beschrieben.

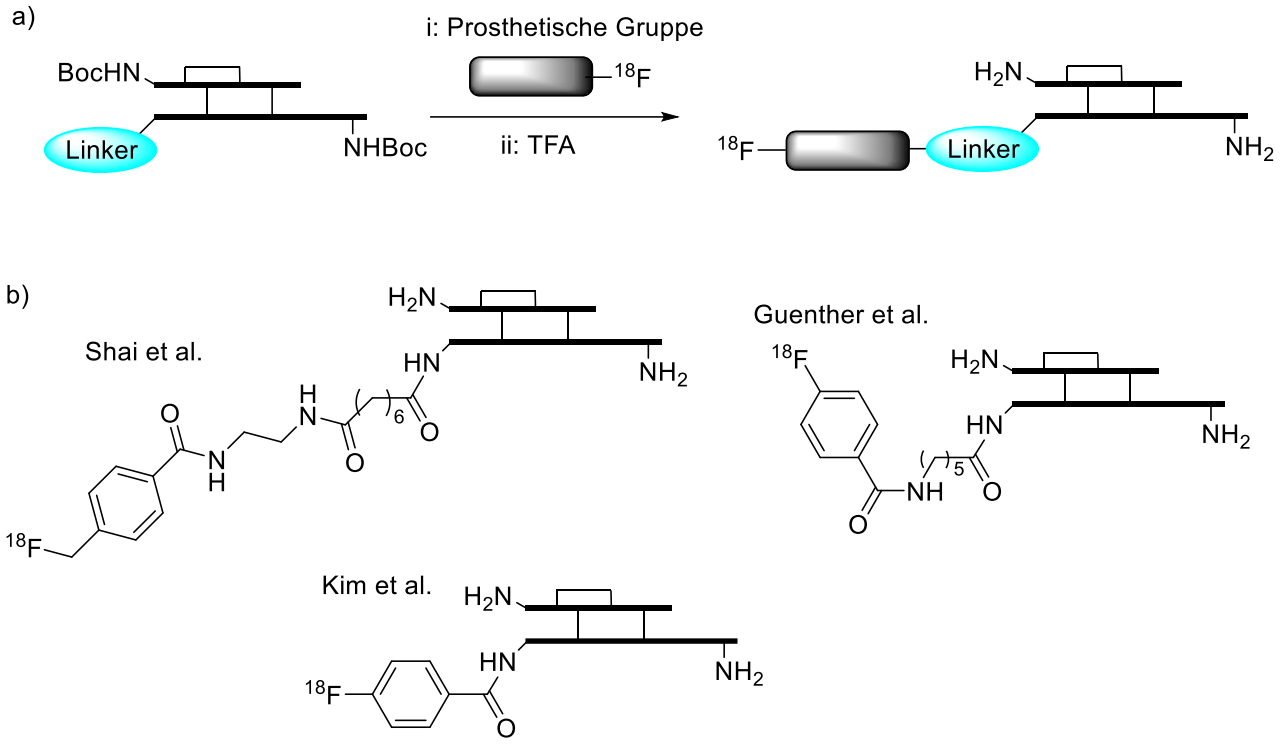

Abbildung 38: Bisher bekannte ^{18}F-markierte Insulinderivate.[123-125]

3.5.1. Indirekte Radiofluorierung von nativem Humaninsulin mittels der prosthetischen Gruppe 1-Methylamino-7-[^{18}F]fluor-8-azaisatosäureanhydrid ([^{18}F]MFA)

Wie in Kapitel 3.3 gezeigt wurde, weist 1-Methylamino-7-[^{18}F]fluor-8-azaisatosäureanhydrid ([^{18}F]MFA)[120] eine gewisse Selektivität hinsichtlich ihrer Aminreaktivität in Bezug auf die räumliche Zugänglichkeit auf, wenn die Konjugation in wässrigem Puffer durchgeführt wird. So ergab ein Kompetitionsexperiment, dass Lysin bei einem pH-Wert von 9 ausschließlich über das Amin in ε-Position mit [^{18}F]MFA Konjugiert wird. Daher sollte die indirekte Radiofluorierung von humanem Insulin (**11**) mit [^{18}F]MFA ([^{18}F]**13**) als PG untersucht werden

(Abbildung 39). Als Puffer wurden 0,2 M Tris-Puffer (pH 7,4), 0,2 M Boratpuffer (pH 9) oder 1 M Natriumhydrogencarbonat (pH 11) mit je 20% MeCN verwendet. Die Konjugation in DMSO ergab alle drei möglichen Radioprodukte [^{18}F]**14–16** mit einem Gesamt-RCU von 74% und einem Produkt-Verhältnis von 49:8:17 ([^{18}F]**14**:[^{18}F]**15**:[^{18}F]**16**) (Abbildung 39). In Boratpufffer wurde ein Gesamt-RCU von 38% erhalten, wobei dieselben Konjugationsprodukte in einem Verhältnis von 17:4:17 erhalten wurden. In HEPES-Puffer (pH 7,4) wurden ausschließlich [^{18}F]**14** und [^{18}F]**16** mit einem Gesamt-RCU von 32% und einem Verhältnis von 26:6 erhalten. Im Gegensatz dazu führte die Konjugation in Na_2CO_3 zur bevorzugten Bildung von [^{18}F]**16** bei einem Gesamt-RCU von 22% und einem Verhältnis zwischen [^{18}F]**15** und [^{18}F]**16** von 2:20. Bei der Reaktion unter basischen Bedingungen (Boratpuffer und Na_2CO_3) wurden bis zu 70% des Anhydrids [^{18}F]**13** hydrolysiert. Diese Ergebnisse führten zu der Überlegung, dass die ε-Aminogruppe teilweise durch die benachbarten Aminosäurenresten räumlich blockiert werden könnte. Daher sollte auch die Radiomarkierung von DesB^{30} Insulin durchgeführt werden. DesB^{30} Insulin, bei dem die letzte Aminosäure der B-Kette (Threonin) entfernt wurde, ähnelt dem nativen humanen Insulin in pharmakologischen Eigenschaften. Es wurde durch Inkubation von nativem humanen Insulin mit Carboxipeptidase A für 16 Stunden bei Raumtemperatur erhalten. Tatsächlich ergab die Markierung von DesB^{30} Insulin mit [^{18}F]**13** in DMSO nur die in A^1 und B^{29} markierten Produkte [^{18}F]**17** und [^{18}F]**19** mit einem Gesamt-RCU von 64% in einem Verhältnis von 28:36. In Boratpuffer betrug der Umsatz der beiden Produkte hingegen nur 20% in einem Verhältnis von 6:14.

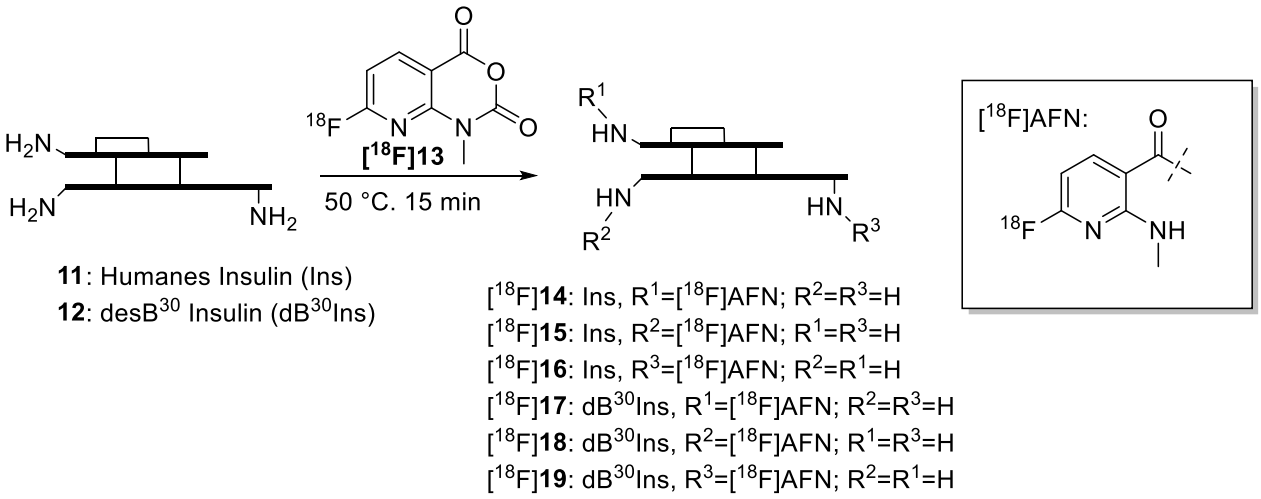

Abbildung 39: Indirekte Radiofluorierung von humanem Insulin und desB^{30}-Insulin mit [^{18}F]**13.**

In einer beispielhaften präparativen Synthese wurden nach Reaktion in DMSO bei 50 °C für 15 min und anschließender Reinigung über semipräparative HPLC die Konjugate [^{18}F]**14** und [^{18}F]**16** in RCAs von 20% und 11% ausgehend von [^{18}F]**13** erhalten.

Tabelle 2: Radiochemische Umsätze der indirekten Radiofluorierung von Insulin (Ins) und desB^{30}-Insulin (DesB^{30}).

EDUKT	PRODUKT	RCU (%)			
		DMSO	Boratpuffer	HEPES	Na_2CO_3
INSULIN	[^{18}F]**14**	49	17	26	n.d.
	[^{18}F]**15**	8	4	n.d.	2
	[^{18}F]**16**	17	17	6%	20
DESB30 INSULIN	[^{18}F]**17**	28	6	-	-
	[^{18}F]**18**	n.d.	n.d	-	-
	[^{18}F]**19**	36	14%.	-	-

Die nicht-radioaktiven Referenzverbindungen **14**–**19** wurden durch Konjugation von Insulin mit 2,5-Dioxopyrrolidin-1-yl 6-fluor-2-(methylamino)nicotinat (**20**) oder **13** entweder in 0,25% Na_2CO_3-Lösung oder 0,5 M HEPES (pH 7,4) durchgeführt (Abbildung 40). Die anschließende Isolation erfolgte über semi-präparative HPLC und Festphasenextraktion.

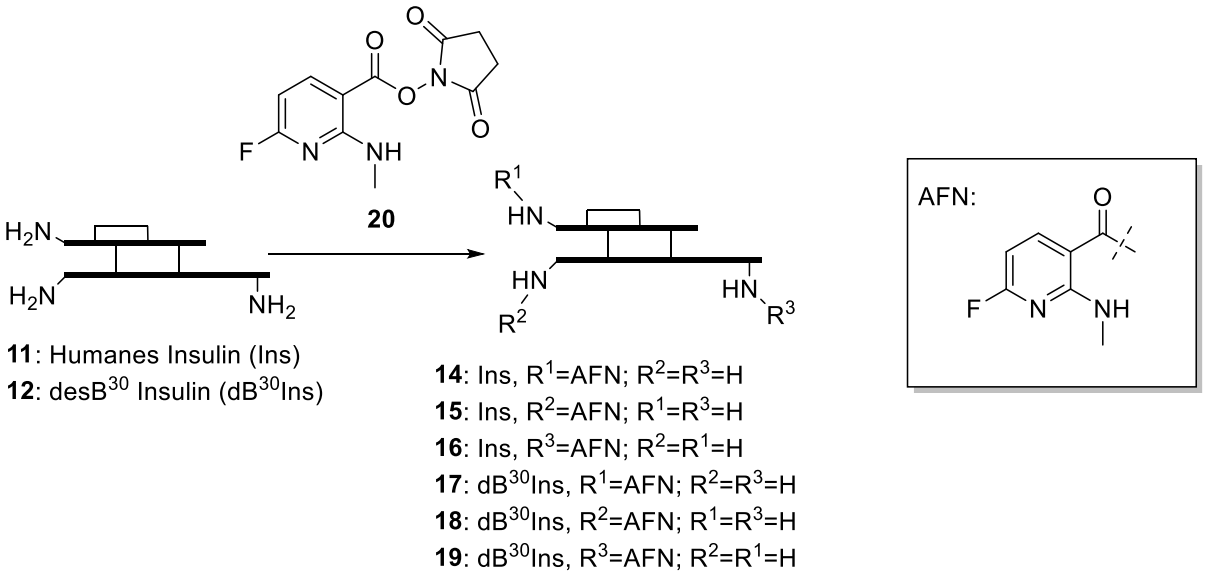

Abbildung 40: Synthese der Referenzverbindungen **14**–**19**.

3.5.2. Direkte Radiofluorierung von Insulinderivaten mittels Al[^{18}F]F-Komplexierung

Die indirekte Radiofluorierung von ungeschütztem Insulin führt zu einem Gemisch von Derivaten, das den verschiedenen Konjugationsstellen in der Peptidkette entspricht. Daher sollte ein entsprechend funktionalisiertes Insulinderivat direkt markiert werden. Viele direkte

Radiofluorierungsmethoden tolerieren jedoch nicht die Vielzahl funktioneller Gruppen, die in Peptiden wie Insulin vorhanden sind. Zudem ist die Löslichkeit von Insulin in vielen der für konventionelle Radiofluorierungsverfahren verwendeten aprotischen Lösungsmitteln gering. Daher wurde die Al[^{18}F]F-Komplexierung als Methode ausgewählt. Diese toleriert funktionelle Gruppen und die Markierung kann in einem Gemisch von H_2O und DMSO durchgeführt werden. Zudem können sehr geringe Mengen des Vorläufers verwendet werden, was gerade für Verbindungen mit hohen Molmassen wie Insulin zu erheblichen Einsparungen führt. Als Chelator wurde NODA ausgewählt, da es stabile Komplexe mit Al[^{18}F] eingeht und bei relativ niedrigen Temperaturen markierbar sein sollte.[59, 61] Der Radiomarkierungsvorläufer wurde von Prof. Dr. Boris D. Zlatopolskiy über Konjugation von Insulin mit NH_2-MPAA-NODA hergestellt.

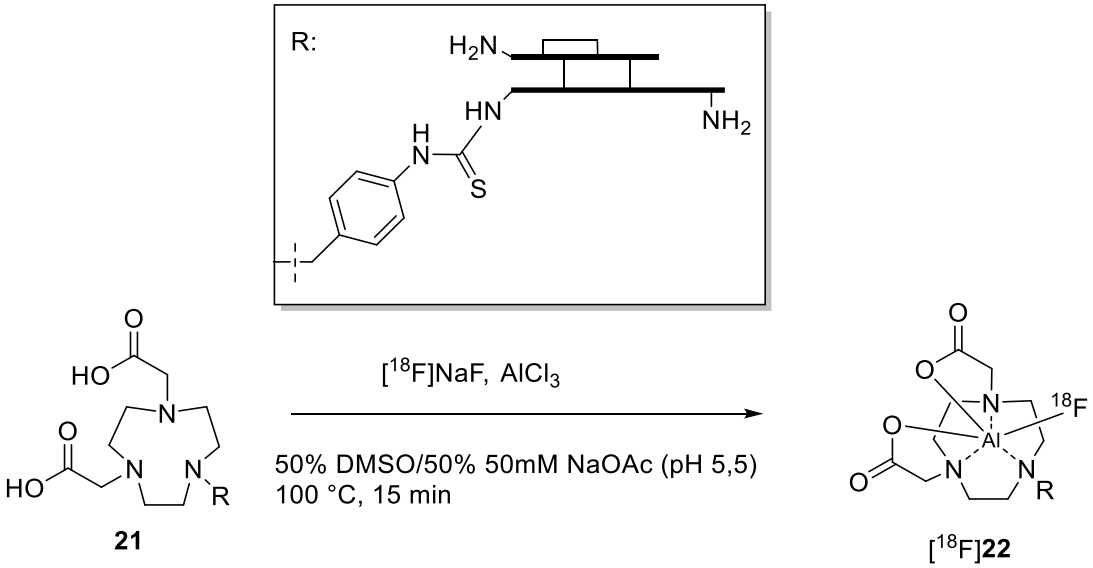

21 [^{18}F]**22**

Abbildung 41: Radiofluorierung von NODA-funktionalisiertem Insulin (**21**) mittels Al[^{18}F]F-Komplexierung.

Für die Radiomarkierung wurde [^{18}F]F^- mit einer 50 mM NaOAc Lösung von einer Anionentauscherkartusche eluiert. Ein Aliquot wurde zu einer Lösung des Vorläufers (**21**) und $AlCl_3$ in DMSO oder EtOH gegeben und anschließend erhitzt (Abbildung 41). Die Ergebnisse einer Optimierung der Reaktionsbedingungen sind in Tabelle 3 dargestellt. Zunächst wurde die Reaktion in EtOH durchgeführt, was jedoch sowohl bei pH 4 als auch bei pH 5,5 nur geringe Umsätze ergab. Ein Wechsel zu DMSO als Lösungsmittel erhöhte den Umsatz deutlich. Es zeigte sich, dass die Reaktion nach 15 min bereits abgeschlossen ist und eine Verlängerung der Reaktionszeit keine höheren Umsätze brachte. Die Erhöhung der Temperatur auf 100 °C brachte schon nach 5 min den höchsten Umsatz von 42±3%. Eine Erhöhung der DMSO-

Konzentration oder die Verwendung geringerer Vorläufermengen führten dagegen zu einer starken Verringerung des Umsatzes.

Tabelle 3: Optimierung der Reaktionsbedingungen für die Radiofluorierung von **21** über Al[^{18}F]F-Komplexierung.

Eintrag	pH	Vorläufermenge [nmol]	T [°C]	Lösungsmittel	t [min]	RCU [%]
1	4	50	50	50% EtOH	15	6±2
2	5,5	50	50	50% EtOH	15	10±3
3	5,5	50	50	50% DMSO	15	25±2
4	5,5	50	50	50% DMSO	30	22±3
5	5,5	50	70	50% DMSO	15	37±6
6	5,5	50	70	50% DMSO	30	38±3
7	5	50	70	50% DMSO	15	36±2
8	5,5	50	70	50% DMSO	15	13±1
9	5,5	50	100	50% DMSO	5	42±3
10	5,5	50	100	50% DMSO	15	41±4
11	5,5	50	100	80% DMSO	15	31±5
12	5,5	25	100	50% DMSO	15	16±3

Mit den optimierten Bedingungen wurde eine Synthese im präparativen Maßstab durchgeführt. Dazu wurde die komplette Elutionslösung von 100 µL NaOAc Puffer mit weiteren 100 µL Puffer sowie einer Lösung des Vorläufers und $AlCl_3$ in 200 µL DMSO versetzt. Die Reaktionslösung wurde dann für 15 min auf 100 °C erhitzt. Das komplexierte Produkt wurde mit einem Umsatz von 31±3% erhalten. Das Rohprodukt wurde über semi-präparative HPLC isoliert und mittels Festphasenextraktion an einer C18 Kartusche formuliert. Die Aktivitätsausbeute betrug 25±3% bei einer Synthesedauer von 50 min.

3.5.3. Bestimmung der Konjugationpositionen in den Referenzverbindungen

Bei der Synthese von Insulinderivaten durch Konjugation mit Amin-Gruppen muss bestimmt werden, an welcher der drei möglichen Positionen die Reaktion stattgefunden hat. Dies kann durch Massenspektrometrie erreicht werden. Dazu wurden parallel ein tryptischer Verdau und die Reduktion der Disulfidbrücken jedes Konjugats nach einem von Dr. Swen Humpert entwickelten Protokoll durchgeführt. Durch die Reduktion von Insulin mit Tris(2-carboxyethyl)phosphin (TCEP) werden die drei Disulfidbrücken zwischen jeweils zwei Cystein-Resten gebrochen (Abbildung 37). Daraus entstehen zwei Fragmente, welche der A-Kette (Fragment I) und der B-Kette (Fragment II) entsprechen. Eine Analyse des Massenspektrums zeigt somit, ob die Konjugation in der A-Kette (und somit in Position A^1) oder in einer der

beiden Positionen in der B-Kette stattgefunden hat. Beim Verdau mit Trypsin werden die Peptidbindungen zwischen B^{21} und B^{22} sowie zwischen B^{29} und B^{30} hydrolysiert. Es entstehen 5 mögliche Fragmente: B^{30} (als einzelne Aminosäure), das Oktapeptid B^{22}–B^{30} (Fragment IV), das Heptapeptid B^{22}–B^{29} (Fragment V), das Hauptfragment nach Abspaltung von B^{30} (desB^{30}-Ins, Fragment VI) sowie das Hauptfragment nach Abspaltung des Oktamers (Fragment III). Das Massenspektrum kann zeigen, ob die Konjugation in Position B^{29} (bei einer Massenzunahme von Fragment V oder IV) oder in einer der beiden Positionen des Hauptfragments (Fragment III) stattgefunden hat. Somit können Insulinderivate mit der Konjugation in Position A^1 oder B^{29} direkt über Reduktion beziehungsweise Verdau nachgewiesen werden, während eine Konjugation in Position B^1 über die Kombination der beiden Verfahren bestimmt wird. Dies wurde für die Referenzverbindungen der vorher beschriebenen Tracer durchgeführt.

3.6. Al[^{18}F]F-Komplexierungen

Radiomarkierung von FAPI-42

2019 haben Haberkorn et al. in einem Patent den FAP-spezifischen Tracer Al[^{18}F]F-FAPI-42 vorgestellt.[126] Allerdings wurden keine RCUs oder RCAs angegeben und bei der beschriebenen Radiosynthese wurde eine Aliquotierung des von der Anionenaustauscherkartusche eluierten [^{18}F]NaF vorgenommen. Auch in dem zwei Jahre später erschienenen Bericht von Lindner et al.[127] wurde für die dort verwendeten Bedingungen keine eindeutige radiochemische Ausbeute angegeben. In einer Synthese unter den im Patent beschriebenen Bedingungen (DMSO-Anteil von 25%) konnte der Tracer nur in einem RCU von unter 20% erhalten werden. Die von Lindner et al. beschriebenen Bedingungen (50% DMSO) ermöglichten einen RCU von etwa 40%.

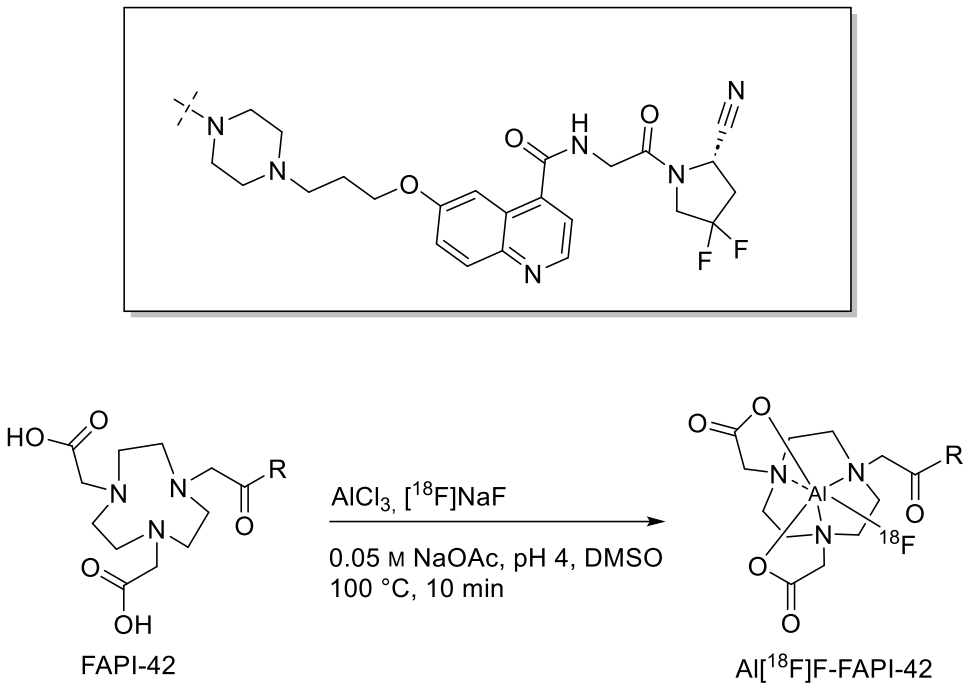

Abbildung 42: Radiosynthese von Al[^{18}F]F-FAPI-42.

Basierend auf diesen Ergebnissen wurden mehrere Parameter der Reaktion verändert, um den Umsatz zu verbessern (Abbildung 42). Zunächst wurde der Anteil des organischen Lösungsmittels in der Reaktionsmischung untersucht, wobei sowohl DMSO als auch EtOH in kleineren Reaktionsvolumina ähnliche Ergebnisse lieferten. Es zeigte sich, dass Lösungsmittelkonzentrationen von 80% oder höher die besten Ergebnisse erzielten. Da die Umsätze oberhalb von 80% nicht weiter stiegen und eine gewisse Menge wässriger Puffer für die Elution des [^{18}F]F$^-$ von der Anionenaustausherkartusche notwendig ist, wurde 80% als optimale Konzentration festgelegt. Obwohl zwischen EtOH und DMSO bei geringeren Reaktionsvolumina kein Unterschied erkennbar war, fiel bei präparativen Synthesen in größeren Volumina auf, dass der Umsatz bei Verwendung von EtOH stark verringert war. Die Reaktionstemperatur von 100 °C liegt über der Siedetemperatur von EtOH, was vermutlich zu Verdunstungseffekten in größeren Reaktoren führte und die genaue Kontrolle der Reaktionstemperatur beeinträchtigte. Daher wurde anschließend ausschließlich DMSO verwendet. Dieses musste vor der Verwendung jedoch destilliert werden, da festgestellt wurde, dass alle vorhandenen DMSO-Gebinde entweder in der Flasche oder scheinbar vor Abfüllung über Molsieben getrocknet wurden. Dabei wurden offensichtlich beträchtliche Mengen an Aluminiumsalzen an das DMSO abgegeben, da vor der Destillation auch ohne Zugabe von $AlCl_3$ Umsätze von 15–60% möglich waren. Untersuchungen der Mengen an Vorläufer und Aluminium mit destilliertem DMSO zeigten, dass 60 nmol Vorläufer ausreichend

für hohe Markierungsumsätze sind, während 0,5 Äqivalente $AlCl_3$ sich als optimal erwiesen. Die Variation des pH-Wertes zwischen 3 und 6 bestätigte ein pH-Optimum bei 4,0. Mit den optimierten Bedingungen wurde Al[^{18}F]F-FAPI-42 in einer Aktivitätsausbeute von 40±5% erhalten.

Radiomarkierung des AMP-Chelators 23

Es wurde ein neuer Chelator für die Al[^{18}F]F-Komplexierung basierend auf dem von Russelli et al.[66] entwickelten Chelator 2-AMPDA-HB (Abbildung 19) untersucht. Im Gegensatz zu diesem sollte der neue Chelator enantiomerenrein sein und eine zweite Funktionalität für die Konjugation an ein Pharmakophor tragen. Der von Dr. Birte Drewes zur Verfügung gestellte Chelator basiert auf 2-Aminopyrrolidin, welches zwei *N*-Acetylgruppen und eine *N*-(2-Hydroxy)benzylgruppe enthält, die an der Komplexierung des Al[^{18}F]F beteiligt sind. Die Position 5 des Benzyls enthält zudem eine Methylpropionatgruppe, über die eine Konjugation ermöglicht wird. Zur Radiomarkierung wurde gemäß der Methode von Russelli et al. zunächst [^{18}F]F^- auf einer Anionenaustauscherkartusche (Clorid-Form) fixiert und mit einer 0,9% Kochsalzlösung eluiert. Ein Aliquot dieser Lösung wurde entnommen und mit einer Lösung von 2 mM $AlCl_3$ in 0,1 M Natriumacetatpuffer für 5 min inkubiert, um den Al[^{18}F]F-Komplex zu bilden. Anschließend wurde der Vorläufer **23** in 0,1 M Natriumacetatpuffer und EtOH zugegeben und die Reaktionsmischung für weitere 12 min inkubiert um den markierten Komplex [^{18}F]**24** zu erhalten (Abbildung 43).

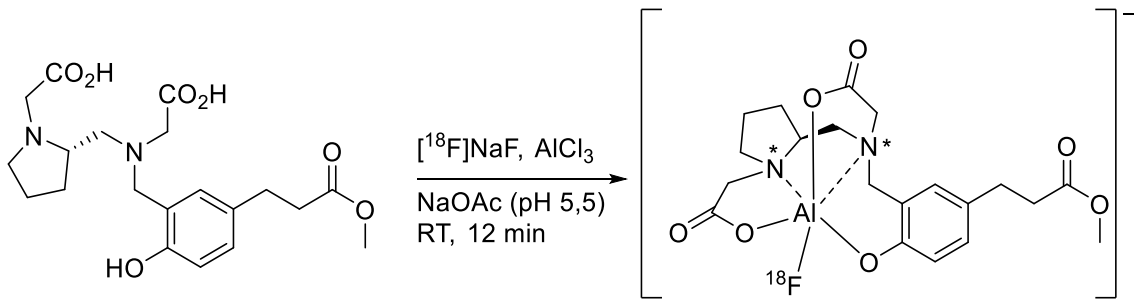

23 [^{18}F]**24**

Abbildung 43: Radiosynthese von [^{18}F]**24**.

Für die Optimierung der Reaktionsbedingungen wurde zunächst die pH-Abhängigkeit untersucht. Dabei wurden 75 nmol **23** in 10% EtOH (0,5 mL) zu 50 µL der Al[^{18}F]F-Lösungen, die auf pH-Werte eingestellt wurden, gegeben und bei Raumtemperatur inkubiert. Bei pH 4

wurde kaum radiochemischer Umsatz beobachtet (Tabelle 4). Erst pH-Werte zwischen 5 und 6,5 brachten bessere Umsätze, wobei das pH Optimum bei 5,5 lag. Für säurelabile Vorläufer wäre auch eine Markierung bei einem fast neutralen pH-Wert von 6,5 denkbar. Frühere Studien mit NOTA legten nahe, dass hohe Konzentrationen eines organischen Lösungsmittels wie EtOH oder DMSO förderlich sind. Jedoch führte eine Erhöhung der EtOH-Konzentration in der Vorläuferlösung zu deutlichen Umsatzeinbrüchen. Die Trennung von Vorläufer und Al[^{18}F]F-Komplex über chromatographische Methoden gestaltet sich oft schwierig. Aufgrund der geringen Vorläufermengen wird die Reinigung häufig mittels Festphasenextraktion durchgeführt. Um die Vorläufermenge im Produkt möglichst gering zu halten, wurde daher versucht, diese zu reduzieren. Die Reduzierung der Vorläufermenge auf 50 und 25 nmol verringerte die Umsätze jedoch auf 28±1% beziehungsweise 19±1%. Eine zusätzliche Steigerung der Reaktionstemperatur auf 100 °C konnte diese zudem nur auf 41±6 und 29±2 erhöhen.

Tabelle 4: Optimierung der Radiosynthese von [^{18}F]**24**.

EINTRAG	pH	VORLÄUFERMENGE [NMOL]	T [°C]	EtOH [%]	RCU [%]
1	4	75	21	10	3±1
2	4,5	75	21	10	11±1
3	5	75	21	10	69±3
4	5,5	75	21	10	86±2
5	6	75	21	10	79±3
6	6,5	75	21	10	65±4
7	5,5	75	21	50	2±0,5
8	5,5	75	21	80	1±0,5
9	5,5	50	21	10	28±1
10	5,5	50	100	10	41±6
11	5,5	25	21	10	19±1
12	5,5	25	100	10	29±2

Die Skalierung von Radiofluorierungen vom analytischem auf ein präparatives Niveau gestaltet sich oft als Herausforderung, da die erforderlichen größeren Reaktionsvolumina sich negativ auf den Umsatz auswirken können. Zur präparativen Markierung von **23** wurde [^{18}F]NaF mit 0,5 mL Kochsalzlösung von der Kartusche eluiert. Anschließend wurden 0,5 mL der Vorläuferlösung mit 75 nmol **23** und 10% EtOH in Puffer (pH 5,5) zugegeben wurden. Trotz des erhöhten Reaktionsvolumens wurde nach 12 min Inkubation bei Raumtemperatur 75±3% Umsatz erzielt. Die Radiofluorierung dieses Chelators eignet sich daher auch für präparative

Radiosynthesen. Um die Stabilität des Komplexes zu beurteilen, wurde der isolierte Tracer in verschiedenen wässrigen Lösungen sowie in Rattenserum über einen Zeitraum von 120 min inkubiert. Dabei schien [^{18}F]**24** in allen verwendeten Medien über den untersuchten Zeitraum hinweg stabil zu sein (Tabelle 5).

Tabelle 5: Stabilitätsuntersuchung von [^{18}F]**24.** a: 0,9 % NaCl; 0,2 M EDTA, 1X PBS (Gibco^{TM}), pH 7,4.

ZEIT [mIN]	**RCR [%]**			
	NaCl[a]	EDTA[b]	PBS[c]	Rattenserum
10	97	98	98	99
30	97	98	98	100
60	99	98	98	100
120	98	99	97	100

Der nächste Schritt wäre die Konjugation des Chelators an ein Pharmakophor über die Propionsäurefunktion, was aus zeitlichen Gründen im Rahmen dieser Arbeit jedoch nicht mehr umgesetzt werden konnte.

4. Zusammenfassung

Im ersten Projekt wurde die kupfervermittelte Radiofluorierung genutzt, um drei [^{18}F]FPhes herzustellen. Die verwendeten Vorläufer bestanden aus einem Ni-Komplex, der gleichzeitig die α-Amino- und α-Carbonylfunktionen schützte und eine stereoselektive Synthese ermöglichte. Der direkte Vergleich von Boronsäuren und Boronsäurepinakolestern als Abgangsgruppen zeigte keinen eindeutigen Trend hinsichtlich höherer Umsätze. Insgesamt wurde RCUs zwischen 69 und 91% erzielt. Darüber hinaus wurden (*S*)- und (*R*)-3-[^{18}F]FPhe mit Aktivitätsausbeuten von 41±2 und 33±1% synthetisiert. Die Synthese von (*S*)-3-[^{18}F]FPhe wurde zusätzlich automatisiert, um eine Routineanwendung zu ermöglichen, wobei eine Aktivitätsausbeute von 18±2% erreicht wurde.

Das zweite Projekt befasste sich mit der Synthese und Bewertung zweier weiterer Aminosäure-basierter Tracer, mit dem Ziel die physikochemischen, pharmakokinetischen und/oder Transporteigenschaften der Leitstruktur [^{18}F]FET zu verbessern. Das *m*-substituierte Analogon *m*-[^{18}F]FET und der Methylester [^{18}F]FET-OMe wurden in guten RCAs von 56±6% beziehungsweise 41±5% hergestellt, was eine präklinische Untersuchung dieser neuen Tracer ermöglichte.

Im Rahmen des dritten Projektes wurden [^{18}F]AFAs als potenzielle PGs entwickelt. Vier verschiedene [^{18}F]AFAs wurden via „on-cartridge“ Radiofluorierung mit RCAs von 65±5% hergestellt. Die *N*-Methyl und *N*-Ethyl-substituierten [^{18}F]AFAs wurden für die Konjugation mit Aminen eingesetzt, wobei abhängig von der sterischen Abschirmung des Amins Umsätze von 11–92% erhalten wurden. Diese Reaktion funktionierte sogar in wässrigem Puffer und zeigte eine Selektivität gegenüber bestimmten Aminen in Abhängigkeit von deren pKs-Wert. Die *N*-Azidopropyl- und *N*-Propargyl-substituierten [^{18}F]AFAs konnten nach Hydrolyse der entsprechenden Anhydride über die kupferkatalysierte Cycloaddition mit Alkinen und Aziden in Umsätzen von 88% und 77% konjugiert werden. Mit den entwickelten Protokollen konnten drei neuen PSMA-spezifischen Tracer ([^{18}F]JK-PSMA-15, [^{18}F]JK-PSMA-16 und [^{18}F]JK-PSMA-18) sowie der neue FAP Ligand [^{18}F]AFA-FAPI in Aktivitätsausbeuten von 16–28% synthetisiert werden. Zusätzlich wurde *N*-Methyl-substituiertes [^{18}F]AFA ([^{18}F]MFA) für die indirekte Radiofluorierung von nativem humanem Insulin und DesB^{30}-Insulin verwendet. Dabei wurden mehrere Produkte in unterschiedlichen Umsätzen, abhängig vom verwendeten Puffer-

Lösungsmittelgemisch erhalten. So wurden in einer beispielhaften Synthese das A^1-konjugierte [^{18}F]**14** und das B^{29}-konjugierte [^{18}F]**16** in RCAs von 20% und 11% erhalten.

Das vierte Projekt behandelte die Radiofluorierung über die Bildung von Al[^{18}F]F-Komplexen. Zunächst sollte diese Methode für die Markierung eines weiteren Insulinderivats eingesetzt werden. Das am Amin in Position B^1 mit dem Chelator NODA modifizierte Insulin **21** wurde mit einer Aktivitätsausbete von 25±3% synthetisiert. Die Optimierung der Reaktionsbedingungen für die Markierung des bekannten FAP-Tracers FAPI-42 ermöglichte eine Aktivitätsausbeute um 40%. Zuletzt wurde der neue Chelator **23** untersucht, welcher auf einer Aminomethylpiperidinstruktur basiert. Bei sehr milden Bedingungen (Raumtemperatur, pH 5,5–6, 10% EtOH) konnten Markierungsumsätze von über 80% erreicht werden. Stabilitätsexperimente zeigten eine gute Stabilität des so erhaltenen Komplexes [^{18}F]**24** über einen Zeitraum von zwei Stunden bei verschiedenen pH-Werten und in Rattenserum.

5. Experimentalteil

5.1. Allgemeines

Alle Synthesen wurden in Glaskolben mit magnetischem Rührer durchgeführt. Wenn angegeben wurde, dass unter Ausschluss von Feuchtigkeit oder Sauerstoff gearbeitet wurde, wurde der Kolben mit Rührer unter vermindertem Druck getrocknet und die Reaktion unter Argon an einer Schlenk-Apparatur durchgeführt. Lösungsmittel wurden unter vermindertem Druck (1–900 mbar) bei 40–50 °C mit einem Rotationsverdampfer (Büche Labortechnik, Essen, Deutschland) entfernt.

Lösungsmittel und Chemikalien wurden von VWR-International, Sigma-Aldrich, Alfa Aeser, Fluorochem Ltd und BLDpharm gekauft und ohne Reinigung verwendet. Dünnschichtchromatographie wurde entweder auf unmodifizierten Si-60-Platten mit Fluoreszenzindikator oder auf C18-modifizierten Platten mit Fluoreszenzindikator durchgeführt. Die Detektion erfolgte über UV-Absorption, ein PerkinElmer Cyclone® Plus Phosphoimager für Radioaktivität oder das Anfärben mittels Kaliumpermanganats, Ninhydrin oder Iod. Präparative Säulenchromatographie wurde auf einem Grace Reveleris™ Chromatographiesystem mit Büchi FlashPure (Si-60, 40 µm) oder Grace Resolv™ (C18. 40 µm) Säulen durchgeführt.

Analytische HPLC wurde auf einem Dionex Ultimate 3000 System mit „Ultimate 3000 variable wavelength detector“ und einem Berthold „LB500 NaI detector“ durchgeführt. Dabei waren Rheodyne 6 Injektoren vor und hinter der Säule verbaut. UV- und Radiodetektor waren in Reihe geschaltet, die Signale haben daher einen zeitlichen Versatz von 0,1–0,2 min je nach Flussrate. Semipräparative HPLC wurde auf einem selbst gebauten System mit einer Knauer K-199 Pumpe, einem Knauer K-2501 UV-Detektor, einem Rheodyne 6 Injektor und einem eigens angefertigten Geiger-Zähler durchgeführt.

NMR-Spektren wurden bei Raumtemperatur in dem angegebenen deuterierten Lösungsmittel mit einem Bruker Ascend™ 400 gemessen. Die bestimmten chemischen Verschiebungen sind als δ [ppm] relativ zu Restpeaks nicht deuterierter Lösungsmittel angegeben. Beobachtete Signale wurden wir folgt charakterisiert: s = Singulett, d = Dublett, t = Triplett, m = Multiplett, dd = Dublett von Dublett. Die Kopplungskonstanten J sind in Hertz angegeben.

Niedrig aufgelöste Massenspektren wurden an einem Thermo Finnigan Surveyor Massenspektrometer (Thermo Fisher Scientific GmbH, Dreieich, Germany) mit einer Flussrate von 200 mL/min aufgenommen. Bei HPLC-MS Messungen war ein Dionex Ultimate 3000 System (Säule: Phenomenex Aeris 3.6 µm Peptide XB-C18, 250 × 4.6 mm, H_2O/MeCN (5–90% über 50 min; 0,2 % Ameisensäure) vorgeschaltet. Hochauflösende Massenspektren wurden mit einem FTICR „LTQ FT Ultra“ (Thermo Fisher Scientific Inc., Bremen, Deutschland) aufgenommen.

5.2. Organische Synthesen

(*S,S*)-**3**, (*S,S*)-**5**, (*R,R*)-**5** und (*S,S*)-**6** wurden entsprechend der Prozedur von Craig et al.[99] hergestellt. Die NMR-Spektren und LRMS-Messungen entsprachen dabei den Literaturangeben.

Synthese von $B(OH)_2$-substituierten Ni(II)-BPX Komplexen – Allgemeine Methode (AM1)

$B(OH)_2$-substituierte Ni(II)-BPX Komplexe wurden entsprechend der Literatur[100] hergestellt. 0,1 M NaOH (0,2 Äq.) wurde zu einer Lösung des entsprechenden BPin-substituierten Ni-BPX Komplex (0,6 M, 1 Äq.) und Methylboronsäure (10 Äq.) in Aceton gegeben und die Reaktionsmischung wurde für 24 h gerührt. Anschließend wurde die Mischung durch Zugabe von 0,1 M HCl (0.15 Äq.) neutralisiert und alle Lösungsmittel unter vermindertem Druck entfernt. Das Rohprodukt wurde säulenchromatographisch auf einer Umkehrphase aufgereinigt (MeCN/H_2O).

(*S,S*)-Ni-BPB-3-$B(OH)_2$Phe [(*S,S*)-**7**]

Das Produkt wurde ausgehend von (*S,S*)-**5** als roter Feststoff erhalten (337 mg, 0.53 mmol, 85%). ^{1}H NMR (400 MHz, THF-d_8) δ = 8.40 (dd, *J* = 8.8, 1.0 Hz, 1H), 8.14 – 8.04 (m, 2H), 7.86 (d, *J* = 7.4 Hz, 1H), 7.69 (s, 1H), 7.62 – 7.42 (m, 4H), 7.37 – 7.20 (m, 6H), 7.10 (ddd, *J* = 7.4, 2.8, 1.5 Hz, 2H), 7.02 (ddd, *J* = 8.7, 6.8, 1.8 Hz, 1H), 6.65 (dd, *J* = 8.3, 1.7 Hz, 1H), 6.56 (ddd, *J* = 8.2, 6.8, 1.2 Hz, 1H), 4.13 (dd, *J* = 11.0, 6.6 Hz, 2H), 3.42 (d, *J* = 12.5 Hz, 1H), 3.23 (t, *J* = 8.3 Hz, 1H), 3.00 (ddd, *J* = 17.5, 11.4, 4.2 Hz, 2H), 2.79 (dd, *J* = 13.5, 5.6 Hz, 1H), 2.20 – 2.13 (m, 3H), 2.02 – 1.92 (m, 1H), 1.58 – 1.49 (m, 1H). ^{13}C NMR (101 MHz, THF-d_8) δ = 181.1, 178.0, 171.8, 145.2, 137.2, 136.2 (×2), 135.4, 134.4, 134.1, 133.4, 132.7, 132.4, 130.4, 130.0, 129.8, 129.4 (×2), 129.3,

128.5 (×2), 127.1, 124.5, 120.3, 72.6, 71.1, 63.9, 58.5, 40.4, 31.7, 24.2. HR-MS: m/z $[M+H]^+$ berechnet für $[C_{34}H_{31}BN_3NiO_5+H]^+$ = 631,18976, gefunden: 631,19052. Passendes Isotopenmuster.

(*R,R*)-Ni-BPB-3-B(OH)$_2$Phe [(*R,R*)-**7**]

Das Produkt wurde ausgehend von (*R,R*)-**5** als roter Feststoff erhalten (357 mg, 0.63 mmol, 90%). ^{1}H NMR (400 MHz, THF-d_8) δ = 8.40 (dd, *J* = 8.8, 0.9 Hz, 1H), 8.12 – 8.06 (m, 2H), 7.85 (t, *J* = 9.5 Hz, 1H), 7.68 (d, *J* = 12.9 Hz, 1H), 7.61 – 7.43 (m, 4H), 7.38 – 7.18 (m, 6H), 7.14 – 7.08 (m, 2H), 7.02 (ddd, *J* = 8.7, 6.8, 1.8 Hz, 1H), 6.65 (dd, *J* = 8.3, 1.7 Hz, 1H), 6.56 (ddd, *J* = 8.2, 6.8, 1.2 Hz, 1H), 4.17 – 4.09 (m, 2H), 3.42 (d, *J* = 12.5 Hz, 1H), 3.22 (d, *J* = 7.2 Hz, 1H), 3.06 – 2.94 (m, 2H), 2.79 (dd, *J* = 13.5, 5.6 Hz, 1H), 2.24 – 2.11 (m, 3H), 1.98 (ddd, *J* = 16.4, 11.1, 5.7 Hz, 1H), 1.53 (td, *J* = 11.0, 5.3 Hz, 1H). ^{13}C NMR (101 MHz, THF-d_8) δ = 181.1, 178.1, 171.8, 145.2, 137.3, 136.2 (×2), 135.4, 134.4, 134.1, 133.4, 132.7, 132.4, 130.5, 130.0, 129.8, 129.7, 129.4, 129.3, 128.5 (×2), 127.1, 124.5, 120.3, 72.6, 71.1, 63.9, 58.5, 40.4, 31.7, 24.2. HR-MS: m/z $[M+H]^+$ berechnet für $[C_{34}H_{31}BN_3NiO_5+H]^+$ = 631,18976, gefunden: 631,19045. Passendes Isotopenmuster.

(*S,S*)-Ni-BPA-α-methyl-3-B(OH)$_2$Phe [(*S,S*)-**8**]

Das Produkt wurde ausgehend von (*S,S*)-**6** als roter Feststoff erhalten (370 mg, 0.65 mmol, 83%). ^{1}H NMR (400 MHz, $CDCl_3$) δ = 8.48 (d, *J* = 8.6 Hz, 1H), 8.03 – 7.90 (m, 3H), 7.72 (d, *J* = 19.9 Hz, 1H), 7.62 – 7.54 (m, 1H), 7.47 – 7.16 (m, 7H), 7.14 (t, *J* = 8.2 Hz, 1H), 7.01 – 6.84 (m, 1H), 4.20 – 4.07 (m, 2H), 3.48 (d, *J* = 12.7 Hz, 1H), 3.35 (d, *J* = 13.4 Hz, 1H), 3.23 (dd, *J* = 9.4, 6.6 Hz, 1H), 2.98 (dd, *J* = 10.1, 5.8 Hz, 1H), 2.86 (d, *J* = 13.5 Hz, 1H), 2.29 – 1.99 (m, 2H), 1.92 – 1.78 (m, 1H), 1.68 – 1.56 (m, 4H), 1.50 – 1.40 (m, 1H), 1.31 – 1.21 (m, 3H), 0.89 (ddt, *J* = 46.7, 43.1, 19.6 Hz, 1H). ^{13}C NMR (101 MHz, $CDCl_3$) δ = 182.2, 181.8, 161.4, 142.8, 136.3, 134.4, 134.1, 133.9, 133.7, 133.3, 132.9, 131.8, 129.1, 128.9, 128.1, 124.0, 123.5, 121.6, 74.9, 70.4, 63.2, 60.5, 60.0, 57.4, 48.3, 30.9, 29.8, 25.4, 23.2, 21.2, 14.3 (×2). HR-MS: m/z $[M+H]^+$ berechnet für $[C_{29}H_{29}BN_3NiO_5+H]^+$ = 569,17411, gefunden: 569,17416. Passendes Isotopenmuster.

Bestimmung der Regioisomere von Insulinderivaten – Allgemeine Methode (AM2)

<u>Reduktion der Disulfidbrücken:</u>

Das Insulinderivat wurde in 0,2% Ameisensäure gelöst (1 mg/mL). TCEP·HCl (40 Äq.) in H_2O (100 mM) wurde zugegeben und bei 37 °C für 2 Stunden inkubiert.

Tryptischer Verdau

Das Insulinderivat wurde in einer Lösung von 0,1 mM $CaCl_2$ und 50 mM NH_4HCO_3 gelöst (1 mg/mL). Trypsin (TPCK behandelt, 10000 BAEE U/mg) wurde in einer Lösung von 1 mM HCl (pH 3) und 0,1 mM $CaCl_2$ gelöst (1 mg/mL). 100 µL der Insulinlösung wurden mit 5 µL der Trypsinlösung kombiniert (Protein/Trypsin 20:1 w/w) und über Nacht bei 37 °C inkubiert.

DesB^{30} Insulin (dB^{30}Ins)

10 mg Insulin wurden in 400 µL H_2O suspendiert und mit NaOH (40%, 20 µL) auf pH 9,2 gebracht. 1 µL (23 U/µL) Carboxypeptidase A-Lösung wurde zugegeben und für 16 Stunden bei Raumtemperatur inkubiert. Vollständiger Umsatz der Reaktion wurde mittels LRMS verifiziert. Die Isolierung fand mittels einer dreifachen Zentrifugenfiltration über Amicon Ultra 0,5 mL Centrifugal Filters (30 kDa Cutoff, Merck) für 15 min statt. LR-MS: m/z $[M+H]^+$ berechnet für $[C_{253}H_{381}N_{64}O_{75}S_6]^{5+}$ =1142,12, gefunden: 1142,24.

2,5-Dioxopyrrolidin-1-yl 6-fluor-2-(methylamino)nicotinat (**20**)

6-Fluor-2-(methylamino)nikotinsäure (100 mg, 0,59 mmol, 1 Äq.) wurde in 400 µL Thionylchlorid gelöst und für 1 Stunde bei Raumtemperatur gerührt. Das Lösungsmittel wurde bei vermindertem Druck im Wasserbad entfernt. Toluol (3 × 1 mL) wurde zugegeben und wiederholt bei vermindertem Druck im Wasserbad entfernt. Der Rückstand wurde in trockenem CH_2Cl_2 (1 mL) aufgenommen und bei 0 °C tropfenweise zu einer Lösung von *N*-Hydrosuccinimid (68 mg, 0,59 mmol, 1 Äq.) und Triethylamin (86 µL, 5,9 mmol, 10 Äq) in trockenem MeCN (0,5 mL) gegeben. Die Reaktionsmischung wurde für 30 min gerührt und anschließend wurde das Lösungsmittel bei vermindertem Druck im Wasserbad entfernt. Der Rückstand wurde in EtOAc aufgenommen (5 mL) und mit gesättigter wässriger NaCl-Lösung (3 × 5 mL), 5% Na_2CO_3 (3 × 5 mL) und H_2O (3 × 5 mL) gewaschen. Die organische Phase wurde mit Na_2SO_4 getrocknet und anschließend wurde das Lösungsmittel bei vermindertem Druck im Wasserbad entfernt. Das Produkt wurde als farbloser Feststoff erhalten (84 mg, 0,30 mmol, 50%). ^{1}H NMR (400 MHz, $CDCl_3$) δ 8.37 (dd, *J* = 8.2, 8.5, 1H), 7.68 (s, 1H), 6.20 (dd, *J* = 8.5, 2.8 Hz, 1H), 3.07 (d, *J* = 4.9 Hz, 3H), 2.93 (s, 4H). ^{13}C NMR (101 MHz, $CDCl_3$) δ 169.3, 166.8 (d, *J* = 248.1 Hz), 161.8 (s), 160.1 (d, *J* = 20.4 Hz), 145.6 (d, *J* = 11.6 Hz), 97.8 (s), 96.2 (d, *J* = 38.8 Hz),

28.2 (s), 25.6 (s). ^{19}F NMR (376 MHz, $CDCl_3$) δ -54.44. HR-MS: m/z $[M+H]^+$ berechnet für $[C_{11}H_{11}FN_3O_4]^+$ = 268,0728, gefunden: 268,0735.

Synthese von Insulin-AFA-Konjugaten **14**–**16**

Methode 1: Insulin (50 mg, 8,6 µmol, 1 Äq.) und **20** (23 mg, 86 µmol, 10 Äq.) wurden bei 0 °C in 0,25 M Na_2CO_3-Lösung (2,5 mL) suspendiert. DMSO (100 µL) wurden tropfenweise zugegeben und für 10 min bei Raumtemperatur gerührt. Nach 5 min wurde erneut DMSO (100 µL) zugegeben. Die Reaktion wurde durch Zugabe von 1 mL Essigsäure/MeCN/H_2O (2:1:1) gestoppt. Das Rohprodukt wurde über semipräparative HPLC (Säule: Synergi Hydro-RP, 19 µm, 100 Å, 250 × 10 mm; Laufmittel: 28% MeCN, 50 mM Na_2SO_4, 0,17% H_3PO_4; Flussrate: 4,5 mL/min) gereinigt. Die drei erhaltenen Fraktionen wurden mittels Festphasenextraktion (SEP-PAK C18, Waters) vom Reaktionsgemisch getrennt und in 50% EtOH aufgenommen. Die Identität der drei erhaltenen Regioisomere wurde mittels HPLC-MS bestimmt.

Methode 2: Insulin (50 mg, 8,6 µmol, 1 Äq.) wurde in 2,5 mL 0,5 M HEPES (pH 7,4) gelöst. **20** (3,5 mg, 13 µmol, 1,5 Äq.) in 200 µL DMSO wurde zugegeben und über Nacht bei Raumtemperatur gerührt. Die Reaktion wurde durch Zugabe von 1 mL Essigsäure/MeCN/H_2O (2:1:1) gestoppt. Das Rohprodukt wurde über semipräparative HPLC (Säule: Synergi Hydro-RP, 19 µm, 100 Å, 250 × 10 mm; Laufmittel: 28% MeCN, 50 mM Na_2SO_4, 0,17% H_3PO_4; Flussrate: 4,5 mL/min) gereinigt. Die drei erhaltenen Fraktionen wurden mittels Festphasenextraktion (SEP-PAK C18, Waters) vom Reaktionsgemisch getrennt und in 50% EtOH aufgenommen. Die Identität der drei erhaltenen Regioisomere wurde mittels HPLC-MS bestimmt.

A^1-AFA-Insulin (**14**)

Vorbehandlung	Detektiertes Fragment	m/z berechnet	m/z gefunden	t_R [min]	ESI Modus	Intensität TIC [%]
Reduktion	I+	1266,03	1266,27	41,6	-	10
Reduktion	II-	858,17	857,73	24,9	+	50

B[1]-AFA-Insulin (**15**)

Vorbehandlung	Detektiertes Fragment	m/z berechnet	m/z gefunden	t_R [min]	ESI Modus	Intensität TIC [%]
Reduktion	I-	1192,5	1192,32	29,07	-	9
Reduktion	II+	896,18	896,31	27,86	+	100
Trypsinierung	III-	974,04	973,87	23,12	+	80
Trypsinierung	IV+	1111,52	1112,65	26,09	+	55

B[29]-AFA-Insulin (**16**)

Vorbehandlung	Detektiertes Fragment	m/z berechnet	m/z gefunden	t_R [min]	ESI Modus	Intensität TIC [%]
Reduktion	I-	1190,5	1190,5	29,07	-	50
Reduktion	II+	896,18	896,34	28,13	+	100
Trypsinierung	III+	1049,464	1049,81	25,32	+	40
Trypsinierung	V-	859,43	859,31	16,17	+	20

Referenzverbindung **22**

21 (1 mg, 0,16 µmol, 1 Äq.) wurde in EtOH (0,5 mL) gelöst. $AlCl_3$ (0,02 mg, 0,16 µmol, 1 Äq) und NaF (0,007 mg, 0,16 µmol, 1 Äq.) in DMSO (100 µL) wurden zugefügt und für 1 h auf 100 °C erhitzt. LR-MS: m/z $[M+6H]^{6+}$ berechnet für $[C_{275}H_{410}AlFN_{68}O_{81}S_7]^{6+}$ = 1038,96, gefunden: 1039,16.

Referenzverbindung **24**

Die Synthese der Referenzverbindung **24** erfolgte laut der Literaturbeschreibung[66]. $AlCl_3$ (1 Äq.) und NaF (1 Äq.) wurden in H_2O (5 mL/mmol) gelöst und durch Zugabe von 0.1 M NaOH auf pH 4 eingestellt. Die Reaktionsmischung wurde für 10 min bei Raumtemperatur gerührt, eine Lösung des Vorläufers (1 Äq.) wurde zugegeben und für 2 Stunden auf 40 °C erhitzt. ^{19}F NMR (376 MHz, D_2O) δ -75.47. LR-MS: m/z $[M]^-$ berechnet für $[C_{20}H_{25}AlFN_2O_7]^-$ = 451,15, gefunden: 451,41.

5.3. Radiofluorierungen

N.c.a [^{18}F]Fluorid ([^{18}F]F^-) wurde aus ^{18}O-angereichertem H_2O mittels der $^{18}O(p,n)^{18}F$ Kernreaktion in einem 1,3 mL Titantarget des JSW BC 1710 Zyklotrons oder in einem 1,6 mL Silbertarget des GE PETtrace am INM-5 erzeugt.

Radiomarkierungsreaktionen wurden in Wheaten V-Vials mit einem PTFE-Magnetrührfisch und einem Silikonseptum als Verschluss durchgeführt. Die Reaktionsgefäße wurden in einem Aluminiumblock mit passenden Bohrlöchern unter Rühren erwärmt. Bei Reaktionen in organischen Lösungsmitteln wurde die Reaktion durch Zugabe von Reinstwasser gestoppt und nicht-reagiertes [^{18}F]F^- in Lösung gebracht. Die Bestimmung des radiochemischem Umsatzes und der radiochemischen Reinheit über analytische HPLC wurde mittels einer Referenzinjektion in das Ventil hinter der Säule, entsprechend dem von Humpert et al. beschriebenen Protokoll durchgeführt.[128] Zur Bestimmung der molaren Aktivität wurde eine Kalibriergerade der ^{19}F-Referenz angefertigt.

Radiofluorierung von Ni-BPX Komplexen mit $B(OH)_2$ oder BPin Abgangsgruppe – Allgemeine Methode (AM3)

[^{18}F]F^- wurde auf einer QMA Anionenaustauschkartusche fixiert und mit 1 mL wasserfreien MeOH gespült. Nachdem die Kartusche mit 10 mL Luft getrocknet wurde, wurde das [^{18}F]F^- mit einer Lösung von Et_4NOTf (1 mg, 3,6 µmol) in *n*BuOH (400 µL) direkt in eine Lösung des Vorläufers (10 µmol) in DMI (800 µL) eluiert. Die Reaktionsmischung wurde für 10 min auf 110 °C erhitzt.

Synthese von (*S*)-3-[^{18}F]FPhe und (*R*)-3-[^{18}F]FPhe – Allgemeine Methode (AM4)

Im Anschluss an die Markierung nach der Allgemeinen Methode AM3 wurde die Reaktionsmischung mit H_2O (5 mL) verdünnt und auf eine ChromaFix C18 ec Kartusche geladen. Die Kartusche wurde mit H_2O (5 mL) gewaschen und mit Luft (10 mL) getrocknet. Anschließend wurde das markierte Zwischenprodukt mit EtOH (1 mL) eluiert und das EtOH bei reduziertem Druck im Argon Strom bei 80 °C über 5 min entfernt. Anschließend wurde 2 M HCl (0,5 mL) zugegeben und die entstandene Reaktionsmischung für 10 min auf 110 °C erhitzt. Nach dem Abkühlen auf Raumtemperatur wurde das Produkt über eine semi-präparative HPLC isoliert (Säule: Synergi Hydro-RP, 19 µm, 100 Å, 250 × 10 mm; 5% EtOH, 0.1% H_3PO_4, 4.5 mL/min t_R = 9,8 min).

Automatisierte Radiosynthese von (*S*)-3-[^{18}F]FPhe

Der Aufbau der Kasette für die automatisierte Radiosynthese ist in Abbildung 36 dargestellt. [^{18}F]F^- wurde von der männlichen Seite her auf die Anionenaustauscherkartusche in Position 5 geladen und von derselben Seite her mit MeCN (1 mL, Vorratsgefäß 2) gespült. Anschließend wurde es über Spritze 1 mit einer Lösung von TBAOH in MeCN (25 mg in 1 mL, Vorratsgefäß 1) in Reaktor 1 eluiert. Das Lösungsmittel wurde bei vermindertem Druck im Stickstoffstrom bei 95 °C über 5 min entfernt. Dann wurde eine Lösung des Vorläufers und des Kupferkomplexes (10 µmol Vorläufer und 15.8 mg Kupferkomplex in 0,25 mL *n*BuOH und 0,5 mL DMI, Vorratsgefäß 3) zugegeben und das Reaktionsgemisch wurde für 15 min auf 110 °C erhitzt. Die Reaktionsmischung wurde mit H_2O (5 mL) in Spritze 2 verdünnt und auf eine Chromafix C18 Extraktionskartusche aufgetragen. Diese wurde mit H_2O (5 mL) gewaschen und im Stickstoffstrom über 1 min getrocknet. Das markierte Zwischenprodukt wurde mit EtOH (1 mL, Vorratsgefäß 5) in Reaktor 2 eluiert und das Lösungsmittel wurde bei vermindertem Druck im Stickstoffstrom bei 100 °C über 10 min entfernt. Anschließend wurde 1 M HCl (0,5 mL, Vorratsgefäß 4) zugegeben und die Entschützung wurde bei 110 °C über 10 min durchgeführt. Das Rohprodukt wurde mit H_2O (5 mL) in Spritze 2 verdünnt und über die interne semipräparative HPLC isoliert (Säule: Hydro RP, 19 µm, 100 Å, 250 × 10 mm; Eluens: 10% EtOH, 0,1% H_3PO_4, 4.5 mL/min t_R = 10,5 min). Das Produkt wurde direkt über einen Sterilfilter in das Produktgefäß geleitet.

Indirekte Radiofluorierung von Insulin und DesB^{30}-Insulin – Allgemeine Methode (AM5)

N-Methyl-substituiertes [^{18}F]AFA wurde wie zuvor beschrieben hergestellt. Von der Lösung des Tracers in MeCN wurde ein Aliquot (20 µL) zu einer Lösung von Insulin oder DesB^{30}-Insulin (0,5 µmol) in 80 µL des Reaktionspuffers gegeben und für 15 min auf 50 °C erhitzt. Als Reaktionspuffer wurden entweder DMSO, Boratpuffer (0,2 M, pH 9), HEPES (0,2 M, pH 7,4) oder Na_2CO_3 (0,25%,) verwendet. Einzelne Produkte wurden über semipräparative HPLC (Säule: Hydro RP, 19 µm, 100 Å, 250 × 10 mm; Eluens: 30% MeCN, 0,05 M Na_2SO_4, 0,17% H_3PO_4, 4.7 mL/min) isoliert.

Radiosynthese von [^{18}F]**22**

[^{18}F]F^- wurde auf einer QMA Anionenaustauschkartusche (vorkonditioniert mit 0,5 M NaOAc, pH 4,7, dann mit 5 mL H_2O gespült) fixiert, mit H_2O (1 mL) gespült und mit 50 mM NaOAc (100

µL, pH 4,7) eluiert. 50 nmol **21** und 29 nmol $AlCl_3$ in 50 mM NaOAc (100 µL, pH 5,5) und DMSO (700 µL) wurden zugegeben und für 15 min auf 50 °C erhitzt. Das Reaktionsgemisch wurde mit H_2O (600 µL) verdünnt und über semipräparative HPLC (Säule: Hydro RP, 19 µm, 100 Å, 250 × 10 mm; Eluens: 30% MeCN, 0,05 M Na_2SO_4, 0,17% H_3PO_4, 4.7 mL/min t_R = 9,3 min) isoliert.

Radiosynthese von Al[^{18}F]F-FAPI-42

[^{18}F]F^- wurde auf einer QMA Anionenaustauschkartusche (vorkonditioniert mit 0,5 M NaOAc, pH 4, dann mit 5 mL H_2O gespült) fixiert, mit H_2O (1 mL) gespült und mit 50 mM NaOAc (350 µL, pH 4) eluiert. Eine Lösung von **25** (60 nmol) und $AlCl_3$ (30 nmol) in DMSO (1,4 mL) wurde zugegeben und die Reaktionsmischung wurde für 12 min auf 100 °C erhitzt. Das Reaktionsgemisch wurde mit H_2O (30 mL) und gesättigter $NaHCO_3$ (1 mL) verdünnt und auf eine Festphasenextraktionskartusche (HLB light) geladen. Die Kartusche wurde mit H_2O (5 mL) gespült und das Produkt mit EtOH (1 mL) eluiert. Das Lösungsmittel wurde bei vermindertem Druck im Argonstrom entfernt und das Produkt in isotonischer Kochsalzlösung formuliert. Al[^{18}F]F-FAPI-42 wurde so in einer Aktivitätsausbeute von 40±5% erhalten (n=7)

Radiosynthese von [^{18}F]**24**

[^{18}F]F^- wurde auf einer QMA Anionenaustauschkartusche (Cl^--Form) fixiert, mit H_2O (1 mL) gespült und mit 0,9% NaCl-Lösung eluiert. Von dieser Lösung wurde ein Aliquot (50 µL) zu einer Lösung von $AlCl_3$ (2 mM, in 0,1 M NaOAc, pH 5,5) gegeben und für 5 min bei Raumtemperatur inkubiert. Dann wurde **23** (75 nmol, in 385 µL 0,1 M NaOAc, pH 5,5) zugegeben und für 12 min bei Raumtemperatur inkubiert. Das Produkt wurde in H_2O (4 mL) verdünnt und auf einer HLB light FPE Kartusche fixiert. Die Kartusche wurde mit H_2O (2 mL) gespült, mit Luft (5 mL) getrocknet und [^{18}F]**24** wurde mit EtOH (0,5 mL) eluiert.

Stabilitätsuntersuchungen von [^{18}F]**24**

Ein Aliquot des Produktes (2 MBq) wurden in einen Kunststoffreaktor überführt und das Lösungsmittel bei 20 °C im Argonstrom entfernt. Anschließend wurden 0,5 mL des entsprechenden Mediums (0,9 % NaCL, PBS pH4, 0,2M EDTA, Rattenserum) zugegeben und bei Raumtemperatur inkubiert. Zu verschiedenen Zeitpunkten (10, 30, 60, 120 min) wurden Proben (0,5 µL) entnommen und die radiochemische Reinheit mittels Radio-Dünnschichtchromatographie (C-18, 20% MeCN, R_f = 0,65) bestimmt.

6. Literatur

(1) Silberstein, E. B. Radioiodine: the classic theranostic agent. *Seminars in nuclear medicine* **2012**, *42* (3), 164-170.
(2) Weineisen, M.; Schottelius, M.; Simecek, J.; Baum, R. P.; Yildiz, A.; Beykan, S.; Kulkarni, H. R.; Lassmann, M.; Klette, I.; Eiber, M.; et al. 68Ga- and 177Lu-Labeled PSMA I&T: Optimization of a PSMA-Targeted Theranostic Concept and First Proof-of-Concept Human Studies. *J Nucl Med* **2015**, *56* (8), 1169-1176.
(3) Yoon, J. K.; Park, B. N.; Ryu, E. K.; An, Y. S.; Lee, S. J. Current Perspectives on (89)Zr-PET Imaging. *Int J Mol Sci* **2020**, *21* (12).
(4) Pandya, D. N.; Bhatt, N. B.; Almaguel, F.; Rideout-Danner, S.; Gage, H. D.; Sai, K. K. S.; Wadas, T. J. 89Zr-Chloride Can Be Used for Immuno-PET Radiochemistry Without Loss of Antigen Reactivity In Vivo. *J Nucl Med* **2019**, *60* (5), 696-701.
(5) Crisan, G.; Moldovean-Cioroianu, N. S.; Timaru, D. G.; Andries, G.; Cainap, C.; Chis, V. Radiopharmaceuticals for PET and SPECT Imaging: A Literature Review over the Last Decade. *Int J Mol Sci* **2022**, *23* (9).
(6) Rong, J.; Haider, A.; Jeppesen, T. E.; Josephson, L.; Liang, S. H. Radiochemistry for positron emission tomography. *Nat Commun* **2023**, *14* (1), 3257.
(7) Langer, O.; Någren, K.; Dolle, F.; Lundkvist, C.; Sandell, J.; Swahn, C.-G.; Vaufrey, F.; Crouzel, C.; Maziere, B.; Halldin, C. Precursor synthesis and radiolabelling of the dopamine D2 receptor ligand [11C]raclopride from [11C]methyl triflate. *J. Labelled Compd. Radiopharm.* **1999**, *42* (12), 1183-1193.
(8) Inoue, M.; Sumii, Y.; Shibata, N. Contribution of Organofluorine Compounds to Pharmaceuticals. *ACS omega* **2020**, *5* (19), 10633-10640.
(9) He, J.; Li, Z.; Dhawan, G.; Zhang, W.; Sorochinsky, A. E.; Butler, G.; Soloshonok, V. A.; Han, J. Fluorine-containing drugs approved by the FDA in 2021. *Chin. Chem. Lett.* **2023**, *34* (1), 107578.
(10) Ido, T.; Wan, C.-N.; Casella, V.; Fowler, J. S.; Wolf, A. P.; Reivich, M.; Kuhl, D. E. Labeled 2-deoxy-D-glucose analogs. 18F-labeled 2-deoxy-2-fluoro-D-glucose, 2-deoxy-2-fluoro-D-mannose and 14C-2-deoxy-2-fluoro-D-glucose. *J. Labelled Compd. Radiopharm.* **1978**, *14* (2), 175-183.
(11) Coenen, H. H. Fluorine-18 labeling methods: Features and possibilities of basic reactions. *Ernst Schering Research Foundation workshop* **2007**, (62), 15-50.
(12) Chirakal, R.; Firnau, G.; Schrobilgen, G. J.; McKay, J.; Garnett, E. S. The synthesis of [18F]Xenon difluoride from [18F]fluoride gas. *Appl. Radiat. Isot.* **1984**, *35* (5), 401-404.
(13) Lerman, O.; Tor, Y.; Rozen, S. Acetyl hypofluorite as a taming carrier of elemental fluorine for novel electrophilic fluorination of activated aromatic rings. *J. Org. Chem.* **1981**, *46* (22), 4629-4631.
(14) Adam, M. J.; Ruth, T. J.; Grierson, J. R.; Abeysekera, B.; Pate, B. D. Routine Synthesis of [18F]6-Fluorodopa with Fluorine-18 Acetyl Hypofluorite. *J. Nucl. Med.* **1986**, *27* (9), 1462-1466.
(15) Banks, R. E.; Mohialdin-Khaffaf, S. N.; Lal, G. S.; Sharif, I.; Syvret, R. G. 1-Alkyl-4-fluoro-1,4-diazoniabicyclo[2.2.2]octane salts: a novel family of electrophilic fluorinating agents. *J. Chem. Soc., Chem. Commun.* **1992**, (8), 595-596.
(16) Füchtner, F.; Preusche, S.; Mäding, P.; Zessin, J.; Steinbach, J. Factors affecting the specific activity of [18F]fluoride from a [18O]water target. *Nuklearmedizin. Nuclear medicine* **2008**, *47* (3), 116-119.

(17) Richarz, R.; Krapf, P.; Zarrad, F.; Urusova, E. A.; Neumaier, B.; Zlatopolskiy, B. D. Neither azeotropic drying, nor base nor other additives: a minimalist approach to (18)F-labeling. *Org Biomol Chem* **2014**, *12* (40), 8094-8099.
(18) Hamacher, K.; Coenen, H. H.; Stöcklin, G. Efficient stereospecific synthesis of no-carrier-added 2-[18F]-fluoro-2-deoxy-D-glucose using aminopolyether supported nucleophilic substitution. *J Nucl Med* **1986**, *27* (2), 235-238.
(19) Ermert, J.; Hamacher, K.; Coenen, H. H. N.C.A. 18F-labelled norephedrine derivatives via α-aminopropiophenones. *J. Labelled Compd. Radiopharm.* **2000**, *43* (14), 1345-1363.
(20) Beringer, F. M.; Brierley, A.; Drexler, M.; Gindler, E. M.; Lumpkin, C. C. Diaryliodonium Salts. II. The Phenylation of Organic and Inorganic Bases1,2. *J. Am. Chem. Soc.* **1953**, *75* (11), 2708-2712.
(21) Pike, V. W.; Aigbirhio, F. I. Reactions of cyclotron-produced [18F]fluoride with diaryliodonium salts—a novel single-step route to no-carrier-added [18]fluoroarenes. *J. Chem. Soc., Chem. Commun.* **1995**, (21), 2215-2216, 10.1039/C39950002215.
(22) Rotstein, B. H.; Stephenson, N. A.; Vasdev, N.; Liang, S. H. Spirocyclic hypervalent iodine(III)-mediated radiofluorination of non-activated and hindered aromatics. *Nat Commun* **2014**, *5*, 4365.
(23) Mu, L.; Fischer, C. R.; Holland, J. P.; Becaud, J.; Schubiger, P. A.; Schibli, R.; Ametamey, S. M.; Graham, K.; Stellfeld, T.; Dinkelborg, L. M.; et al. 18F-Radiolabeling of Aromatic Compounds Using Triarylsulfonium Salts. *Eur. J. Org. Chem.* **2012**, *2012* (5), 889-892.
(24) Sander, K.; Gendron, T.; Yiannaki, E.; Cybulska, K.; Kalber, T. L.; Lythgoe, M. F.; Arstad, E. Sulfonium salts as leaving groups for aromatic labelling of drug-like small molecules with fluorine-18. *Sci Rep* **2015**, *5*, 9941.
(25) Gendron, T.; Sander, K.; Cybulska, K.; Benhamou, L.; Sin, P. K. B.; Khan, A.; Wood, M.; Porter, M. J.; Arstad, E. Ring-Closing Synthesis of Dibenzothiophene Sulfonium Salts and Their Use as Leaving Groups for Aromatic (18)F-Fluorination. *J. Am. Chem. Soc.* **2018**, *140* (35), 11125-11132.
(26) Xu, P.; Zhao, D.; Berger, F.; Hamad, A.; Rickmeier, J.; Petzold, R.; Kondratiuk, M.; Bohdan, K.; Ritter, T. Site-Selective Late-Stage Aromatic [(18) F]Fluorination via Aryl Sulfonium Salts. *Angew. Chem. Int. Ed. Engl.* **2020**, *59* (5), 1956-1960.
(27) Chen, W.; Huang, Z.; Tay, N. E. S.; Giglio, B.; Wang, M.; Wang, H.; Wu, Z.; Nicewicz, D. A.; Li, Z. Direct arene C-H fluorination with (18)F(-) via organic photoredox catalysis. *Science* **2019**, *364* (6446), 1170-1174.
(28) Chen, W.; Wang, H.; Tay, N. E. S.; Pistritto, V. A.; Li, K. P.; Zhang, T.; Wu, Z.; Nicewicz, D. A.; Li, Z. Arene radiofluorination enabled by photoredox-mediated halide interconversion. *Nat Chem* **2022**, *14* (2), 216-223.
(29) Shetty, D.; Choi, S. Y.; Jeong, J. M.; Lee, J. Y.; Hoigebazar, L.; Lee, Y. S.; Lee, D. S.; Chung, J. K.; Lee, M. C.; Chung, Y. K. Stable aluminium fluoride chelates with triazacyclononane derivatives proved by X-ray crystallography and 18F-labeling study. *Chem. Commun.* **2011**, *47* (34), 9732-9734.
(30) Curnock, E.; Levason, W.; Light, M. E.; Luthra, S. K.; McRobbie, G.; Monzittu, F. M.; Reid, G.; Williams, R. N. Group 3 metal trihalide complexes with neutral N-donor ligands - exploring their affinity towards fluoride. *Dalton Trans* **2018**, *47* (17), 6059-6068.
(31) Askenasy, H. M.; Anbar, M.; Laor, Y.; Lewitus, Z.; Kosary, I. Z.; Guttmann, S. The localization of intracranial space-occupying lesions by fluoroborate ions labelled with fluorine 18. *Am J Roentgenol Radium Ther Nucl Med* **1962**, *88*, 350-354.

(32) Entzian, W.; Aronow, S.; Soloway, A. H.; Sweet, W. H. A Preliminary Evaluation of F¹⁸-Labeled Tetrafluoroborate As A Scanning Agent For Intracranial Tumors. *J. Nucl. Med.* **1964**, *5* (7), 542-550.
(33) Ting, R.; Adam, M. J.; Ruth, T. J.; Perrin, D. M. Arylfluoroborates and Alkylfluorosilicates as Potential PET Imaging Agents: High-Yielding Aqueous Biomolecular 18F-Labeling. *J. Am. Chem. Soc.* **2005**, *127* (38), 13094-13095.
(34) Ting, R.; Harwig, C.; auf dem Keller, U.; McCormick, S.; Austin, P.; Overall, C. M.; Adam, M. J.; Ruth, T. J.; Perrin, D. M. Toward [18F]-Labeled Aryltrifluoroborate Radiotracers: In Vivo Positron Emission Tomography Imaging of Stable Aryltrifluoroborate Clearance in Mice. *J. Am. Chem. Soc.* **2008**, *130* (36), 12045-12055.
(35) Liu, Z.; Li, Y.; Lozada, J.; Schaffer, P.; Adam, M. J.; Ruth, T. J.; Perrin, D. M. Stoichiometric leverage: rapid 18F-aryltrifluoroborate radiosynthesis at high specific activity for click conjugation. *Angew. Chem. Int. Ed. Engl.* **2013**, *52* (8), 2303-2307.
(36) Li, Z.; Chansaenpak, K.; Liu, S.; Wade, C. R.; Conti, P. S.; Gabbaï, F. P. Harvesting 18F-fluoride ions in water via direct 18F–19F isotopic exchange: radiofluorination of zwitterionic aryltrifluoroborates and in vivo stability studies. *MedChemComm* **2012**, *3* (10).
(37) Liu, Z.; Pourghiasian, M.; Radtke, M. A.; Lau, J.; Pan, J.; Dias, G. M.; Yapp, D.; Lin, K. S.; Benard, F.; Perrin, D. M. An organotrifluoroborate for broadly applicable one-step 18F-labeling. *Angew. Chem. Int. Ed. Engl.* **2014**, *53* (44), 11876-11880.
(38) An, F.; Nurili, F.; Sayman, H.; Ozer, Z.; Cakiroglu, H.; Aras, O.; Ting, R. One-Step, Rapid, (18)F-(19)F Isotopic Exchange Radiolabeling of Difluoro-dioxaborinins: Substituent Effect on Stability and In Vivo Applications. *J. Med. Chem.* **2020**, *63* (21), 12693-12706.
(39) Krishnan, H. S.; Ma, L.; Vasdev, N.; Liang, S. H. (18) F-Labeling of Sensitive Biomolecules for Positron Emission Tomography. *Chemistry* **2017**, *23* (62), 15553-15577.
(40) Schirrmacher, R.; Bradtmoller, G.; Schirrmacher, E.; Thews, O.; Tillmanns, J.; Siessmeier, T.; Buchholz, H. G.; Bartenstein, P.; Wangler, B.; Niemeyer, C. M.; et al. 18F-labeling of peptides by means of an organosilicon-based fluoride acceptor. *Angew. Chem. Int. Ed. Engl.* **2006**, *45* (36), 6047-6050.
(41) Ilhan, H.; Lindner, S.; Todica, A.; Cyran, C. C.; Tiling, R.; Auernhammer, C. J.; Spitzweg, C.; Boeck, S.; Unterrainer, M.; Gildehaus, F. J.; et al. Biodistribution and first clinical results of (18)F-SiFAlin-TATE PET: a novel (18)F-labeled somatostatin analog for imaging of neuroendocrine tumors. *Eur. J. Nucl. Med. Mol. Imaging.* **2020**, *47* (4), 870-880.
(42) Mu, L.; Höhne, A.; Schubiger, P. A.; Ametamey, S. M.; Graham, K.; Cyr, J. E.; Dinkelborg, L.; Stellfeld, T.; Srinivasan, A.; Voigtmann, U.; et al. Siliciumbausteine für eine einstufige 18F-Radiomarkierung von Peptiden für die PET-Bildgebung. *Angew. Chem.* **2008**, *120* (26), 5000-5003.
(43) Mawick, M.; Jaworski, C.; Bittermann, J.; Iovkova, L.; Pu, Y.; Wangler, C.; Wangler, B.; Jurkschat, K.; Krause, N.; Schirrmacher, R. CycloSiFA: The Next Generation of Silicon-Based Fluoride Acceptors for Positron Emission Tomography (PET). *Angew. Chem. Int. Ed. Engl.* **2023**, e202309002.
(44) Hong, H.; Zhang, L.; Xie, F.; Zhuang, R.; Jiang, D.; Liu, H.; Li, J.; Yang, H.; Zhang, X.; Nie, L.; et al. Rapid one-step (18)F-radiolabeling of biomolecules in aqueous media by organophosphine fluoride acceptors. *Nat Commun* **2019**, *10* (1), 989.
(45) Wang, C.; Zhang, L.; Mou, Z.; Feng, W.; Li, Z.; Yang, H.; Chen, X.; Lv, S.; Li, Z. Direct (18)F-Labeling of Biomolecules via Spontaneous Site-Specific Nucleophilic Substitution by F(-) on Phosphonate Prostheses. *Org. Lett.* **2021**, *23* (11), 4261-4266.

(46) Inkster, J. A.; Liu, K.; Ait-Mohand, S.; Schaffer, P.; Guerin, B.; Ruth, T. J.; Storr, T. Sulfonyl fluoride-based prosthetic compounds as potential 18F labelling agents. *Chemistry* **2012**, *18* (35), 11079-11087.
(47) Zhang, B.; Pascali, G.; Wyatt, N.; Matesic, L.; Klenner, M. A.; Sia, T. R.; Guastella, A. J.; Massi, M.; Robinson, A. J.; Fraser, B. H. Synthesis, bioconjugation and stability studies of [(18) F]ethenesulfonyl fluoride. *J. Labelled. Comp. Radiopharm.* **2018**, *61* (11), 847-856.
(48) Matesic, L.; Wyatt, N. A.; Fraser, B. H.; Roberts, M. P.; Pham, T. Q.; Greguric, I. Ascertaining the suitability of aryl sulfonyl fluorides for [18F]radiochemistry applications: a systematic investigation using microfluidics. *J. Org. Chem.* **2013**, *78* (22), 11262-11270.
(49) Al-Momani, E.; Israel, I.; Buck, A. K.; Samnick, S. Improved synthesis of [(1)(8)F]FS-PTAD as a new tyrosine-specific prosthetic group for radiofluorination of biomolecules. *Appl. Radiat. Isot.* **2015**, *104*, 136-142.
(50) Pascali, G.; Matesic, L.; Zhang, B.; King, A. T.; Robinson, A. J.; Ung, A. T.; Fraser, B. H. Sulfur - fluorine bond in PET radiochemistry. *EJNMMI Radiopharm. Chem.* **2017**, *2* (1), 9.
(51) Scroggie, K. R.; Perkins, M. V.; Chalker, J. M. Reaction of [(18)F]Fluoride at Heteroatoms and Metals for Imaging of Peptides and Proteins by Positron Emission Tomography. *Front Chem* **2021**, *9*, 687678.
(52) Zheng, Q.; Xu, H.; Wang, H.; Du, W. H.; Wang, N.; Xiong, H.; Gu, Y.; Noodleman, L.; Sharpless, K. B.; Yang, G.; et al. Sulfur [(18)F]Fluoride Exchange Click Chemistry Enabled Ultrafast Late-Stage Radiosynthesis. *J. Am. Chem. Soc.* **2021**, *143* (10), 3753-3763.
(53) Walter, N.; Bertram, J.; Drewes, B.; Bahutski, V.; Timmer, M.; Schutz, M. B.; Kramer, F.; Neumaier, F.; Endepols, H.; Neumaier, B.; et al. Convenient PET-tracer production via SuFEx (18)F-fluorination of nanomolar precursor amounts. *Eur. J. Med. Chem.* **2022**, *237*, 114383.
(54) Bruce Martin, R. Ternary complexes of Al3+ and F− with a third ligand. *Coord. Chem. Rev.* **1996**, *149*, 23-32.
(55) Solomonik, V. G.; Mukhanov, A. A. Ab initio study of scandium fluoride molecules: ScF, ScF2, AND ScF3. *J. Struct. Chem.* **2012**, *53* (1), 28-34.
(56) Lemal, D. M. Perspective on Fluorocarbon Chemistry. *J. Org. Chem.* **2004**, *69* (1), 1-11.
(57) McBride, W. J.; Sharkey, R. M.; Karacay, H.; D'Souza, C. A.; Rossi, E. A.; Laverman, P.; Chang, C. H.; Boerman, O. C.; Goldenberg, D. M. A novel method of 18F radiolabeling for PET. *J. Nucl. Med.* **2009**, *50* (6), 991-998.
(58) McBride, W. J.; D'Souza, C. A.; Sharkey, R. M.; Karacay, H.; Rossi, E. A.; Chang, C.-H.; Goldenberg, D. M. Improved 18F Labeling of Peptides with a Fluoride-Aluminum-Chelate Complex. *Bioconjugate Chem.* **2010**, *21* (7), 1331-1340.
(59) D'Souza, C. A.; McBride, W. J.; Sharkey, R. M.; Todaro, L. J.; Goldenberg, D. M. High-yielding aqueous 18F-labeling of peptides via Al18F chelation. *Bioconjugate Chem.* **2011**, *22* (9), 1793-1803.
(60) McBride, W. J.; D'Souza, C. A.; Sharkey, R. M.; Goldenberg, D. M. The radiolabeling of proteins by the [18F]AlF method. *Appl. Radiat. Isot.* **2012**, *70* (1), 200-204.
(61) Huynh, P. T.; Soni, N.; Pal, R.; Sarkar, S.; Jung, J.-M.; Lee, W.; Yoo, J. Direct radiofluorination of a heat-sensitive antibody by Al–18F complexation. *New J. Chem.* **2019**, *43* (38), 15389-15395.
(62) Malik, N.; Baur, B.; Winter, G.; Reske, S. N.; Beer, A. J.; Solbach, C. Radiofluorination of PSMA-HBED via Al(18)F(2+) Chelation and Biological Evaluations In Vitro. *Mol. Imaging. Biol.* **2015**, *17* (6), 777-785.
(63) Kersemans, K.; De Man, K.; Courtyn, J.; Van Royen, T.; Piron, S.; Moerman, L.; Brans, B.; De Vos, F. Automated radiosynthesis of Al[(18)F]PSMA-11 for large scale routine use. *Appl. Radiat. Isot.* **2018**, *135*, 19-27.

(64) Cleeren, F.; Lecina, J.; Bridoux, J.; Devoogdt, N.; Tshibangu, T.; Xavier, C.; Bormans, G. Direct fluorine-18 labeling of heat-sensitive biomolecules for positron emission tomography imaging using the Al(18)F-RESCA method. *Nat Protoc* **2018**, *13* (10), 2330-2347.
(65) Cleeren, F.; Lecina, J.; Ahamed, M.; Raes, G.; Devoogdt, N.; Caveliers, V.; McQuade, P.; Rubins, D. J.; Li, W.; Verbruggen, A.; et al. Al(18)F-Labeling Of Heat-Sensitive Biomolecules for Positron Emission Tomography Imaging. *Theranostics* **2017**, *7* (11), 2924-2939.
(66) Russelli, L.; Martinelli, J.; De Rose, F.; Reder, S.; Herz, M.; Schwaiger, M.; Weber, W.; Tei, L.; D'Alessandria, C. Room Temperature Al(18) F Labeling of 2-Aminomethylpiperidine-Based Chelators for PET Imaging. *ChemMedChem* **2020**, *15* (3), 284-292.
(67) Bhalla, R.; Darby, C.; Levason, W.; Luthra, S. K.; McRobbie, G.; Reid, G.; Sanderson, G.; Zhang, W. Triaza-macrocyclic complexes of aluminium, gallium and indium halides: fast18F and19F incorporation via halide exchange under mild conditions in aqueous solution. *Chem. Sci.* **2014**, *5* (1), 381-391.
(68) Bhalla, R.; Levason, W.; Luthra, S. K.; McRobbie, G.; Sanderson, G.; Reid, G. Radiofluorination of a pre-formed gallium(III) aza-macrocyclic complex: towards next-generation positron emission tomography (PET) imaging agents. *Chemistry* **2015**, *21* (12), 4688-4694.
(69) Whetter, J. N.; Vaughn, B. A.; Koller, A. J.; Boros, E. An Unusual Pair: Facile Formation and In Vivo Validation of Robust Sc-(18) F Ternary Complexes for Molecular Imaging. *Angew. Chem. Int. Ed. Engl.* **2022**, *61* (7), e202114203.
(70) Liu, Z.; Sun, Y.; Liu, T. Recent Advances in Synthetic Methodologies to Form C-(18)F Bonds. *Front Chem* **2022**, *10*, 883866.
(71) Wang, C.; Lin, R.; Yao, S. Recent Advances in (18)F-Labeled Amino Acids Synthesis and Application. *Pharmaceutics* **2022**, *14* (10).
(72) Luu, T. G.; Kim, H.-K. Recent progress on radiofluorination using metals: strategies for generation of C–18F bonds. *Org. Chem. Frot.* **2023**, *10* (22), 5746-5781.
(73) Ichiishi, N.; Brooks, A. F.; Topczewski, J. J.; Rodnick, M. E.; Sanford, M. S.; Scott, P. J. Copper-catalyzed [18F]fluorination of (mesityl)(aryl)iodonium salts. *Org. Lett.* **2014**, *16* (12), 3224-3227.
(74) Mossine, A. V.; Brooks, A. F.; Makaravage, K. J.; Miller, J. M.; Ichiishi, N.; Sanford, M. S.; Scott, P. J. Synthesis of [18F]Arenes via the Copper-Mediated [18F]Fluorination of Boronic Acids. *Org. Lett.* **2015**, *17* (23), 5780-5783.
(75) Makaravage, K. J.; Brooks, A. F.; Mossine, A. V.; Sanford, M. S.; Scott, P. J. H. Copper-Mediated Radiofluorination of Arylstannanes with [(18)F]KF. *Org. Lett.* **2016**, *18* (20), 5440-5443.
(76) Sharninghausen, L. S.; Brooks, A. F.; Winton, W. P.; Makaravage, K. J.; Scott, P. J. H.; Sanford, M. S. NHC-Copper Mediated Ligand-Directed Radiofluorination of Aryl Halides. *J. Am. Chem. Soc.* **2020**, *142* (16), 7362-7367.
(77) Lee, S. J.; Makaravage, K. J.; Brooks, A. F.; Scott, P. J. H.; Sanford, M. S. Copper-Mediated Aminoquinoline-Directed Radiofluorination of Aromatic C-H Bonds with K(18) F. *Angew. Chem. Int. Ed. Engl.* **2019**, *58* (10), 3119-3122.
(78) Tredwell, M.; Preshlock, S. M.; Taylor, N. J.; Gruber, S.; Huiban, M.; Passchier, J.; Mercier, J.; Genicot, C.; Gouverneur, V. A general copper-mediated nucleophilic 18F fluorination of arenes. *Angew. Chem. Int. Ed. Engl.* **2014**, *53* (30), 7751-7755.
(79) Zlatopolskiy, B. D.; Zischler, J.; Krapf, P.; Zarrad, F.; Urusova, E. A.; Kordys, E.; Endepols, H.; Neumaier, B. Copper-mediated aromatic radiofluorination revisited: efficient production of PET tracers on a preparative scale. *Chemistry* **2015**, *21* (15), 5972-5979.

(80) Zischler, J.; Kolks, N.; Modemann, D.; Neumaier, B.; Zlatopolskiy, B. D. Alcohol-Enhanced Cu-Mediated Radiofluorination. *Chemistry* **2017**, *23* (14), 3251-3256.
(81) Hoffmann, C.; Kolks, N.; Smets, D.; Haseloer, A.; Groner, B.; Urusova, E. A.; Endepols, H.; Neumaier, F.; Ruschewitz, U.; Klein, A.; et al. Next Generation Copper Mediators for the Efficient Production of (18) F-Labeled Aromatics. *Chemistry* **2023**, *29* (2), e202202965.
(82) Kuchar, M.; Pretze, M.; Kniess, T.; Steinbach, J.; Pietzsch, J.; Löser, R. Site-selective radiolabeling of peptides by 18F-fluorobenzoylation with [18F]SFB in solution and on solid phase: a comparative study. *Amino Acids* **2012**, *43* (4), 1431-1443.
(83) Kiesewetter, D. O.; Jacobson, O.; Lang, L.; Chen, X. Automated radiochemical synthesis of [18F]FBEM: A thiol reactive synthon for radiofluorination of peptides and proteins. *Appl. Radiat. Isot.* **2011**, *69* (2), 410-414.
(84) Cai, W.; Zhang, X.; Wu, Y.; Chen, X. A Thiol-Reactive ¹⁸F-Labeling Agent, N-[2-(4-¹⁸F-Fluorobenzamido)Ethyl]Maleimide, and Synthesis of RGD Peptide-Based Tracer for PET Imaging of α_vβ₃ Integrin Expression. *J. Nucl. Med.* **2006**, *47* (7), 1172-1180.
(85) Koniev, O.; Wagner, A. Developments and recent advancements in the field of endogenous amino acid selective bond forming reactions for bioconjugation. *Chem. Soc. Rev.* **2015**, *44* (15), 5495-5551, 10.1039/C5CS00048C.
(86) Humpert, S.; Omrane, M. A.; Urusova, E. A.; Gremer, L.; Willbold, D.; Endepols, H.; Krasikova, R. N.; Neumaier, B.; Zlatopolskiy, B. D. Rapid (18)F-labeling via Pd-catalyzed S-arylation in aqueous medium. *Chem. Commun.* **2021**, *57* (29), 3547-3550.
(87) Al-Shuaeeb, R. A. A.; Kolodych, S.; Koniev, O.; Delacroix, S.; Erb, S.; Nicolaÿ, S.; Cintrat, J.-C.; Brion, J.-D.; Cianférani, S.; Alami, M.; et al. Palladium-Catalyzed Chemoselective and Biocompatible Functionalization of Cysteine-Containing Molecules at Room Temperature. *Chem. Eur. J.* **2016**, *22* (32), 11365-11370.
(88) Ma, G.; McDaniel, J. W.; Murphy, J. M. One-Step Synthesis of [(18)F]Fluoro-4-(vinylsulfonyl)benzene: A Thiol Reactive Synthon for Selective Radiofluorination of Peptides. *Org. Lett.* **2021**, *23* (2), 530-534.
(89) Chiotellis, A.; Sladojevich, F.; Mu, L.; Muller Herde, A.; Valverde, I. E.; Tolmachev, V.; Schibli, R.; Ametamey, S. M.; Mindt, T. L. Novel chemoselective (18)F-radiolabeling of thiol-containing biomolecules under mild aqueous conditions. *Chem. Commun.* **2016**, *52* (36), 6083-6086.
(90) Kettenbach, K.; Schieferstein, H.; Ross, T. L. 18F-labeling using click cycloadditions. *Biomed. Res. Int.* **2014**, *2014*, 361329.
(91) Marik, J. Click for PET: rapid preparation of 18F fluoropeptides using CuI catalyzed 1,3-dipolar cycloaddition. *Tetrahedron* **2006**, *47* (37).
(92) Li, Y.; Liu, Z.; Harwig, C. W.; Pourghiasian, M.; Lau, J.; Lin, K. S.; Schaffer, P.; Benard, F.; Perrin, D. M. (18)F-click labeling of a bombesin antagonist with an alkyne-(18)F-ArBF(3) (-): in vivo PET imaging of tumors expressing the GRP-receptor. *Am. J. Nucl. Med. Mol. Imag.* **2013**, *3* (1), 57-70.
(93) Agard, N. J.; Prescher, J. A.; Bertozzi, C. R. A Strain-Promoted [3 + 2] Azide−Alkyne Cycloaddition for Covalent Modification of Biomolecules in Living Systems. *J. Am. Chem. Soc.* **2004**, *126* (46), 15046-15047.
(94) Xu, M.; Ma, X.; Pigga, J. E.; Zhang, H.; Wang, S.; Zhao, W.; Deng, H.; Wu, A. M.; Liu, R.; Wu, Z.; et al. Development of 18F-Labeled hydrophilic trans-cyclooctene as a bioorthogonal tool for PET probe construction. *Chem. Commun.* **2023**, 10.1039/D3CC04212J.

(95) Keinanen, O.; Fung, K.; Pourat, J.; Jallinoja, V.; Vivier, D.; Pillarsetty, N. K.; Airaksinen, A. J.; Lewis, J. S.; Zeglis, B. M.; Sarparanta, M. Pretargeting of internalizing trastuzumab and cetuximab with a (18)F-tetrazine tracer in xenograft models. *EJNMMI Res* **2017**, *7* (1), 95.
(96) Belokon, Y. N.; Bakhmutov, V. I.; Chernoglazova, N. I.; Kochetkov, K. A.; Vitt, S. V.; Garbalinskaya, N. S.; Belikov, V. M. General method for the asymmetric synthesis of α-amino acids via alkylation of the chiral nickel(II) Schiff base complexes of glycine and alanine. *J. Chem. Soc., Perkin Trans. 1* **1988**, (2), 305-312, 10.1039/P19880000305.
(97) Langen, K. J.; Stoffels, G.; Filss, C.; Heinzel, A.; Stegmayr, C.; Lohmann, P.; Willuweit, A.; Neumaier, B.; Mottaghy, F. M.; Galldiks, N. Imaging of amino acid transport in brain tumours: Positron emission tomography with O-(2-[(18)F]fluoroethyl)-L-tyrosine (FET). *Methods* **2017**, *130*, 124-134.
(98) Wiriyasermkul, P.; Nagamori, S.; Tominaga, H.; Oriuchi, N.; Kaira, K.; Nakao, H.; Kitashoji, T.; Ohgaki, R.; Tanaka, H.; Endou, H.; et al. Transport of 3-Fluoro-l-α-Methyl-Tyrosine by Tumor-Upregulated L-Type Amino Acid Transporter 1: A Cause of the Tumor Uptake in PET. *J. Nucl. Med.* **2012**, *53* (8), 1253-1261.
(99) Craig, A.; Kolks, N.; Urusova, E. A.; Zischler, J.; Brugger, M.; Endepols, H.; Neumaier, B.; Zlatopolskiy, B. D. Preparation of labeled aromatic amino acids via late-stage (18)F-fluorination of chiral nickel and copper complexes. *Chem. Commun.* **2020**, *56* (66), 9505-9508.
(100) Hinkes, S. P. A.; Klein, C. D. P. Virtues of Volatility: A Facile Transesterification Approach to Boronic Acids. *Org. Lett.* **2019**, *21* (9), 3048-3052.
(101) Habermeier, A.; Graf, J.; Sandhofer, B. F.; Boissel, J. P.; Roesch, F.; Closs, E. I. System L amino acid transporter LAT1 accumulates O-(2-fluoroethyl)-L-tyrosine (FET). *Amino Acids* **2015**, *47* (2), 335-344.
(102) Verhoeven, J.; Hulpia, F.; Kersemans, K.; Bolcaen, J.; De Lombaerde, S.; Goeman, J.; Descamps, B.; Hallaert, G.; Van den Broecke, C.; Deblaere, K.; et al. New fluoroethyl phenylalanine analogues as potential LAT1-targeting PET tracers for glioblastoma. *Sci. Rep.* **2019**, *9* (1), 2878.
(103) Augustyn, E.; Finke, K.; Zur, A. A.; Hansen, L.; Heeren, N.; Chien, H. C.; Lin, L.; Giacomini, K. M.; Colas, C.; Schlessinger, A.; et al. LAT-1 activity of meta-substituted phenylalanine and tyrosine analogs. *Bioorg. Med. Chem. Lett.* **2016**, *26* (11), 2616-2621.
(104) Henna, Y.; Lauri, P.; Kalle, M.; Jukka, L.; Krista, L.; Antti, P.; Maija, L.-K.; Jarkko, R. Structure–activity relationship study of compounds binding to large amino acid transporter 1 (LAT1) based on pharmacophore modeling and in situ rat brain perfusion. *Eur. J. Pharm. Sci.* **2013**, *48* (3), 523-531.
(105) Jussi, K.; Mikko, G.; Tarja, K.; Aleksanteri, P.; Seppo, A.; Maija, L.-K.; Krista, L.; Jarkko, R.; Kristiina, M. H. Structural properties for selective and efficient l-type amino acid transporter 1 (LAT1) mediated cellular uptake. *Int. J. Pharm.* **2018**, *544* (1), 91-99.
(106) Peura, L.; Malmioja, K.; Laine, K.; Leppänen, J.; Gynther, M.; Isotalo, A.; Rautio, J. Large Amino Acid Transporter 1 (LAT1) Prodrugs of Valproic Acid: New Prodrug Design Ideas for Central Nervous System Delivery. *Mol. Pharmaceutics* **2011**, *8* (5), 1857-1866.
(107) Venteicher, B.; Merklin, K.; Ngo, H. X.; Chien, H.-C.; Hutchinson, K.; Campbell, J.; Way, H.; Griffith, J.; Alvarado, C.; Chandra, S.; et al. The Effects of Prodrug Size and a Carbonyl Linker on l-Type Amino Acid Transporter 1-Targeted Cellular and Brain Uptake. *ChemMedChem* **2021**, *16* (5), 869-880.
(108) Zur, A. A.; Chien, H. C.; Augustyn, E.; Flint, A.; Heeren, N.; Finke, K.; Hernandez, C.; Hansen, L.; Miller, S.; Lin, L.; et al. LAT1 activity of carboxylic acid bioisosteres: Evaluation of hydroxamic acids as substrates. *Bioorg. Med. Chem. Lett.* **2016**, *26* (20), 5000-5006.

(109) Ristau, B. T.; O'Keefe, D. S.; Bacich, D. J. The prostate-specific membrane antigen: Lessons and current clinical implications from 20 years of research. *Urol. Oncol.* **2014**, *32* (3), 272-279.
(110) Siegel, R. L.; Miller, K. D.; Wagle, N. S.; Jemal, A. Cancer statistics, 2023. *CA Cancer J. Clin.* **2023**, *73* (1), 17-48.
(111) Houshmand, S.; Lawhn-Heath, C.; Behr, S. PSMA PET imaging in the diagnosis and management of prostate cancer. *Abdom Radiol (NY)* **2023**.
(112) Chen, Y.; Foss, C. A.; Byun, Y.; Nimmagadda, S.; Pullambhatla, M.; Fox, J. J.; Castanares, M.; Lupold, S. E.; Babich, J. W.; Mease, R. C.; et al. Radiohalogenated Prostate-Specific Membrane Antigen (PSMA)-Based Ureas as Imaging Agents for Prostate Cancer. *J. Med. Chem.* **2008**, *51* (24), 7933-7943.
(113) Endepols, H.; Morgenroth, A.; Zlatopolskiy, B. D.; Krapf, P.; Zischler, J.; Richarz, R.; Munoz Vasquez, S.; Neumaier, B.; Mottaghy, F. M. Peripheral ganglia in healthy rats as target structures for the evaluation of PSMA imaging agents. *BMC Cancer* **2019**, *19* (1), 633.
(114) Fitzgerald, A. A.; Weiner, L. M. The role of fibroblast activation protein in health and malignancy. *Cancer Metastasis Rev.* **2020**, *39* (3), 783-803.
(115) Hamson, E. J.; Keane, F. M.; Tholen, S.; Schilling, O.; Gorrell, M. D. Understanding fibroblast activation protein (FAP): substrates, activities, expression and targeting for cancer therapy. *Proteom. Clin. Appl.* **2014**, *8* (5-6), 454-463.
(116) Jansen, K.; Heirbaut, L.; Cheng, J. D.; Joossens, J.; Ryabtsova, O.; Cos, P.; Maes, L.; Lambeir, A. M.; De Meester, I.; Augustyns, K.; et al. Selective Inhibitors of Fibroblast Activation Protein (FAP) with a (4-Quinolinoyl)-glycyl-2-cyanopyrrolidine Scaffold. *ACS Med. Chem. Lett.* **2013**, *4* (5), 491-496.
(117) Jansen, K.; Heirbaut, L.; Verkerk, R.; Cheng, J. D.; Joossens, J.; Cos, P.; Maes, L.; Lambeir, A. M.; De Meester, I.; Augustyns, K.; et al. Extended structure-activity relationship and pharmacokinetic investigation of (4-quinolinoyl)glycyl-2-cyanopyrrolidine inhibitors of fibroblast activation protein (FAP). *J. Med. Chem.* **2014**, *57* (7), 3053-3074.
(118) Hu, K.; Li, J.; Wang, L.; Huang, Y.; Li, L.; Ye, S.; Han, Y.; Huang, S.; Wu, H.; Su, J.; et al. Preclinical evaluation and pilot clinical study of [(18)F]AlF-labeled FAPI-tracer for PET imaging of cancer associated fibroblasts. *Acta Pharm Sin B* **2022**, *12* (2), 867-875.
(119) Zhang, N.; Pan, F.; Pan, L.; Diao, W.; Su, F.; Huang, R.; Yang, B.; Li, Y.; Qi, Z.; Zhang, W.; et al. Synthesis, radiolabeling, and evaluation of a (4-quinolinoyl)glycyl-2-cyanopyrrolidine analogue for fibroblast activation protein (FAP) PET imaging. *Front. Bioeng. Biotechnol.* **2023**, *11*, 1167329.
(120) Gröner, B.; Willmann, M.; Donnerstag, L.; Urusova, E. A.; Neumaier, F.; Humpert, S.; Endepols, H.; Neumaier, B.; Zlatopolskiy, B. D. 7-[(18)F]Fluoro-8-azaisatoic Anhydrides: Versatile Prosthetic Groups for the Preparation of PET Tracers. *J. Med. Chem.* **2023**, *66* (17), 12629-12644.
(121) Agrawal, R.; Reno, C. M.; Sharma, S.; Christensen, C.; Huang, Y.; Fisher, S. J. Insulin action in the brain regulates both central and peripheral functions. *Am. J. Physiol. Endocrinol. Metab.* **2021**, *321* (1), E156-E163.
(122) Xiang, Y.; Su, B.; Liu, D.; Webber, M. J. Managing Diabetes with Hydrogel Drug Delivery. *Advanced Therapeutics* **2024**, *7* (1), 2300127.
(123) Kim, D. H.; Blacker, M.; Valliant, J. F. Preparation and evaluation of fluorine-18-labeled insulin as a molecular imaging probe for studying insulin receptor expression in tumors. *J. Med. Chem.* **2014**, *57* (9), 3678-3686.
(124) Shai, Y.; Kirk, K. L.; Channing, M. A.; Dunn, B. B.; Lesniak, M. A.; Eastman, R. C.; Finn, R. D.; Roth, J.; Jacobson, K. A. Fluorine-18 labeled insulin: a prosthetic group methodology for

incorporation of a positron emitter into peptides and proteins. *Biochemistry* **1989**, *28* (11), 4801-4806.
(125) Guenther, K. J.; Yoganathan, S.; Garofalo, R.; Kawabata, T.; Strack, T.; Labiris, R.; Dolovich, M.; Chirakal, R.; Valliant, J. F. Synthesis and in Vitro Evaluation of 18F- and 19F-Labeled Insulin: A New Radiotracer for PET-based Molecular Imaging Studies. *J. Med. Chem.* **2006**, *49* (4), 1466-1474.
(126) Haberkorn, U.; Loktev, A.; Lindner, T.; Mier, W.; Giesel, F.; Kratochwil, C. FAP INHIBITOR. WO 2019/154886 A1, 2019.
(127) Lindner, T.; Altmann, A.; Giesel, F.; Kratochwil, C.; Kleist, C.; Krämer, S.; Mier, W.; Cardinale, J.; Kauczor, H.-U.; Jäger, D.; et al. 18F-labeled tracers targeting fibroblast activation protein. *EJNMMI Radiopharm. Chem.* **2021**, *6* (1).
(128) Humpert, S.; Hoffmann, C.; Neumaier, F.; Zlatopolskiy, B. D.; Neumaier, B. Validation of analytical HPLC with post-column injection as a method for rapid and precise quantification of radiochemical yields. *J. Chromatogr. B. Analyt. Technol. Biomed. Life. Sci.* **2023**, *1228*, 123847.

7. Anhang

7.1. NMR-Spektren

Verbindung (*S,S*)-**7**

^{1}H NMR (400 MHz, THF-d8)

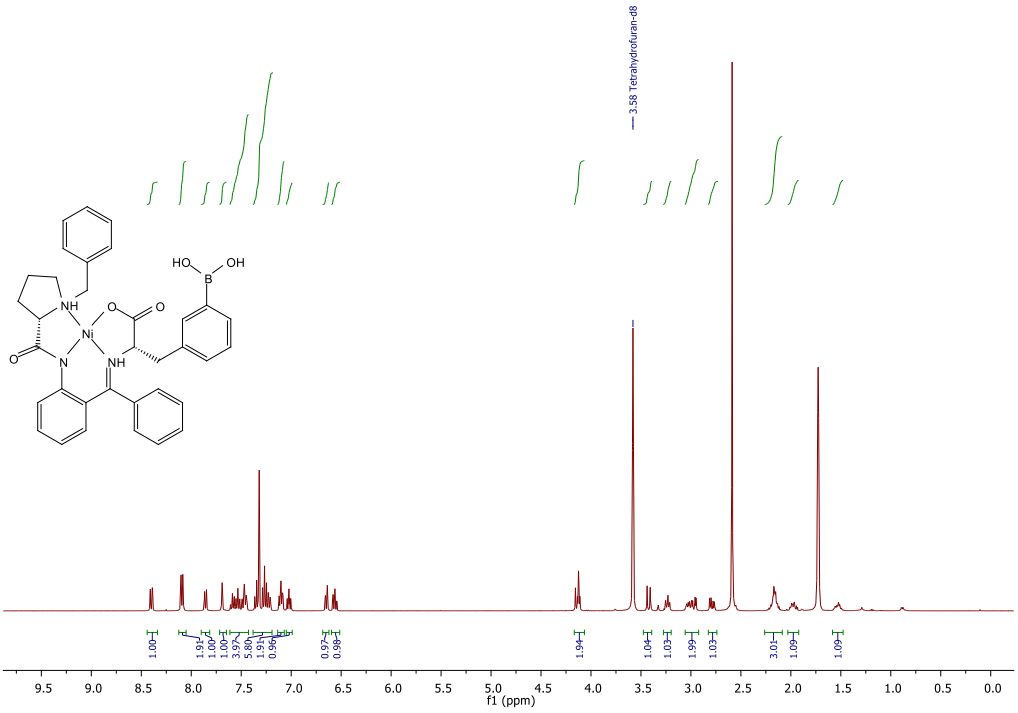

^{13}C NMR (101 MHz, THF-d8)

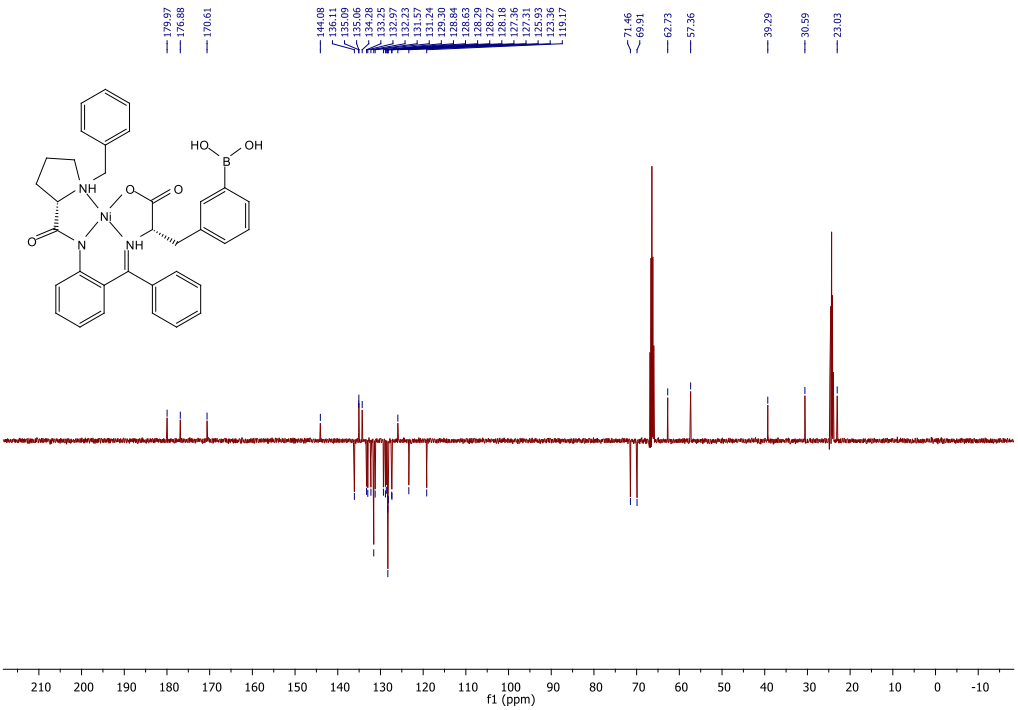

Verbindung (*R*,*R*)-**7**

^{1}H NMR (400 MHz, THF-d8)

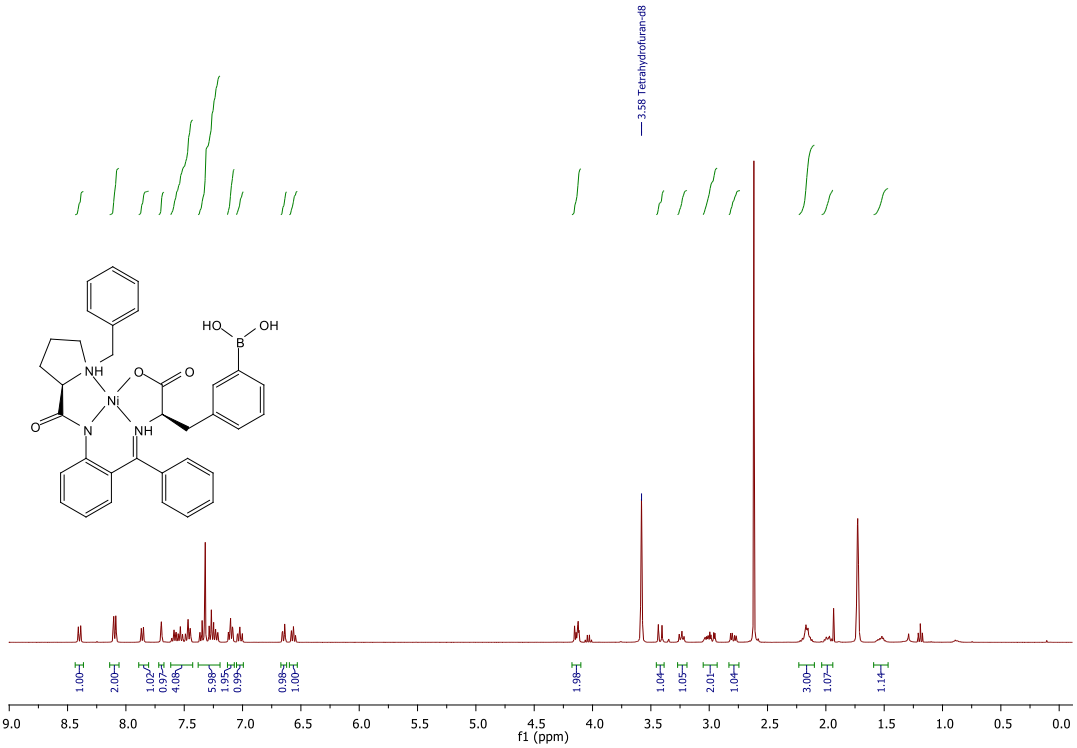

^{13}C NMR (101 MHz, THF-d8)

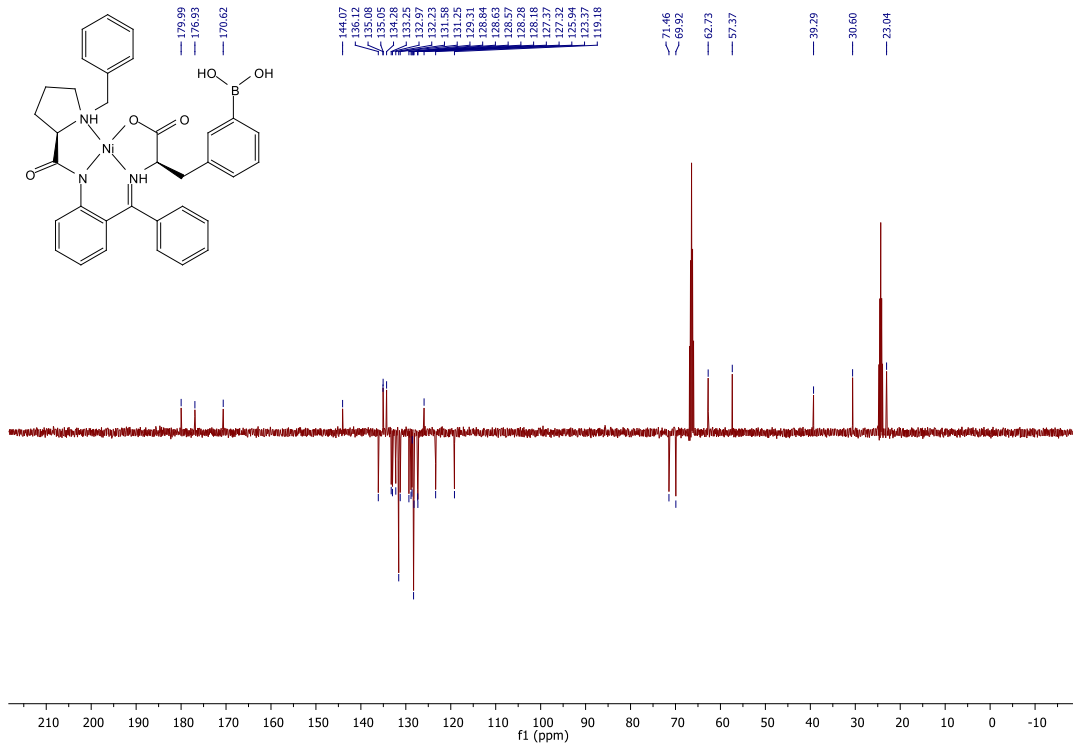

Verbindung (*S,S*)-**8**

^{1}H NMR (400 MHz, $CDCl_3$)

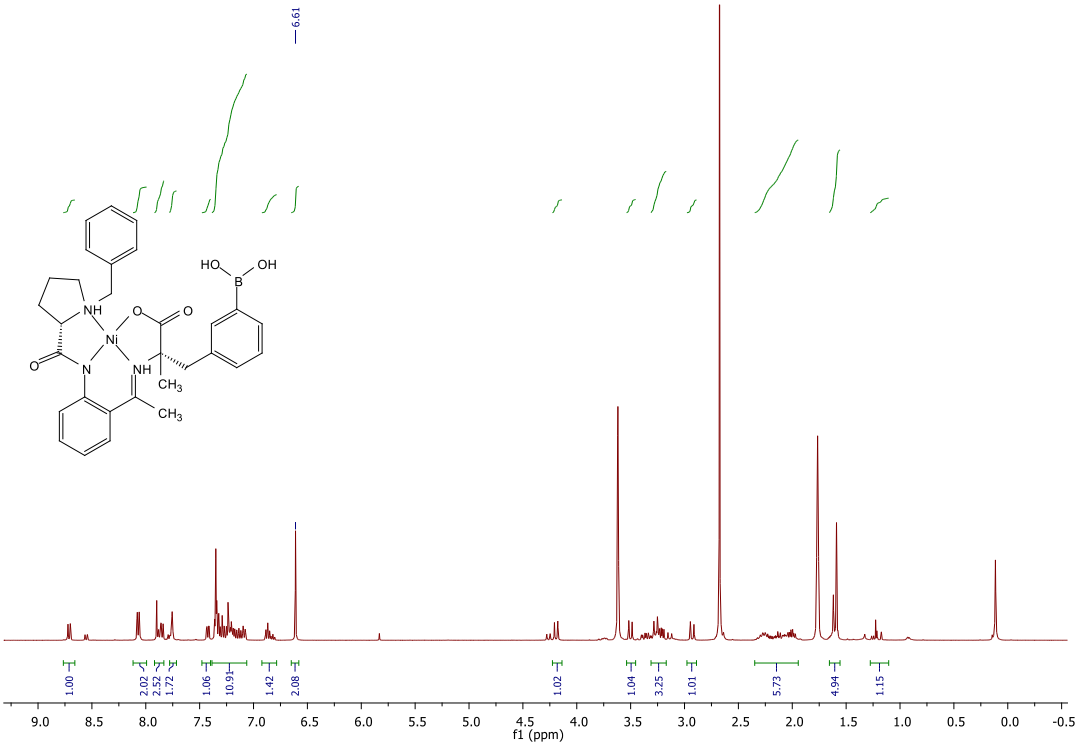

^{13}C NMR (101 MHz, $CDCl_3$)

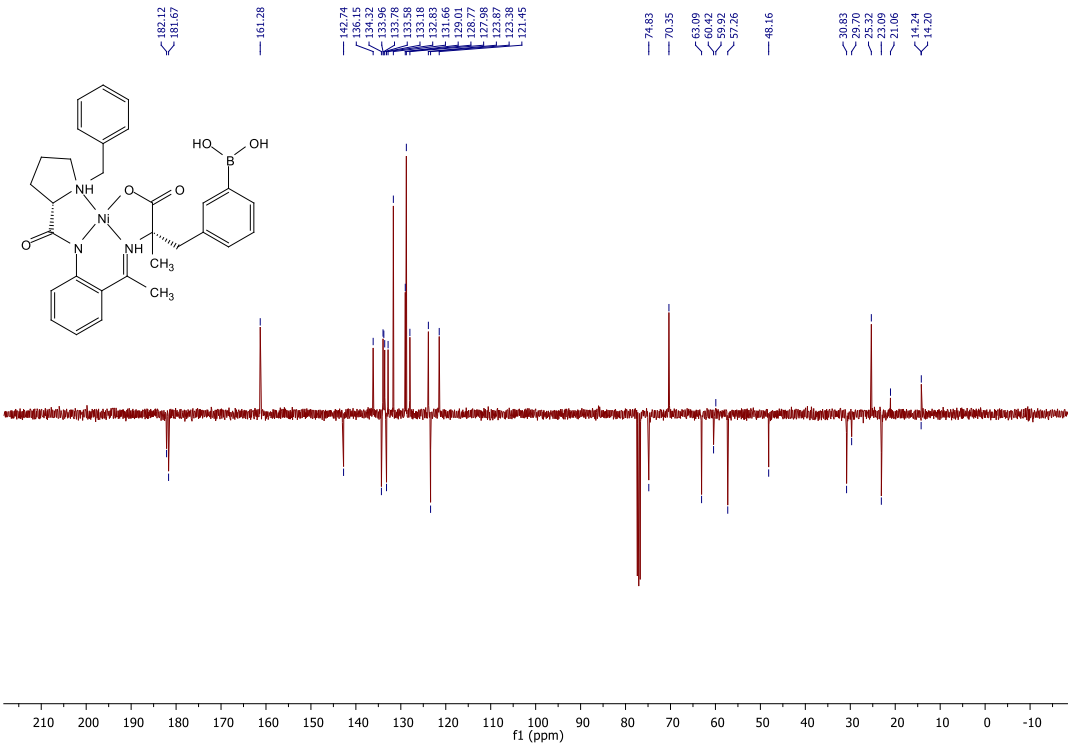

Verbindung **20**

^{1}H NMR (400 MHz, $CDCl_3$)

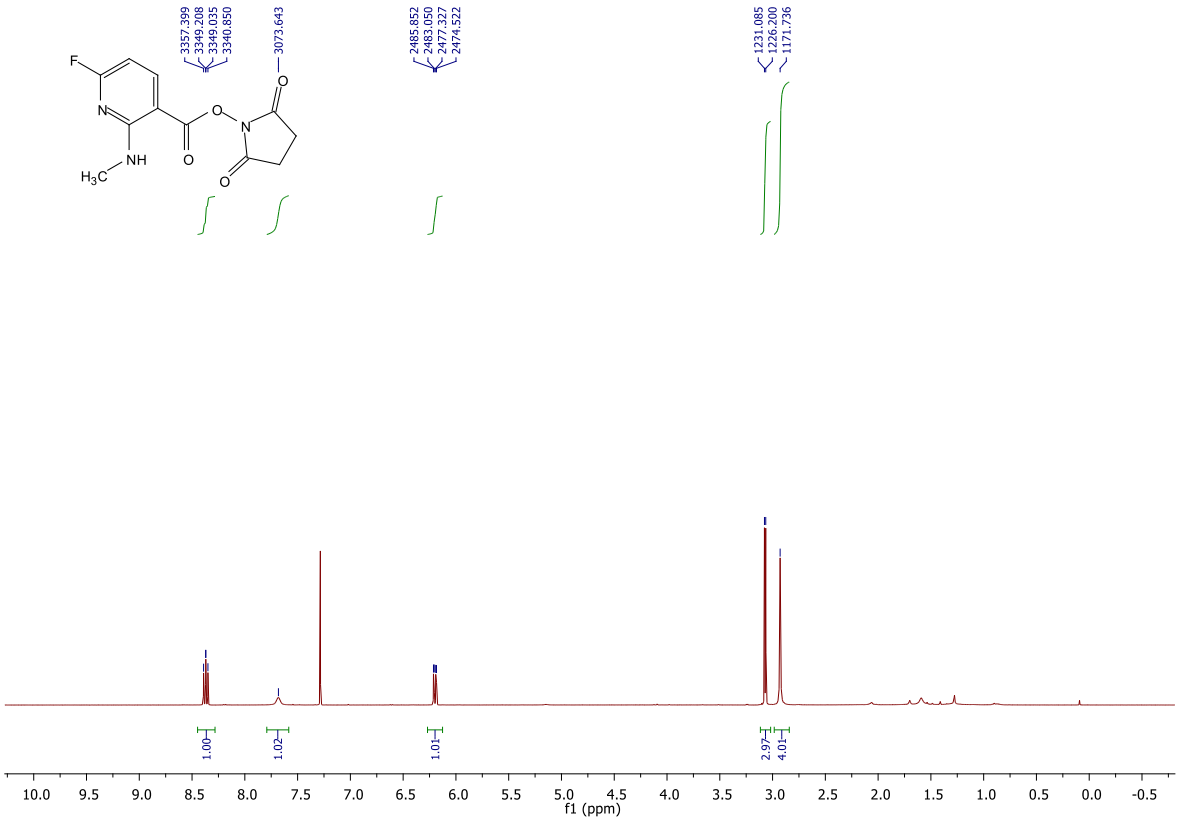

^{13}C NMR (101 MHz, $CDCl_3$)

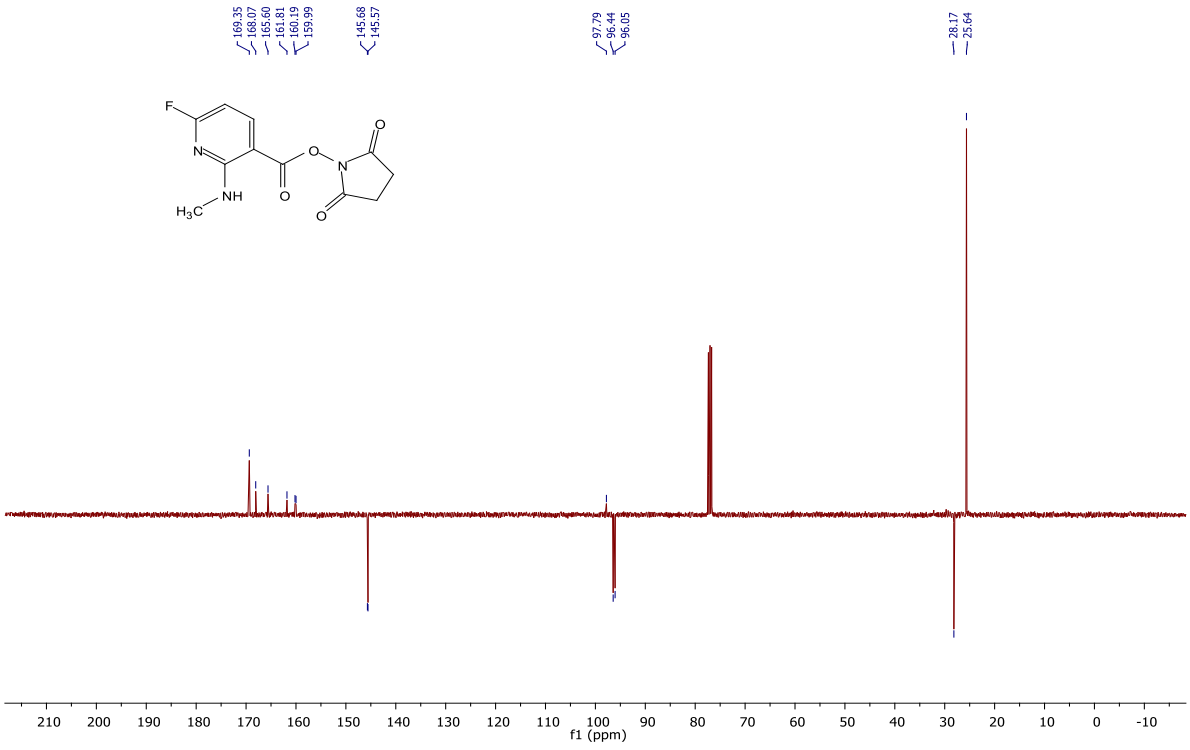

^{19}F NMR (376 MHz, $CDCl_3$)

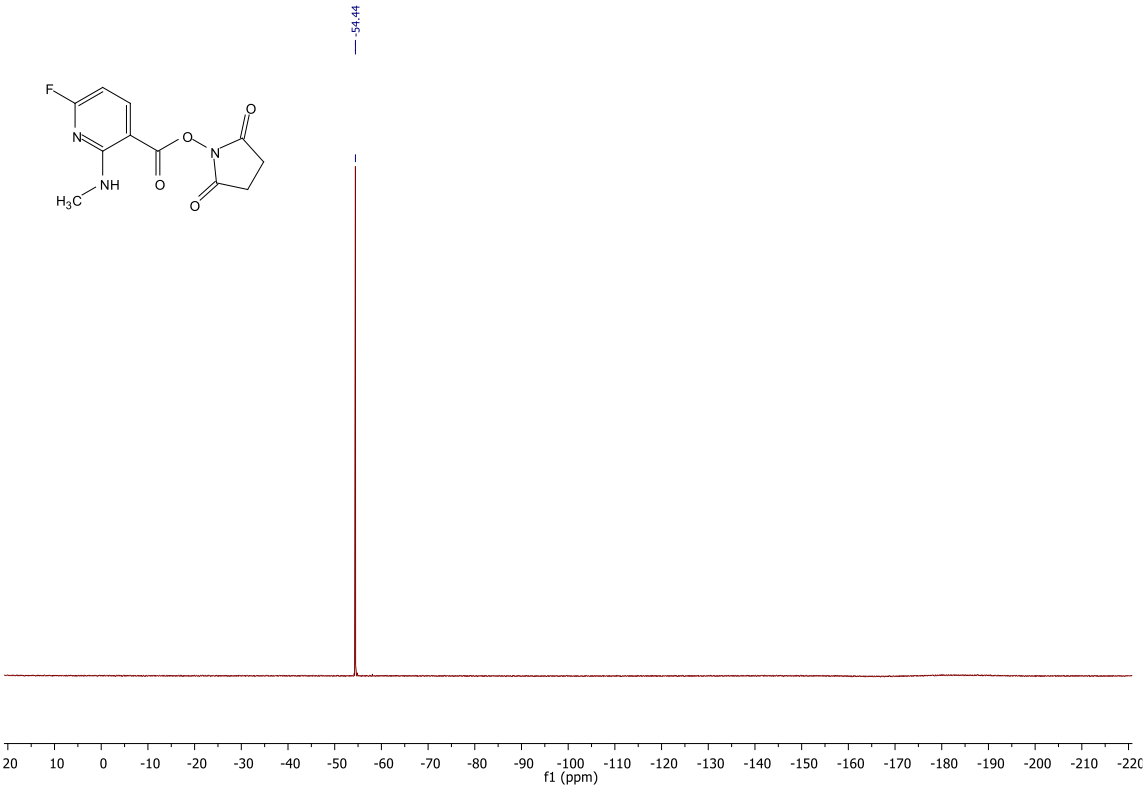

Verbindung **24**

^{19}F NMR (376 MHz, $CDCl_3$)

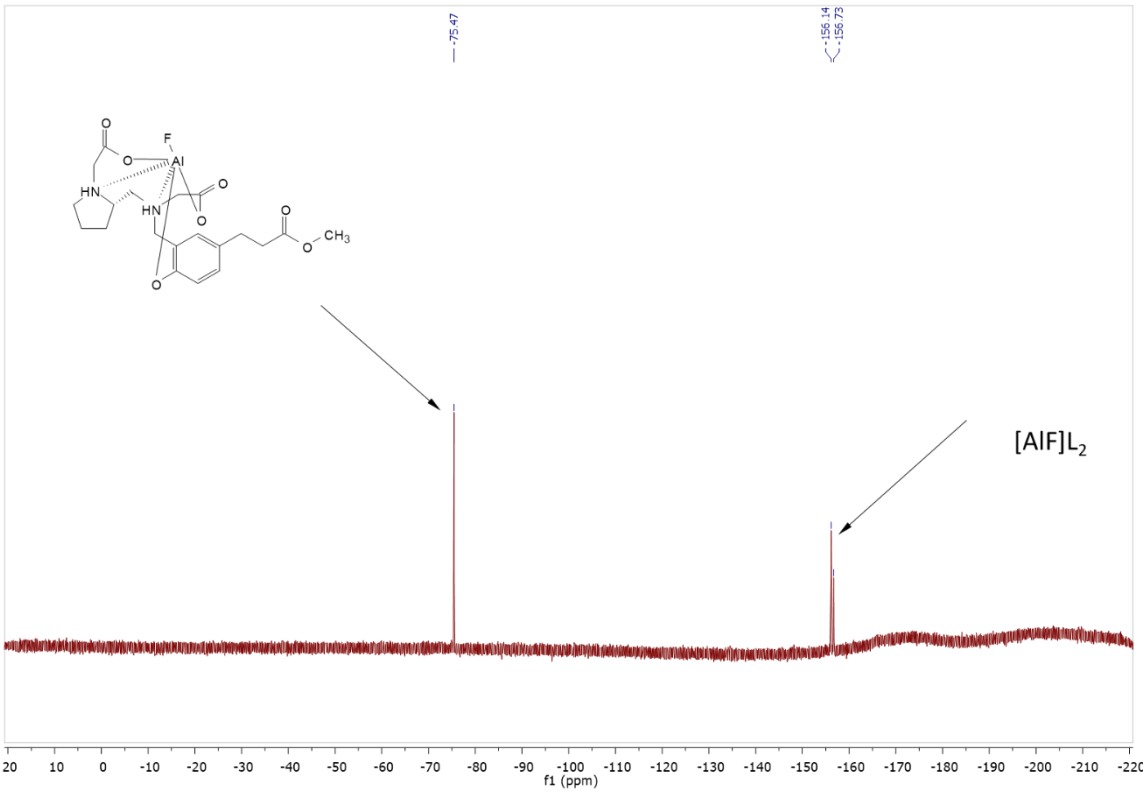

7.2. Massenspektren

Verbindung **22**

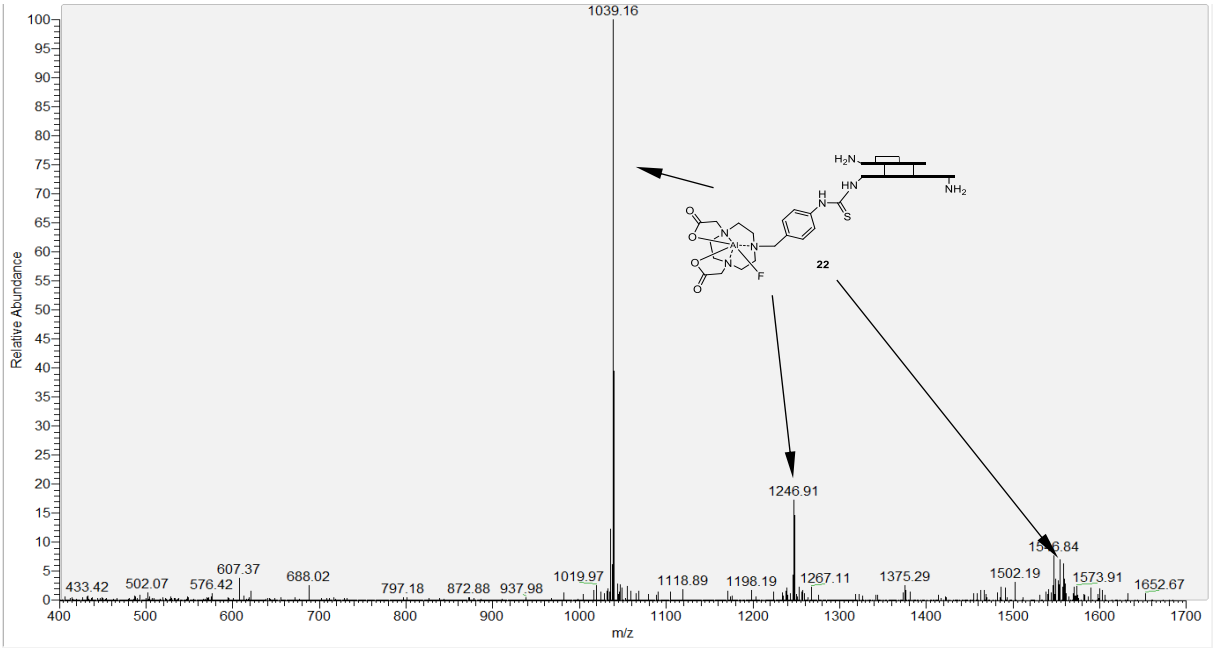

Verbindung **24**

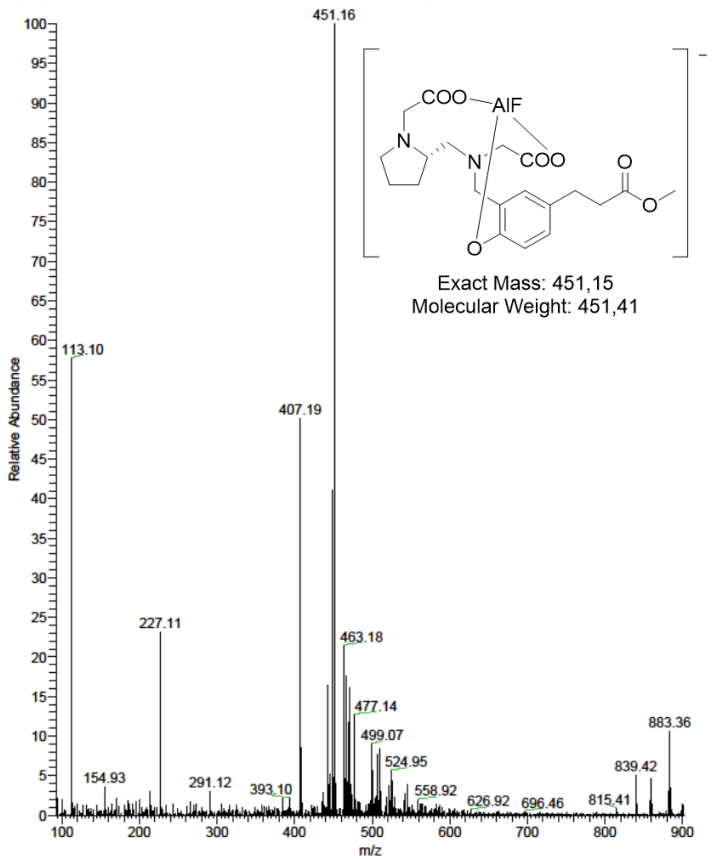

7.3. HPLC-Chromatogramme

Verbindung (*S*)-[^{18}F]FPhe

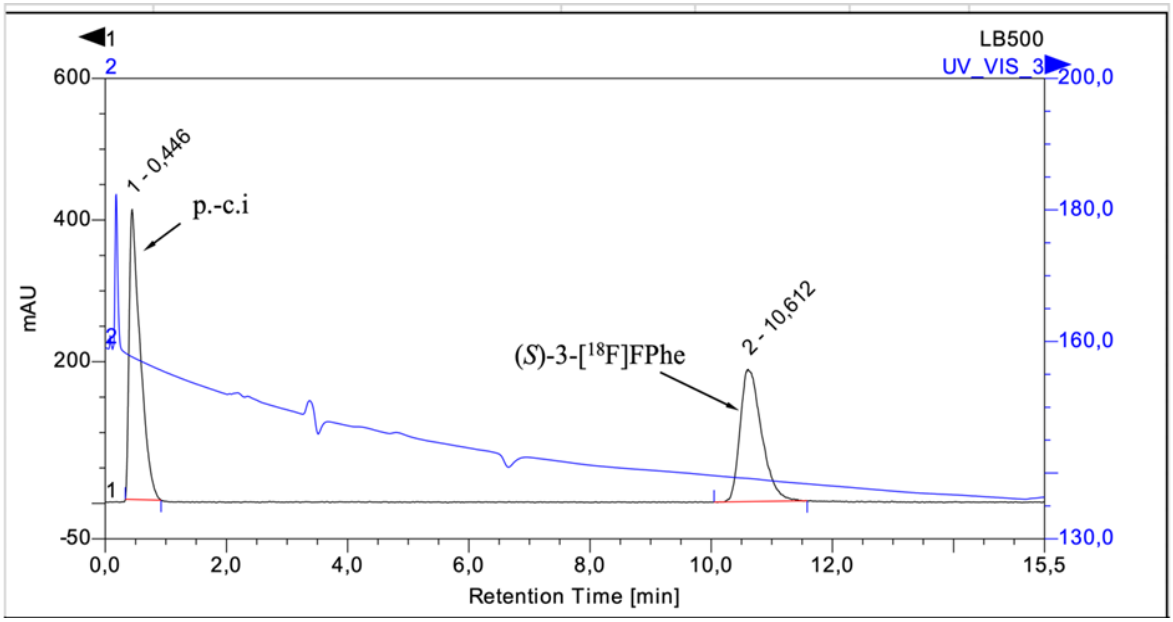

Abbildung 44: HPLC-Chromatogramm von (*S*)-[^{18}F]FPhe. Blau: UV-Kanal, Schwarz: Radioaktivitätskanal, p.-c.i: Referenzinjektion.

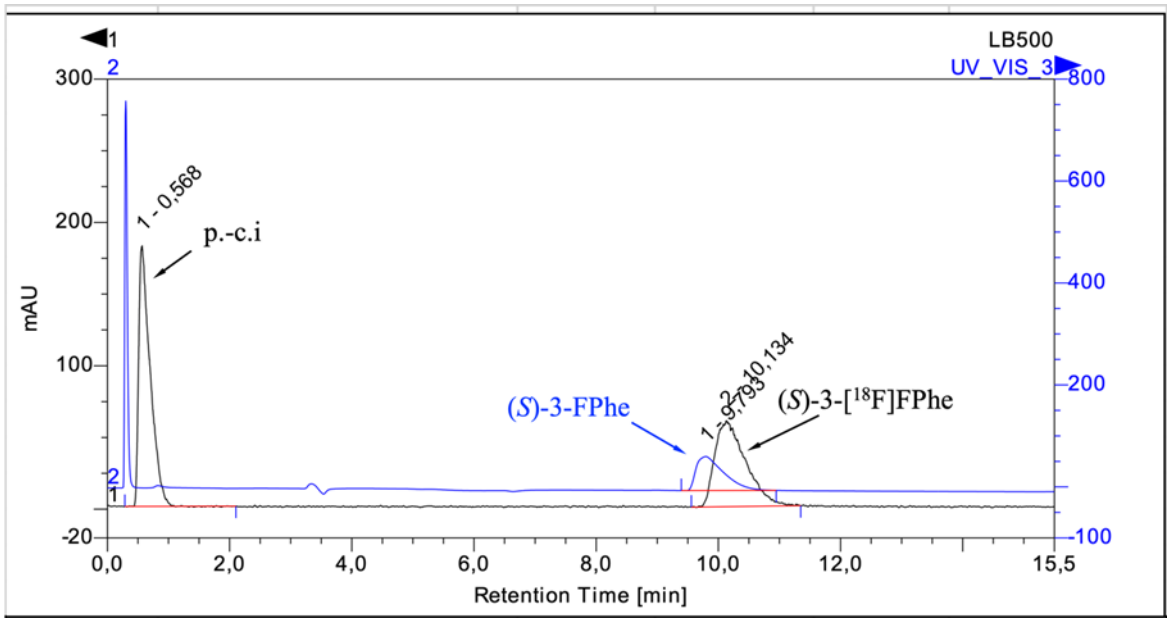

Abbildung 45: HPLC-Chromatogramm von (*S*)-[^{18}F]FPhe mit Koinjektion der Referenzverbindung. Blau: UV-Kanal, Schwarz: Radioaktivitätskanal, p.-c.i: Referenzinjektion.

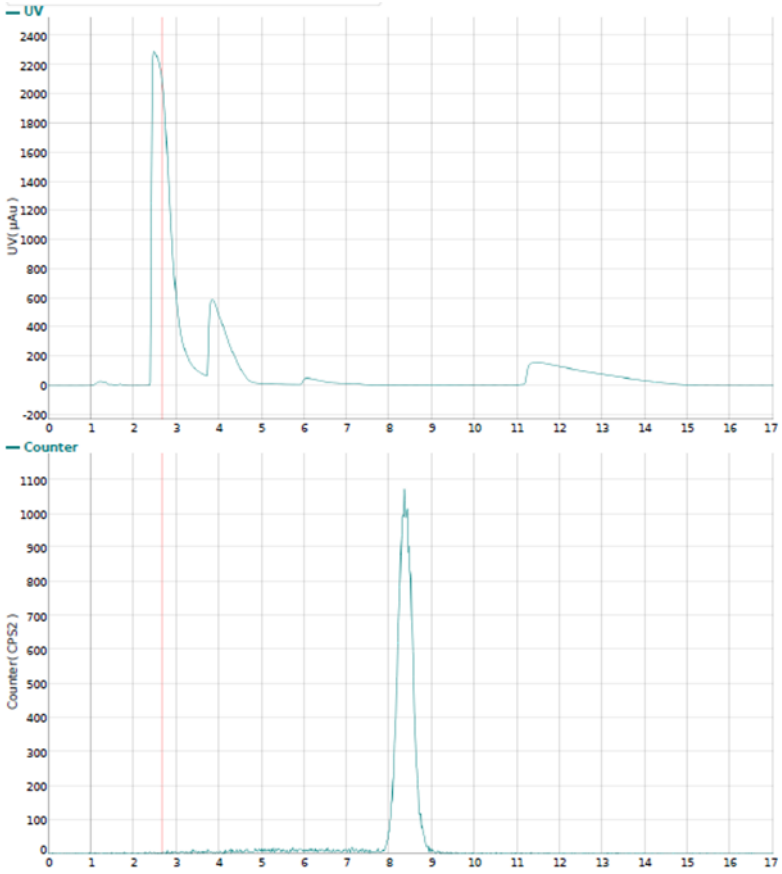

Abbildung 46: HPLC-Chromatogramm der semipräparativen Isolierung von (*S*)-[^{18}F]FPhe. Oben: UV-Kanal, Unten: Radioaktivitätskanal.

Verbindung (*R*)-[^{18}F]FPhe

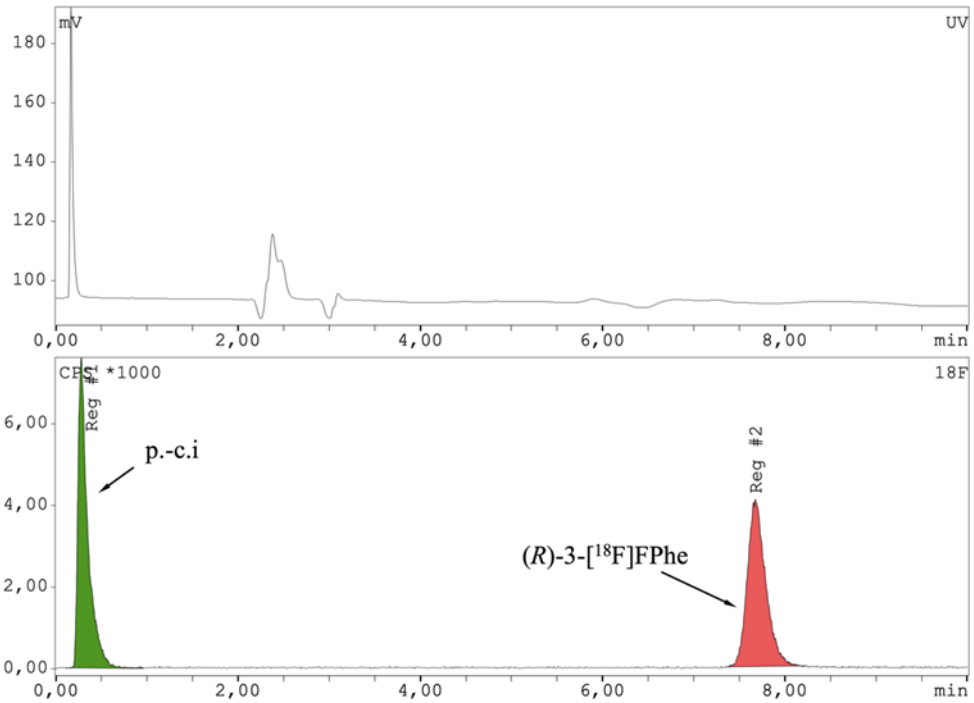

Abbildung 47: HPLC-Chromatogramm von (*R*)-[^{18}F]FPhe. Oben: UV-Kanal, Unten: Radioaktivitätskanal, p.-c.i: Referenzinjektion.

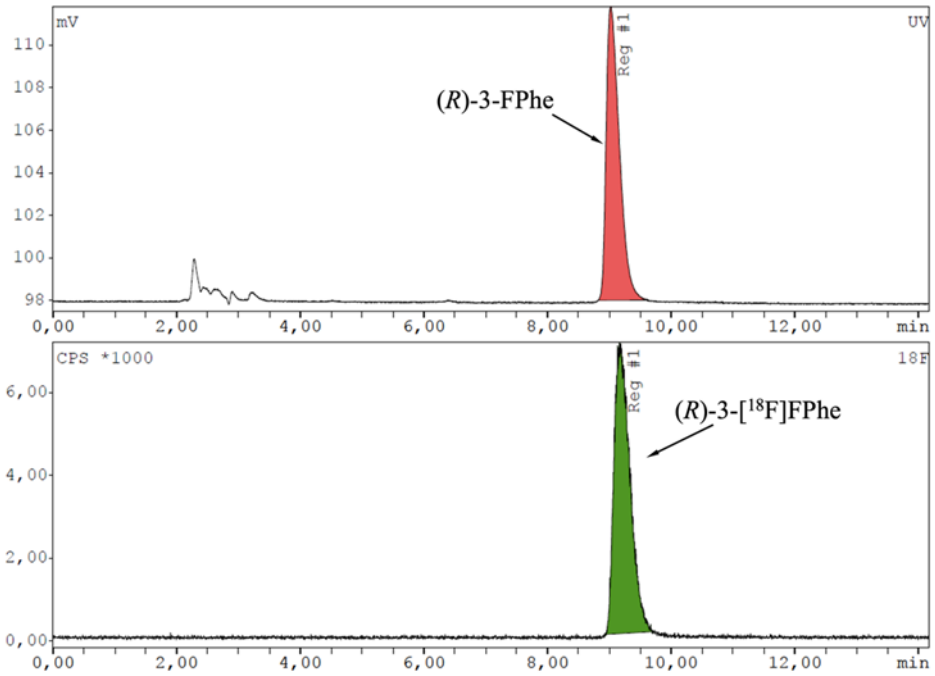

Abbildung 48: HPLC-Chromatogramm von (*R*)-[^{18}F]FPhe mit Koinjektion der Referenzverbindung. Oben: UV-Kanal, Unten: Radioaktivitätskanal.

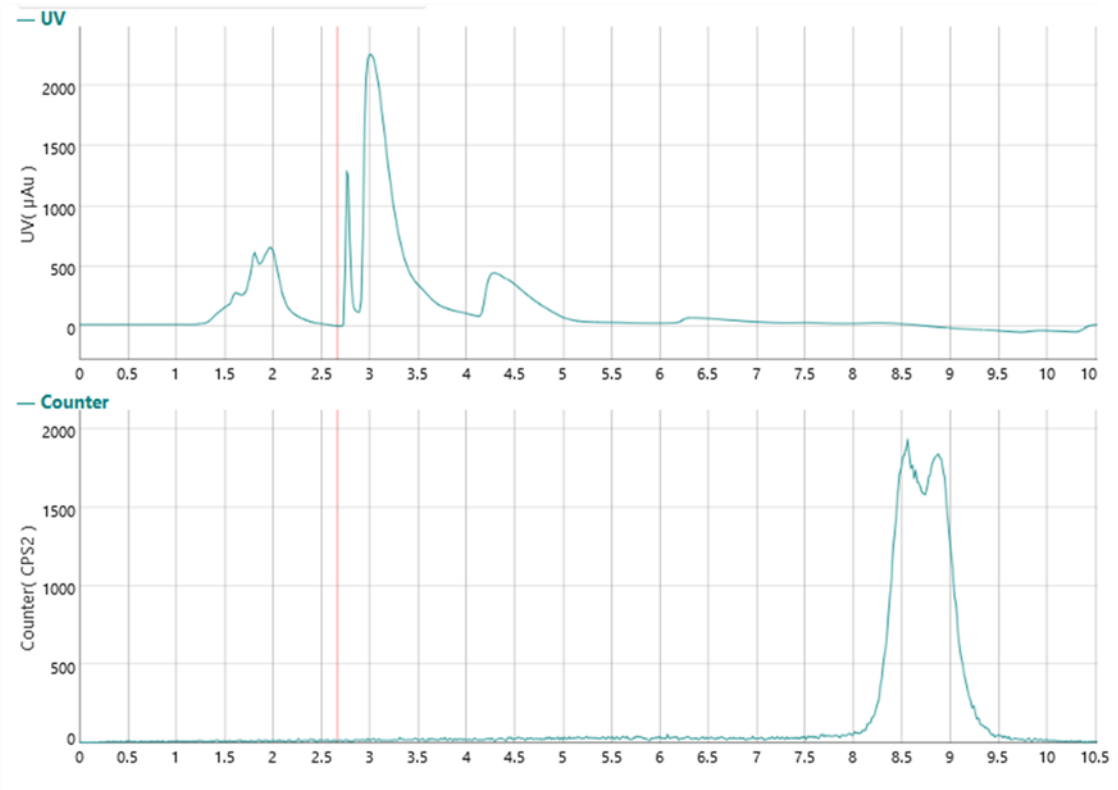

Abbildung 49: HPLC-Chromatogramm der semipräparativen Isolierung von (*R*)-[^{18}F]FPhe. Oben: UV-Kanal, Unten: Radioaktivitätskanal.

Verbindungen [^{18}F]**14** und [^{18}F]**16**

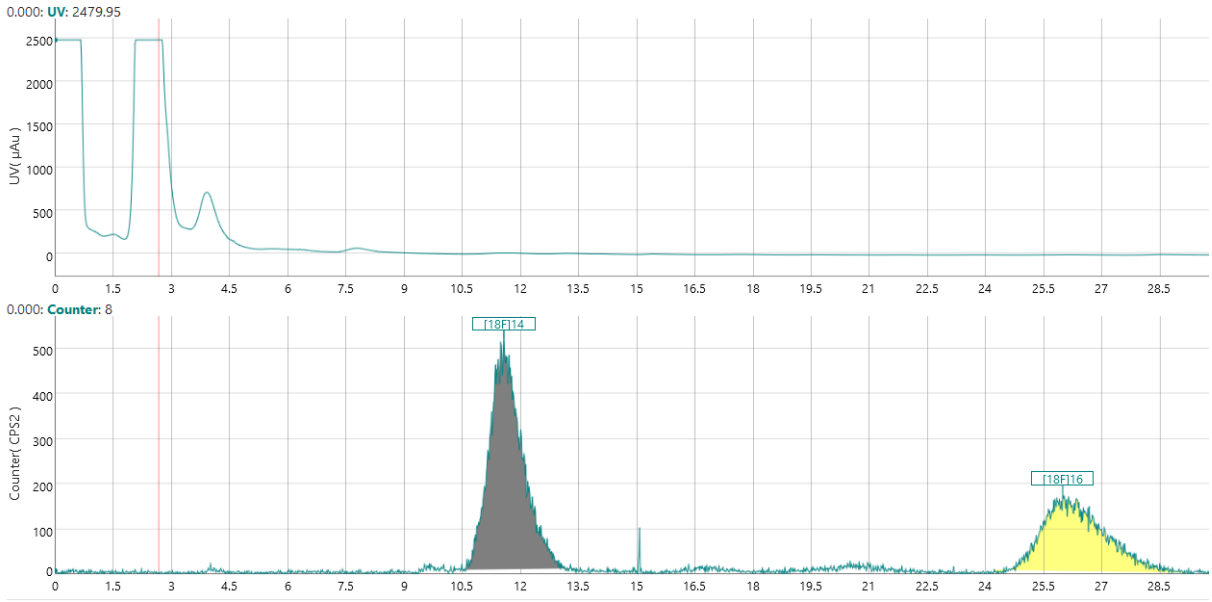

Abbildung 50: HPLC-Chromatogramm der semipräparativen Isolierung von [^{18}F]**14** (grau) und [^{18}F]**16** (gelb). Oben: UV-Kanal, Unten: Radioaktivitätskanal.

Verbindung [^{18}F]**22**

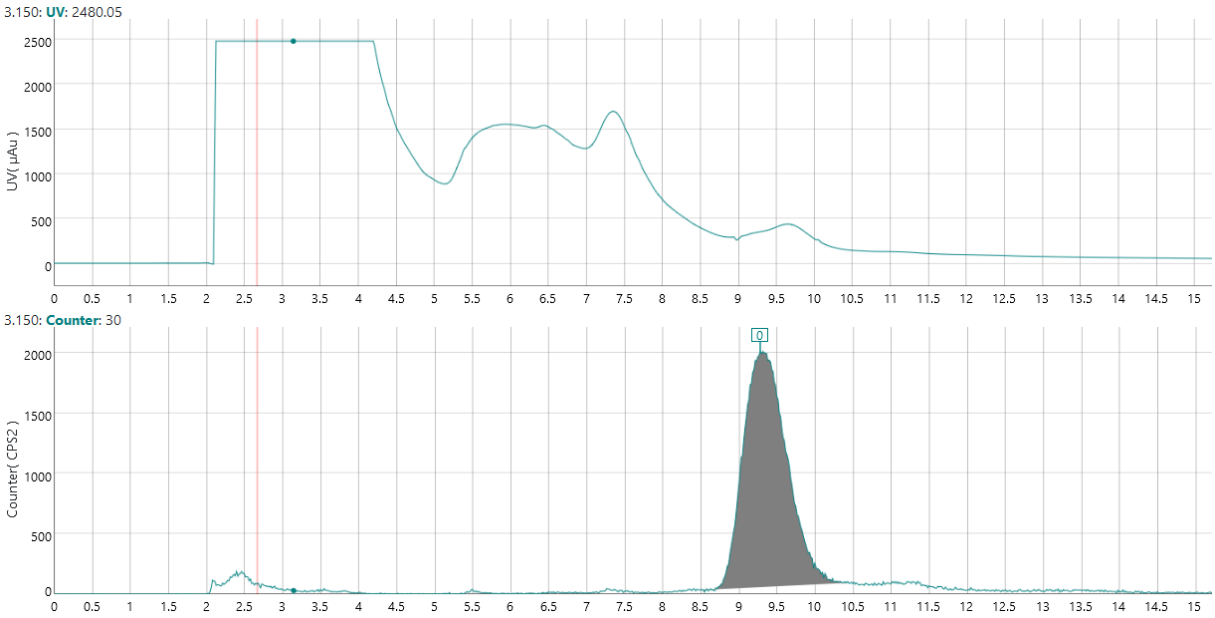

Abbildung 51: HPLC-Chromatogramm der semipräparativen Isolierung von [^{18}F]22. Oben: UV-Kanal, Unten: Radioaktivitätskanal.

7.4. Radio-DC

Verbindung [^{18}F]**24**

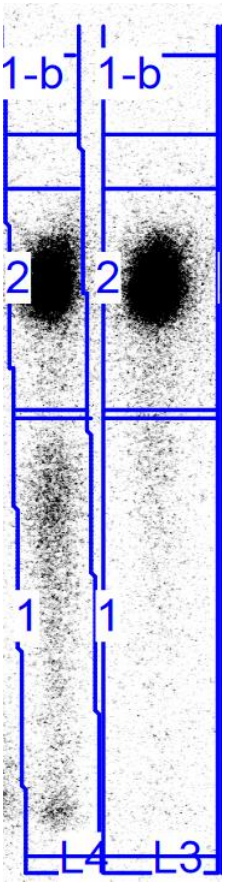

Abbildung 52: Radio DC von Verbindung [^{18}F]**24**. L4: Rohprodukt, L3: Isoliertes Produkt, Region 1: [^{18}F]F^- und Al[^{18}F]F^{2+}, Region 2: [^{18}F]**24.**

7.5. Abkürzungen

[^{18}F]AFA	1-Amino-7-[^{18}F]fluor-8-azaisatosäureanhydrid
[^{18}F]FDG	2-[^{18}F]Fluor-2-desoxy-D-Glucose
[^{18}F]FET	*O*-[^{18}F]Fluorethyltyrosin
[^{18}F]FET-OMe	*O*-[^{18}F]Fluorethyltyrosin-methylester
[^{18}F]FPhe	[^{18}F]Fluorphenylalanin
[^{18}F]MFA	1-Methylamino-7-[^{18}F]fluor-8-azaisatosäureanhydrid
[^{18}F]SFB	*N*-Succinimidyl-4-[^{18}F]fluorbenzoat
2-AMPDA-HB	2-(Hydroxybenzyl)-Aminomethylpiperidindiessigsäure
AAS	Aromatische Aminosäuren
AG	Abgangsgruppe
AMP	Aminomethylpiperidin
CT	Computer-Tomographie
CycloSiFA	2-(2,6-Diisopropylphenyl)-1,1-diisopropyl-2,3-dihydro-1*H*-benzo[*c*][1,2]azasilol
DABCO	1,4-Diazabicyclo[2.2.2]octan
DMA	*N*,*N*-Dimethylacetamid
DMF	*N,N*-Dimethylformamid
DMI	1,3-Dimethyl-2-imidazolidinon
DMSO	Dimethylsulfoxid
DTPA	Diethylentriaminpentaessigsäure
ESI	Elektrospray-Ionisation
EtOH	Ethanol
EZG	Elektronenziehende Gruppe
FAP	Fibroblasten-Aktivierungsprotein
FDA	U. S. Food and Drug Administration
FPE	Festphasenextraktion
FPhe	Fluorphenylalanin
HBED	*N*,*N*′-Di(2-hydroxybenzyl)ethylendiamin-*N*,*N*′-diessigsäure
HEPES	2-[4-(2-Hydroxyethyl)-1-piperazinyl]-ethansulfonsäure
HOAc	Essigsäure
HPLC	Hochleistungsflüssigkeitschromatographie
HRMS	Hochauflösende Massenspektrometrie
IEDDA	Inverse electron demand Diels-Alder
K_{222}	Kryptofix® 222
LAT1	*Large Amino Acid Transporter 1*
LRMS	Niedrigauflösende Massenspektrometrie
***m*-[^{18}F]FET**	4-*O*-[^{18}F]Fluorethyltyrosin
MeCN	Acetonitril
MeOH	Methanol
***m*-FET**	4-*O*-Fluorethyltyrosin

MPAA-NODA	2,2'-(7-(4-(2-((2-aminoethyl)amino)-2-oxoethyl)benzyl)-1,4,7-triazonane-1,4-diyl)diacetic acid
MRT	Magnet-Resonanz-Tomographie
NCS	*N*-Chlorsuccinimid
Ni-BPA	Ni-2-[*N*-(*N*'-benzylprolyl)amino]acetophenon
Ni-BPB	Ni-2-[*N*-(*N*'-benzylprolyl)amino]benzophenon
Ni-BPX	Ni-2-[*N*-(*N*'-benzylprolyl)amino]acetophenone oder Ni-2-[*N*-(*N*'-benzylprolyl)amino]acetophenon
NODA	1,4,7-Triazazyclononan-1,4-diessigsäure
NOTA	1,4,7-Triazazyclononan-1,4,7-triessigsäure
PET	Positronen-Emissions-Tomographie
PG	Prosthetische Gruppe
PSMA	Prostata-spezifisches Membranantigen
PSMA I&T	Prostata-spezifisches Membranantigen Bildgebung und Therapie
RCA	Radiochemische Ausbeute
RCU	Radiochemischer Umsatz
RESCA	*Restrained complexing agent*
SiFA	Silizium-Fluorid-Akzeptor
SPECT	Einzelphotonen-Emissions-Computertomographie
Tacn	Triazazyclononan
TBAF	Tetrabutylammoniumfluorid
TBAOH	Tetrabutylammoniumhydroxid
TCEP	Tris(2-carboxyethyl)phosphin
TEMPO	2,2,6,6-Tetramethylpiperidinyloxyl
TFA	Trifluoressigsäure
TFAA	Trifluoressigsäureanhydrid
TPCK	Tosyl-L-phenylalaninchloromethylketon
UAMC1110	(S)-*N*-(2-(2-cyano-4,4-difluoropyrrolidin-1-yl)-2-oxoethyl)quinolin-4-carboxamid

7.6. SI von Manuskripten

Supporting Information for

Radiosynthesis and preclinical evaluation of *m*-[^{18}F]FET and [^{18}F]FET-OMe as novel [^{18}F]FET analogs for brain tumor imaging

Benedikt Gröner[1,2], Heike Endepols[1,2,3], Elizaveta A. Urusova[1,2], Melanie Brugger[1], Felix Neumaier[1,2], Marco Timmer[4], Bernd Neumaier[1,2], Boris D. Zlatopolskiy[1,2]*

[1] *Forschungszentrum Jülich GmbH, Institute of Neuroscience and Medicine, Nuclear Chemistry (INM-5), Wilhelm-Johnen-Straße, 52428 Jülich, Germany.*

[2] *University of Cologne, Faculty of Medicine and University Hospital Cologne, Institute of Radiochemistry and Experimental Molecular Imaging, Kerpener Straße 62, 50937 Cologne, Germany.*

[3] *University of Cologne, Faculty of Medicine and University Hospital Cologne, Department of Nuclear Medicine, Kerpener Straße 62, 50937 Cologne, Germany.*

[4] *University of Cologne, Faculty of Medicine and University Hospital Cologne, Center for Neurosurgery, Department of General Neurosurgery, Kerpener Straße 62, 50937 Cologne, Germany.*

[*] *Corresponding author; e-mail: b.neumaier@fz-juelich.de*

Table of contents

1 NMR spectra

1.1 Compound **2**

^{1}H-NMR spectrum of **2**

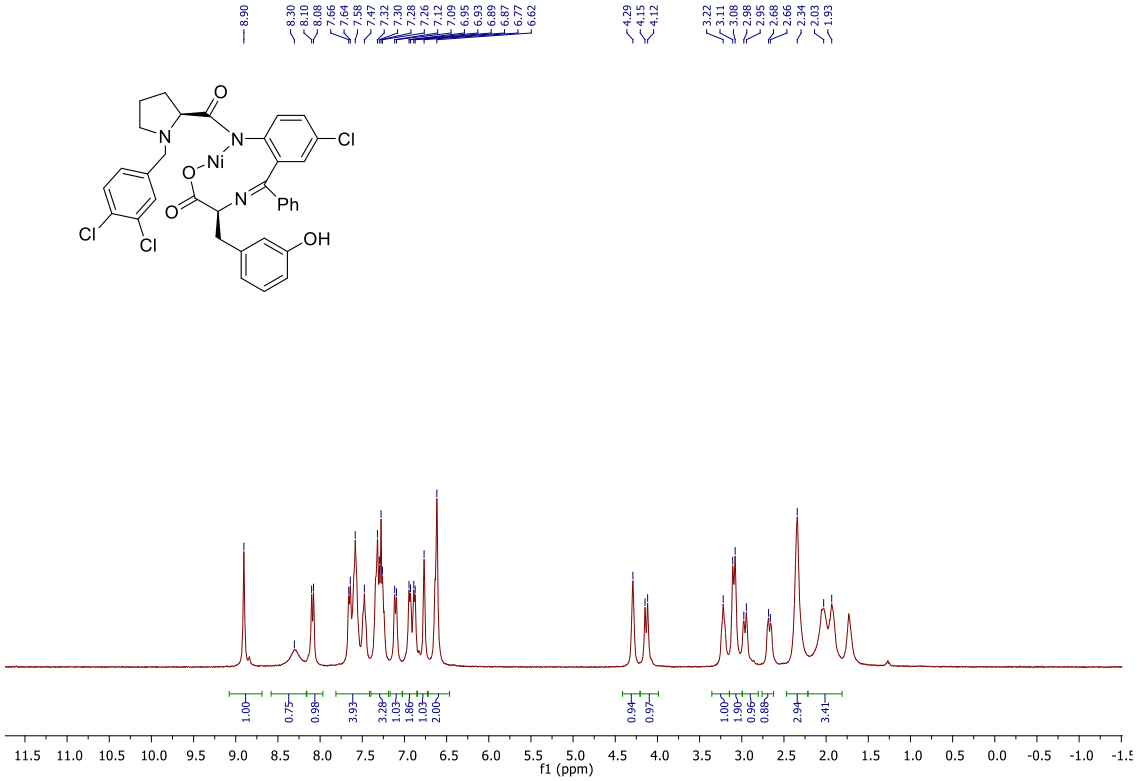

^{13}C-NMR spectrum of **2**

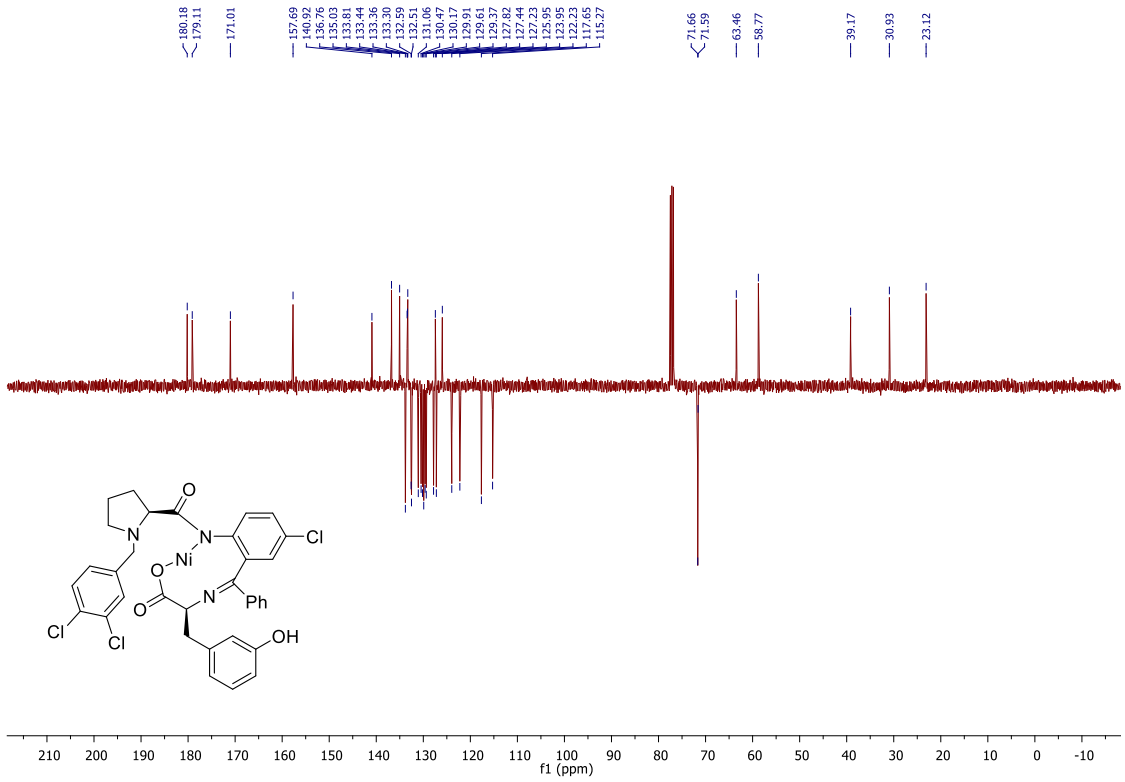

1.2 Compound **3**

^{1}H-NMR spectrum of **3**

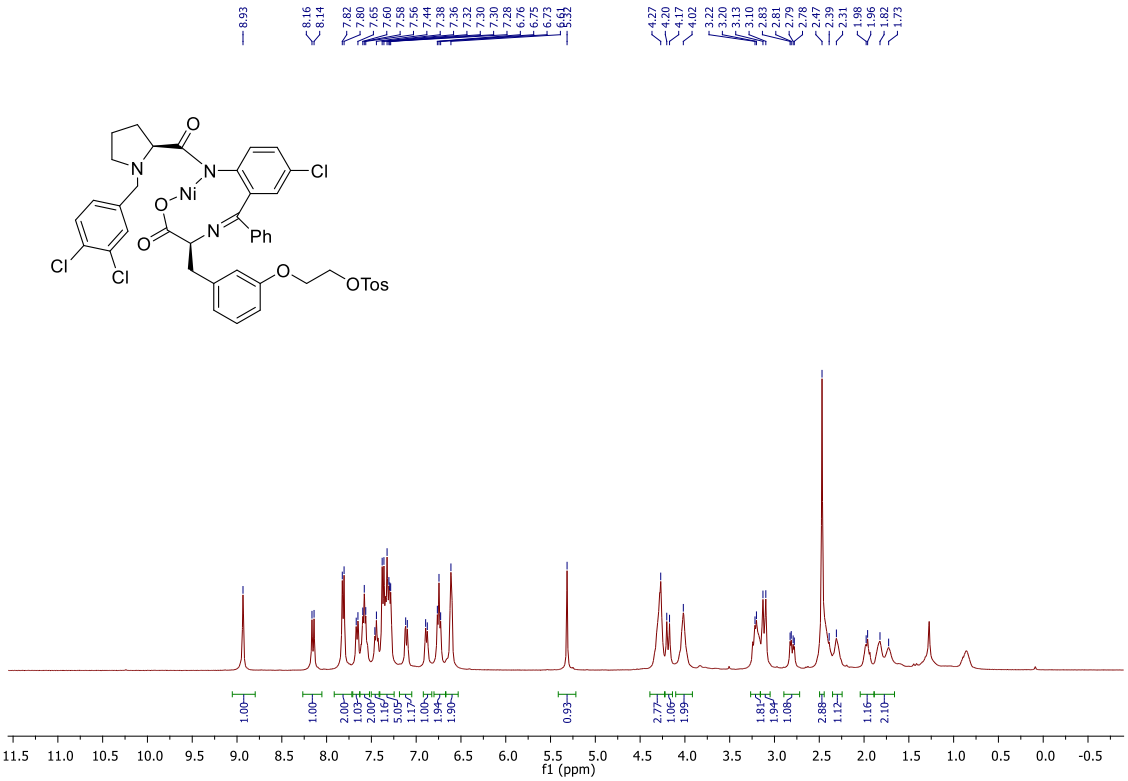

^{13}C-NMR spectrum of **3**

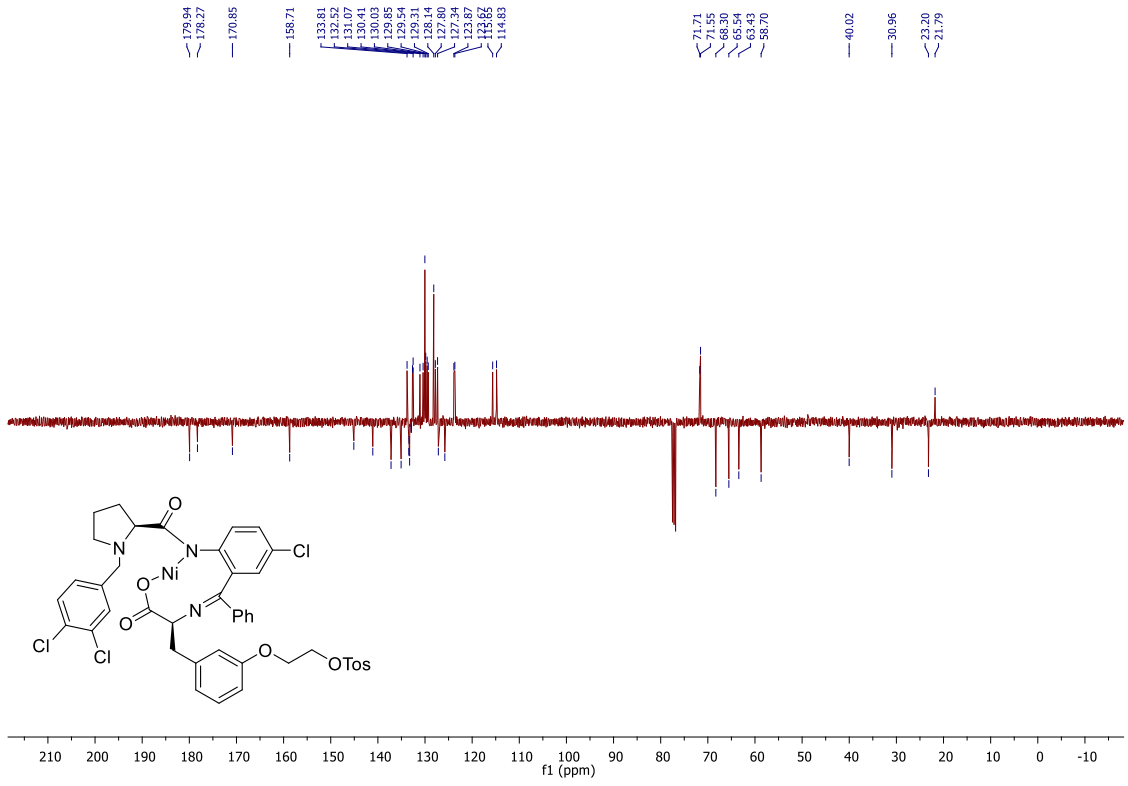

1.3 Compound **4**

^{1}H-NMR spectrum of **4**

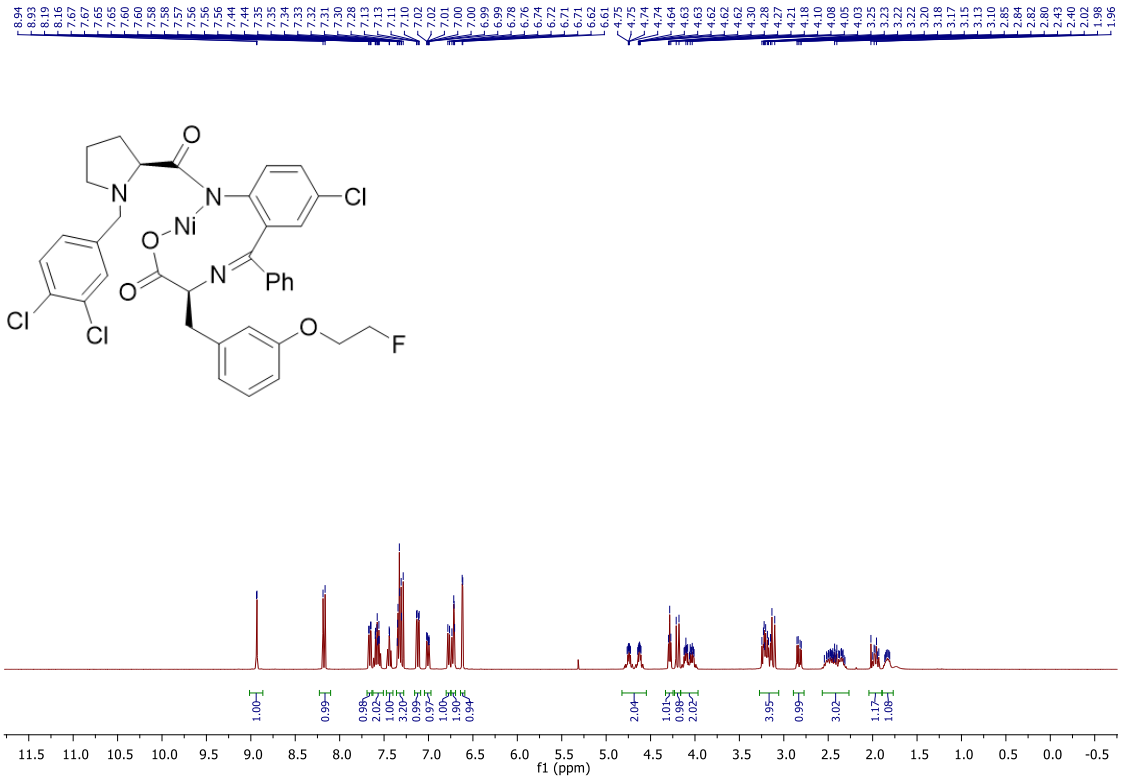

^{13}C-NMR spectrum of **4**

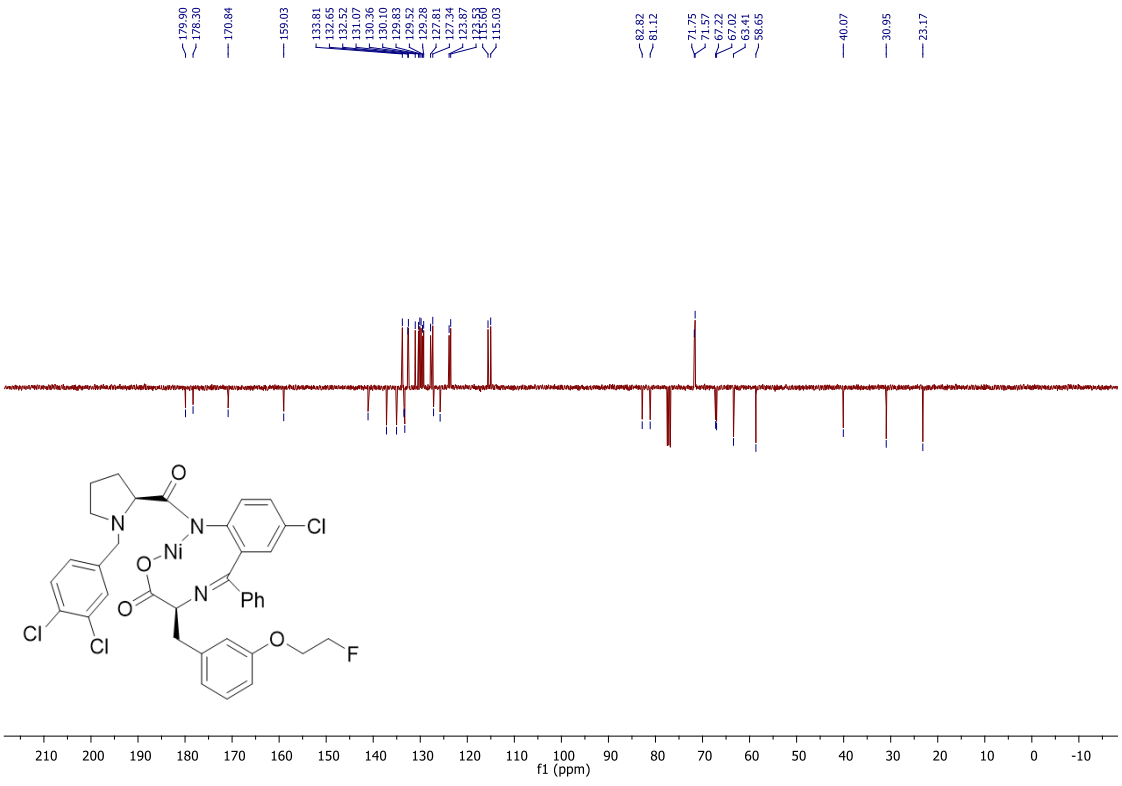

^{19}F-NMR spectrum of **4**

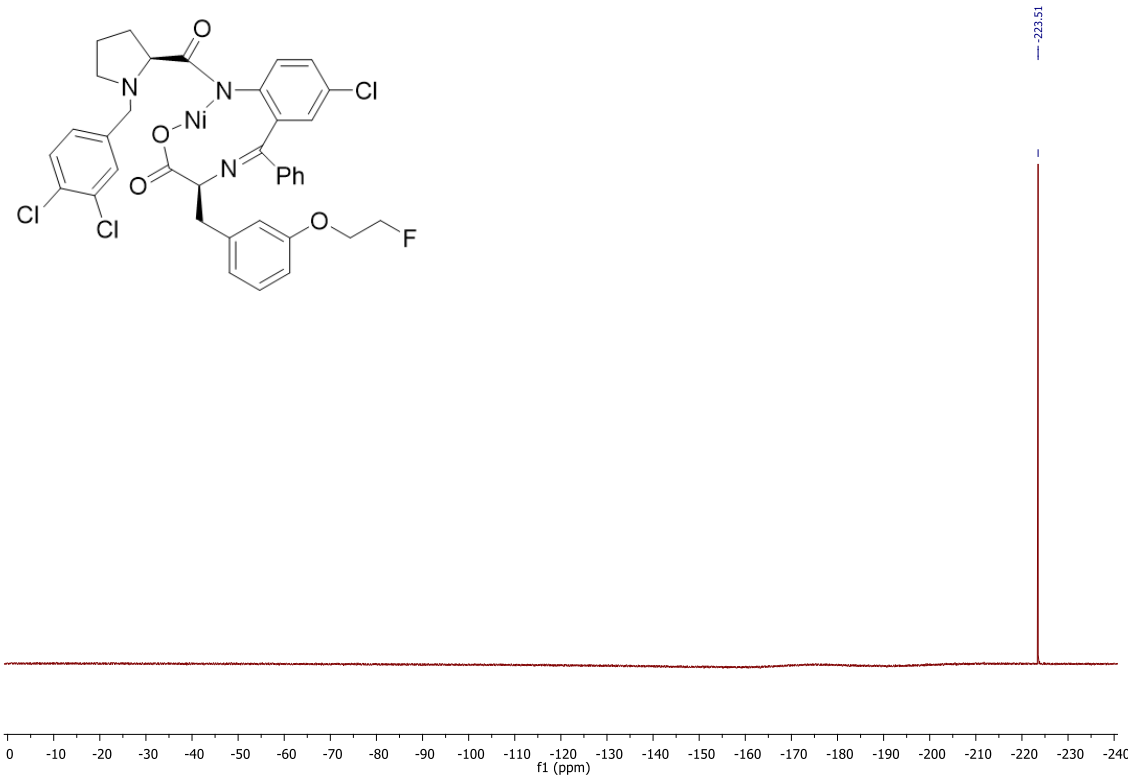

1.4 *m*-FET

^{1}H-NMR spectrum of *m*-FET

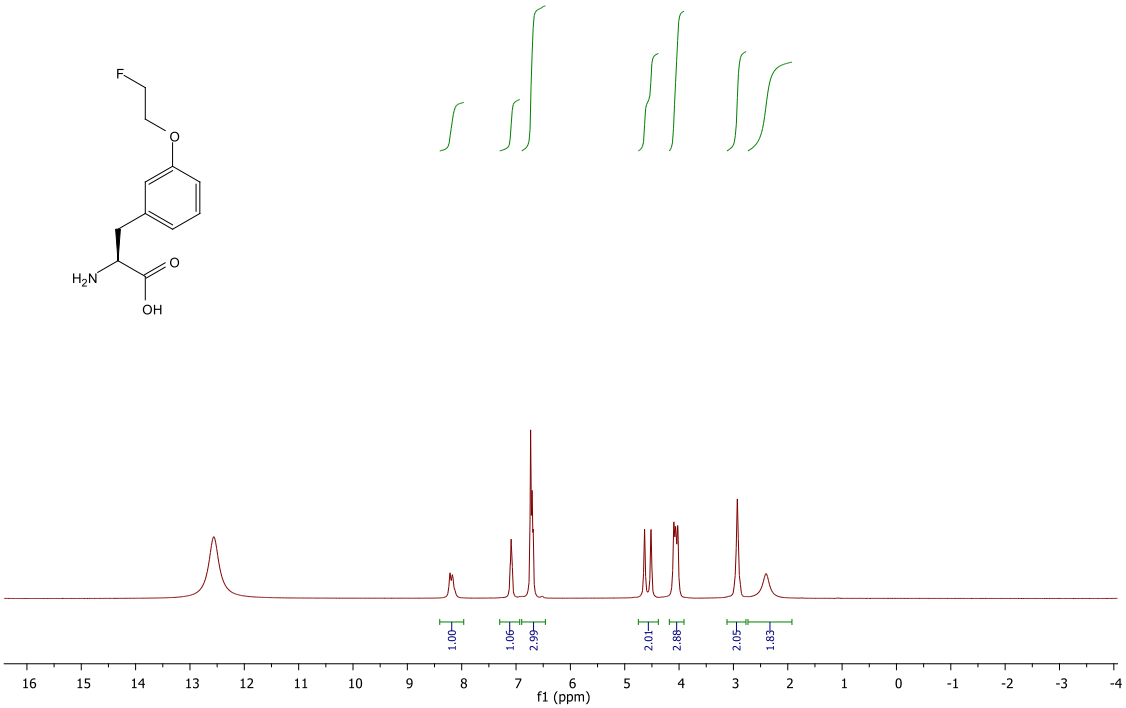

^{13}C-NMR spectrum of *m*-FET

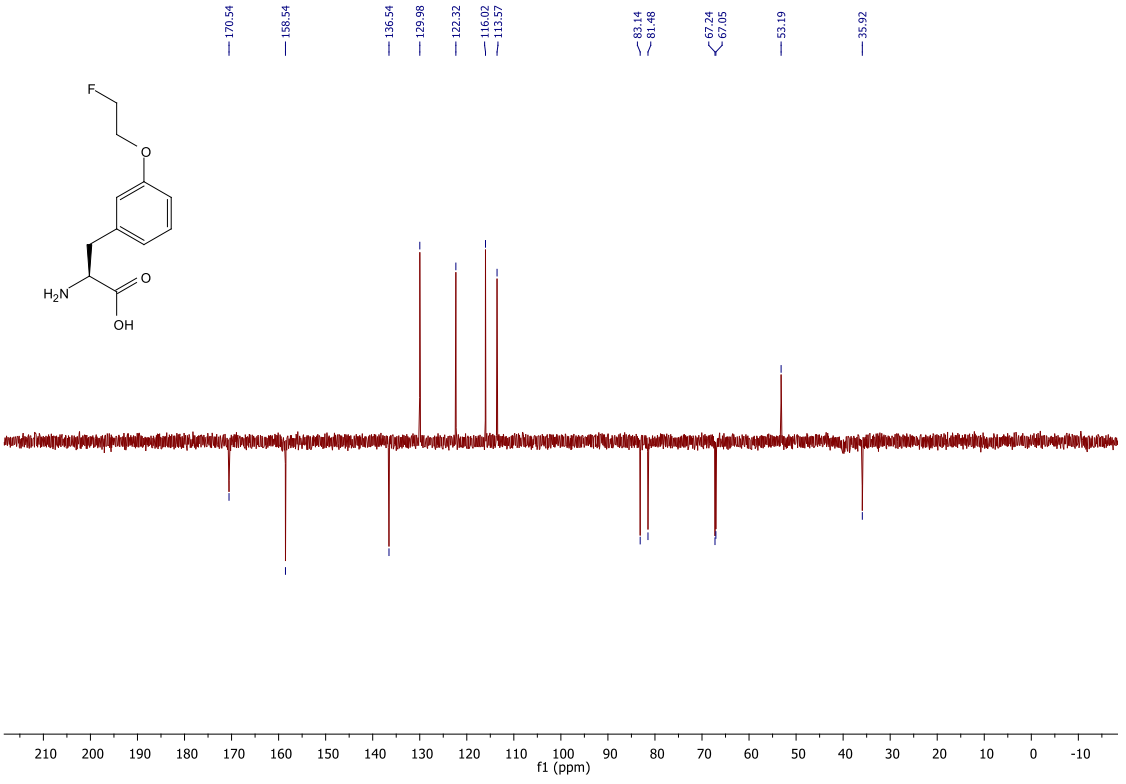

^{19}F-NMR spectrum of *m*-FET

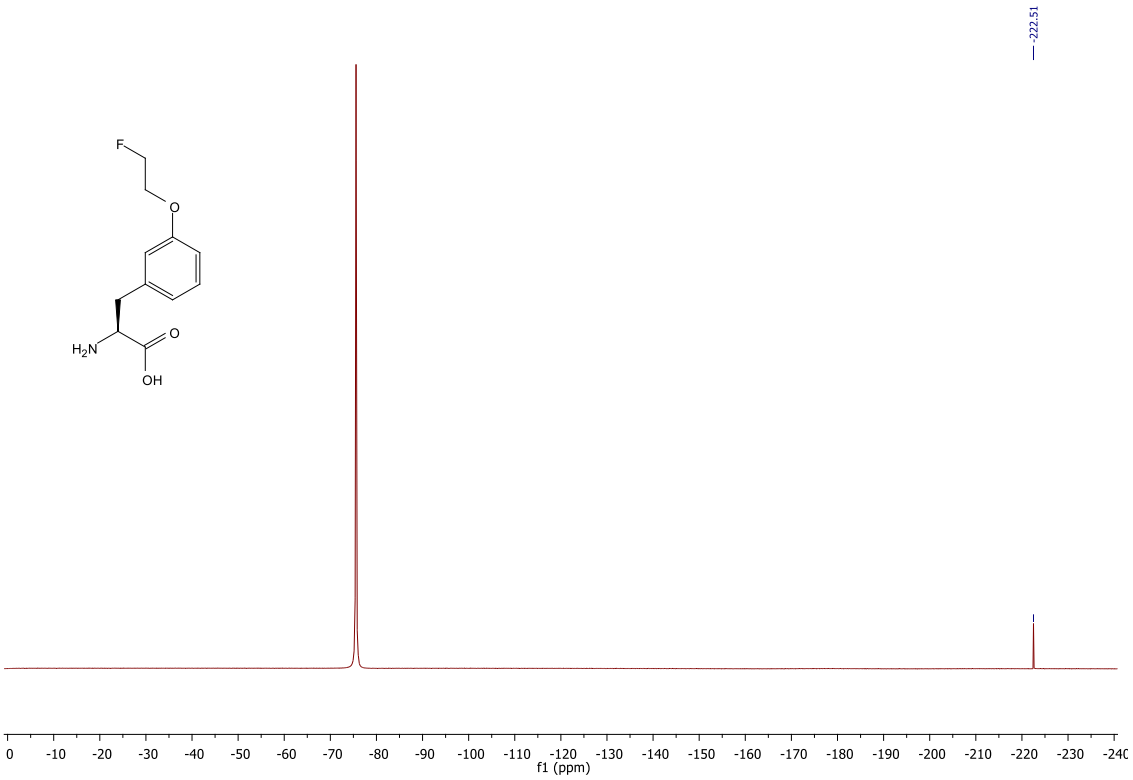

1.5 Compound **6**

^{1}H-NMR spectrum of **6**

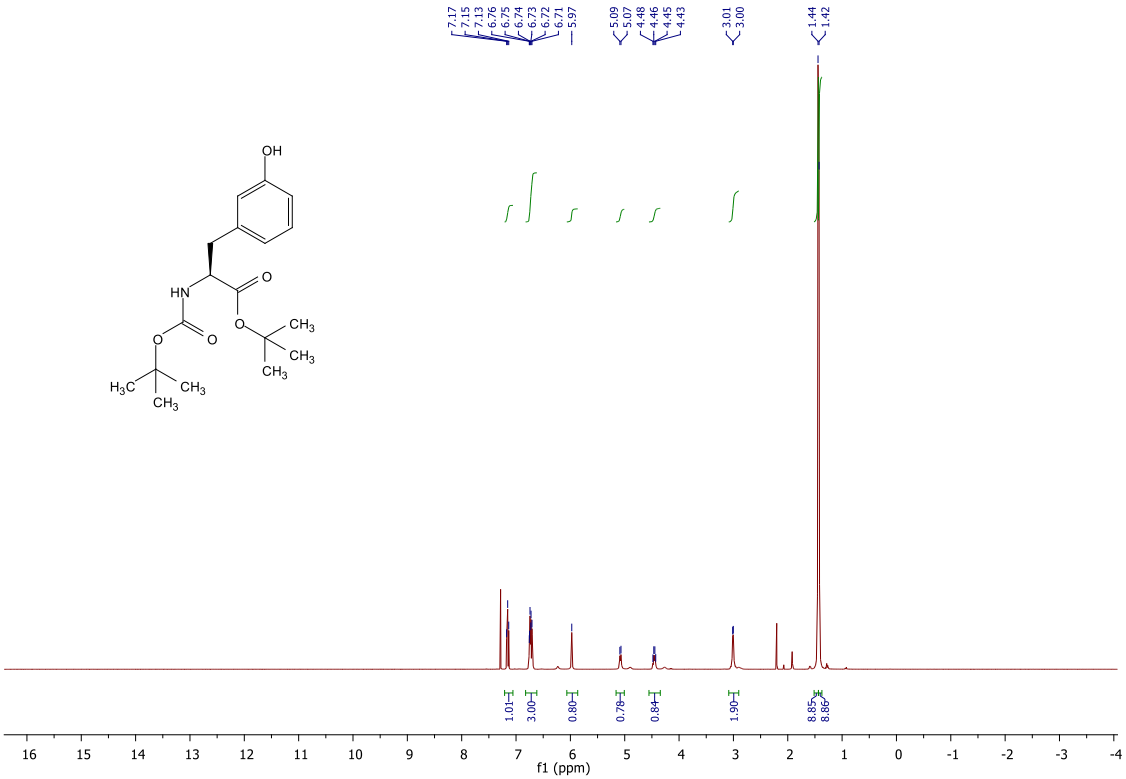

^{13}C-NMR spectrum of **6**

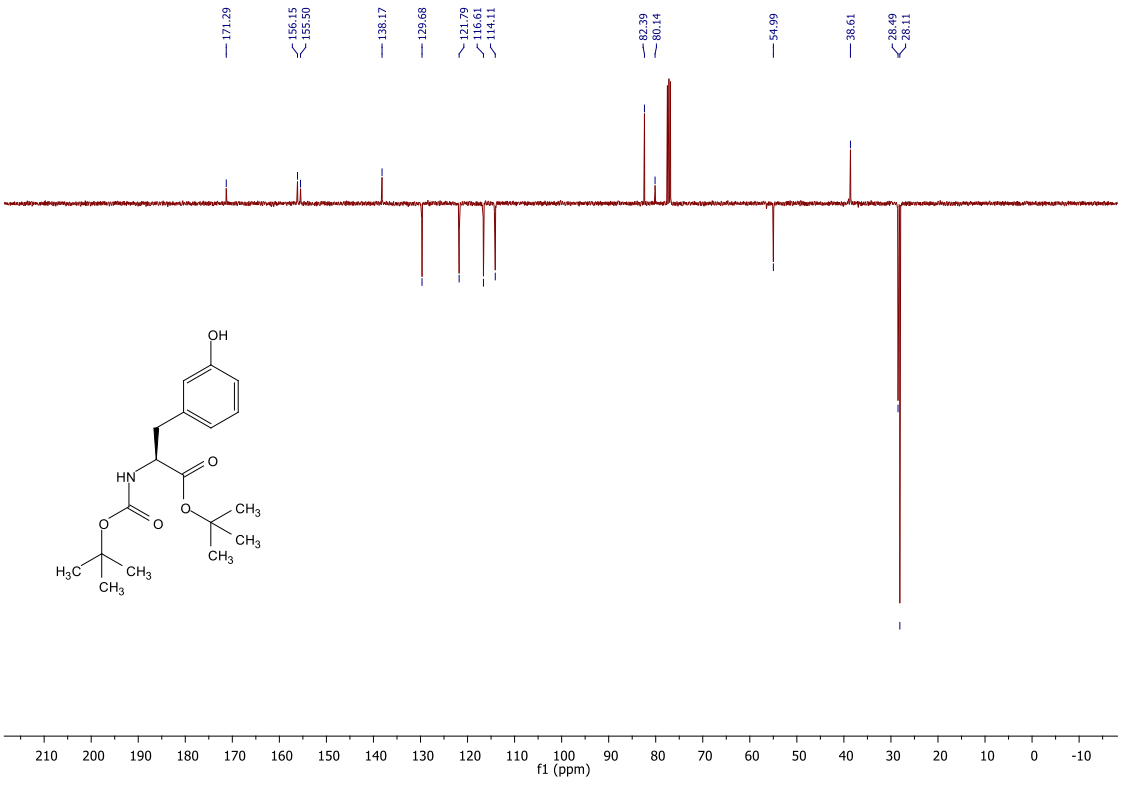

1.6 Compound **5**

^{1}H-NMR spectrum of **5**

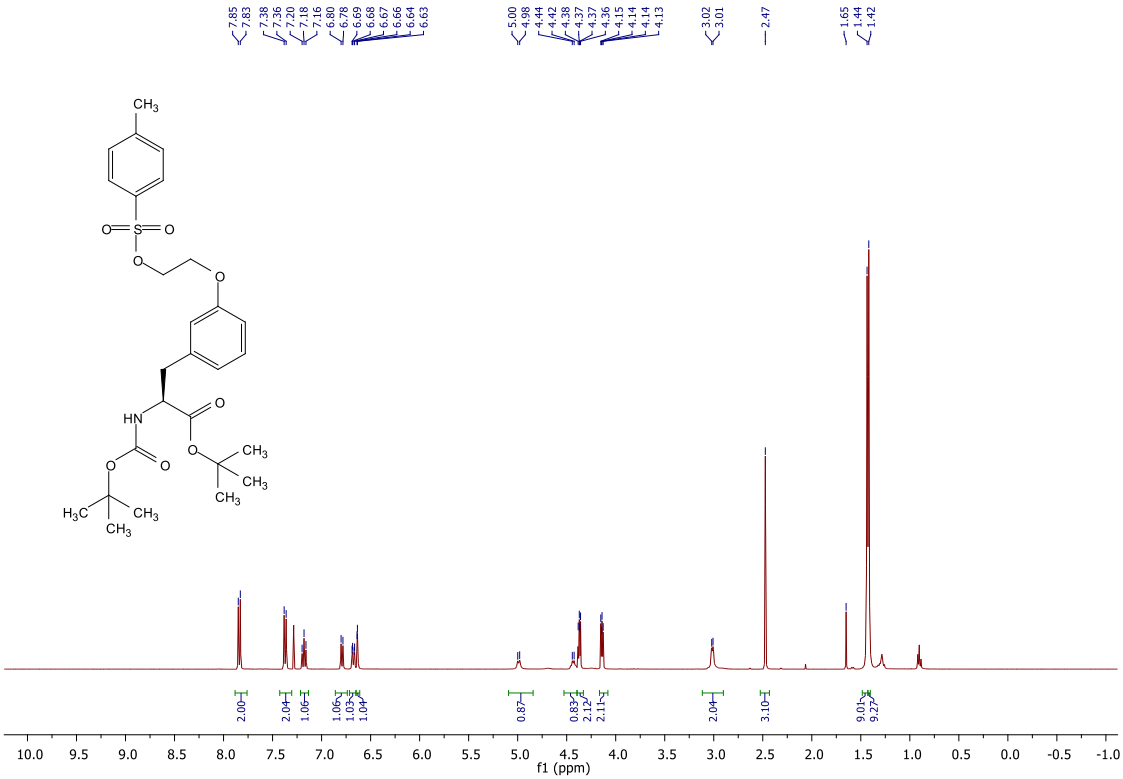

^{13}C-NMR spectrum of **5**

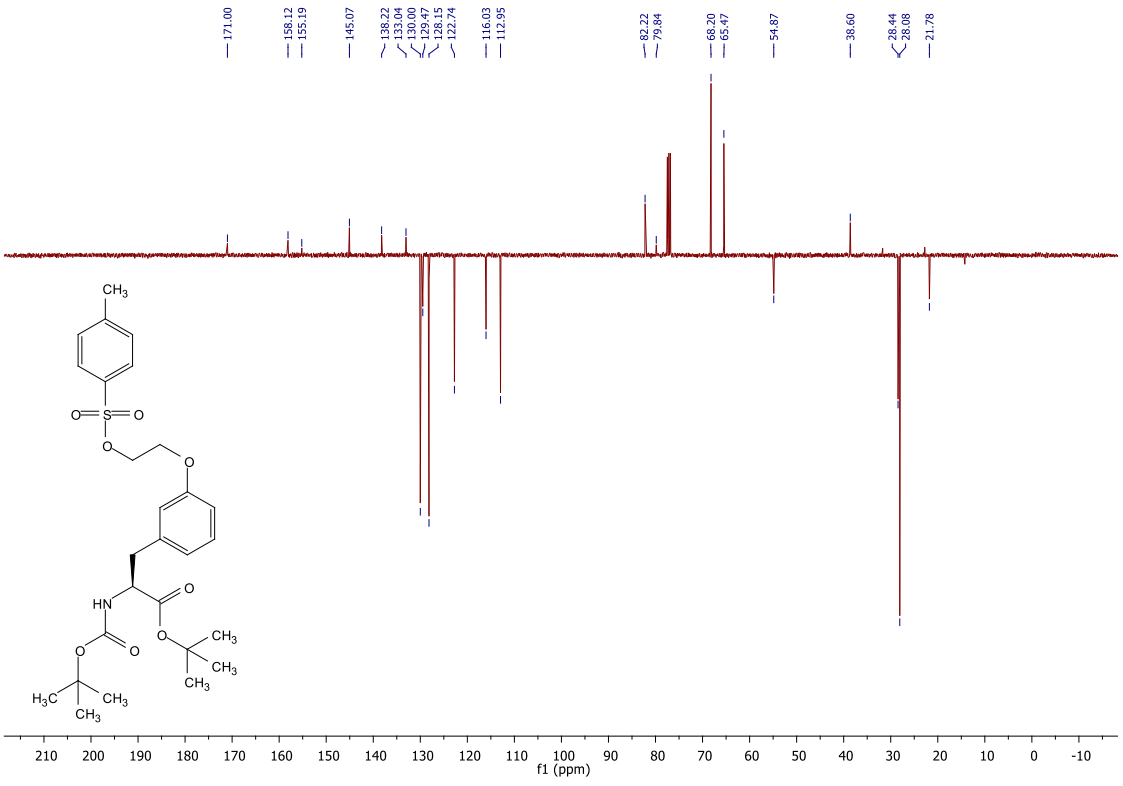

1.7 Compound **7**

^{1}H-NMR spectrum of **7**

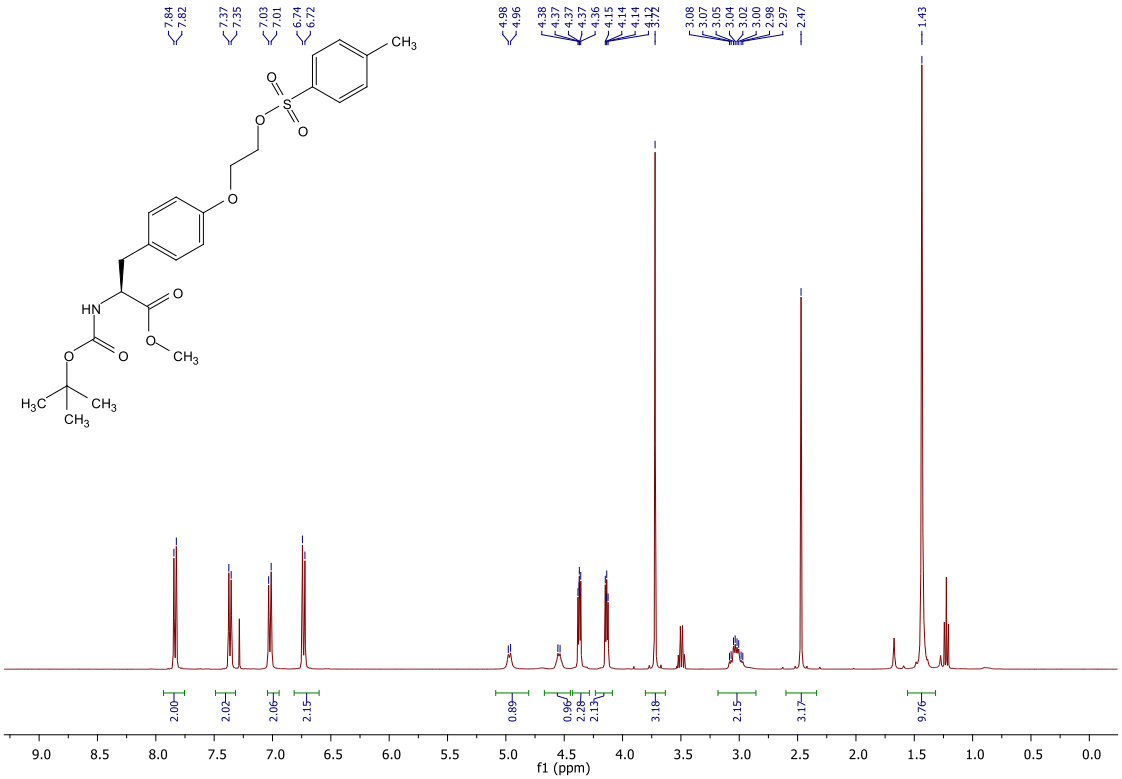

^{13}C-NMR spectrum of **7**

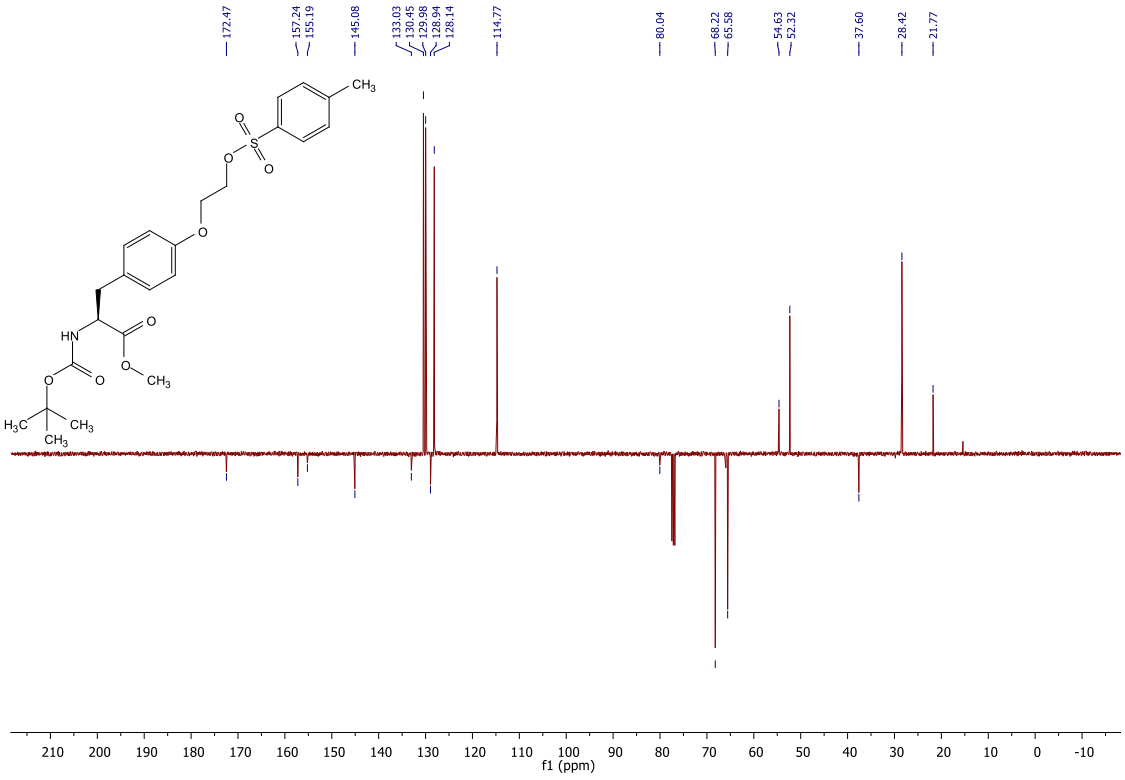

1.8 HCl·FET-OMe

^{1}H-NMR spectrum of HCl·FET-OMe

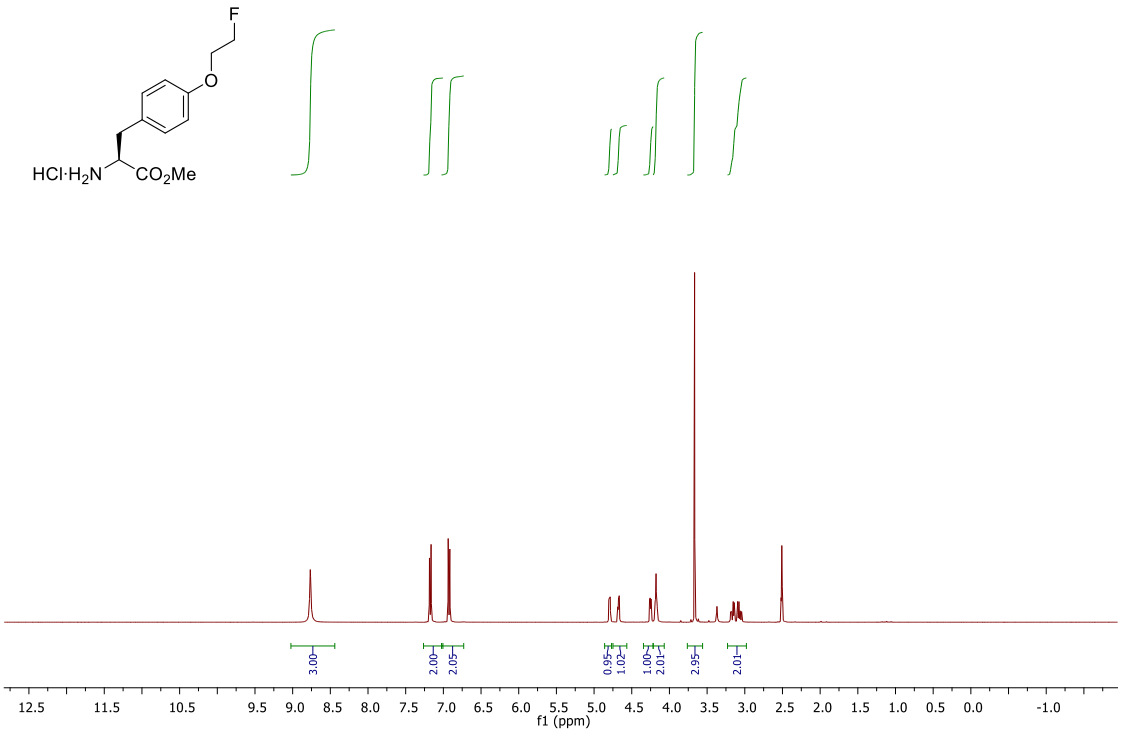

^{13}C-NMR spectrum of HCl·FET-OMe

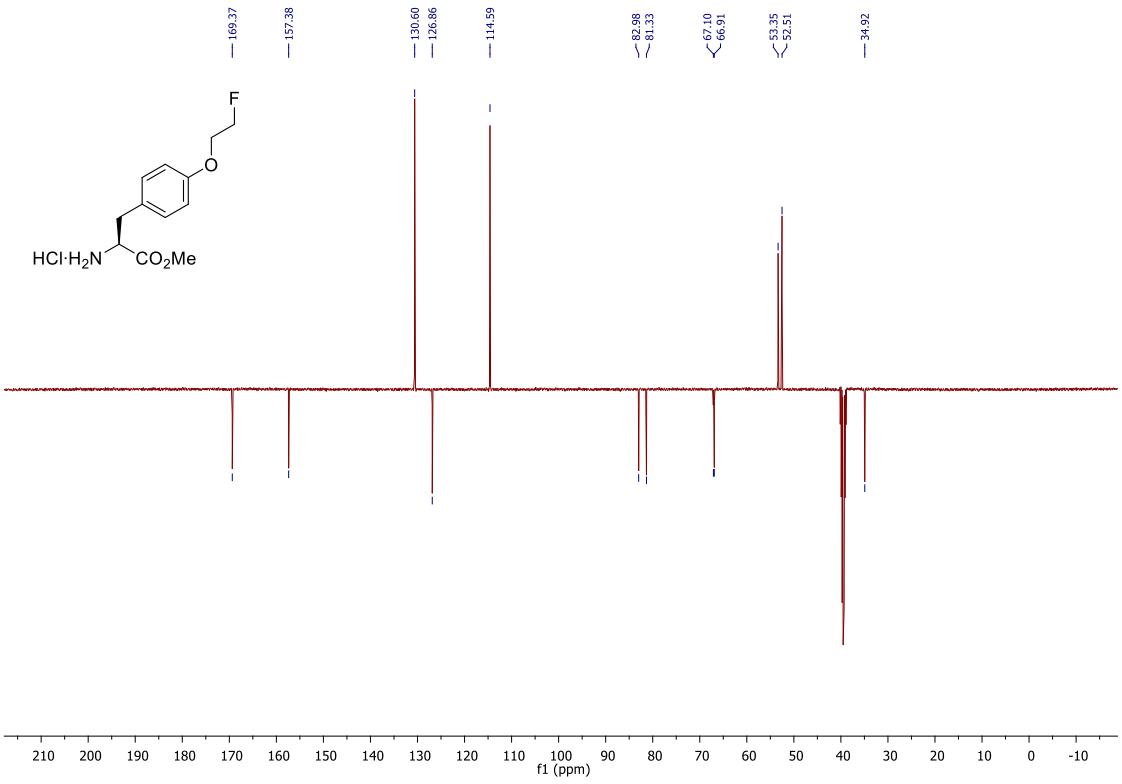

^{19}F-NMR spectrum of HCl·FET-OMe

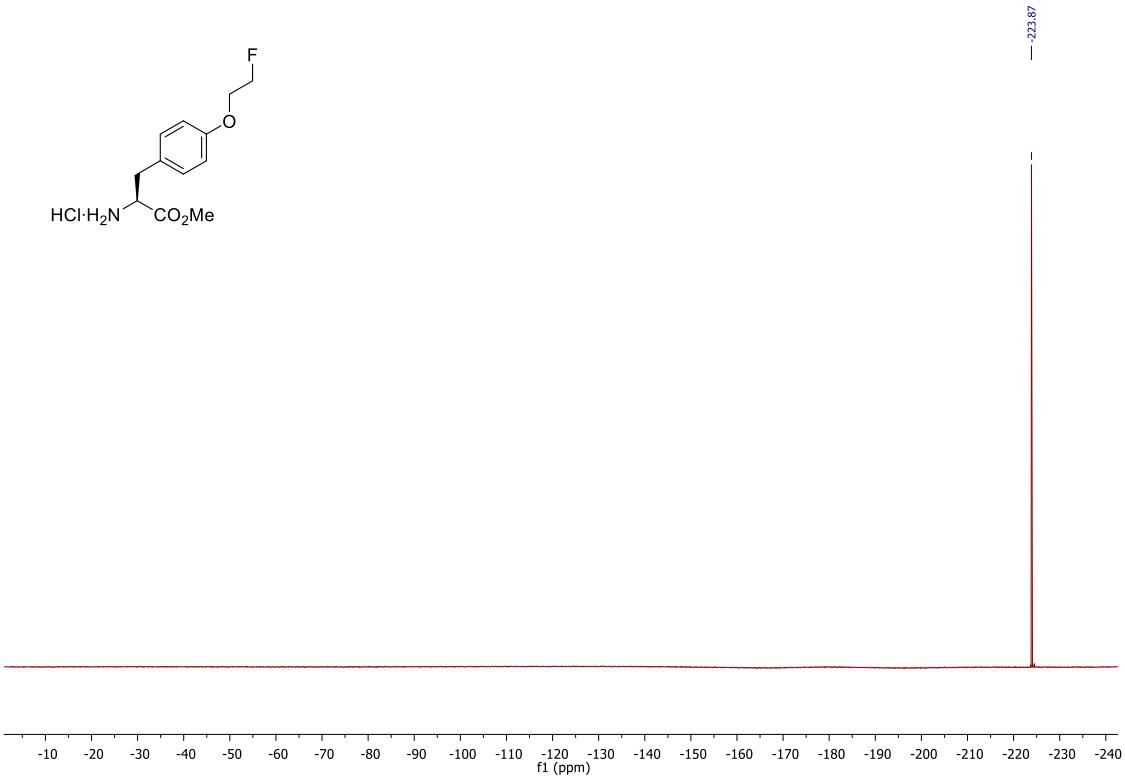

2 HPLC chromatograms

2.1 HPLC chromatograms of *m*-[^{18}F]FET

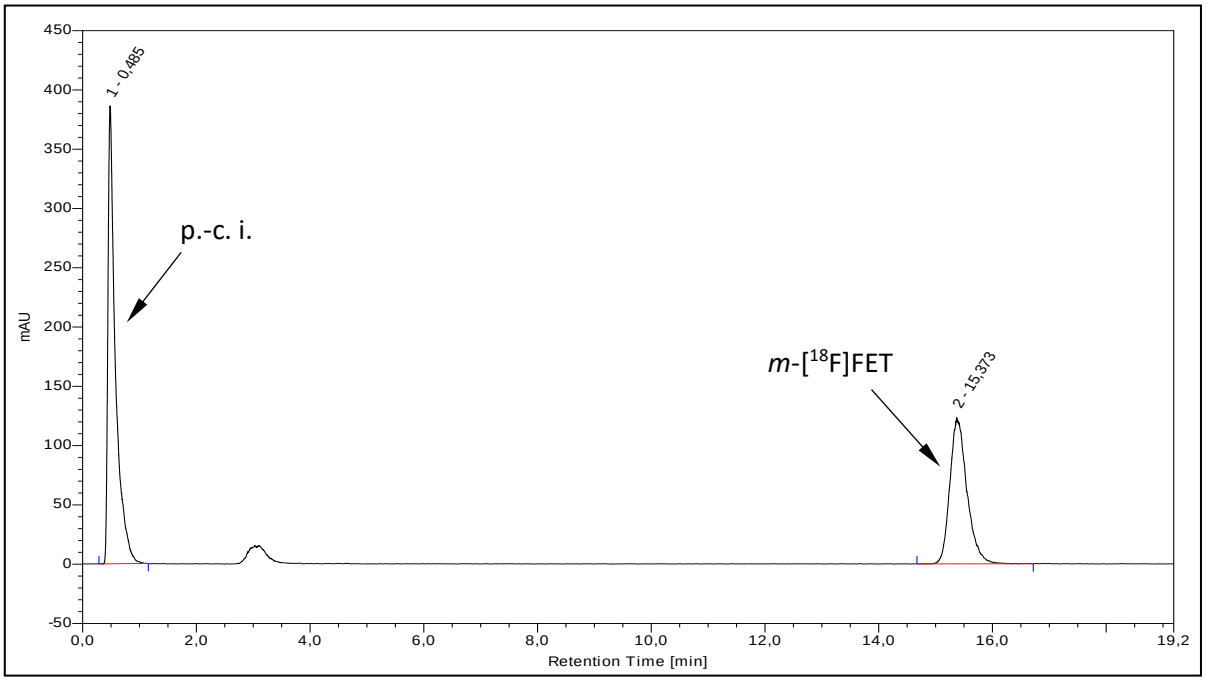

HPLC trace of crude *m*-[^{18}F]FET [eluent: 10% MeCN (0.1% TFA); flow rate: 1 mL/min]. Abbreviation: p.-c.i. – post column injection.

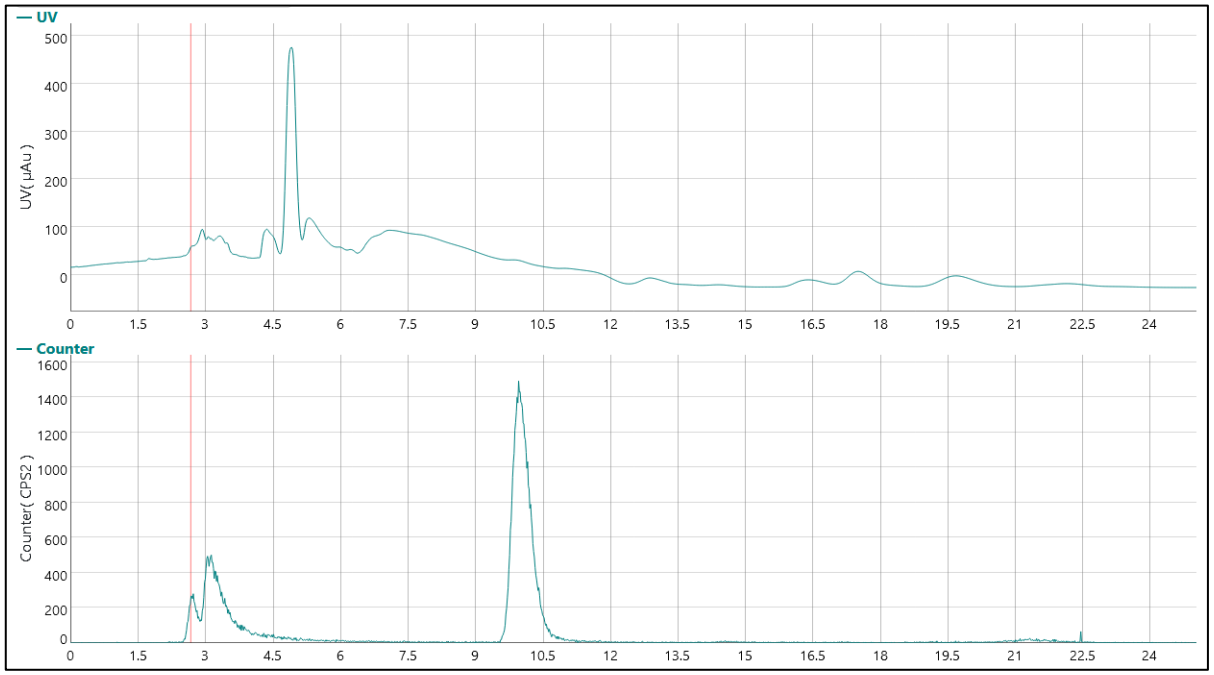

HPLC traces for purification of *m*-[^{18}F]FET by semi-preparative HPLC (top trace: UV, λ = 254 nm; bottom trace: radioactivity; column: Hydro-RP, 250×10 mm; eluent: 10% EtOH [300 mg/L NH_4OAc]; flow rate: 4.7 mL/min; t_R = 10.1 min).

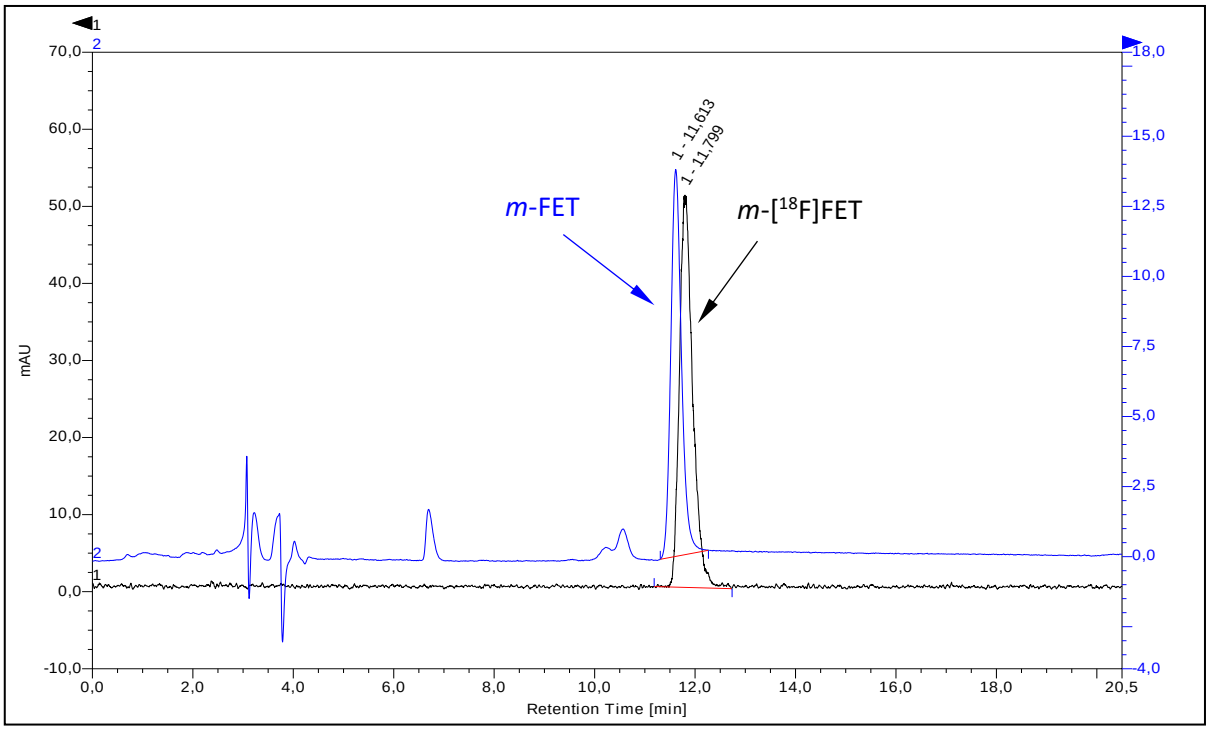

HPLC traces of purified *m*-[^{18}F]FET spiked with the non-radioactive reference compound *m*-FET (eluent: 10% EtOH [300 mg/L NH_4OAc]; flow rate: 1 mL/min). Blue trace: UV, $\lambda = 254$ nm; black trace: radioactivity.

2.2 HPLC chromatograms of [^{18}F]FET-OMe

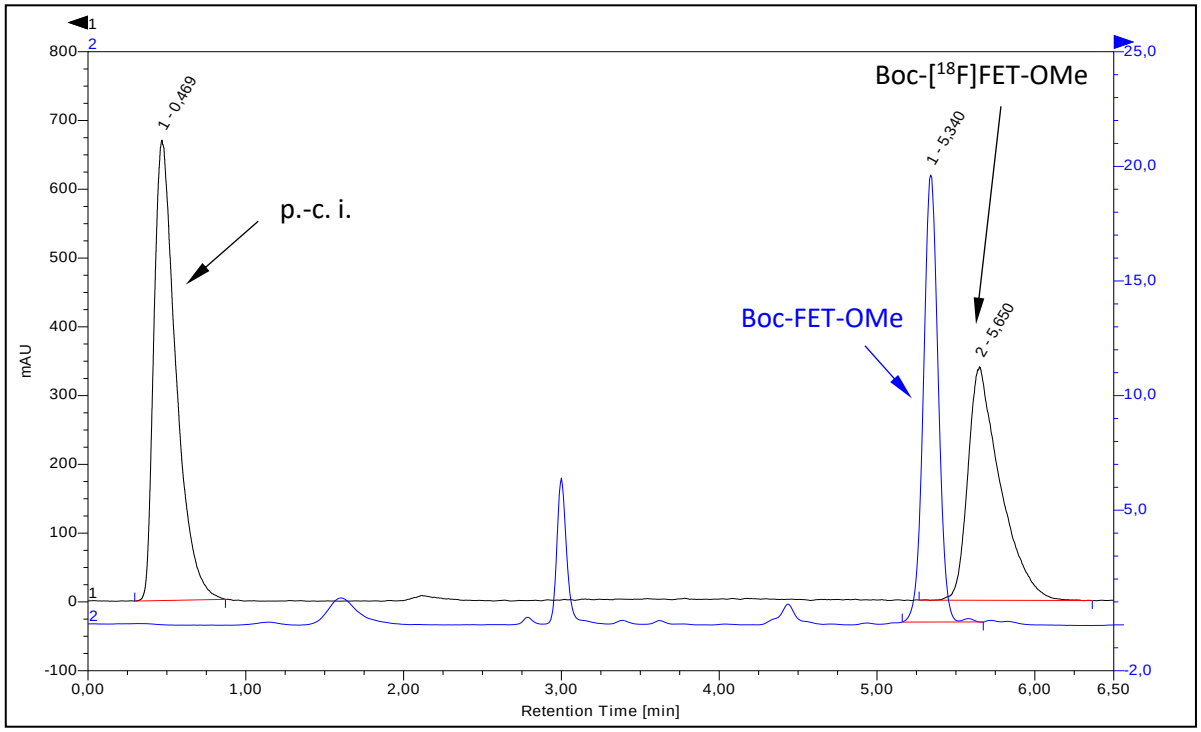

HPLC traces of Boc-[^{18}F]FET-OMe spiked with the non-radioactive reference compound Boc-FET-OMe (eluent: 65% MeCN; flow rate: 1 mL/min). Blue trace: UV, λ = 254 nm; black trace: radioactivity. Abbreviation: p.-c. i. – post column injection.

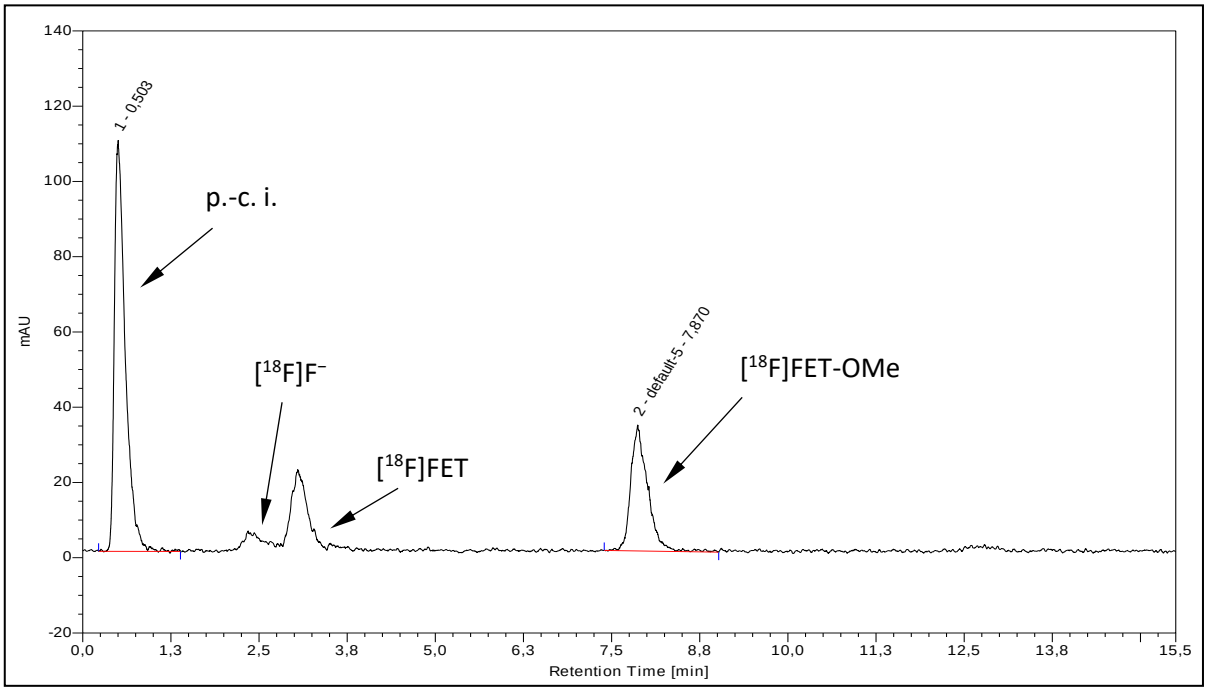

HPLC trace of [^{18}F]FET-OMe [eluent: 15% MeCN (0.1% TFA); flow rate: 1 mL/min]. Abbreviation: p.-c.i. – post column injection.

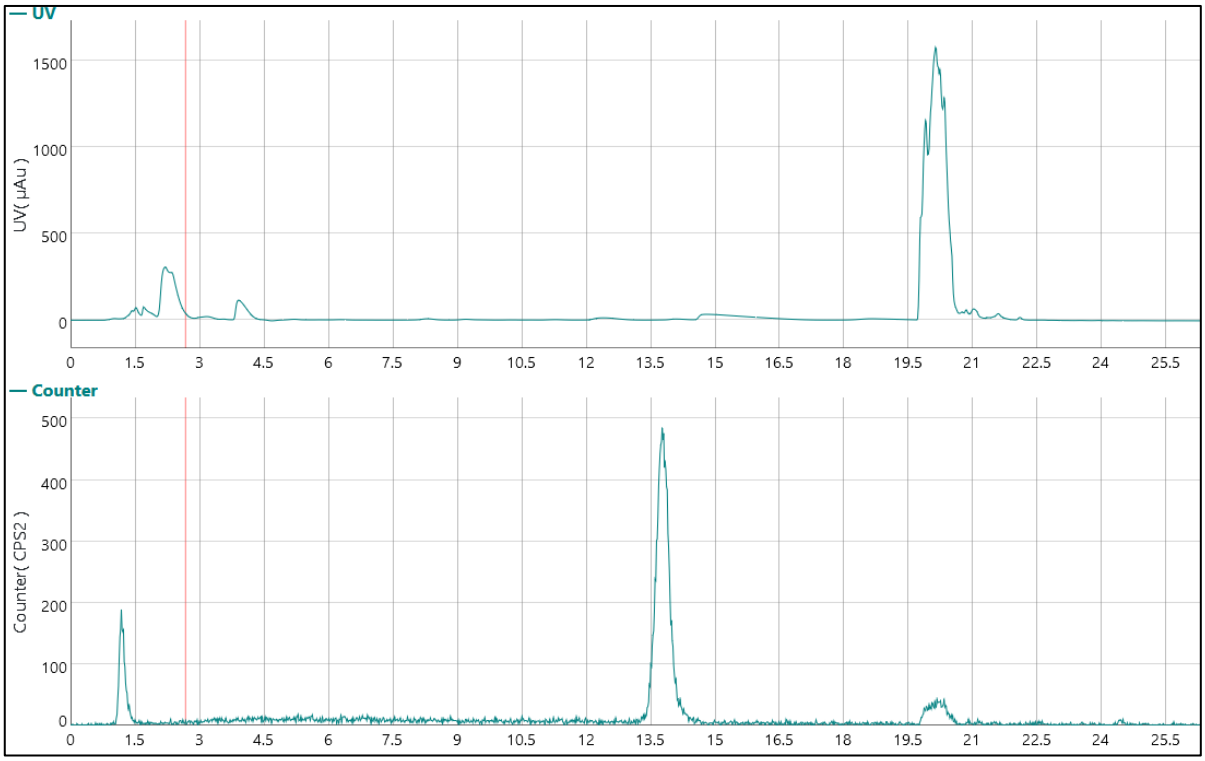

HPLC traces for purification of [^{18}F]FET-OMe by semi-preparative HPLC (top trace: UV, λ = 254 nm; bottom trace: radioactivity; column: Hydro-RP, 250×10 mm; eluent: 15% MeCN (0.1% TFA); flow rate: 4.7 mL/min; t_R = 13.8 min).

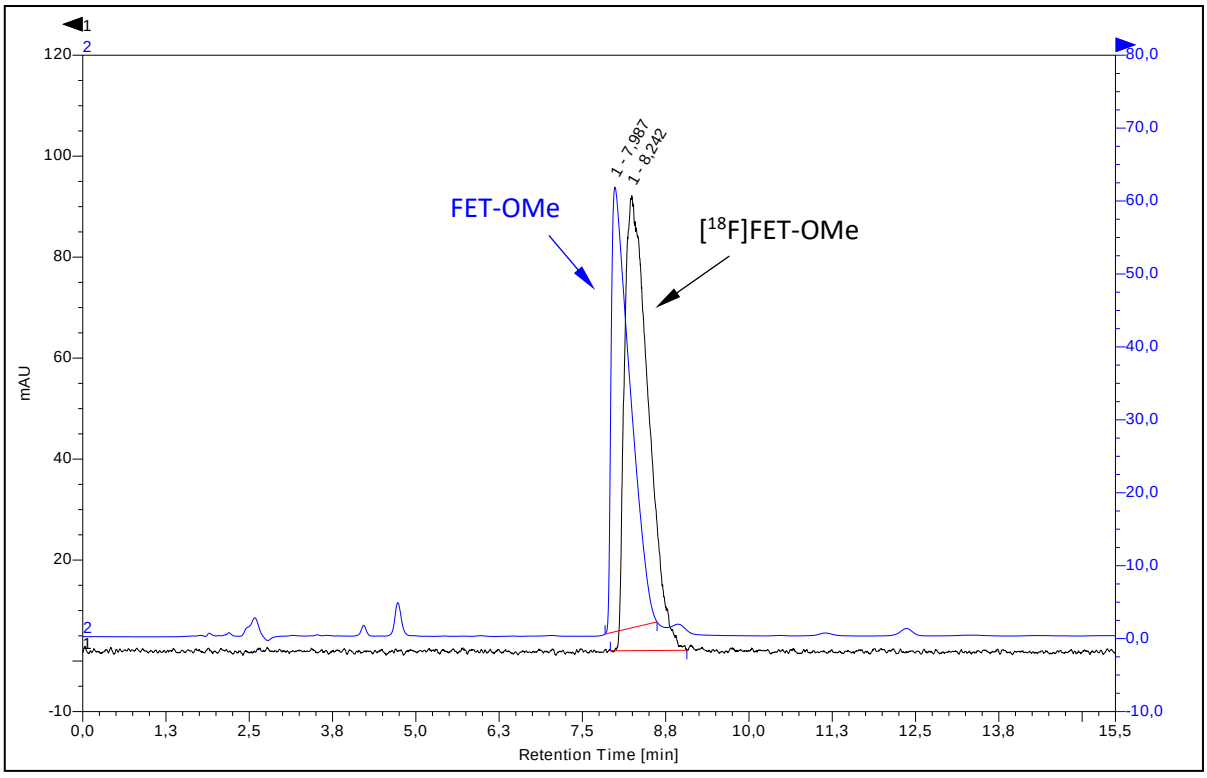

HPLC traces of purified [^{18}F]FET-OMe spiked with the non-radioactive reference compound FET-OMe [eluent: 15% MeCN (0.1% TFA); flow rate: 1 mL/min]. Blue trace: UV, λ = 254 nm; black trace: radioactivity.

3 Determination of molar activity of *m*-[^{18}F]FET and [^{18}F]FET-OMe

A sample of the purified tracer solution (20 µL) was analysed by analytical HPLC and the carrier amount was determined from the peak area according to the respective calibration curve. The molar activity (A_M) was calculated according to following formula:

$$A_M = \frac{(GBq)}{(\mu mol)}$$

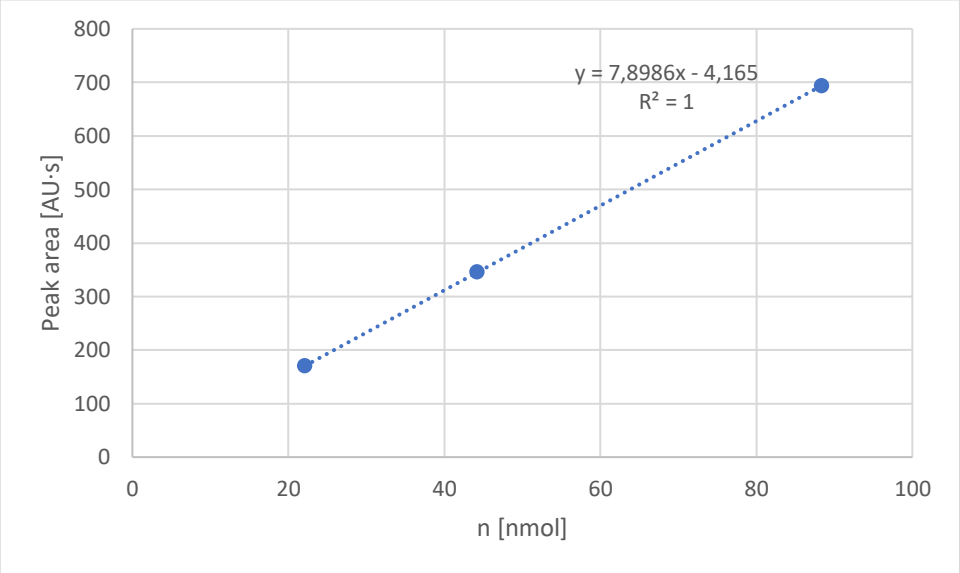

Figure S1: Calibration curve for determination of carrier amount of *m*-[^{18}F]FET. Raw data are shown in Table S1.

Table S1: Calibration data (measured at 254 nm) for determination of carrier amount of *m*-[^{18}F]FET.

Concentration [µM]	n [nmol]	Peak area [AU·s]
1	88.4	693.83
0.5	44.2	345.72
0.25	22.1	169.89

Table S2: Calculation of molar activity of *m*-[^{18}F]FET.

Activity in 20 µL [GBq]	6.36×10^{-4}
Peak area [AU·s]	0.053
Carrier amount [nmol]	6.71×10^{-4}
Molar activity [GBq/µmol]	94.8

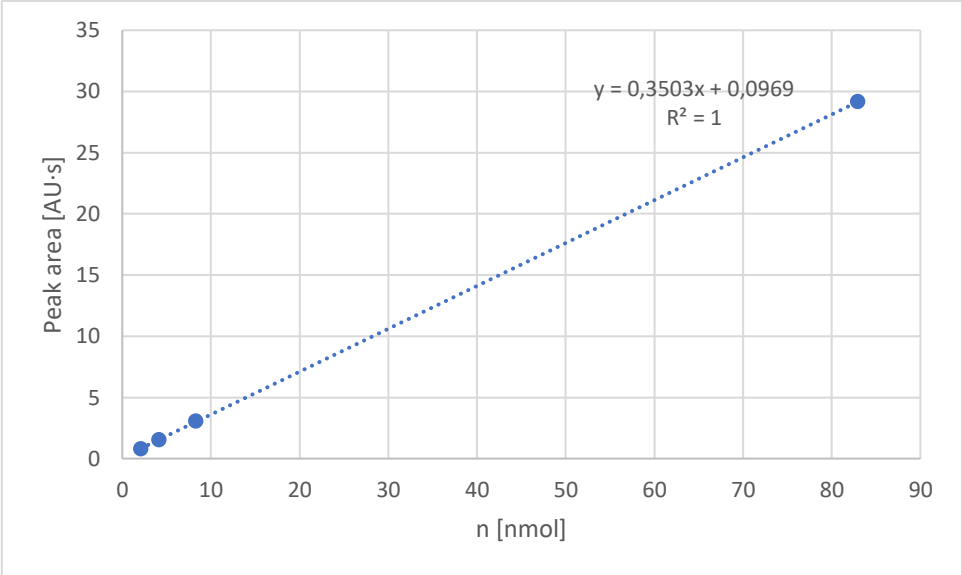

Figure S2: Calibration curve for determination of carrier amount of [^{18}F]FET-OMe. Raw data are shown in Table S3.

Table S3: Calibration data (measured at 254 nm) for determination of carrier amount of [^{18}F]FET-OMe.

Concentration [µM]	n [nmol]	Peak area [AU·s]
1	82.9	29.15
0.1	8.3	3.06
0.05	4.1	1.54
0.025	2.1	0.78

Table S4: Calculation of molar activity of [^{18}F]FET-OMe.

Activity in 20 µL [GBq]	1.17×10^{-3}
Peak area [AU·s]	0.0026
Carrier amount [nmol]	7.42×10^{-4}
Molar activity [GBq/µmol]	157.4

4 Protein incorporation

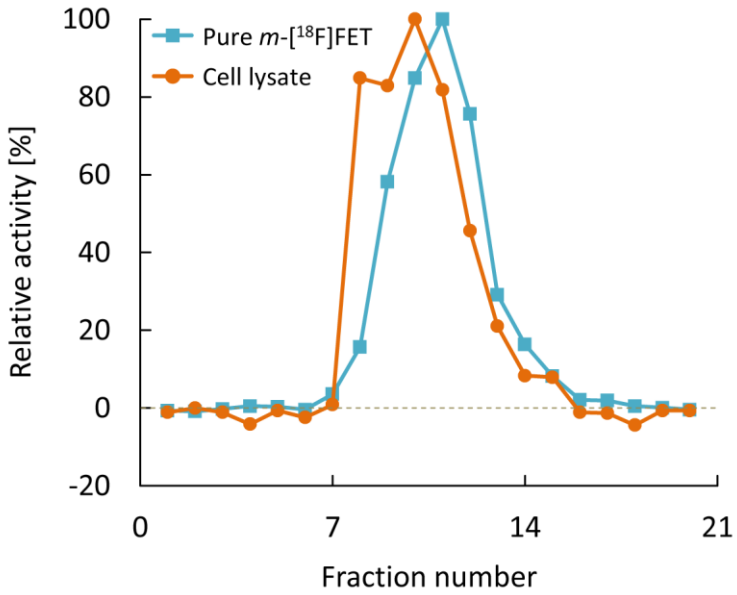

Figure S3: Elution profile of radioactivity from PD 10 cartridges loaded with the soluble fraction of homogenized U87 MG cells incubated with *m*-[^{18}F]FET for 1 h (orange) or with pure *m*-[^{18}F]FET (control experiments without incubation, turquoise). The cartridges were eluted with 20 × 1 mL of Earle's balanced salt solution (EBSS) and the radioactivity in each fraction was measured with a gamma counter, corrected for background activity and normalized by the maximum activity value. Note that the apparently negative values observed in some cases are an artefact introduced by the background subtraction that can be attributed to slight variations in background radioactivity.

Supporting Information

7-[^{18}F]Fluoro-8-azaisatoic Anhydrides: Versatile Prosthetic Groups for the Preparation of PET-Tracers

Benedikt Gröner[a,b#], Michael Willmann[a#], Lisa Donnerstag[a,b], Elizaveta A. Urusova[a,b], Felix Neumaier[a,b], Swen Humpert[a], Heike Endepols[a,b,c], Bernd Neumaier[a,b,d*], and Boris D. Zlatopolskiy[a,b,d]

[a] Forschungszentrum Jülich GmbH, Institute of Neuroscience and Medicine, Nuclear Chemistry (INM-5), Wilhelm-Johnen-Straße, 52428 Jülich, Germany.

[b] University of Cologne, Faculty of Medicine and University Hospital Cologne, Institute of Radiochemistry and Experimental Molecular Imaging, Kerpener Straße 62, 50937 Cologne, Germany.

[c] University of Cologne, Faculty of Medicine and University Hospital Cologne, Department of Nuclear Medicine, Kerpener Straße 62, 50937 Cologne, Germany.

[d] Max Planck Institute for Metabolism Research, Gleueler Straße 50, 50931, Cologne, Germany.

* Corresponding author: b.neumaier@fz-juelich.de;

# B.G. and M.W. contributed equally

Table of contents

1 Synthesis schemes

1.1 Compounds **7** and **9**[1] (**Scheme S1**)

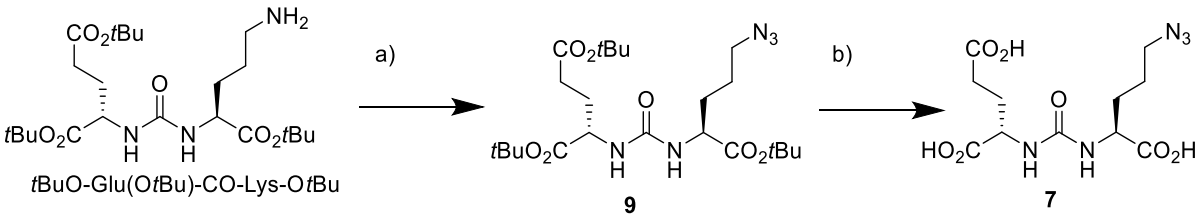

Scheme S1: Preparation of 1,5-di-*tert*-butyl (*S*)-2-({[(*S*)-6-azido-1-(*tert*-butoxy)-1-oxohexan-2-yl]carbamoyl}amino)pentanedioate (**9**) and (*S*)-2-({[(*S*)-5-azido-1-carboxypentyl]carbamoyl}amino)pentanedioic acid (**7**). Reaction conditions: a) K_2CO_3, $CuSO_4$, MeOH, imidazole-1-sulfonyl azide hydrochloride, r.t., 24 h, 64%; b) TFA, H_2O, TIPS (95:2.5:2.5), r.t., 2 h, 92%.

1.2 Compounds **8** and **11** (**Scheme S2**)

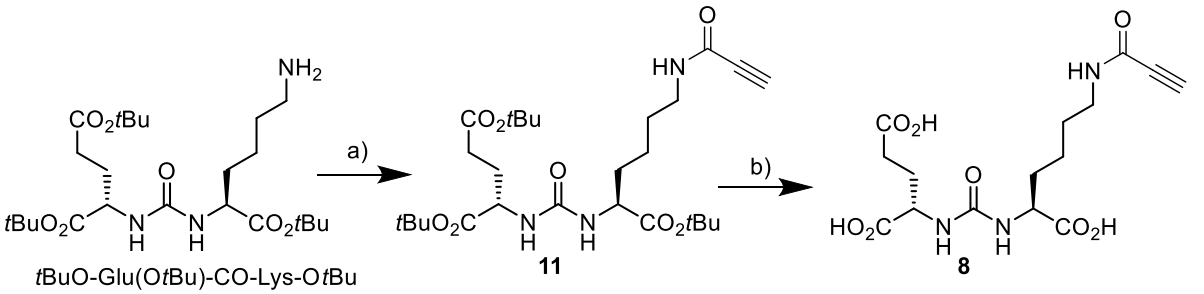

Scheme S2: Preparation of di-*tert*-butyl {[(*S*)-1-(*tert*-butoxy)-1-oxo-6-propiolamidohexan-2-yl]carbamoyl}-(*S*)-glutamate (**11**) and {[(*S*)-1-carboxy-5-propiolamidopentyl]carbamoyl}-(*S*)-glutamic acid (**8**). Reaction conditions: a) pentafluorophenyl propiolate, DIPEA, DMF, -10 °C to rt, 2 h, 87%; b) TFA, H_2O, TIPS (95:2.5:2.5), rt, 1 h, 57%.

2 NMR-spectra

2.1 Compound **2a**

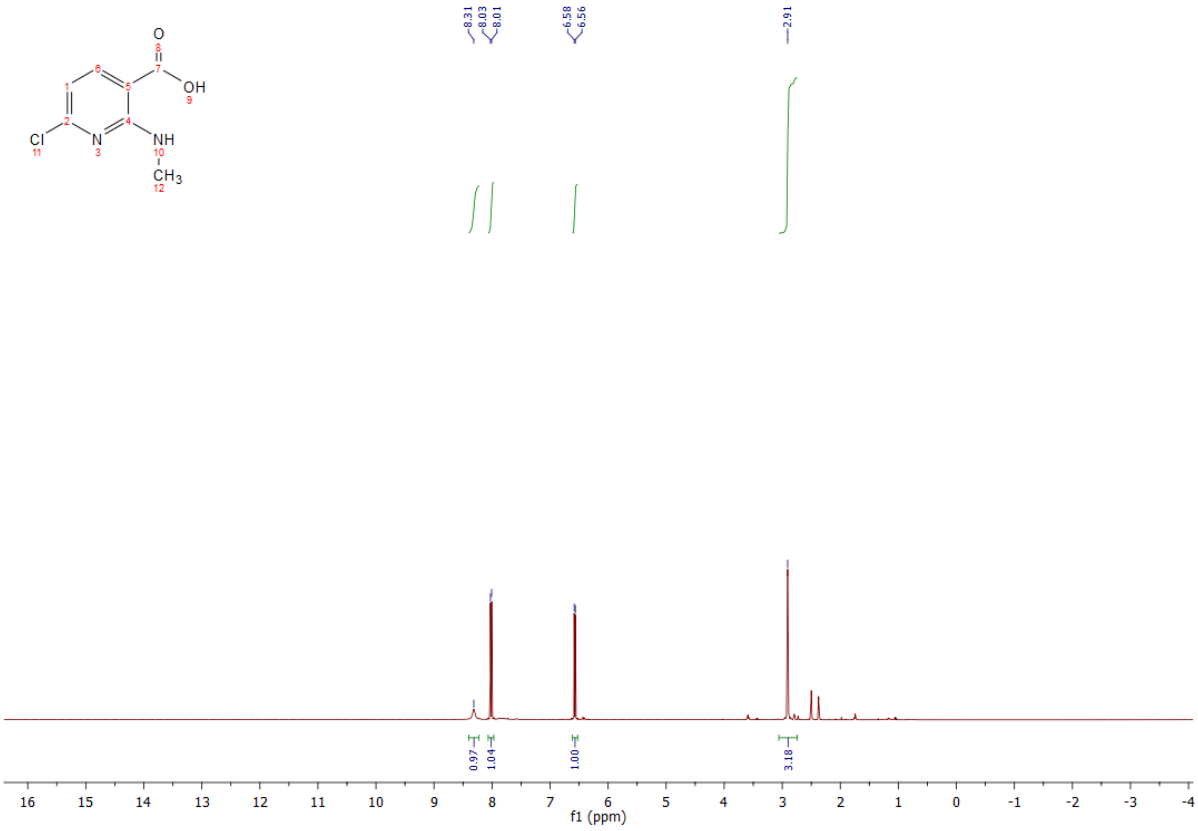

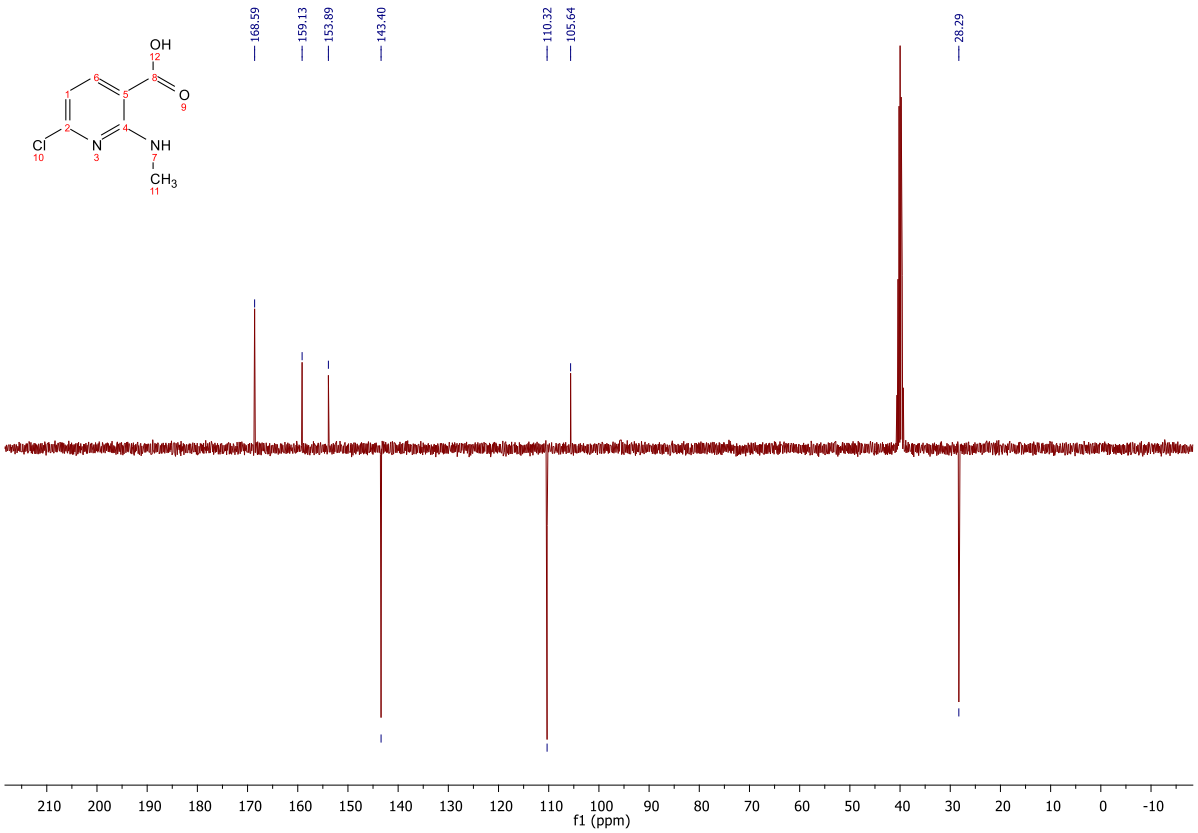

2.2 Compound **2b**

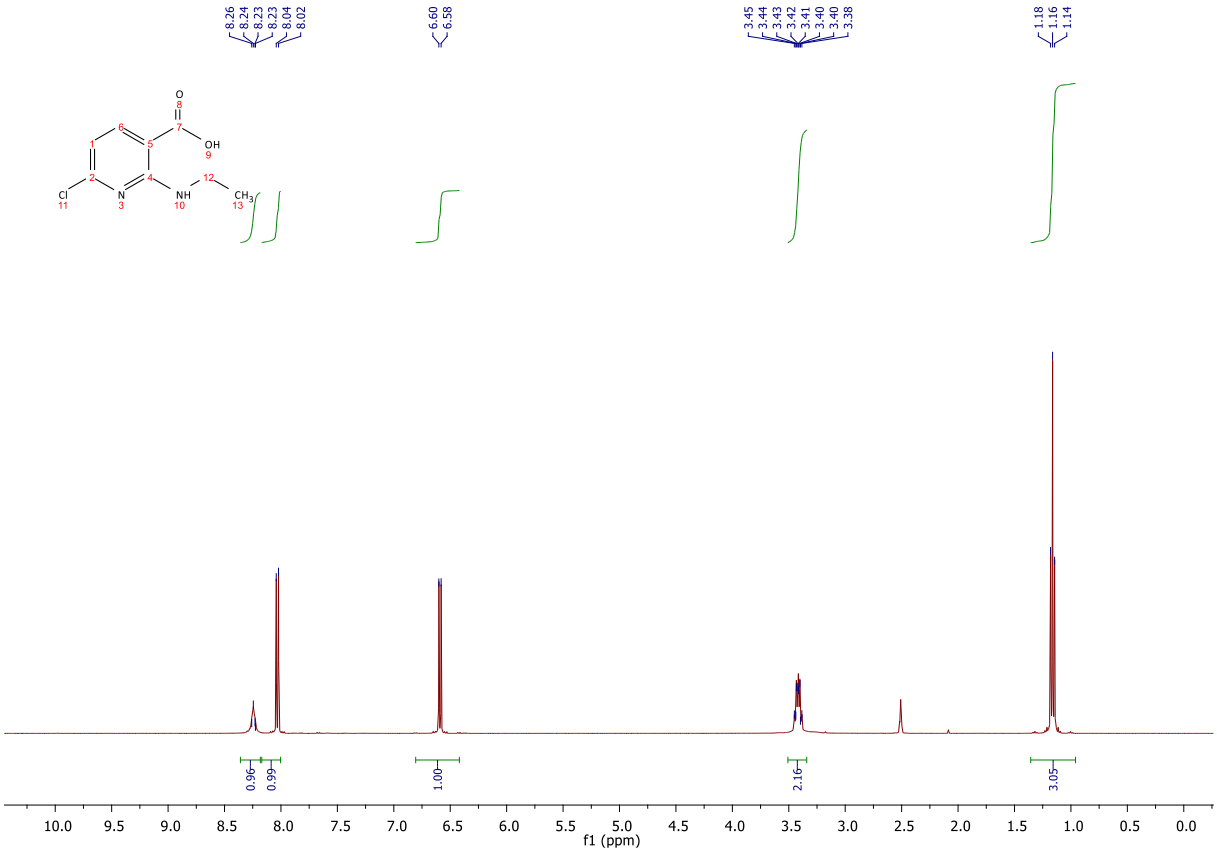

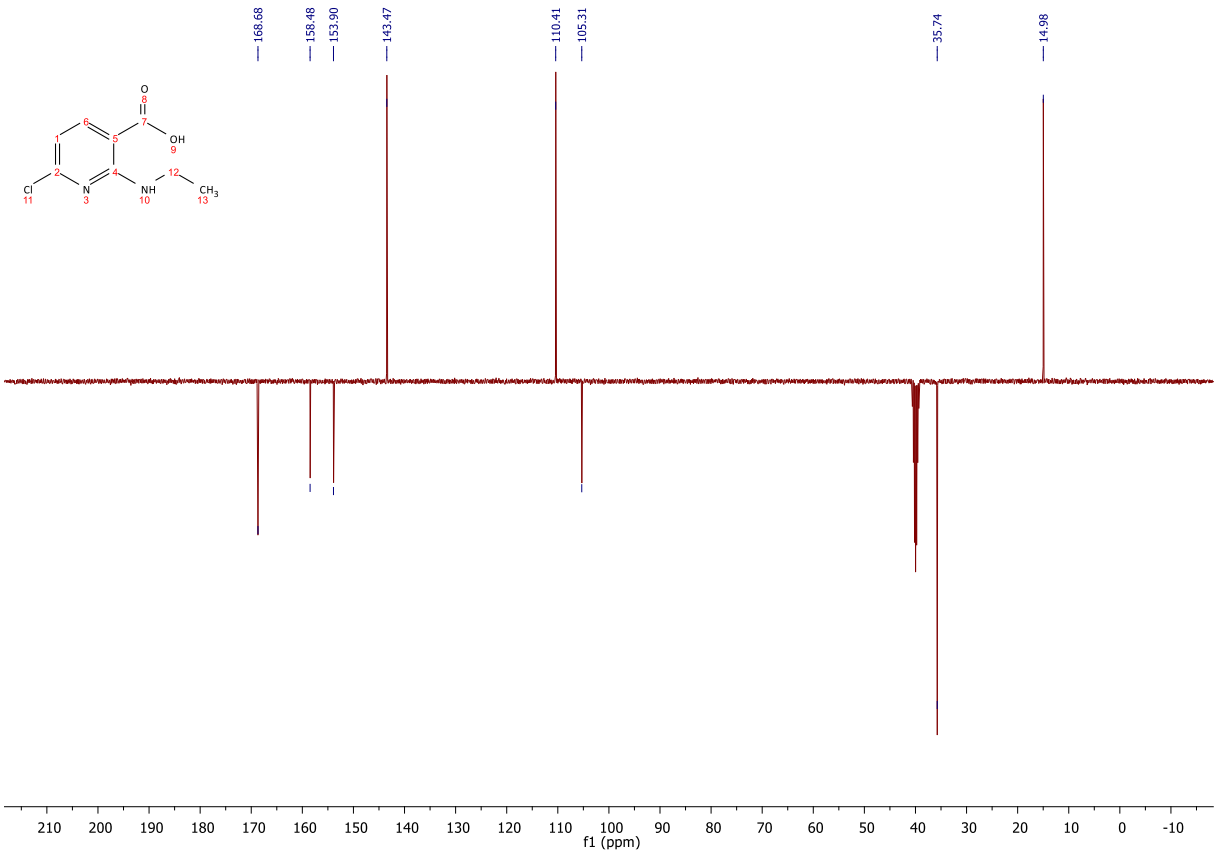

2.3 Compound **2c**

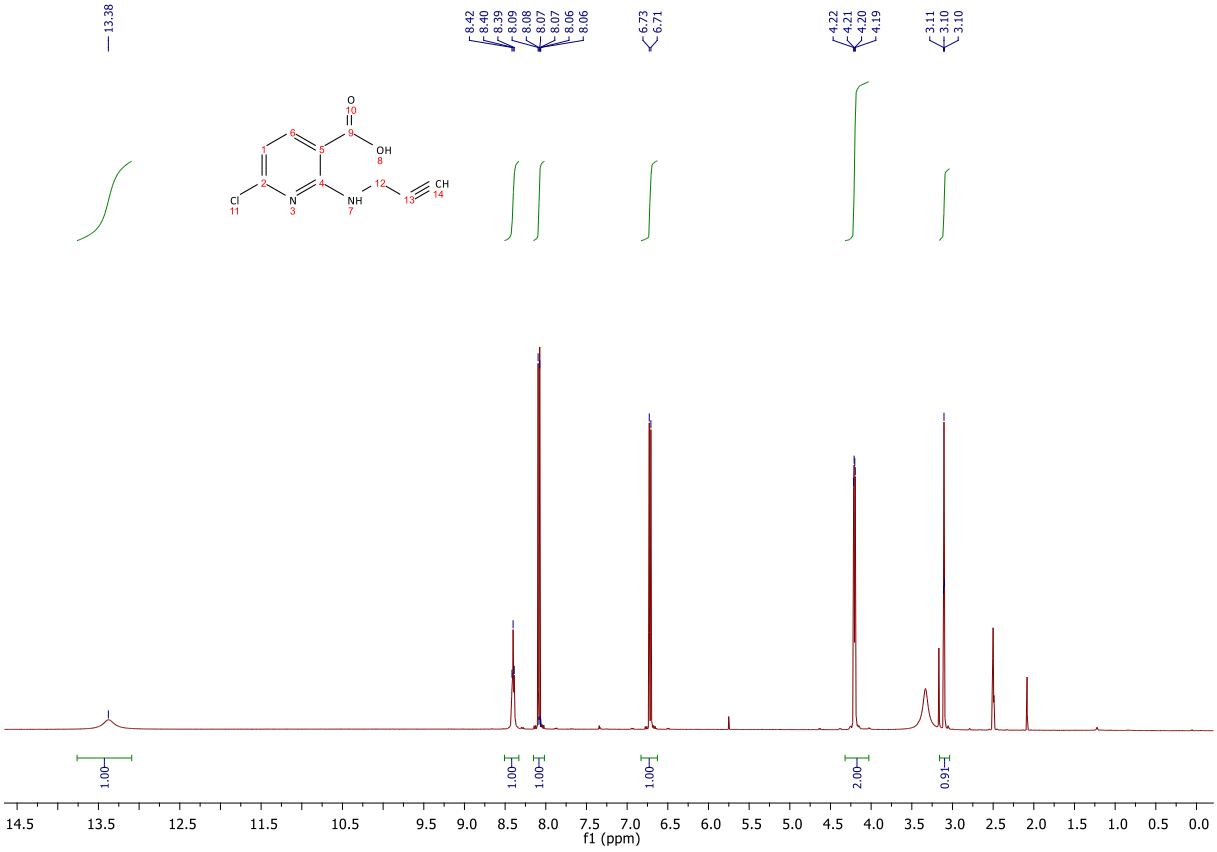

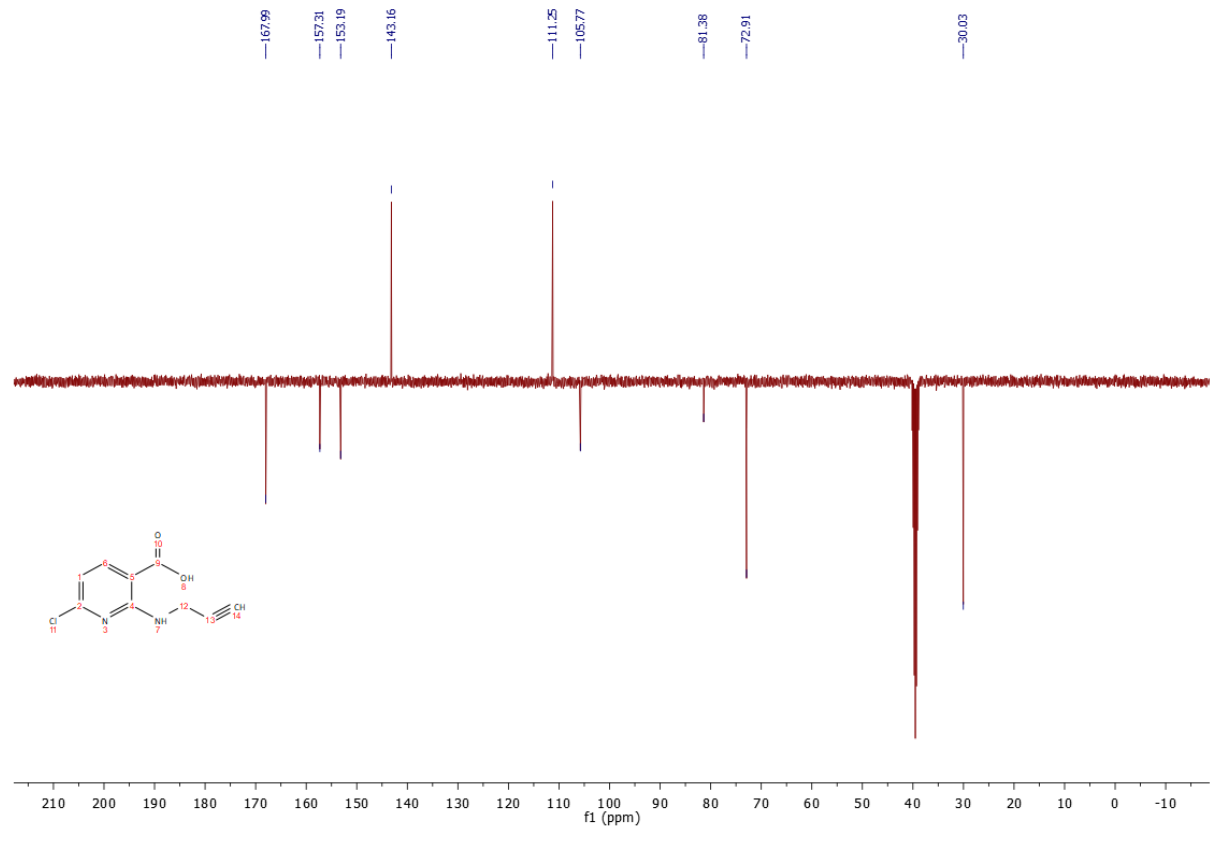

2.4 Compound **2d**

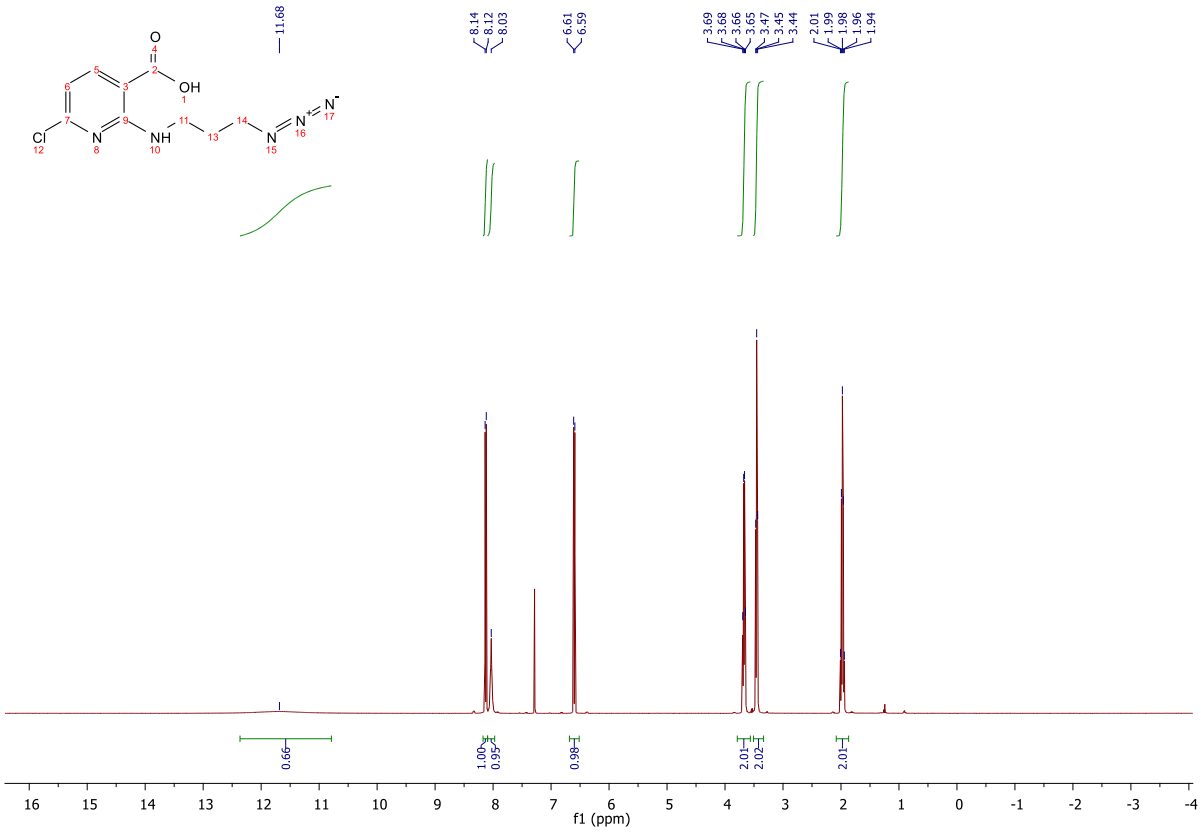

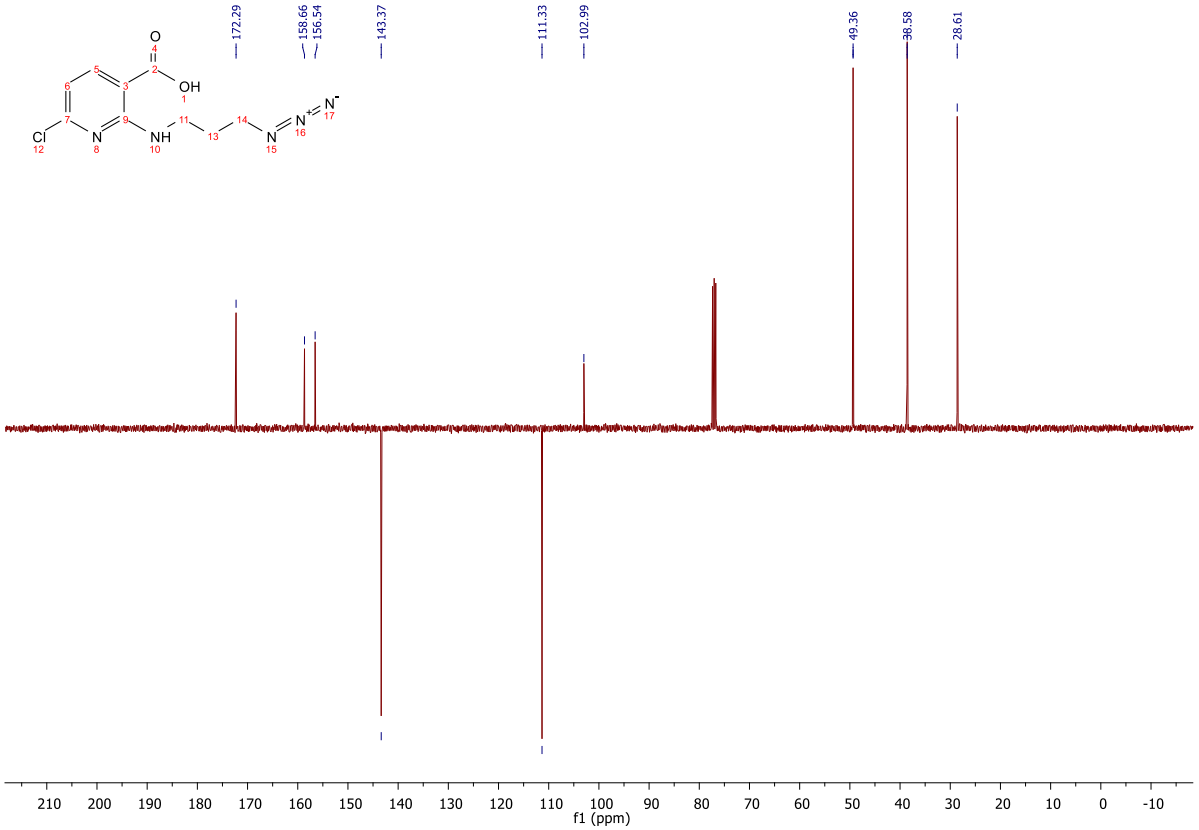

2.5 Compound **2e**

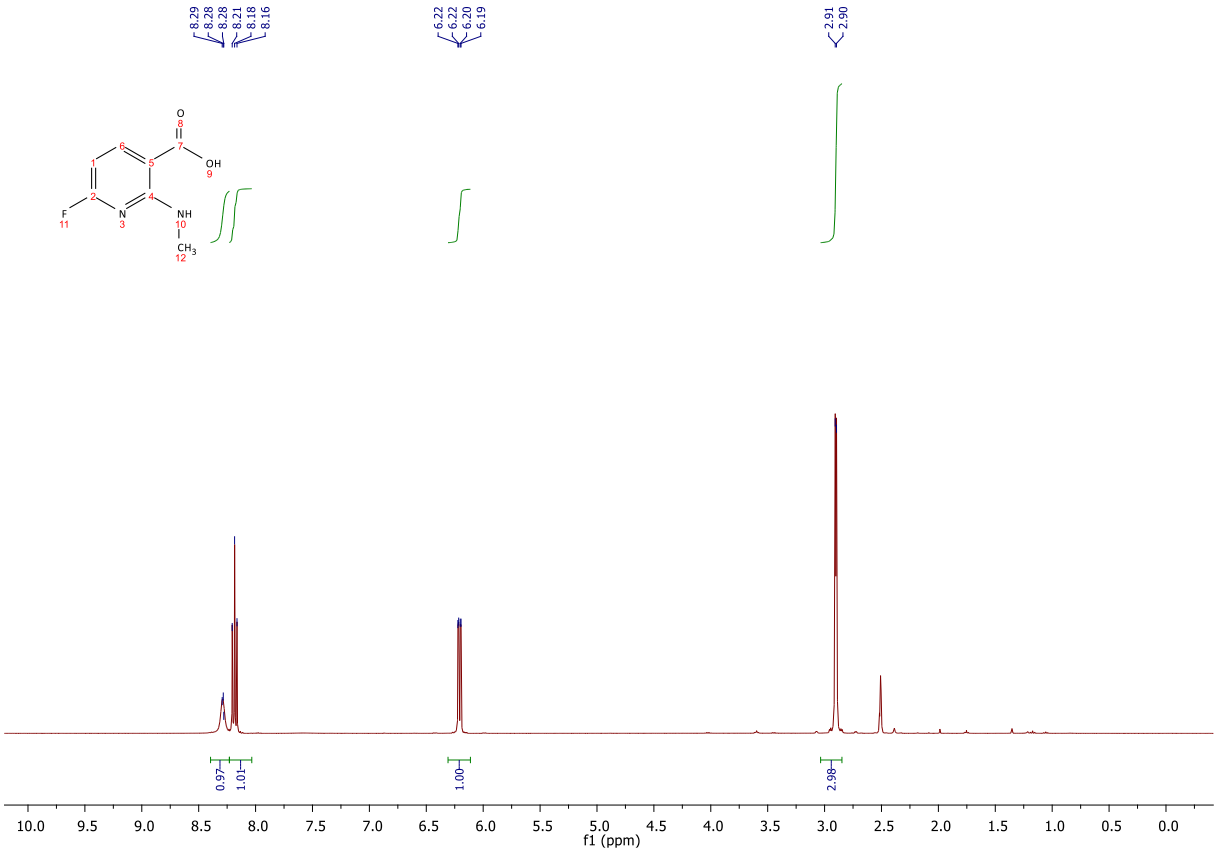

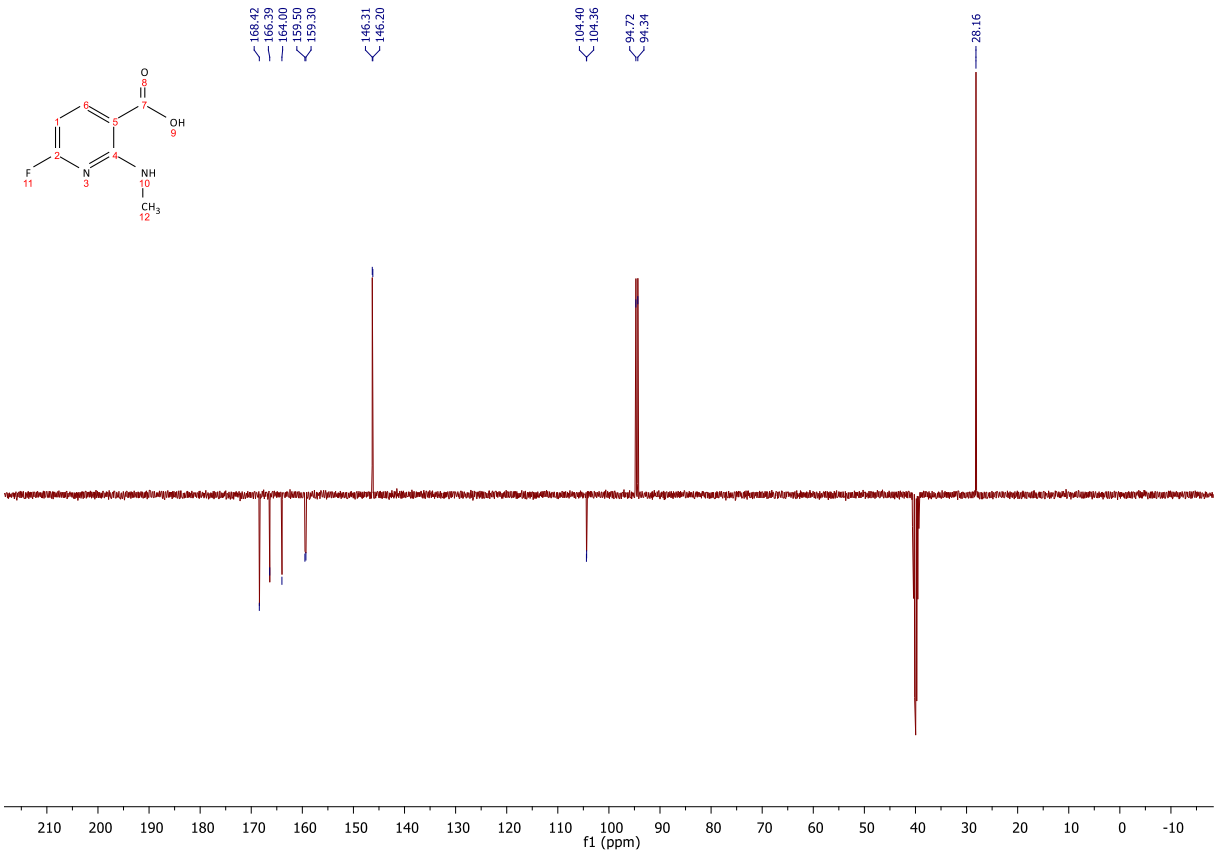

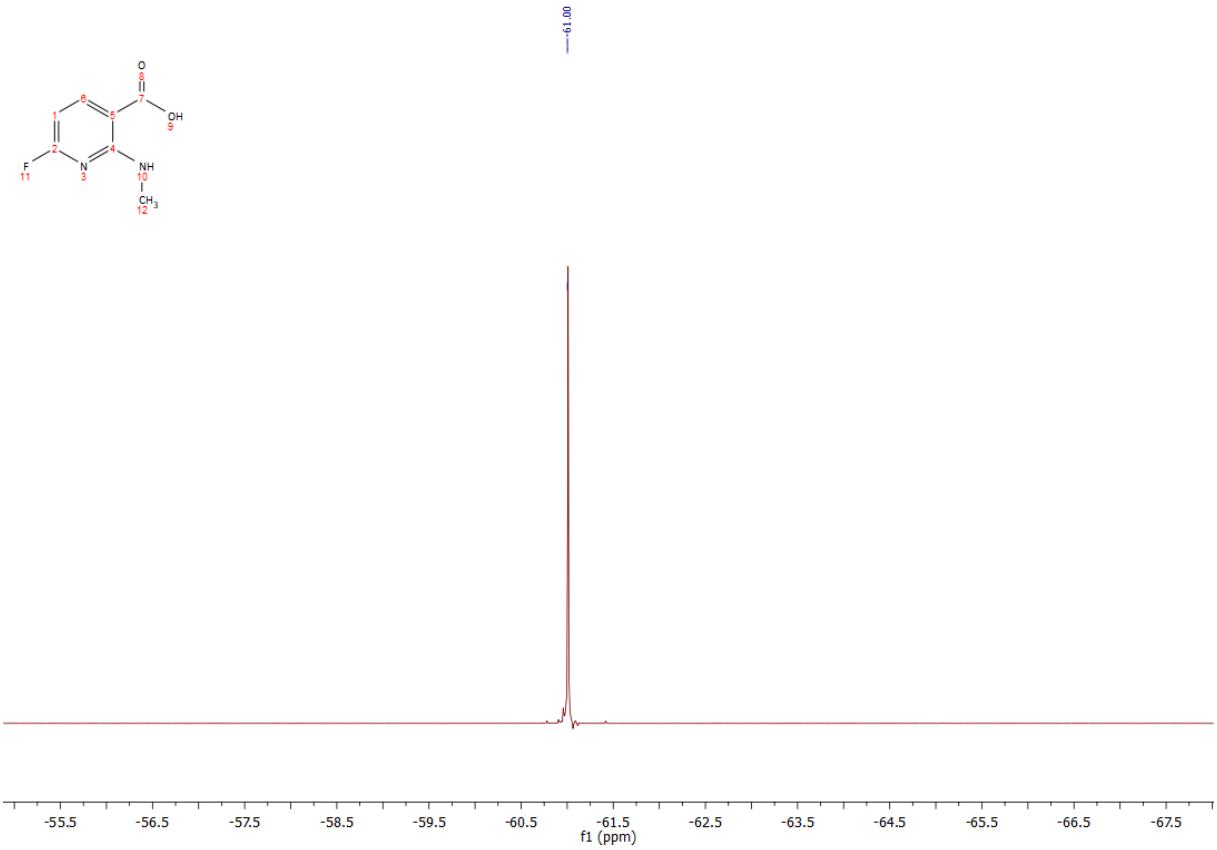
-61.00
-55.5
-56.5
-57.5
-58.5
-59.5
-60.5
-61.5
-62.5
-63.5
-64.5
-65.5
-66.5
-67.5
f1 (ppm)

2.6 Compound **2f**

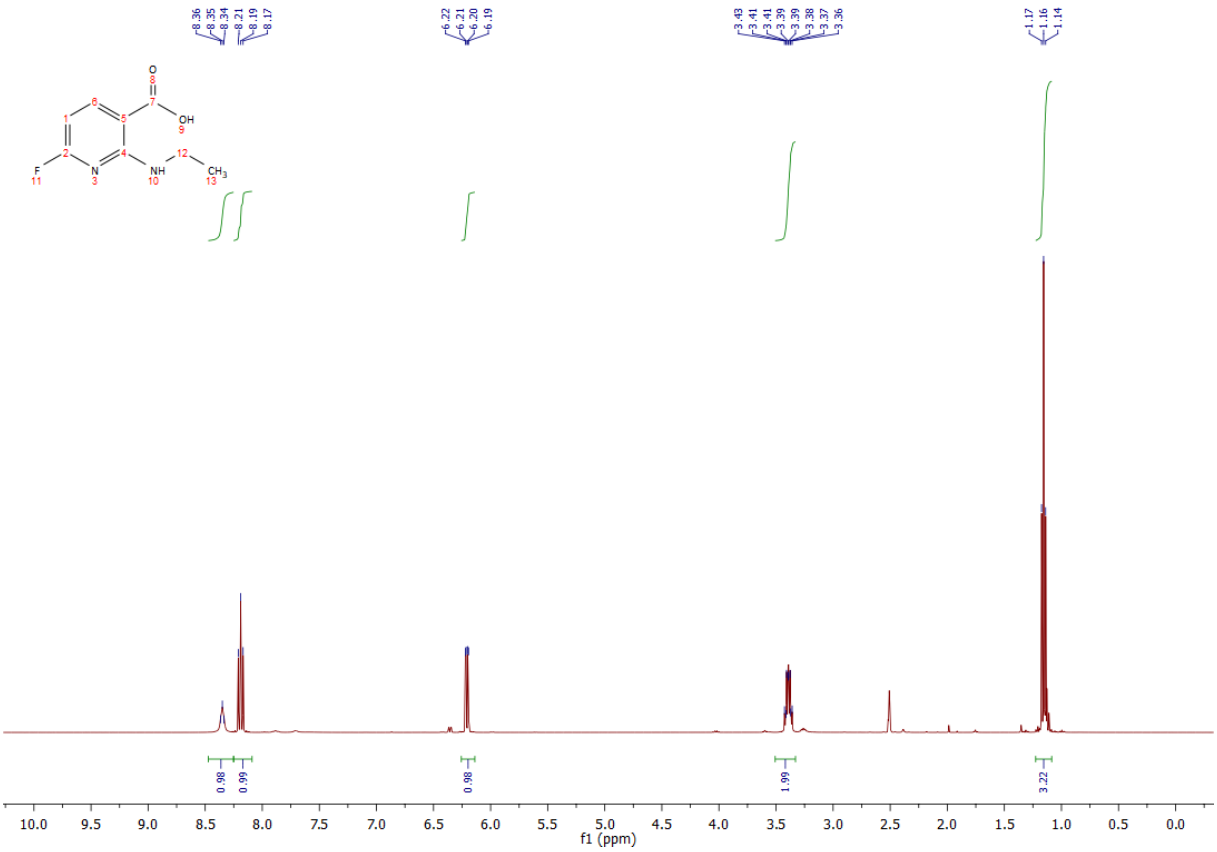

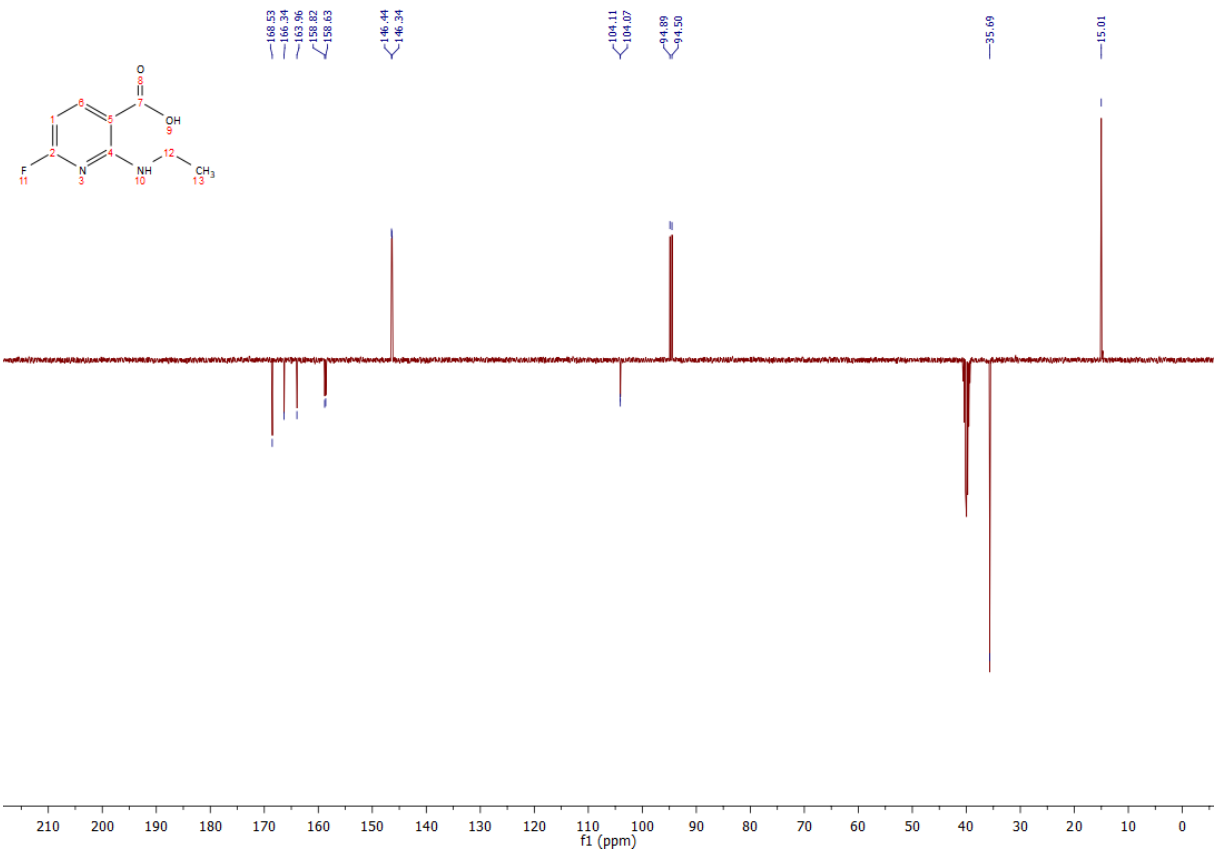

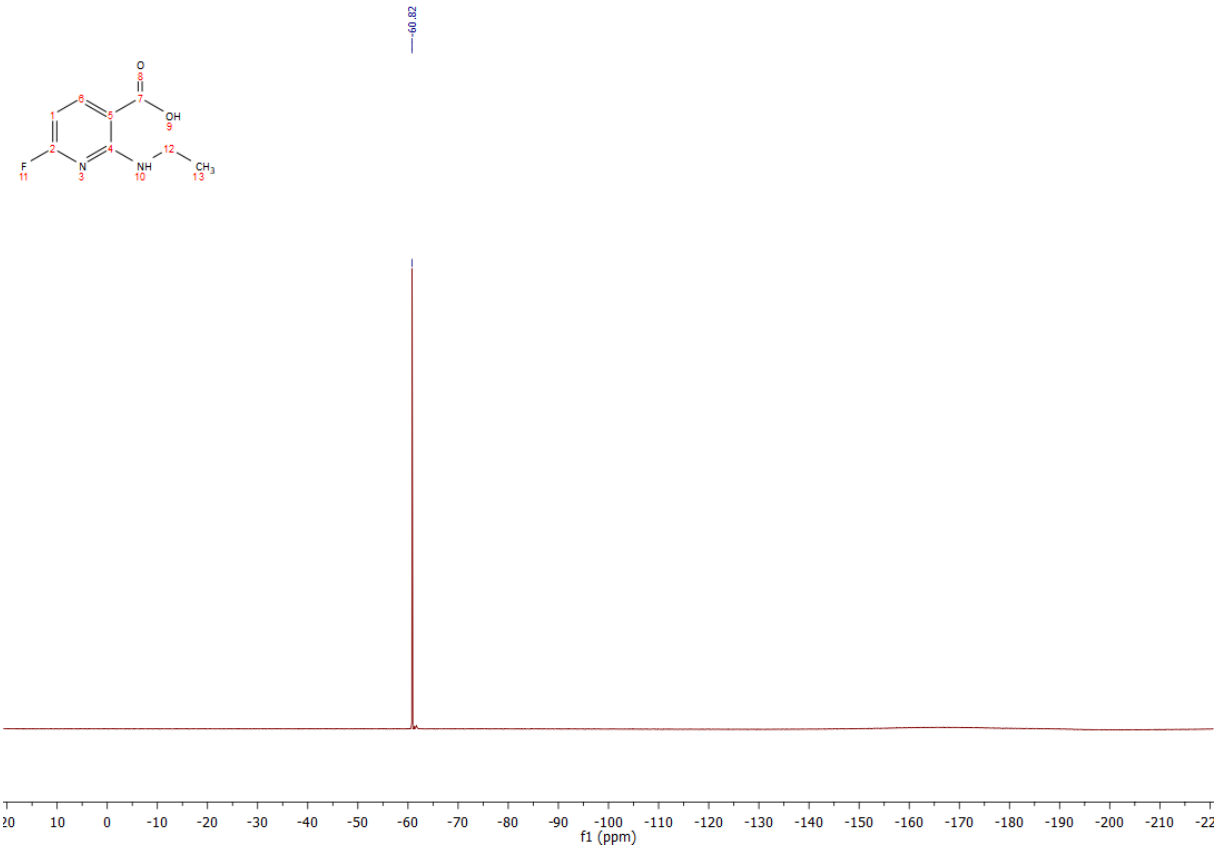
-60.82
O
8
7
OH
9
6
5
1
2
4
12
F
11
N
3
NH
10
CH3
13
20
10
0
-10
-20
-30
-40
-50
-60
-70
-80
-90
-100
-110
-120
-130
-140
-150
-160
-170
-180
-190
-200
-210
-22
f1 (ppm)

2.7 Compound **2g**

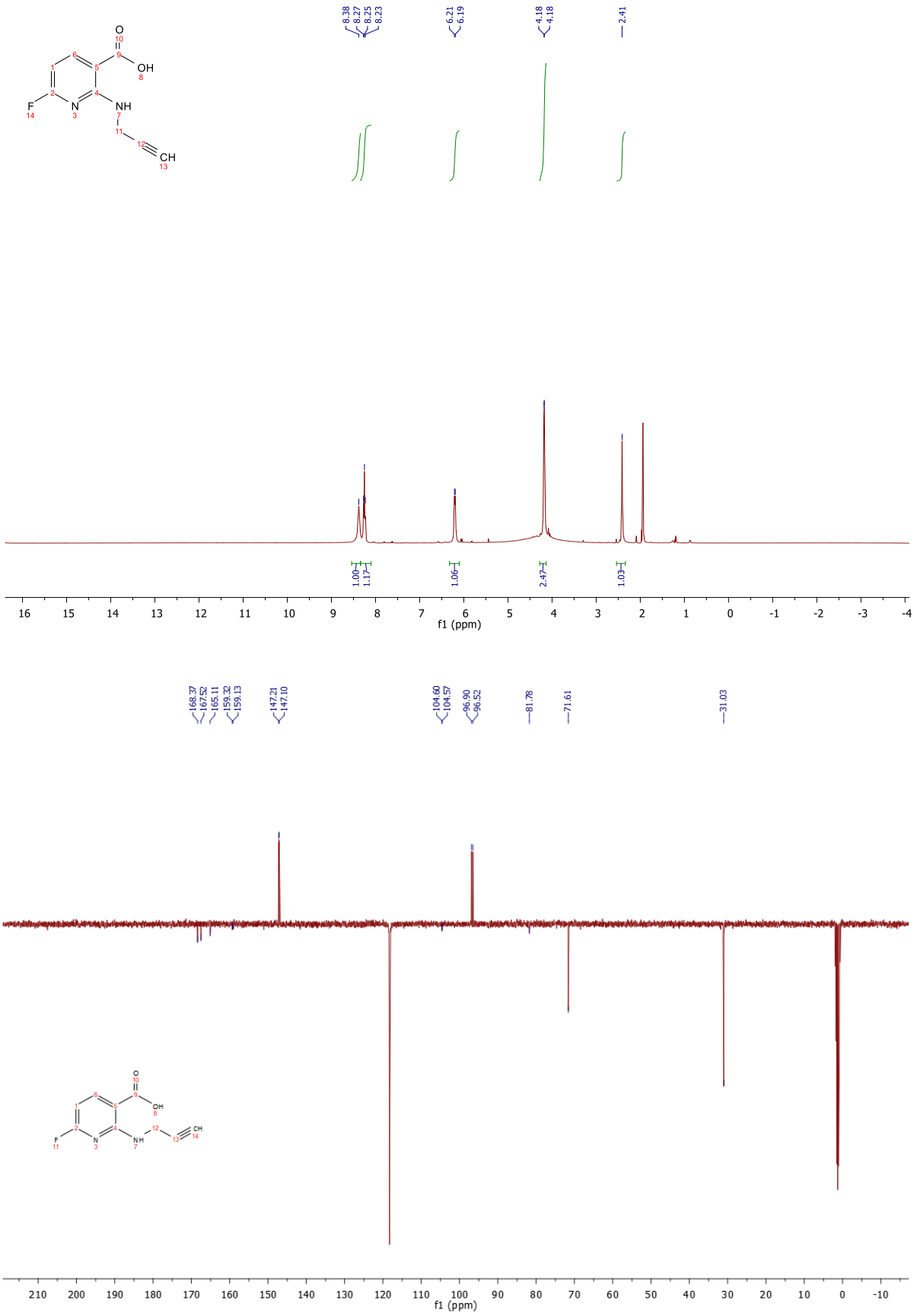

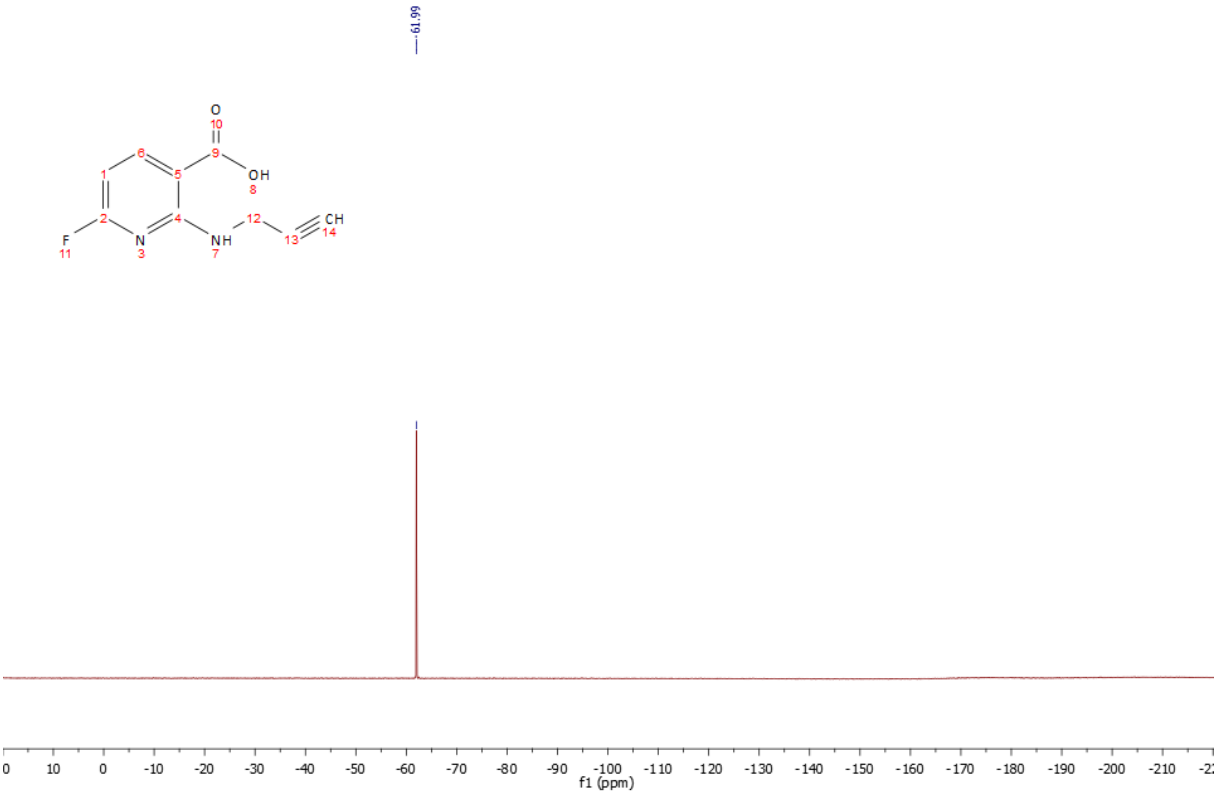
61.99
O
10
6
9
1
5
OH
8
2
4
12
CH
14
F
11
N
3
NH
7
13
0
10
0
-10
-20
-30
-40
-50
-60
-70
-80
-90
-100
-110
-120
-130
-140
-150
-160
-170
-180
-190
-200
-210
f1 (ppm)

2.8 Compound **2h**

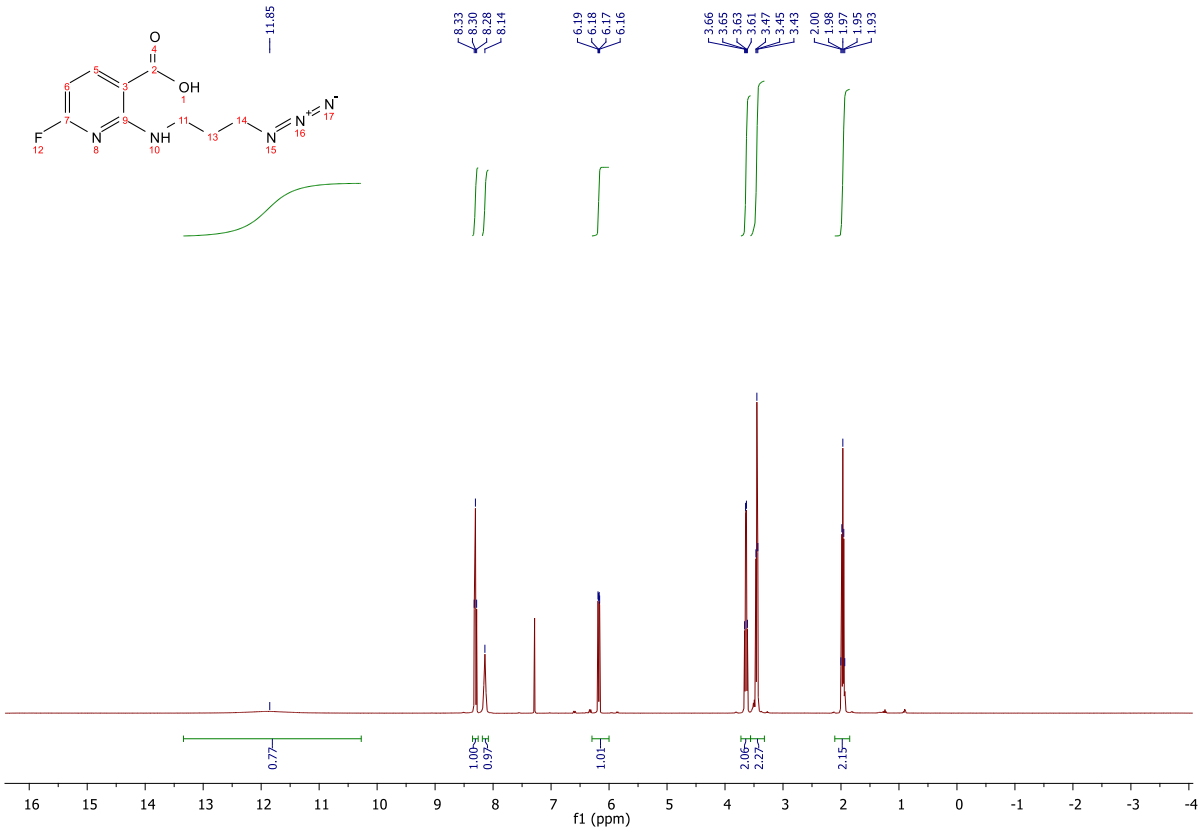

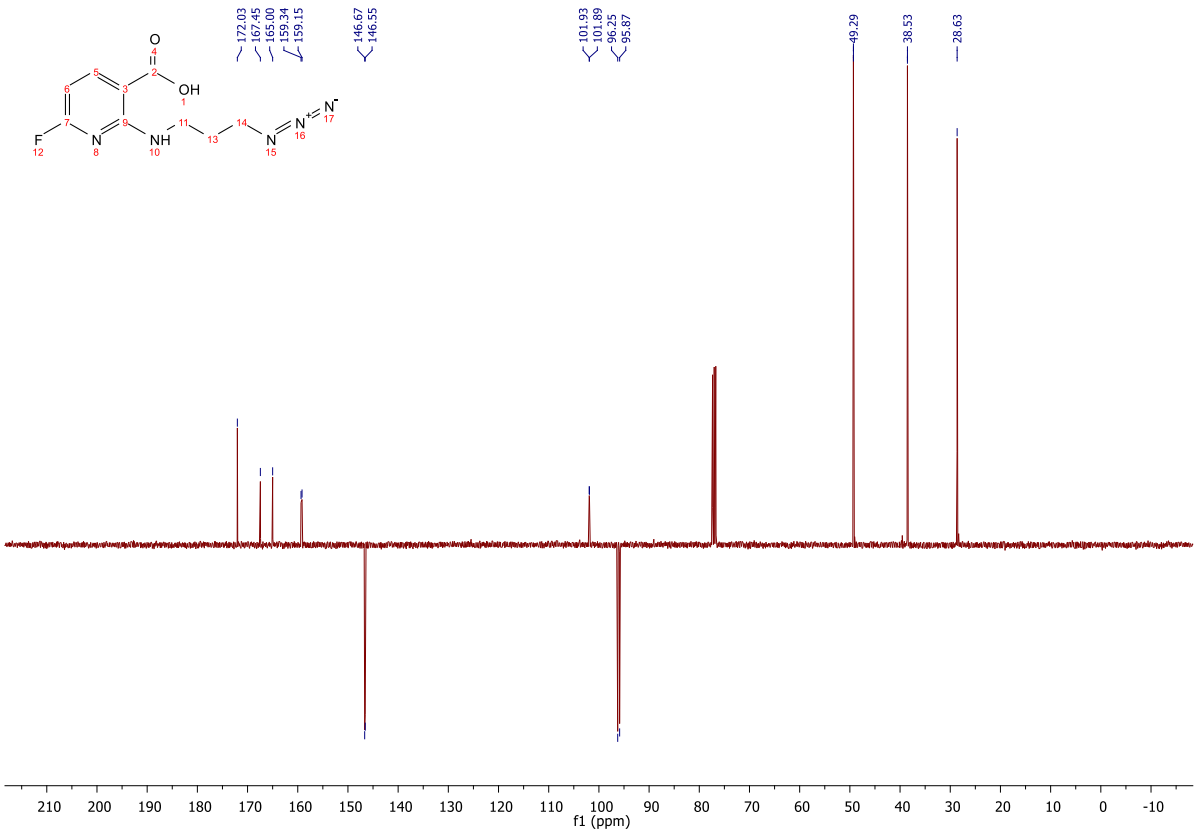

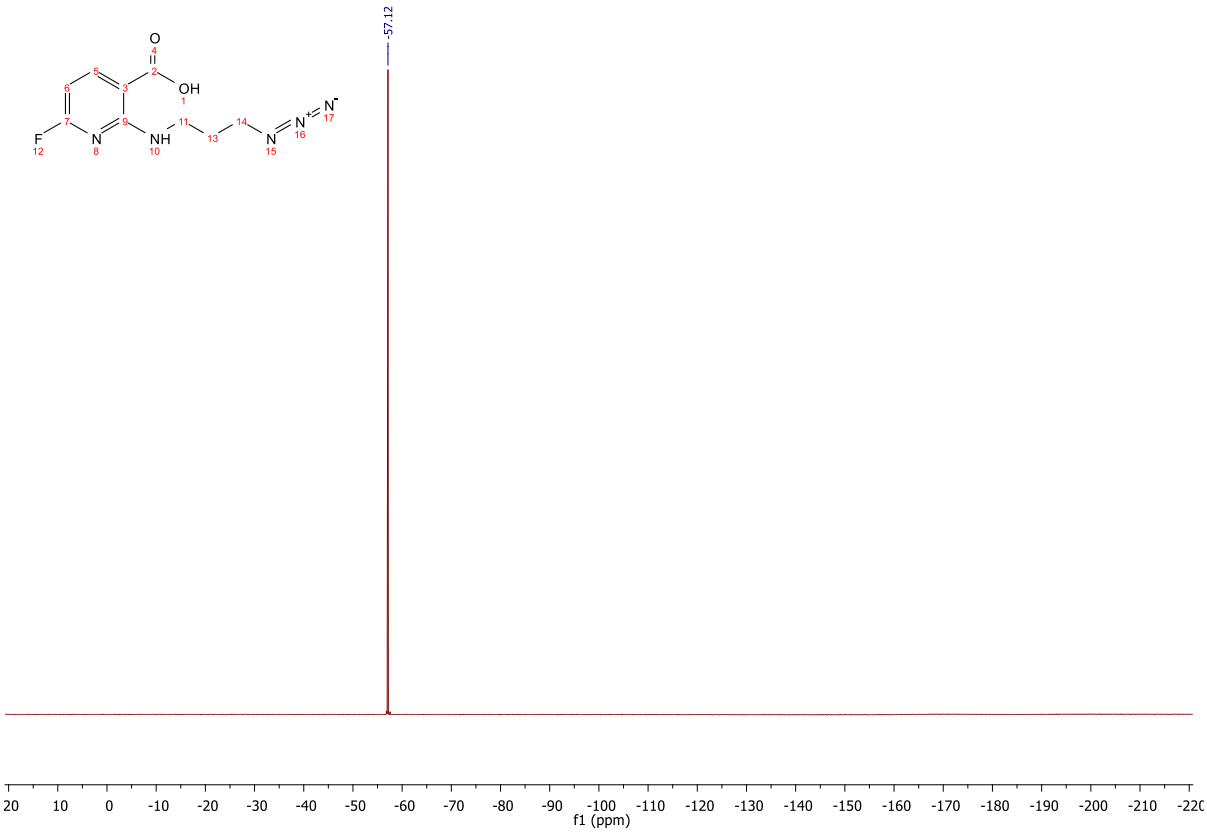
-57.12
O
4
2
OH
1
5
6
3
7
9
F
12
N
8
NH
10
11
13
14
N
15
N
16
N
17
20
10
0
-10
-20
-30
-40
-50
-60
-70
-80
-90
-100
-110
-120
-130
-140
-150
-160
-170
-180
-190
-200
-210
-220
f1 (ppm)

2.9 Compound **3a**

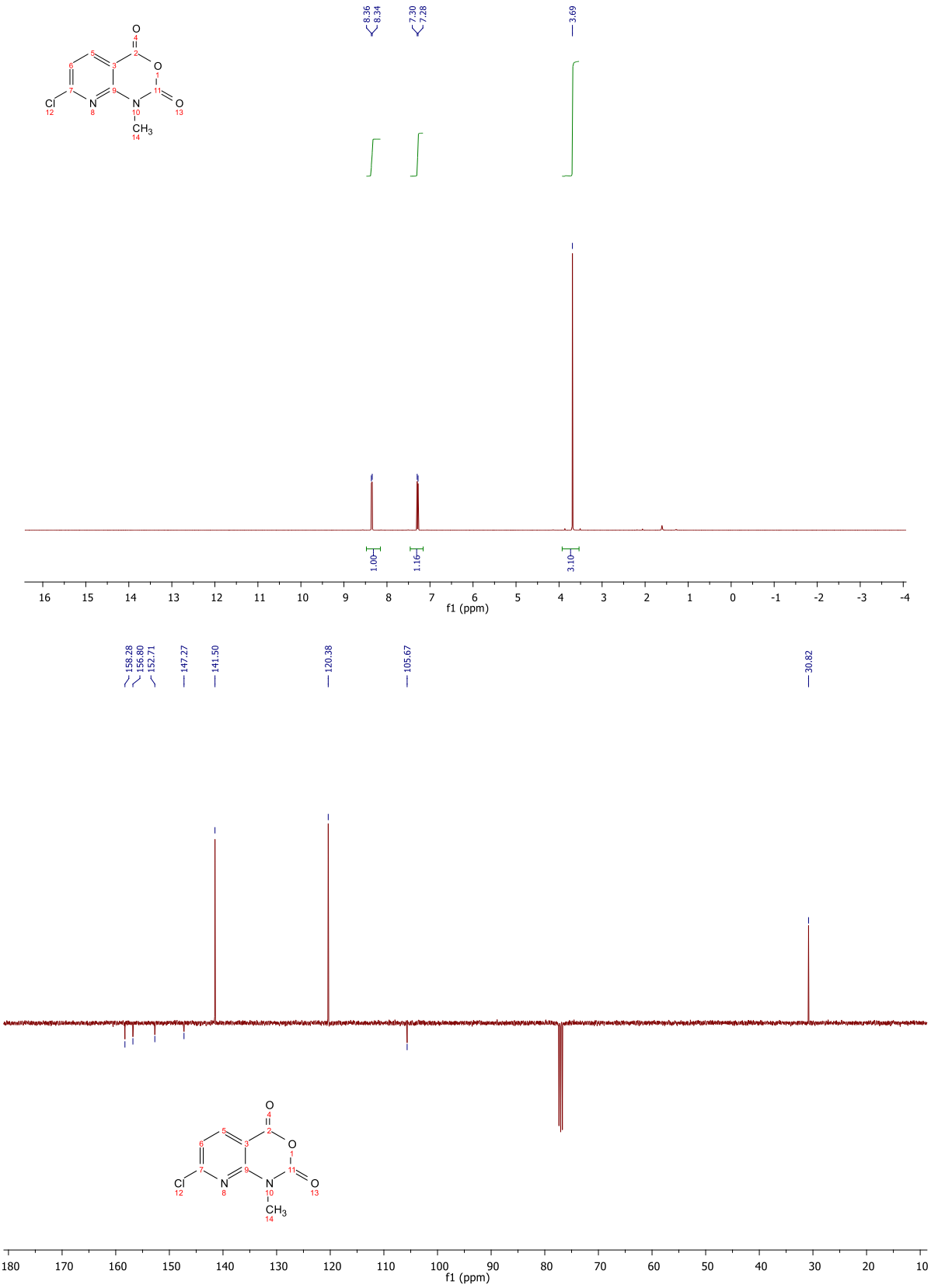

2.10 Compound **3b**

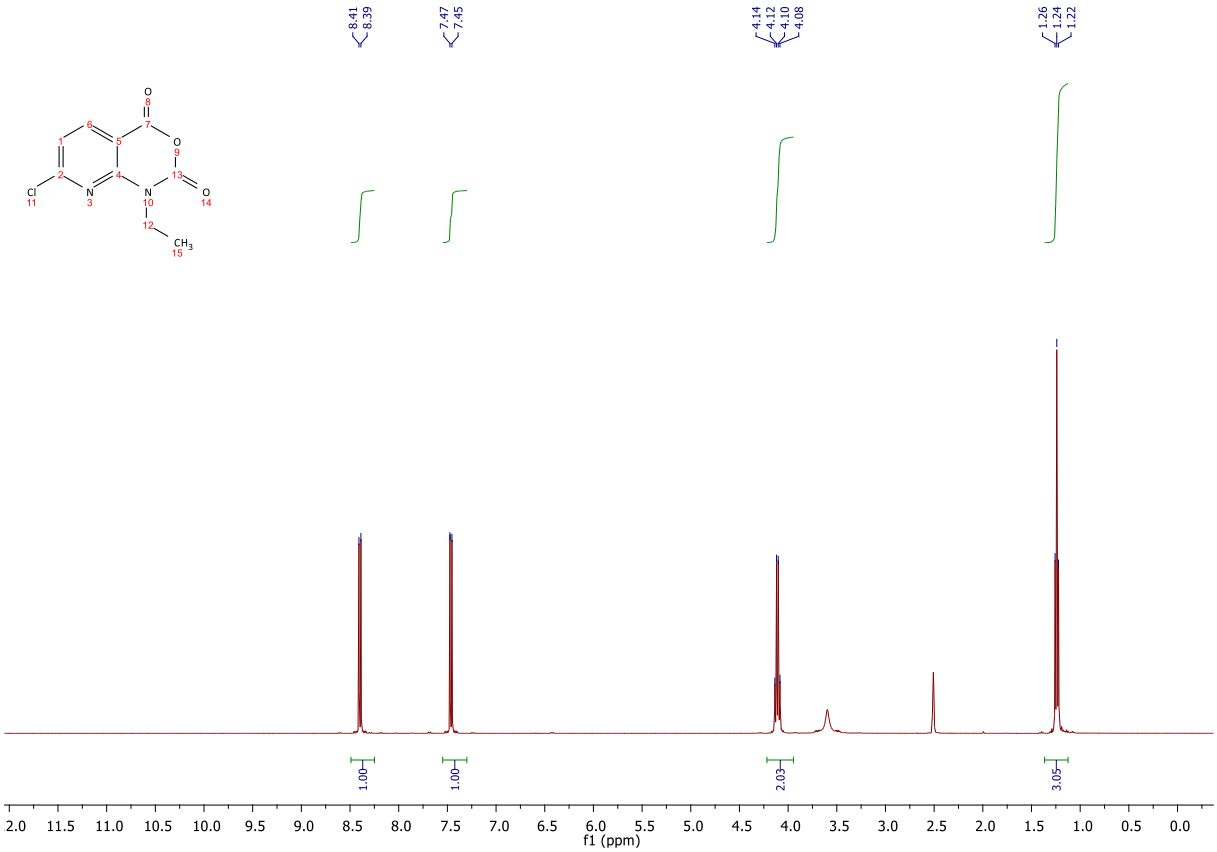

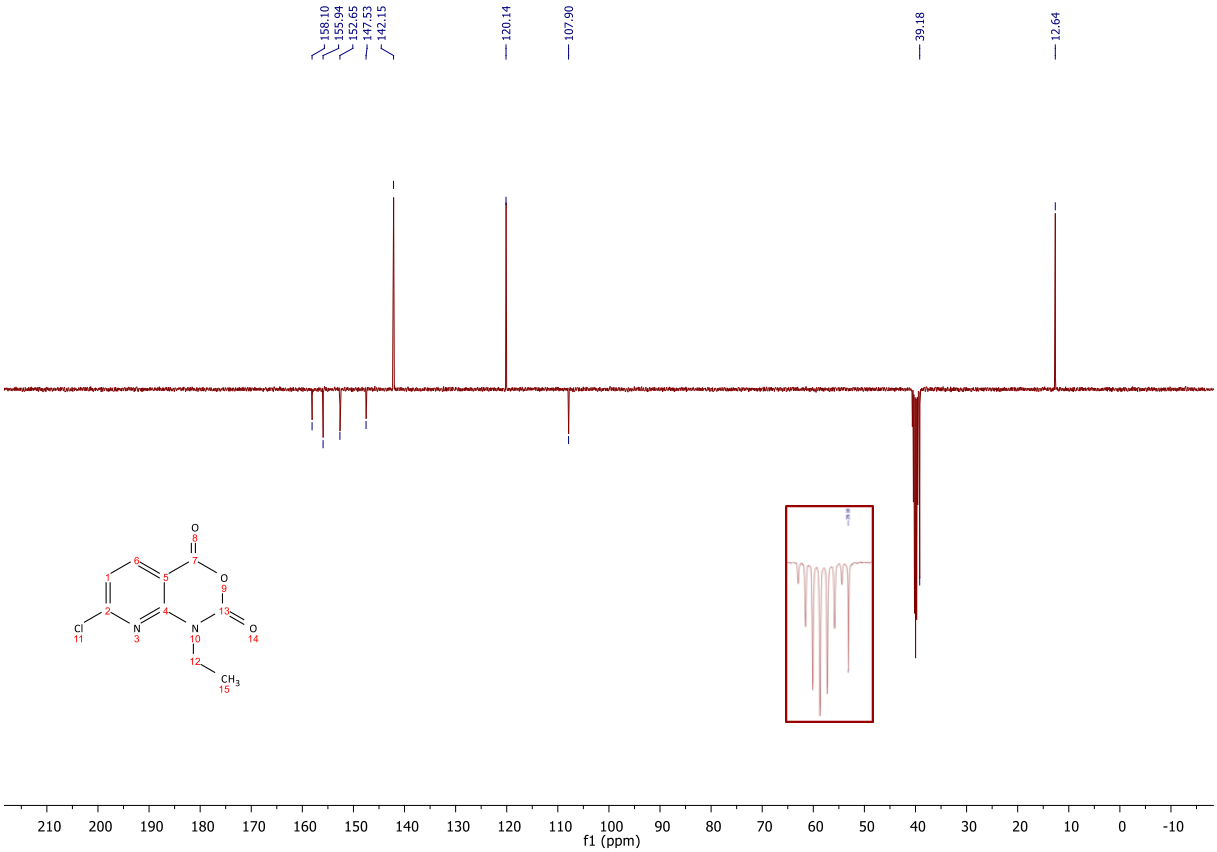

2.11 Compound **3c**

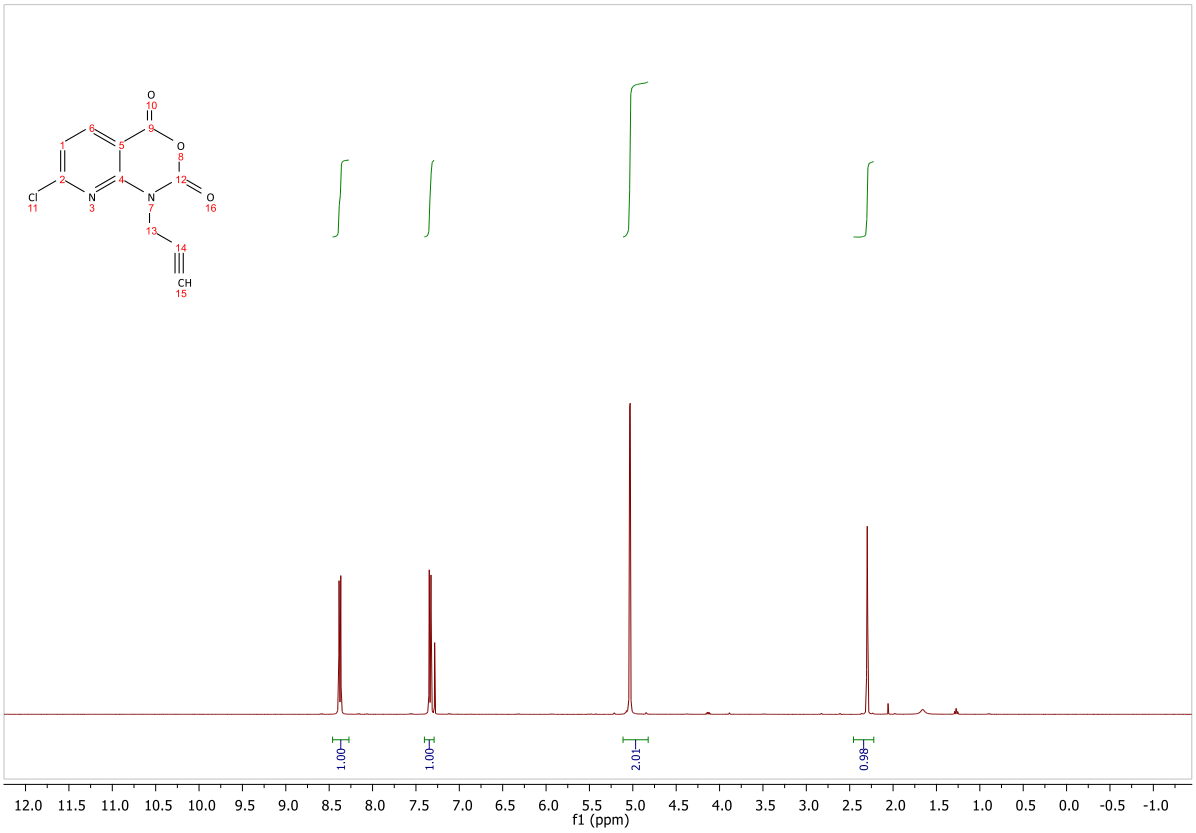

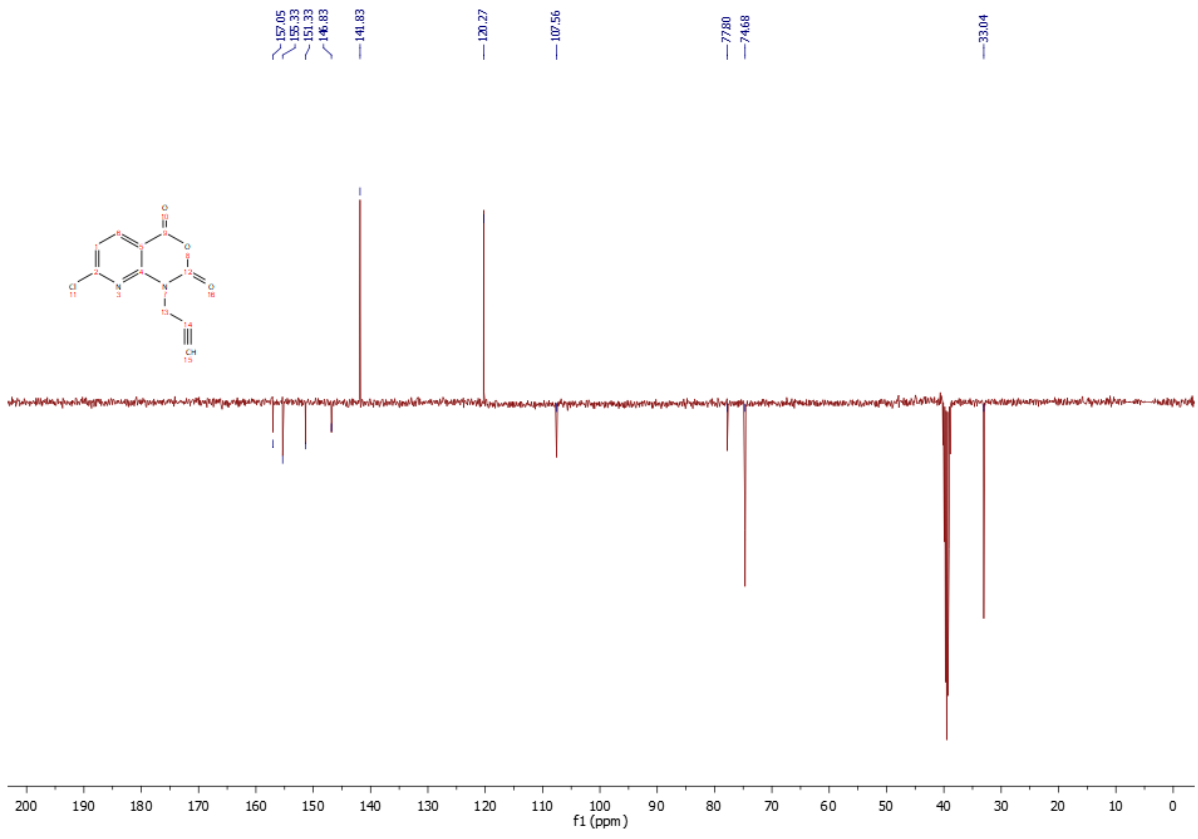

2.12 Compound **3d**

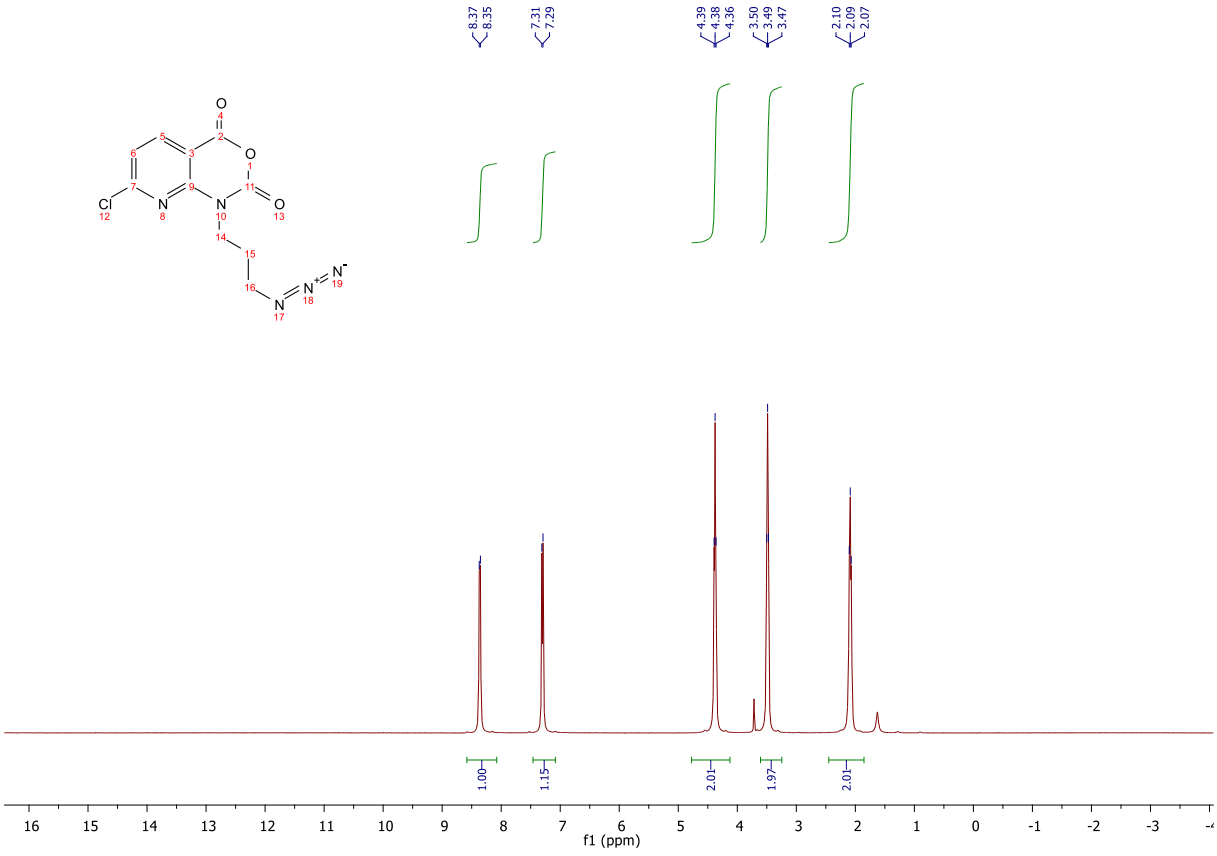

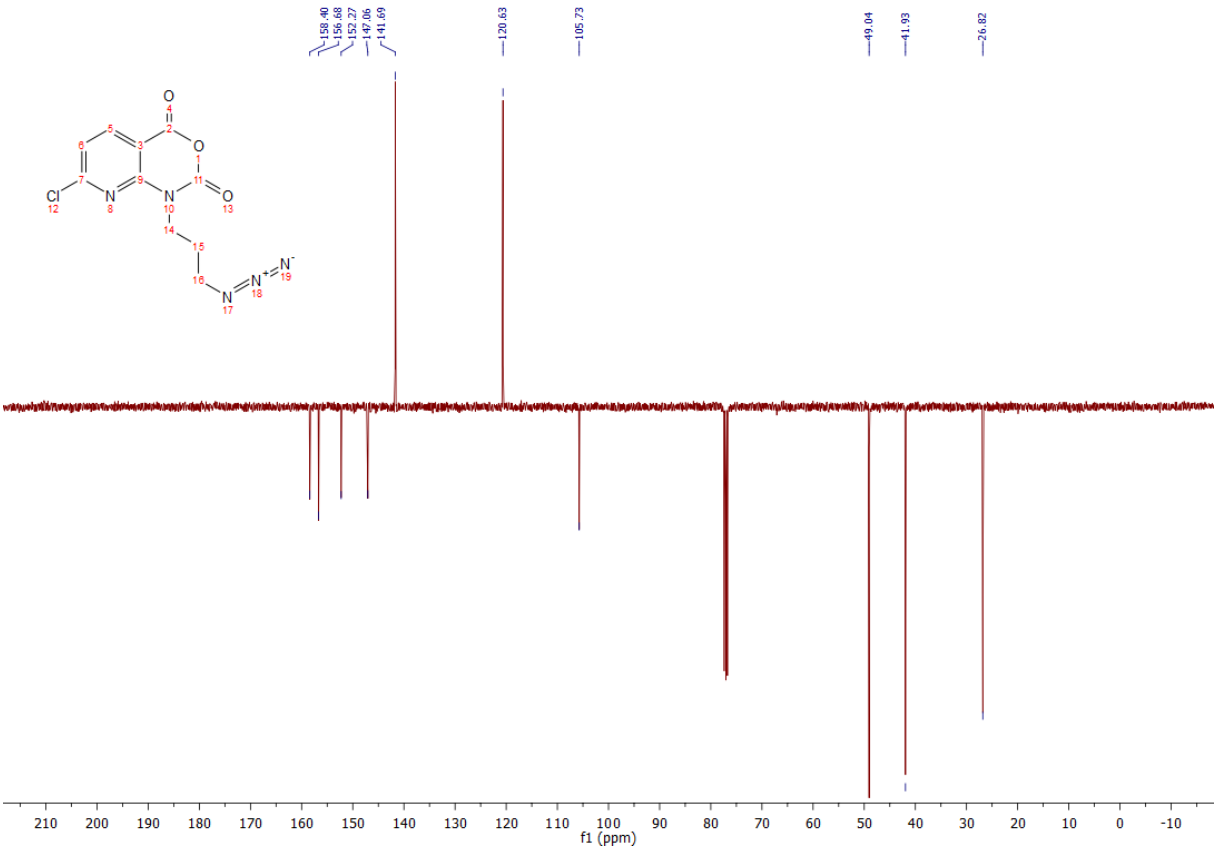

2.13 Compound **3e**

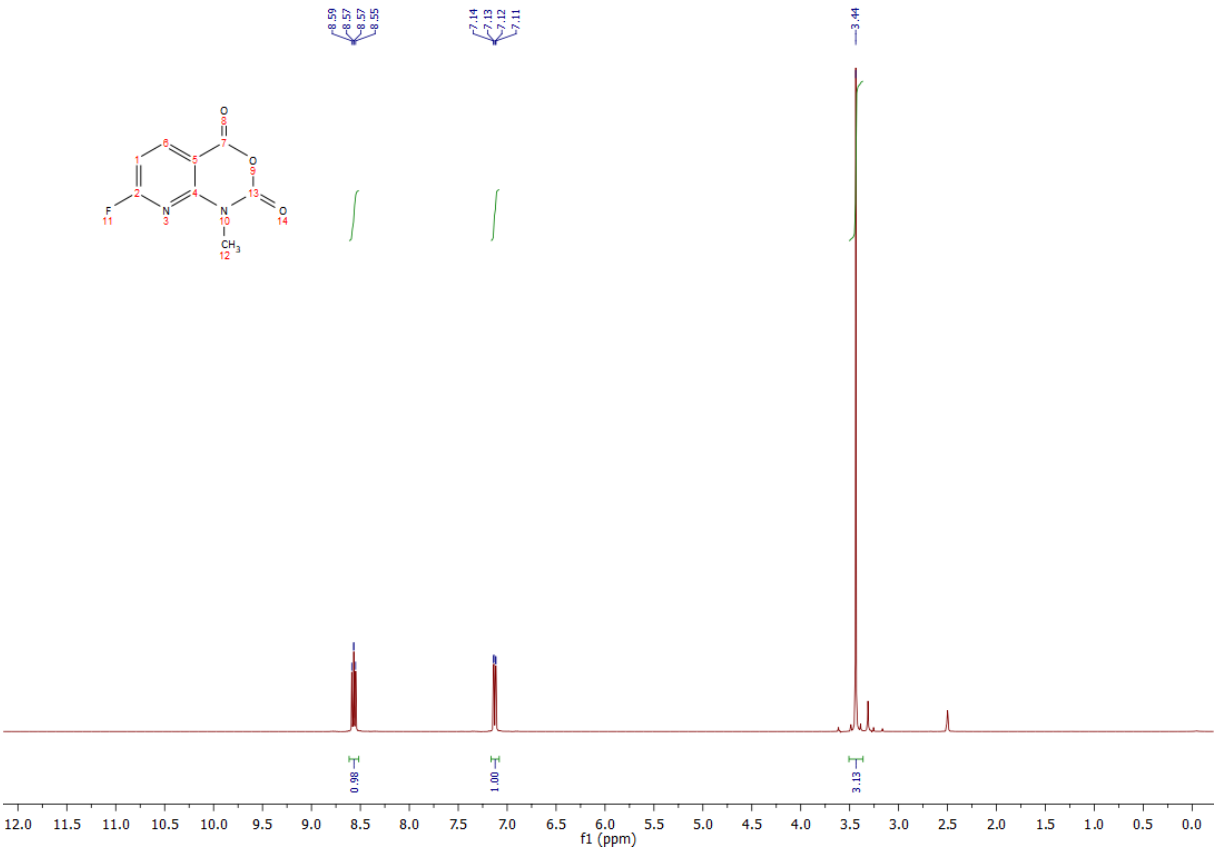

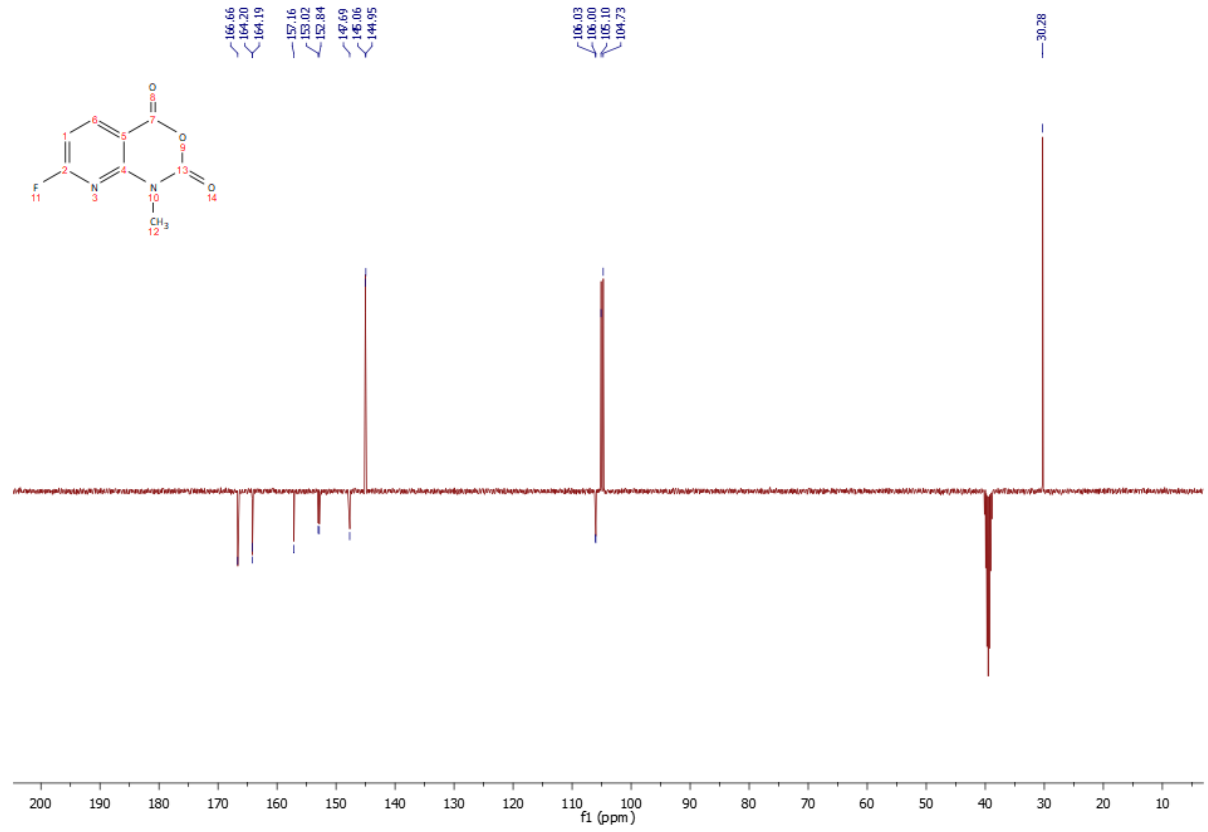

^{19}F NMR (376 MHz, DMSO) δ -56.82.

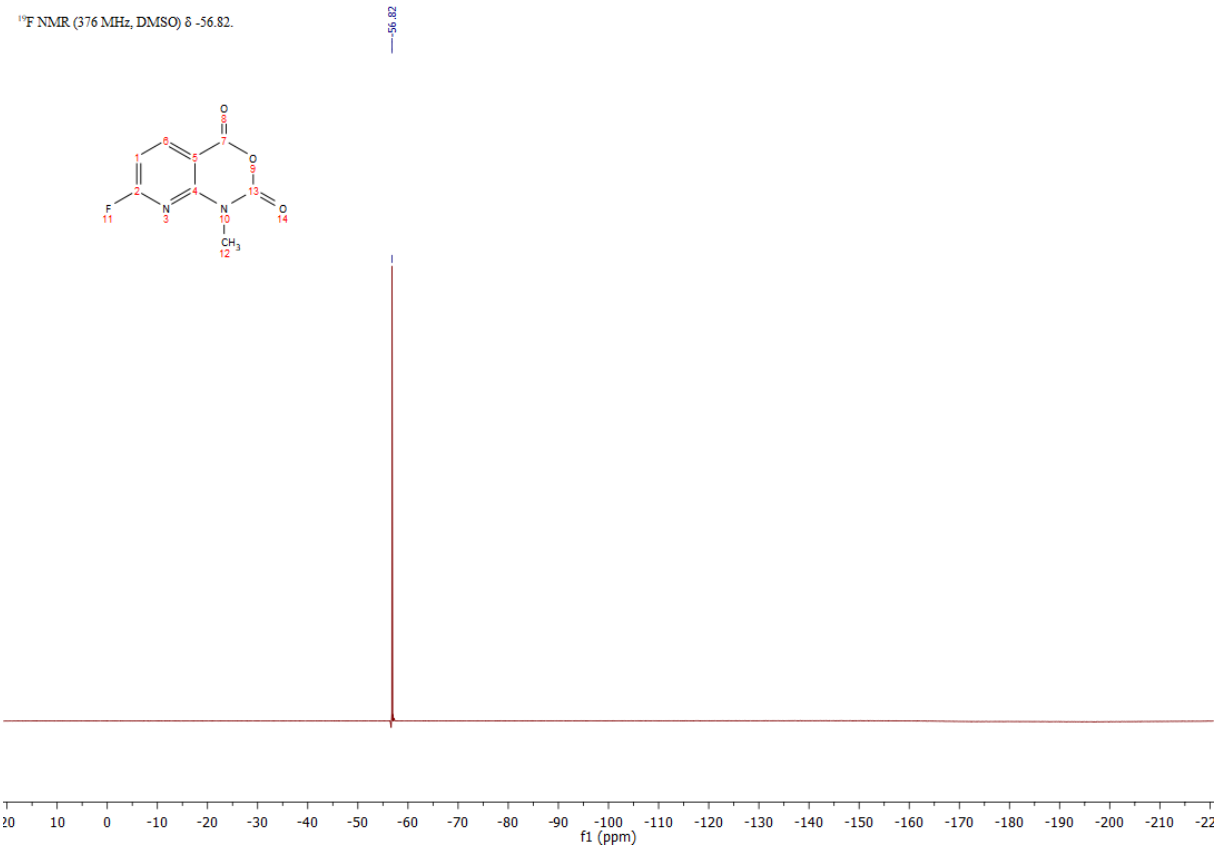

2.14 Compound **3f**

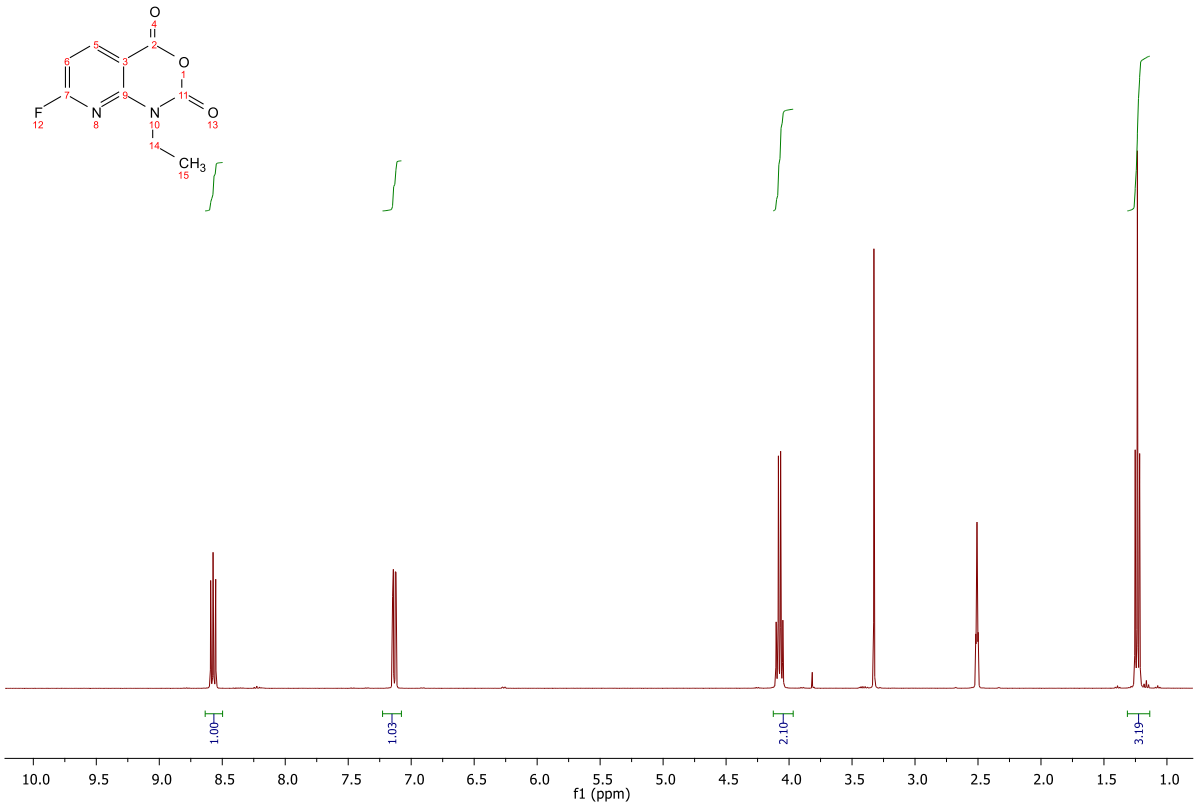

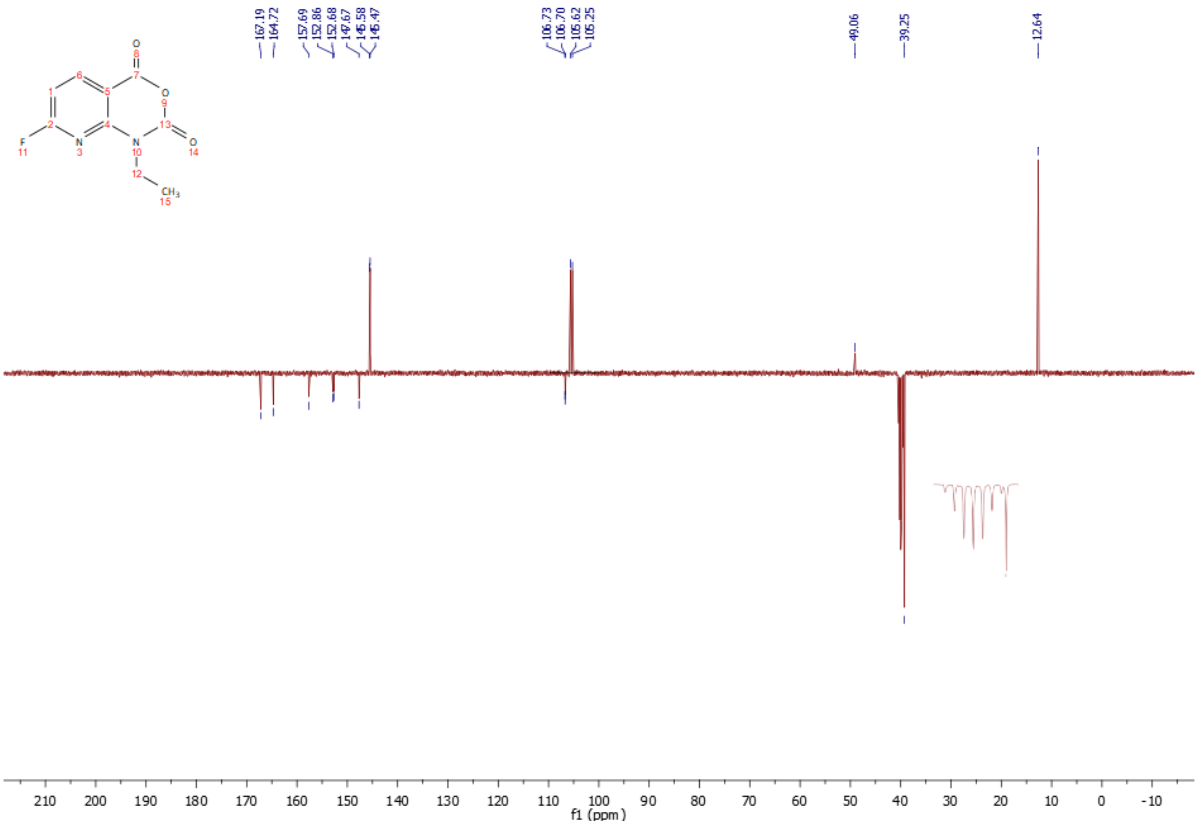

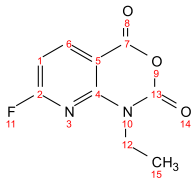
O
8
6
7
1
5
O
9
2
4
13
F
11
N
3
N
10
O
14
12
CH3
15

-56.86
20
10
0
-10
-20
-30
-40
-50
-60
-70
-80
-90
-100
-110
-120
-130
-140
-150
-160
-170
-180
-190
-200
-210
f1 (ppm)

2.15 Compound **3g**

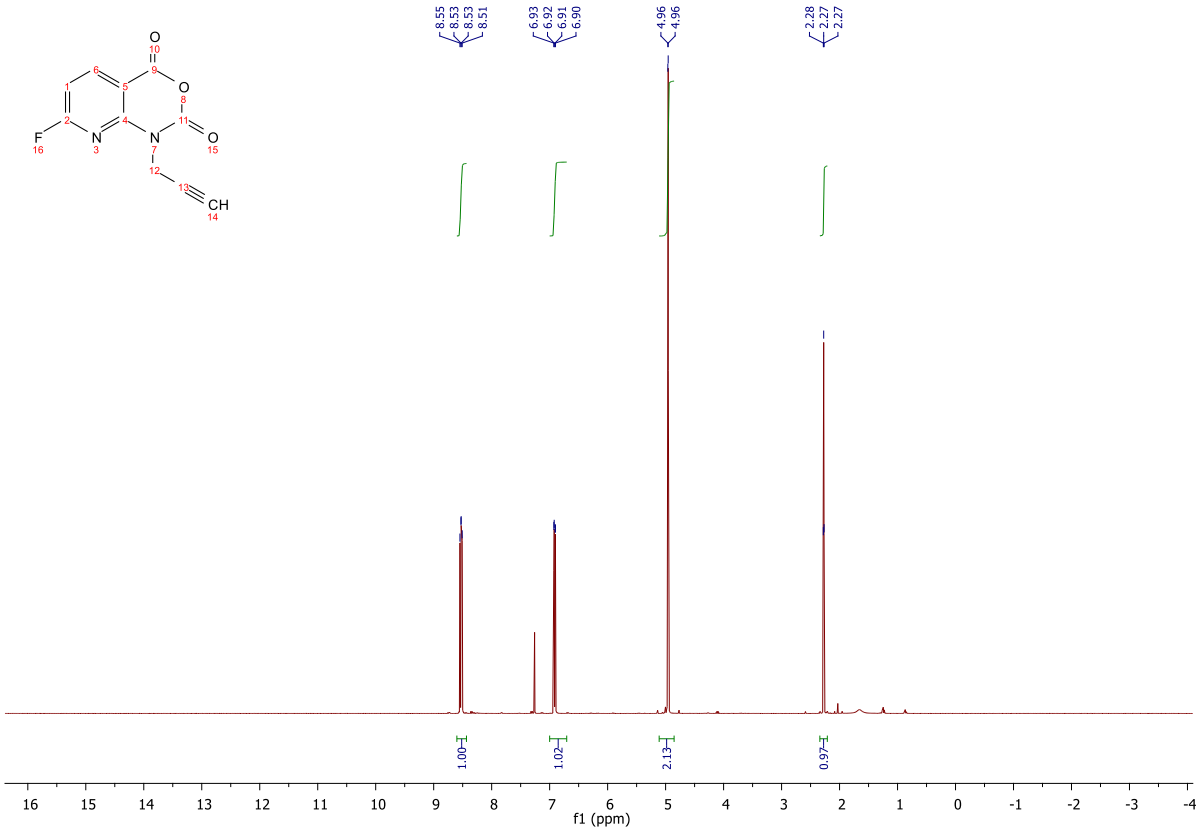

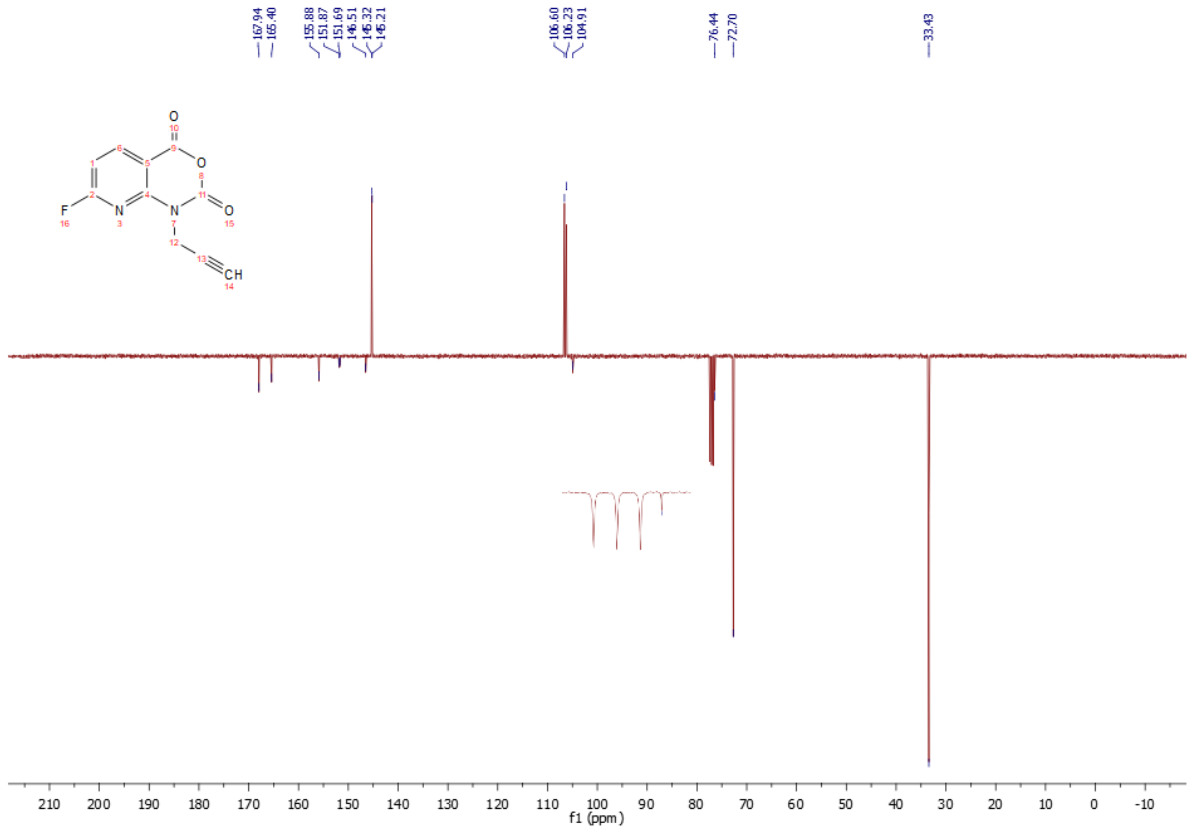

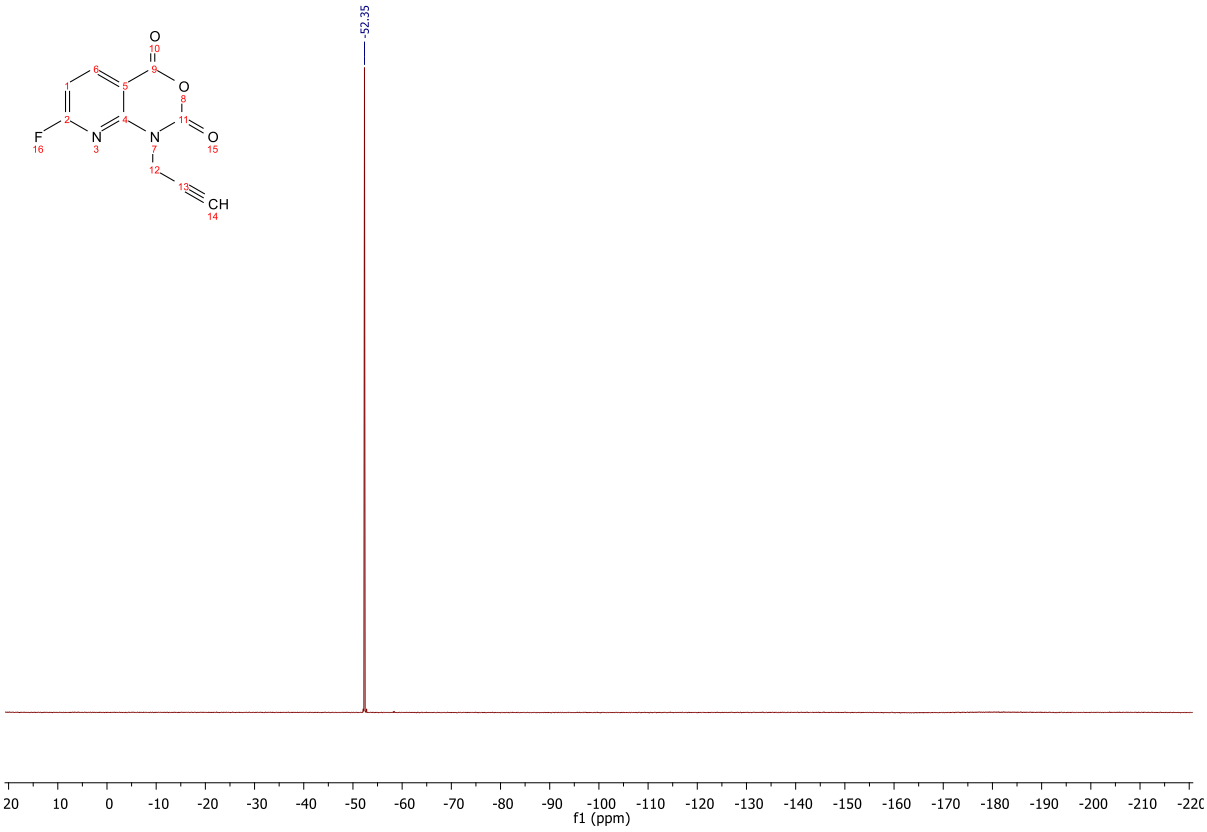
-52.35
20 10 0 -10 -20 -30 -40 -50 -60 -70 -80 -90 -100 -110 -120 -130 -140 -150 -160 -170 -180 -190 -200 -210 -220
f1 (ppm)

2.16 Compound **3h**

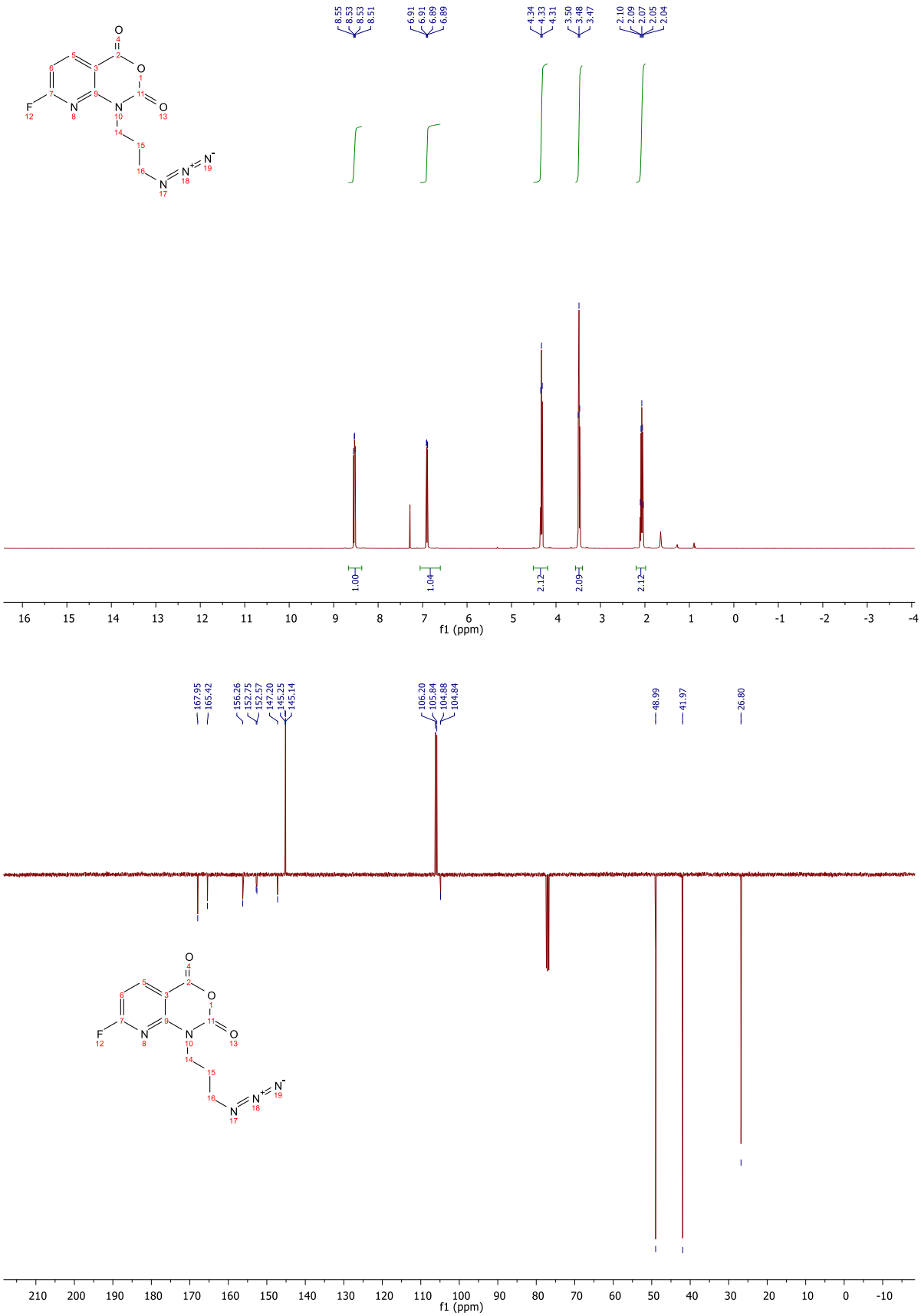

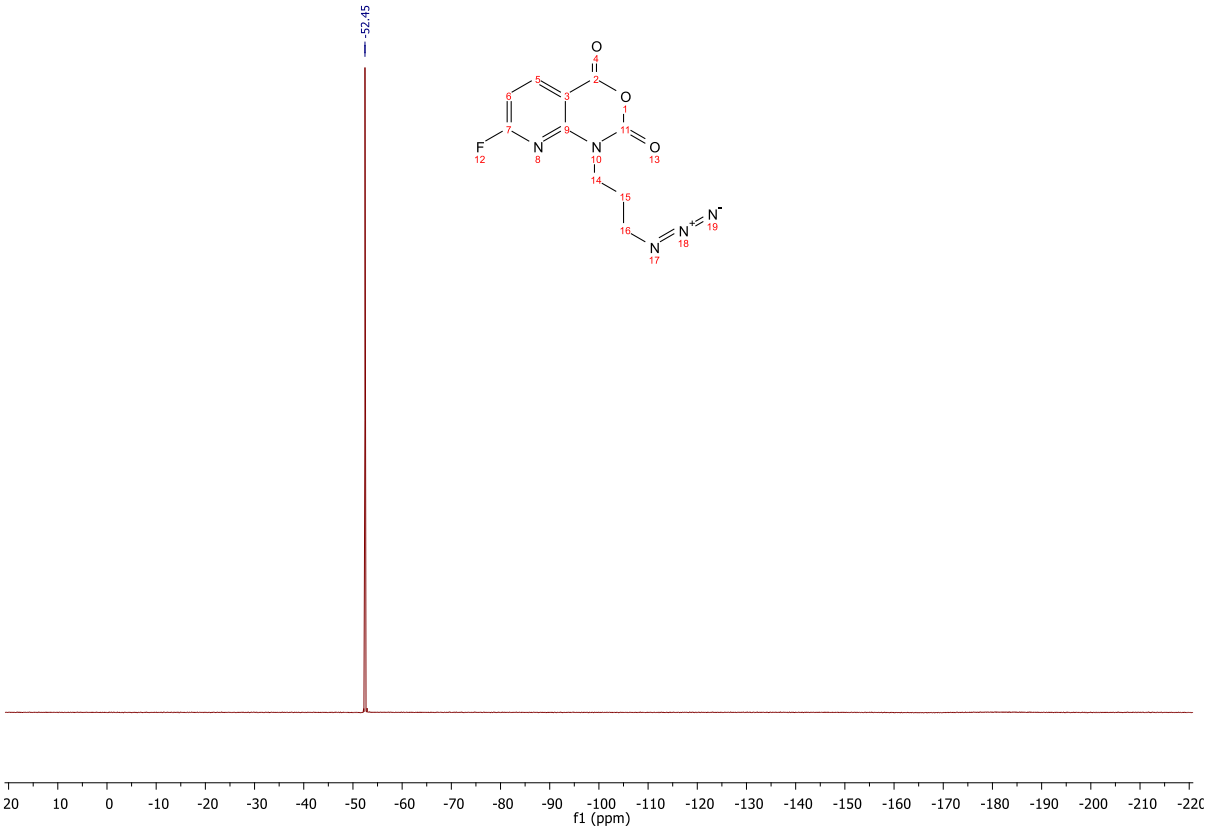
-52.45
O
4
2
5
3
6
O
1
7
9
11
F
12
N
8
N
10
O
13
14
15
16
N
17
N
18
N
19
20
10
0
-10
-20
-30
-40
-50
-60
-70
-80
-90
-100
-110
-120
-130
-140
-150
-160
-170
-180
-190
-200
-210
-220
f1 (ppm)

2.17 Compound **4a**

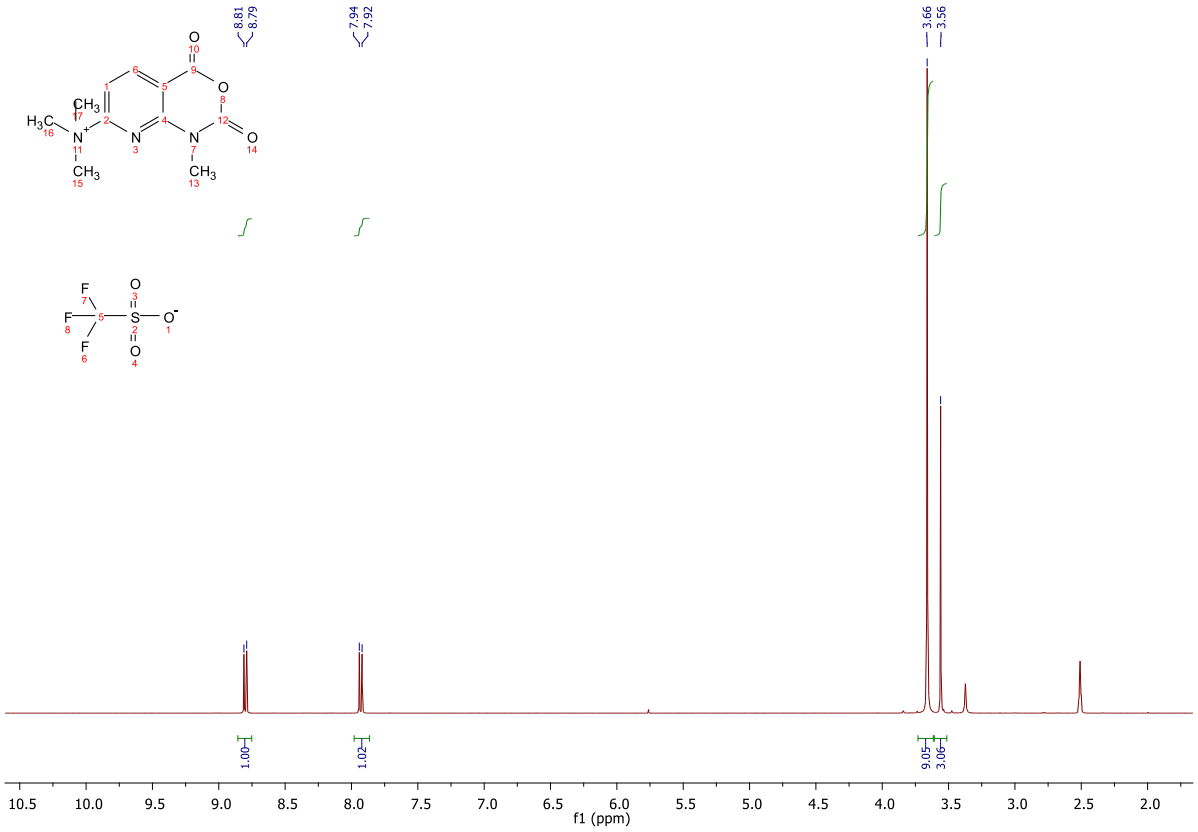

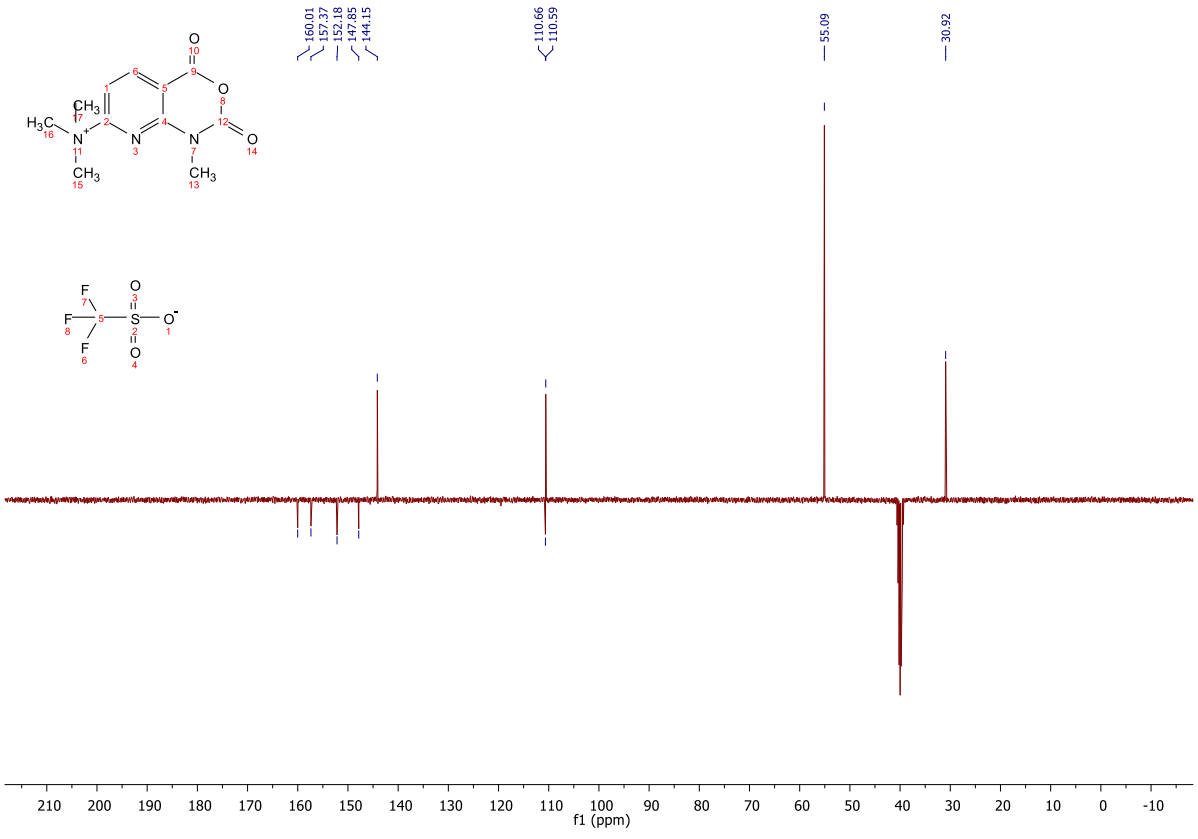

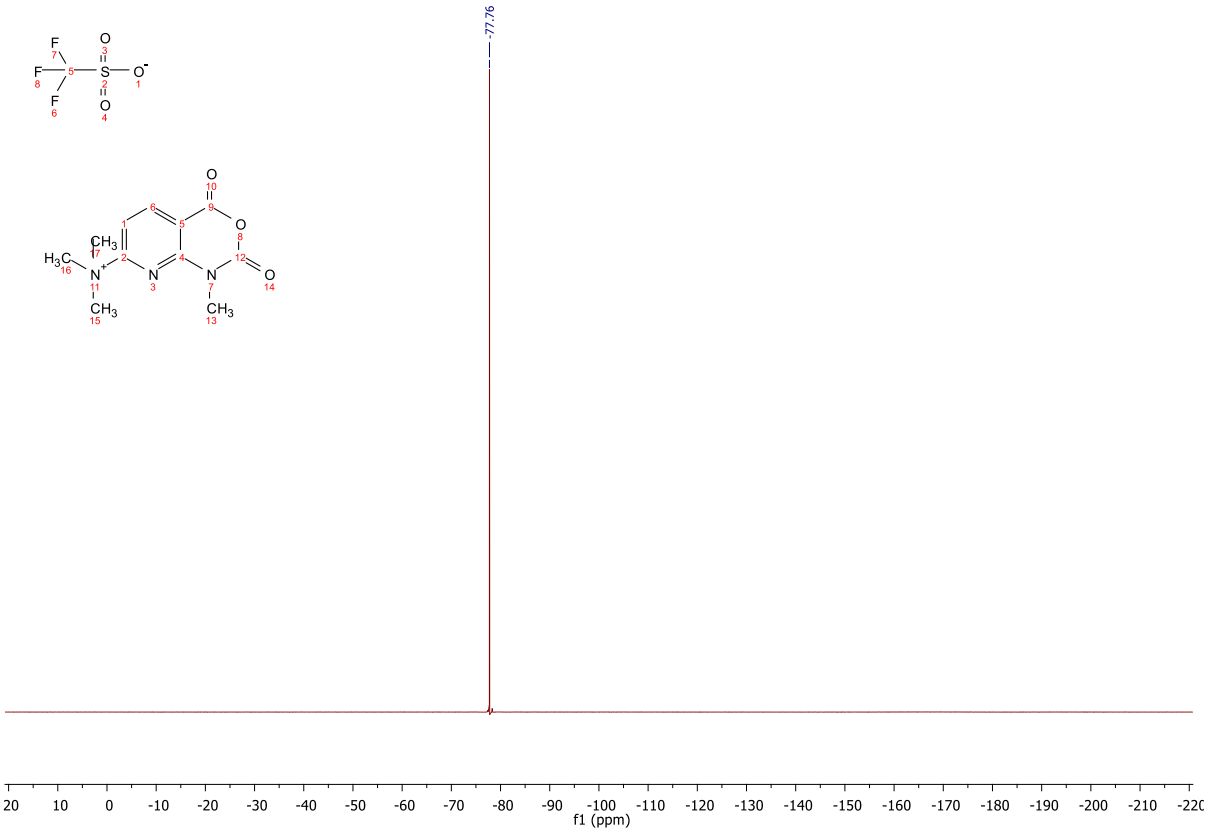
-77.76
20
10
0
-10
-20
-30
-40
-50
-60
-70
-80
-90
-100
-110
-120
-130
-140
-150
-160
-170
-180
-190
-200
-210
f1 (ppm)

2.18 Compound **4b**

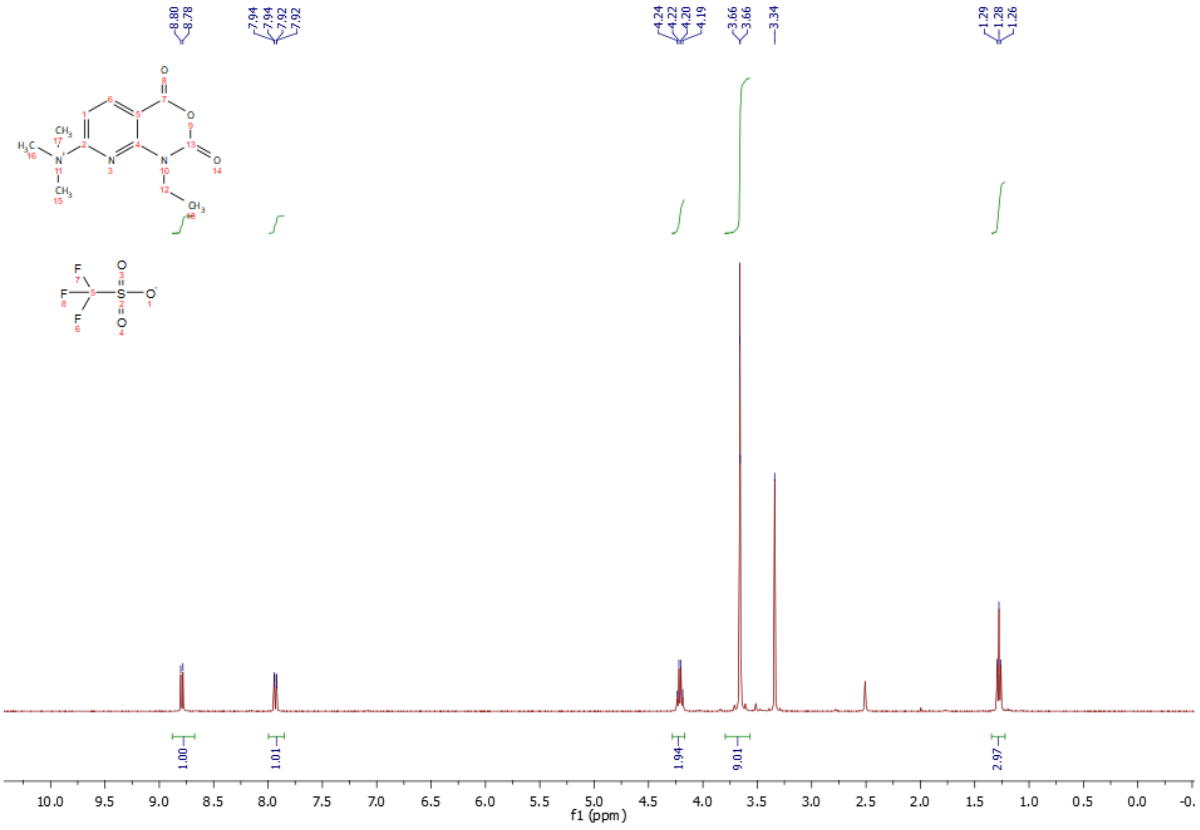

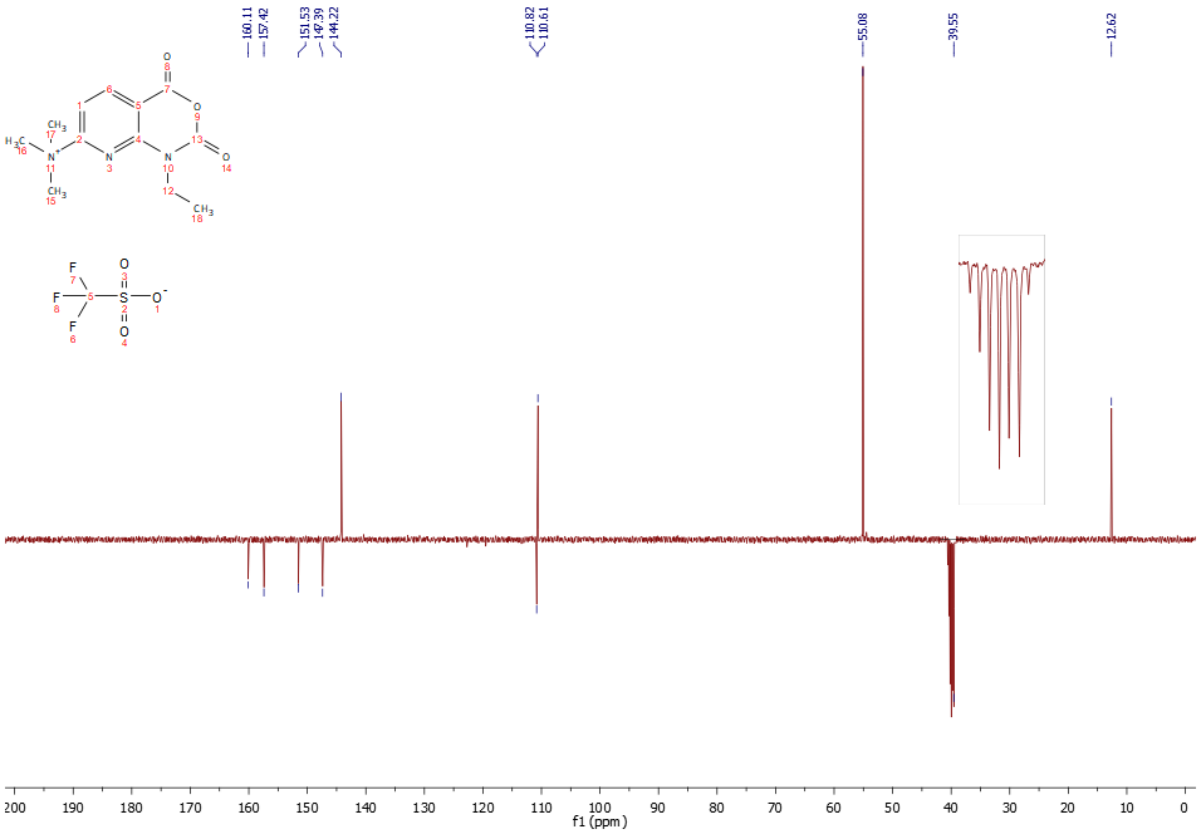

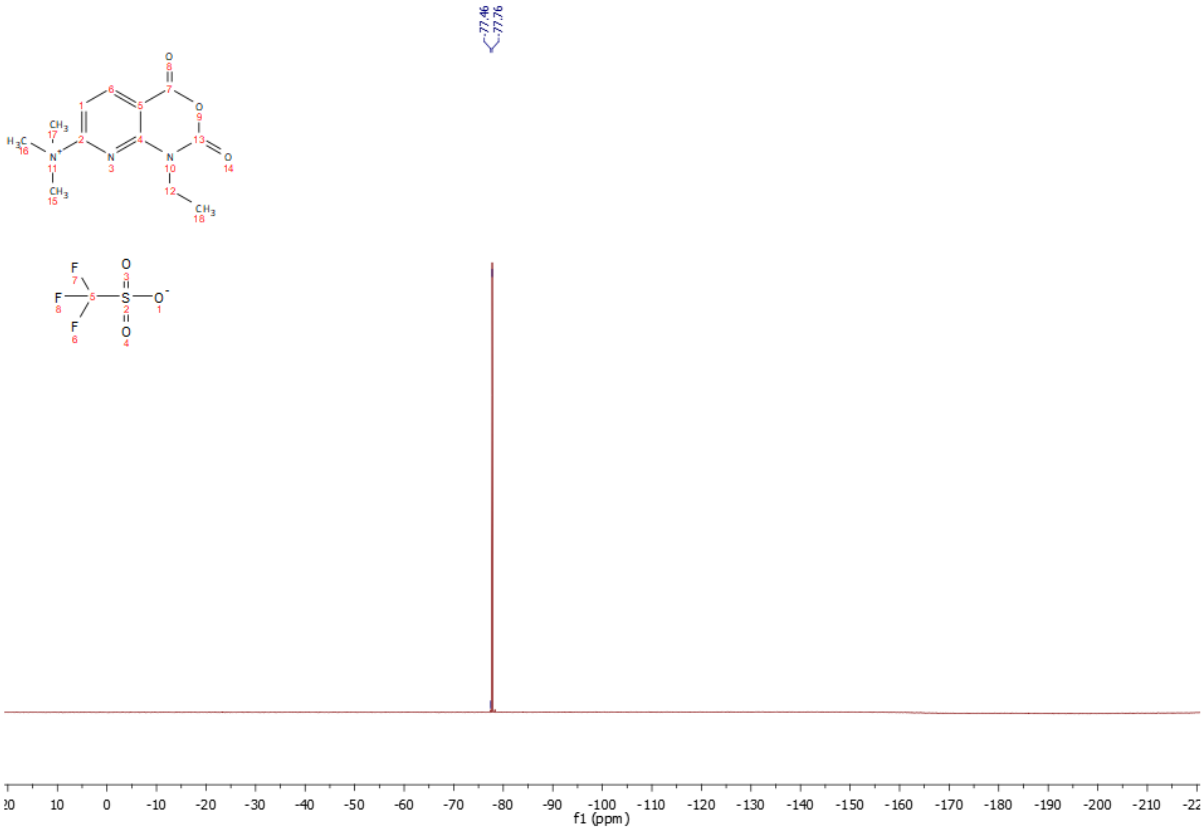
77.46
77.76
f1 (ppm)

2.19 Compound **4c**

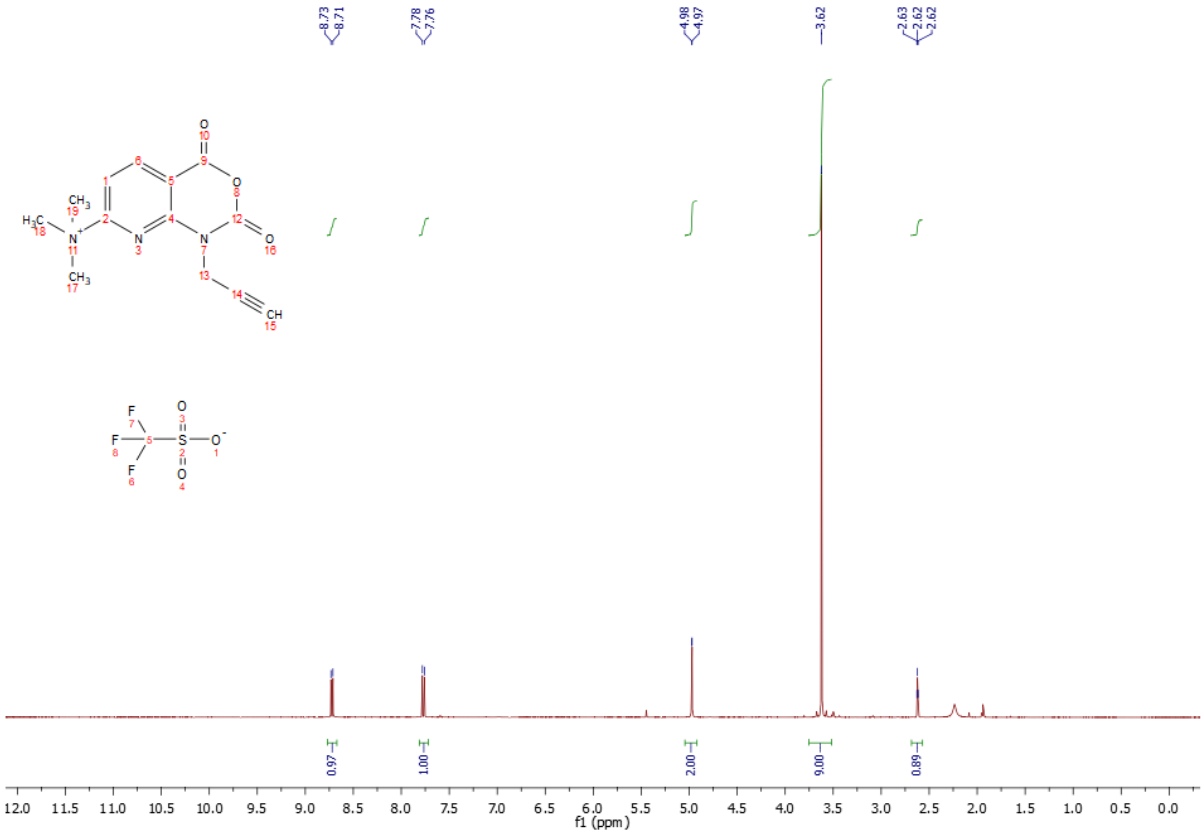

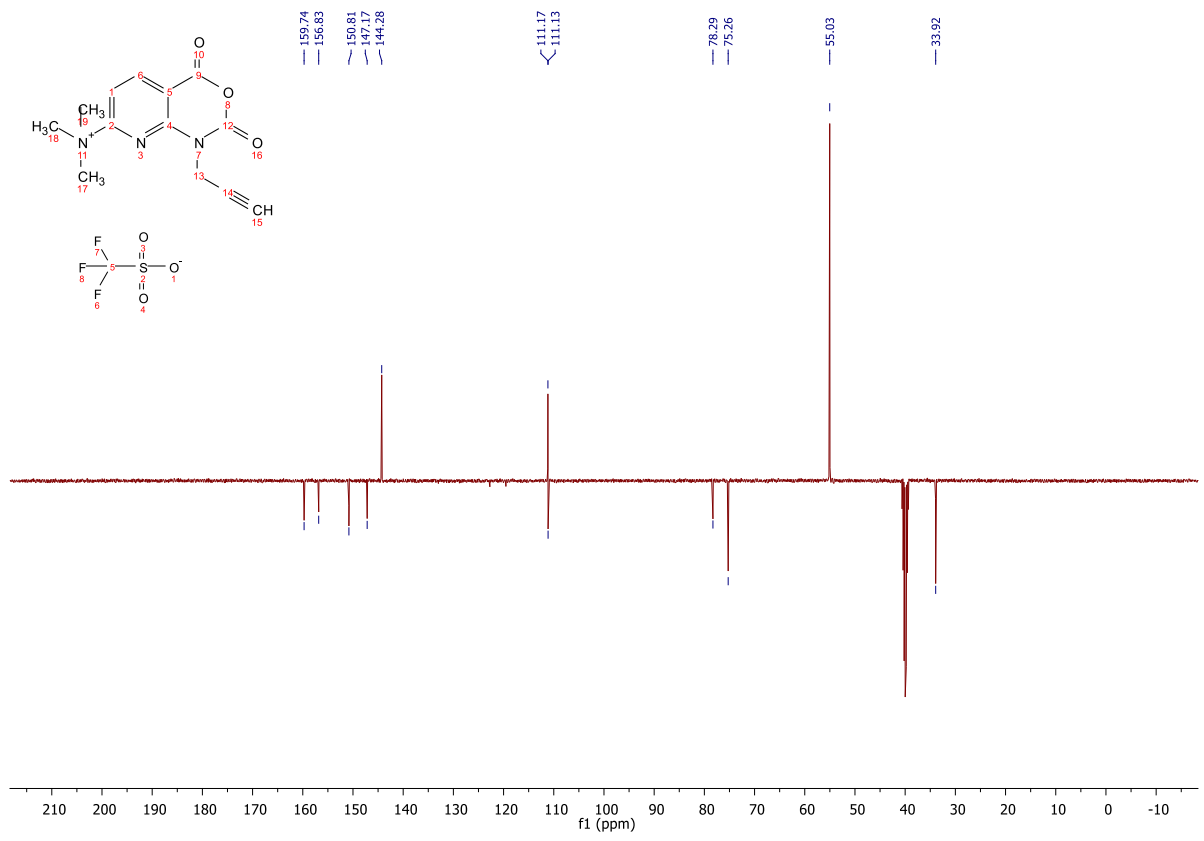

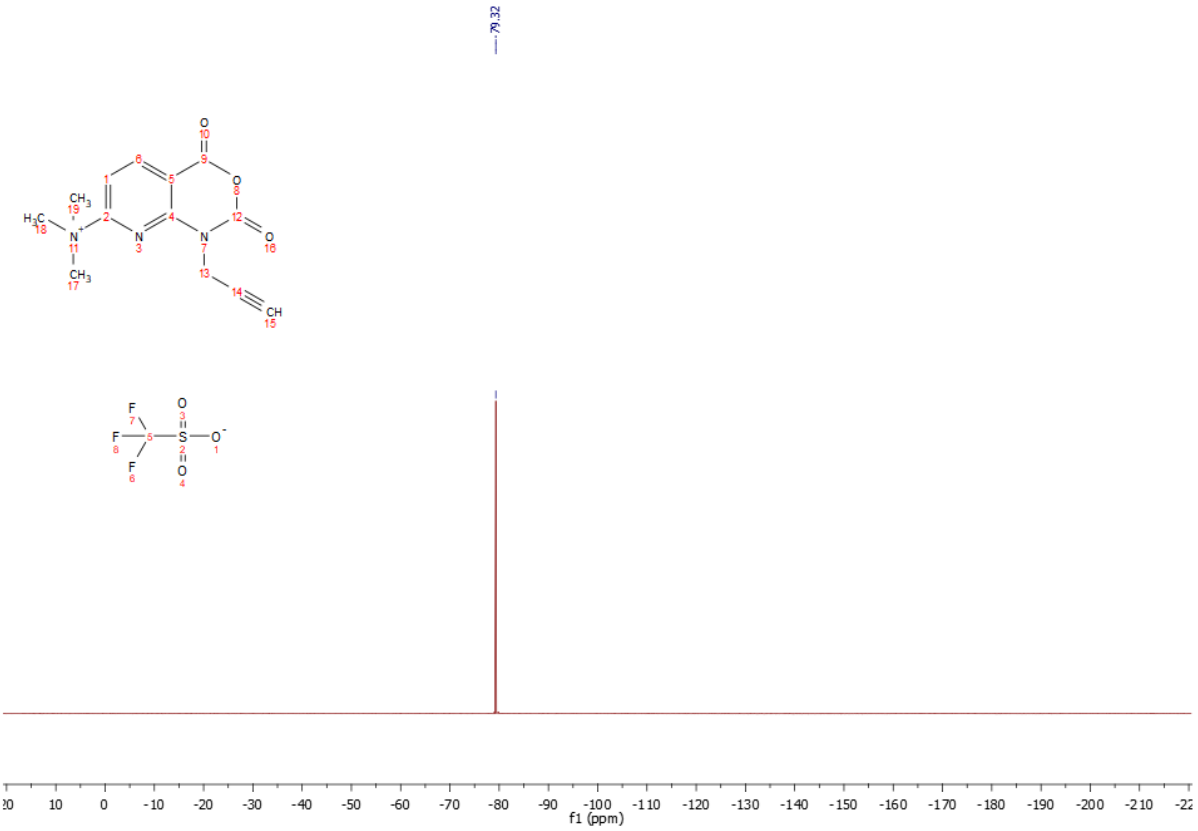
-79.32
f1 (ppm)

2.20 Compound **4d**

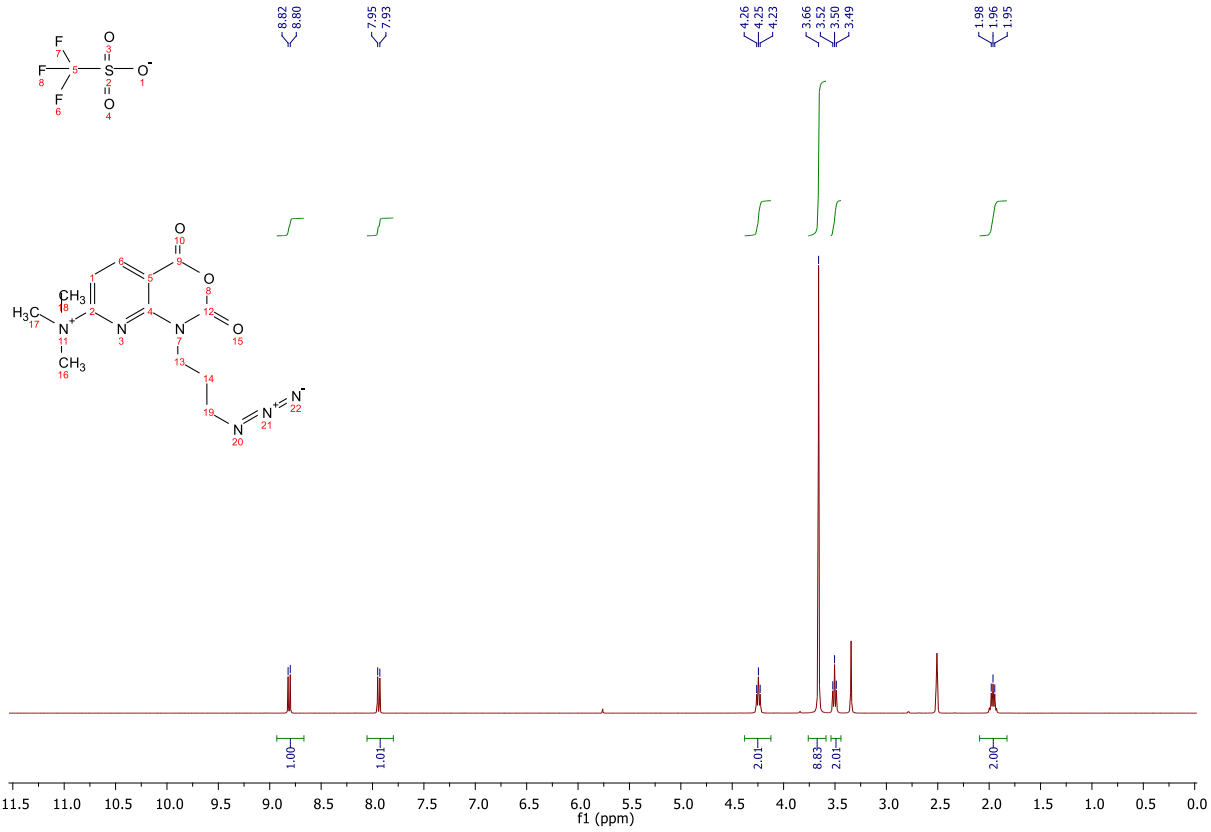

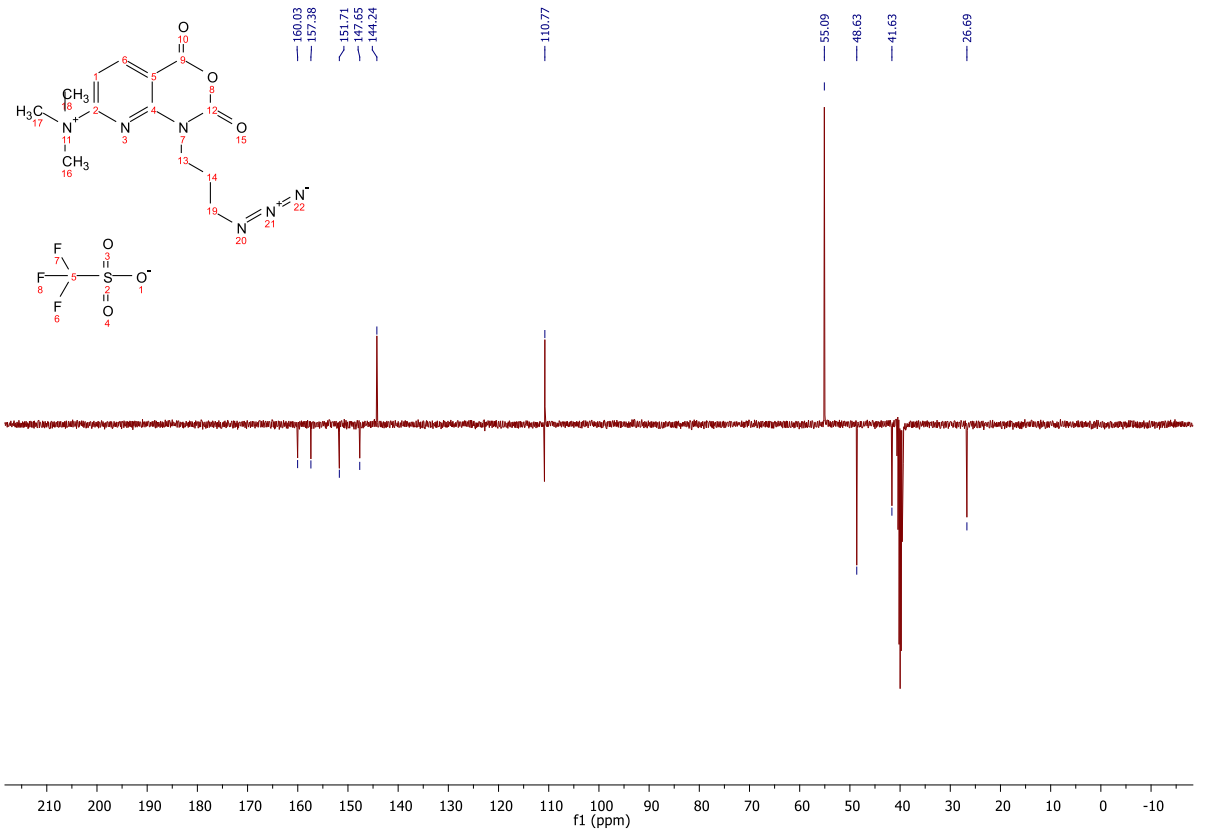

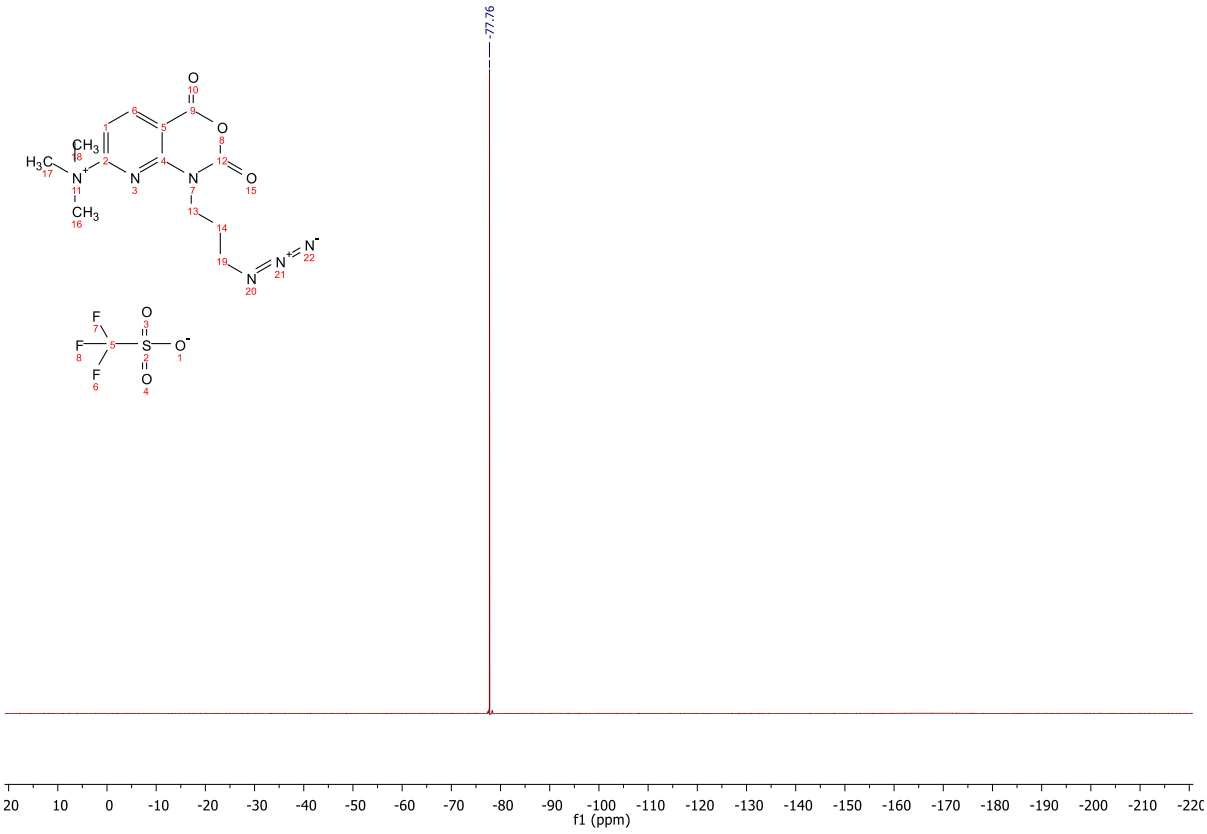
-77.76
20
10
0
-10
-20
-30
-40
-50
-60
-70
-80
-90
-100
-110
-120
-130
-140
-150
-160
-170
-180
-190
-200
-210
-220
f1 (ppm)

2.21 Compound **5a**

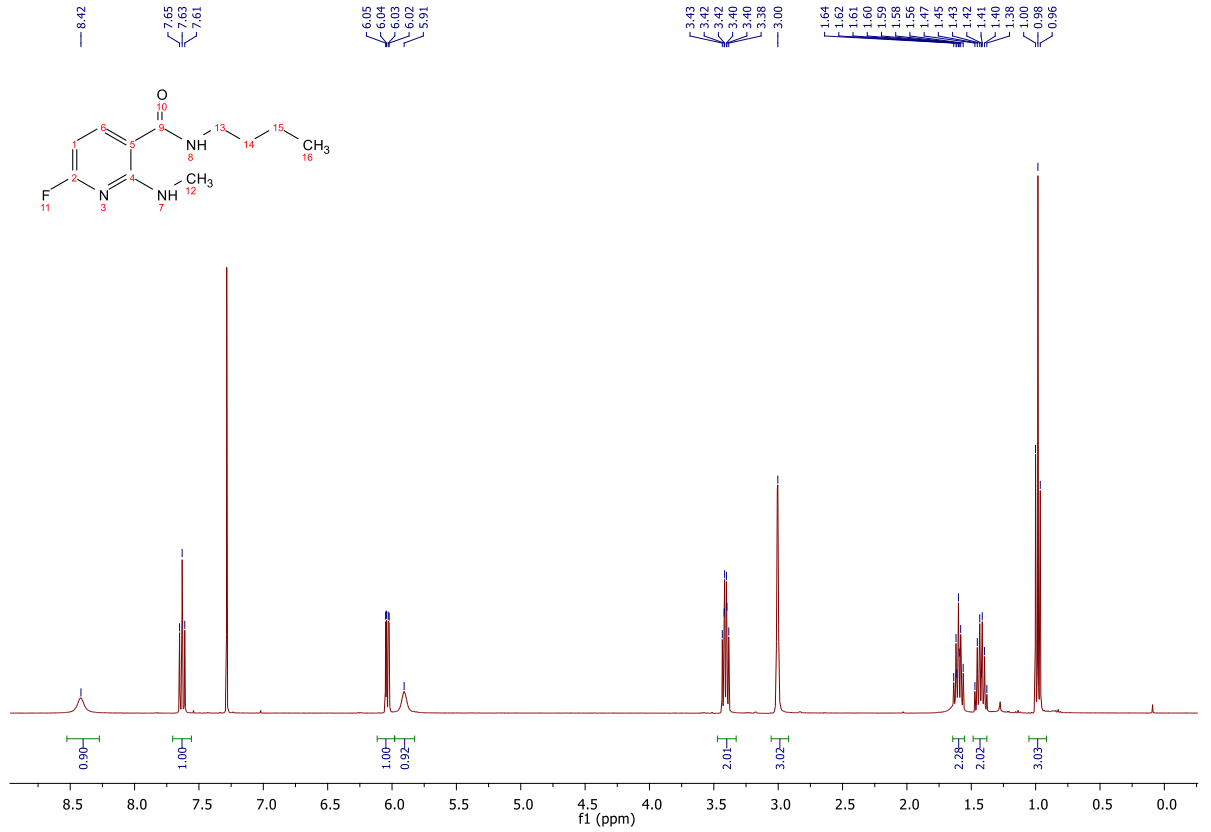

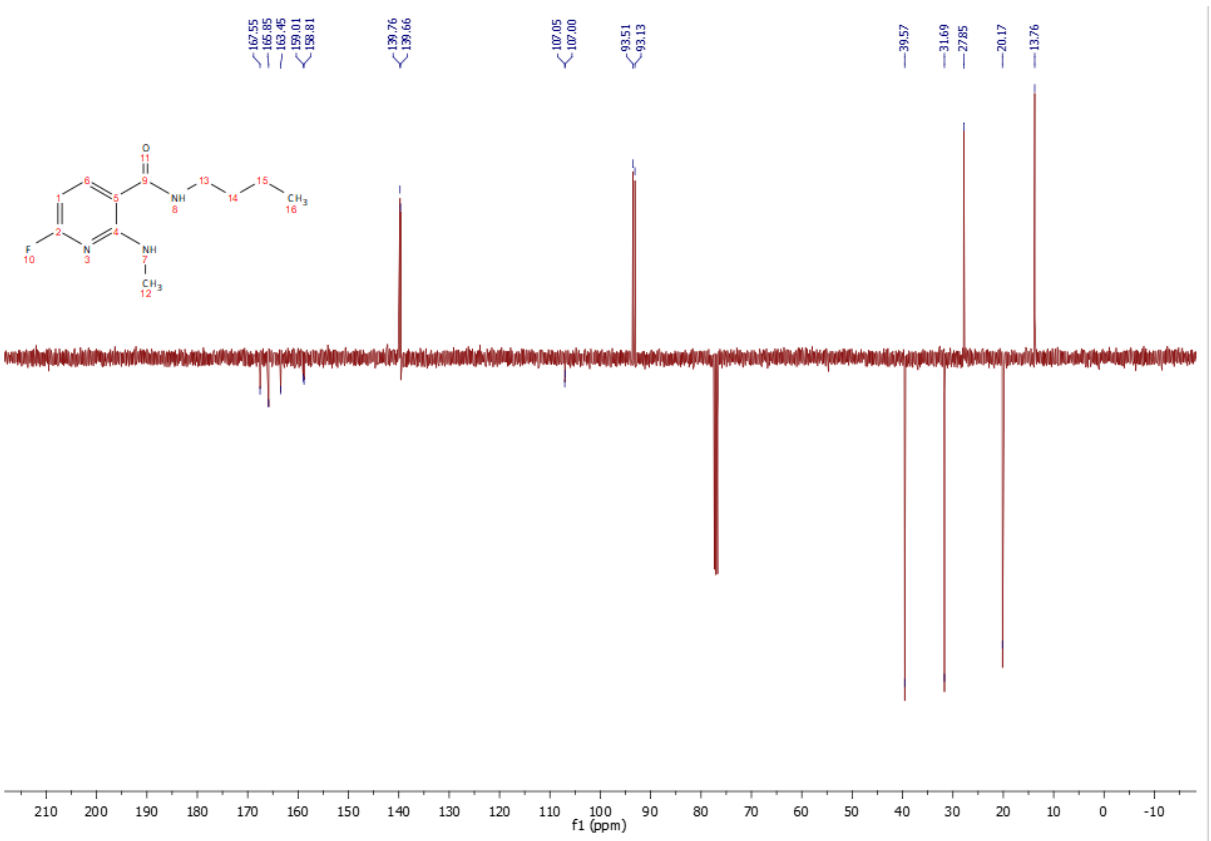

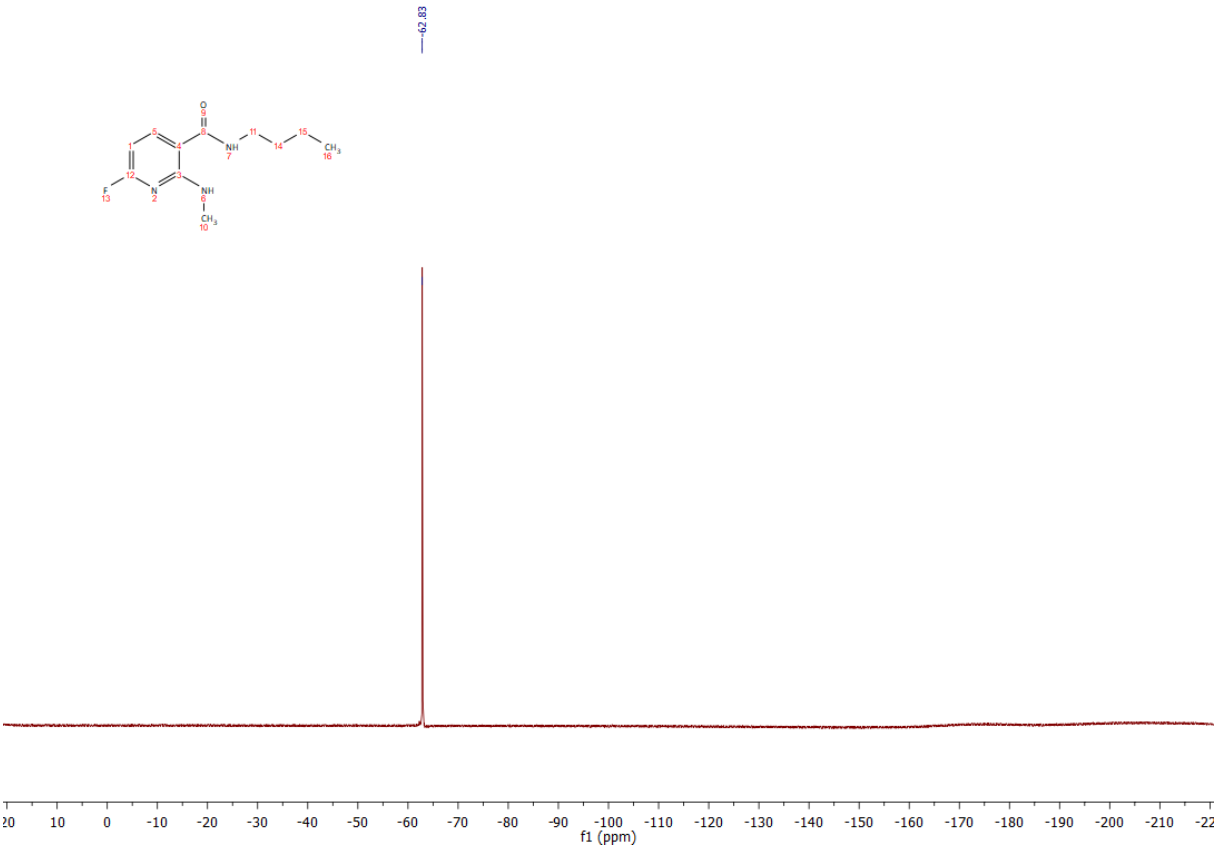
-62.83
f1 (ppm)

2.22 Compound **5b**

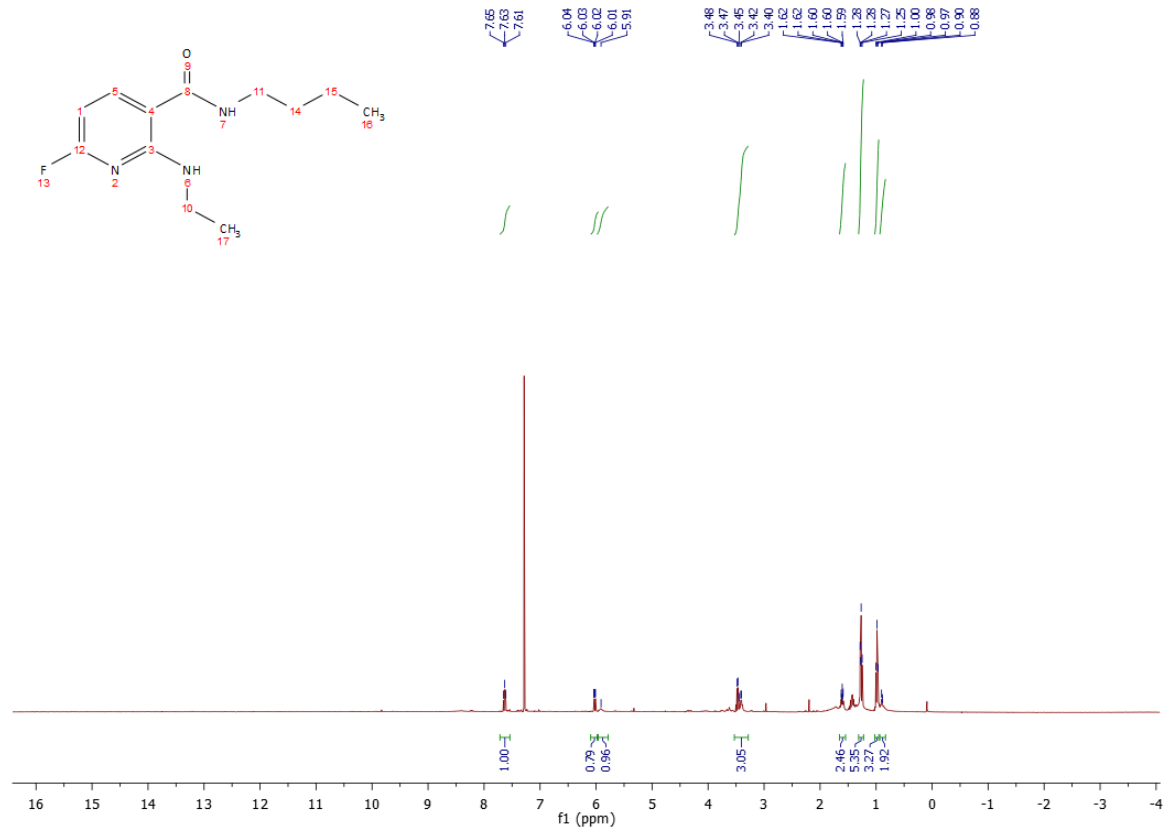

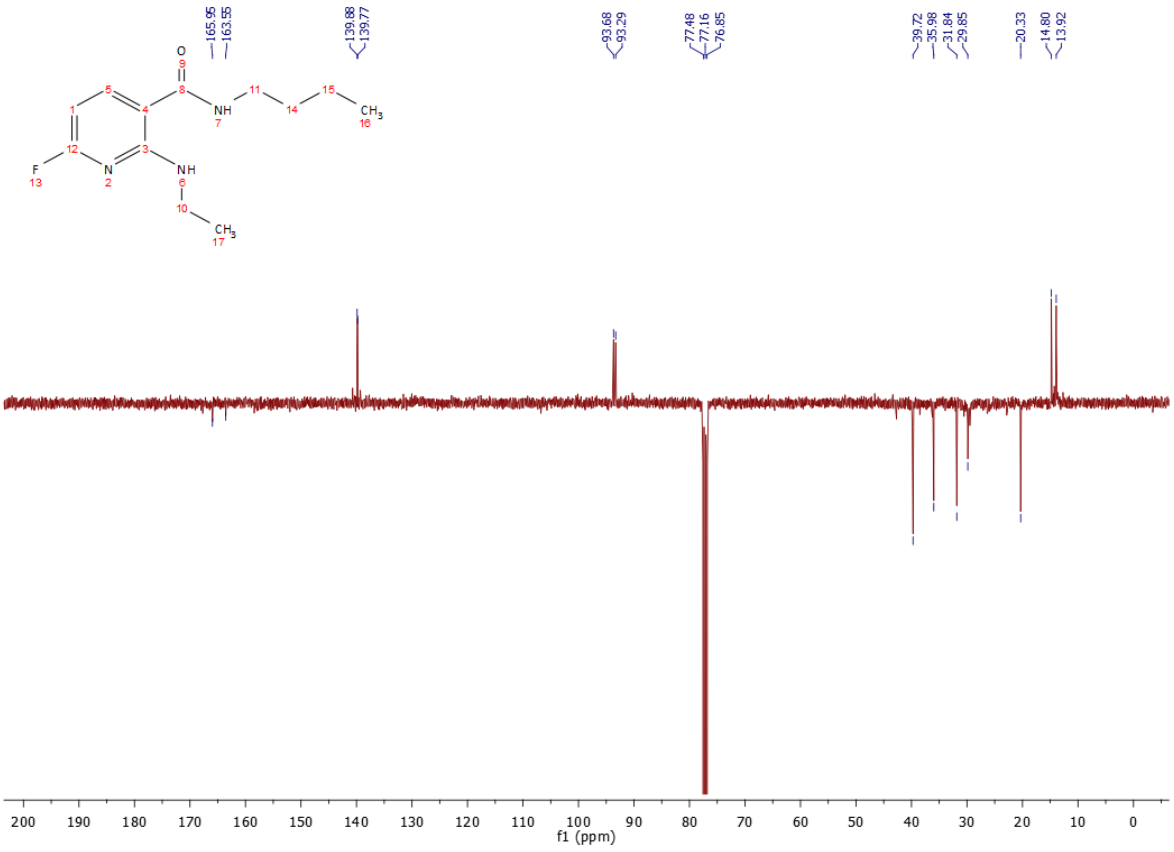

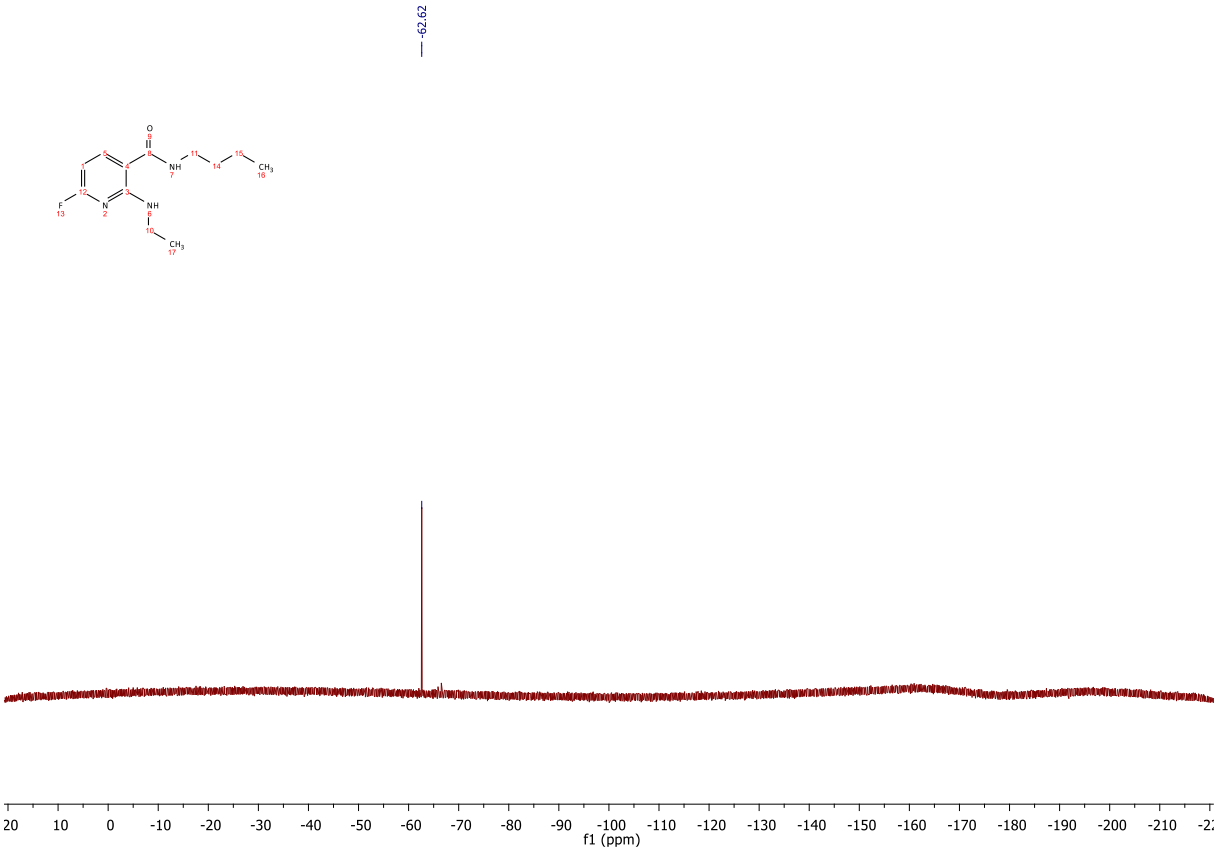
-62.62
O
9
5
6
4
8
NH
7
11
14
15
CH3
16
F
13
12
N
2
3
NH
1
10
CH3
17
20
10
0
-10
-20
-30
-40
-50
-60
-70
-80
-90
-100
-110
-120
-130
-140
-150
-160
-170
-180
-190
-200
-210
f1 (ppm)

2.23 Compound **5c**

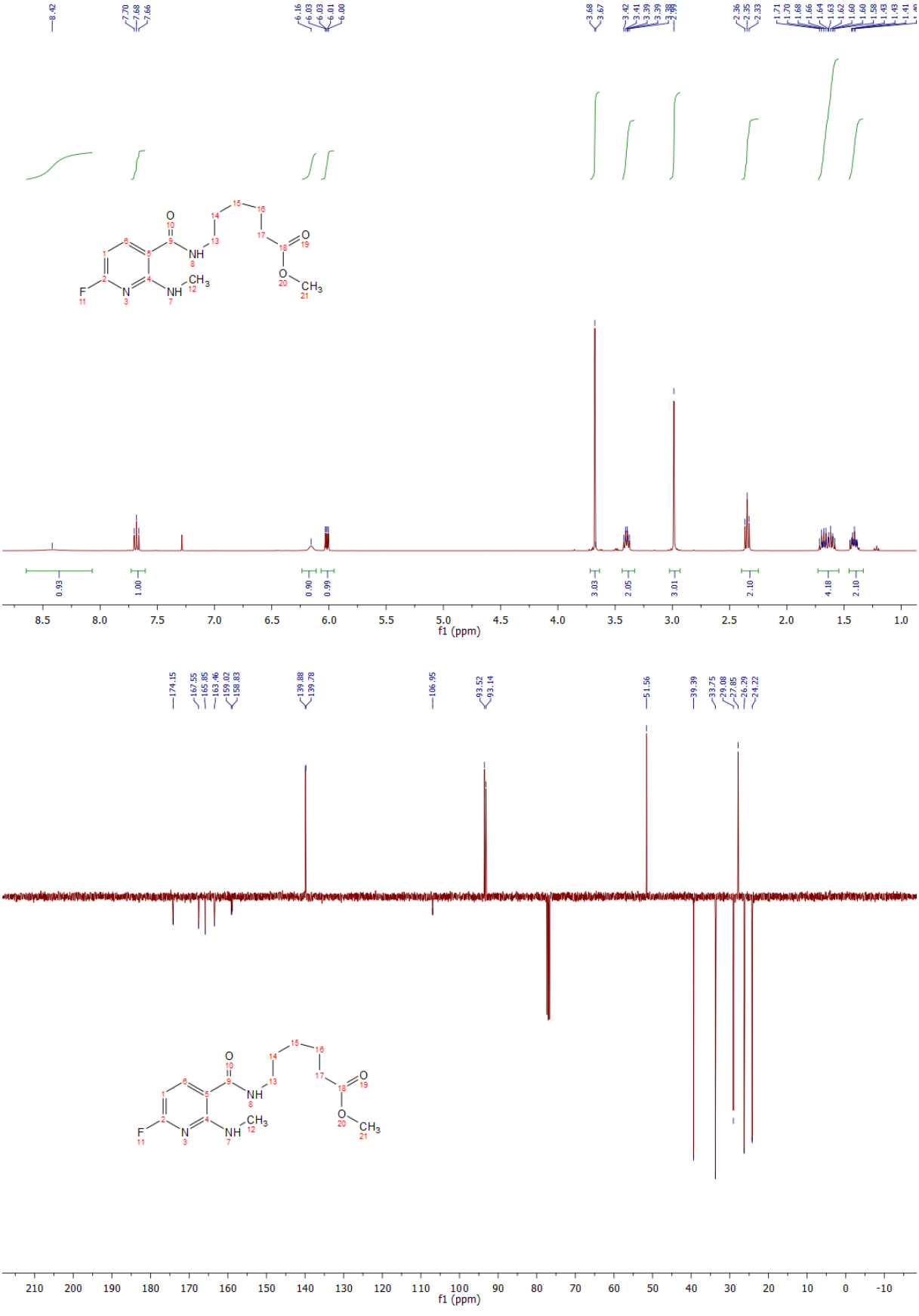

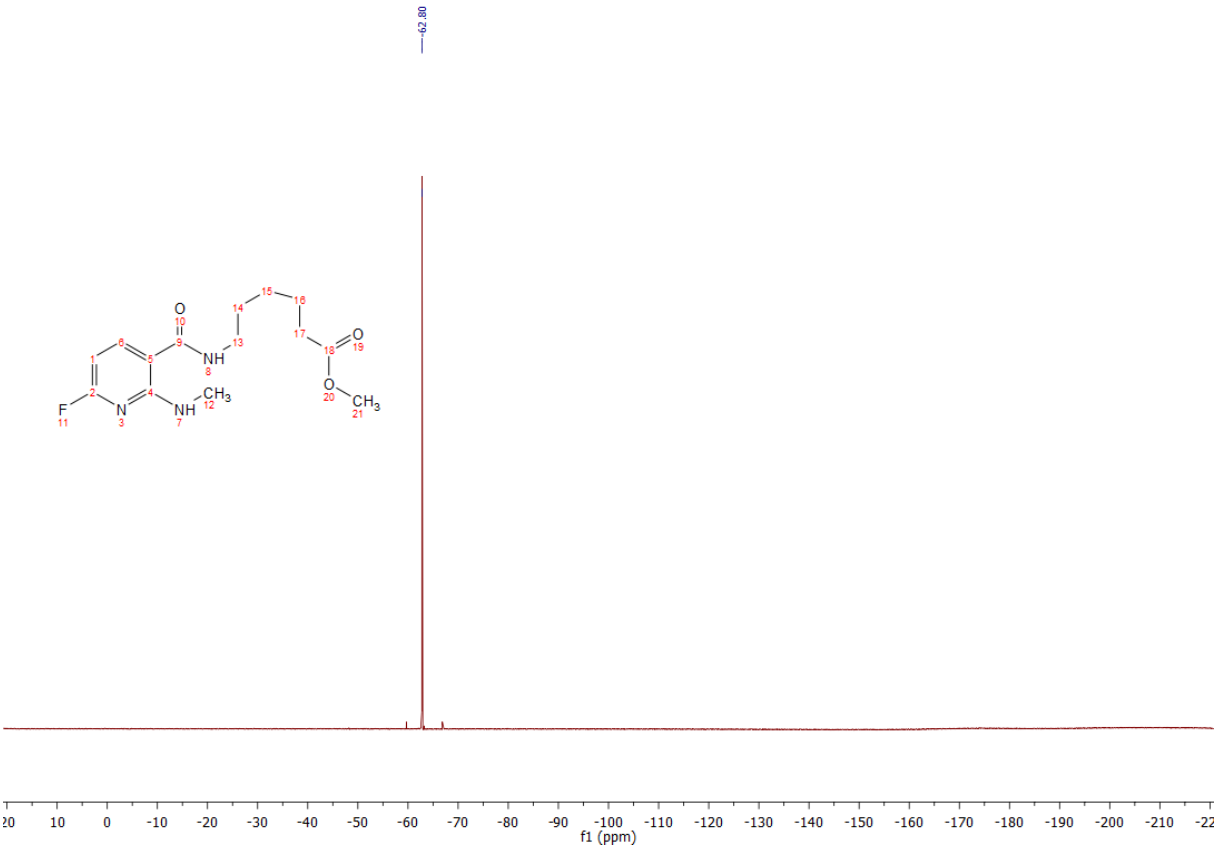
-62.80
F
N
NH
CH3
O
NH
O
O
CH3
f1 (ppm)

2.24 Compound **5d**

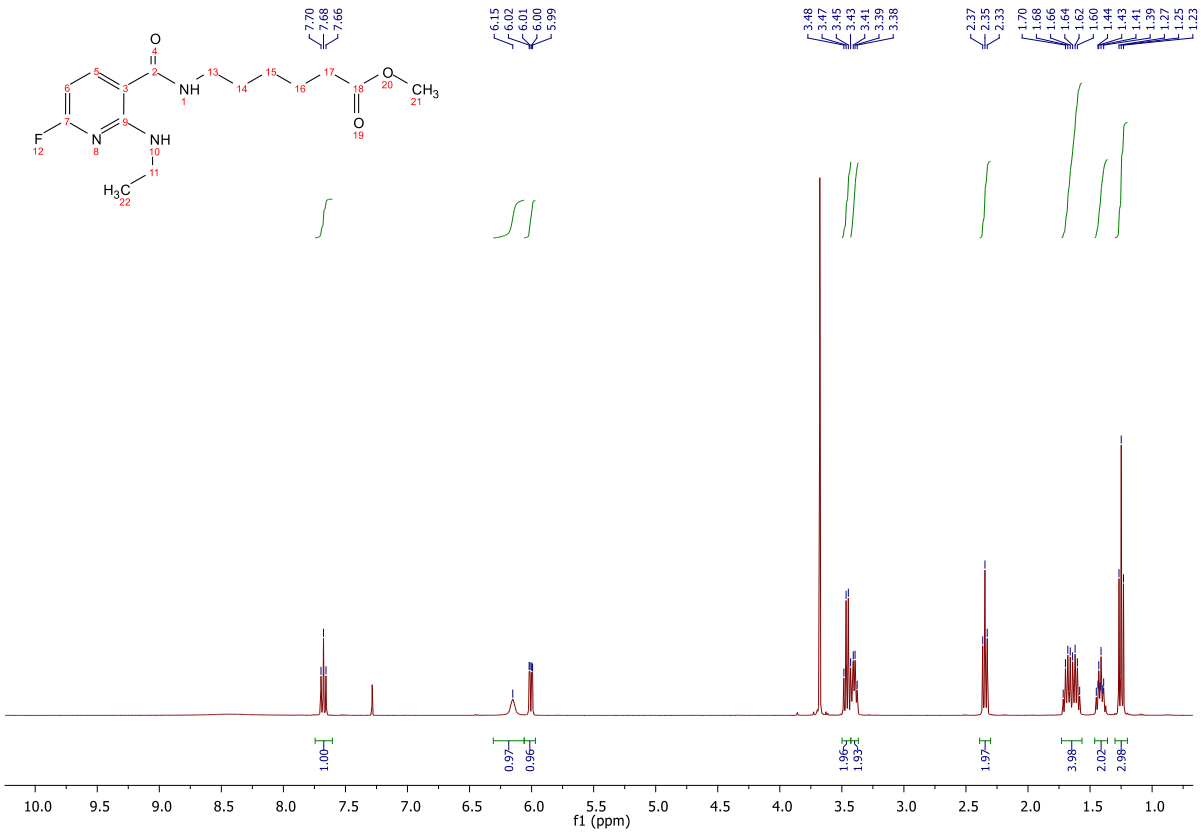

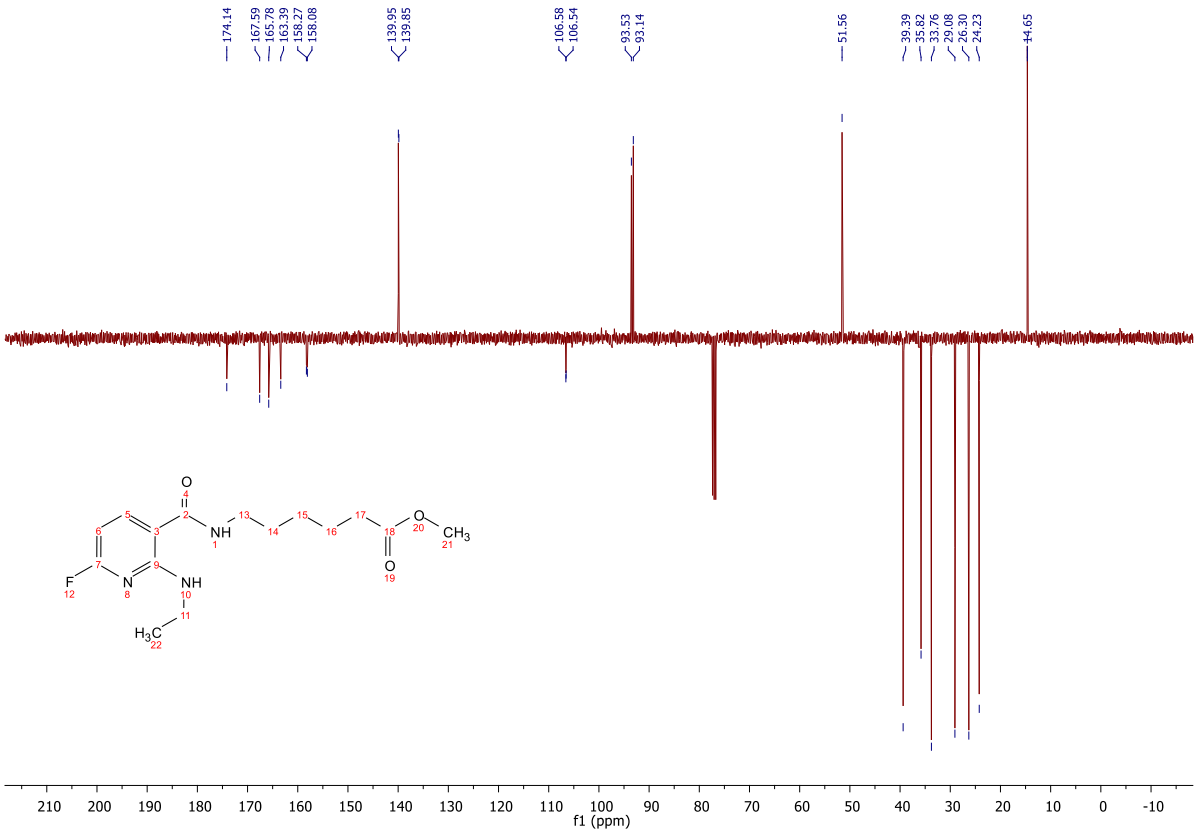

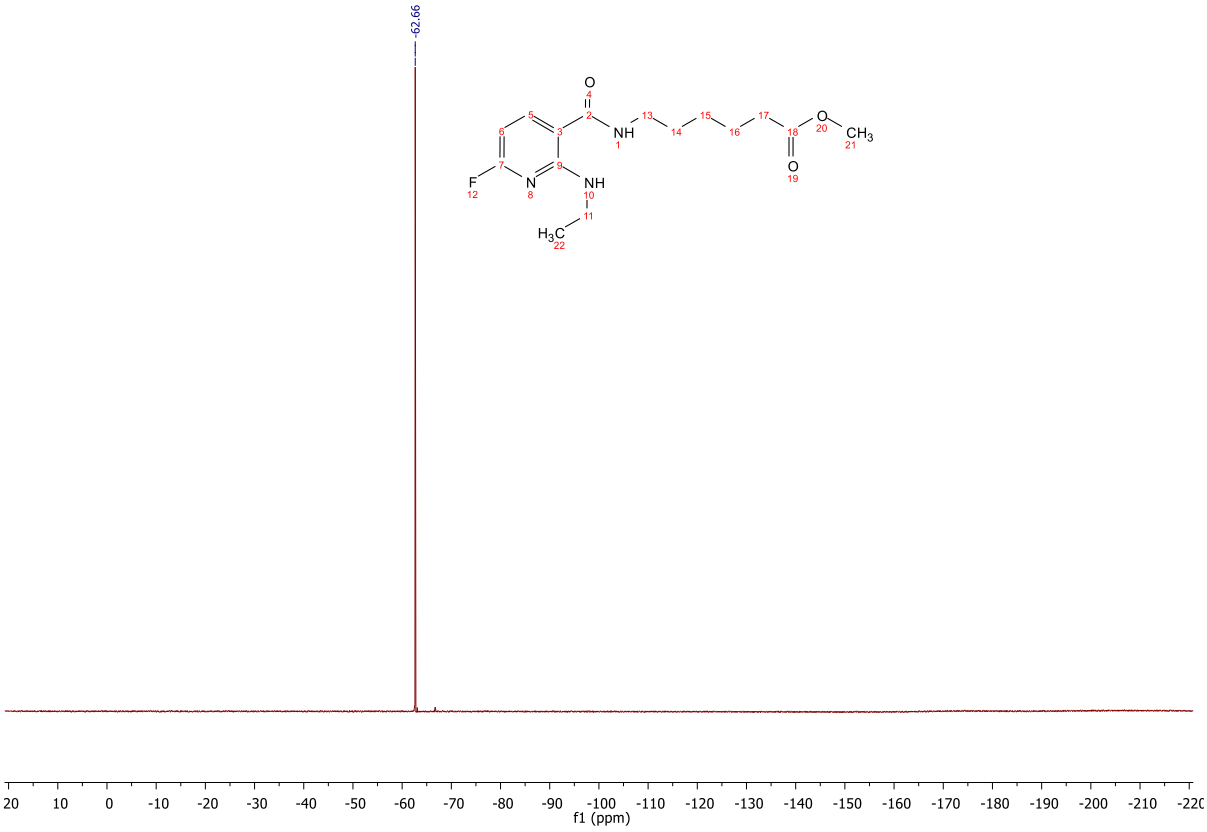
-62.66
O
4
2
3
5
6
NH
1
13
14
15
16
17
18
O
19
O
20
CH3
21
7
F
12
N
8
9
NH
10
11
H3C
22
20
10
0
-10
-20
-30
-40
-50
-60
-70
-80
-90
-100
-110
-120
-130
-140
-150
-160
-170
-180
-190
-200
-210
-220
f1 (ppm)

2.25 Compound **5e**

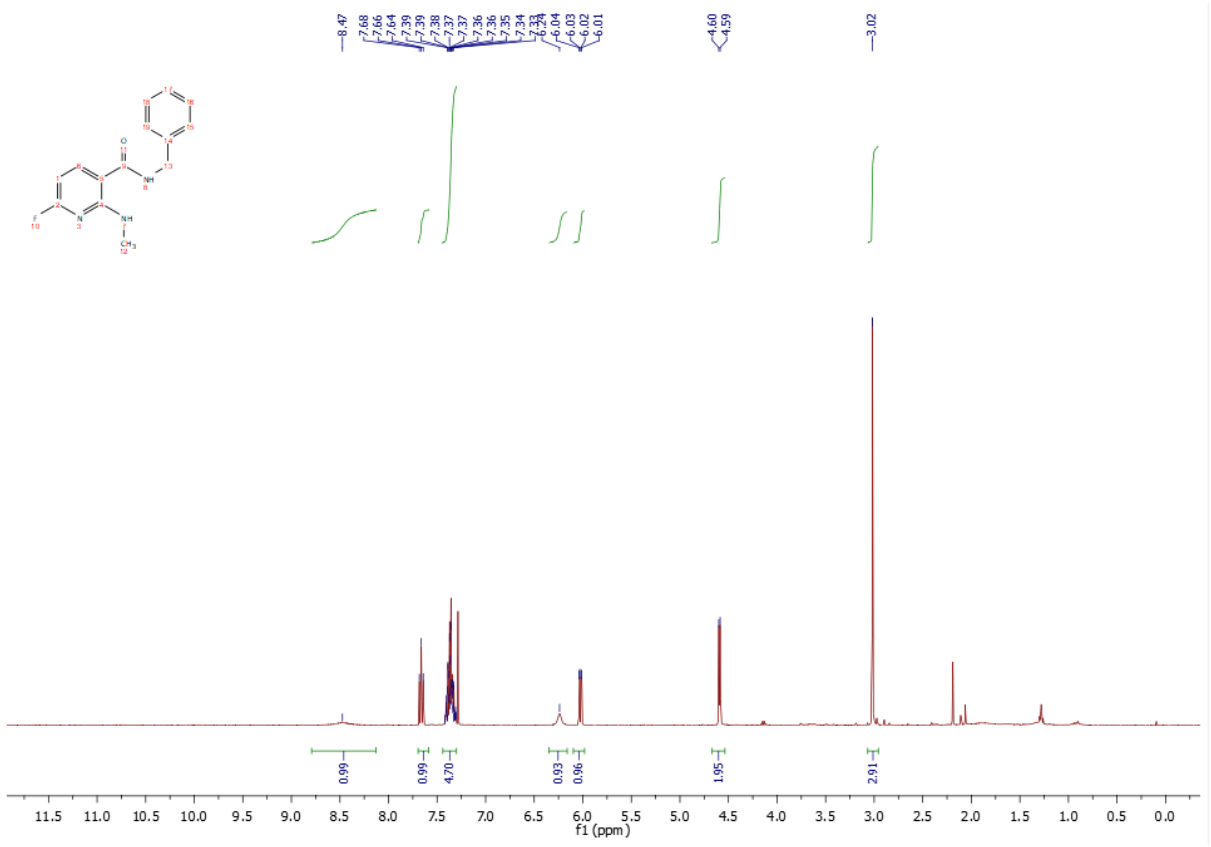

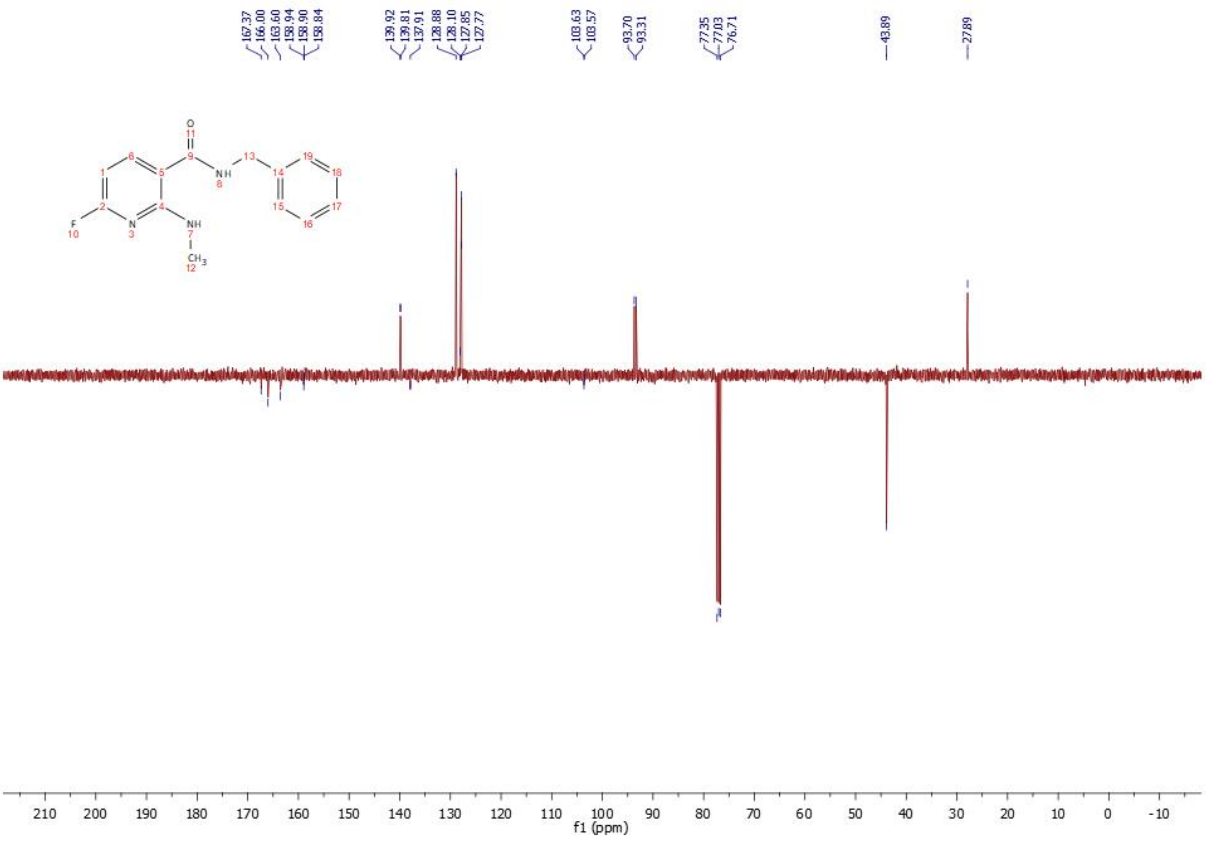

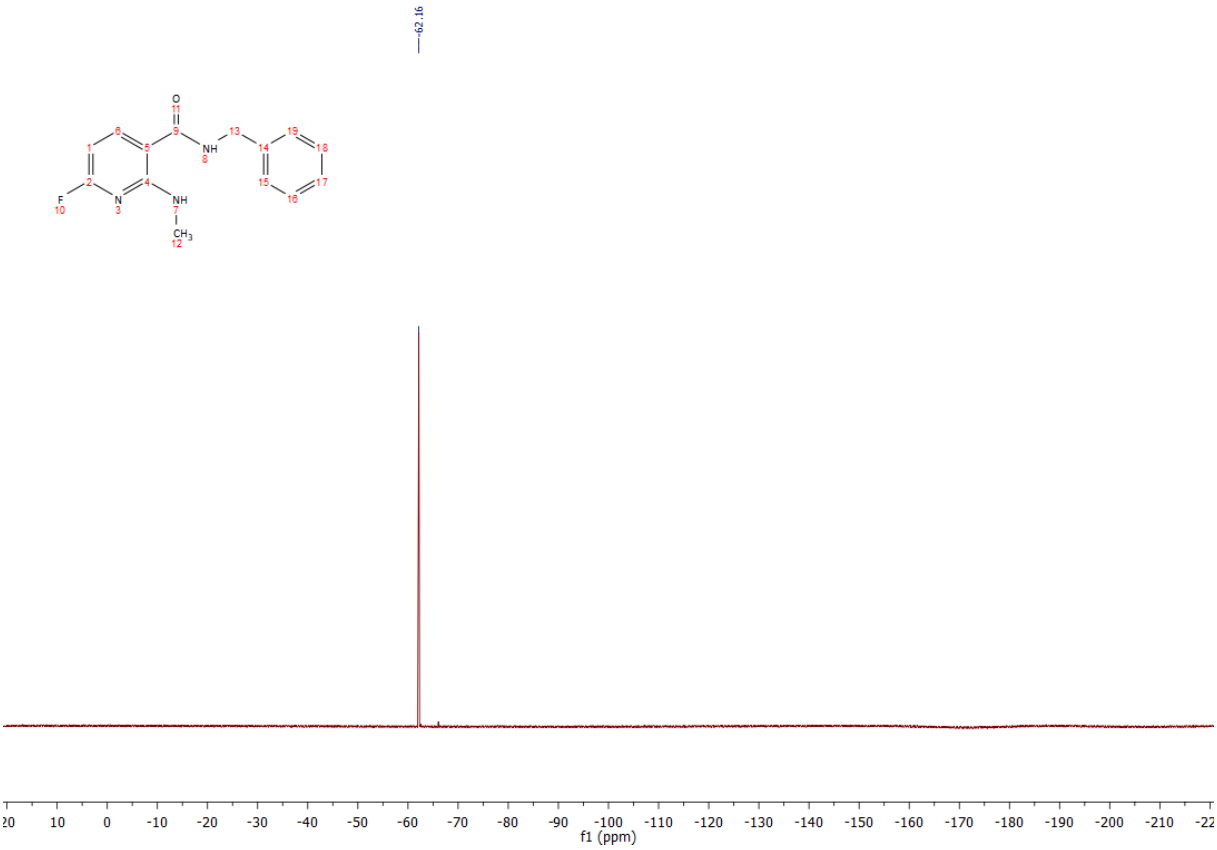
-62.16
O
11
9
NH
8
13
14
19
18
15
17
16
1
6
5
2
4
F
10
N
3
NH
7
CH3
12
20
10
0
-10
-20
-30
-40
-50
-60
-70
-80
-90
-100
-110
-120
-130
-140
-150
-160
-170
-180
-190
-200
-210
-22
f1 (ppm)

2.26 Compound **5f**

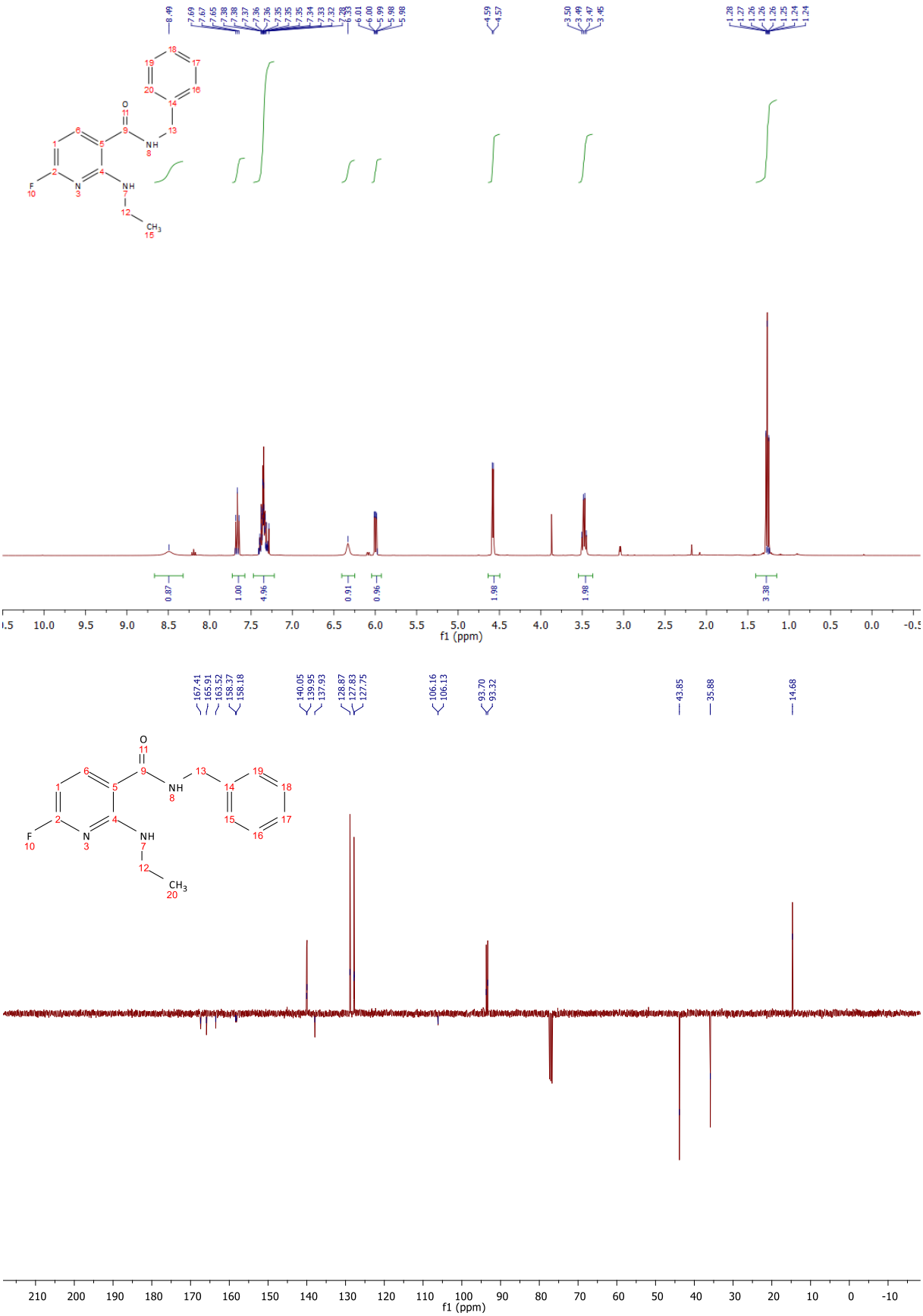

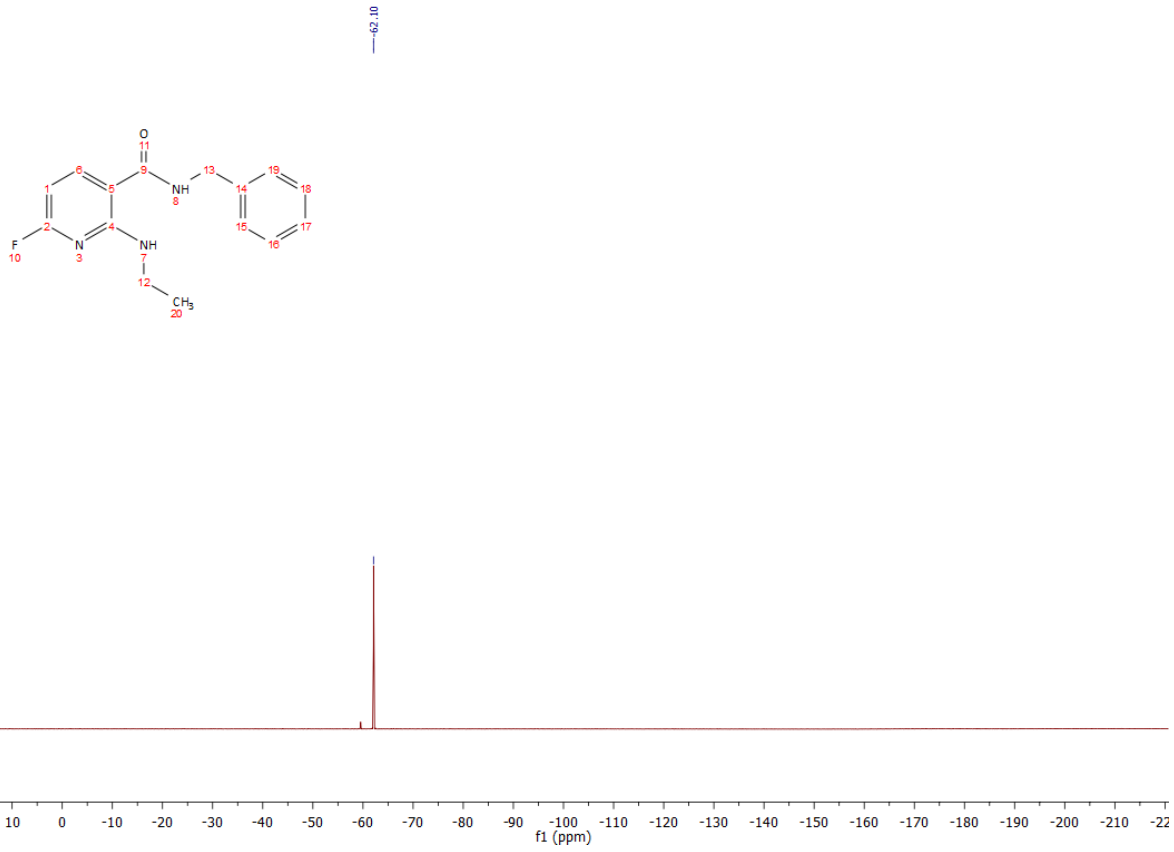
-62.10
O
11
1
6
5
9
NH
8
13
14
19
18
15
16
17
2
4
F
10
N
3
NH
7
12
CH3
20
20
10
0
-10
-20
-30
-40
-50
-60
-70
-80
-90
-100
-110
-120
-130
-140
-150
-160
-170
-180
-190
-200
-210
-22
f1 (ppm)

2.27 Compound **5g**

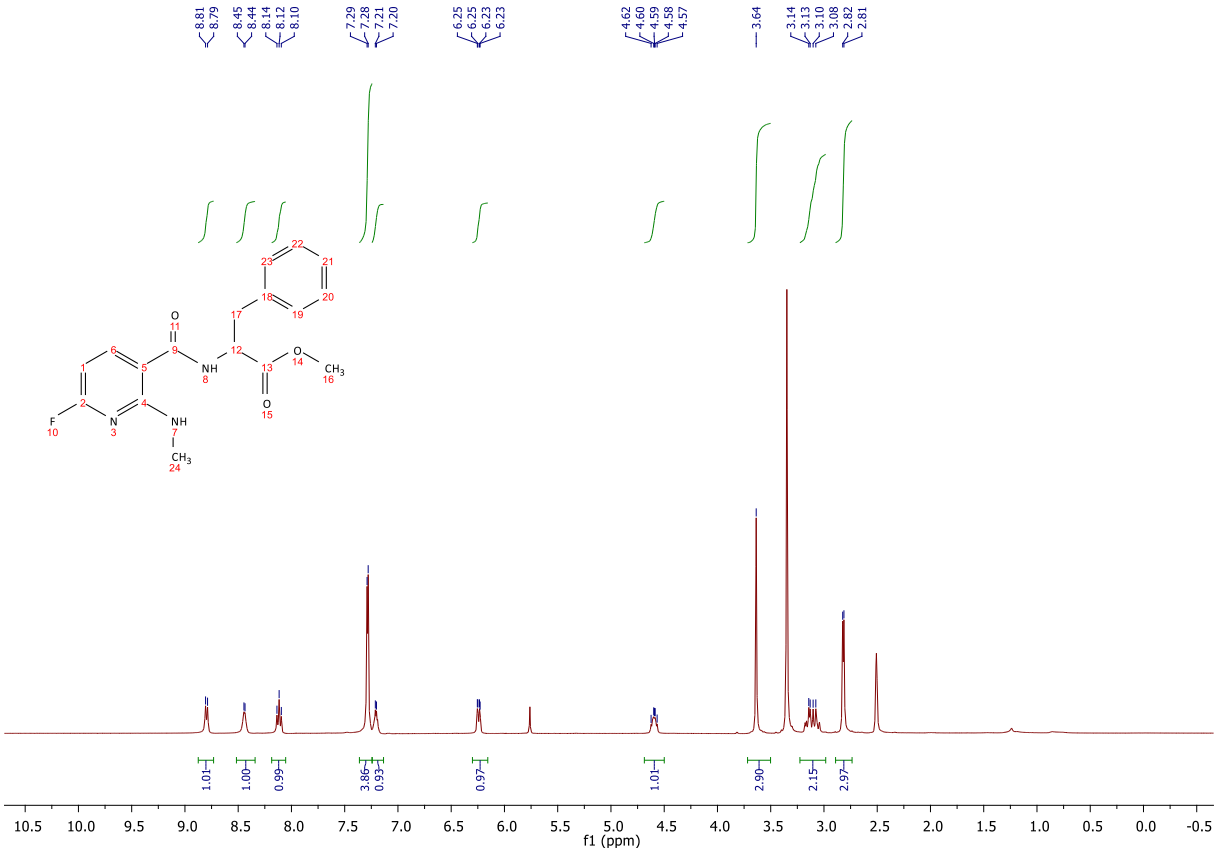

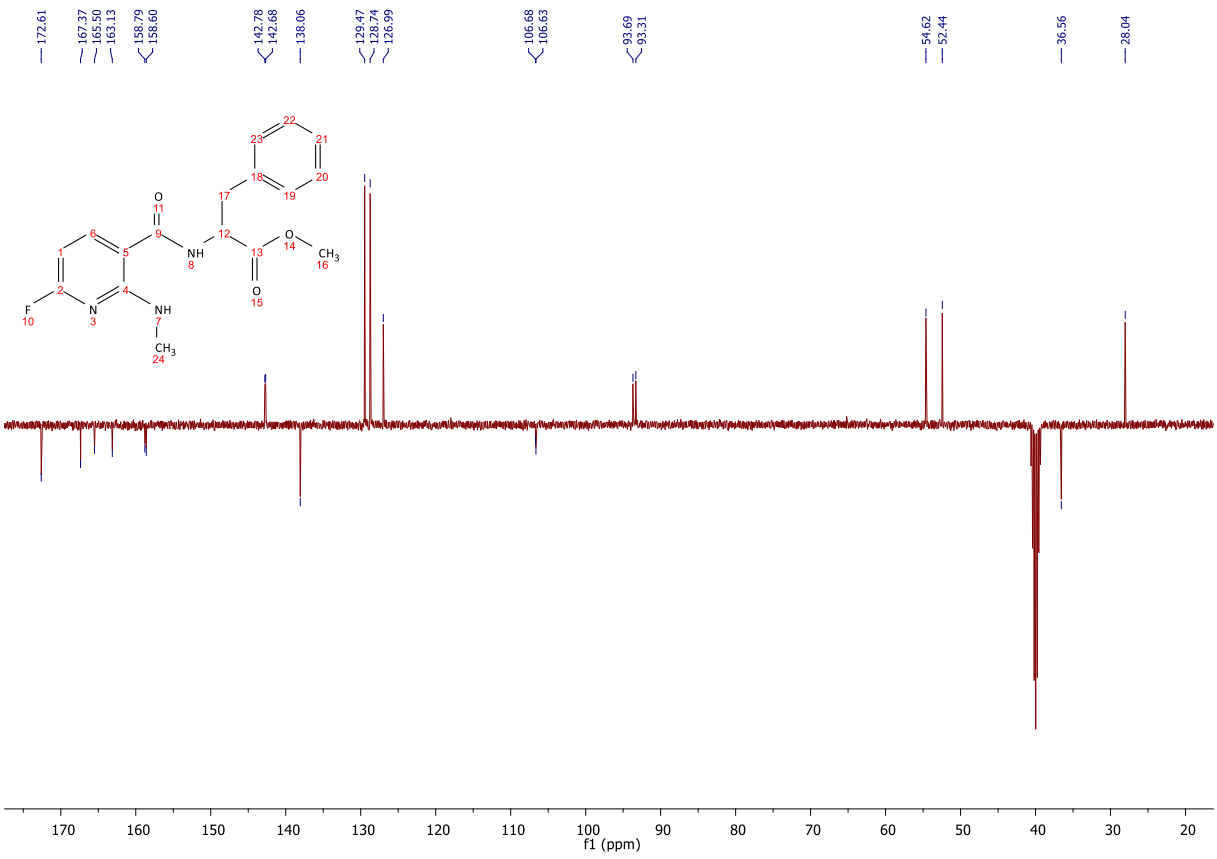

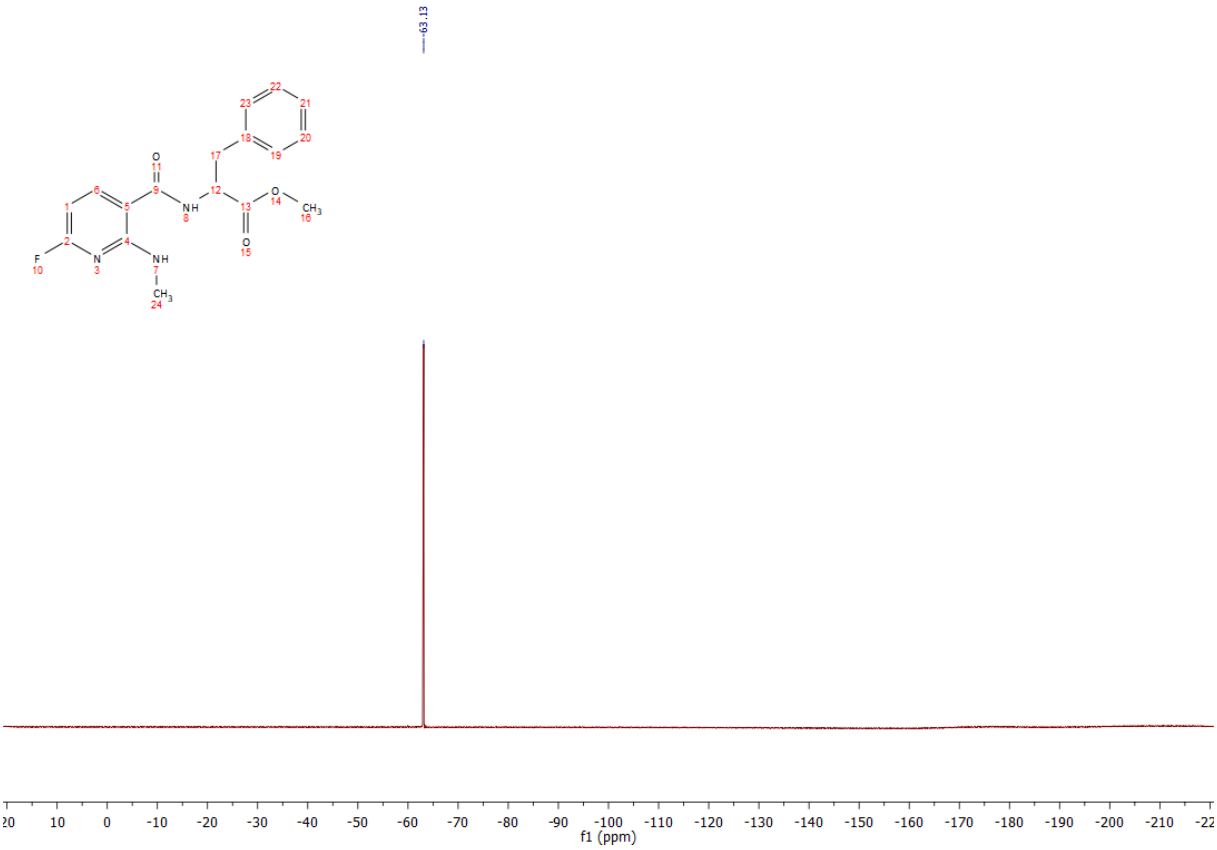
-63.13
f1 (ppm)

2.28 Compound **5h**

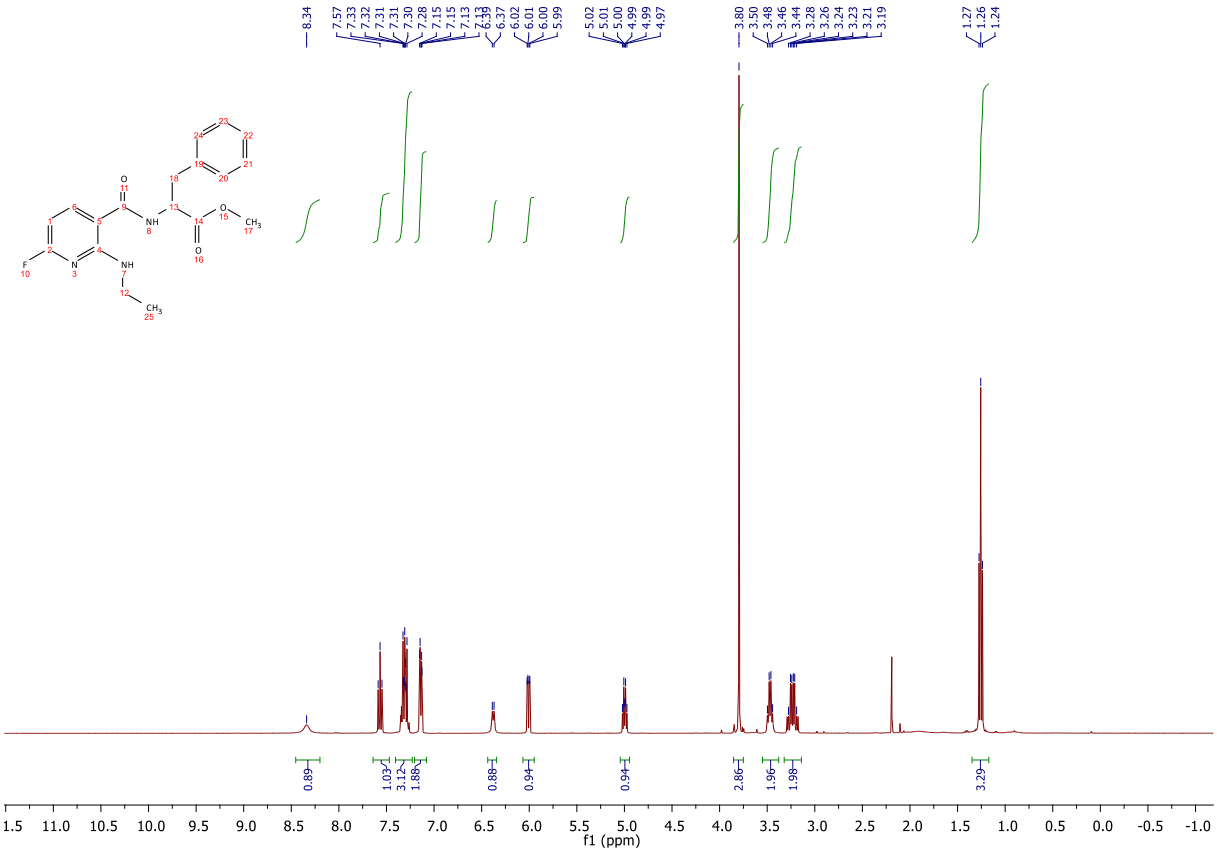

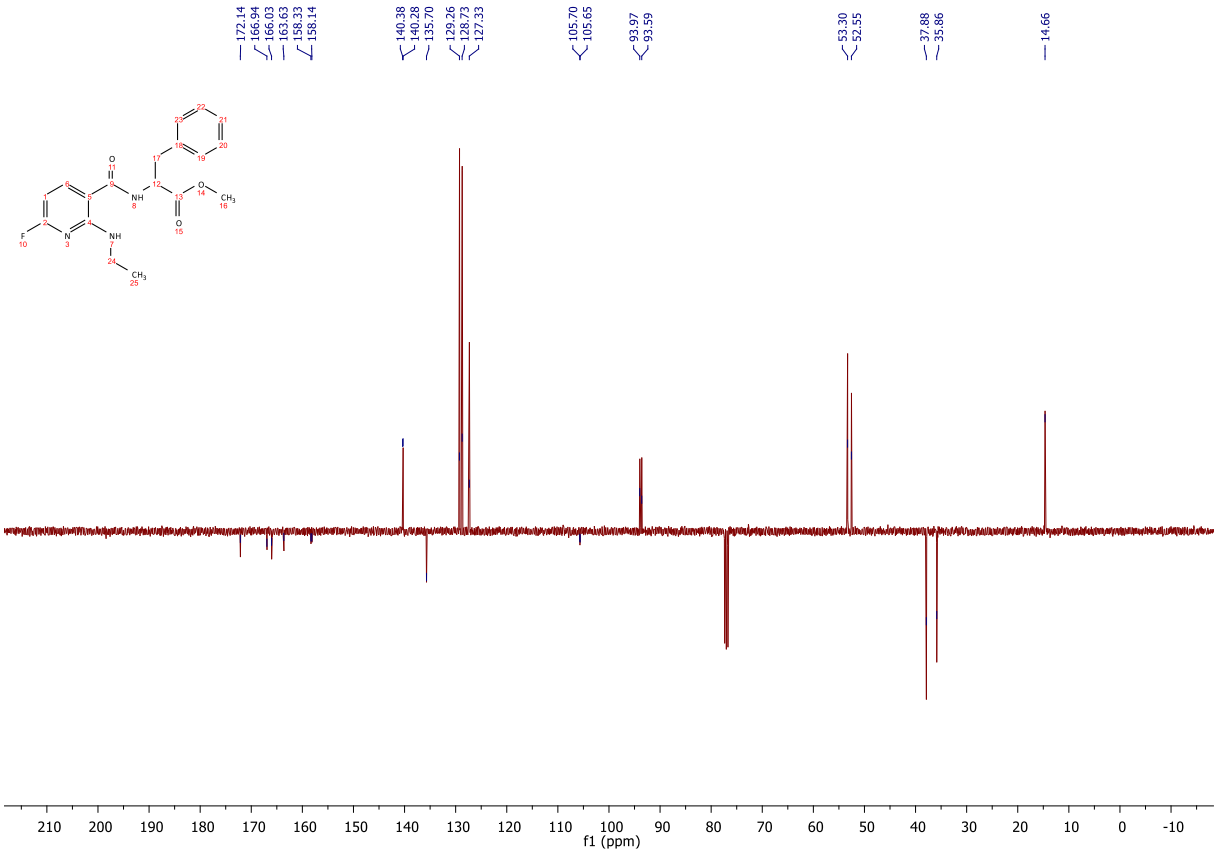

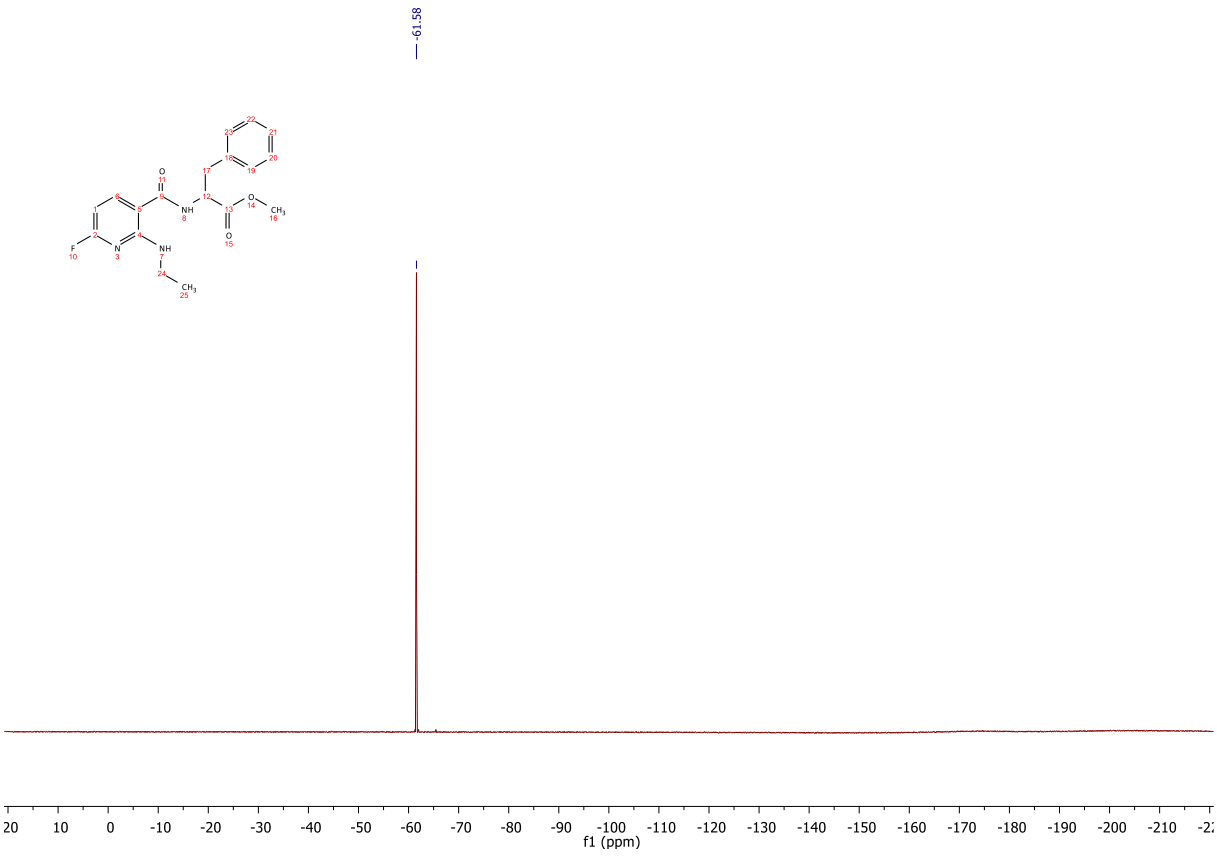
-61.58
20
10
0
-10
-20
-30
-40
-50
-60
-70
-80
-90
-100
-110
-120
-130
-140
-150
-160
-170
-180
-190
-200
-210
f1 (ppm)

2.29 Compound **5i**

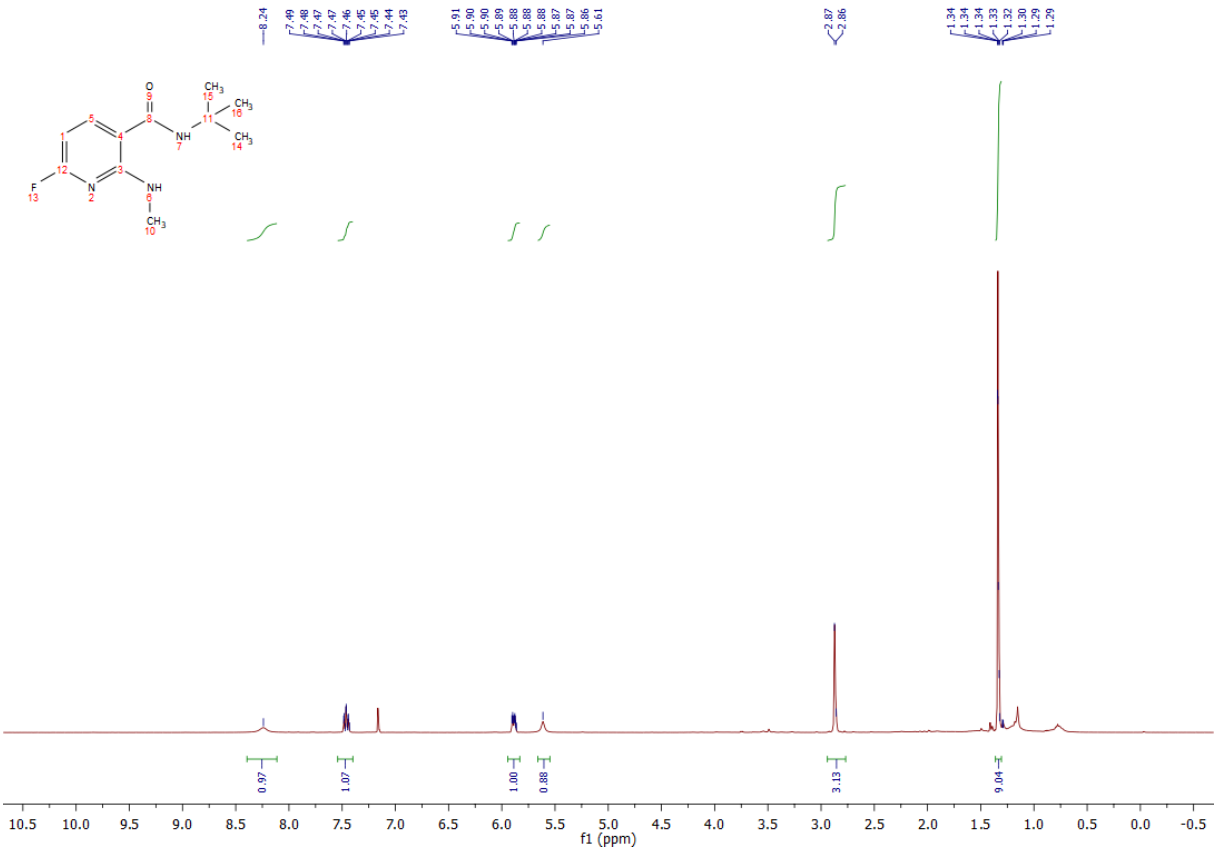

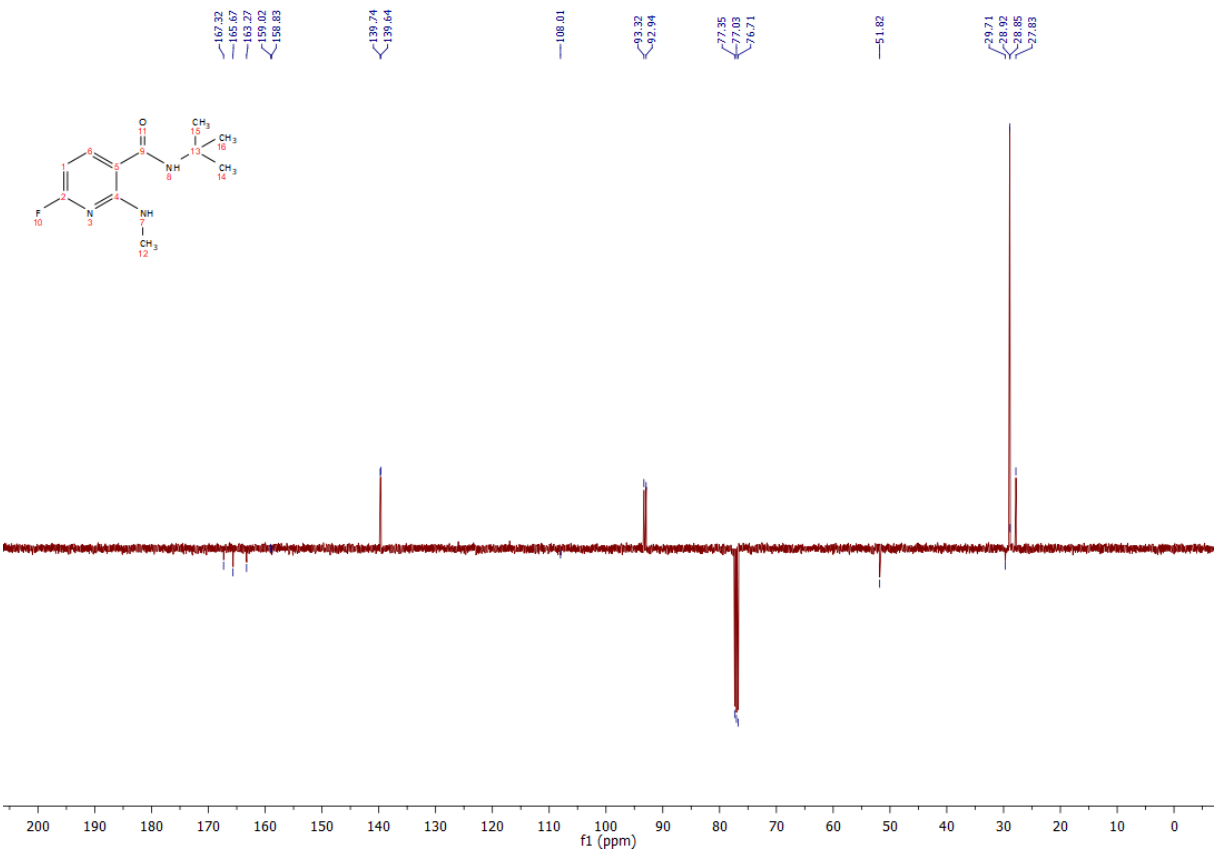

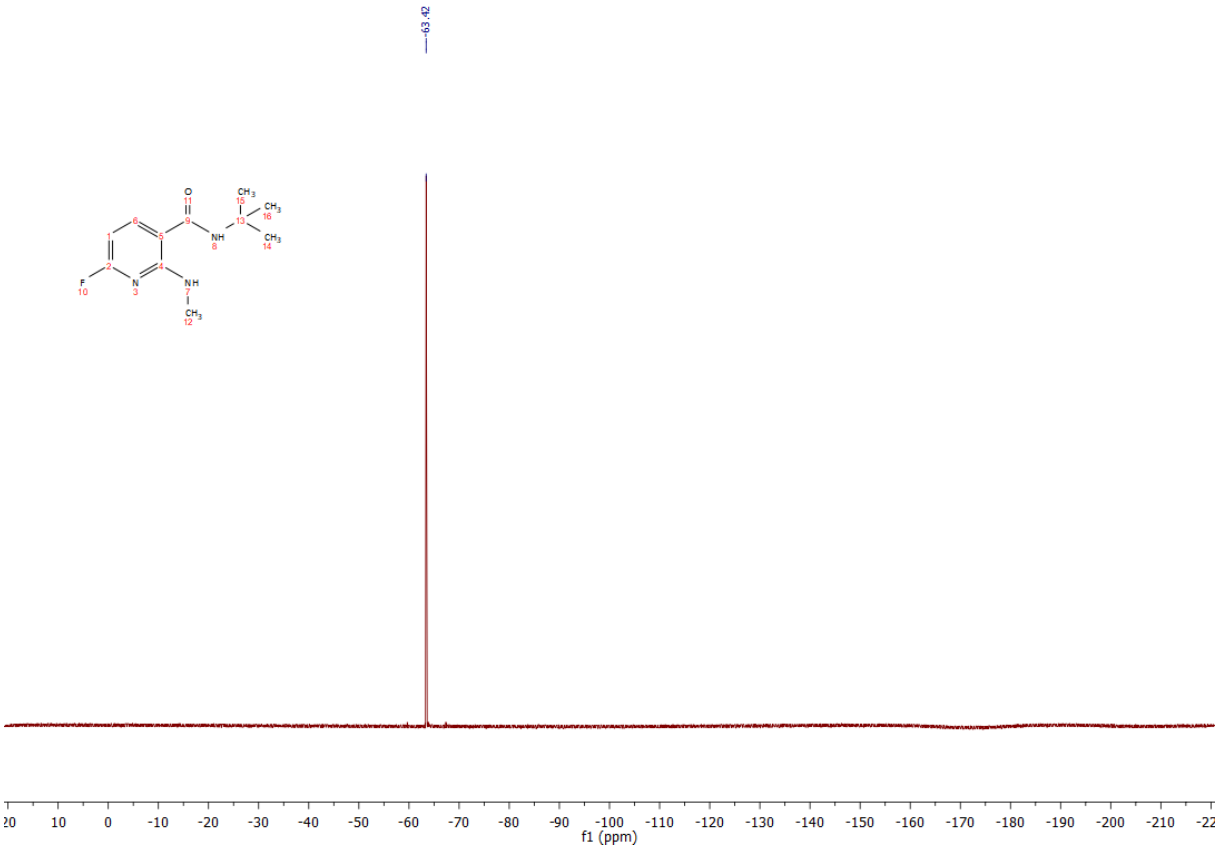
-63.42
O
11
CH3
15
CH3
16
CH3
14
NH
8
13
9
6
5
1
2
4
F
10
N
3
NH
7
CH3
12
20
10
0
-10
-20
-30
-40
-50
-60
-70
-80
-90
-100
-110
-120
-130
-140
-150
-160
-170
-180
-190
-200
-210
-22
f1 (ppm)

2.30 Compound **5j**

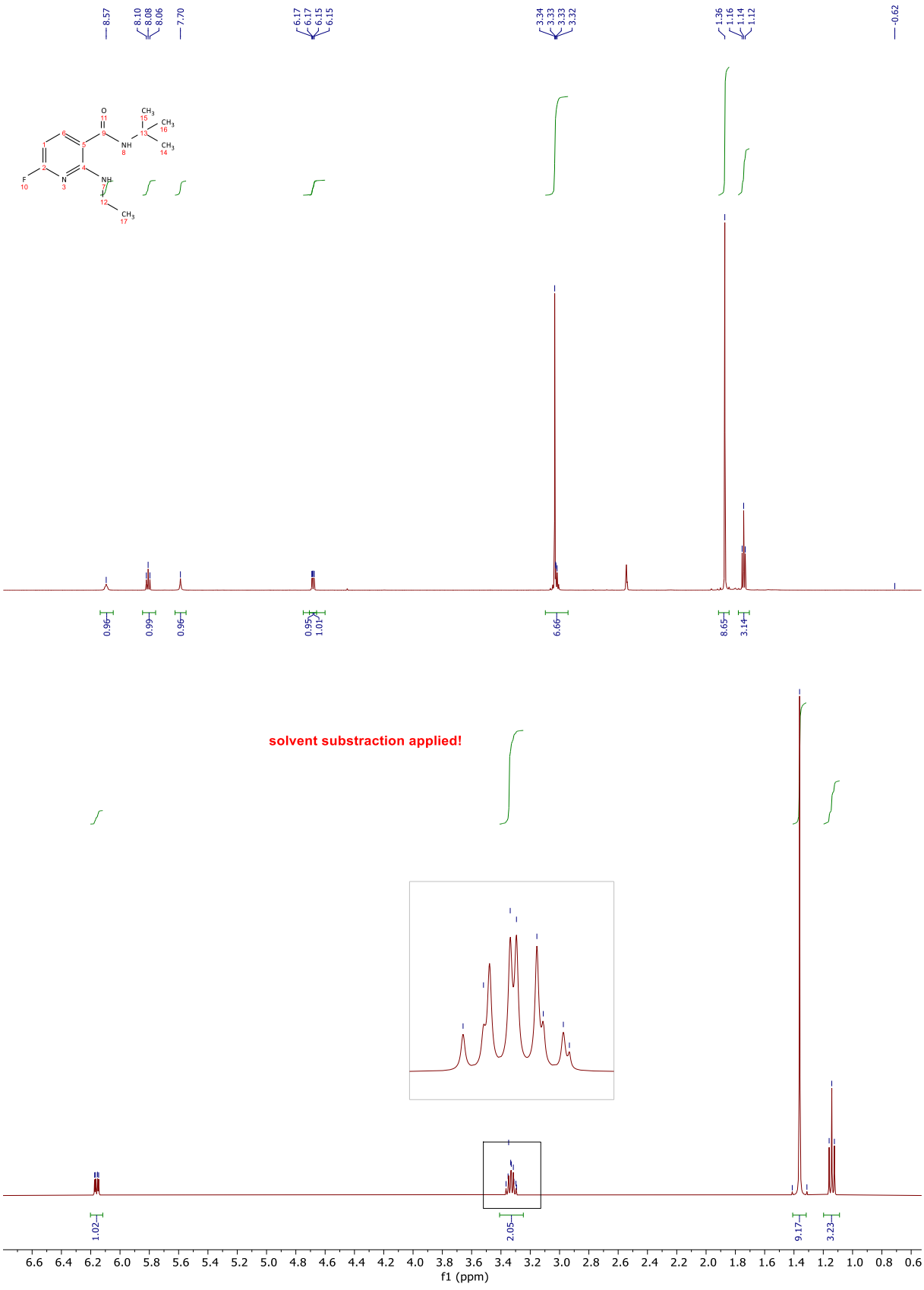

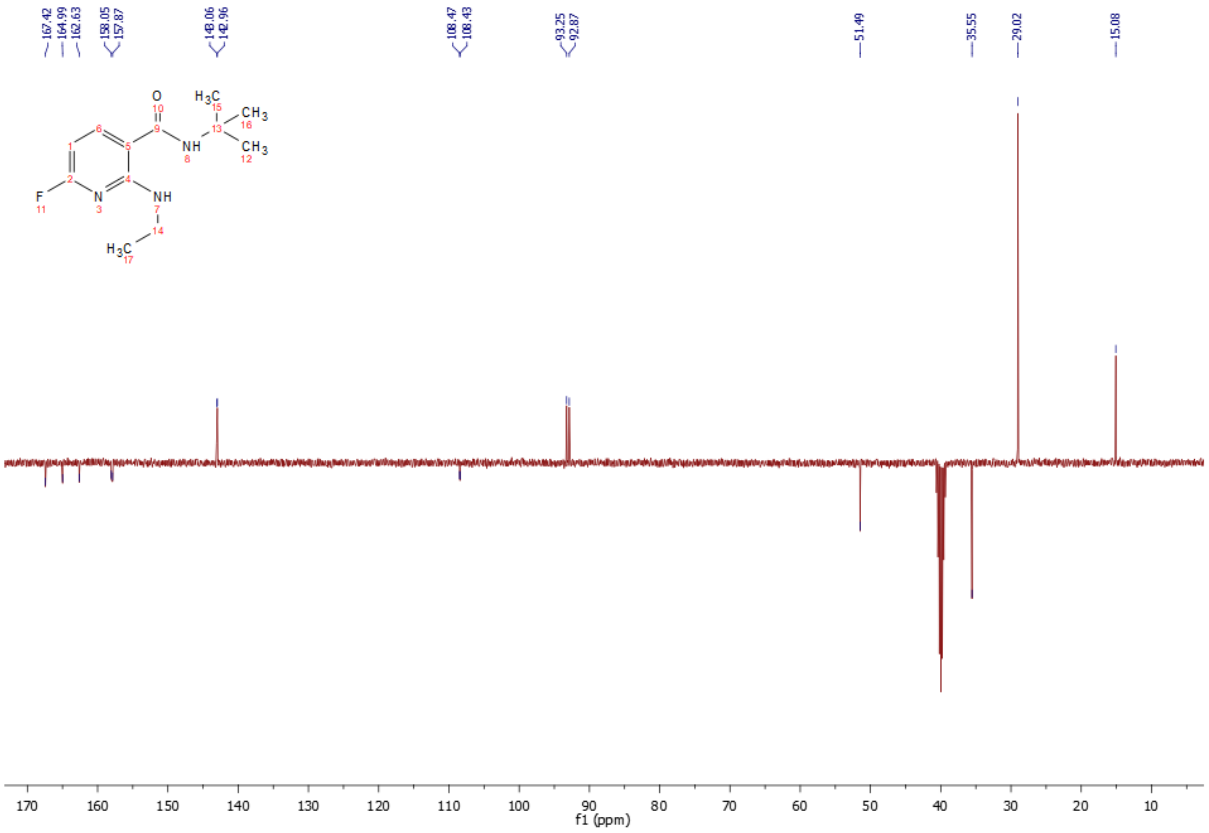
167.42
164.99
162.63
158.05
157.87
148.06
147.96
108.47
108.43
93.25
92.87
51.49
35.55
29.02
15.08
f1 (ppm)

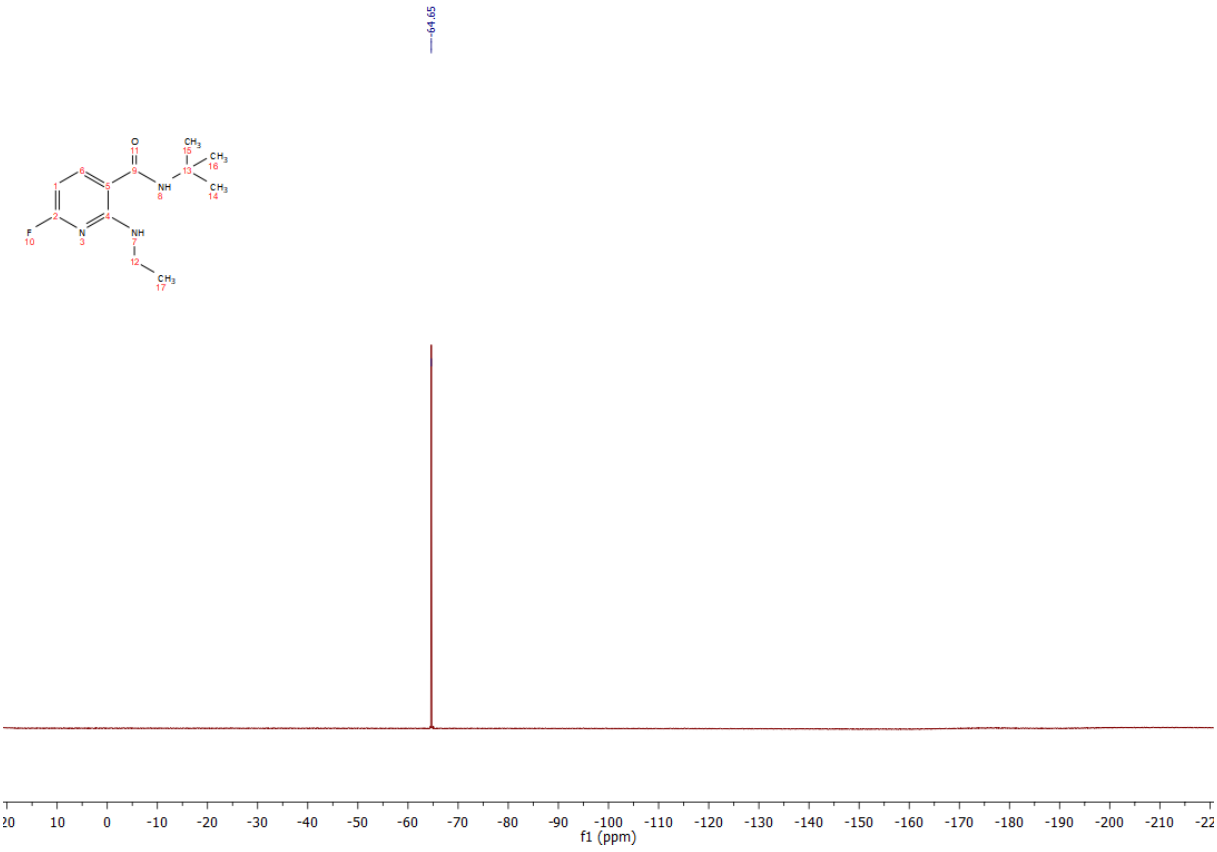
64.65
f1 (ppm)

2.31 Compound **5k**

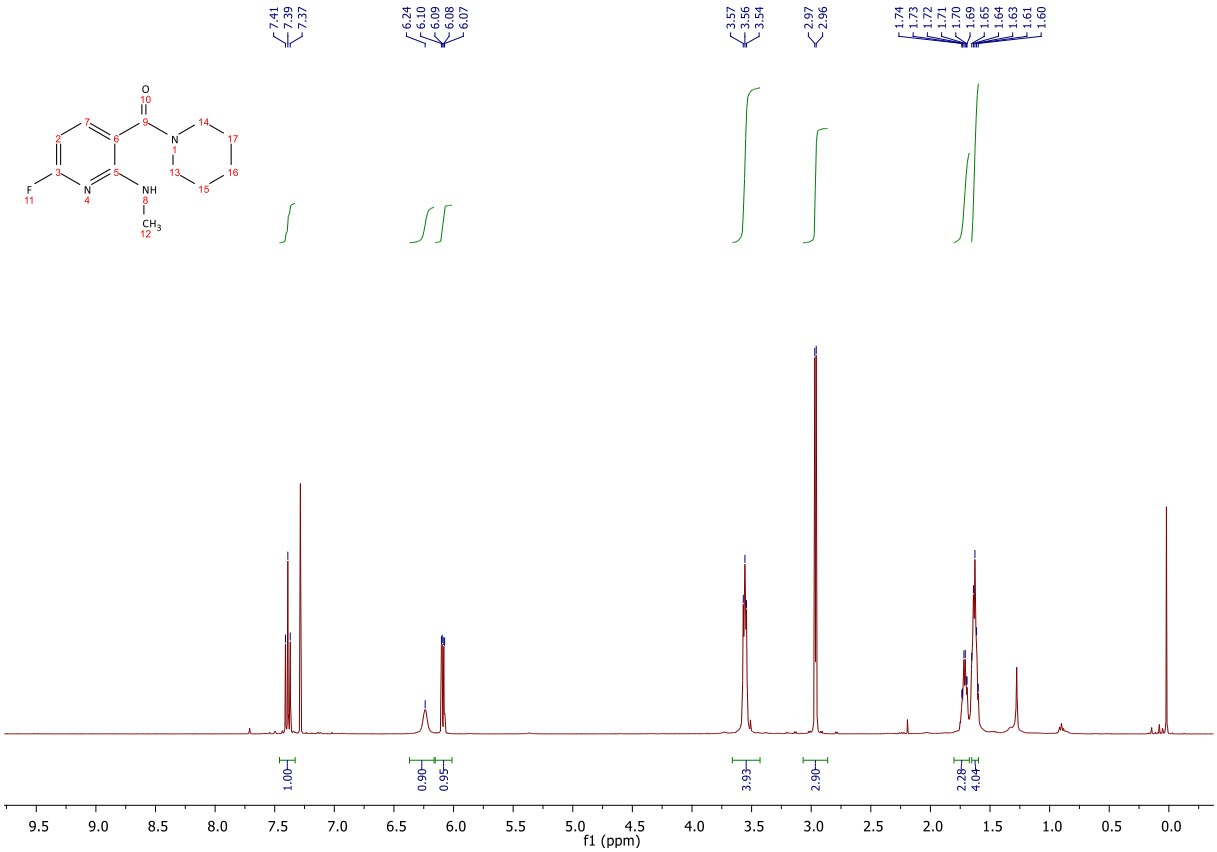

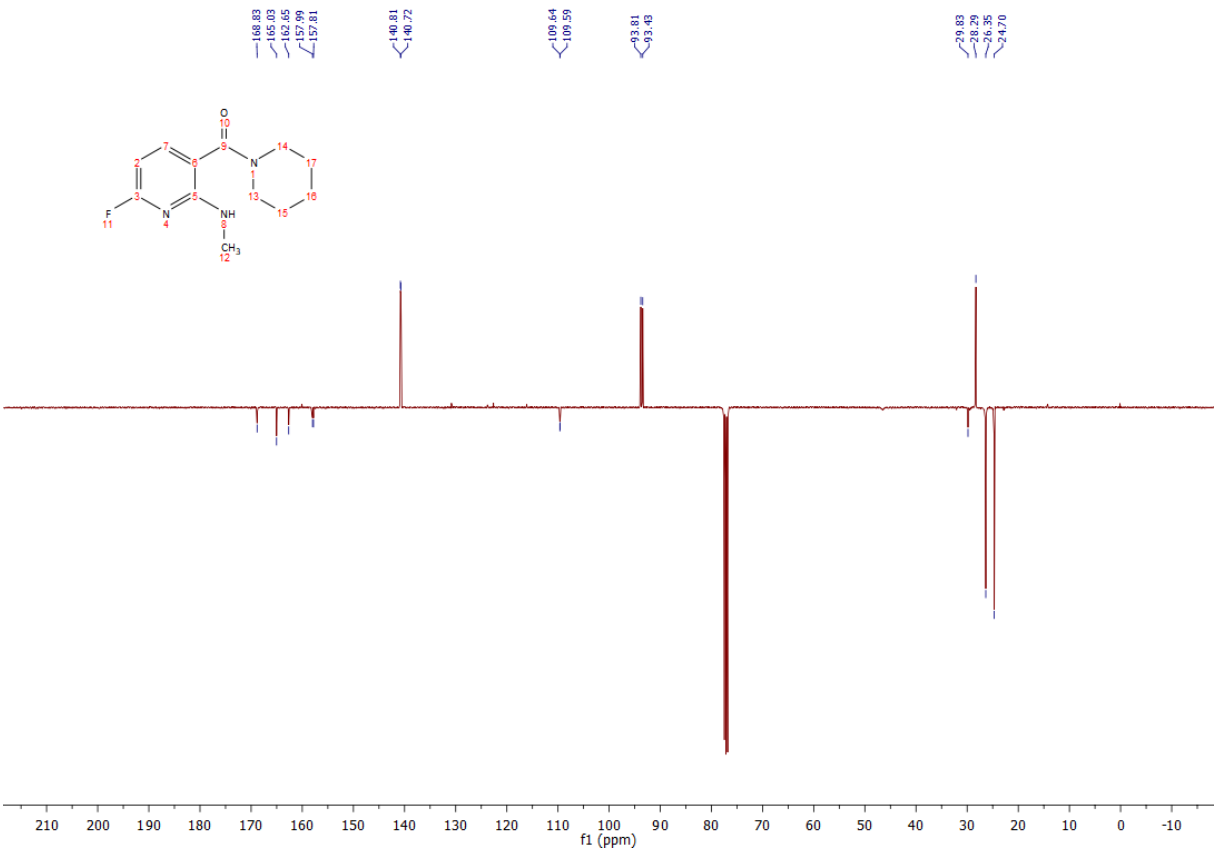

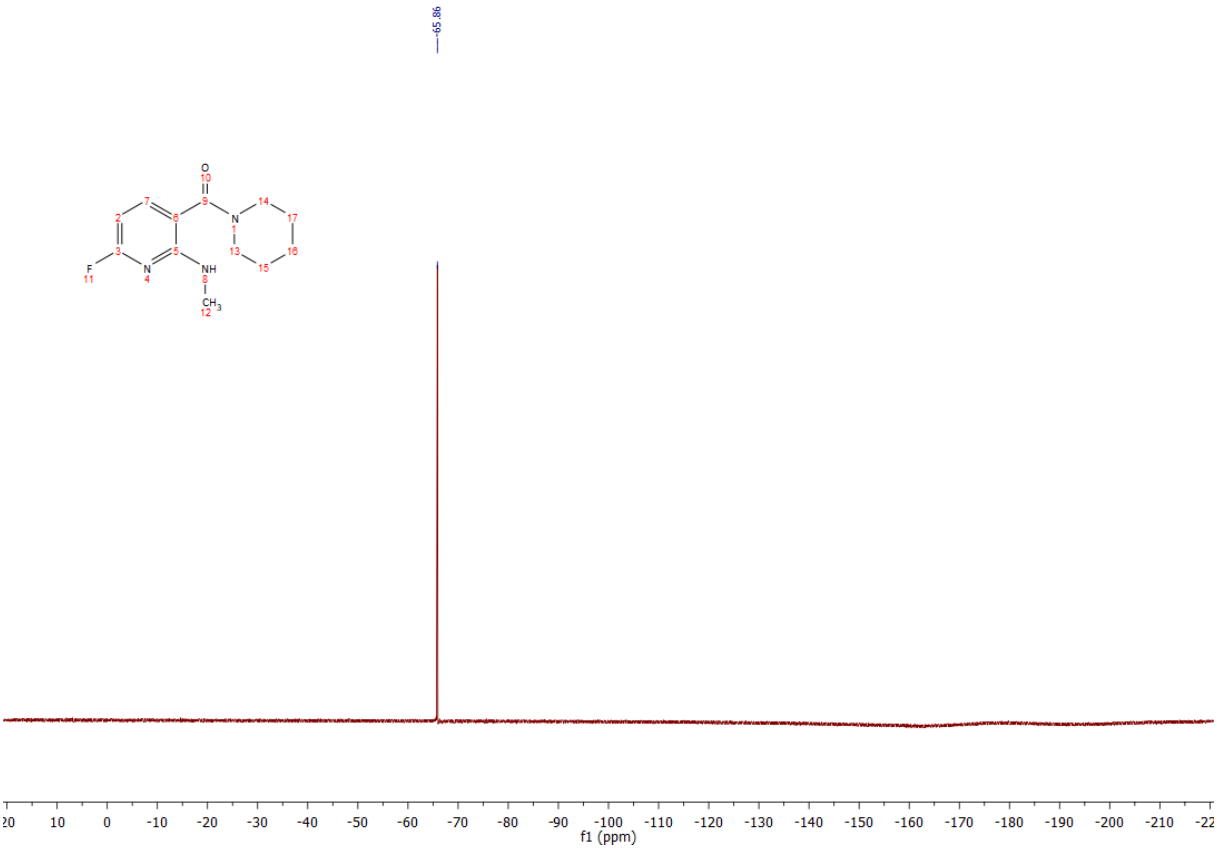
-65.86
O
10
9
7
2
6
N
1
14
17
13
16
15
3
5
F
11
N
4
NH
8
CH3
12
20 10 0 -10 -20 -30 -40 -50 -60 -70 -80 -90 -100 -110 -120 -130 -140 -150 -160 -170 -180 -190 -200 -210 -22
f1 (ppm)

2.32 Compound **5l**

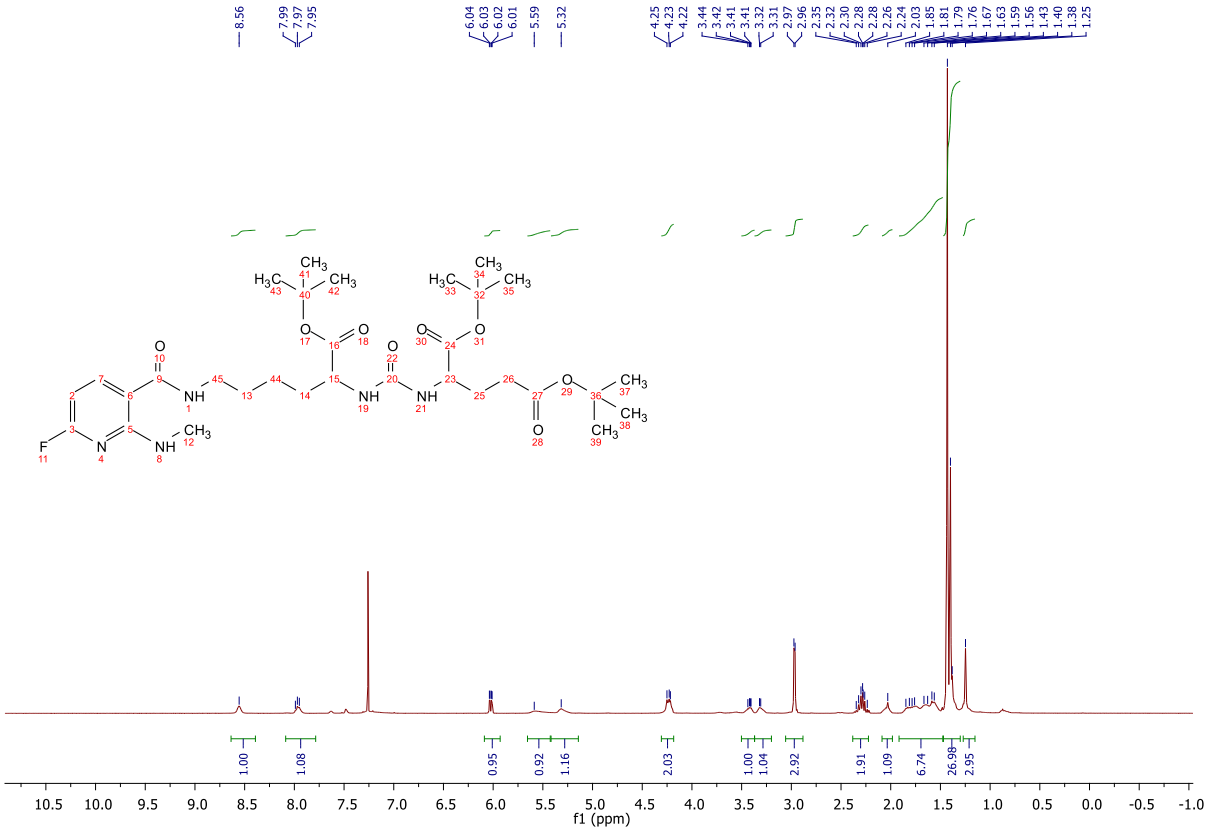

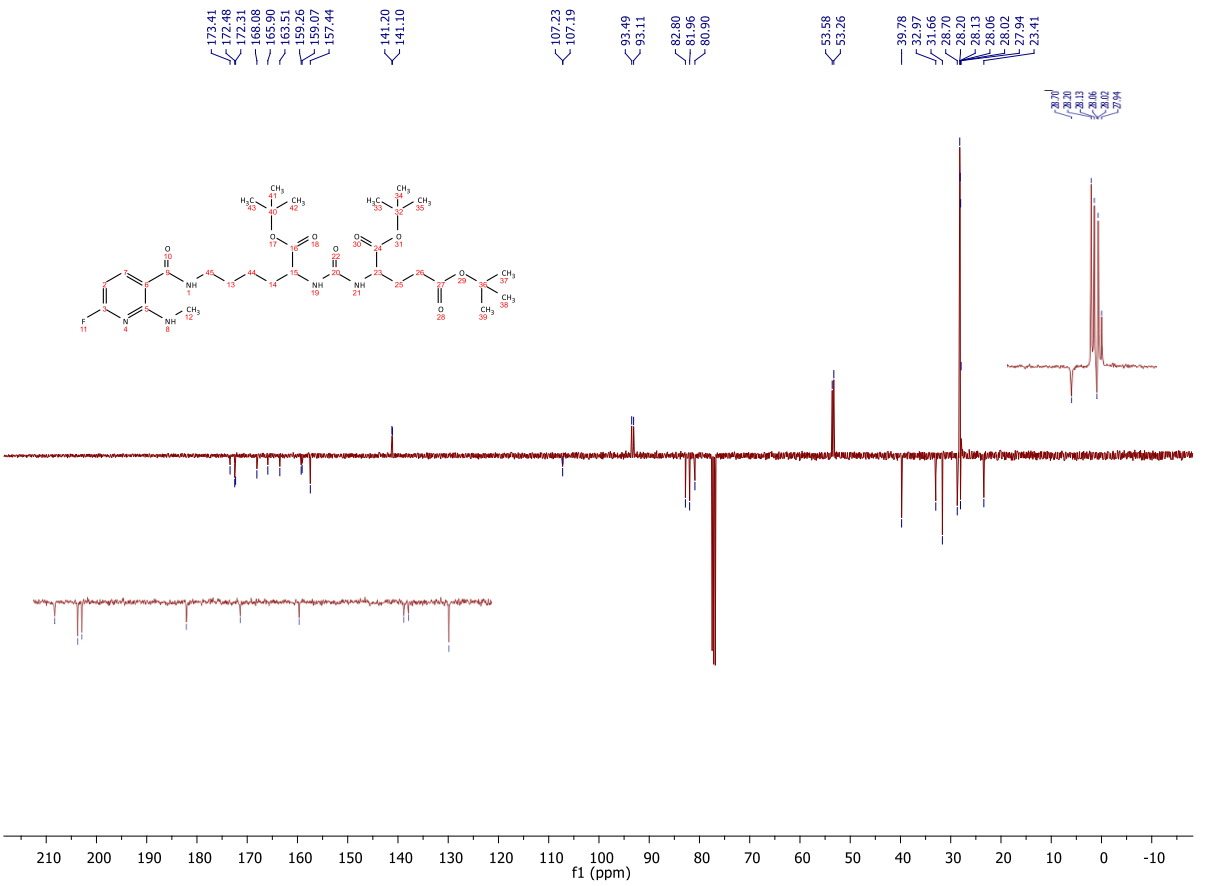

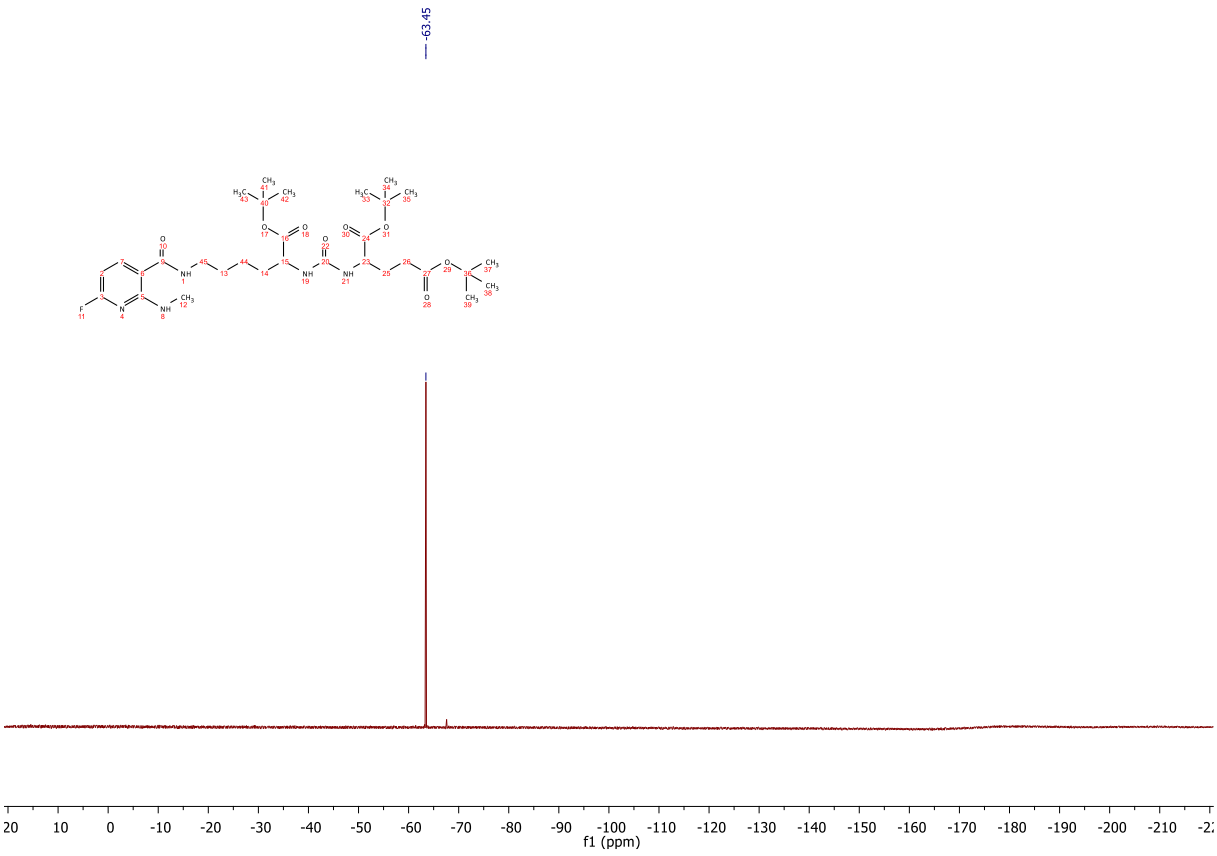
-63.45
20
10
0
-10
-20
-30
-40
-50
-60
-70
-80
-90
-100
-110
-120
-130
-140
-150
-160
-170
-180
-190
-200
-210
f1 (ppm)

2.33 Compound **5m**

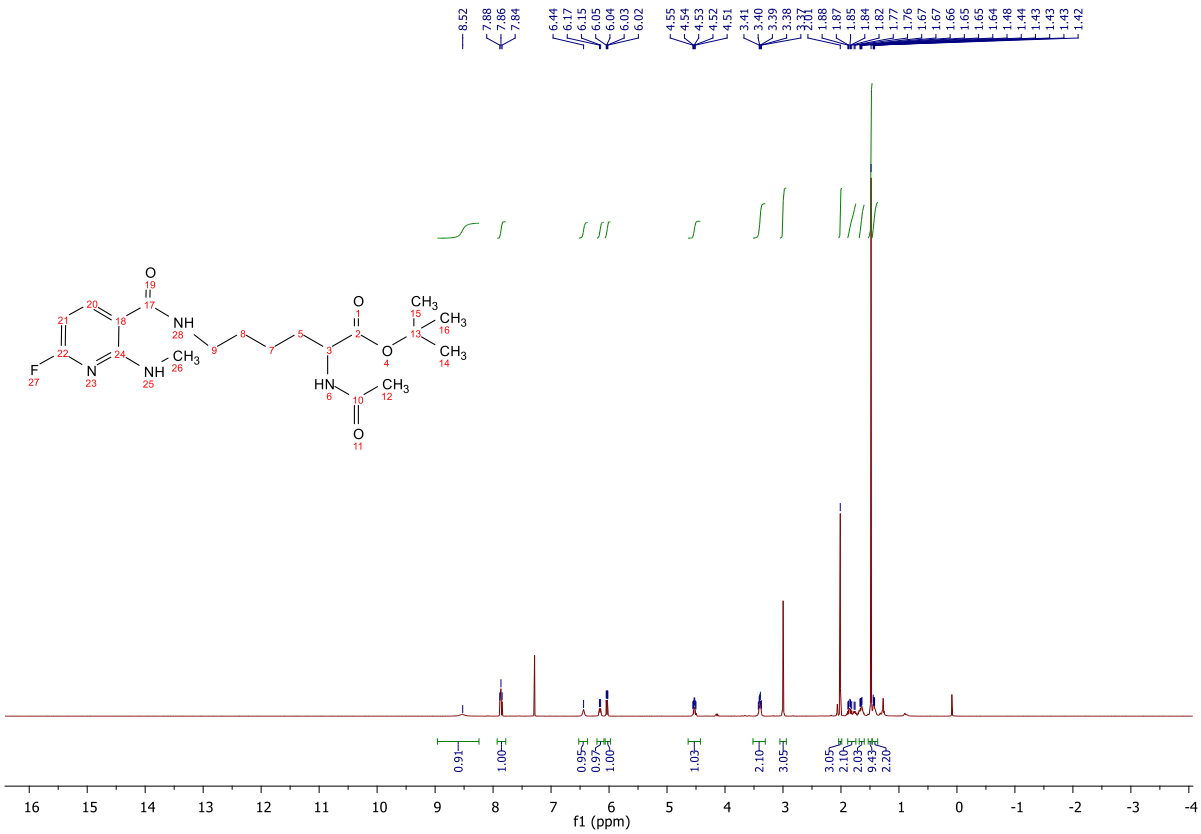

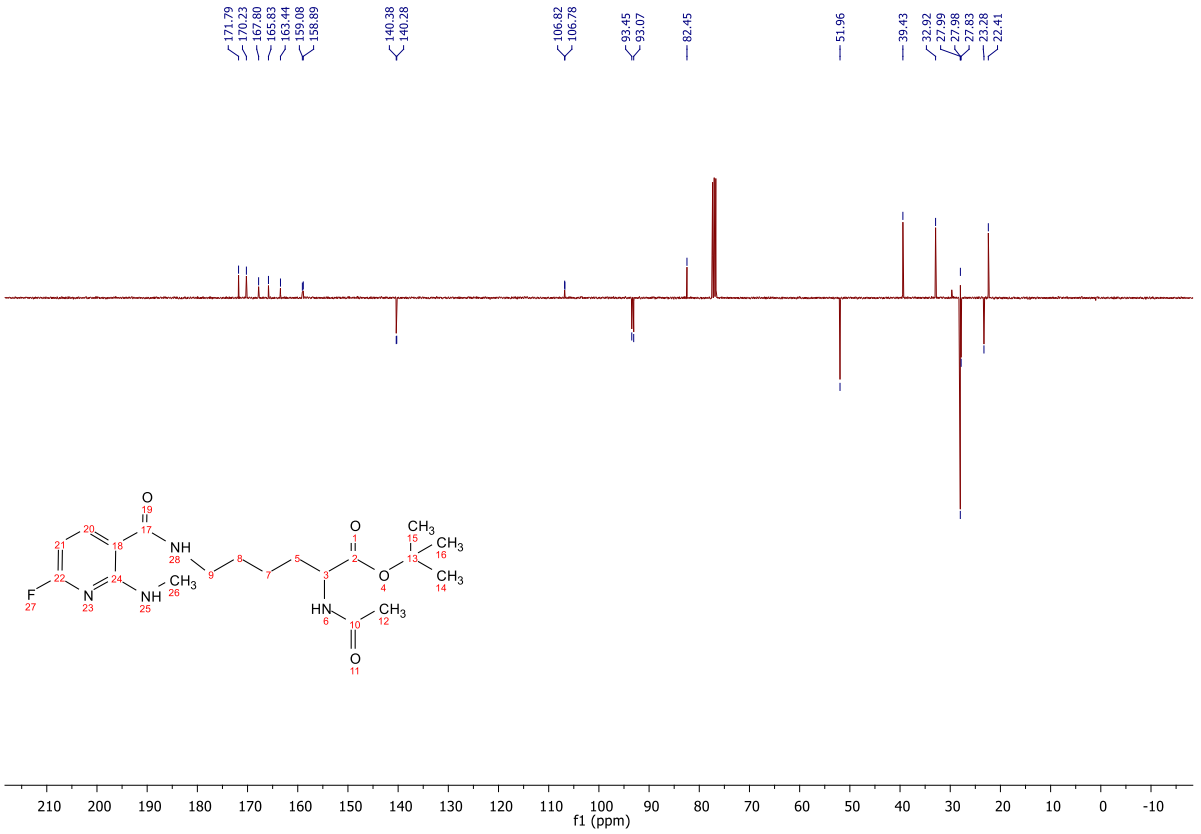

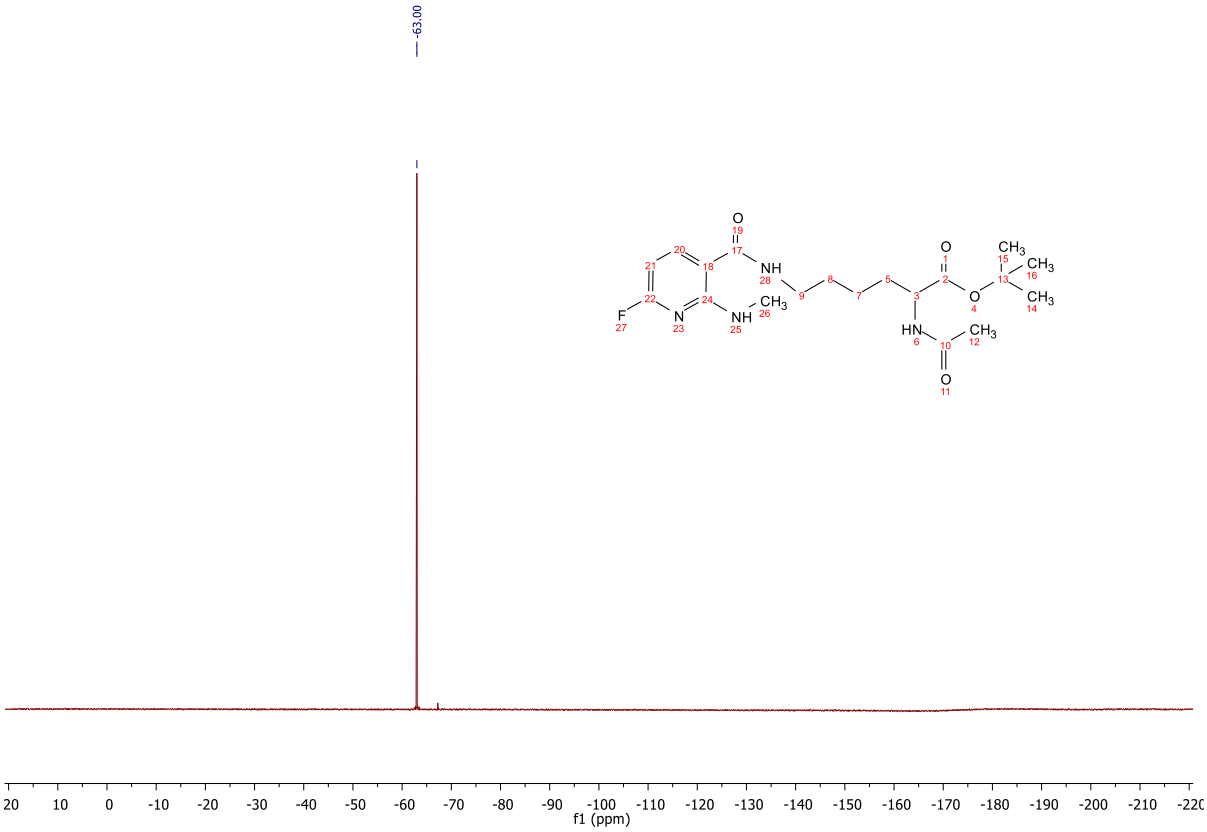
-63.00
20
10
0
-10
-20
-30
-40
-50
-60
-70
-80
-90
-100
-110
-120
-130
-140
-150
-160
-170
-180
-190
-200
-210
-220
f1 (ppm)

2.34 Compound **5n**

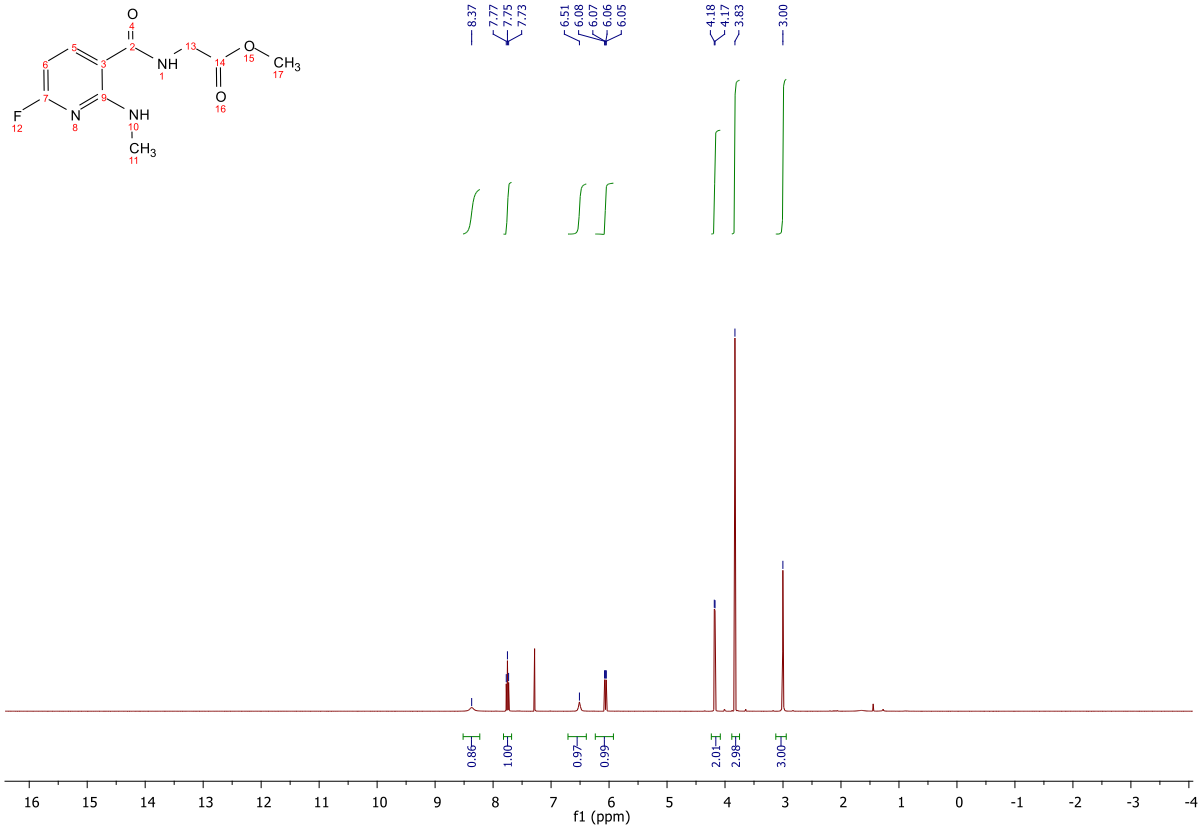

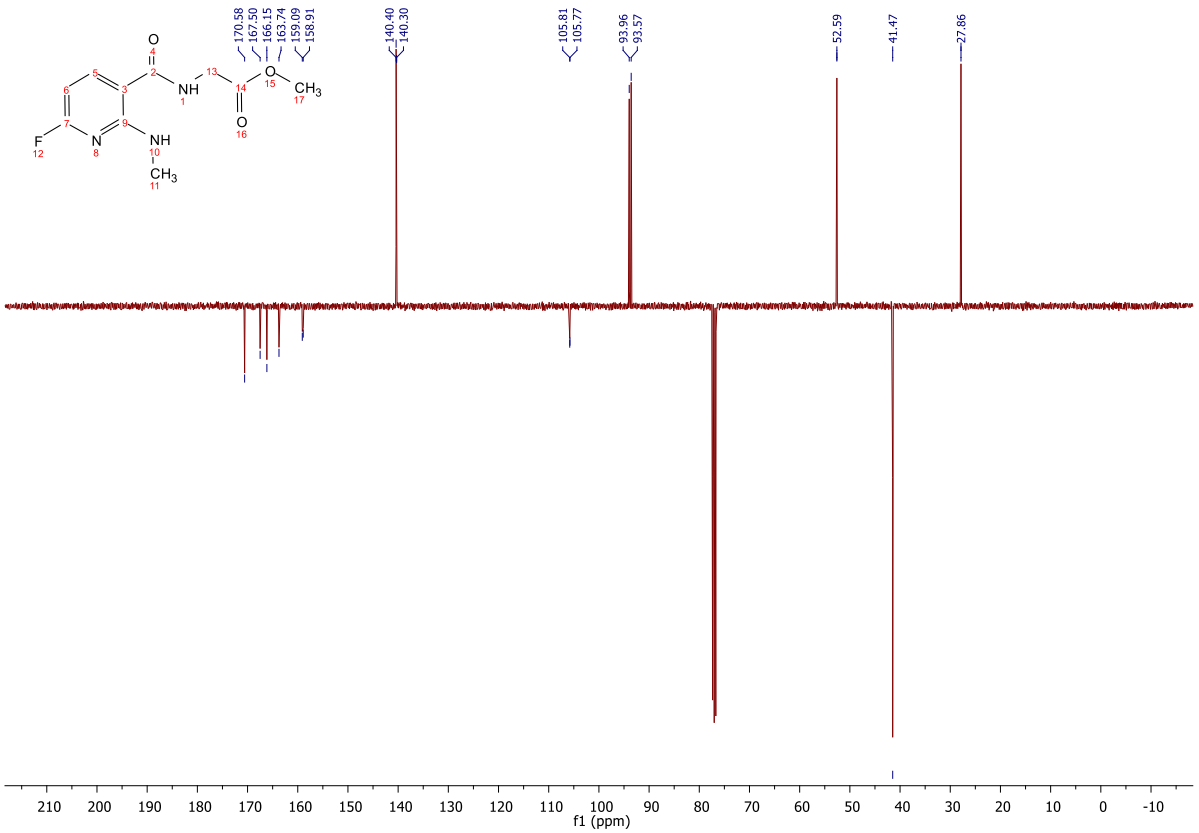

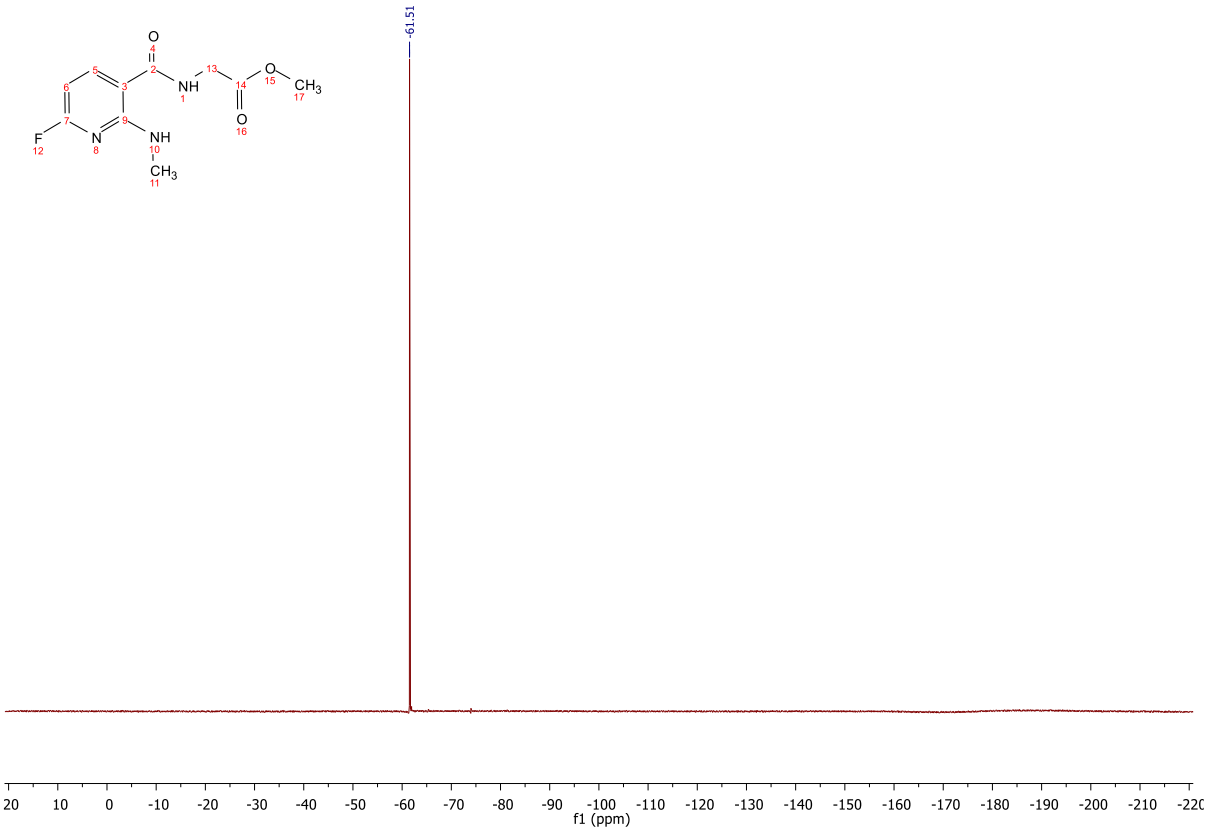
-61.51
O
4
2
NH
1
13
14
O
15
CH3
17
O
16
3
5
6
7
F
12
N
8
9
NH
10
CH3
11
20
10
0
-10
-20
-30
-40
-50
-60
-70
-80
-90
-100
-110
-120
-130
-140
-150
-160
-170
-180
-190
-200
-210
-220
f1 (ppm)

2.35 Compound **5o**

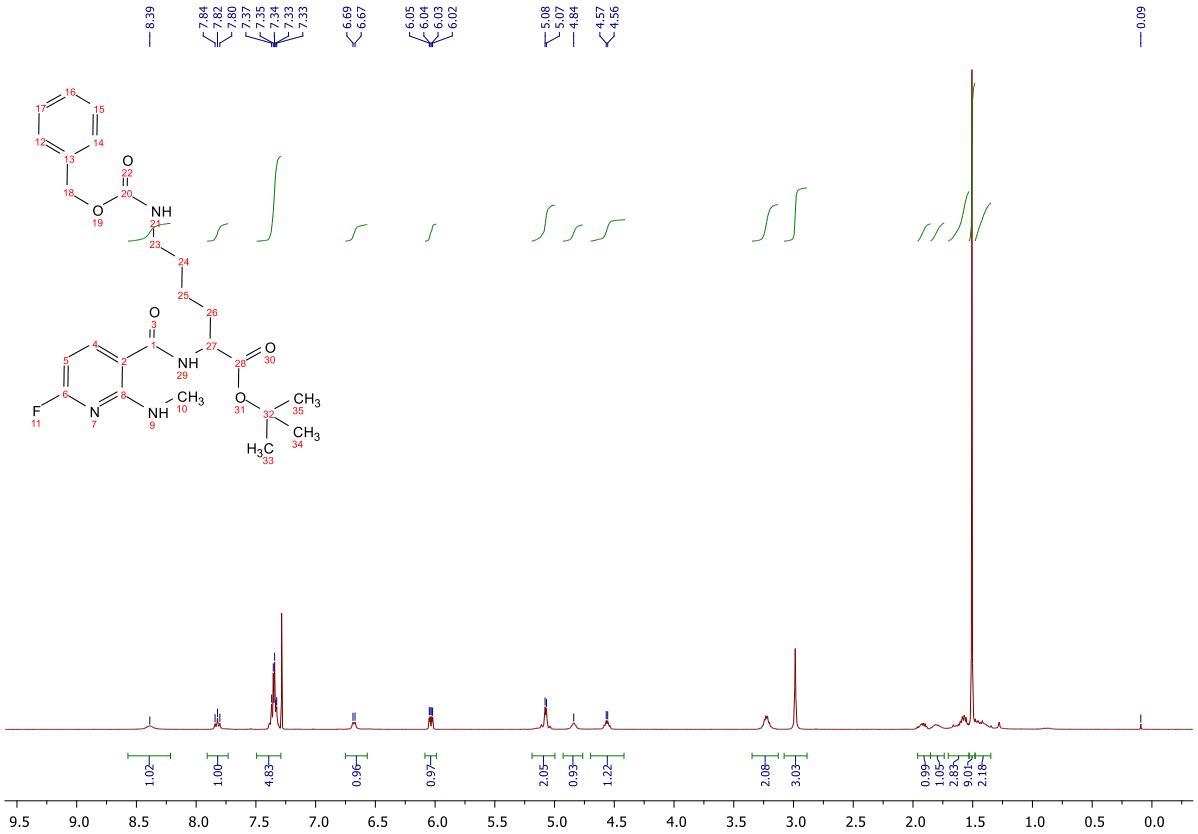

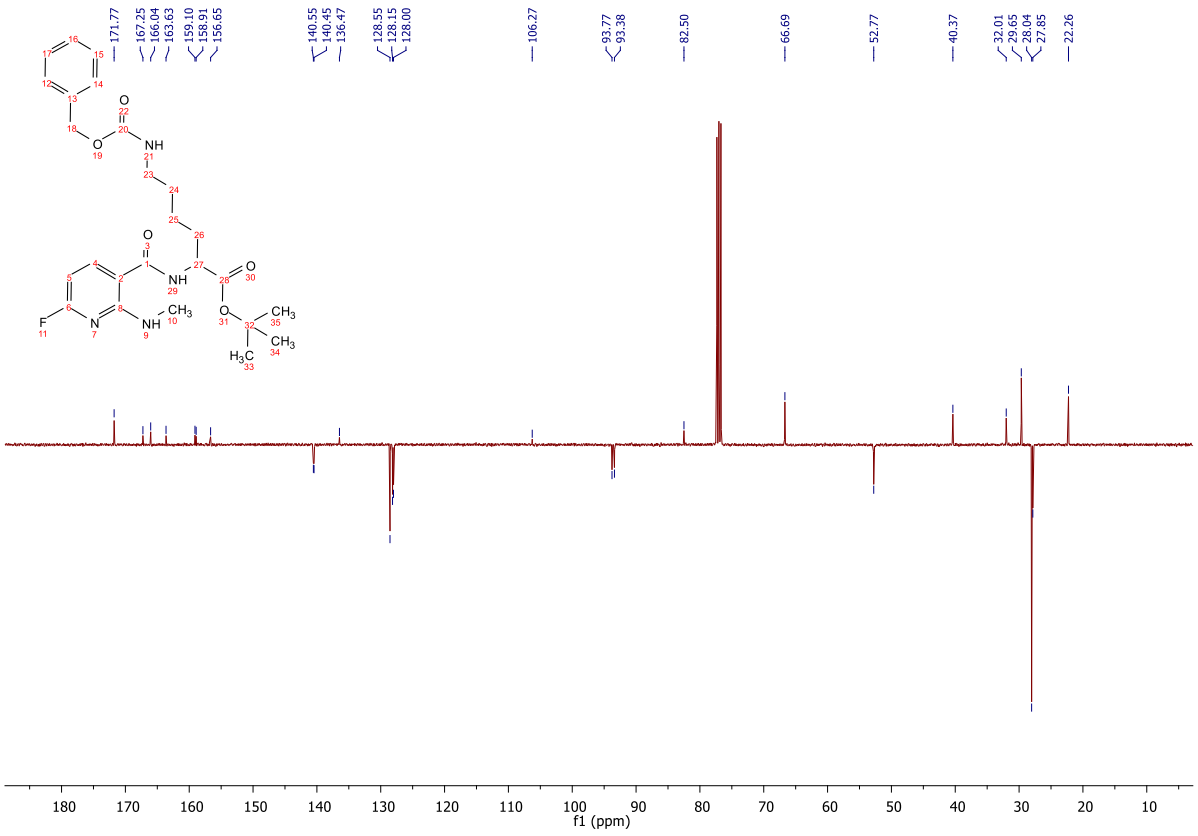

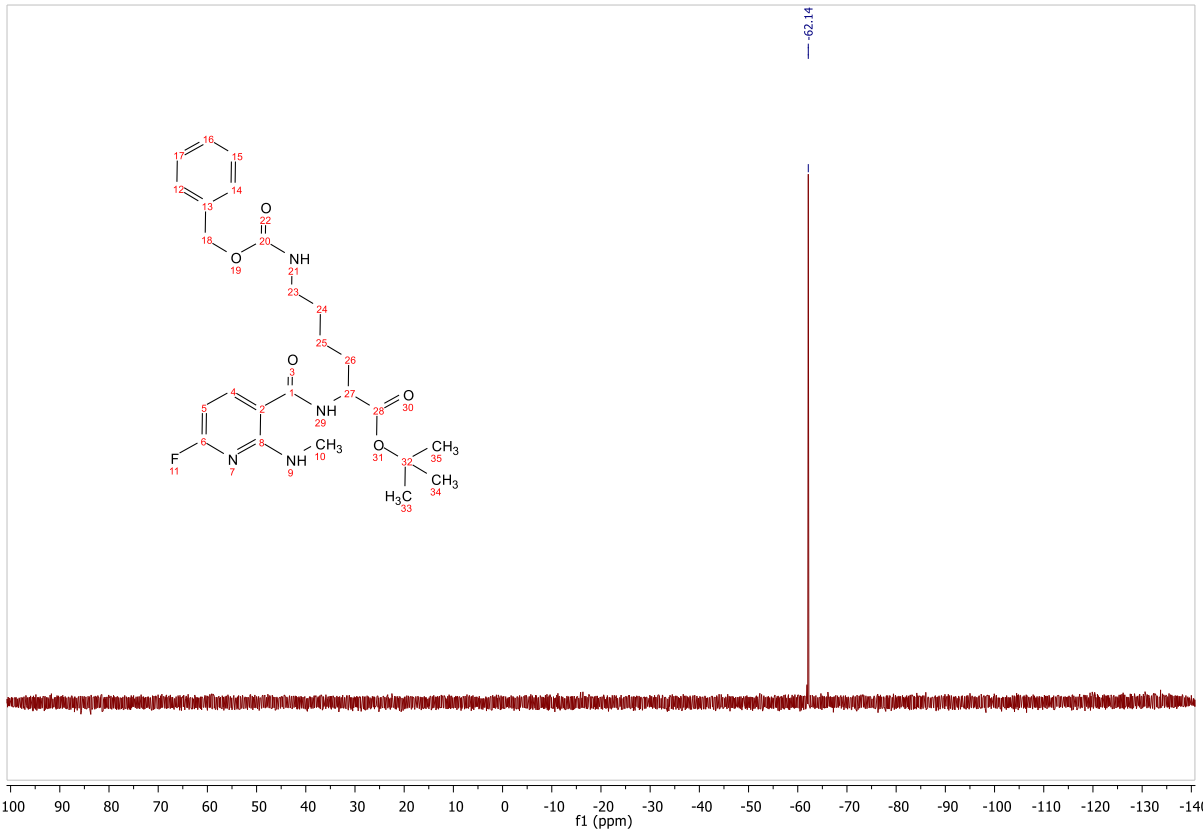
-62.14
100 90 80 70 60 50 40 30 20 10 0 -10 -20 -30 -40 -50 -60 -70 -80 -90 -100 -110 -120 -130 -140
f1 (ppm)

2.36 Compound **5p** (JK-PSMA-15)

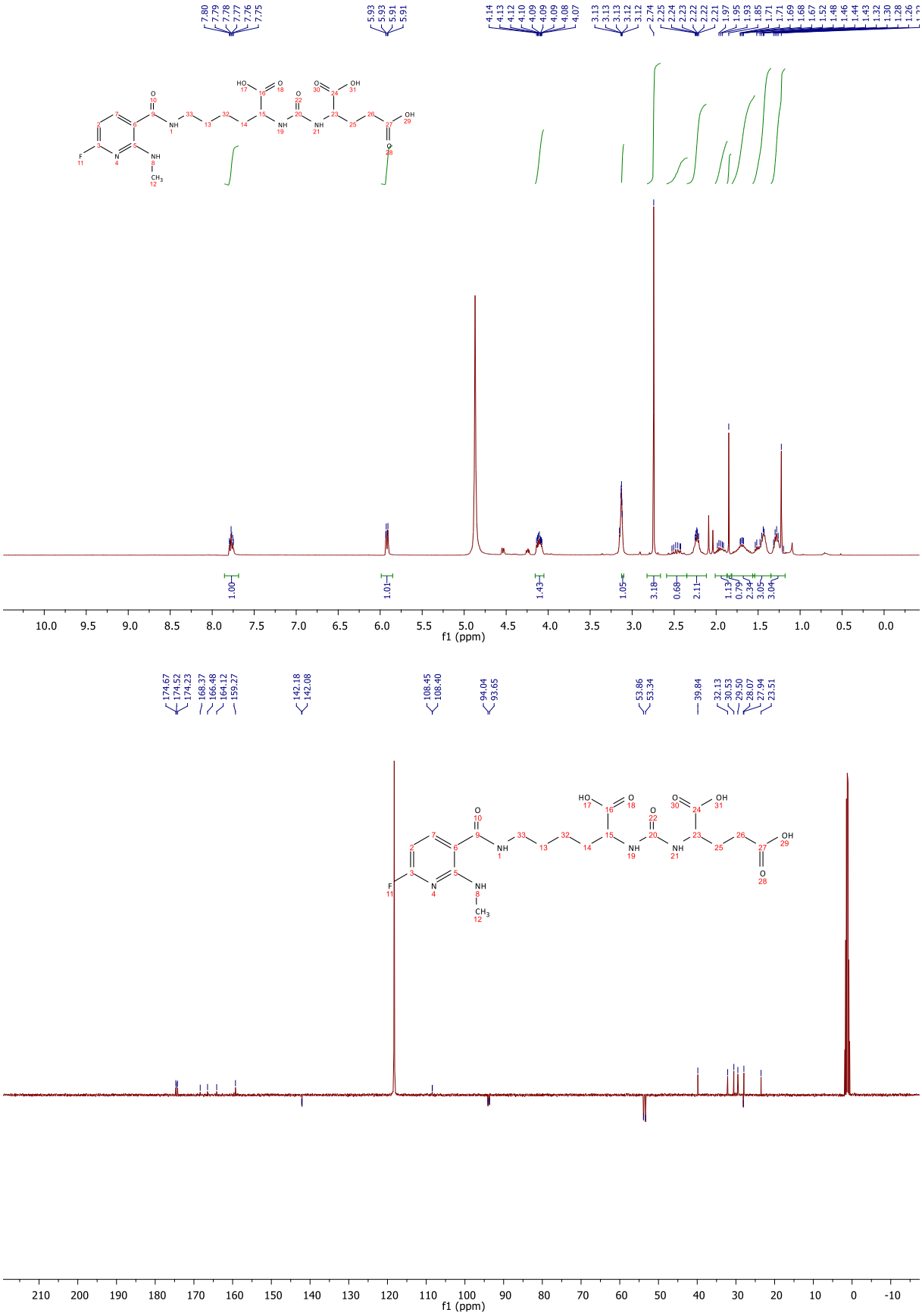

2.37 Compound **6a**

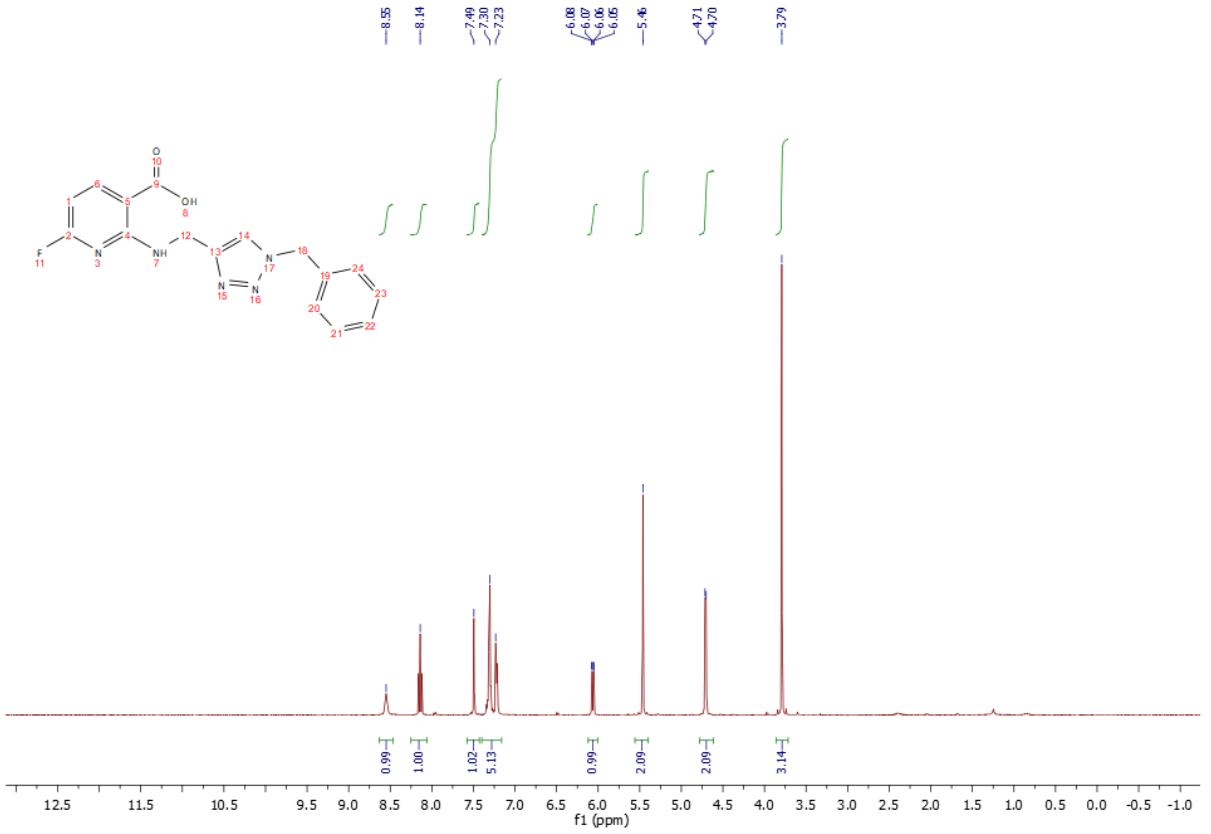

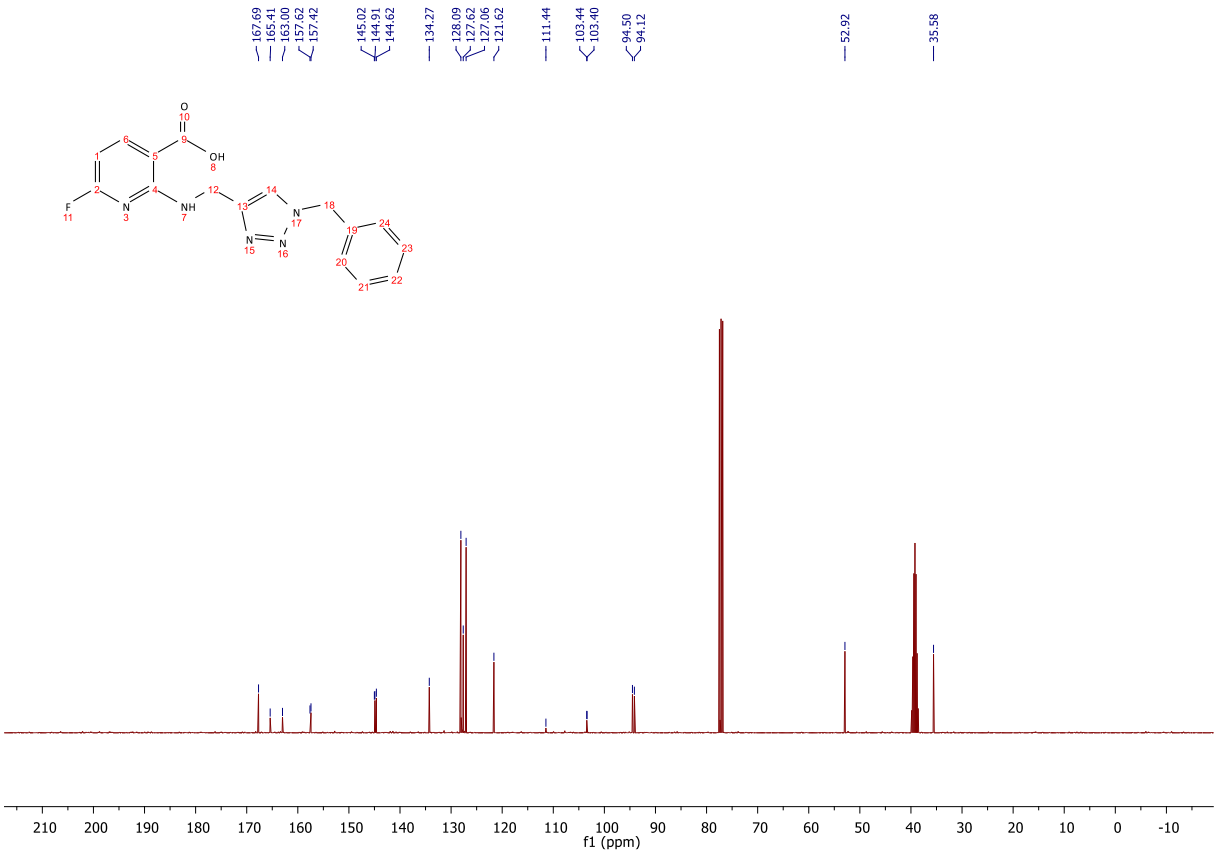


-59.80
O
10
9
OH
8
6
5
1
2
4
F
11
N
3
NH
7
12
13
14
N
17
18
19
24
23
N
15
N
16
20
21
22
20 10 0 -10 -20 -30 -40 -50 -60 -70 -80 -90 -100 -110 -120 -130 -140 -150 -160 -170 -180 -190 -200 -210 -220
f1 (ppm)

2.38 Compound **10**

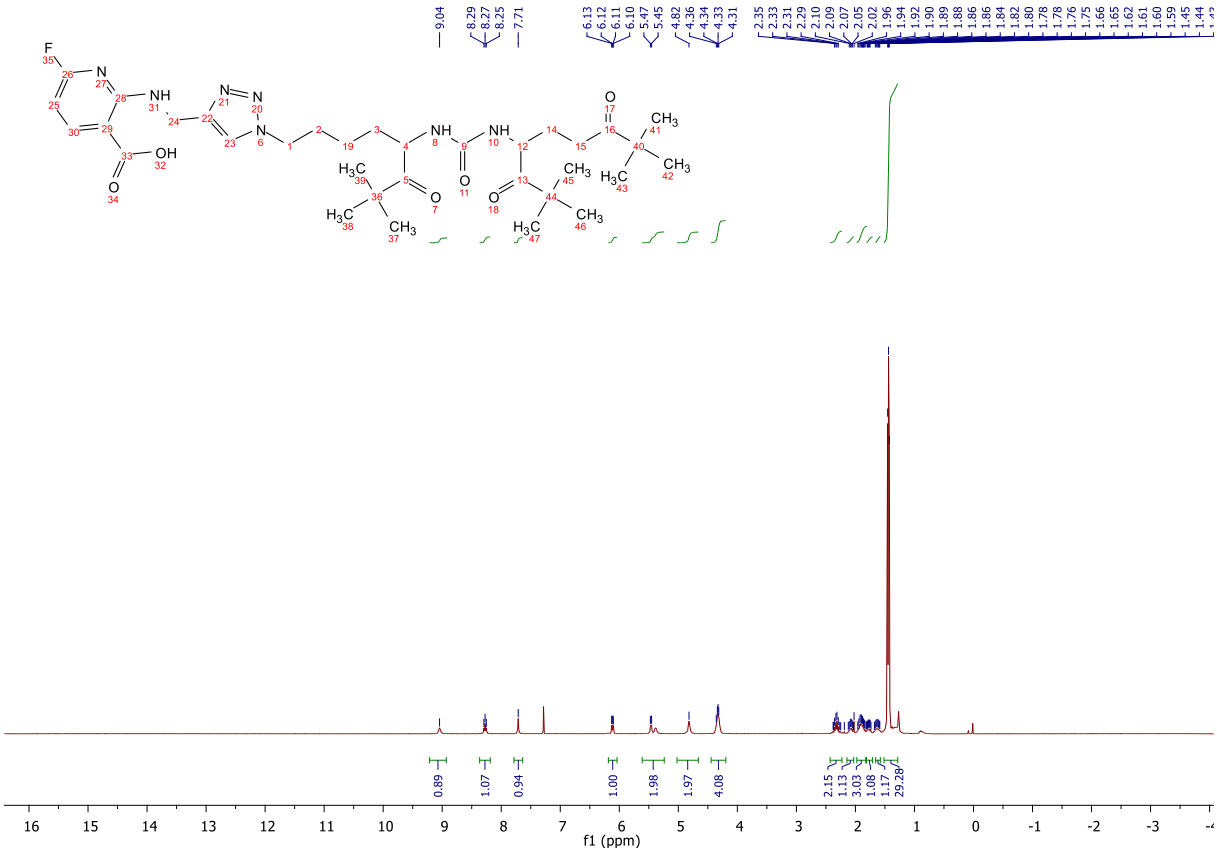

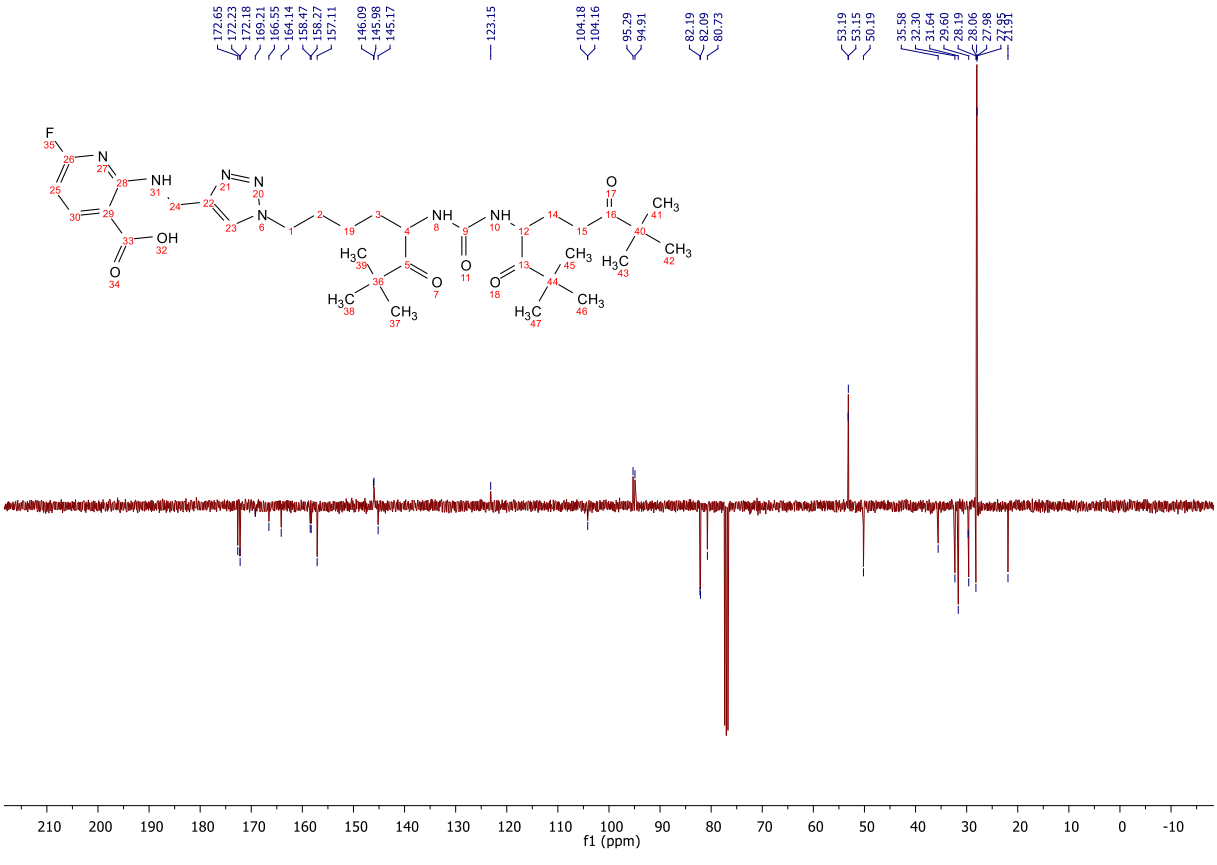

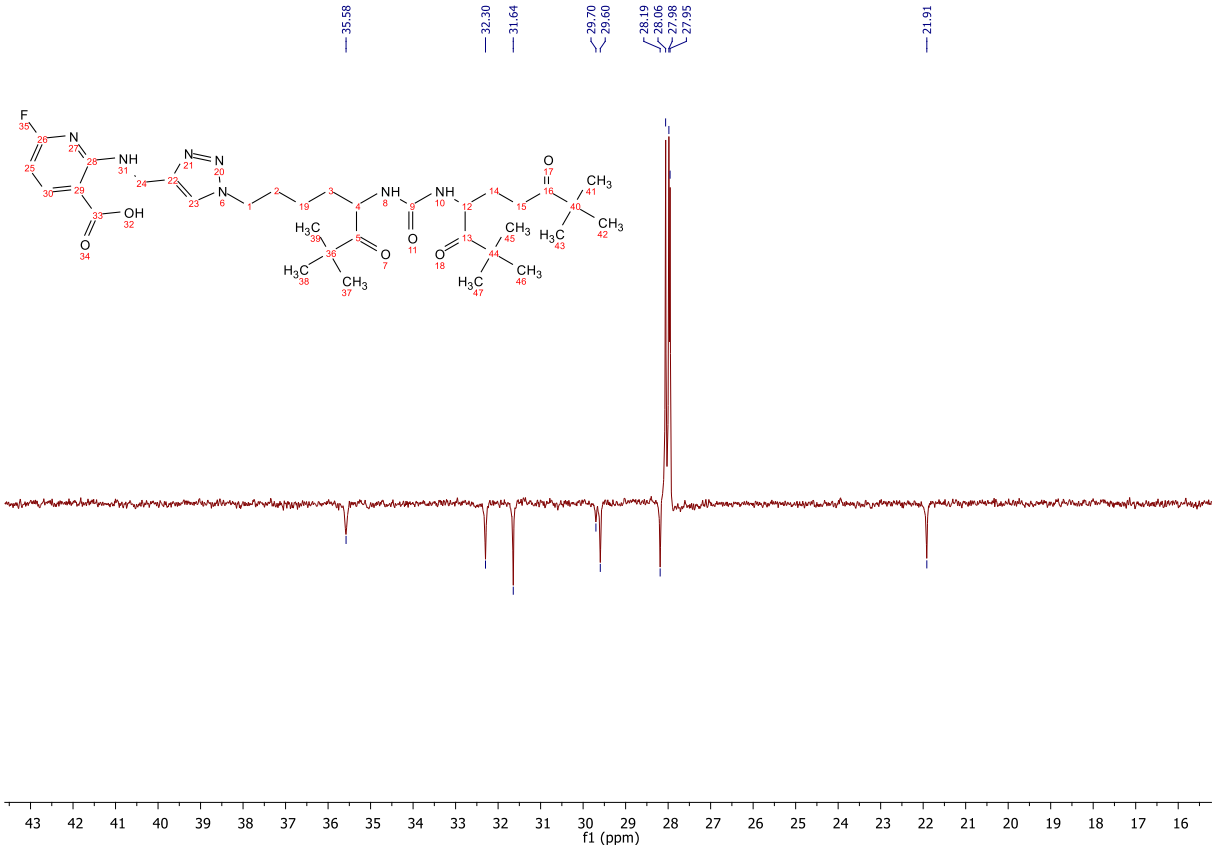
35.58
32.30
31.64
29.70
29.60
28.19
28.06
27.98
27.95
21.91
43 42 41 40 39 38 37 36 35 34 33 32 31 30 29 28 27 26 25 24 23 22 21 20 19 18 17 16
f1 (ppm)

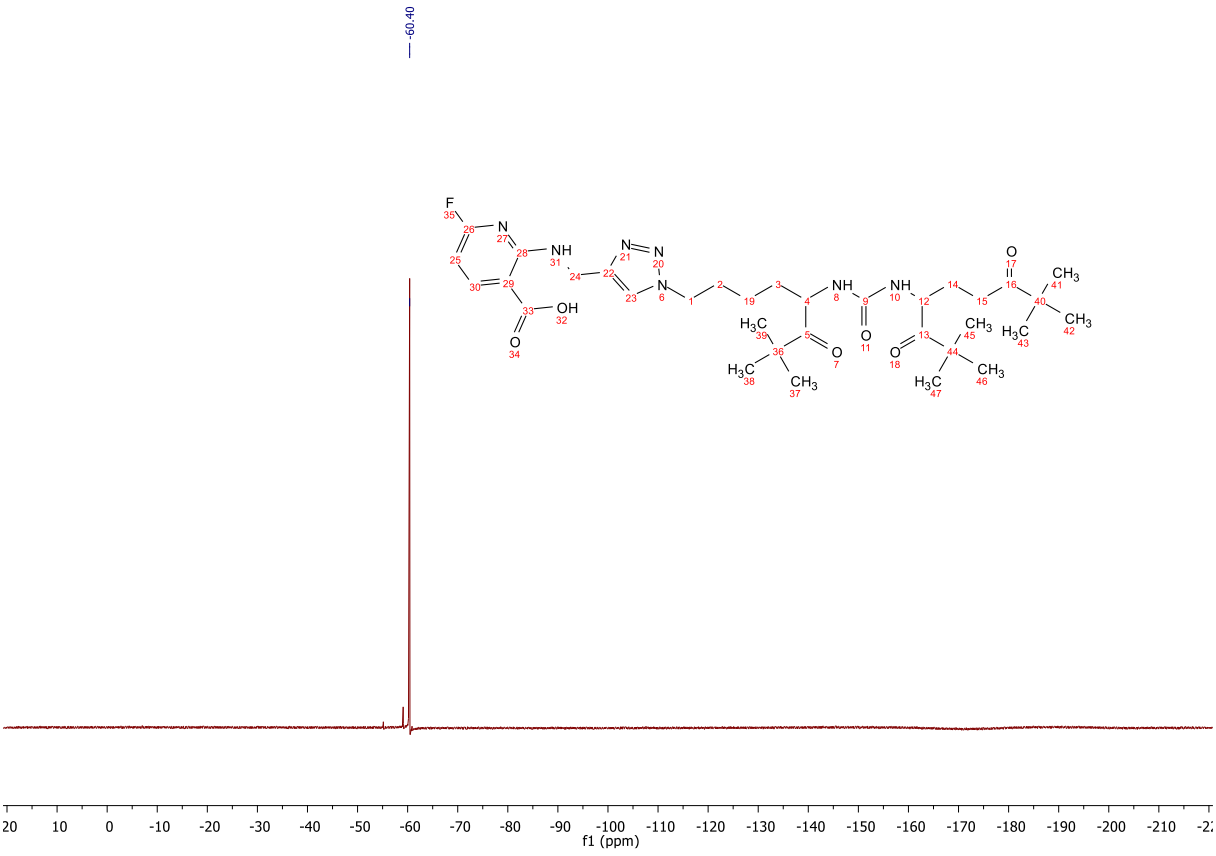
-60.40
20 10 0 -10 -20 -30 -40 -50 -60 -70 -80 -90 -100 -110 -120 -130 -140 -150 -160 -170 -180 -190 -200 -210
f1 (ppm)

2.39 Compound **6b** (JK-PSMA-16)

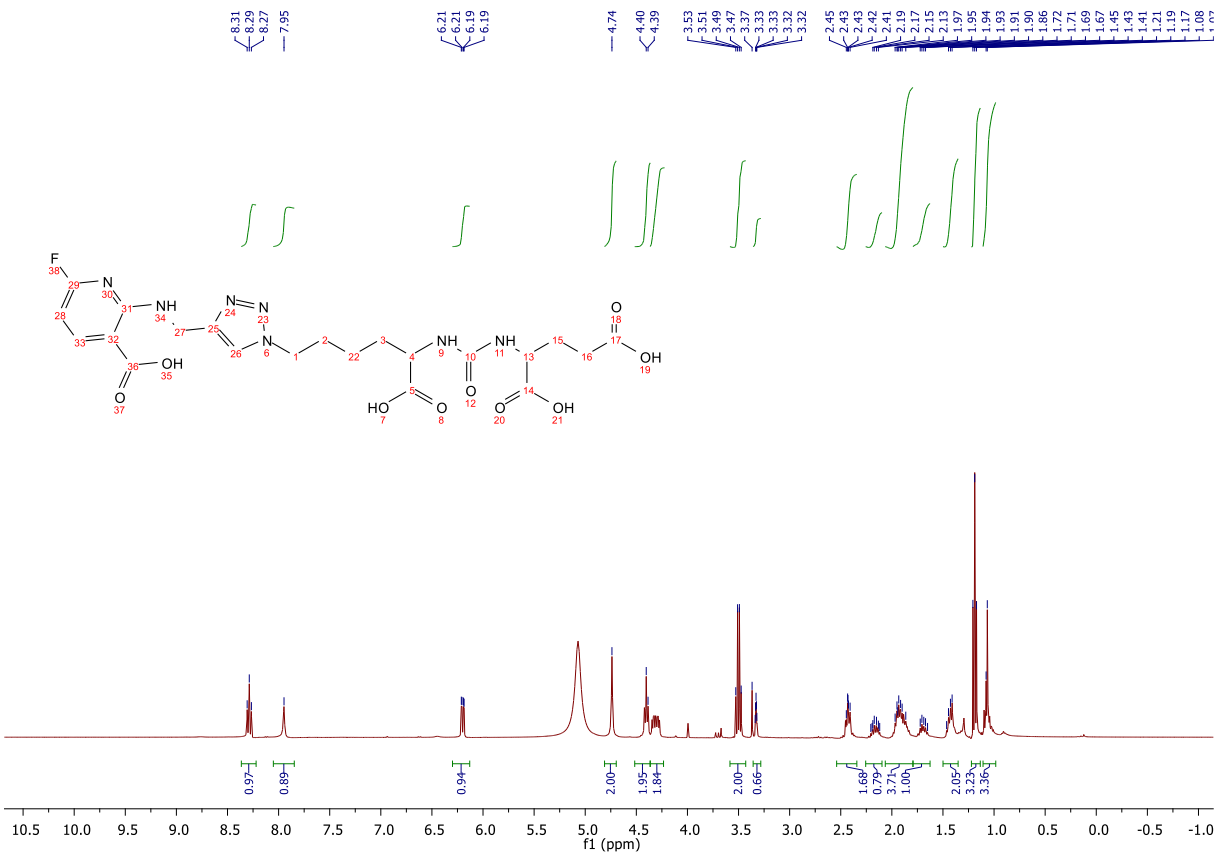

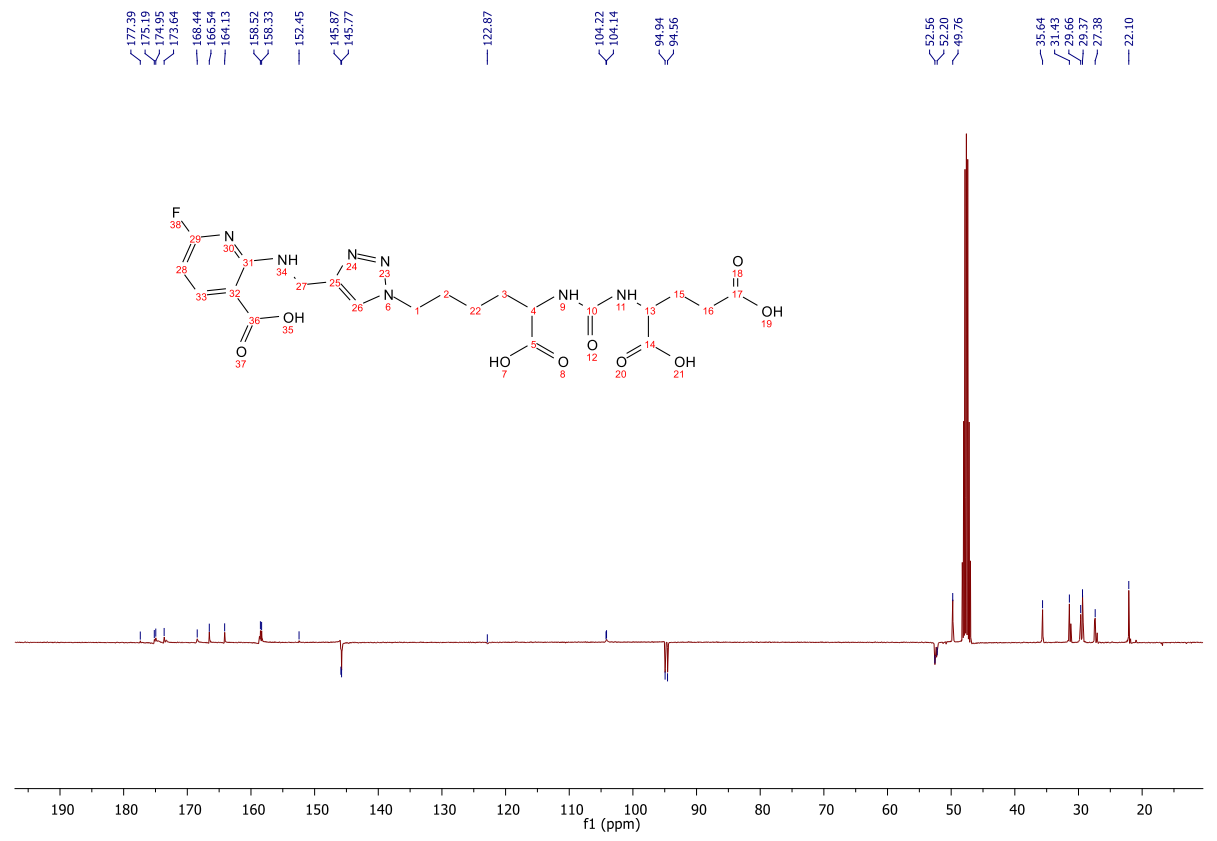

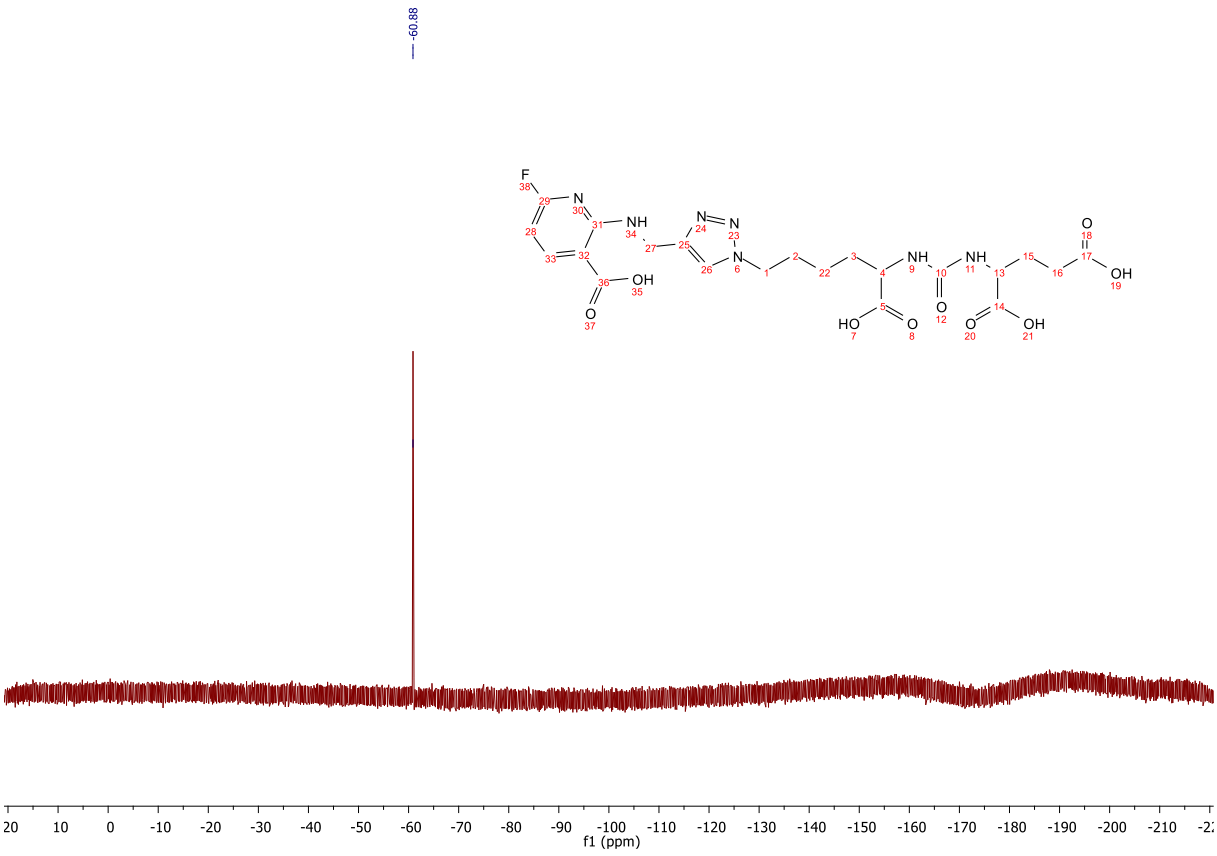
-60.88
F
38
N
29
30
NH
31
34
28
33
32
36
OH
35
O
37
N
24
N
23
27
25
26
N
6
1
2
22
3
4
NH
9
10
NH
11
13
15
16
O
18
17
OH
19
5
HO
7
O
8
O
12
14
O
20
OH
21
20
10
0
-10
-20
-30
-40
-50
-60
-70
-80
-90
-100
-110
-120
-130
-140
-150
-160
-170
-180
-190
-200
-210
f1 (ppm)

2.40 Compound **6c**

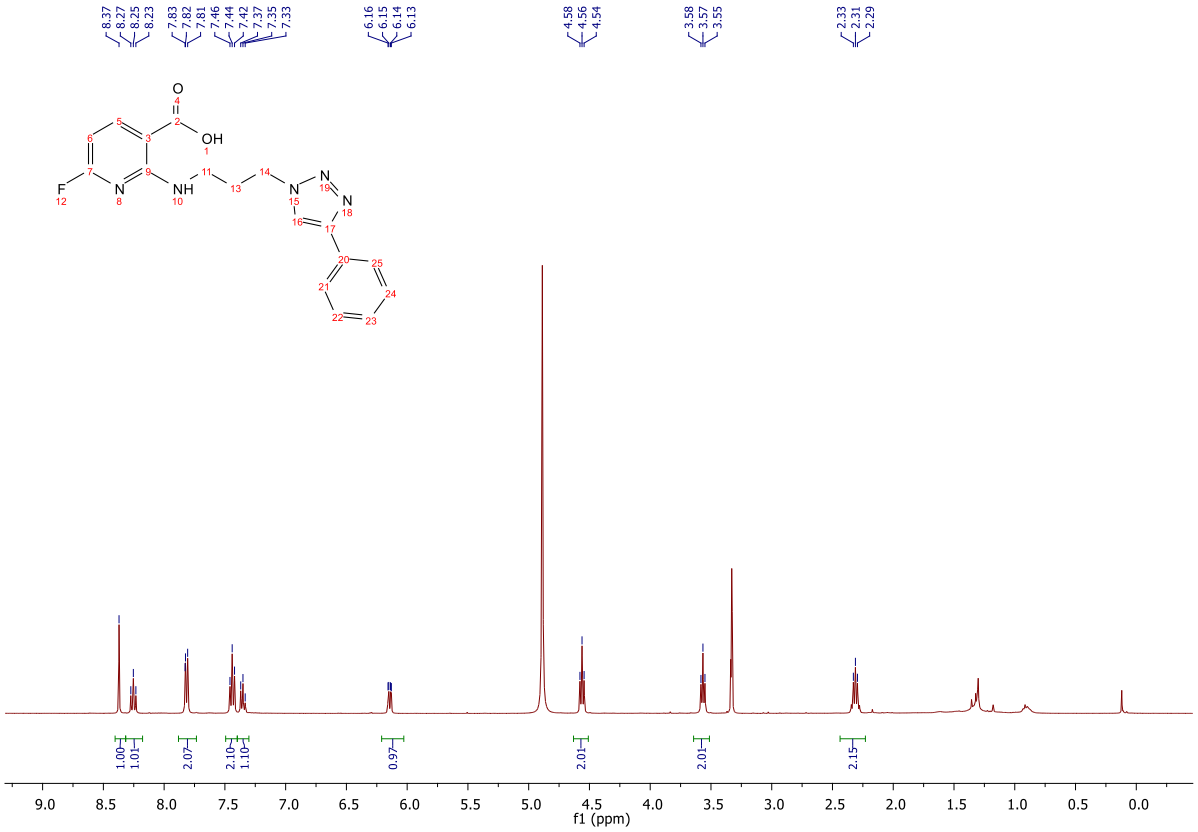

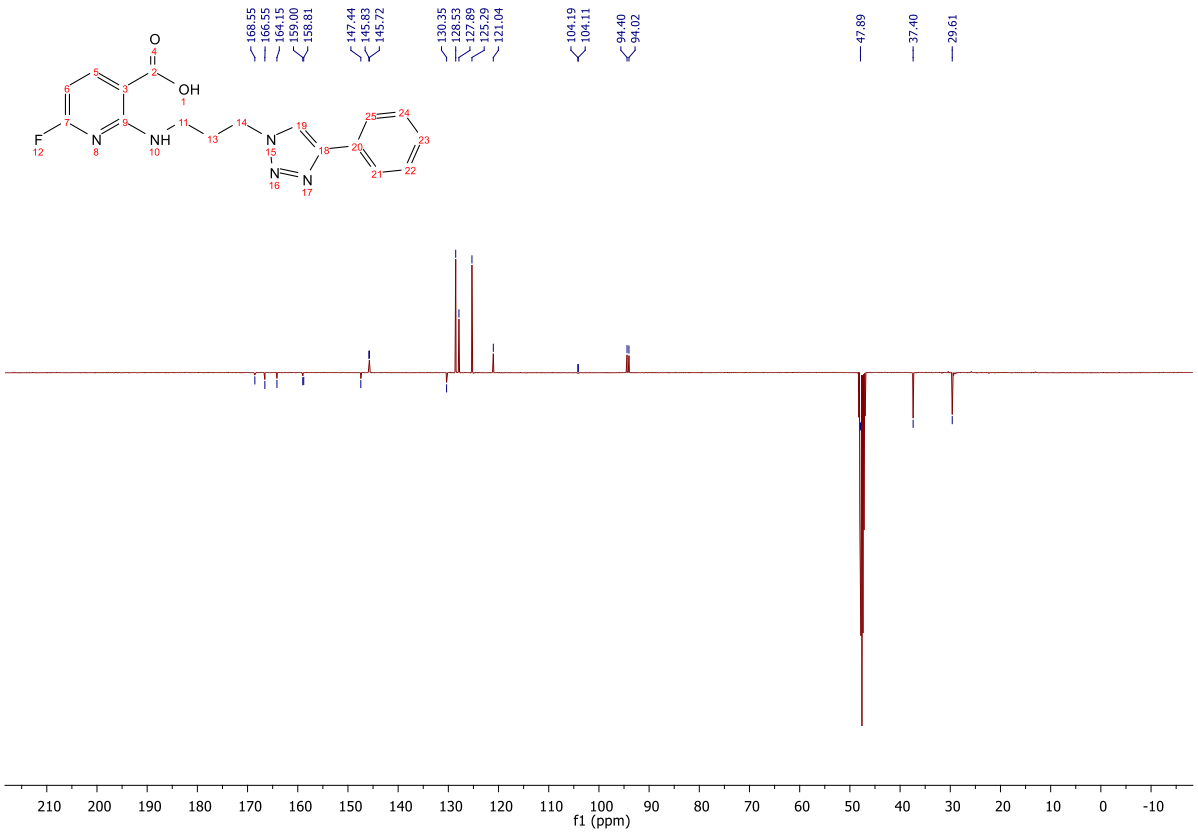

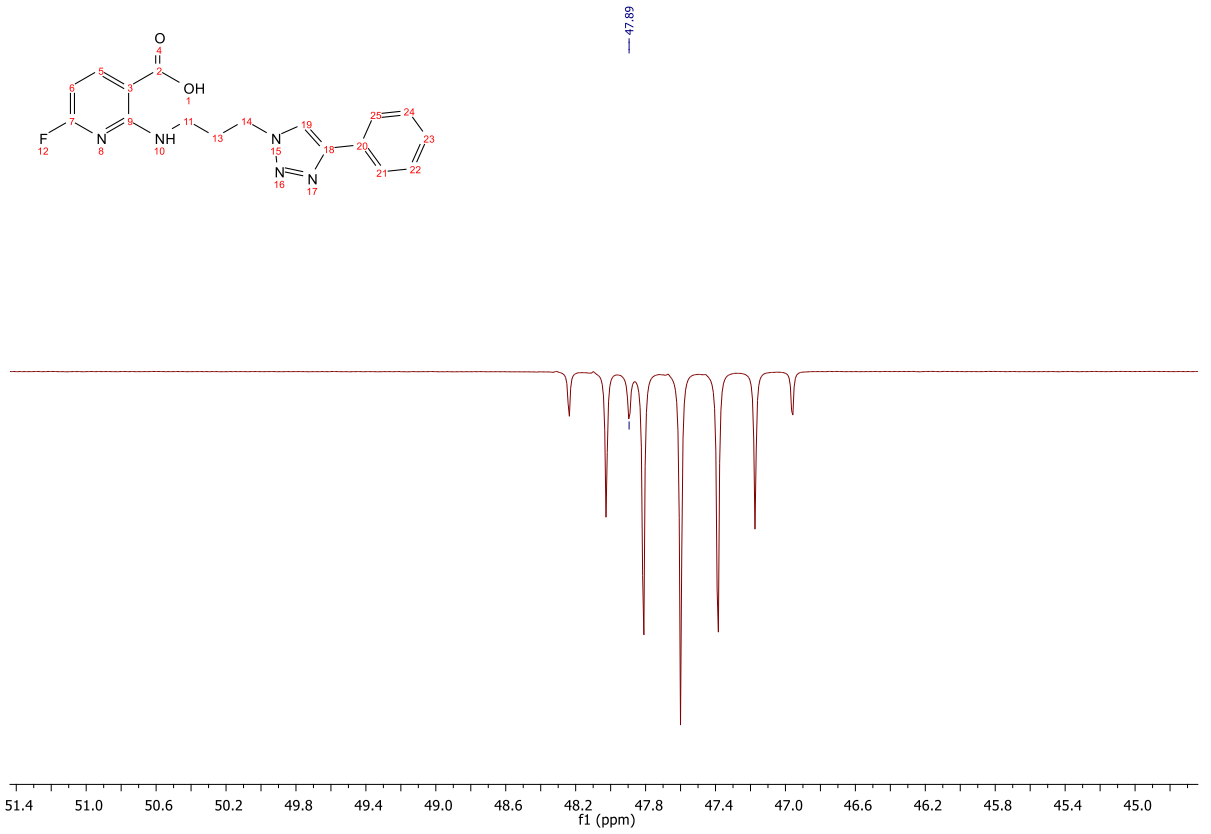
47.89
51.4
51.0
50.6
50.2
49.8
49.4
49.0
48.6
48.2
47.8
47.4
47.0
46.6
46.2
45.8
45.4
45.0
f1 (ppm)

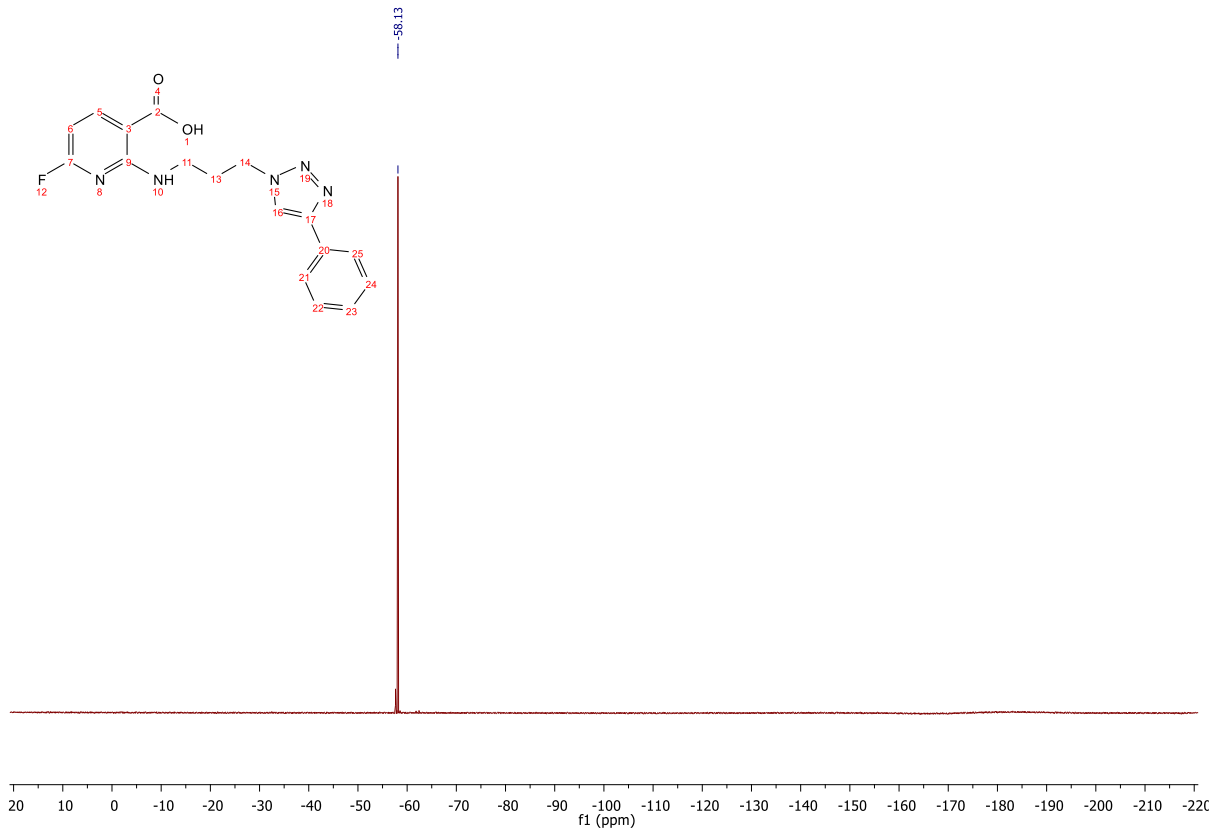
-58.13
20
10
0
-10
-20
-30
-40
-50
-60
-70
-80
-90
-100
-110
-120
-130
-140
-150
-160
-170
-180
-190
-200
-210
f1 (ppm)

2.41 Compound **11**

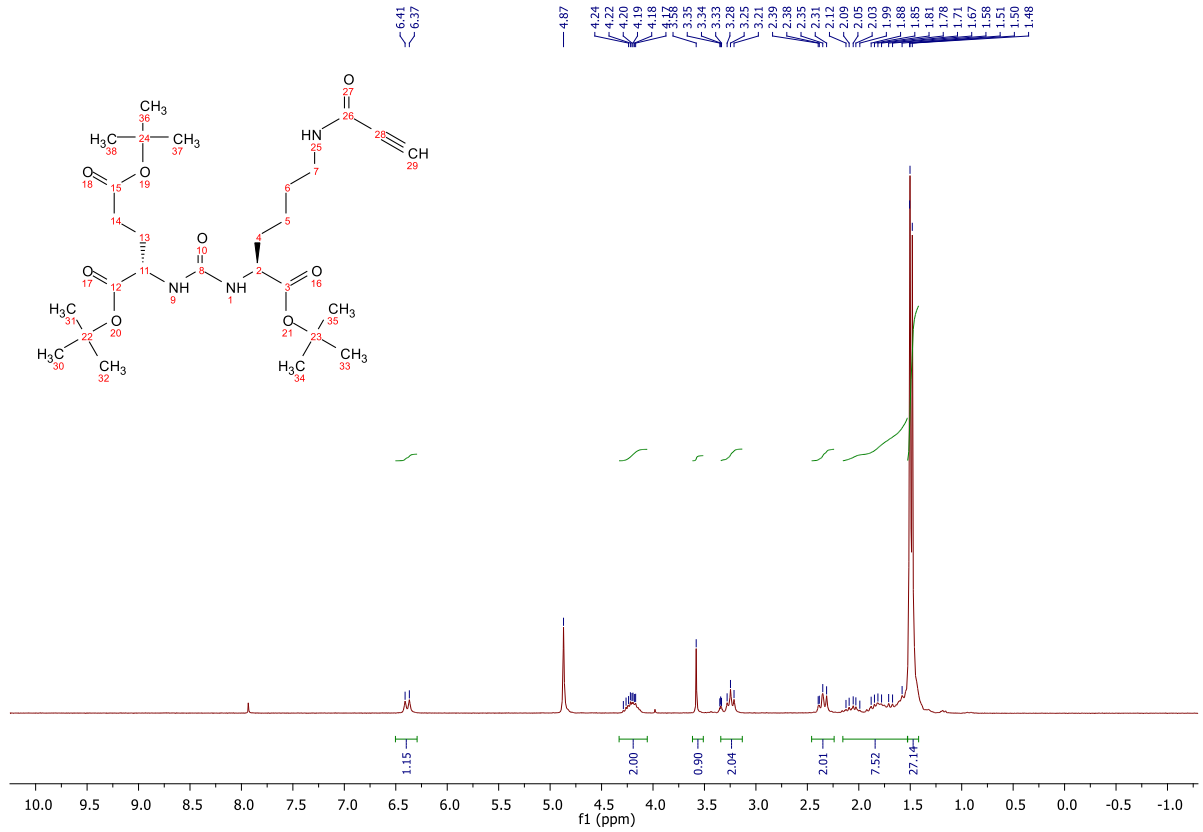

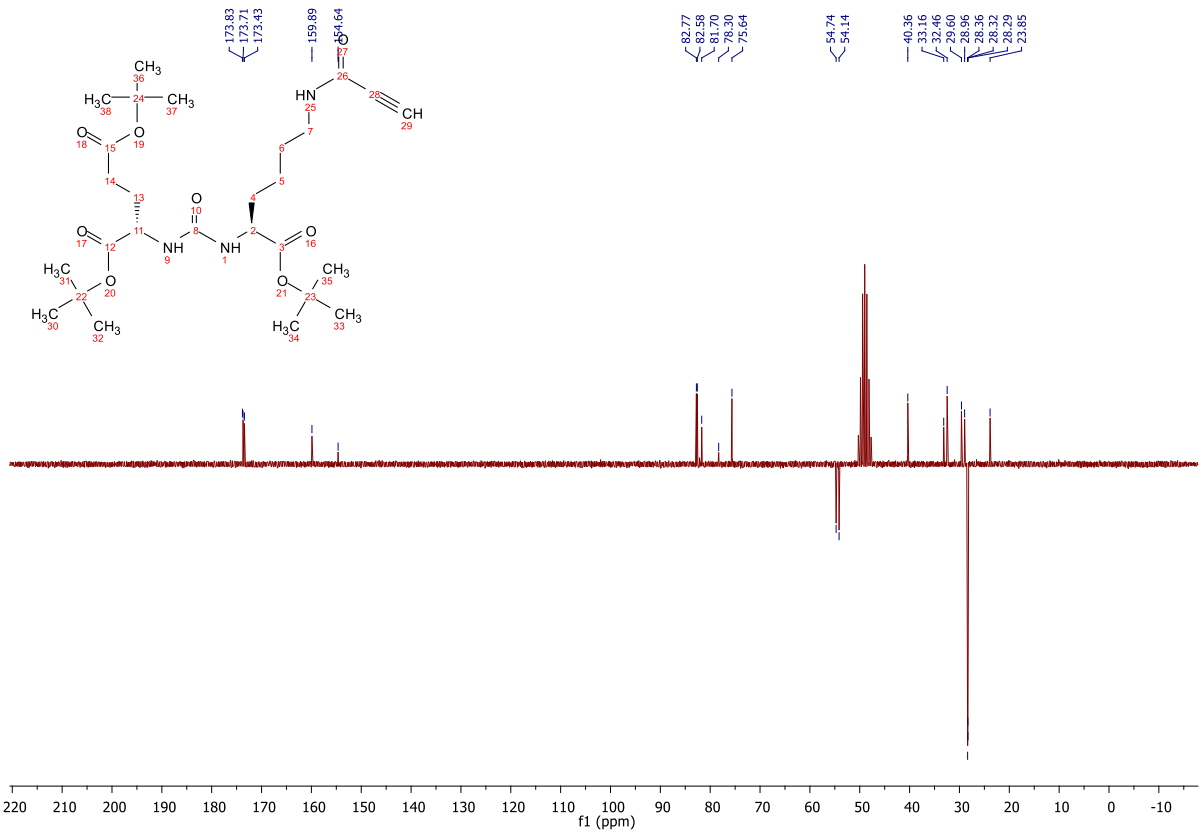

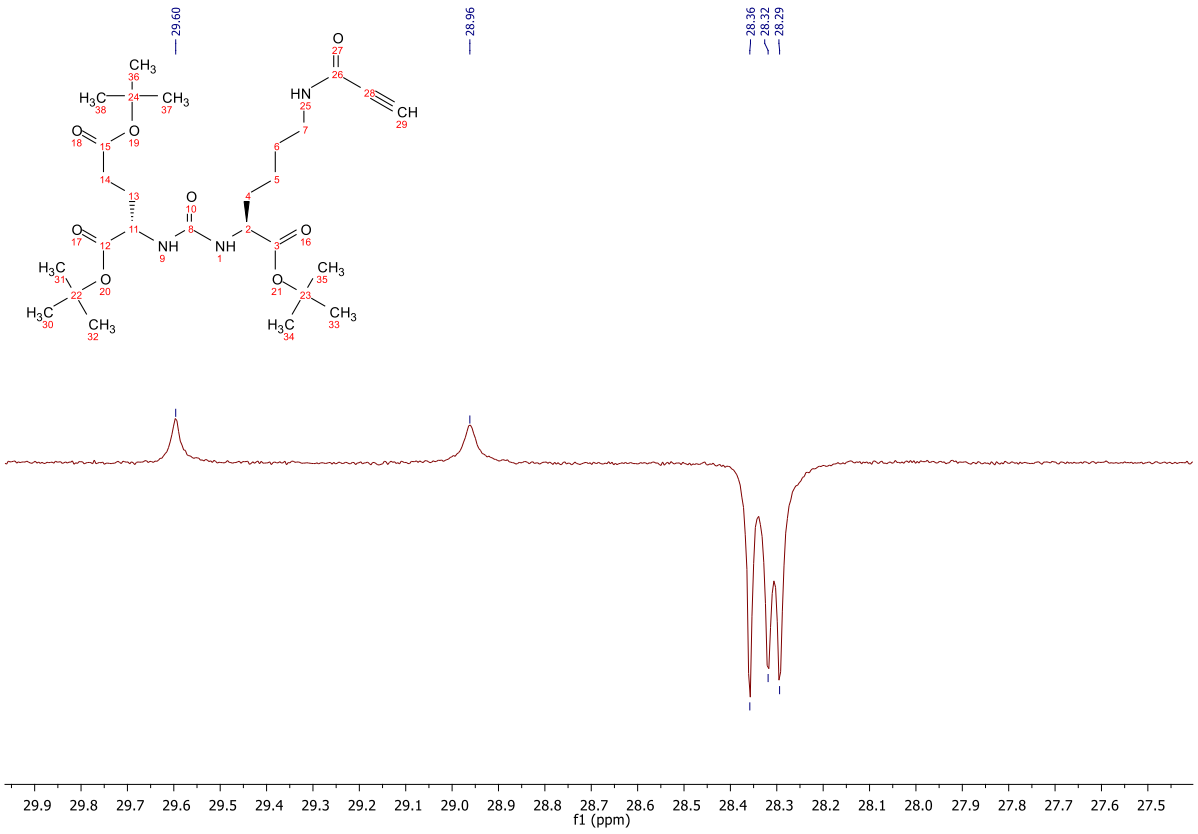
29.60
28.96
28.36
28.32
28.29
29.9 29.8 29.7 29.6 29.5 29.4 29.3 29.2 29.1 29.0 28.9 28.8 28.7 28.6 28.5 28.4 28.3 28.2 28.1 28.0 27.9 27.8 27.7 27.6 27.5
f1 (ppm)

2.42 Compound **8**

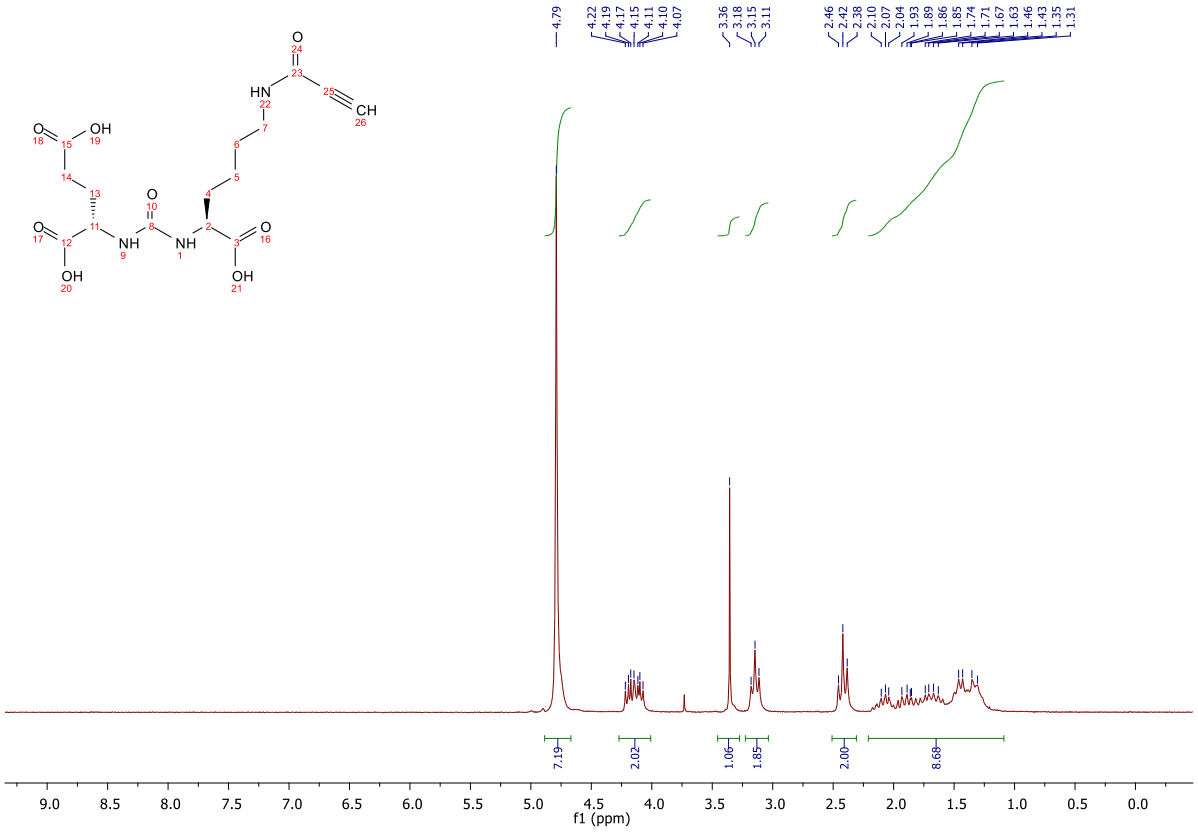

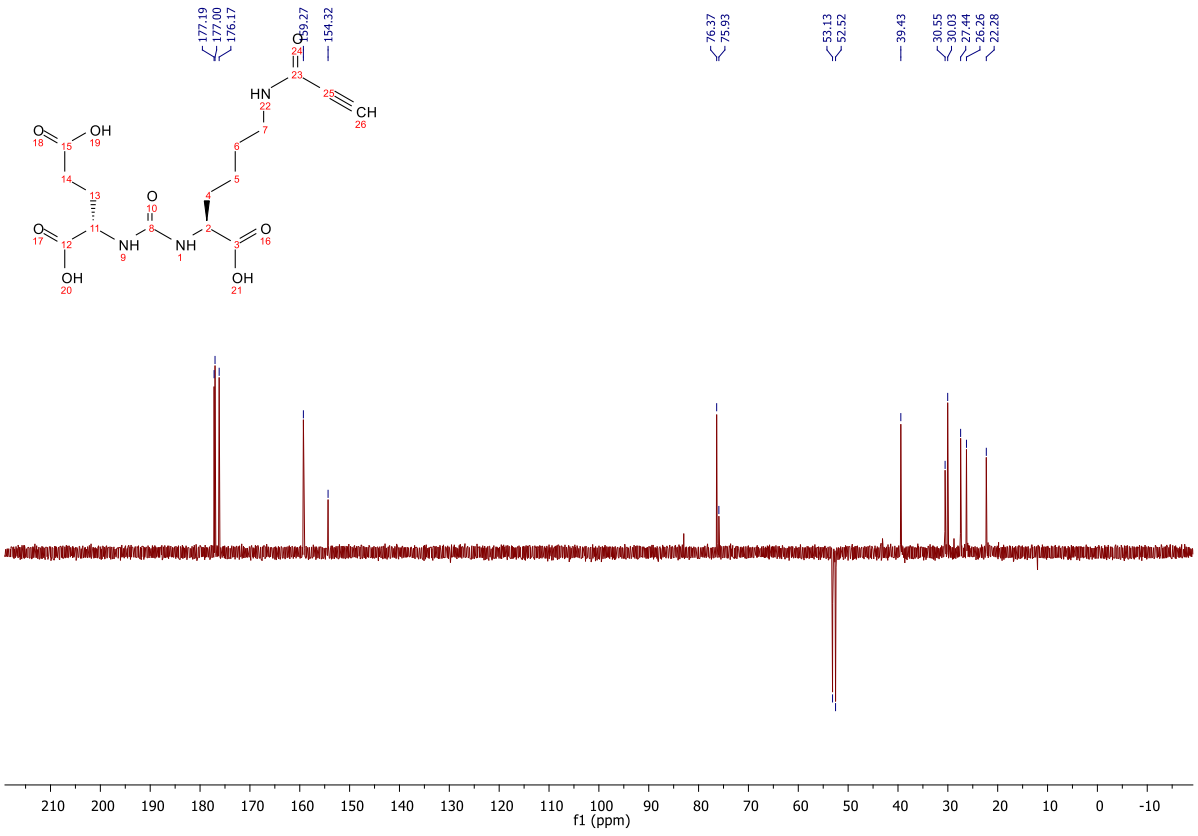

2.43 Compound **6d** (JK-PSMA-18)

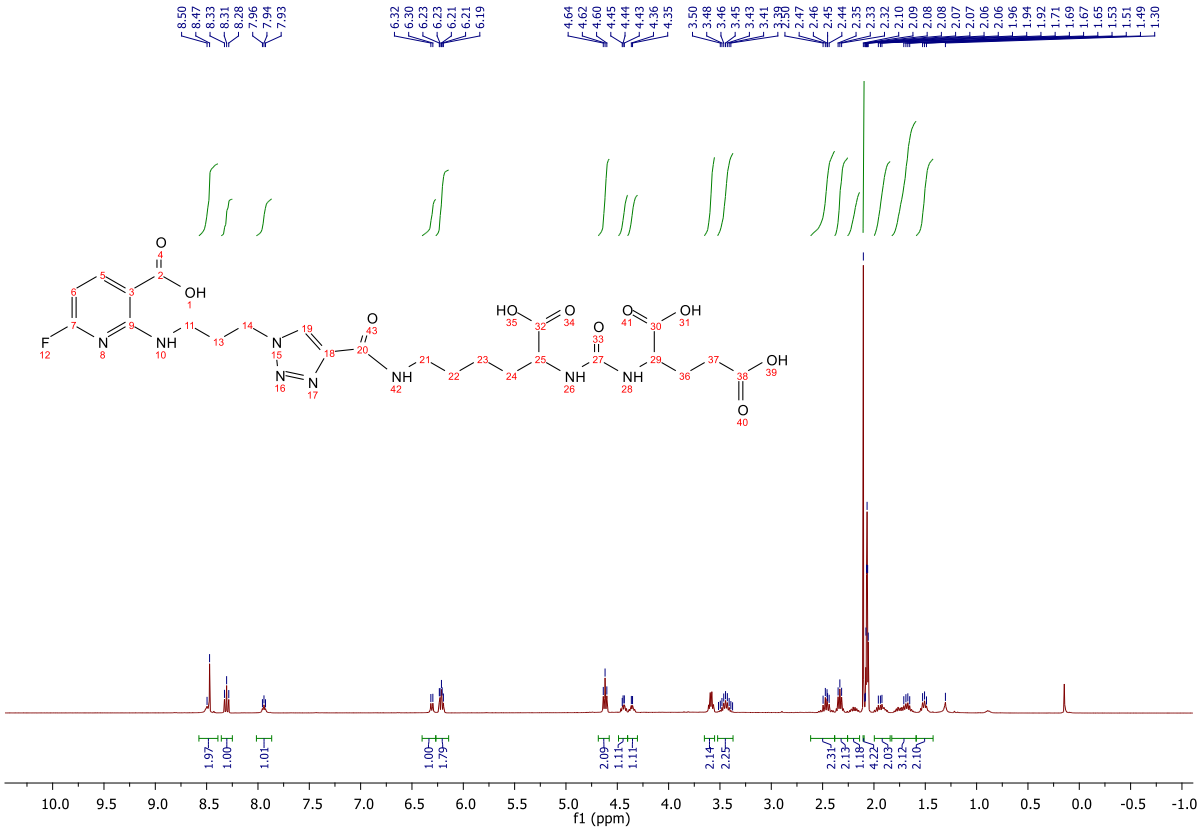

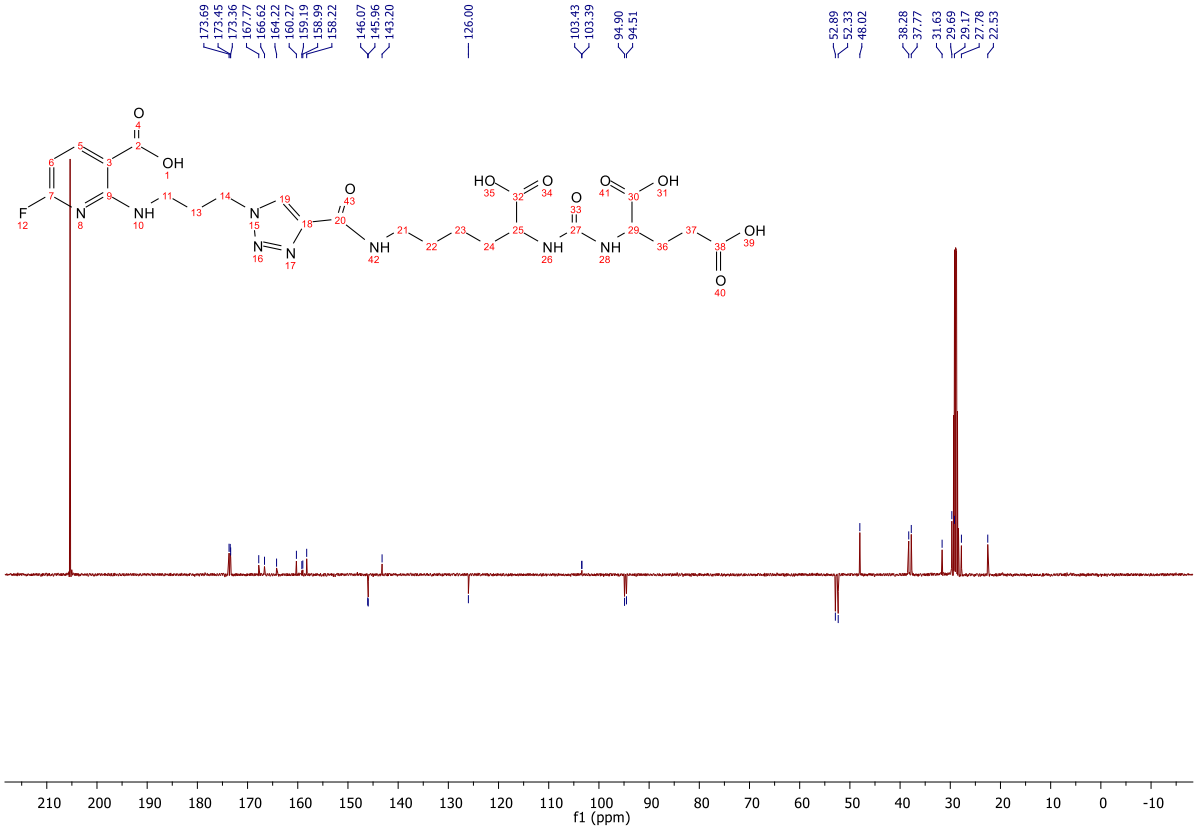

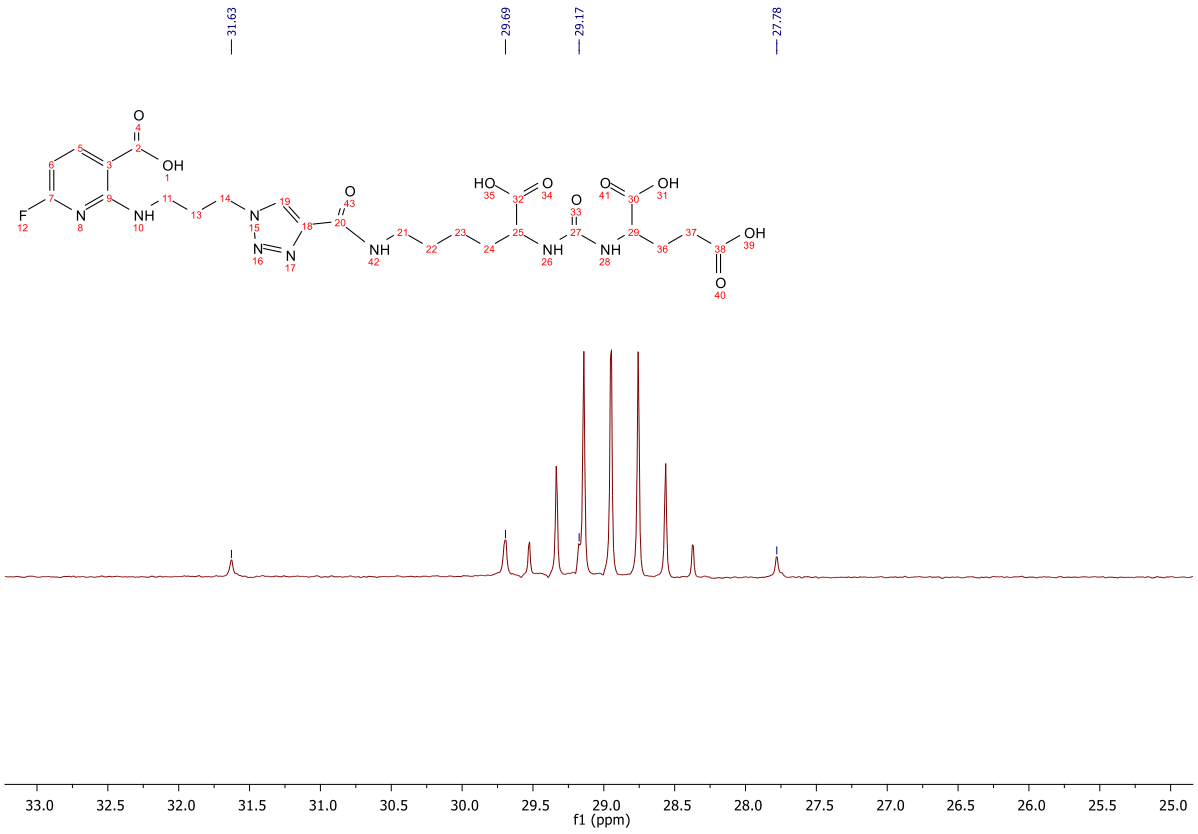
31.63
29.69
29.17
27.78
33.0
32.5
32.0
31.5
31.0
30.5
30.0
29.5
29.0
28.5
28.0
27.5
27.0
26.5
26.0
25.5
25.0
f1 (ppm)

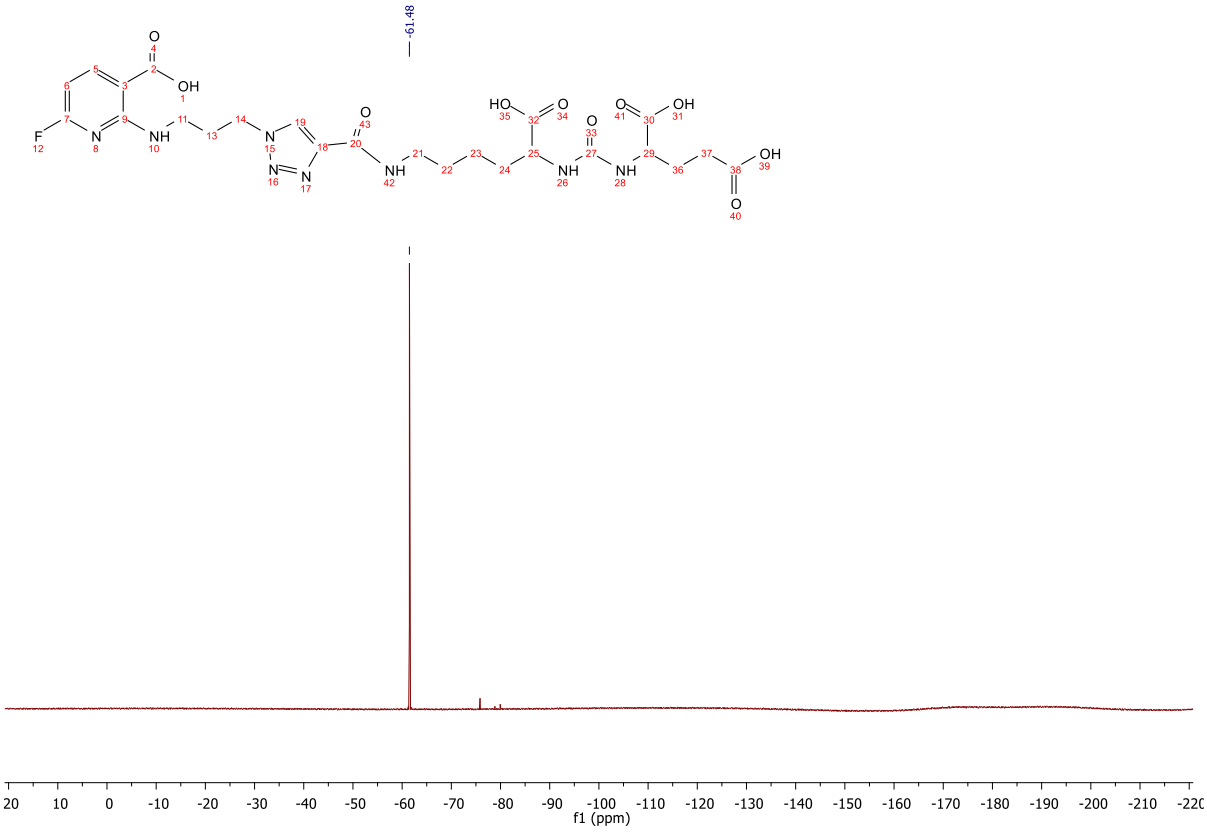
-61.48
20
10
0
-10
-20
-30
-40
-50
-60
-70
-80
-90
-100
-110
-120
-130
-140
-150
-160
-170
-180
-190
-200
-210
f1 (ppm)

3 General Methods for Analytical HPLC:

Column: Multokrom 250×4.6 mm 100-5 C18 AQ column (CS Chromatographie Service GmbH, Langerwehe, Germany)

Method A: 0–10 min 50% MeCN, 11–15 min 90% MeCN, flow rate 1 mL/min.

Method B: 0–20 min 50% MeCN, 21–25 min 90 % MeCN, flow rate 1.5 mL/min.

Method C: 0–20 min 50% MeCN, 21–25 min 90 % MeCN, flow rate 1 mL/min.

Method D: 0–5 min 50% MeCN, 7–12.5 min 70% MeCN, flow rate 1 mL/min.

Method E: 0–15 min 20% to 90% MeCN, 15–20 min 90% MeCN, flow rate 1 mL/min.

Method F: 0–12 min 30% MeCN, 15–20 min 80% MeCN, flow rate 1 mL/min.

4 HPLC chromatograms of ^{18}F-labeled AFAs:

4.1 HPLC traces of [^{18}F]**3e** (**Figs. S1** & **S2**)

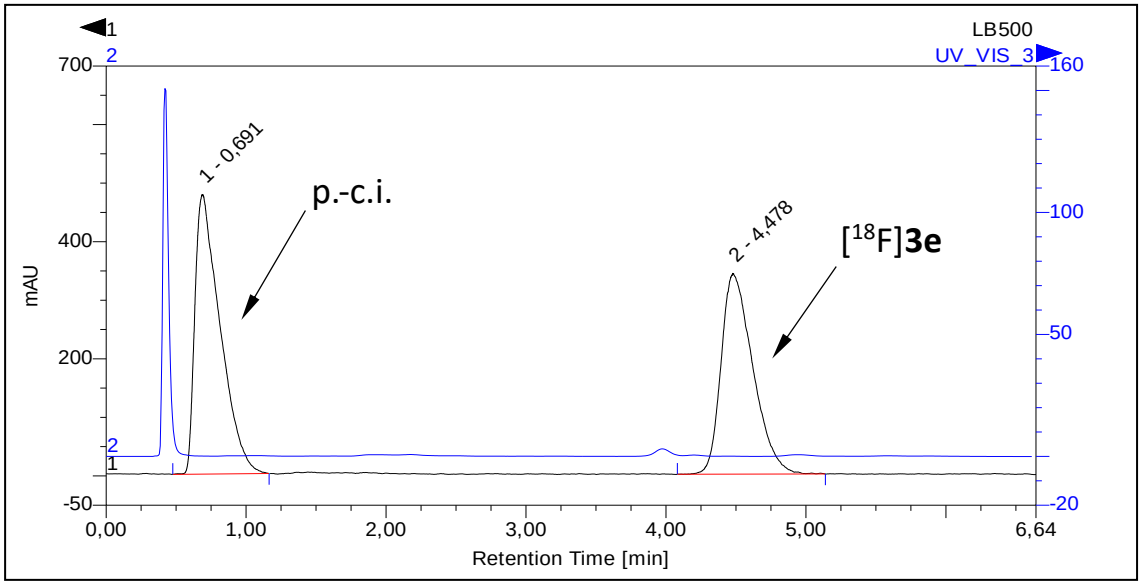

Figure S1: HPLC traces of SPE-purified [^{18}F]**3e**, Method C (0.1% TFA). Blue trace: UV, λ = 254 nm; black trace: radioactivity. Abbreviation: p.-c.i. – post-column injection.

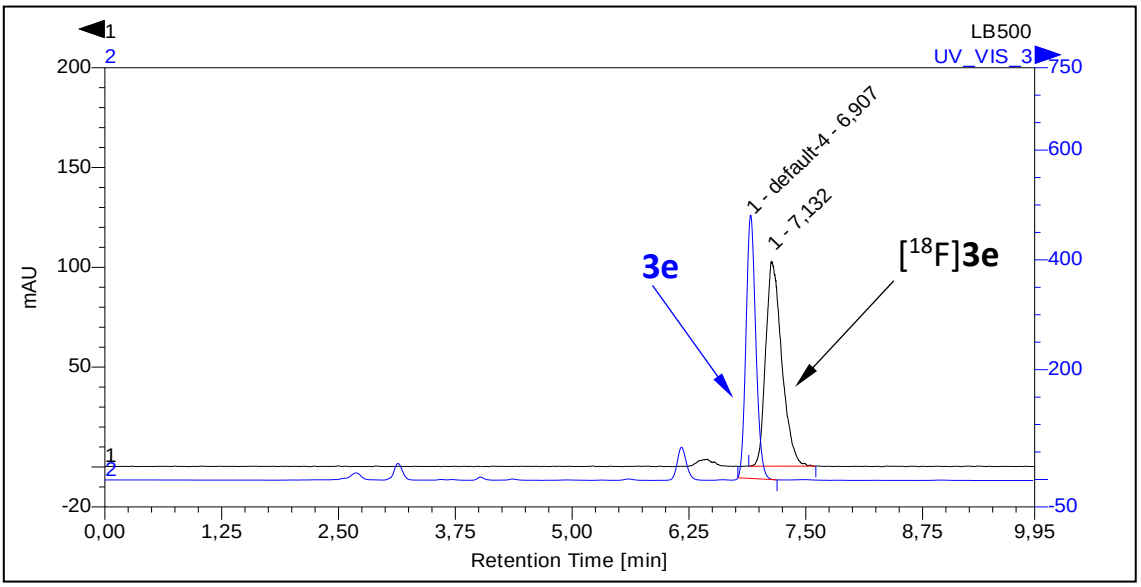

Figure S2: HPLC traces of [^{18}F]**3e** spiked with the non-radioactive reference compound, Method A (0.1% TFA). Blue trace: UV, λ = 254 nm; black trace: radioactivity.

4.2 HPLC traces of [^{18}F]**3f** (**Figs. S3** & **S4**)

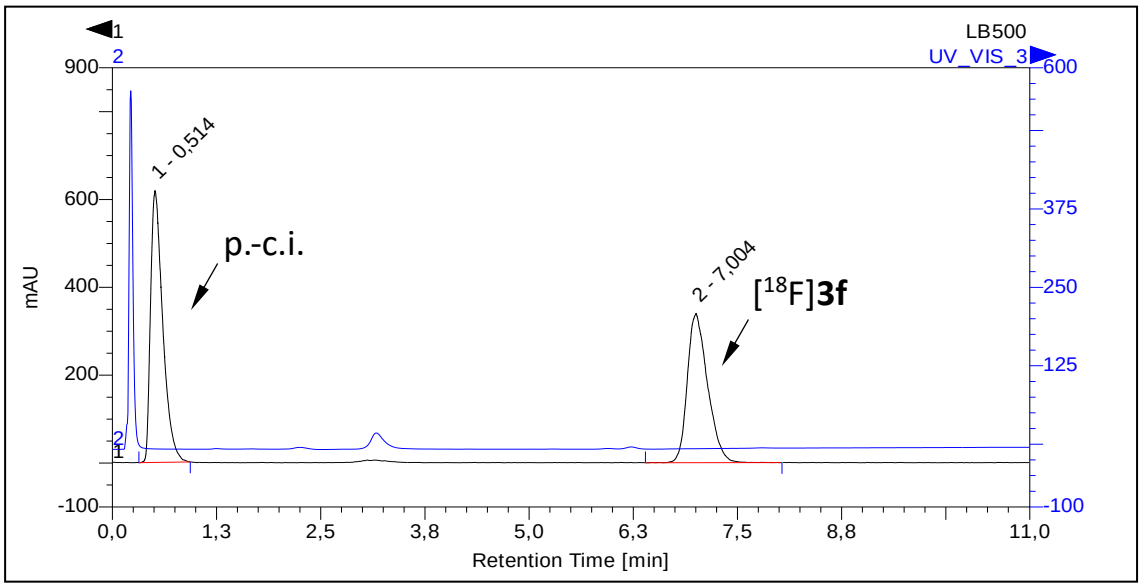

Figure S3: HPLC traces of [^{18}F]**3f**, Method C (0.1% TFA). Blue trace: UV, λ = 254 nm; black trace: radioactivity. Abbreviation: p.-c.i. – post-column injection.

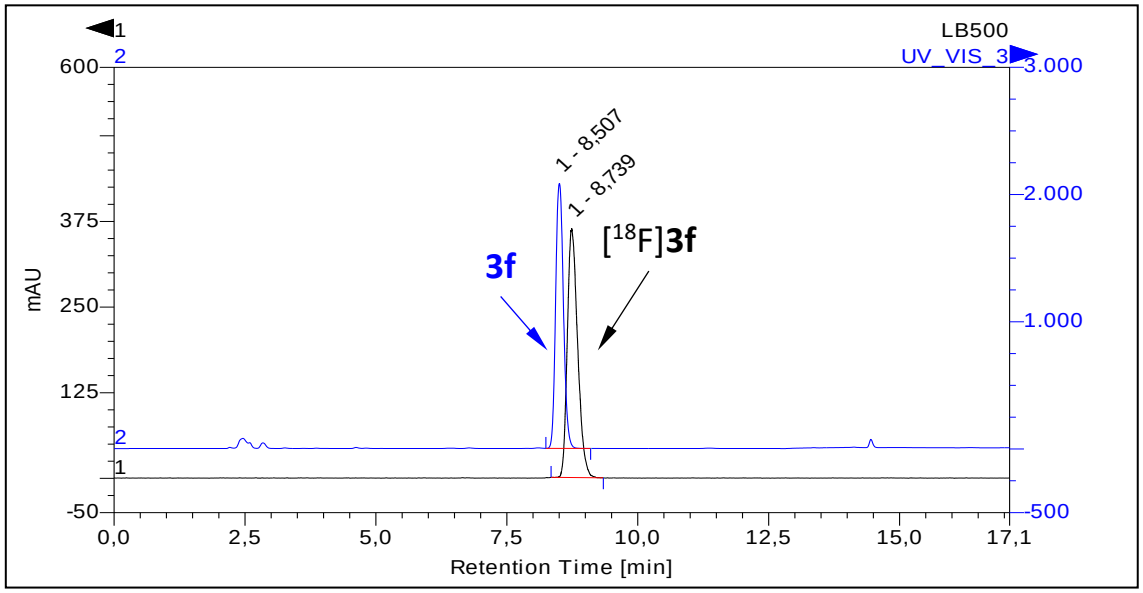

Figure S4: HPLC traces of [^{18}F]**3f** spiked with the non-radioactive reference compound, Method A (0.1% TFA). Blue trace: UV, λ = 254 nm; black trace: radioactivity.

4.3 HPLC traces of [^{18}F]**3g** (**Figs. S5** & **S6**)

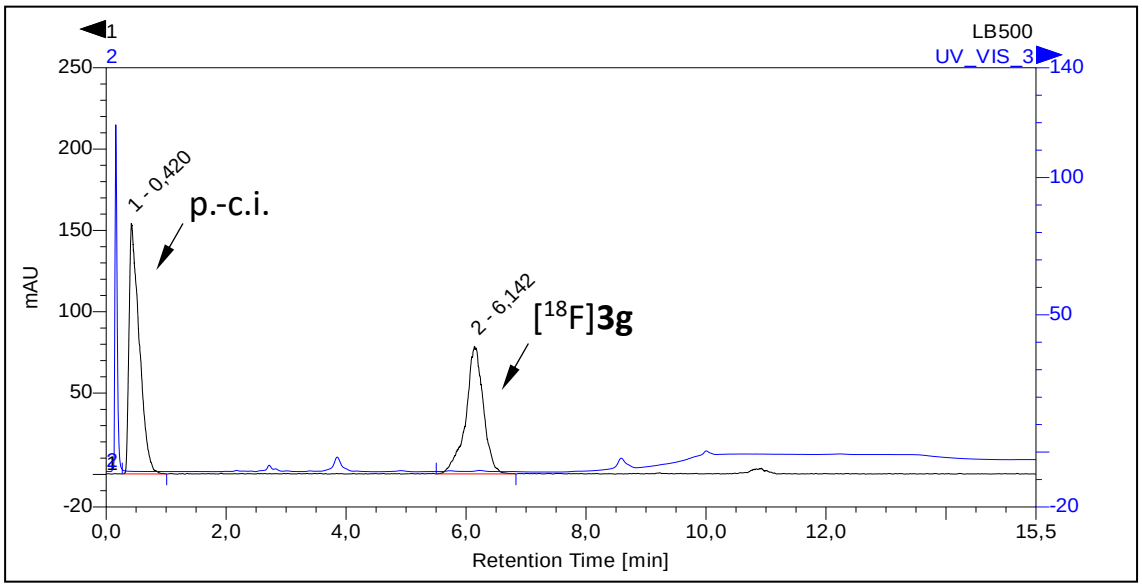

Figure S5: HPLC traces of [^{18}F]**3g**, Method D (0.1% TFA). Blue trace: UV, λ = 254 nm; black trace: radioactivity. Abbreviation: p.-c.i. – post-column injection.

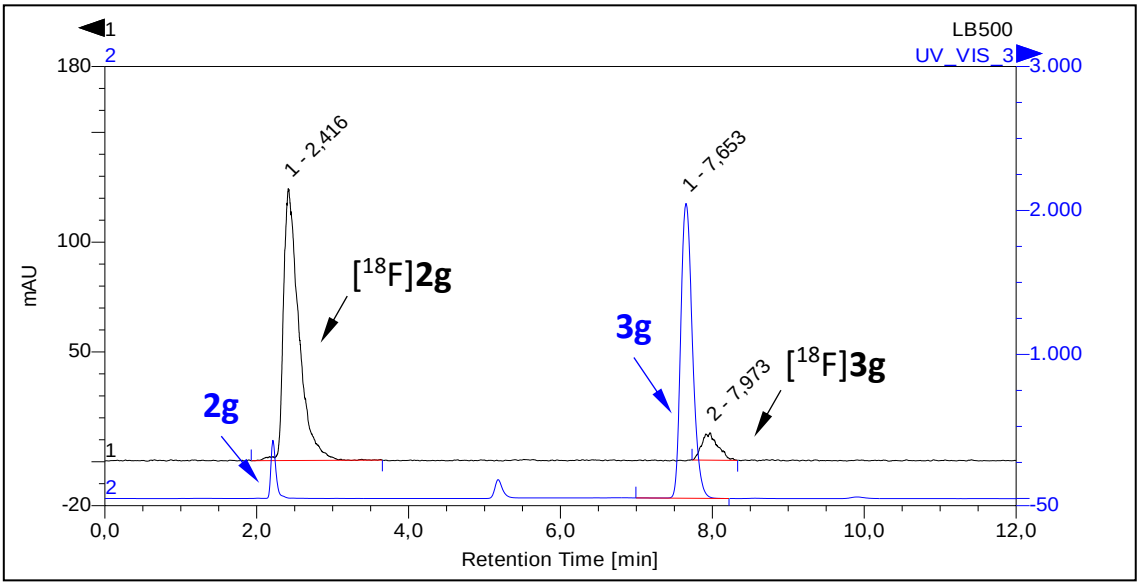

Figure S6: HPLC traces of [^{18}F]**3g** spiked with the non-radioactive reference compounds, Method A (with 300 mg/L NaOAc added to the eluent). Chromatogram shows almost complete (>90%) hydrolysis of the anhydride [^{18}F]**3g** to the acid [^{18}F]**2g** (R_t = 2.4 min). Blue trace: UV, λ = 254 nm; black trace: radioactivity.

4.4 HPLC traces of [^{18}F]**3h** (**Figs. S7** & **S8**)

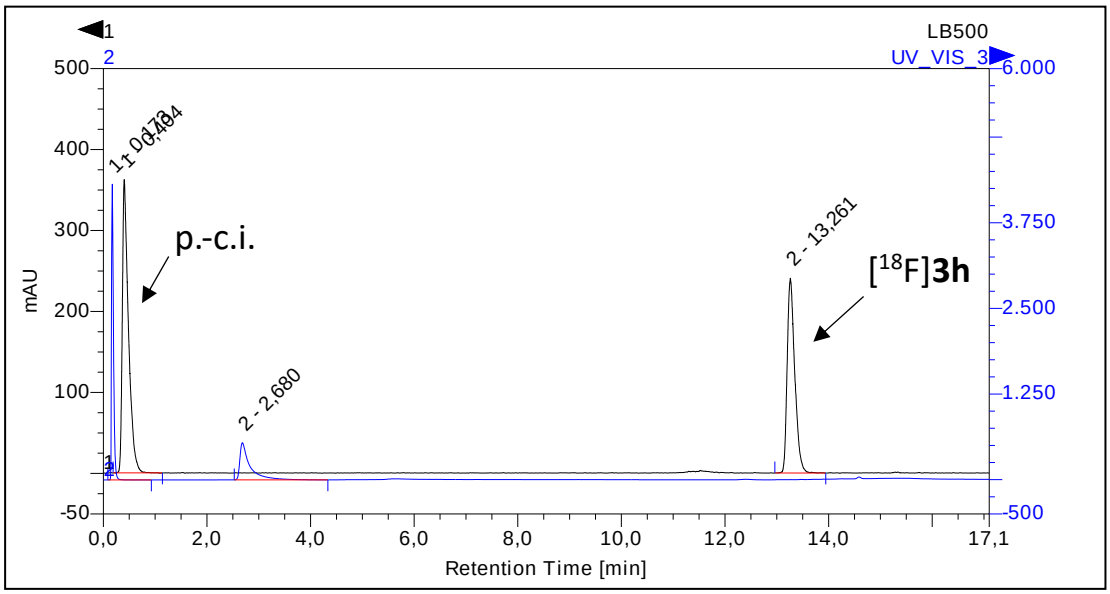

Figure S7: HPLC traces of [^{18}F]**3h**, Method A (0.1% TFA). Blue trace: UV, λ = 254 nm; black trace: radioactivity. Abbreviation: p.-c.i. – post-column injection.

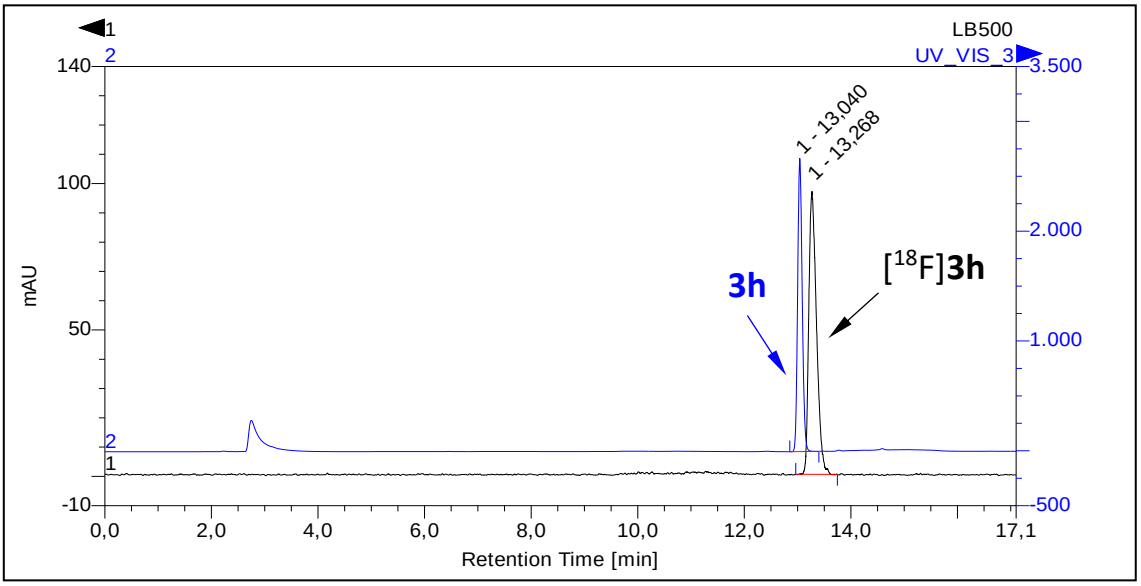

Figure S8: HPLC traces of [^{18}F]**3h** spiked with the non-radioactive reference compound, Method A (with 300 mg/L NaOAc added to the eluent). Blue trace: UV, λ = 254 nm; black trace: radioactivity.

5 HPLC chromatograms of radiolabeled model compounds und PET-tracers:

5.1 HPLC traces of [^{18}F]**5a** (**Figs. S9** & **S10**)

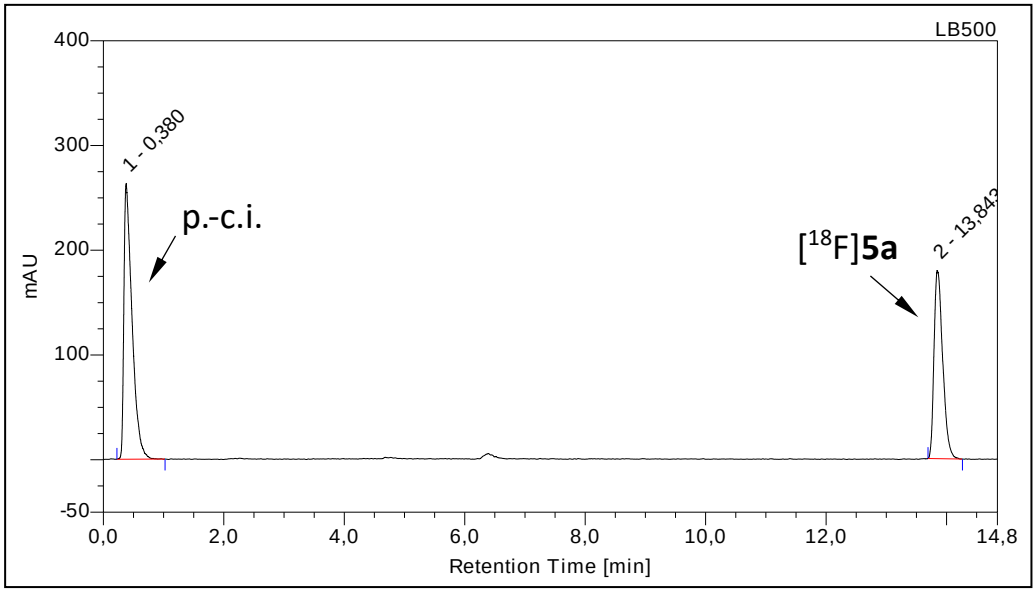

Figure S9: Radio-HPLC trace of crude [^{18}F]**5a**, Method A (0.1% TFA). Abbreviation: p.-c.i. – post-column injection.

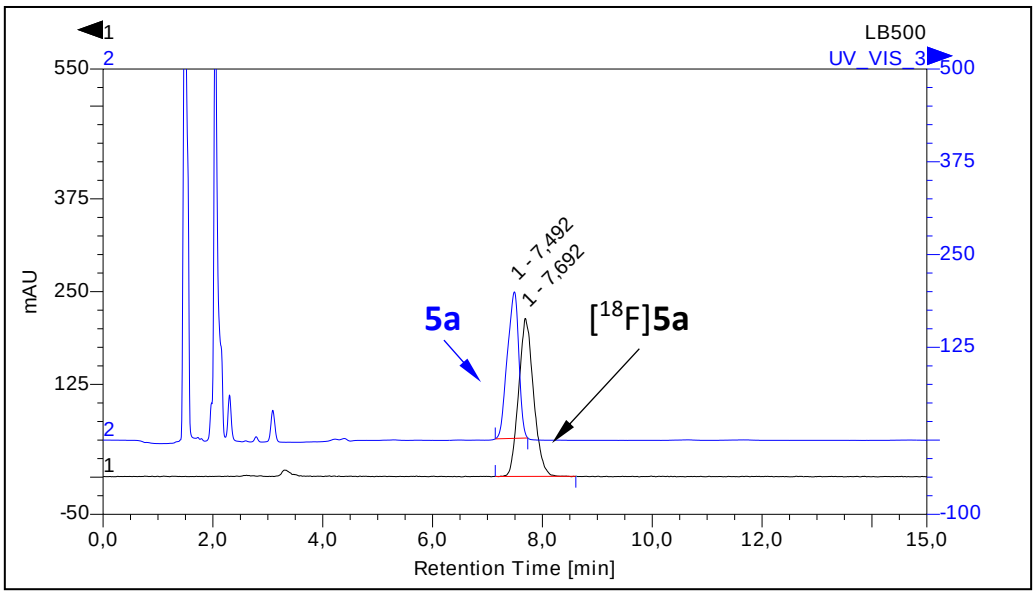

Figure S10: HPLC traces of [^{18}F]**5a** spiked with the non-radioactive reference compound, Method C. Blue trace: UV, λ = 254 nm; black trace: radioactivity.

5.2 HPLC traces of [^{18}F]**5b** (**Figs. S11** & **S12**)

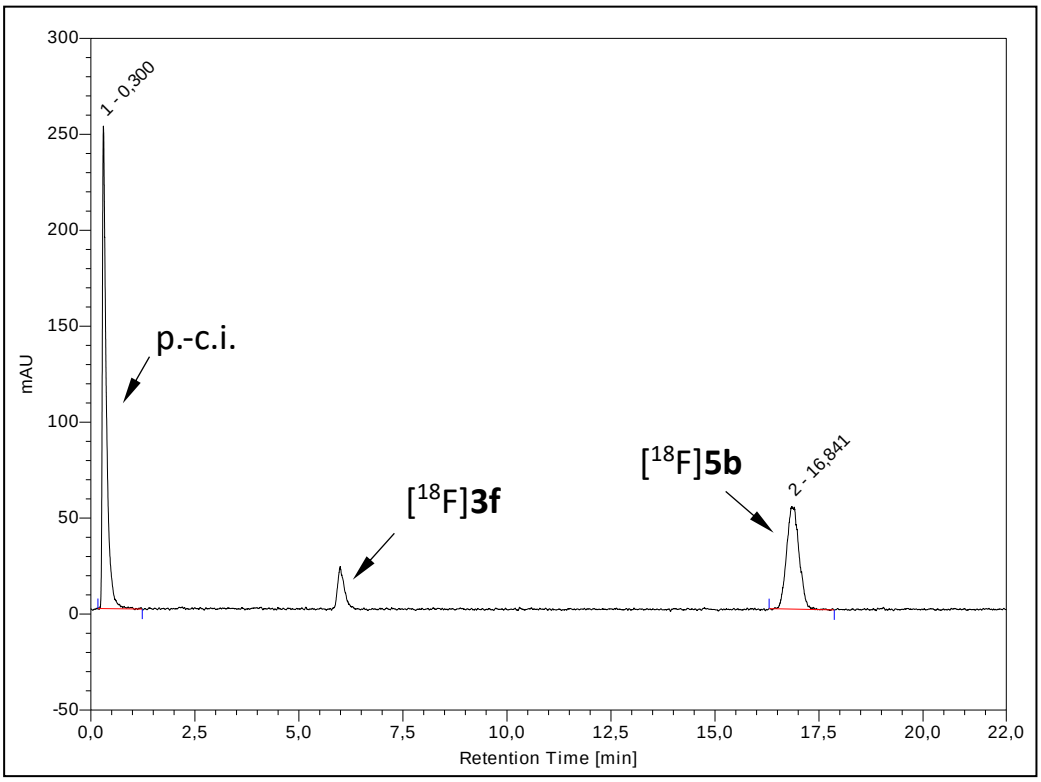

Figure S11: Radio-HPLC trace of crude [^{18}F]**5b**, Method A. Abbreviation: p.-c.i. – post-column injection.

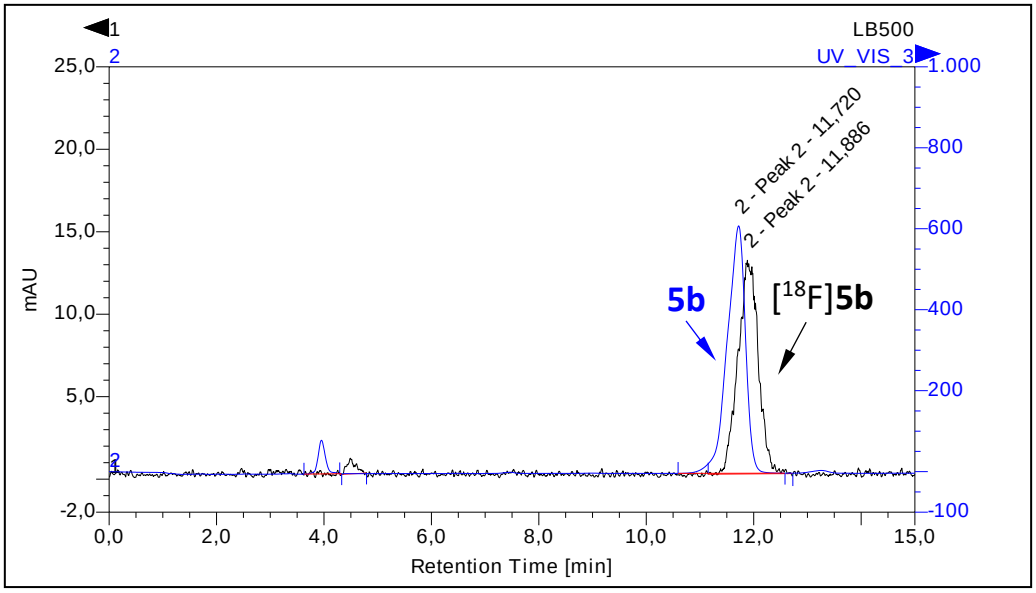

Figure S12: HPLC traces of [^{18}F]**5b** spiked with the non-radioactive reference compound, Method B. Blue trace: UV, λ = 254 nm; black trace: radioactivity.

5.3 HPLC traces of [^{18}F]**5c** (**Figs. S13** & **S14**)

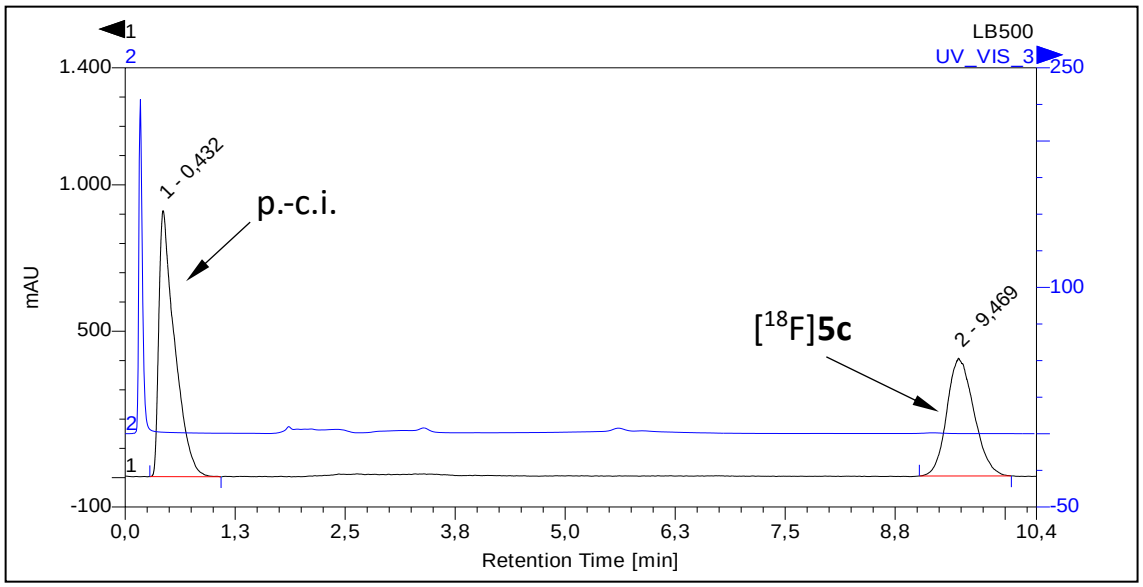

Figure S13: HPLC traces of crude [^{18}F]**5c**, Method C (0.1% TFA). Blue trace: UV, λ = 254 nm; black trace: radioactivity. Abbreviation: p.-c.i. – post-column injection.

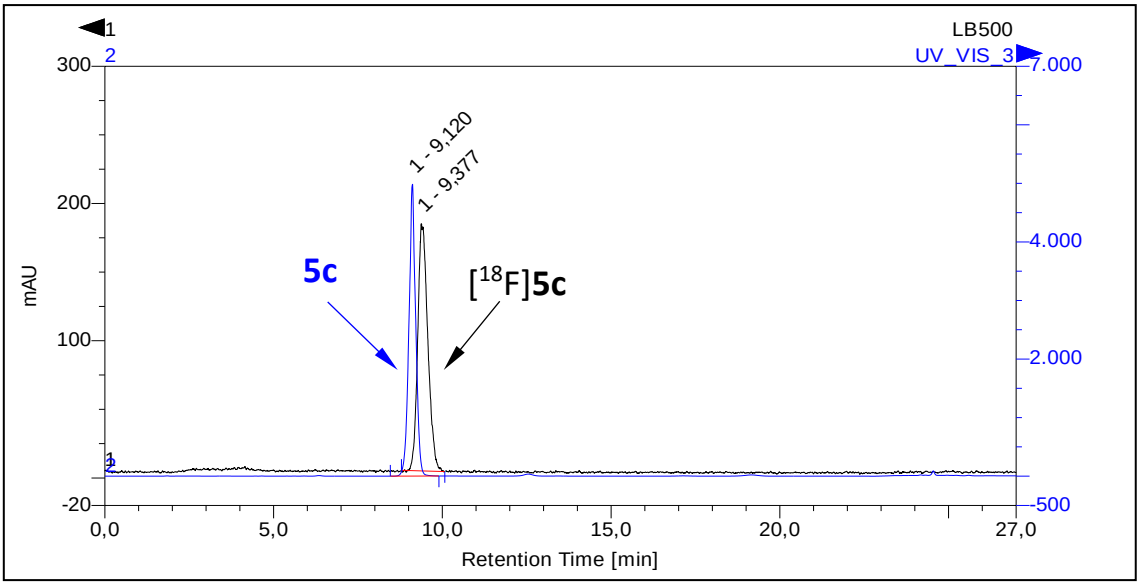

Figure S14: HPLC traces of [^{18}F]**5c** spiked with the non-radioactive reference compound, Method C (0.1% TFA). Blue trace: UV, λ = 254 nm; black trace: radioactivity.

5.4 HPLC traces of [^{18}F]**5d** (**Figs. S15** & **S16**)

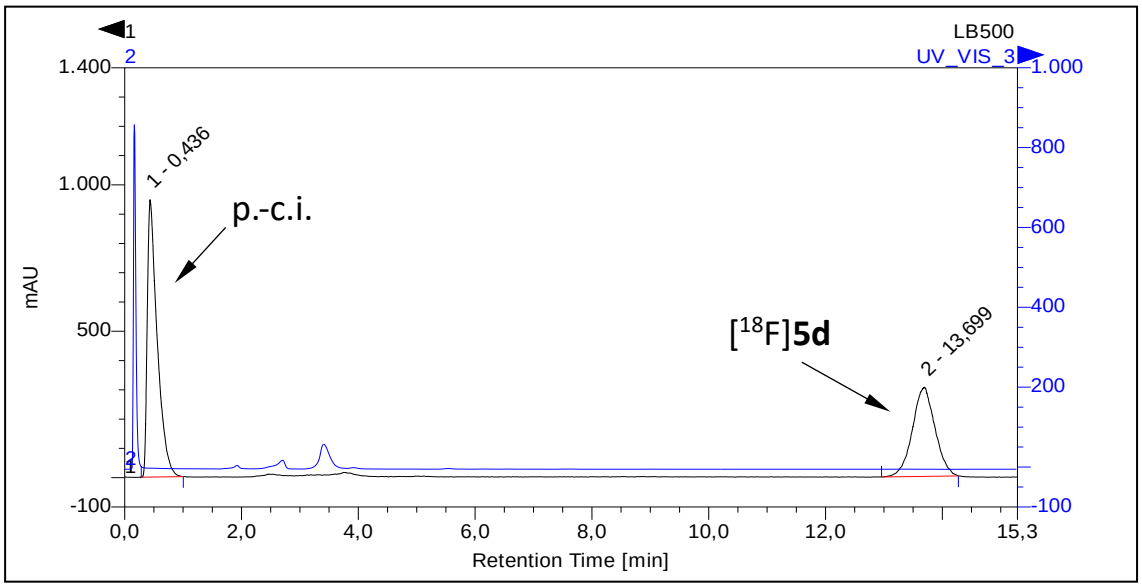

Figure S15: HPLC traces of crude [^{18}F]**5d**, Method C (0.1% TFA). Blue trace: UV, λ = 254 nm; black trace: radioactivity. Abbreviation: p.-c.i. – post-column injection.

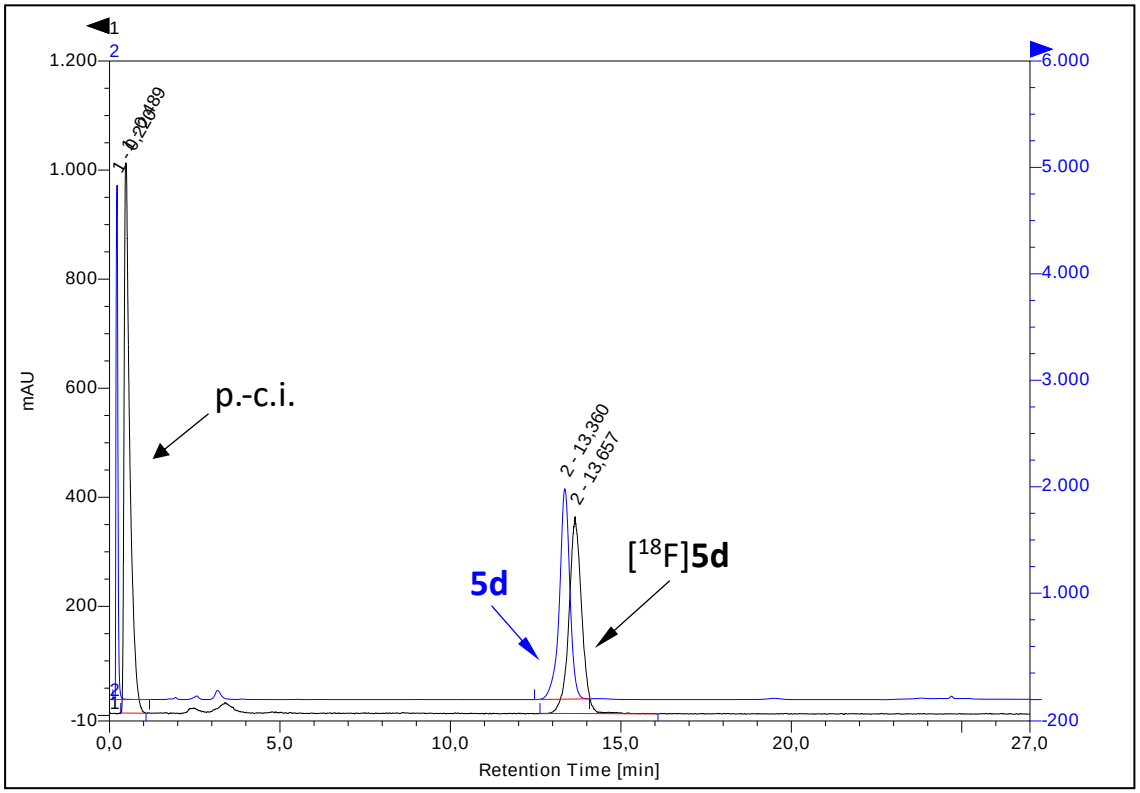

Figure S16: HPLC traces of crude [^{18}F]**5d** spiked with the non-radioactive reference compound, Method C (0.1% TFA). Blue trace: UV, λ = 254 nm; black trace: radioactivity. Abbreviation: p.-c.i. – post-column injection.

5.5 HPLC traces of [^{18}F]**5e** (**Figs. S17** & **S18**)

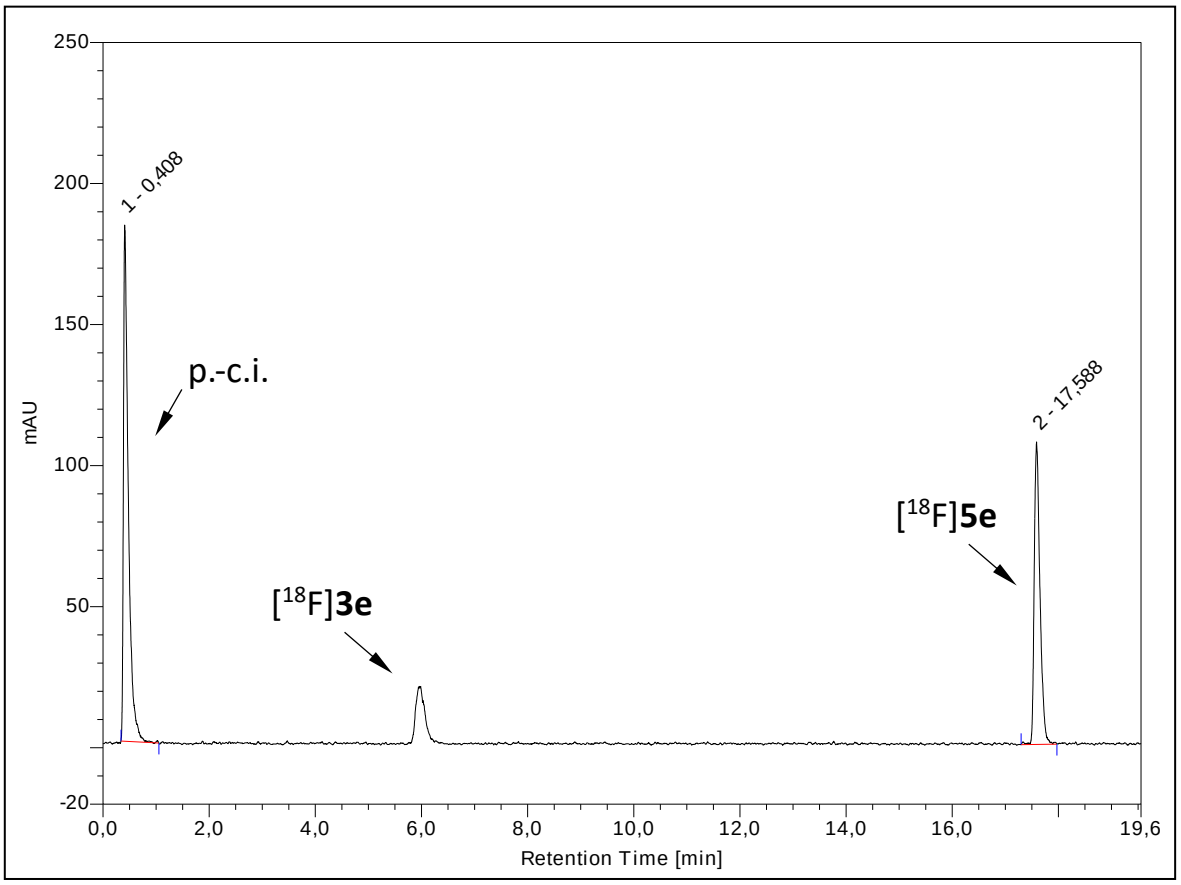

Figure S17: Radio-HPLC trace of [^{18}F]**5e**, Method B. Abbreviation: p.-c.i. – post-column injection.

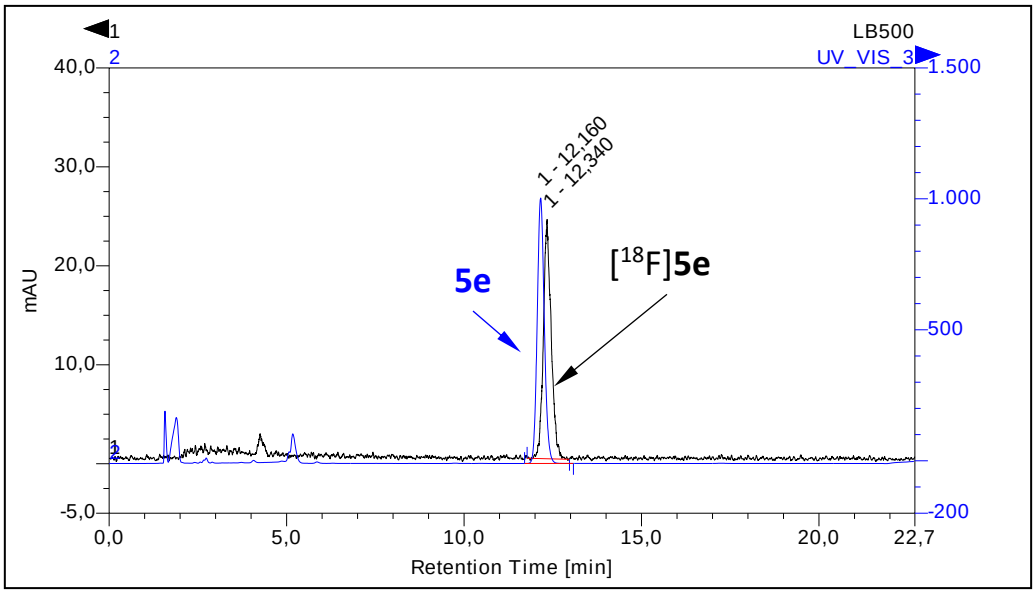

Figure S18: HPLC traces of [^{18}F]**5e** spiked with the non-radioactive reference compound, Method A. Blue trace: UV, λ = 254 nm; black trace: radioactivity.

5.6 HPLC traces of [^{18}F]**5f** (**Figs. S19** & **S20**)

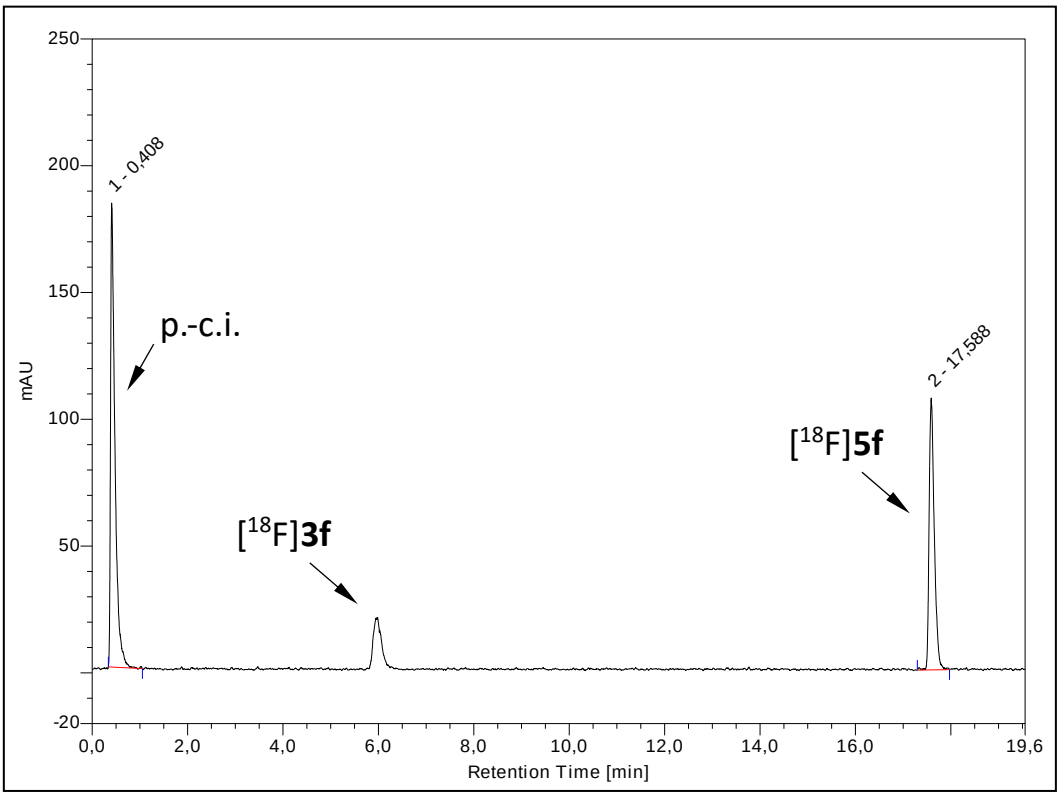

Figure S19: Radio-HPLC trace of crude [^{18}F]**5f**, Method B. Abbreviation: p.-c.i. – post-column injection.

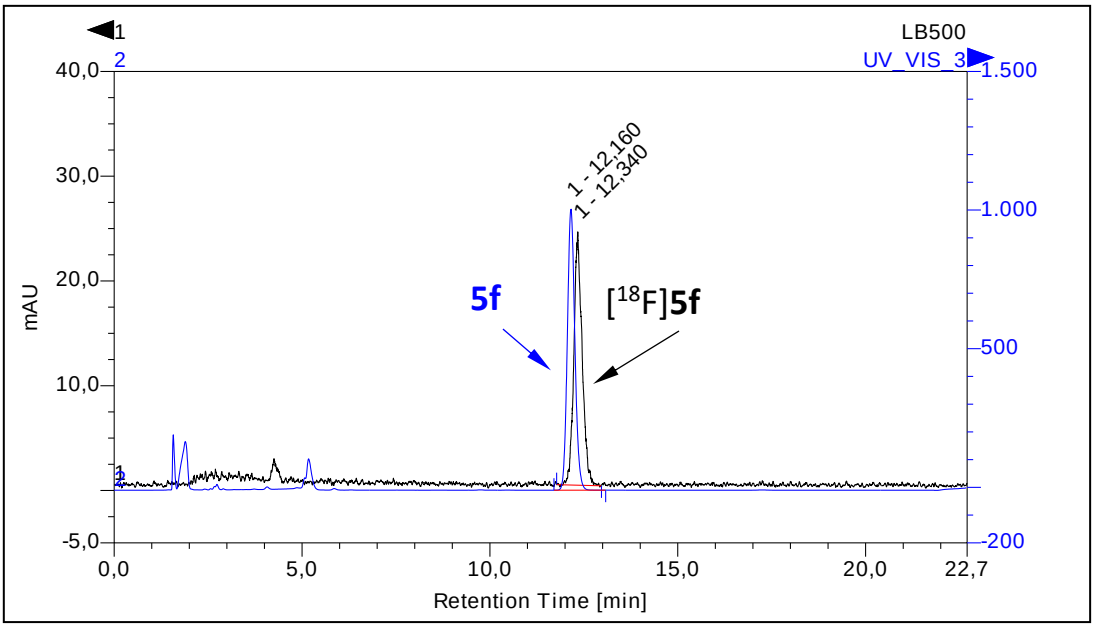

Figure S20: HPLC traces of crude [^{18}F]**5f** spiked with the non-radioactive reference compound, Method A. Blue trace: UV, λ = 254 nm; black trace: radioactivity.

5.7 HPLC traces of [^{18}F]**5g** (**Figs. S21** & **S22**)

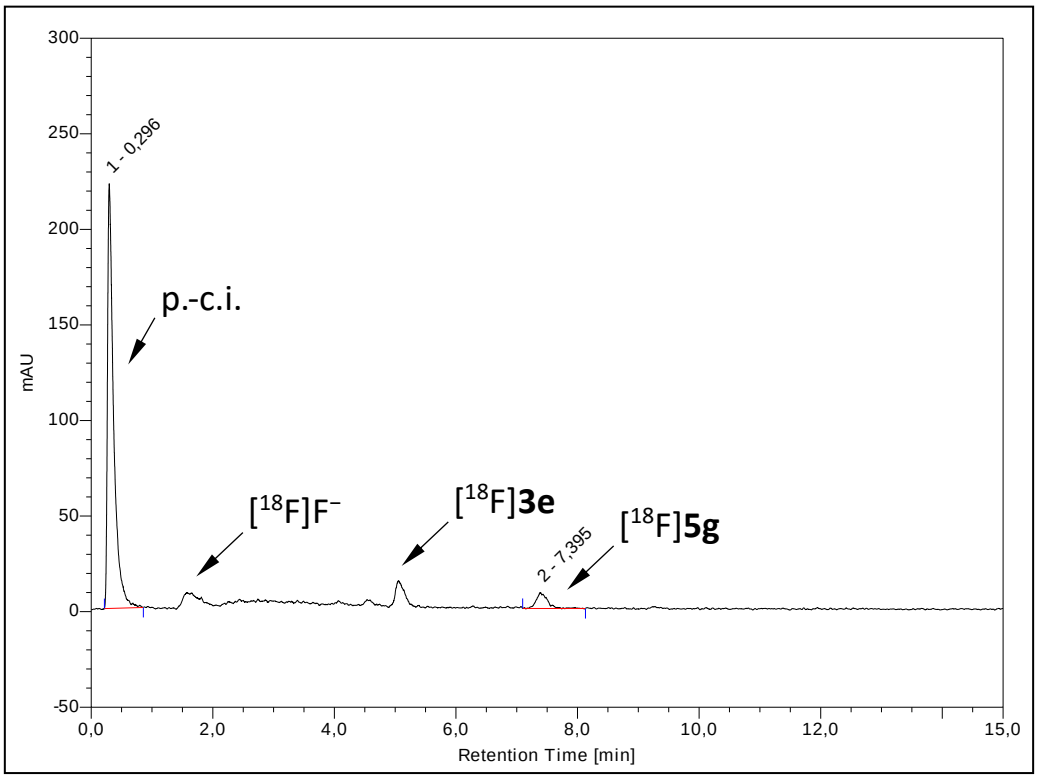

Figure S21: Radio-HPLC trace of crude [^{18}F]**5g**, Method B (0.1% TFA). Abbreviation: p.-c.i. – post-column injection.

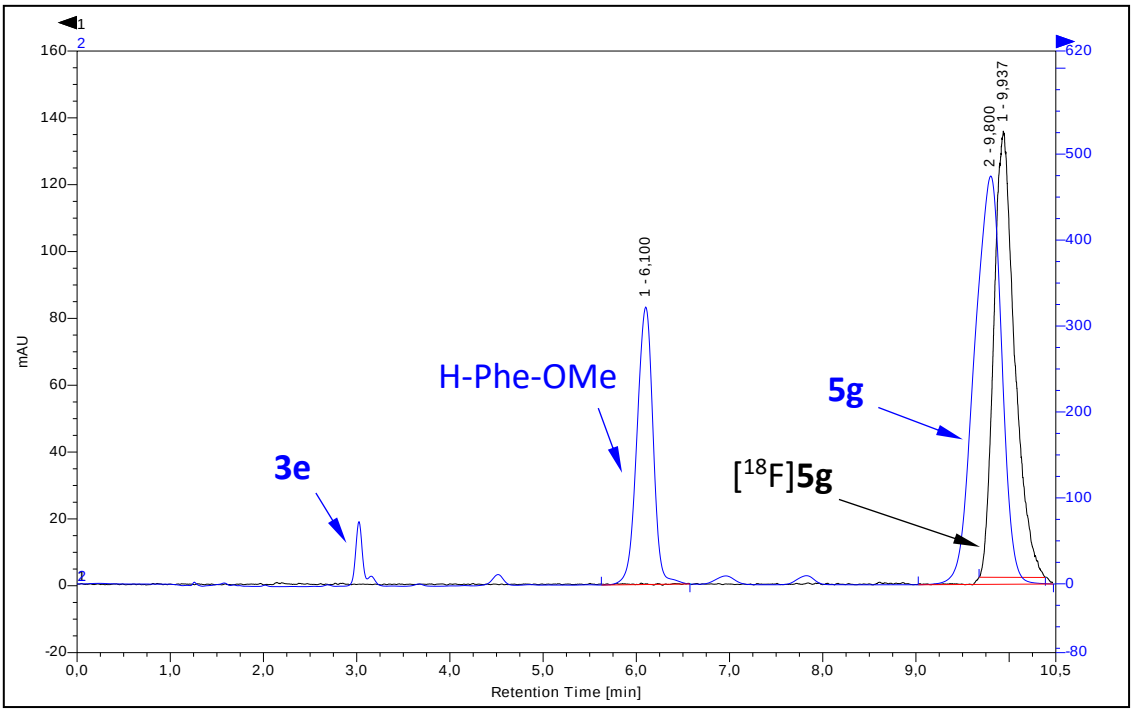

Figure S22: HPLC traces of isolated [^{18}F]**5g** spiked with the non-radioactive reference compounds, Method B. Blue trace: UV, λ = 254 nm; black trace: radioactivity.

5.8 HPLC traces of [^{18}F]**5h** (**Figs. S23** & **S24**)

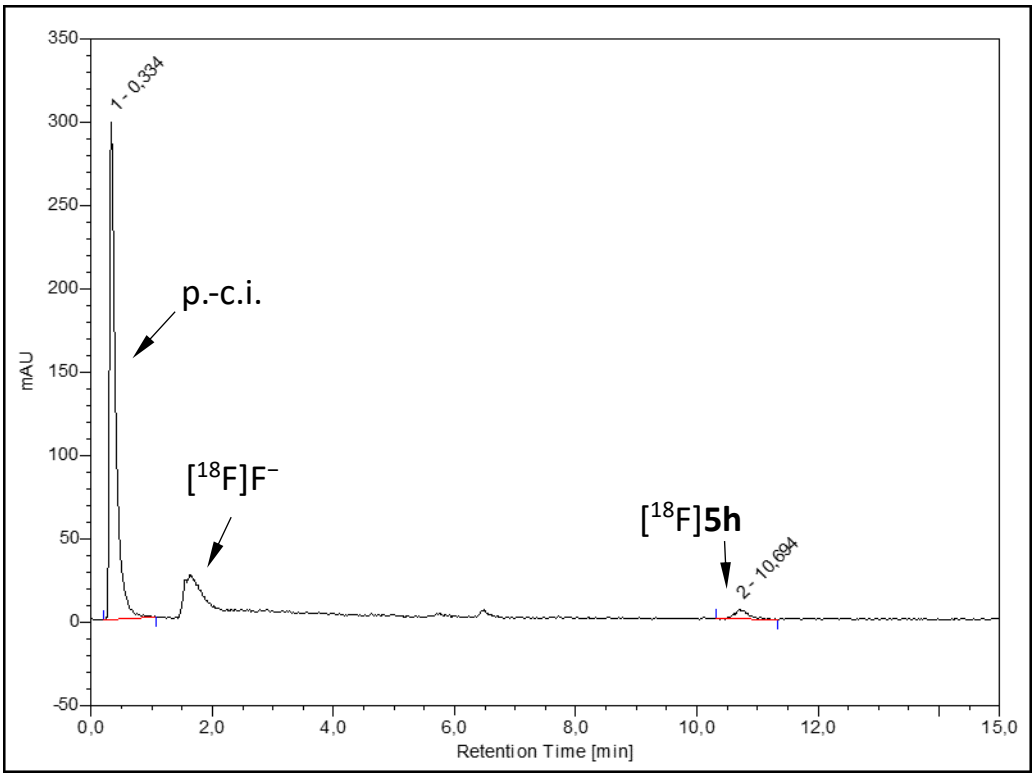

Figure S23: Radio-HPLC trace of crude [^{18}F]**5h**, Method B. Abbreviation: p.-c.i. – post-column injection.

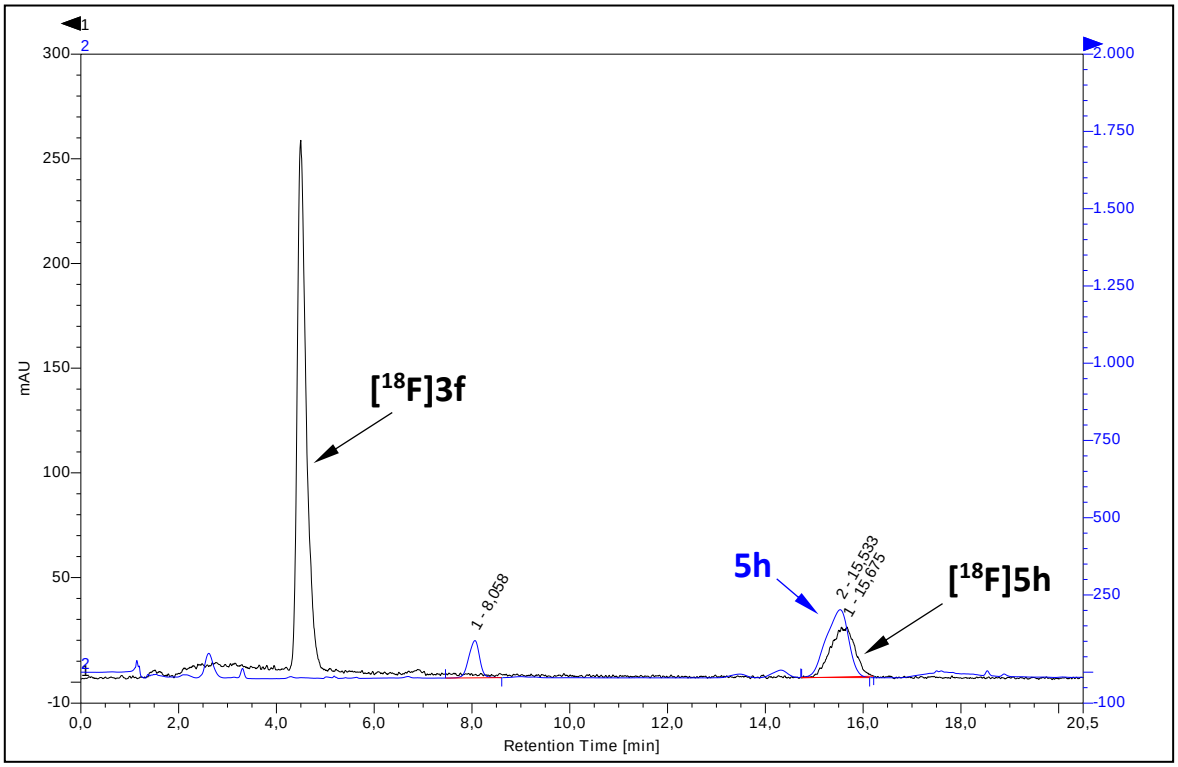

Figure S24: HPLC traces of crude [^{18}F]**5h** spiked with the non-radioactive reference compound, Method B. Blue trace: UV, λ = 254 nm; black trace: radioactivity.

5.9 HPLC traces of [^{18}F]**5i** (**Figs. S25** & **S26**)

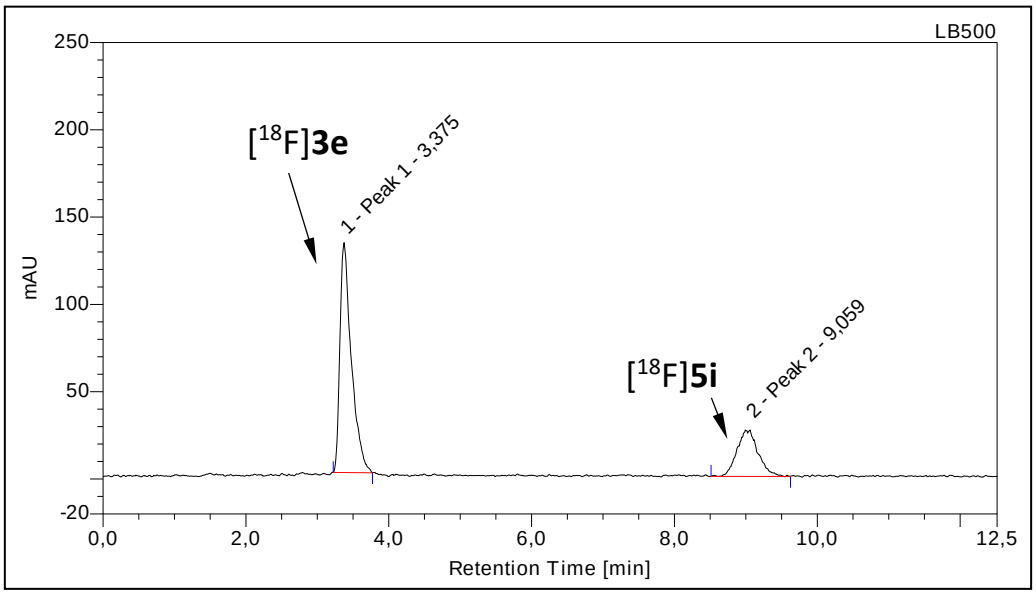

Figure S25: Radio-HPLC trace of crude [^{18}F]**5i**, Method A.

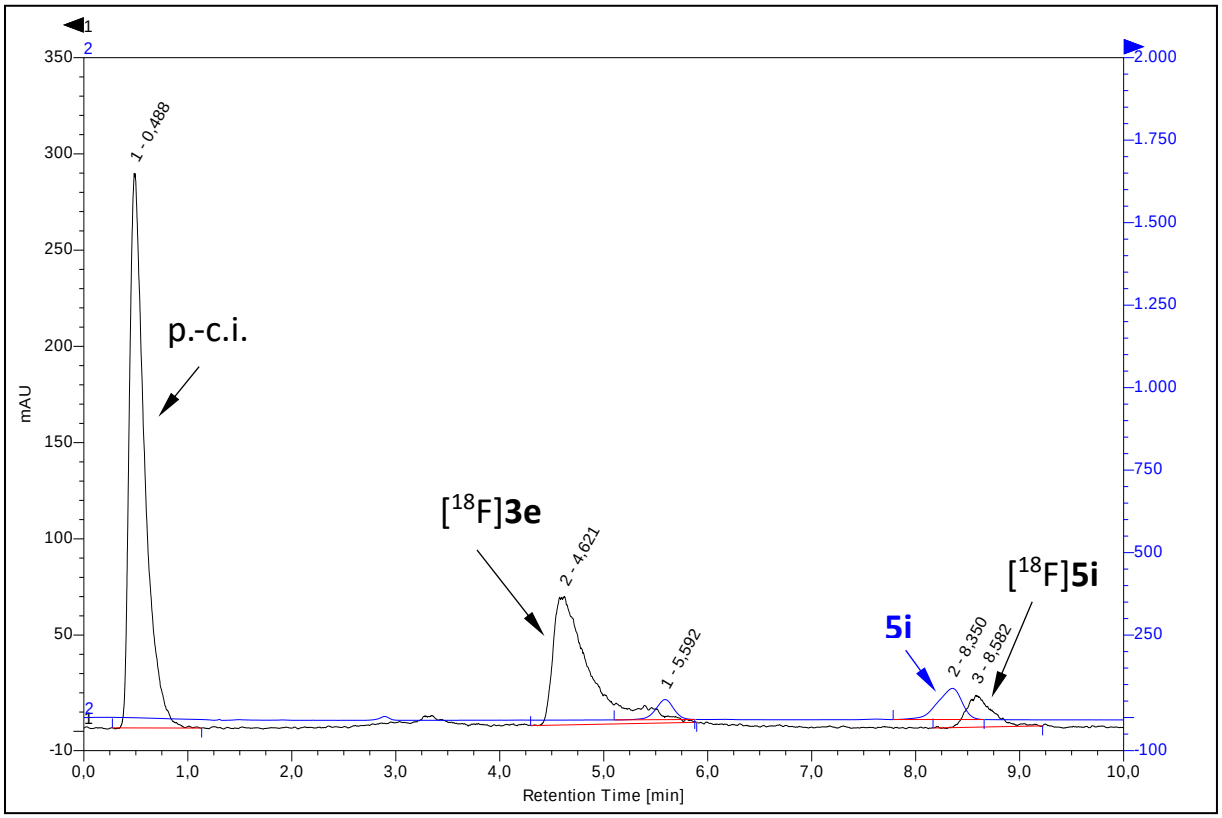

Figure S26: HPLC traces of crude [^{18}F]**5i** spiked with the non-radioactive reference compound, Method B. Blue trace: UV, λ = 254 nm; black trace: radioactivity. Abbreviation: p.-c.i. – post-column injection.

5.10 HPLC traces of [^{18}F]**5j** (**Figs. S27** & **S28**)

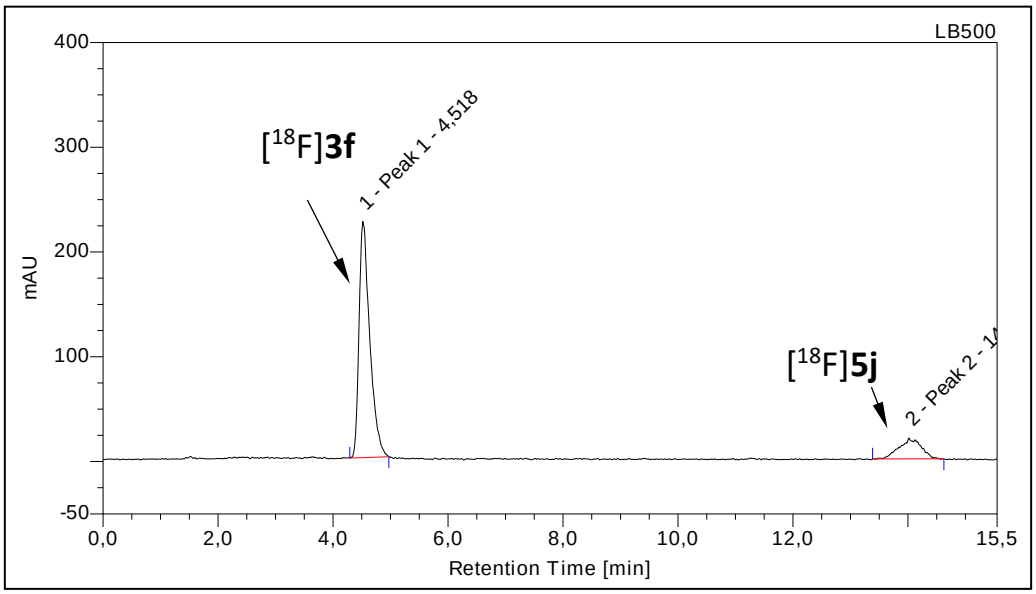

Figure S27: Radio-HPLC trace of crude [^{18}F]**5j**, Method A.

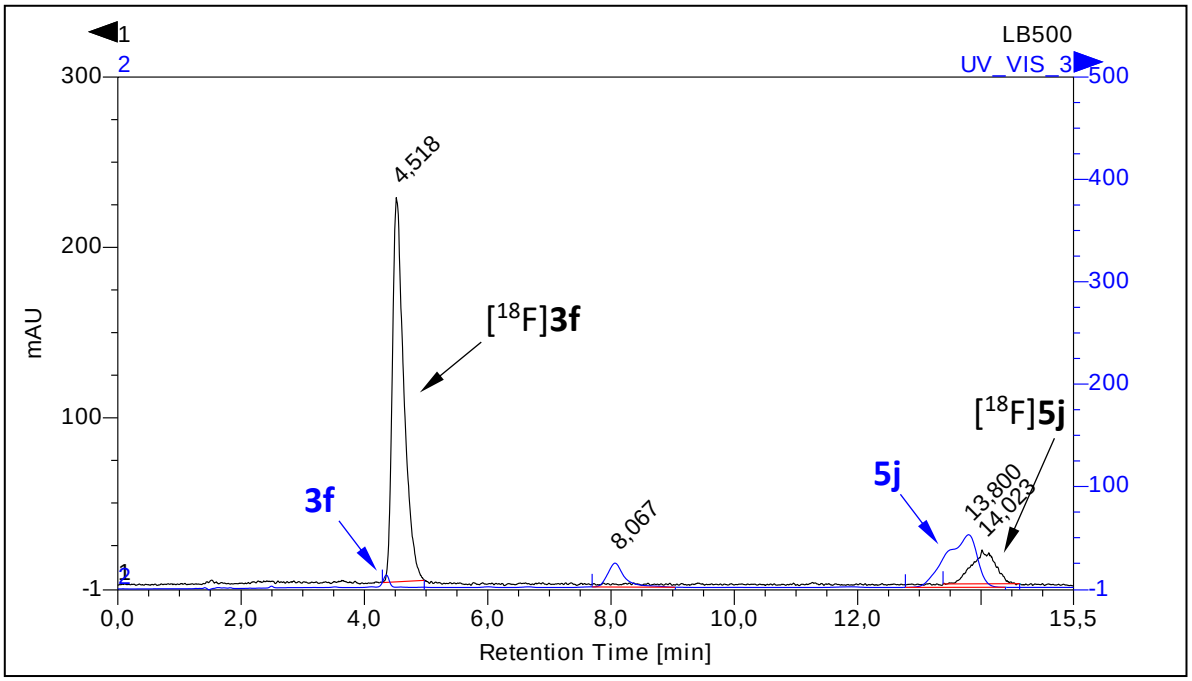

Figure S28: HPLC traces of crude [^{18}F]**5j** spiked with the non-radioactive reference compounds, Method B. Blue trace: UV, λ = 254 nm; black trace: radioactivity.

5.11 HPLC traces of [^{18}F]**5k** (**Figs. S29** & **S30**)

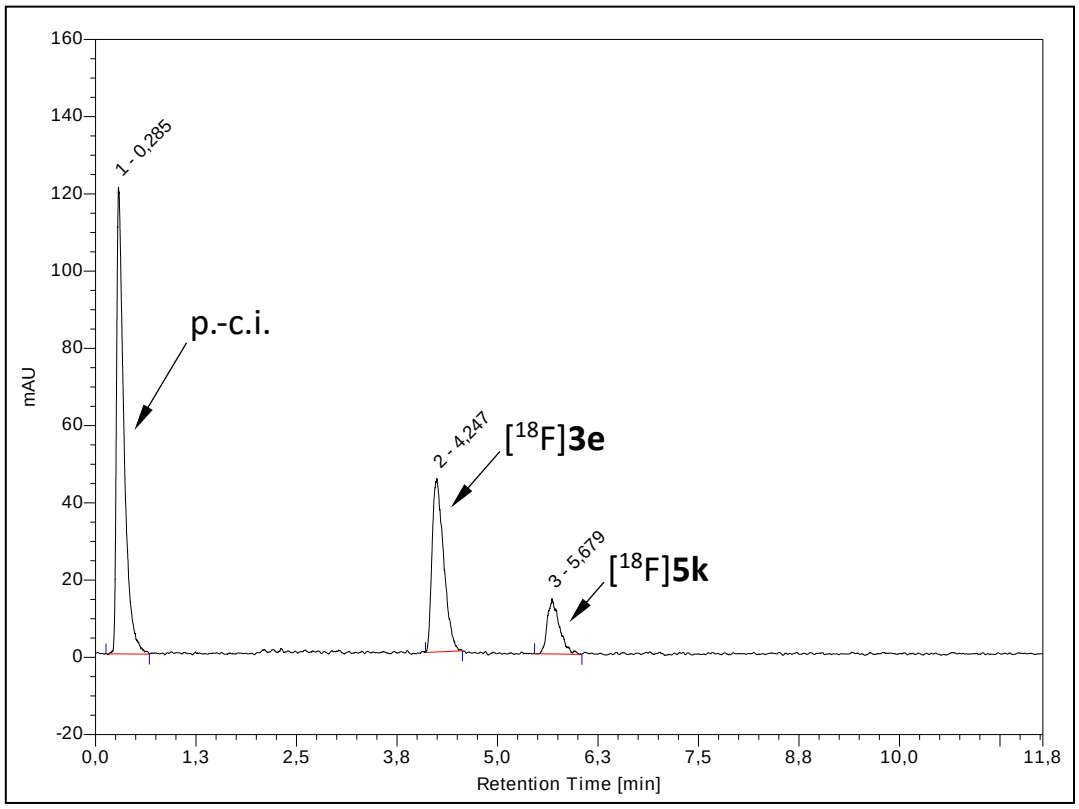

Figure S29: Radio-HPLC trace of [^{18}F]**5k**, Method A. Abbreviation: p.-c.i. – post-column injection.

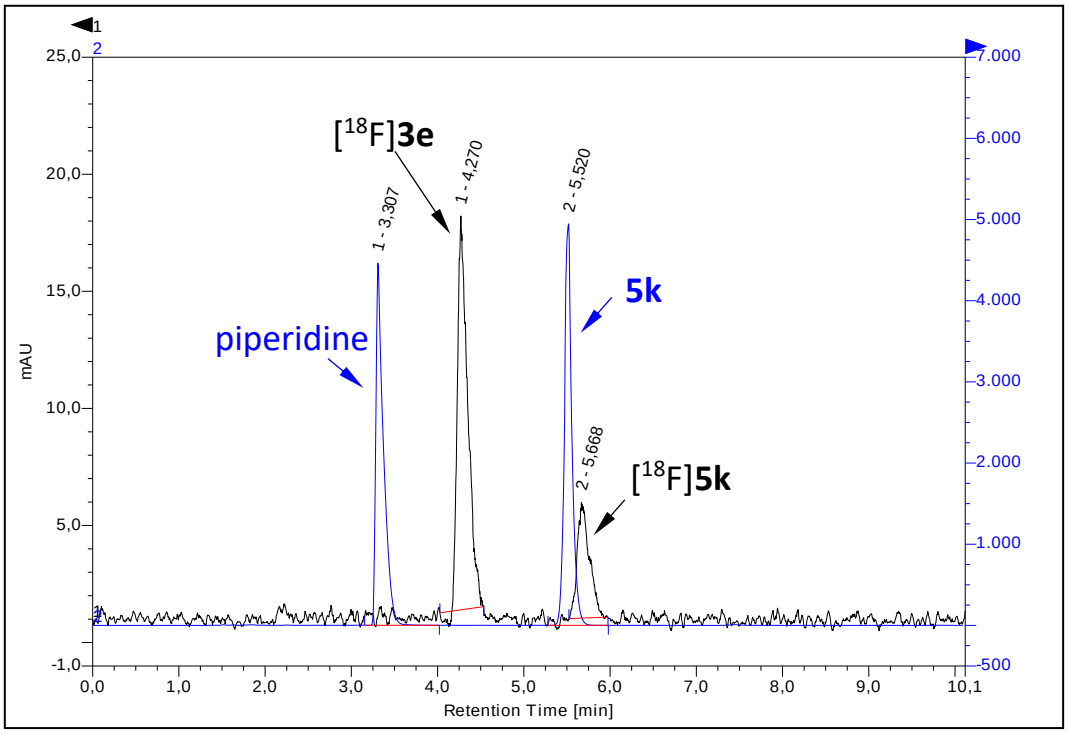

Figure S30: HPLC traces of crude [^{18}F]**5k** spiked with the non-radioactive reference compound, Method B. Blue trace: UV, λ = 254 nm; black trace: radioactivity.

5.12 HPLC trace of [^{18}F]**5l** (**Fig. S31**)

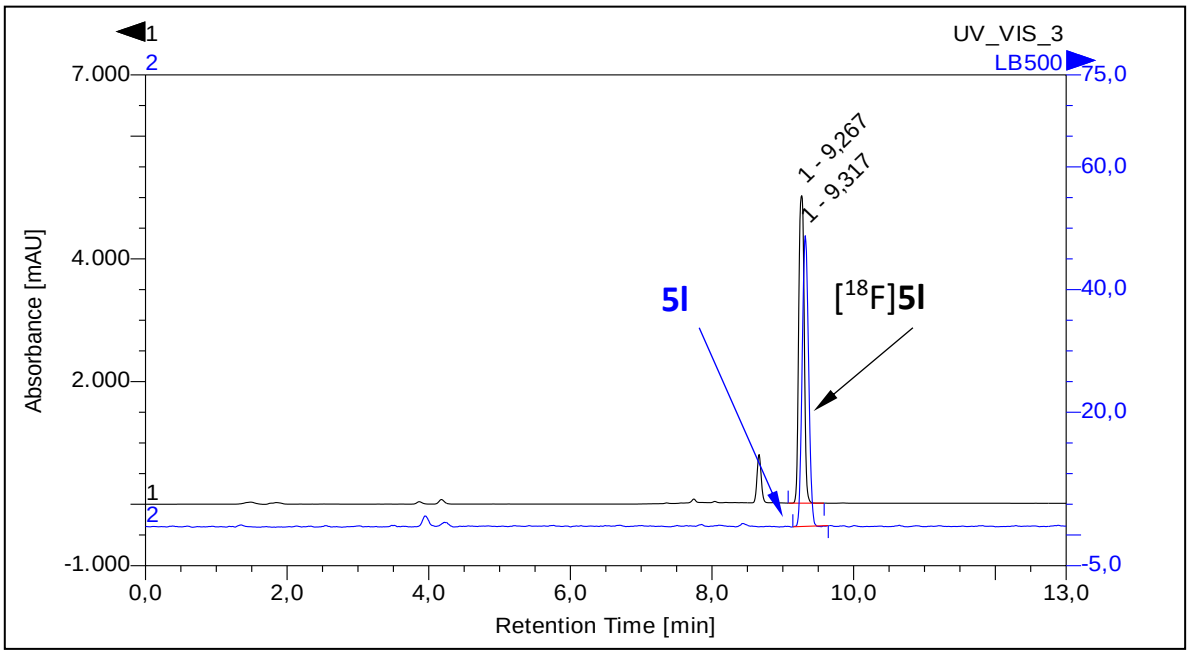

Figure S31: HPLC traces of crude [^{18}F]**5l** spiked with the non-radioactive reference compound, Method A (0.1% TFA). Blue trace: UV, λ = 254 nm; black trace: radioactivity.

5.13 HPLC trace of [^{18}F]**5m** (**Fig. S32**)

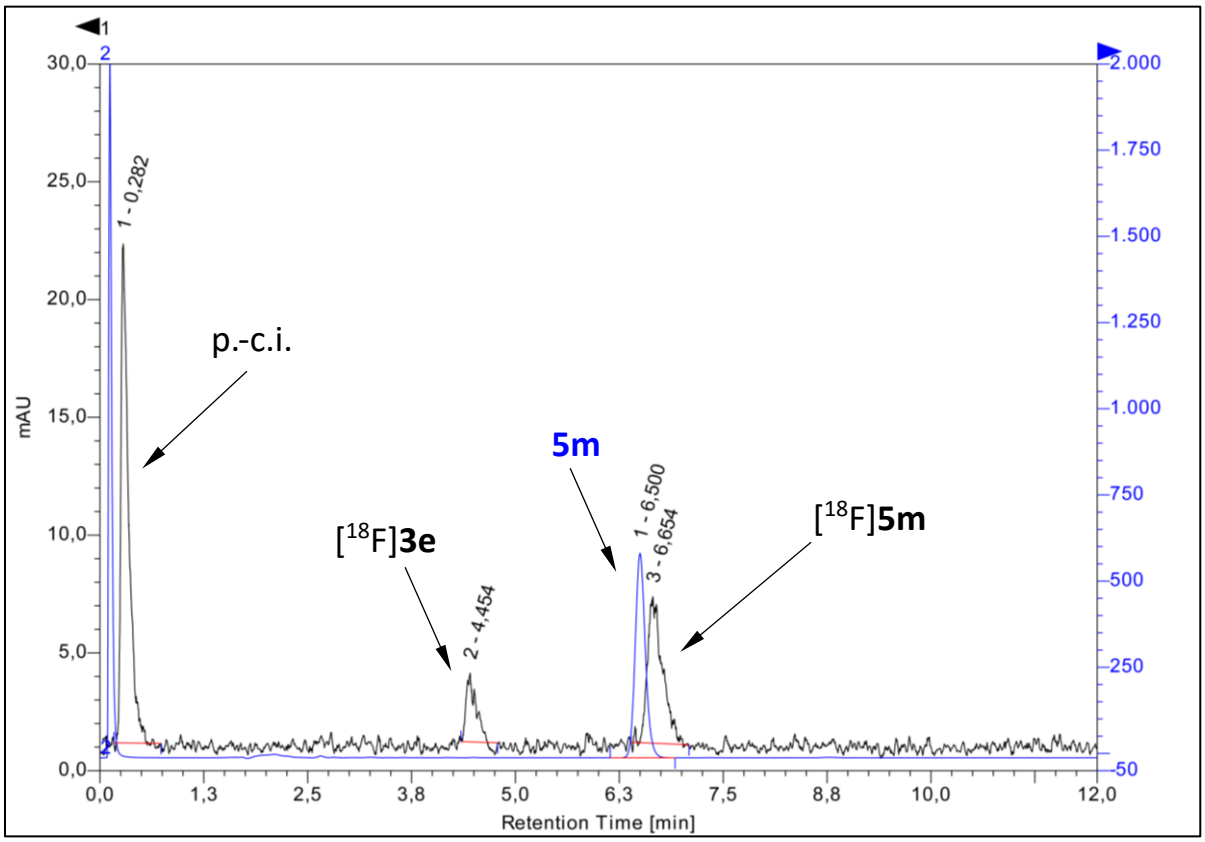

Figure S32: HPLC traces of crude [^{18}F]**5m** spiked with the non-radioactive reference compound, Method B. Blue trace: UV, λ = 254 nm; black trace: radioactivity. Abbreviation: p.-c.i. – post-column injection.

5.14 HPLC trace of [^{18}F]**5o** (**Fig. S33**)

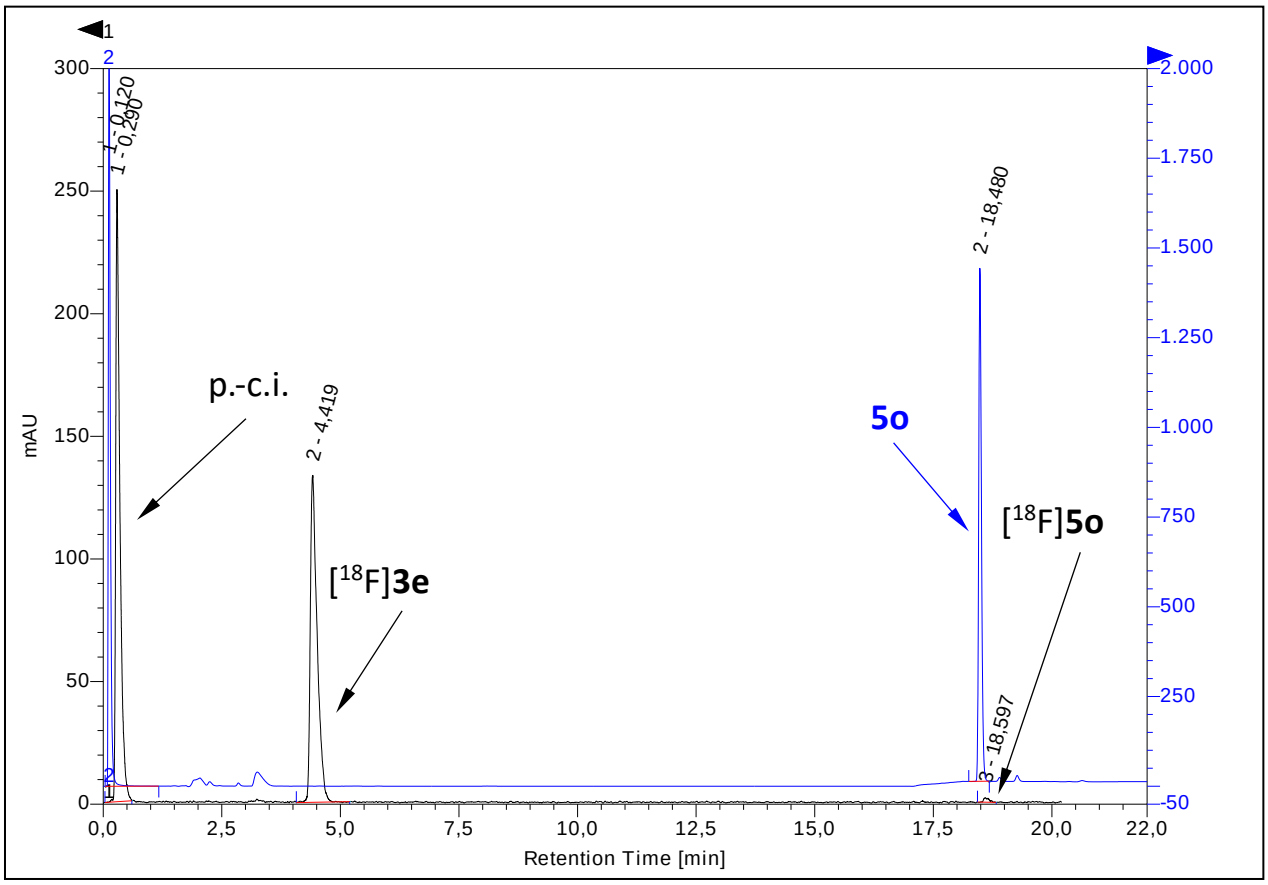

Figure S33: HPLC traces of crude [^{18}F]**5o** spiked with the non-radioactive reference compound, Method B. Blue trace: UV, λ = 254 nm; black trace: radioactivity. Abbreviation: p.-c.i. – post-column injection.

5.15 HPLC trace for competition between Ac-Lys(H)-O*t*Bu and H-Lys(Z)-O*t*Bu (4:1) (**Fig. S34**)

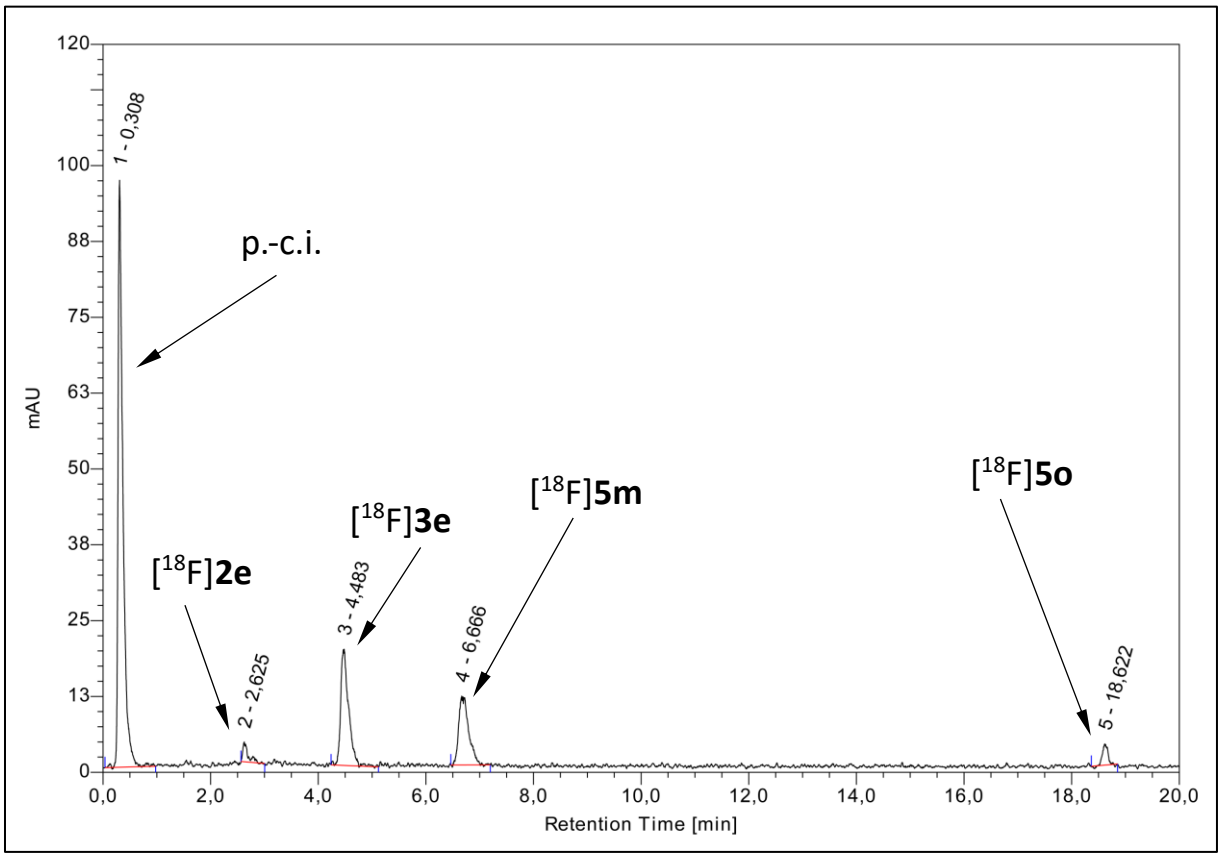

Figure S34: HPLC trace of the competition experiment, Method B. Blue trace: UV, λ = 254 nm; black trace: radioactivity. Abbreviation: p.-c.i. – post-column injection.

5.16 HPLC trace for competition between *n*-butylamine and H-Gly-OMe (**Fig. S35**)

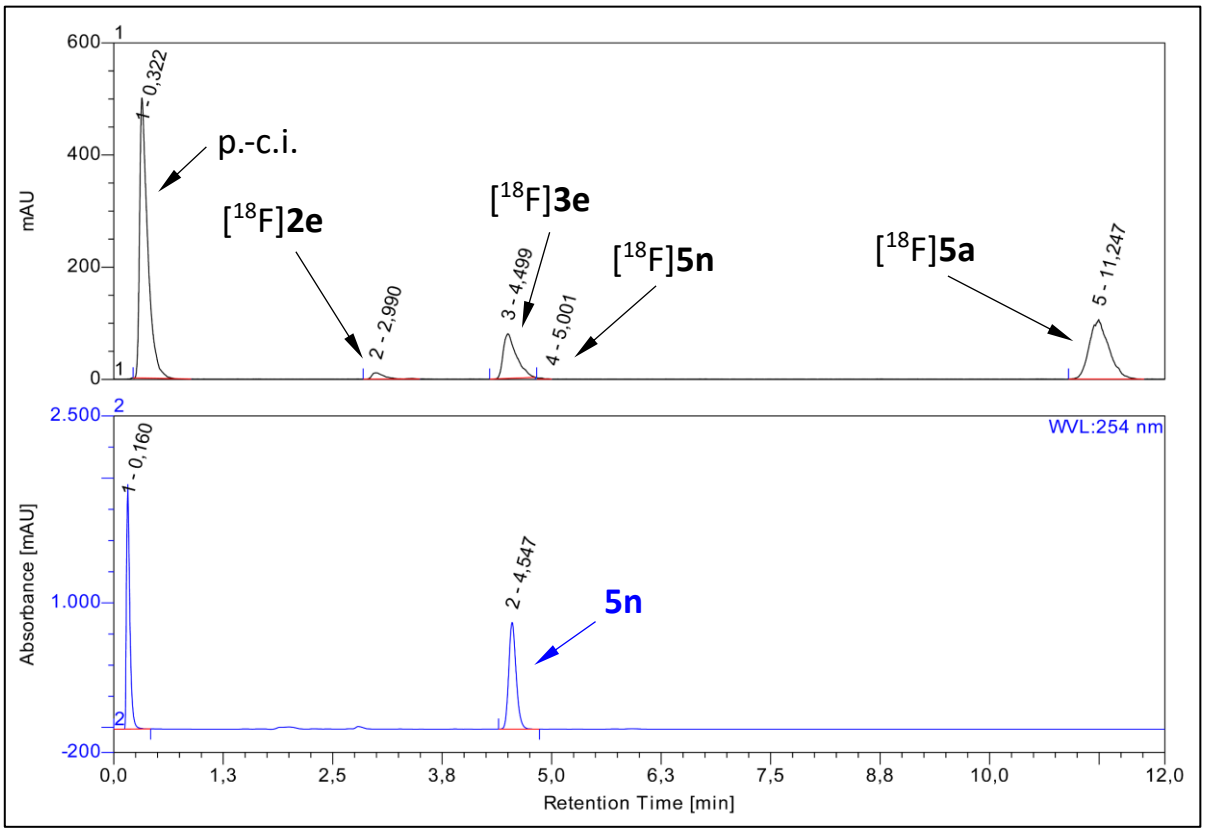

Figure S35: HPLC traces of competition experiment spiked with the non-radioactive reference compound **5n**, Method A (0.1% TFA). Blue trace: UV, λ = 254 nm; black trace: radioactivity. Abbreviation: p.-c.i. – post-column injection.

5.17 HPLC traces of [^{18}F]**5p** ([^{18}F]JK-PSMA-15) (**Figs. S36-S38**)

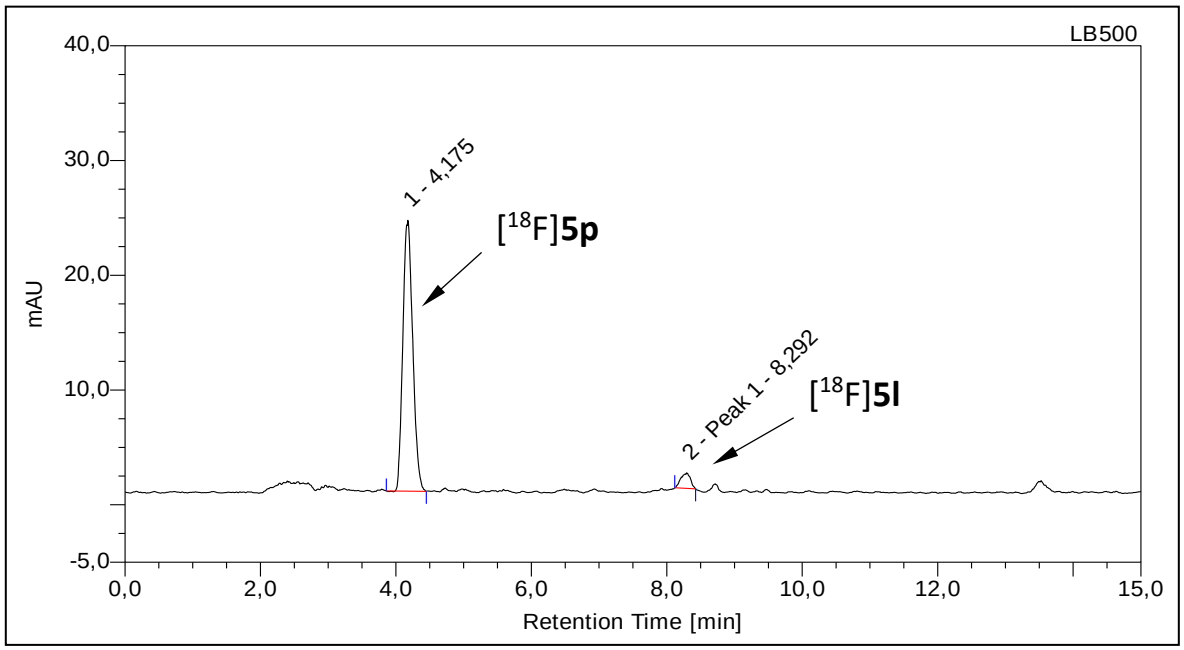

Figure S36: Radio-HPLC trace of crude [^{18}F]**5p** ([^{18}F]JK-PSMA-15), Method E (0.1% TFA).

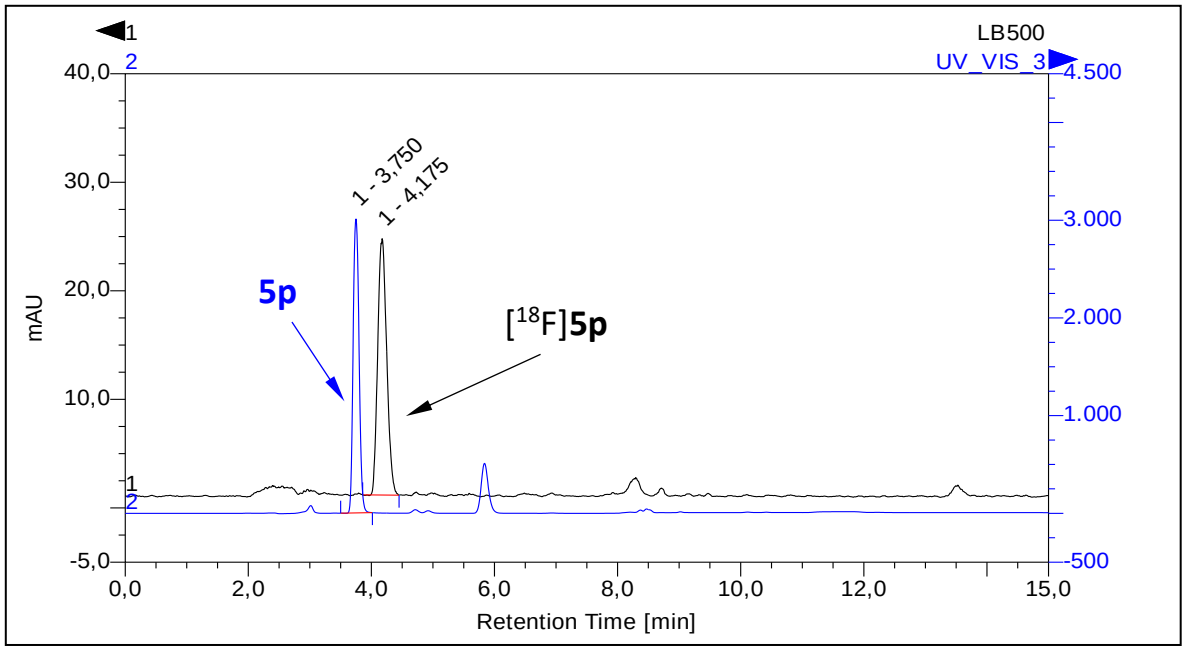

Figure S37: HPLC traces of crude [^{18}F]**5p** ([^{18}F]JK-PSMA-15) spiked with the non-radioactive reference compound, Method E (0.1% TFA). Blue trace: UV, λ = 254 nm; black trace: radioactivity.

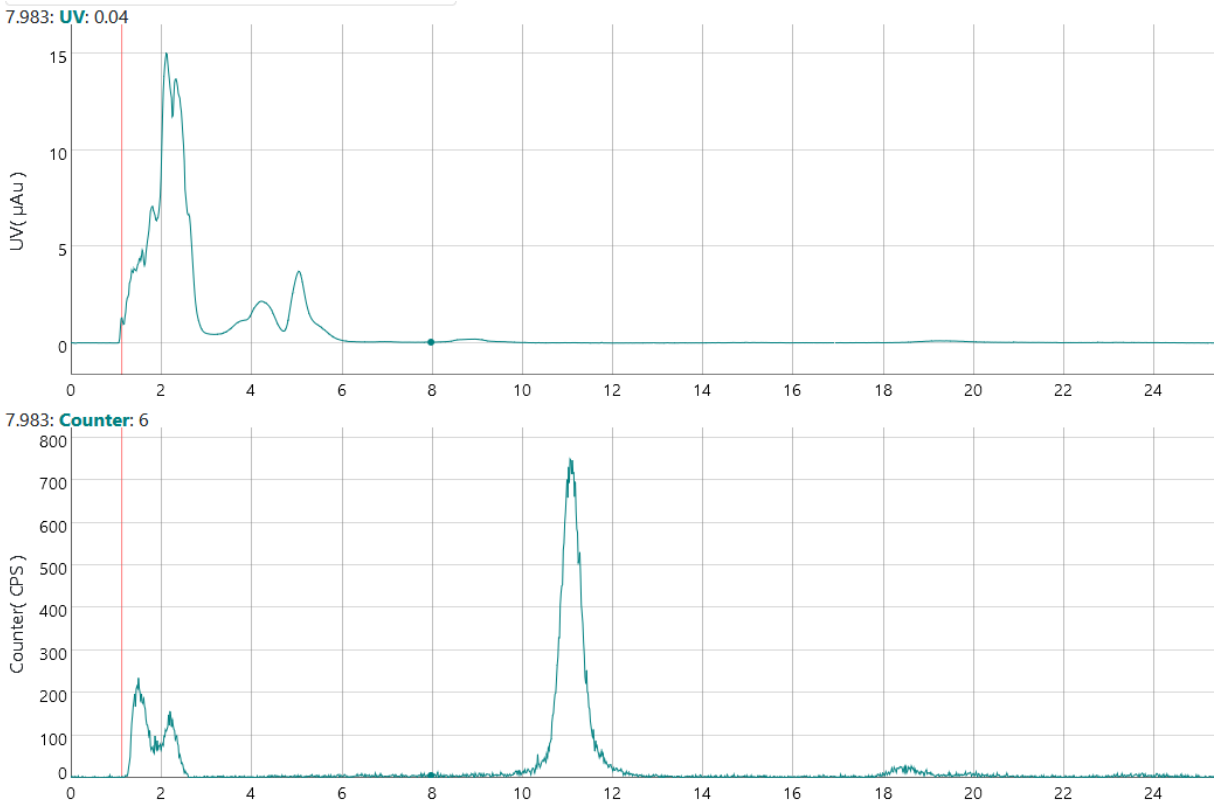

Figure S38: Purification of [^{18}F]**5p** ([^{18}F]JK-PSMA-15) by preparative HPLC (top: UV chromatogram, λ=254 nm; bottom: radio-chromatogram; column: Hydro-RP, 250×10 mm; eluent: 30% MeCN (0.1% TFA); flow rate: 4.7 mL/min; t_R = 11 min).

5.18 HPLC traces of [^{18}F]**6a** (**Figs. S39** & **S40**)

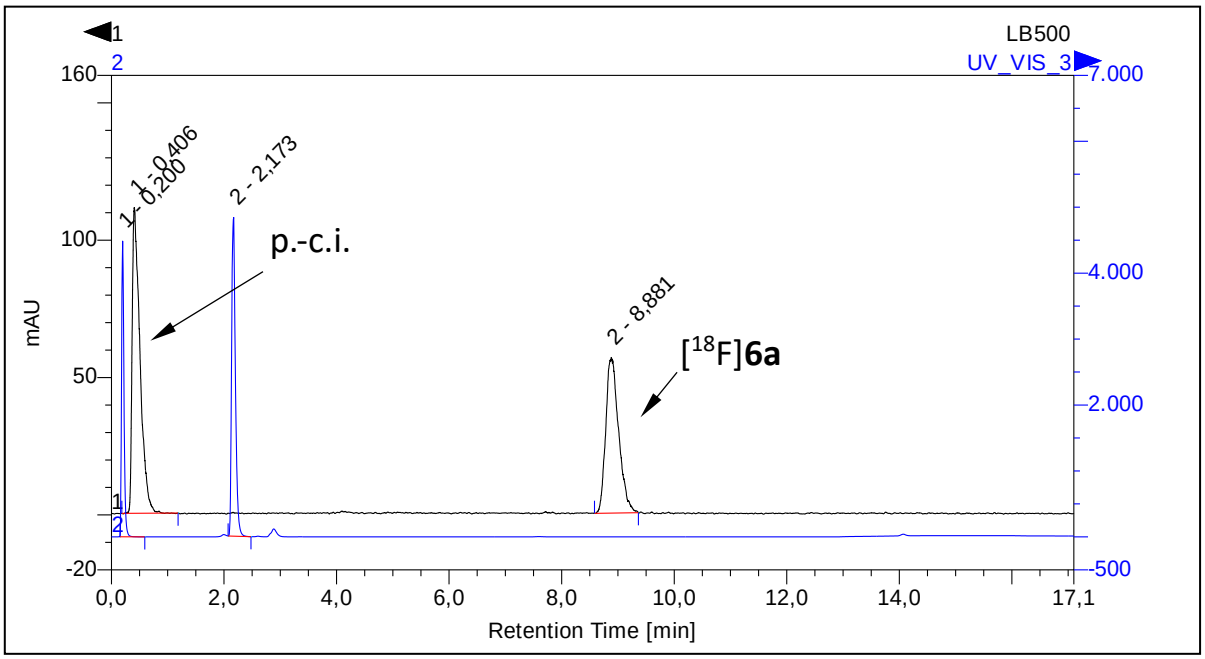

Figure S39: HPLC traces of crude [^{18}F]**6a**, Method A (0.1% TFA). Blue trace: UV, λ = 254 nm; black trace: radioactivity. Abbreviation: p.-c.i. – post-column injection.

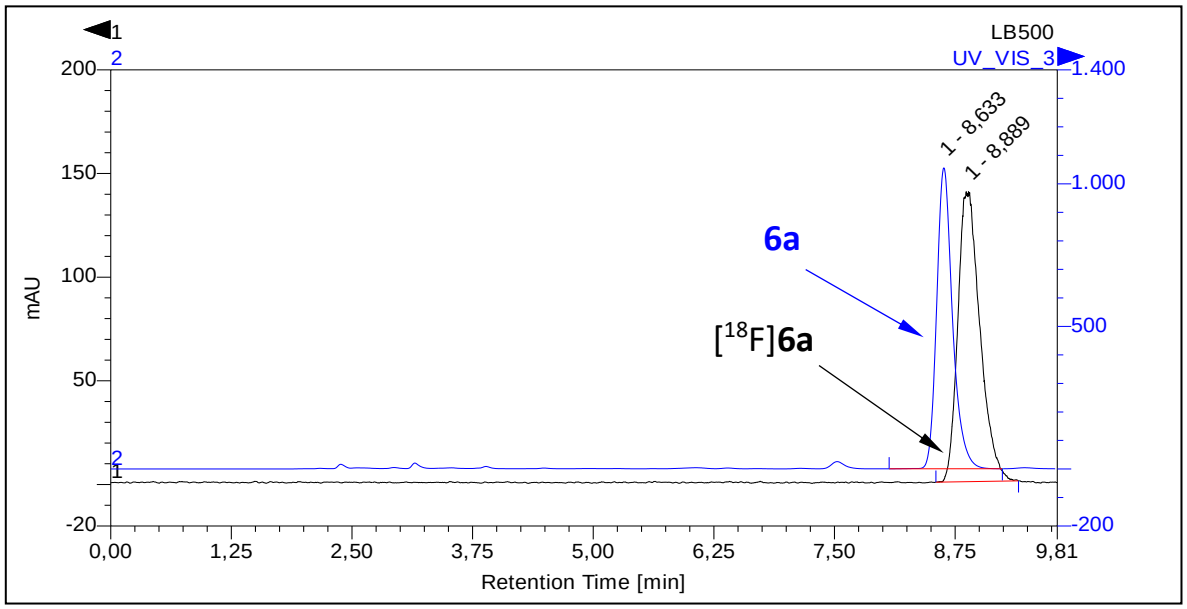

Figure S40: HPLC traces of crude [^{18}F]**6a** spiked with the non-radioactive reference compound, Method A (0.1% TFA). Blue trace: UV, λ = 254 nm; black trace: radioactivity.

5.19 HPLC traces of [^{18}F]**6b** ([^{18}F]JK-PSMA-16) (**Figs. S41-S43**)

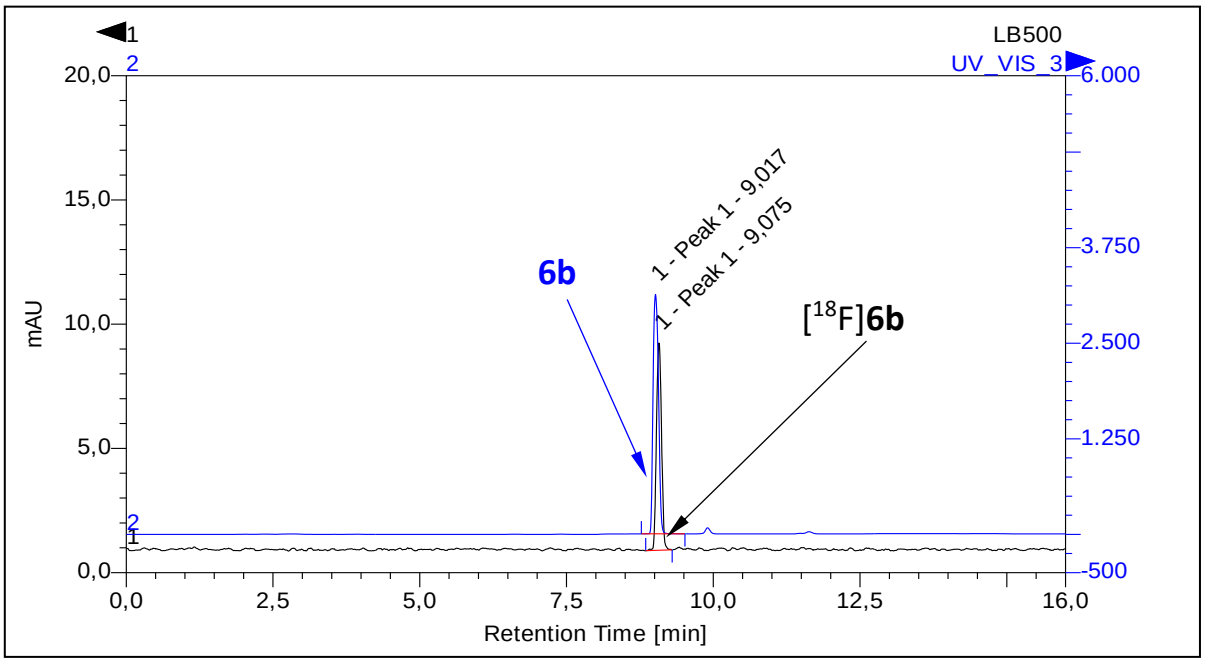

Figure S41: HPLC traces of purified [^{18}F]**6b** ([^{18}F]JK-PSMA-16) spiked with the non-radioactive reference compound, Method E (0.1% TFA). Blue trace: UV, λ = 254 nm; black trace: radioactivity.

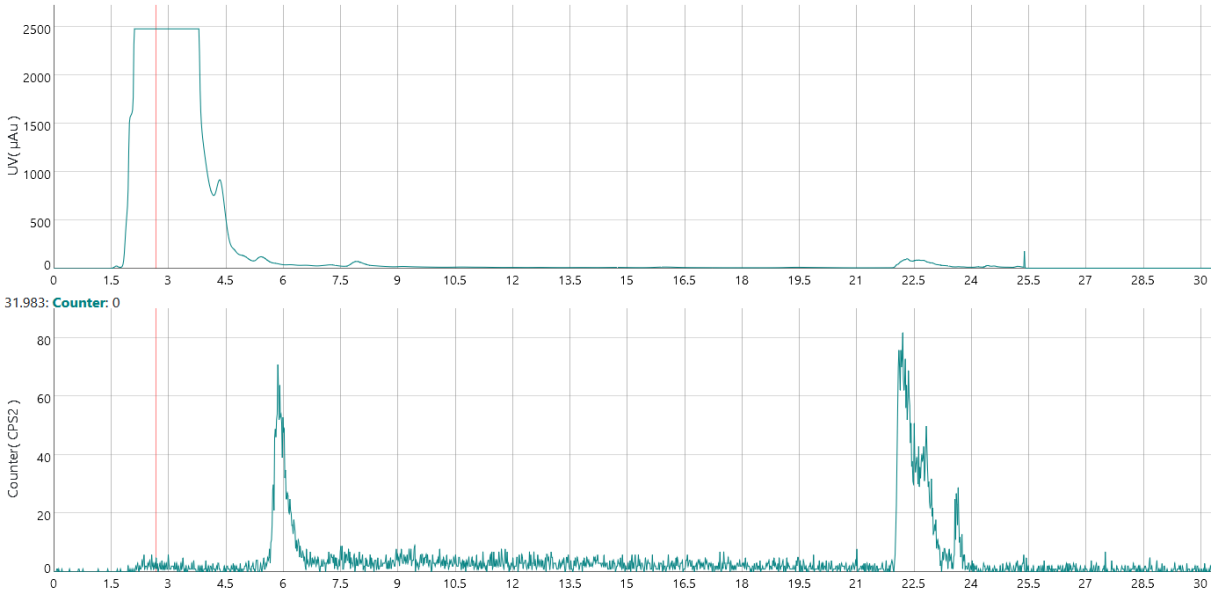

Figure S42: Purification of [^{18}F]**6b** ([^{18}F]JK-PSMA-16) by preparative HPLC (top: UV chromatogram, λ=254 nm; bottom: radio-chromatogram; column: Hydro-RP, 250×10 mm; eluent: 30% MeCN (0.1% TFA); flow rate: 4.7 mL/min; t_R = 22 min).

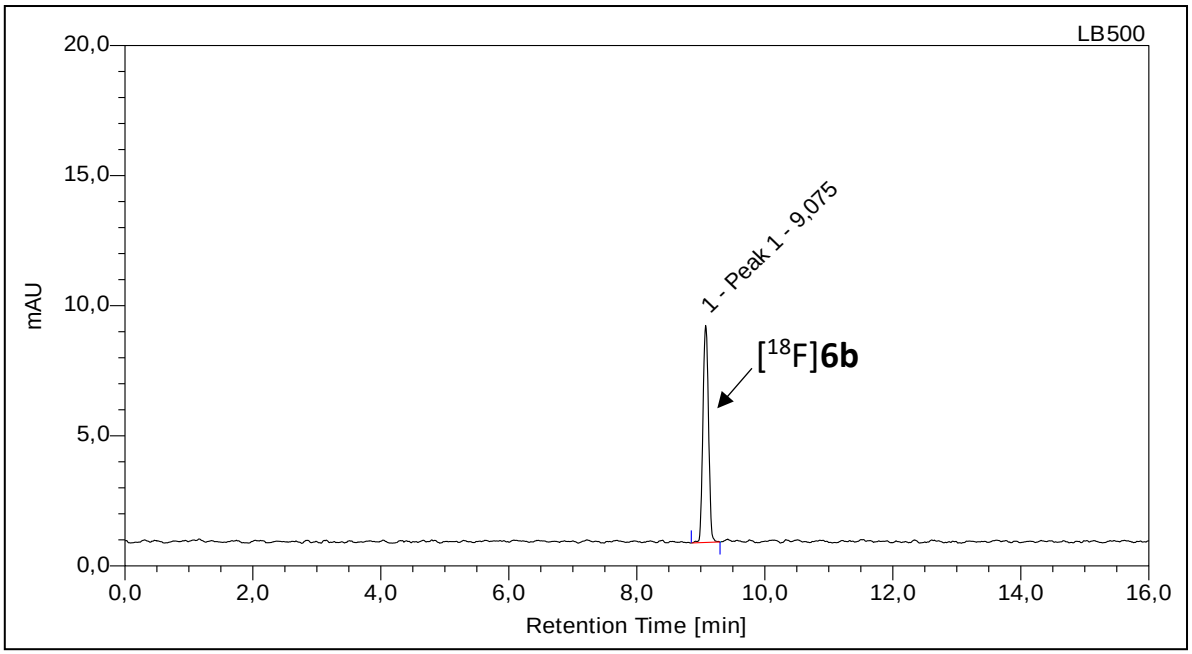

Figure S43: Radio-HPLC of purified [^{18}F]**6b** ([^{18}F]JK-PSMA-16), Method E (0.1% TFA).

5.20 HPLC traces of [^{18}F]**6c** (**Figs. S44** & **S45**)

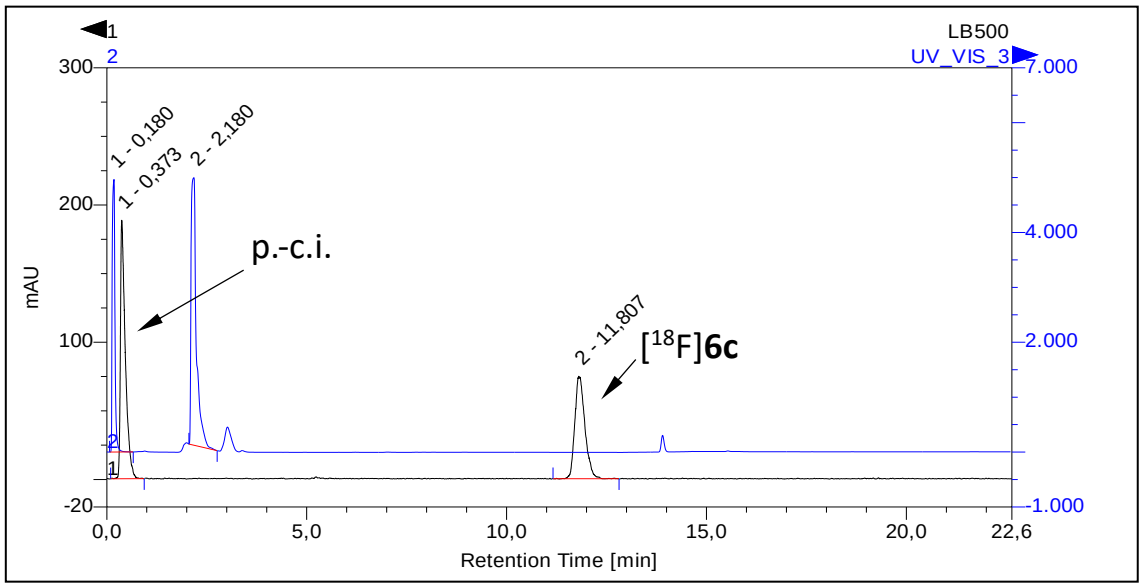

Figure S44: HPLC traces of crude [^{18}F]**6c**, Method A (0.1% TFA). Blue trace: UV, λ = 254 nm; black trace: radioactivity. Abbreviation: p.-c.i. – post-column injection.

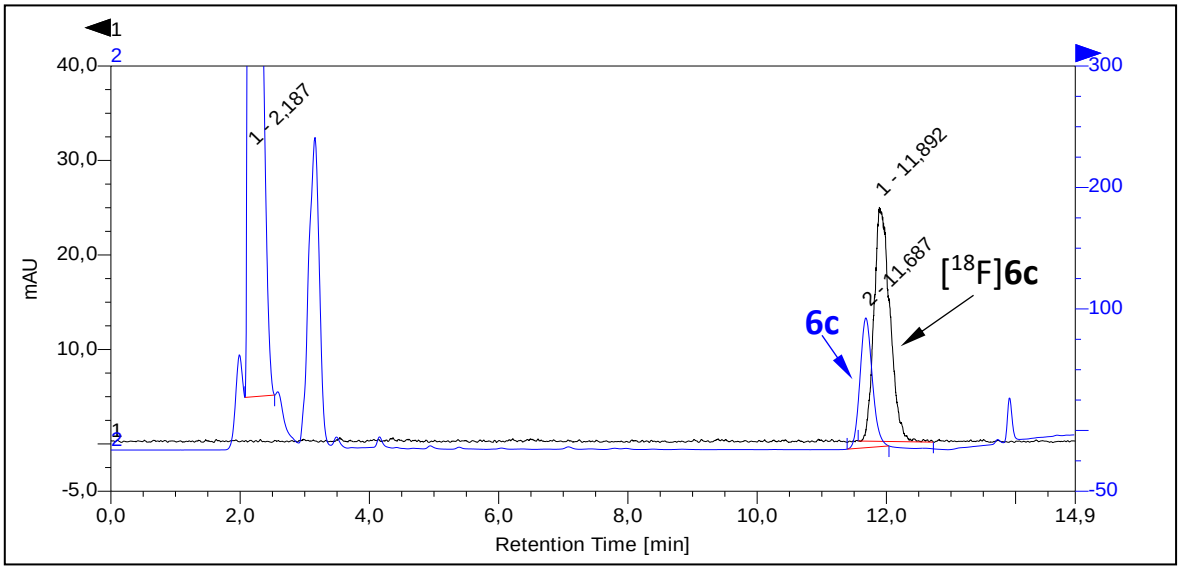

Figure S45: HPLC traces of crude [^{18}F]**6c** spiked with the non-radioactive reference compound, Method A (0.1% TFA). Blue trace: UV, λ = 254 nm; black trace: radioactivity.

5.21 HPLC traces of [^{18}F]**6d** ([^{18}F]JK-PSMA-18) (**Figs. S46-S49**)

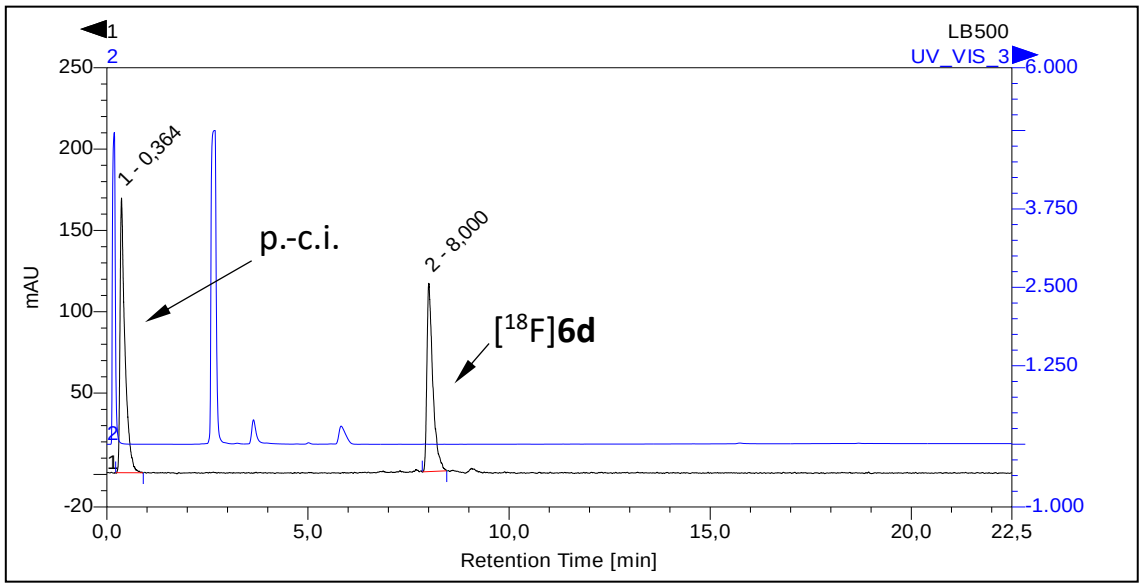

Figure S46: HPLC traces of crude [^{18}F]**6d** ([^{18}F]JK-PSMA-18), Method E (0.1% TFA). Blue trace: UV, λ = 254 nm; black trace: radioactivity. Abbreviation: p.-c.i. – post-column injection.

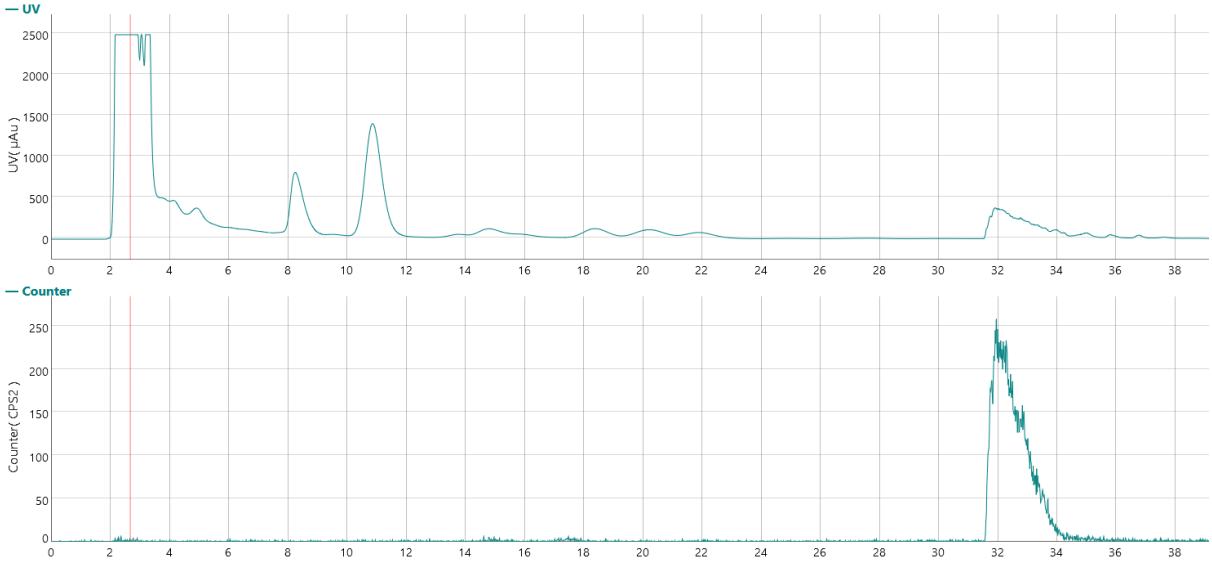

Figure S47: Purification of [^{18}F]**6d** ([^{18}F]JK-PSMA-18) by preparative HPLC (top: UV chromatogram, λ=254 nm; bottom: radio-chromatogram; column: Hydro-RP, 250×10 mm; eluent: 30% MeCN (0.1% TFA); flow rate: 4.7 mL/min; t_R = 32 min).

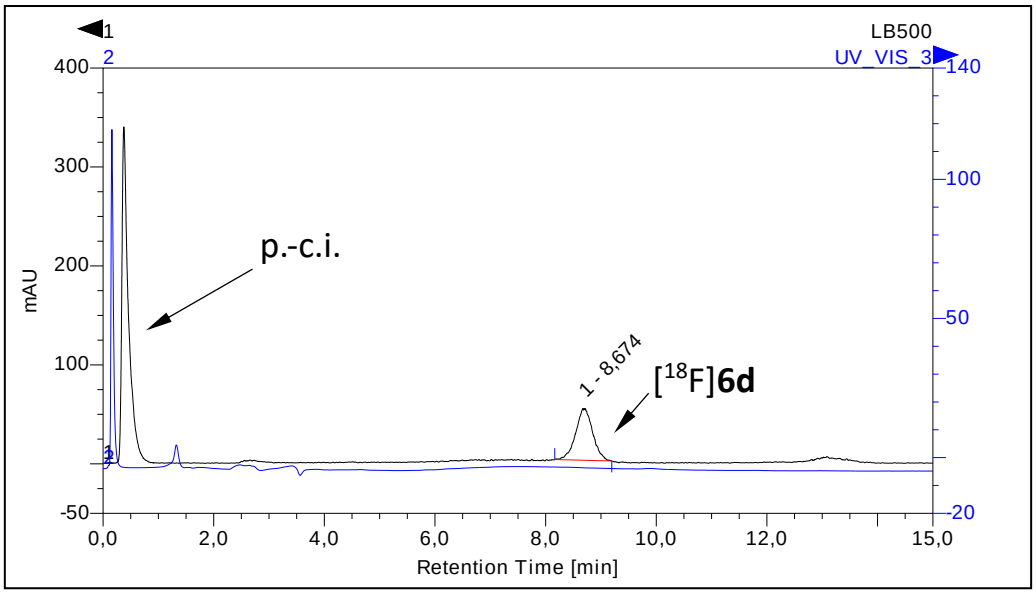

Figure S48: HPLC traces of purified [^{18}F]**6d** ([^{18}F]JK-PSMA-18), Method E (0.1% TFA). Blue trace: UV, λ = 254 nm; black trace: radioactivity. Abbreviation: p.-c.i. – post-column injection.

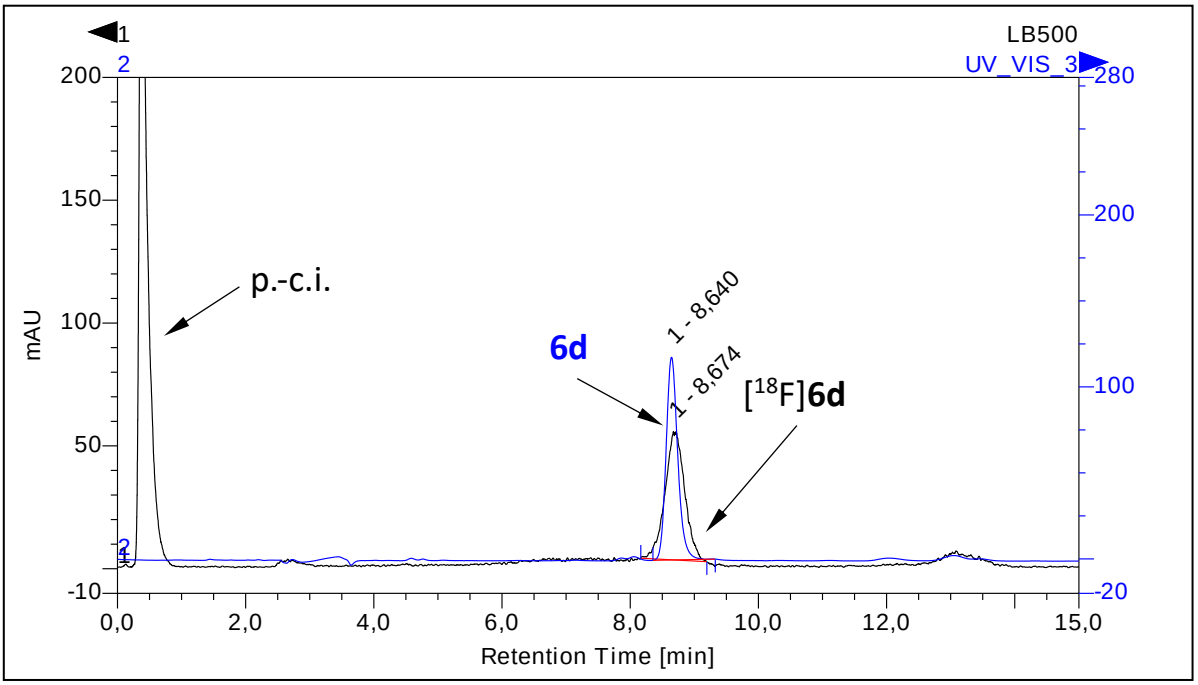

Figure S49: HPLC traces of [^{18}F]**6d** ([^{18}F]JK-PSMA-18) spiked with the non-radioactive reference compound, Method E (0.1% TFA). Blue trace: UV, λ = 254 nm; black trace: radioactivity. Abbreviation: p.-c.i. – post-column injection.

6 Calibration curves

6.1 Calibration curve for JK-PSMA-15

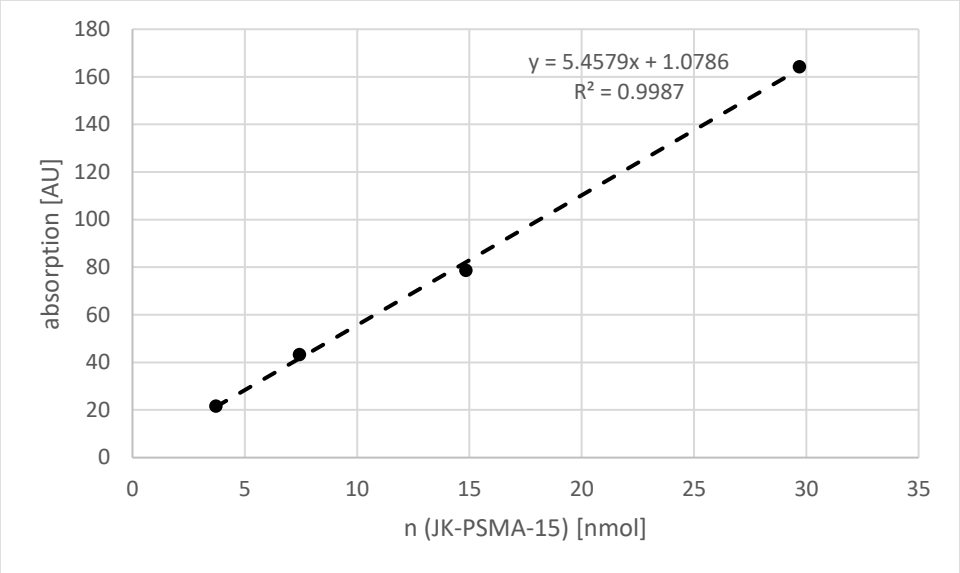

6.2 Calibration curve for JK-PSMA-16

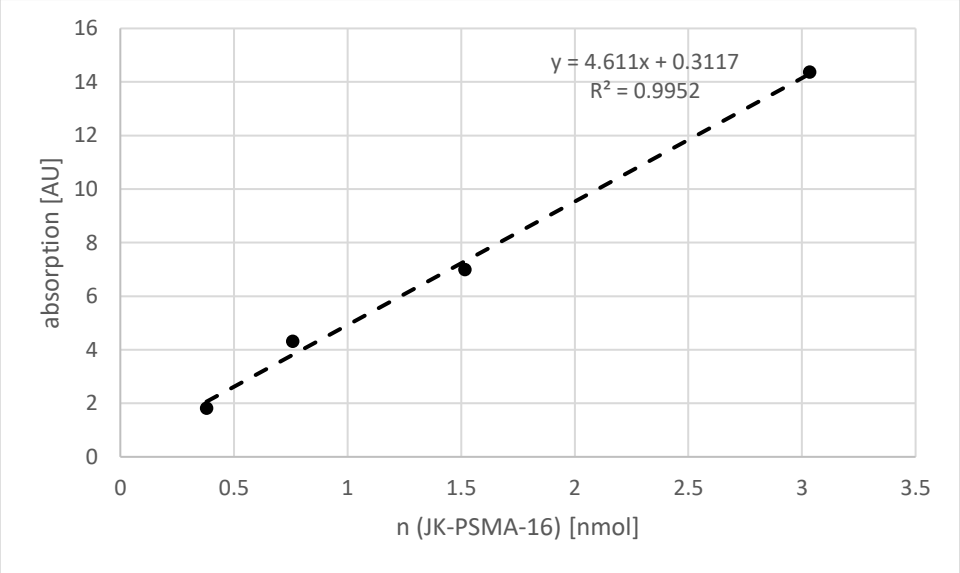

6.3 Calibration curve for JK-PSMA-18

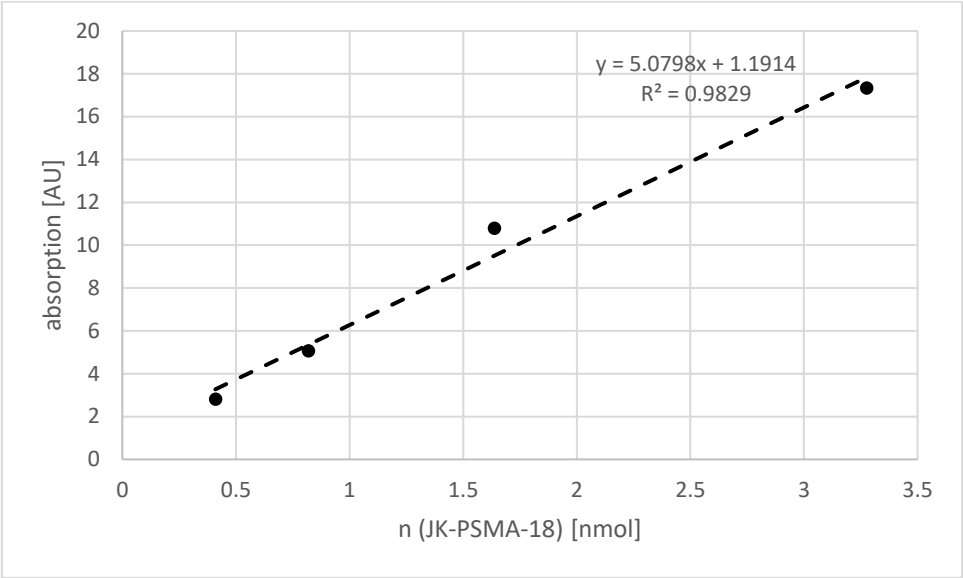

7 In vivo experiments

7.1 Methods

7.1.1 Signal-to-background ratio (SCG/background)

This parameter describes the difference between tracer uptake into the PSMA-positive ganglia and tracer uptake into PSMA-negative background tissues. It was calculated as the ratio of mean SUV_{bw} values determined in elliptical volumes of interest (VOIs) drawn over the PSMA-positive superior cervical ganglion (SCG: 150 voxels) and the PSMA-negative neck region dorsal from the spinal cord (background: 1600 voxels).

7.1.2 Acutance

The image intensity of a PSMA-positive ganglion decreases gradually towards surrounding background tissues, forming a slope which reflects the edge contrast or acutance. Accordingly, the acutance provides a measure for the perceived sharpness of the image and the ability to reliably measure the size of small PSMA-expressing tissues, which are important criteria for, e.g., the delineation of PSMA-positive metastases from surrounding PSMA-negative tissues. For quantification of the acutance in VINCI 5.21 (Max Planck Institute for Metabolism Research, Cologne, Germany), an 8 mm profile (1 pixel width) was placed over the middle of the SCG (diameter approx. 3.5 mm) in the horizontal plane. The slope of the profile plot was determined by dividing the maximum height of the SCG profile (peak minus background) by its full width at half maximum (FWHM). The time frame used for this analysis was 60–120 min p.i.

7.1.3 Resolution

The dorsal root ganglia (DRG) are arranged in pairs along the spinal cord, and the resolution describes how well the two ganglia of a pair can be separated from each other. Accordingly, the resolution provides a measure for the ability to distinguish two adjacent PSMA-expressing tissues, which is an important criterion for, e.g., the delineation of PSMA-positive metastases located close to each other or to other structures with high radioactivity retention. For quantification of the resolution in VINCI 5.21, a 12 mm profile was placed over the first cervical pair of the DRG (ganglion diameter approx. 2.5 mm; distance from center to center approx. 4 mm) in the horizontal plane. The resolution R was then calculated from the profile plot according to:

$$R = \frac{2(P1 - P2)}{1.7(FWHM1 + FWHM2)}$$

where P1-P2 is the distance between the two peaks corresponding to the ganglia and FWHM1 and FWHM2 are their full widths at half maximum.

7.2 Results (**Tab. S1-S5 & Fig. S50**)

Table S1: Values of injected dose and animal weight for the experiments with the newly developed PSMA-tracers.

Tracer	Injected dose [MBq]	Animal weight [g]	n
[^{18}F]JK-PSMA-15	62.8 ± 8.1	334 ± 31	3
[^{18}F]JK-PSMA-15 + 2-PMPA	62.4	302	1
[^{18}F]JK-PSMA-16	56.3 ± 8.1	290 ± 17	3
[^{18}F]JK-PSMA-16 + 2-PMPA	60.2	268	1
[^{18}F]JK-PSMA-18	61.8 ± 1.5	260 ± 25	3
[^{18}F]JK-PSMA-18 + 2-PMPA	58.4	237	1

Table S2: Properties of the newly developed PSMA-tracers in comparison to [^{18}F]JK-PSMA-7 at 90-120 min p.i.

	[^{18}F]JK-PSMA-7[a]	[^{18}F]JK-PSMA-15	[^{18}F]JK-PSMA-16	[^{18}F]JK-PSMA-18
SCG uptake, SUV_{bw}	31.3 ± 10.5	45.2 ± 8.2	19.1 ± 9.4	46.2 ± 9.7
Background uptake, SUV_{bw}	4.03 ± 1.00	4.05 ± 0.79	6.17 ± 3.02	6.78 ± 1.03
Acutance, %ID/g/mm	0.075 ± 0.027	0.079 ± 0.024	0.026 ± 0.015	0.086 ± 0.019
Resolution	1.095 ± 0.042	1.089 ± 0.144	1.032 ± 0.115	0.961 ± 0.157
Signal-to-background ratio	8.15 ± 1.71	11.49 ± 3.29	2.27 ± 0.24	7.04 ± 2.32

[a] Values for [^{18}F]JK-PSMA-7 are from[2].

Table S3: Statistical comparison of the tracer properties at 90-120 min p.i. using one-way ANOVA followed by Dunnett's multiple comparison test.

	ANOVA main effect	[^{18}F]JK-PSMA-15 vs. [^{18}F]JK-PSMA-7	[^{18}F]JK-PSMA-16 vs. [^{18}F]JK-PSMA-7	[^{18}F]JK-PSMA-18 vs. [^{18}F]JK-PSMA-7
SCG uptake, SUV_{bw}	F(3,8)=5.5; p=0.0239	p=0.2438	p=0.3283	p=0.2040
Background uptake, SUV_{bw}	F(3,8)=2.2; p=0.1608	not tested	not tested	not tested
Acutance, %ID/g/mm	F(3,8)=3.5; p=0.0698	not tested	not tested	not tested
Resolution	F(3,7)=0.8; p=0.5516	not tested	not tested	not tested
Signal-to-background ratio	F(3,8)=9.1; p=0.0058	p=0.2209	p=0.0273*	p=0.8656

* significant difference compared to [^{18}F]JK-PSMA-7.

Table S4: Signal-to-background ratios (mean±SD) measured during four consecutive 30 min time frames.

Tracer	0-30 min p.i.	30-60 min p.i.	60-90 min p.i.	90-120 min p.i.
[^{18}F]JK-PSMA-7[a]	3.82 ± 0.23	5.44 ± 0.56	7.04 ± 1.31	9.27 ± 2.12
[^{18}F]JK-PSMA-15	4.71 ± 0.54	7.57 ± 1.73	10.28 ± 2.95	14.02 ± 4.37
[^{18}F]JK-PSMA-16	2.54 ± 0.65	2.52 ± 0.65	2.86 ± 0.25	2.86 ± 0.16
[^{18}F]JK-PSMA-18	3.83 ± 0.55	4.71 ± 1.18	6.45 ± 2.11	8.02 ± 3.04

[a] Values for [^{18}F]JK-PSMA-7 are from[2].

Table S5: Comparison of signal-to-background ratios using 2-way ANOVA with factors "tracer" and "uptake period". Main effect for factor "tracer": F(3,8)=10.08; p=0.0043. Shown are results from Dunnett's multiple comparison test, where each novel tracer is compared with [^{18}F]JK-PSMA-7.

Tracer	0-30 min p.i.	30-60 min p.i.	60-90 min p.i.	90-120 min p.i.
[^{18}F]JK-PSMA-15	p=0.6554	p=0.4187	p=0.1303	p=0.0162*
[^{18}F]JK-PSMA-16	p=0.0708	p=0.1916	p=0.0378*	p=0.0011*
[^{18}F]JK-PSMA-18	p=0.3167	p=0.9428	p=0.9678	p=0.7813

* significant difference compared to [^{18}F]JK-PSMA-7.

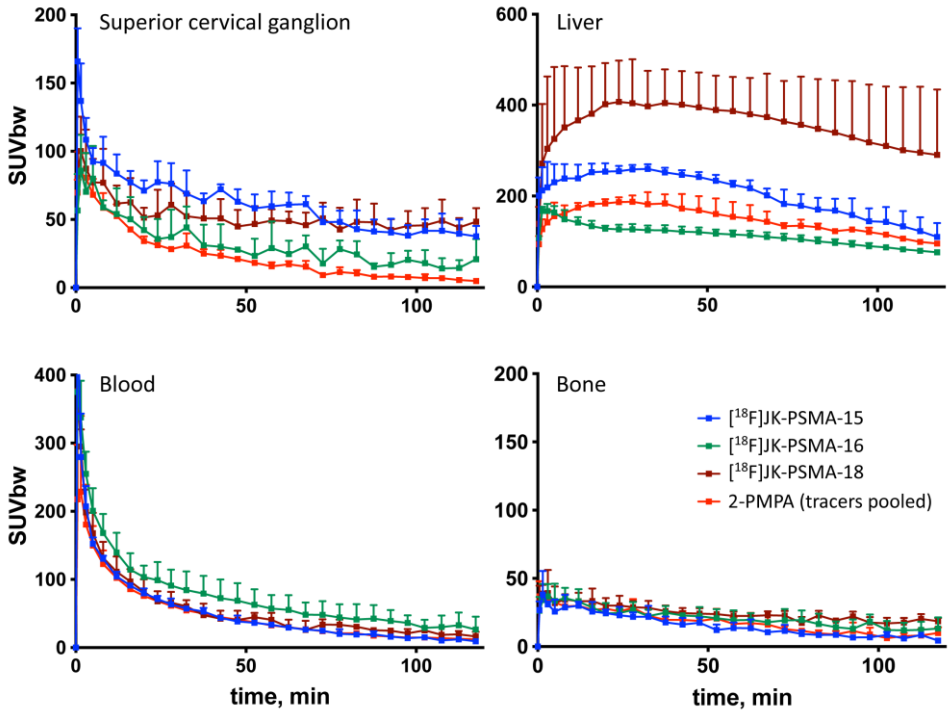

Figure S50: Comparison of time-activity curves (TACs) for the new PSMA-targeting tracers in the indicated volumes of interest (VOIs) measured without (n=3 per tracer) or with (n=1 per tracer, averaged across tracers) co-injection of the PSMA-inhibitor 2-PMPA. Note that one of the animals in the [^{18}F]JK-PSMA-18 group without co-injection of 2-PMPA showed unusually high liver uptake, as reflected in the higher variability of liver uptake for this tracer and the apparent difference between liver uptake with and without 2-PMPA co-injection.

8 References

(1) Krapf, P.; Richarz, R.; Urusova, E. A.; Neumaier, B.; Zlatopolskiy, B. D. Seyferth-Gilbert Homologation as a Route to ^{18}F-Labeled Building Blocks: Preparation of Radiofluor-inated Phenylacetylenes and Their Application in PET Chemistry. *European J. Org. Chem.* **2016**, *2016* (3), 430–433. https://doi.org/10.1002/ejoc.201501377.

(2) Zlatopolskiy, B. D.; Endepols, H.; Krapf, P.; Guliyev, M.; Urusova, E. A.; Richarz, R.; Hohberg, M.; Dietlein, M.; Drzezga, A.; Neumaier, B. Discovery of ^{18}F-JK-PSMA-7, a PET Probe for the Detection of Small PSMA-Positive Lesions. *J. Nucl. Med.* **2019**, *60* (6), 817–823. https://doi.org/10.2967/jnumed.118.218495.

Preclinical comparison of known and novel radiofluorinated FAP ligands prepared using different ^{18}F-labeling methods

Benedikt Gröner[1,2], Chris Hoffmann[1,2], Heike Endepols[1,2,3], Johannes Lindemeyer[4], Marco Timmer[5], Otari Gokhadze[2], Melanie Brugger[2], Felix Neumaier[1,2], Bernd Neumaier*[1,2], Boris D. Zlatopolskiy[1,2]

[1] *University of Cologne, Faculty of Medicine and University Hospital Cologne, Institute of Radiochemistry and Experimental Molecular Imaging, Kerpener Straße 62, 50937 Cologne, Germany.*

[2] *Forschungszentrum Jülich GmbH, Institute of Neuroscience and Medicine, Nuclear Chemistry (INM-5), Wilhelm-Johnen-Straße, 52428 Jülich, Germany.*

[3] *University of Cologne, Faculty of Medicine and University Hospital Cologne, Department of Nuclear Medicine, Kerpener Straße 62, 50937 Cologne, Germany.*

[4] *University of Cologne, Faculty of Medicine and University Hospital Cologne, Department of Radiology, Kerpener Straße 62, 50937 Cologne, Germany.*

[5] *University of Cologne, Faculty of Medicine and University Hospital Cologne, Center for Neurosurgery, Kerpener Straße 62, 50937 Cologne, Germany.*

* *Corresponding author; e-mail: b.neumaier@fz-juelich.de*

Table of content

1 NMR spectra

^{1}H NMR of compound 2

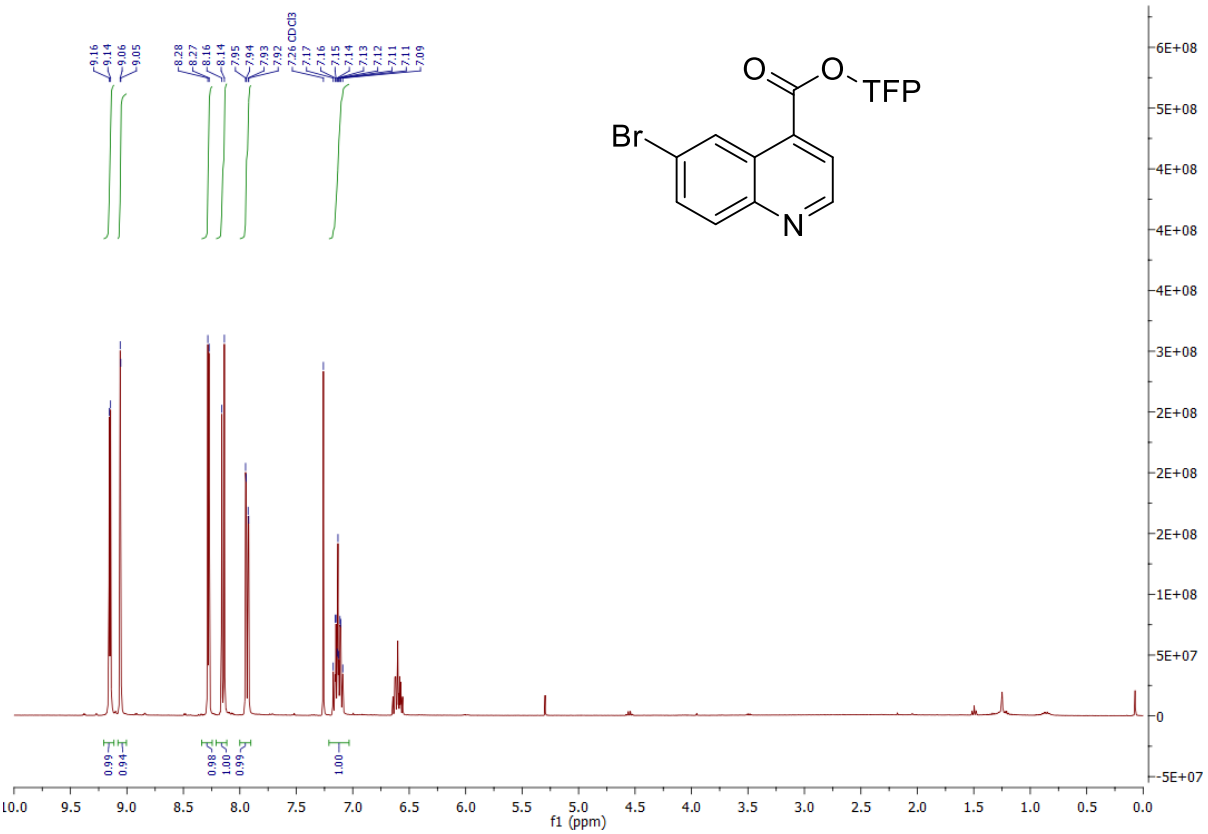

^{13}C NMR of compound 2

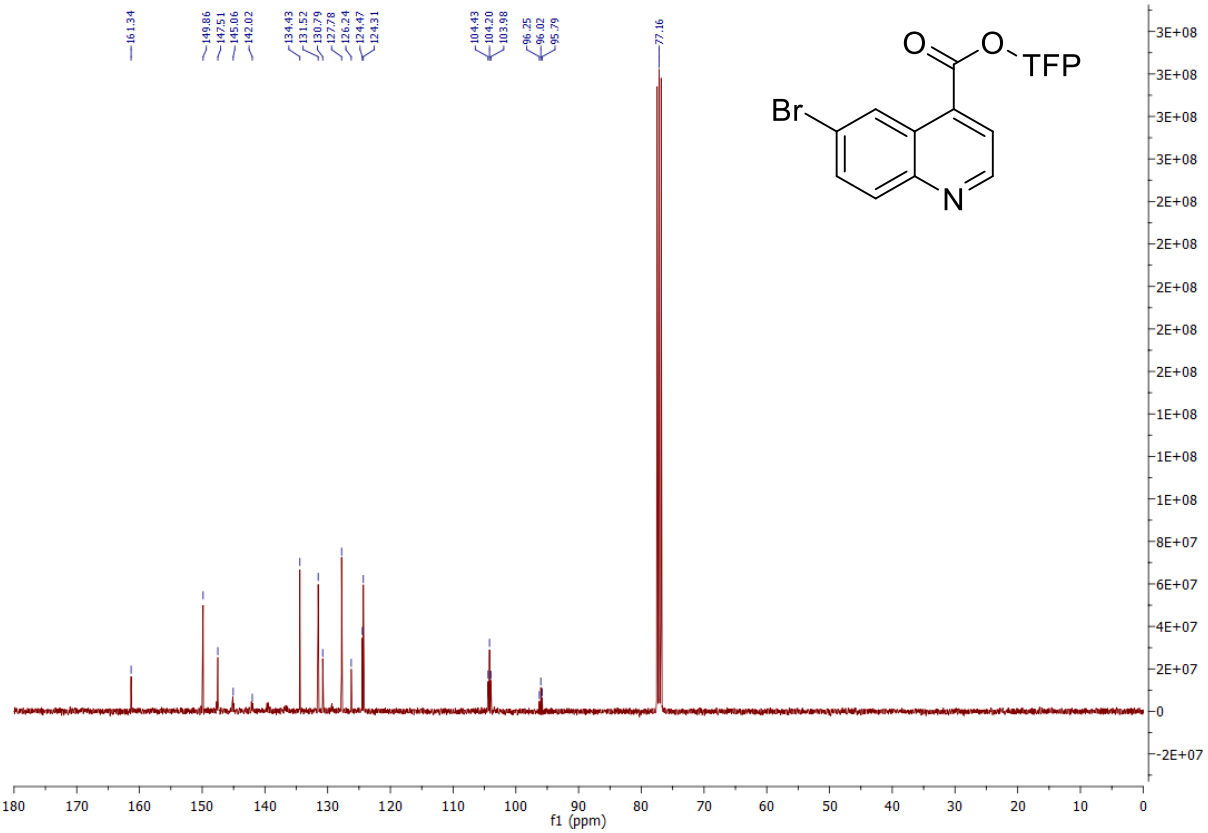

^{19}F NMR of compound 2

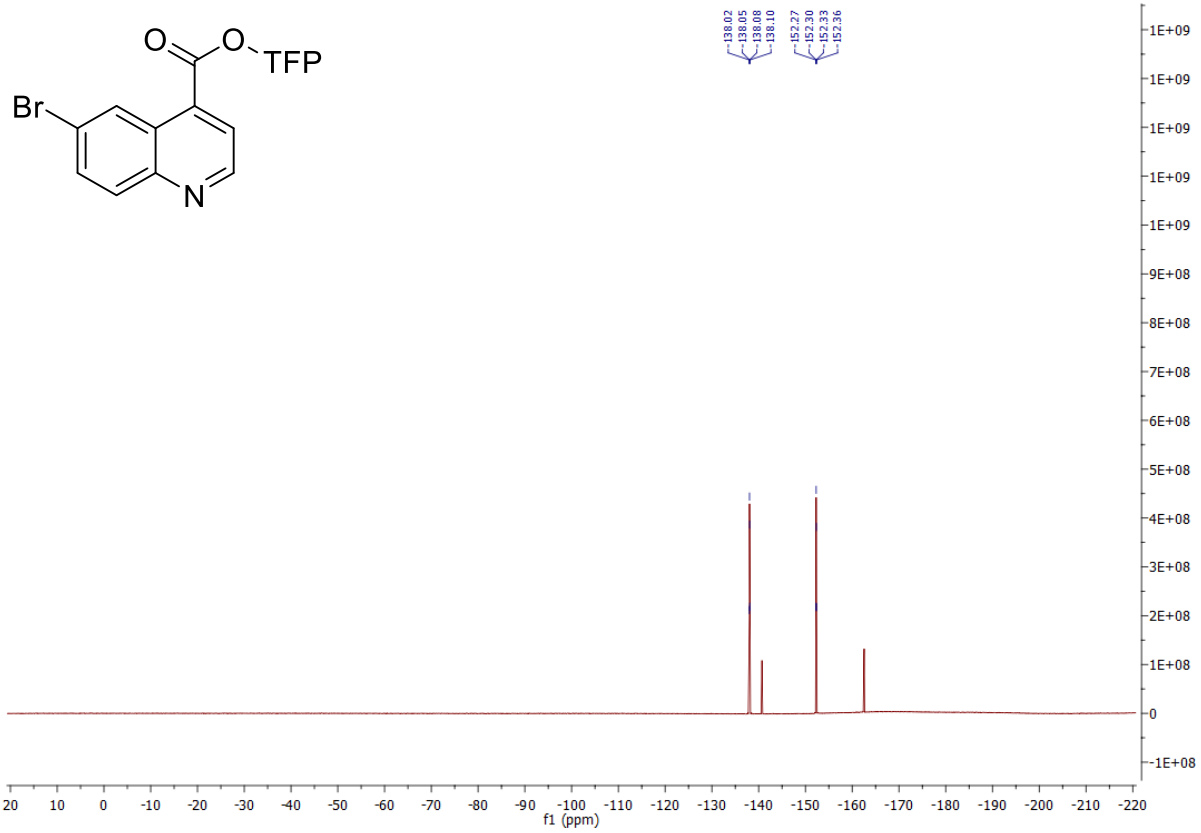

^{1}H NMR of compound 3

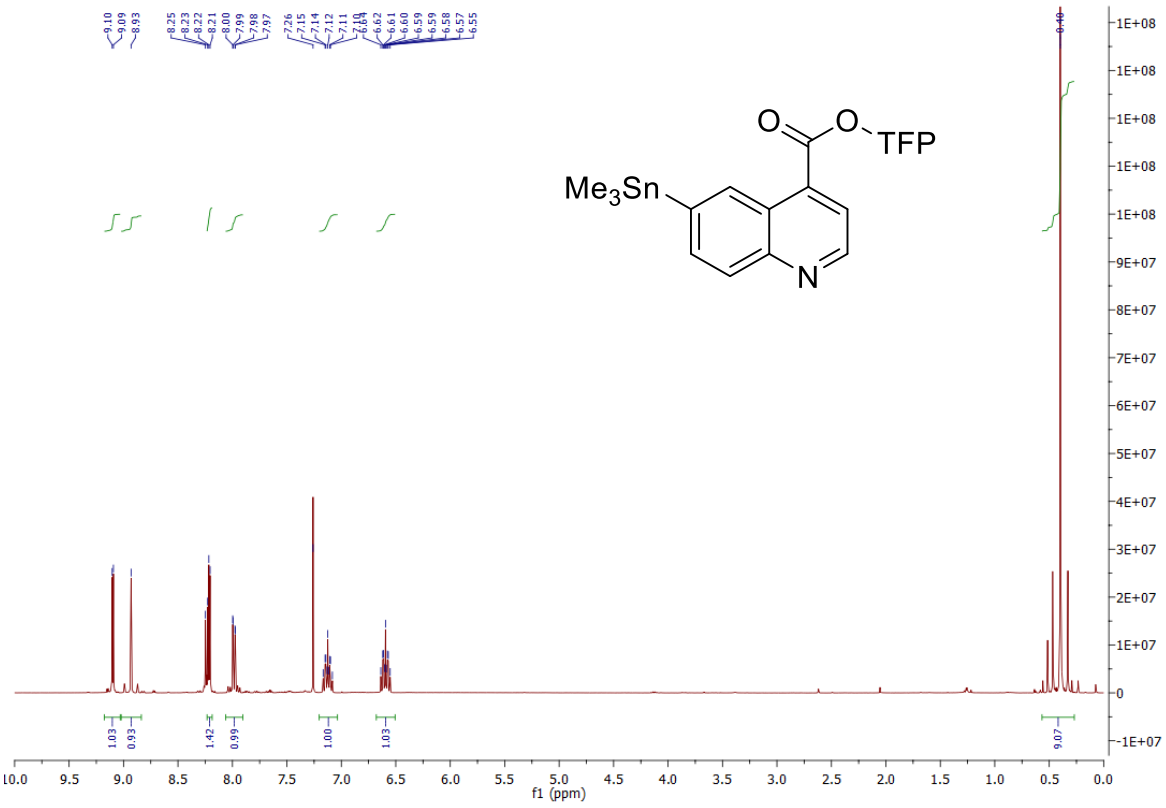

^{13}C NMR of compound 3

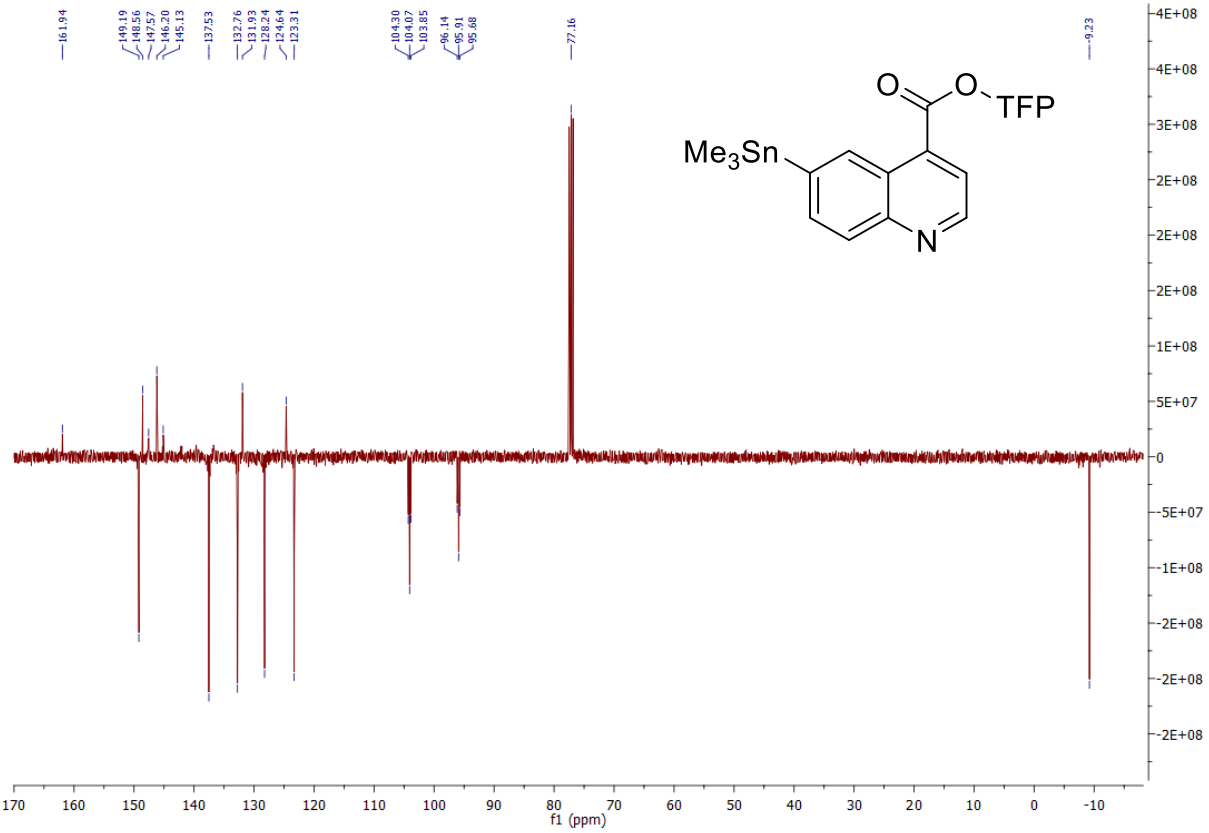

^{19}F NMR of compound 3

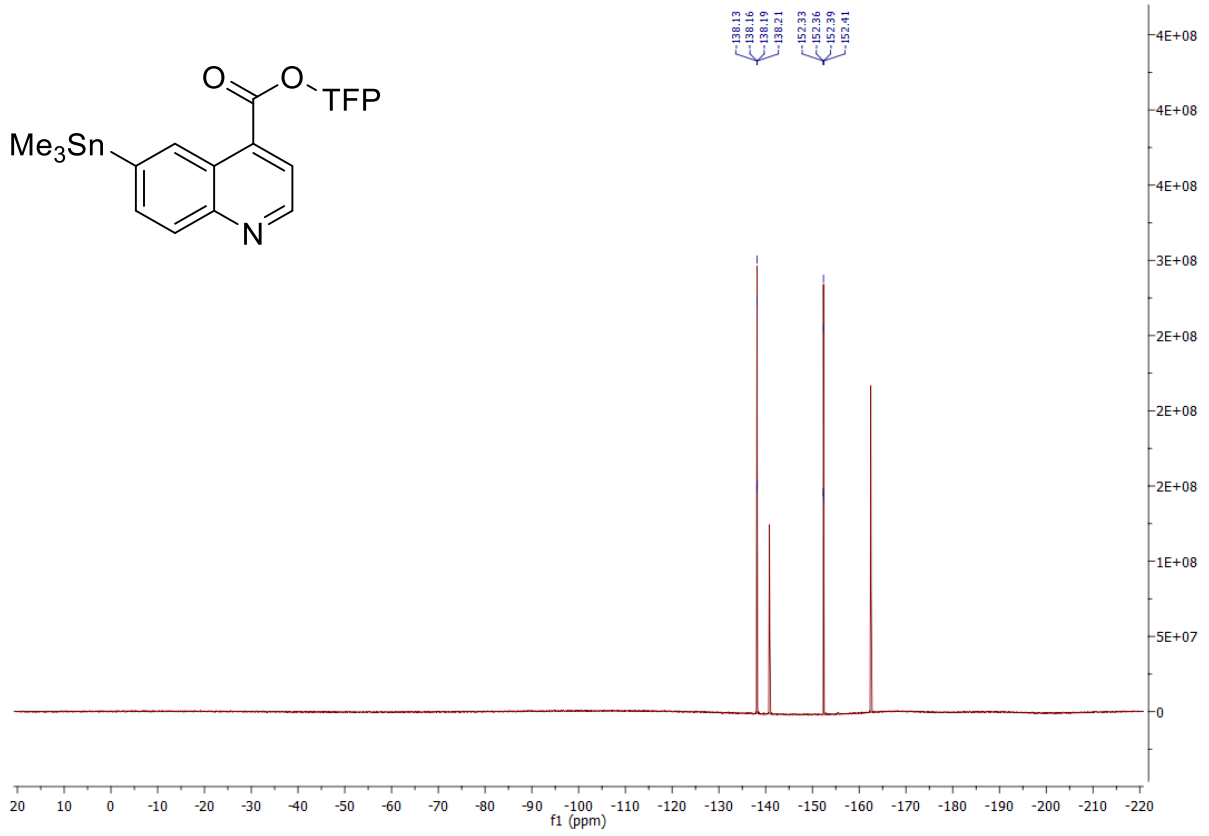

^{1}H NMR of compound 5

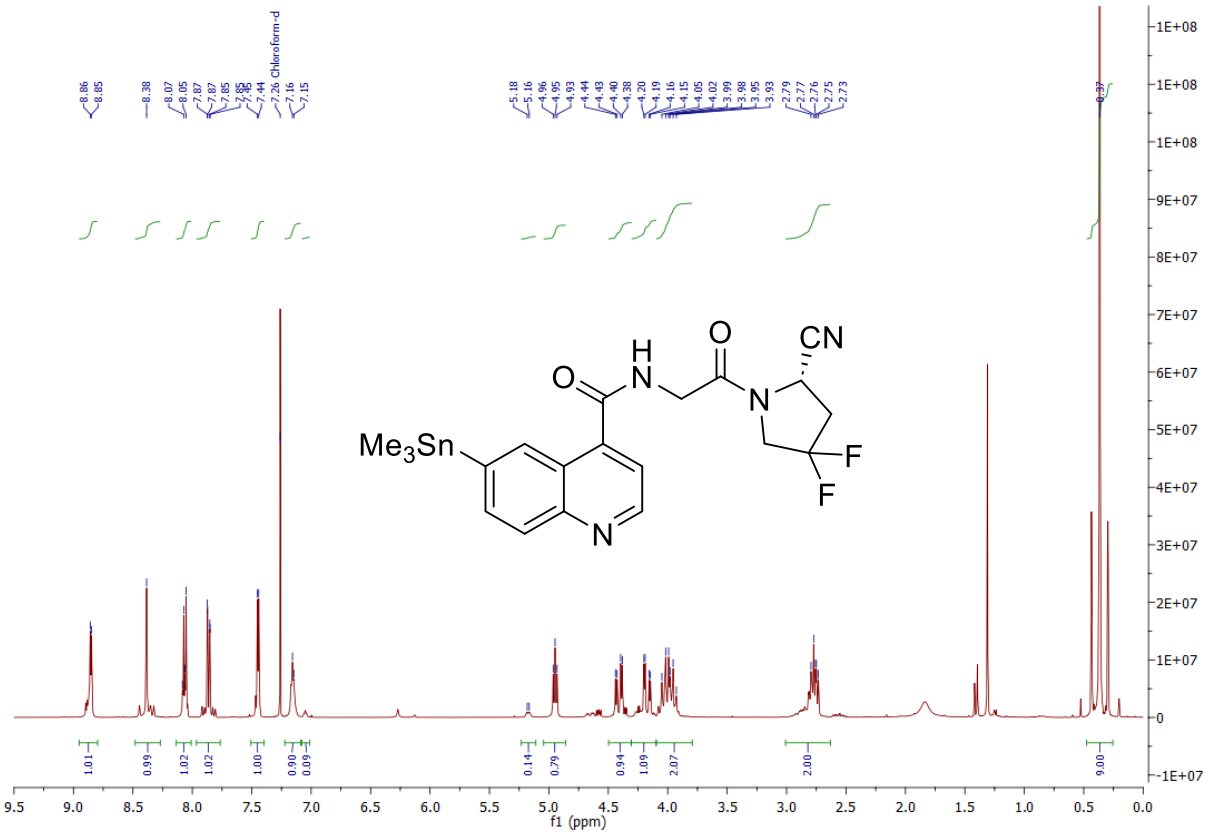

^{13}C NMR of compound 5

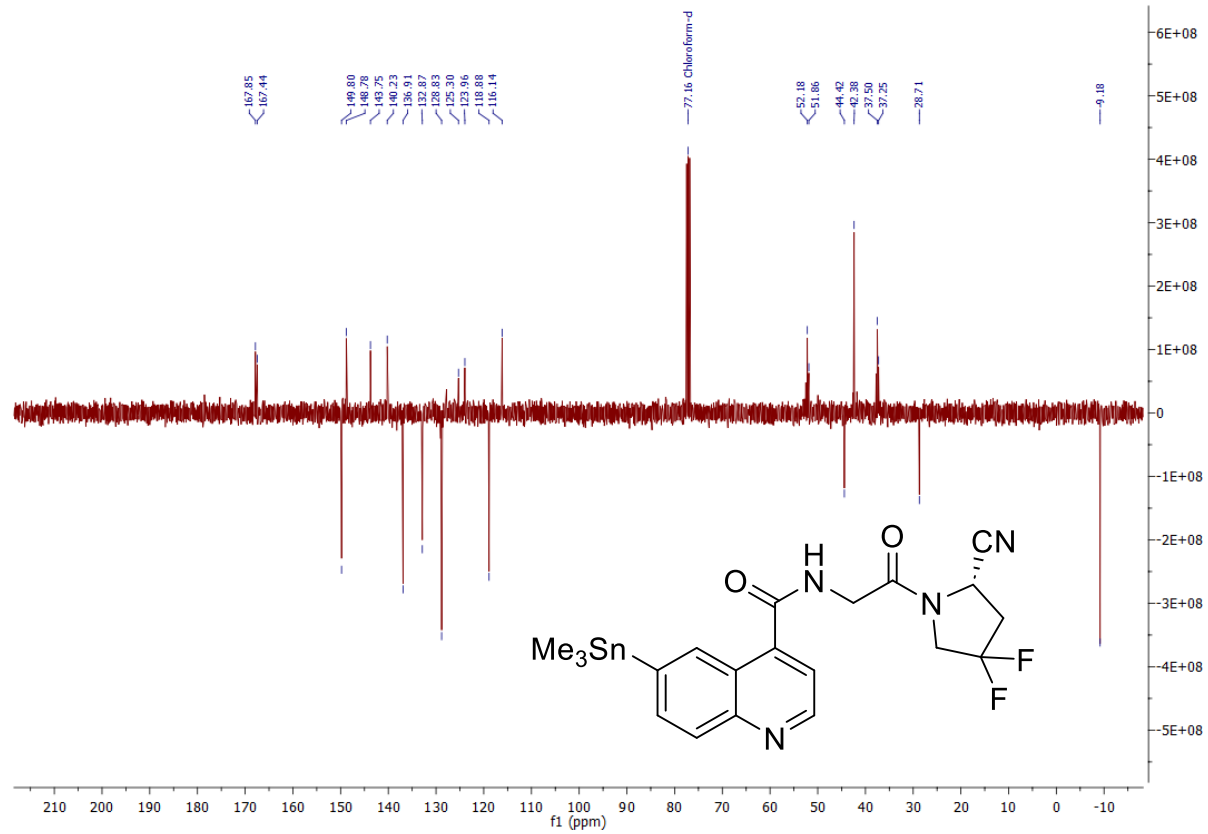

^{19}F NMR of compound 5

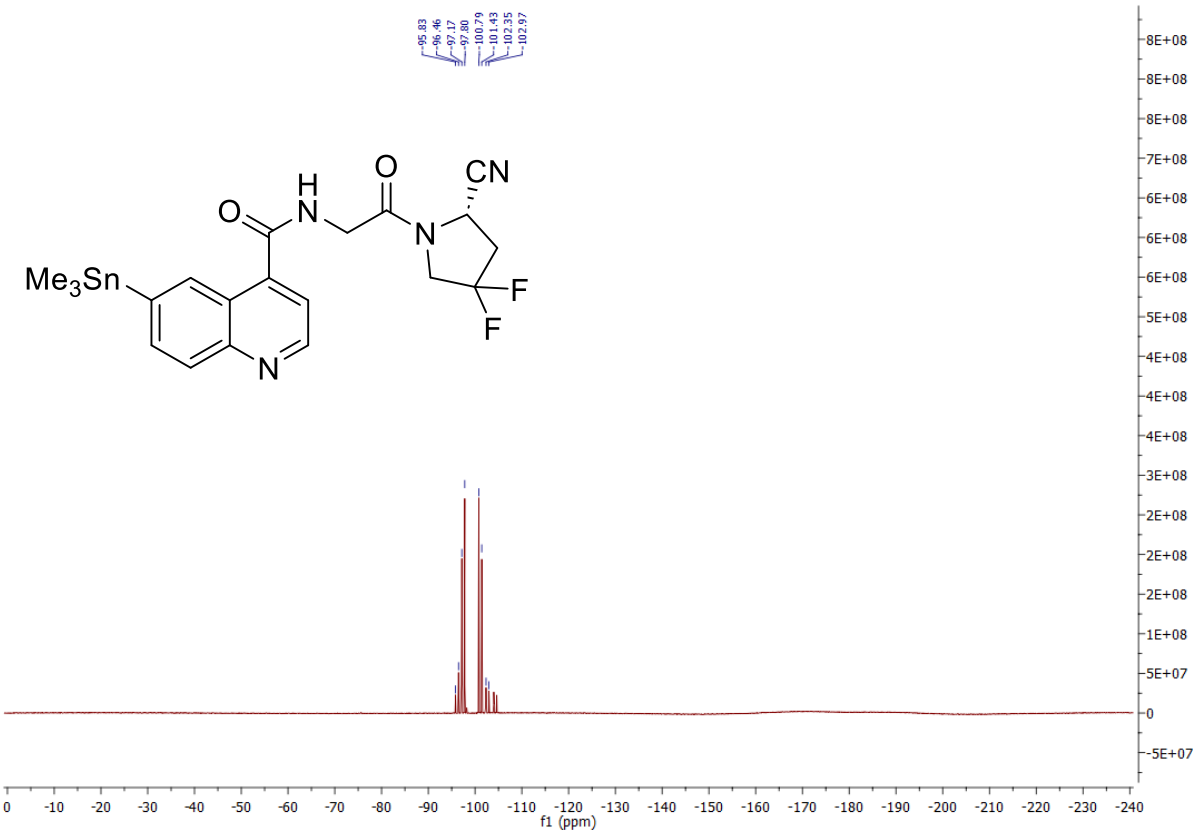

^{1}H NMR of compound 8

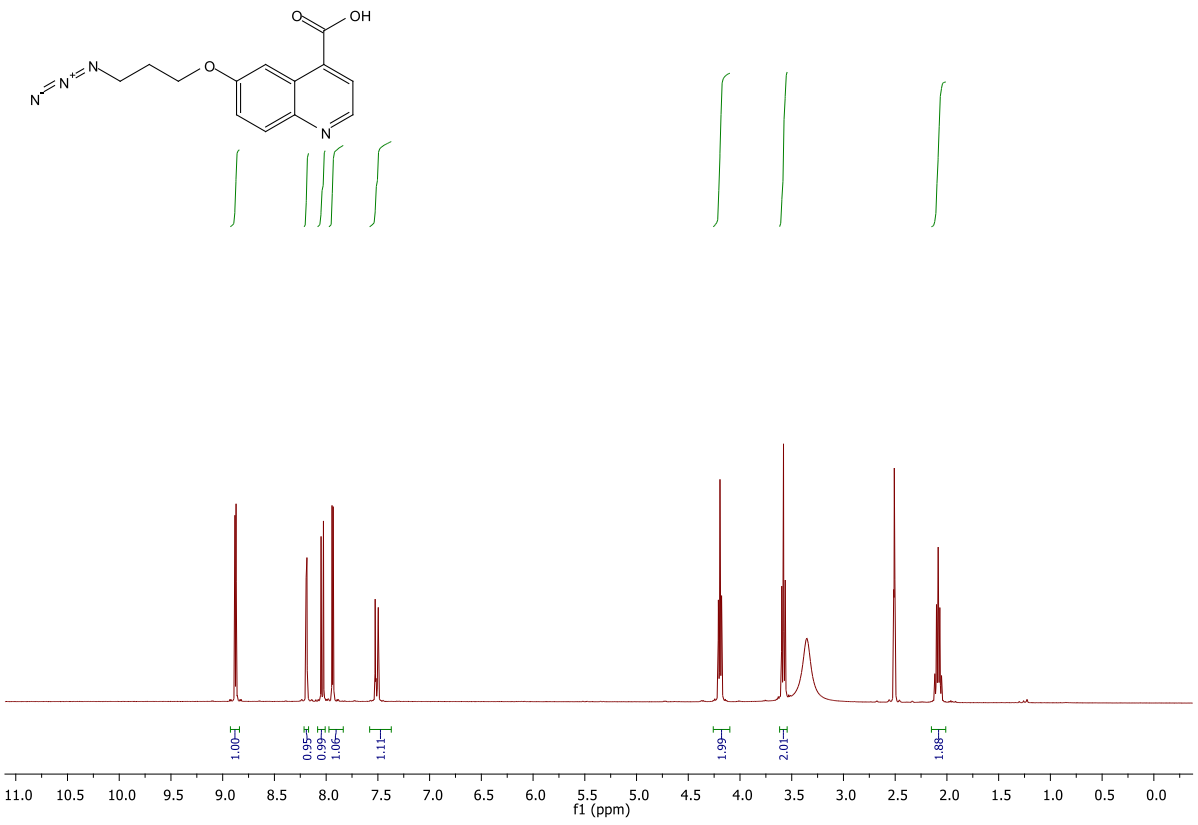

^{13}C NMR of compound 8

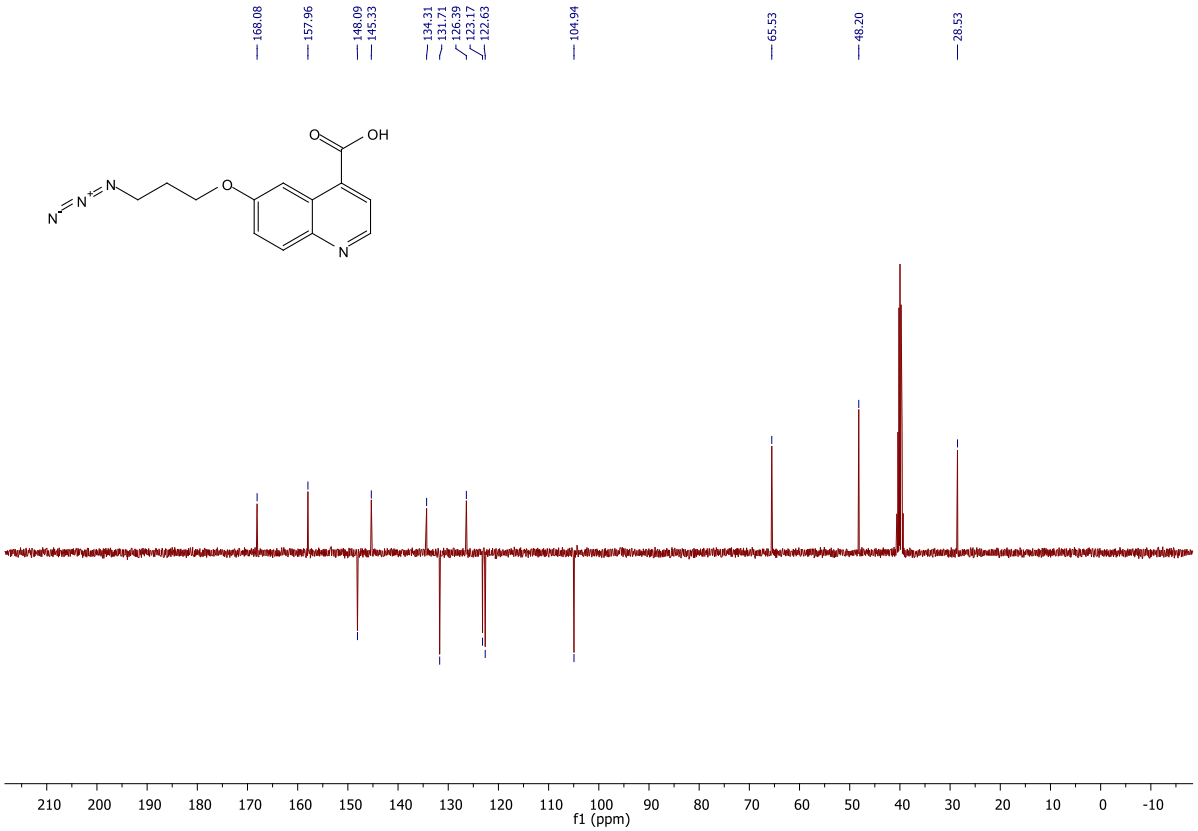

^{1}H NMR of compound 9

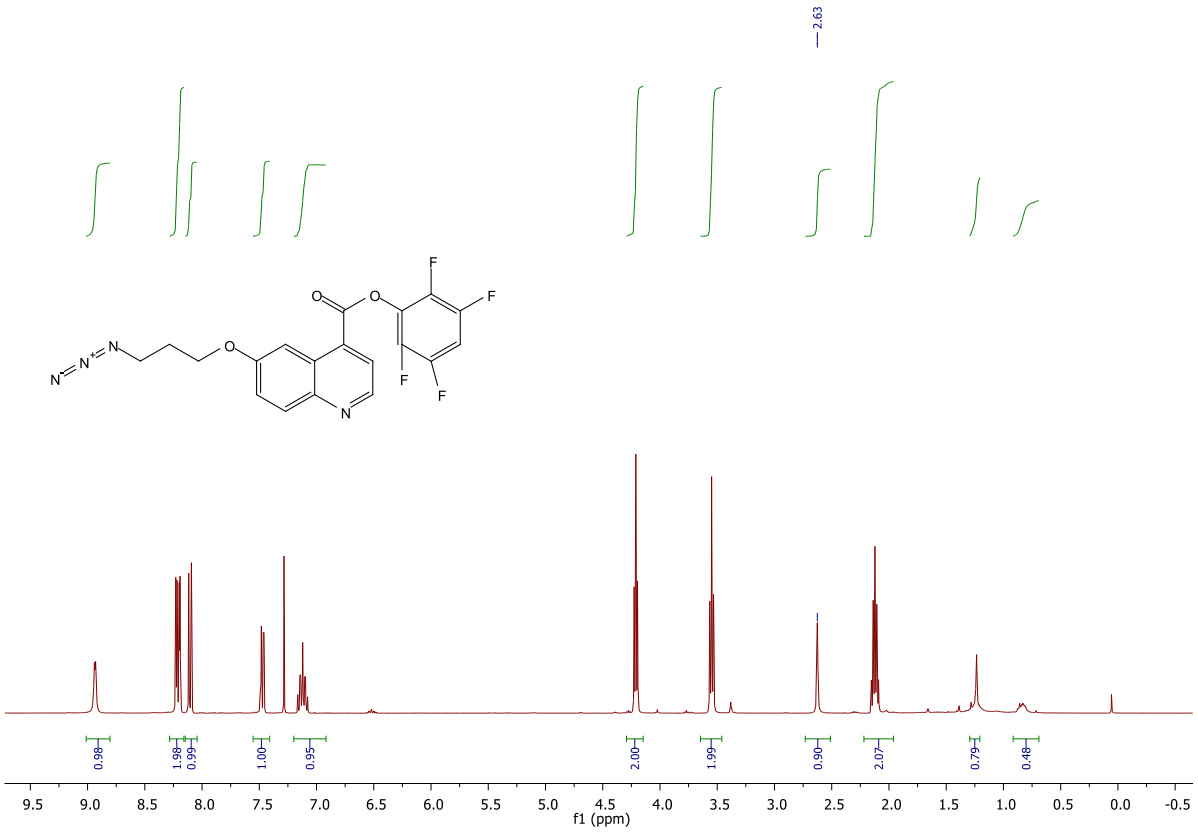

^{13}C NMR of compound 9

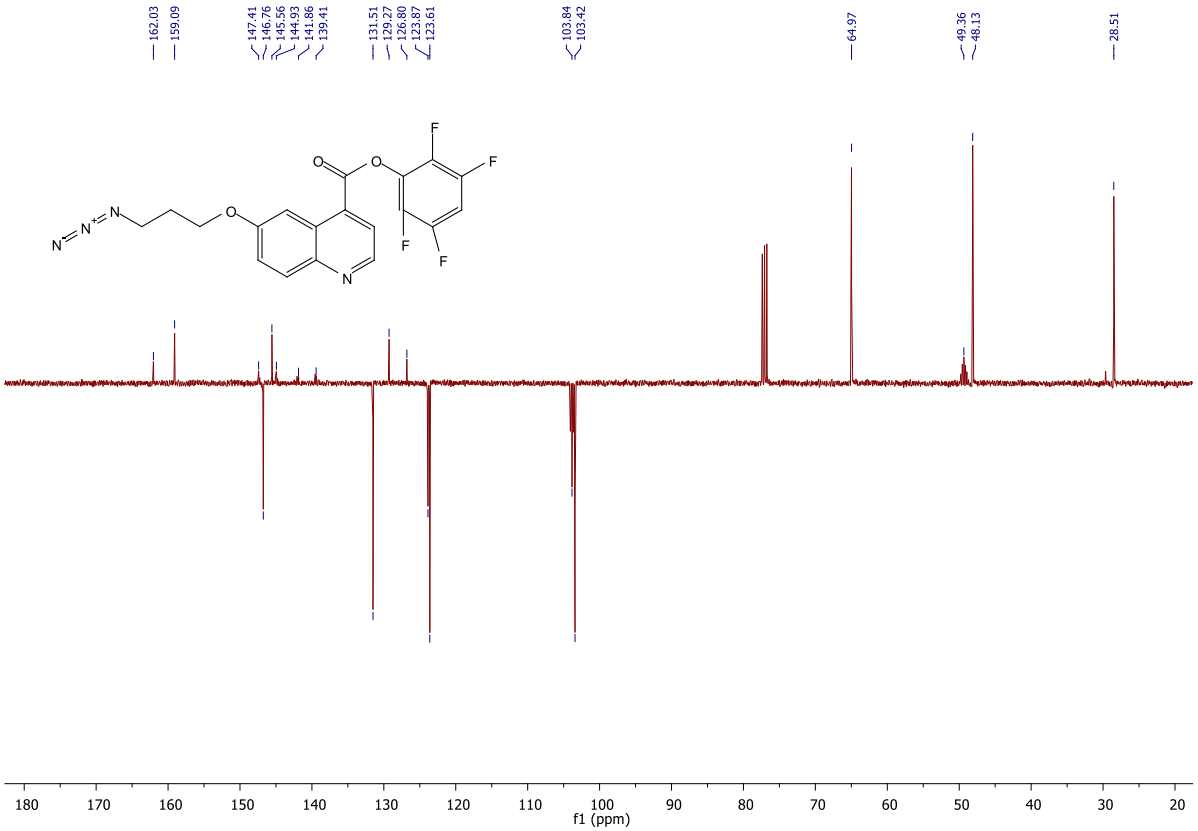

^{19}F NMR of compound 9

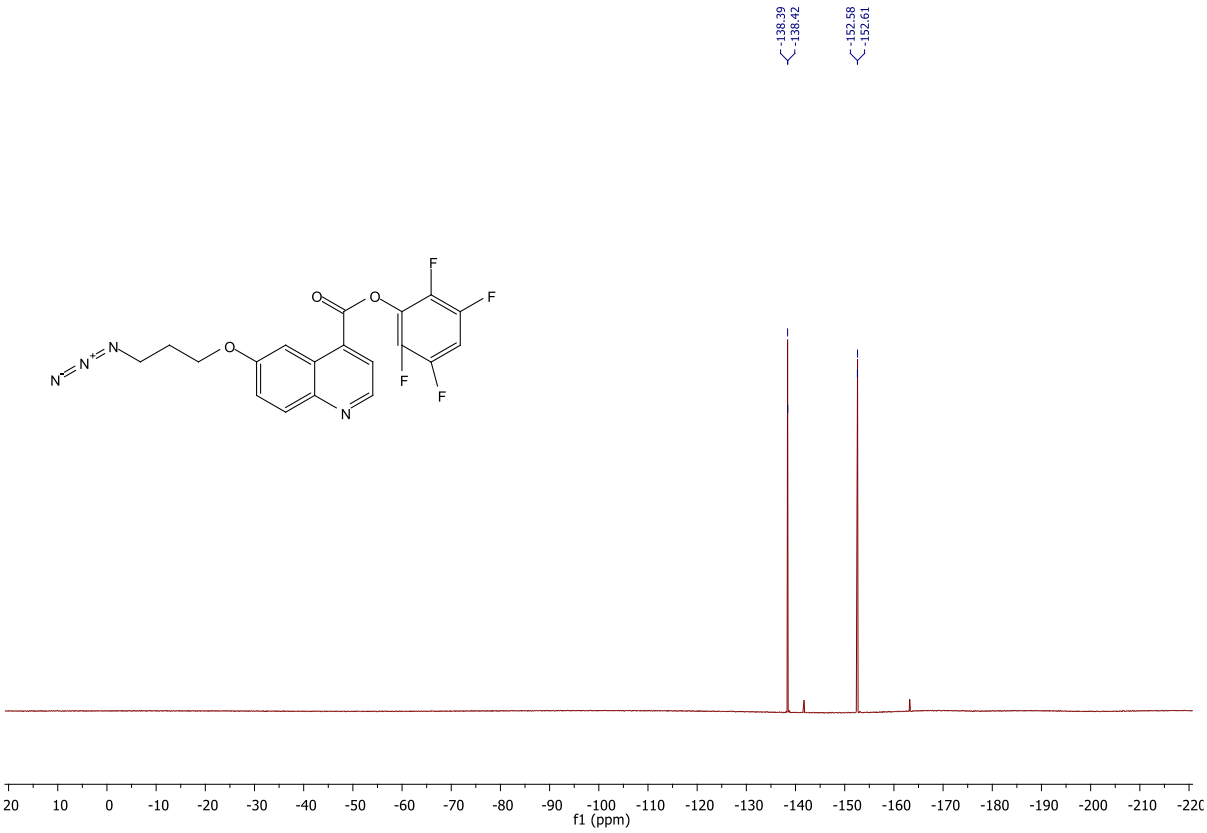

^{1}H NMR of compound 11

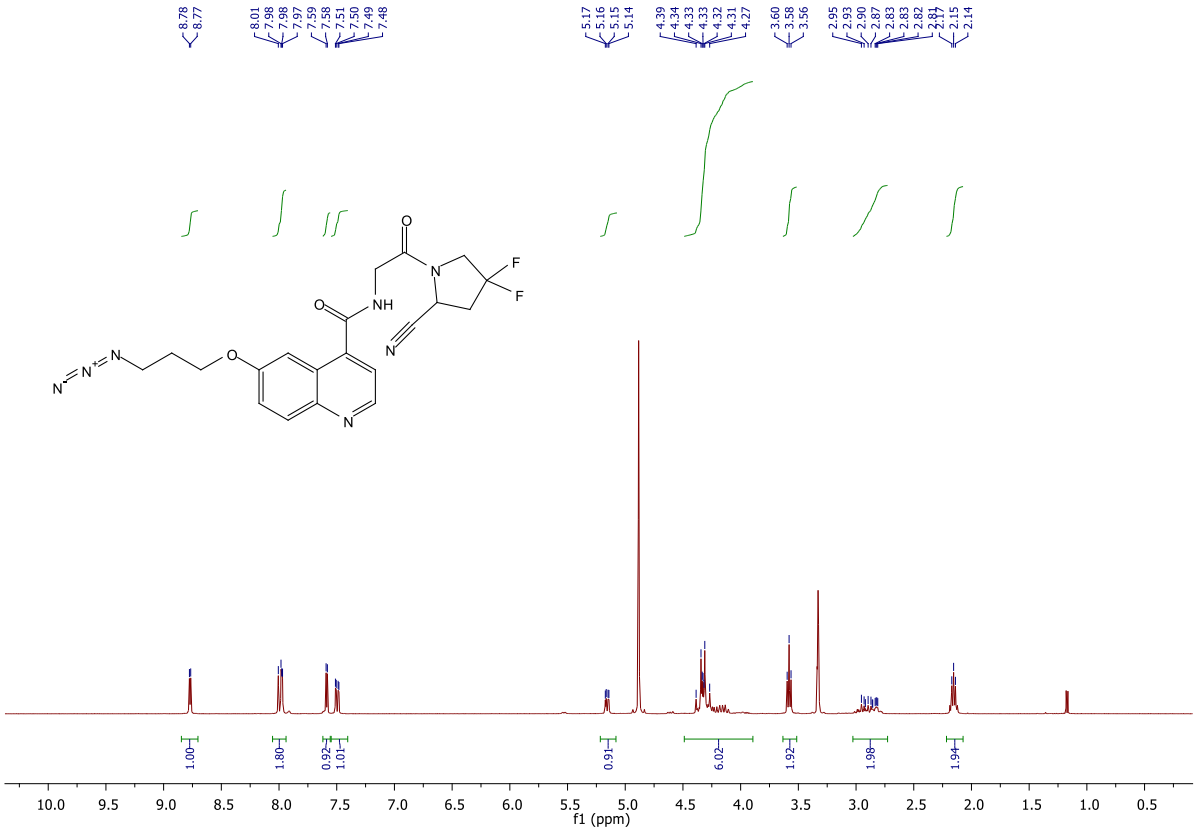

^{13}C NMR of compound 11

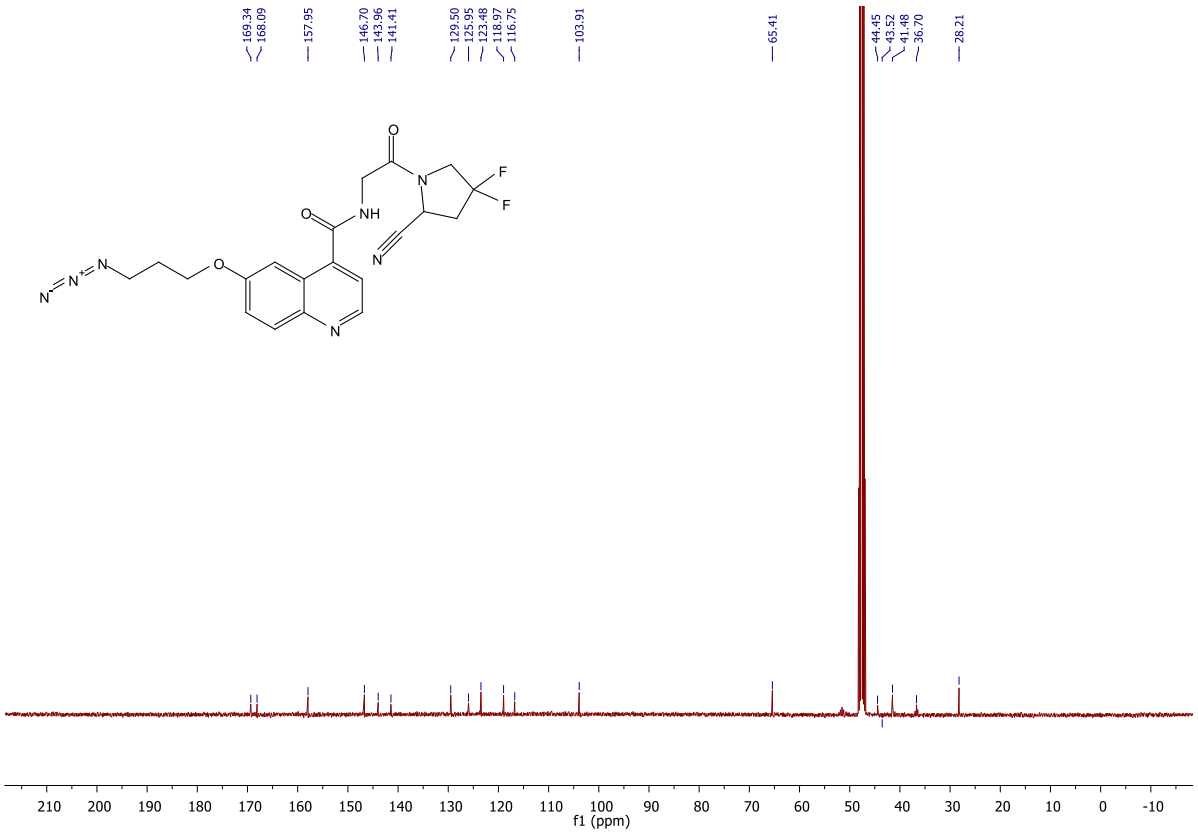

^{19}F NMR of compound 11

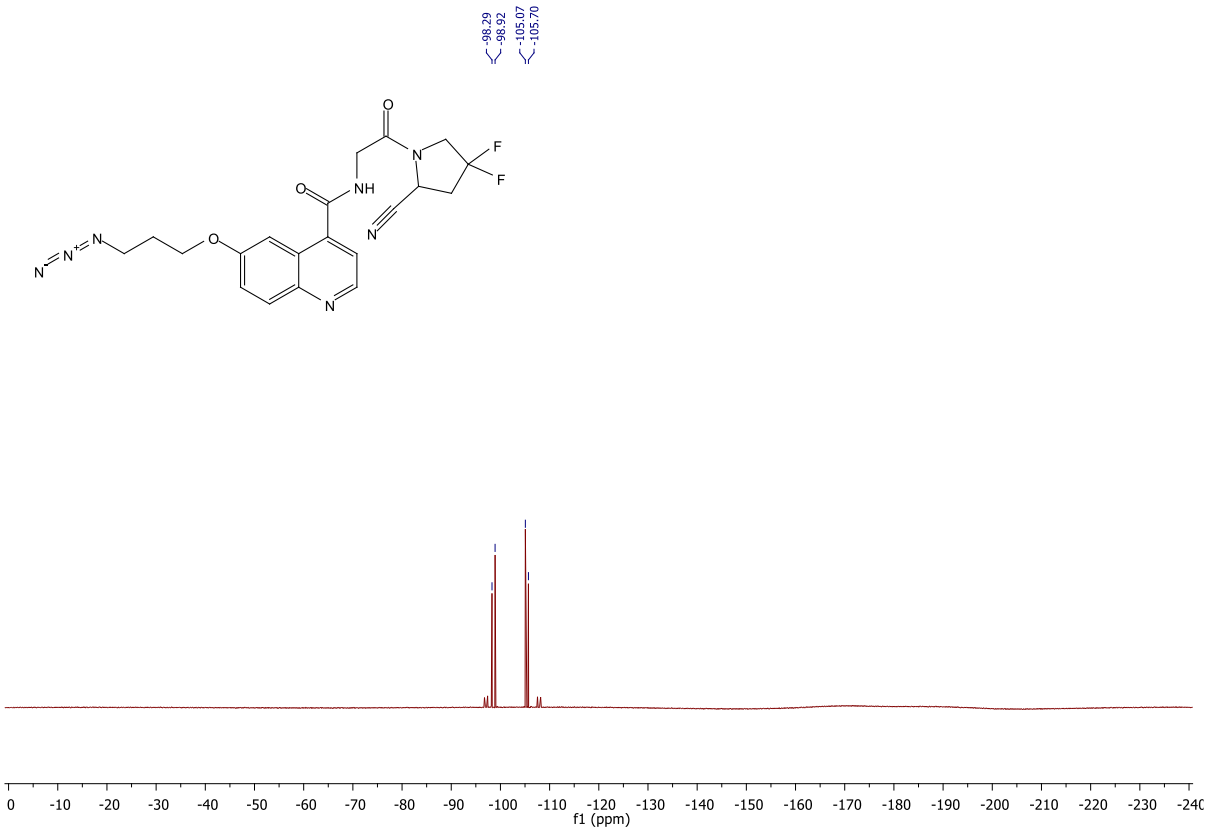

^{1}H NMR of compound 12

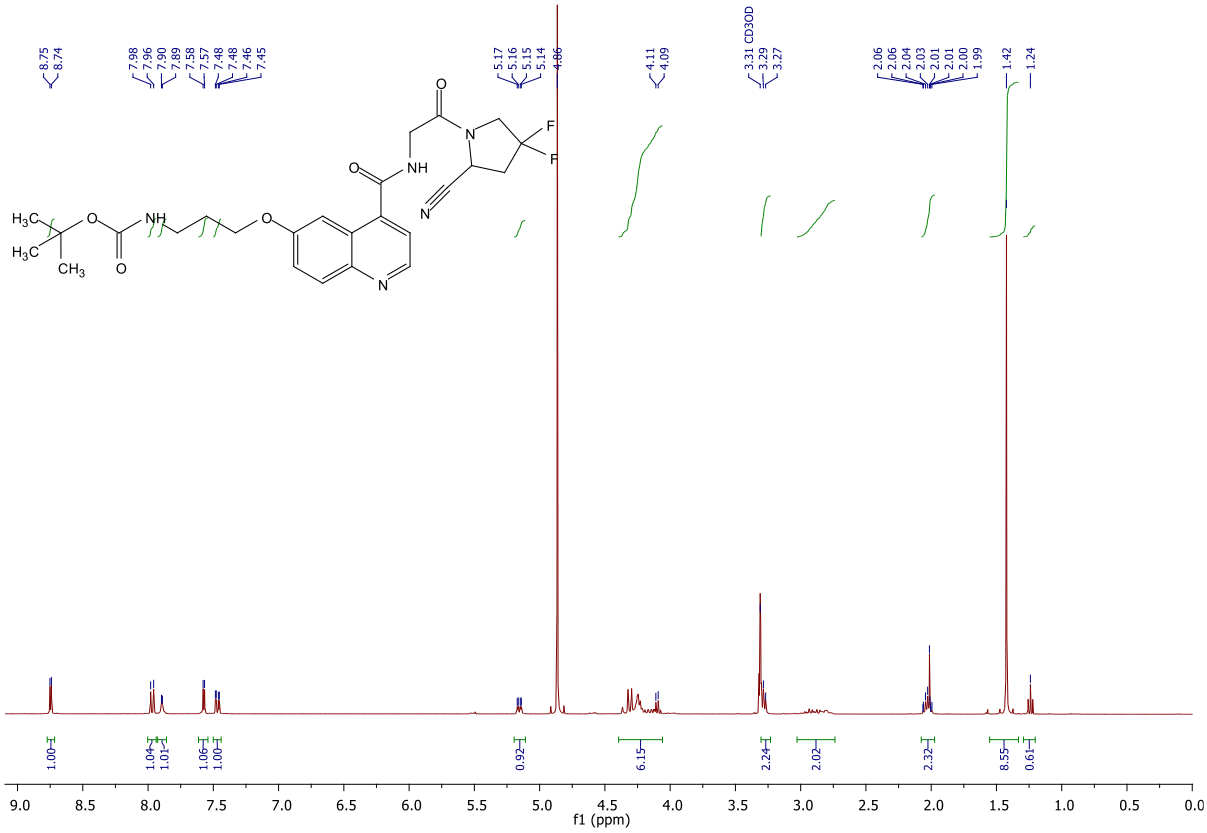

^{13}C NMR of compound 12

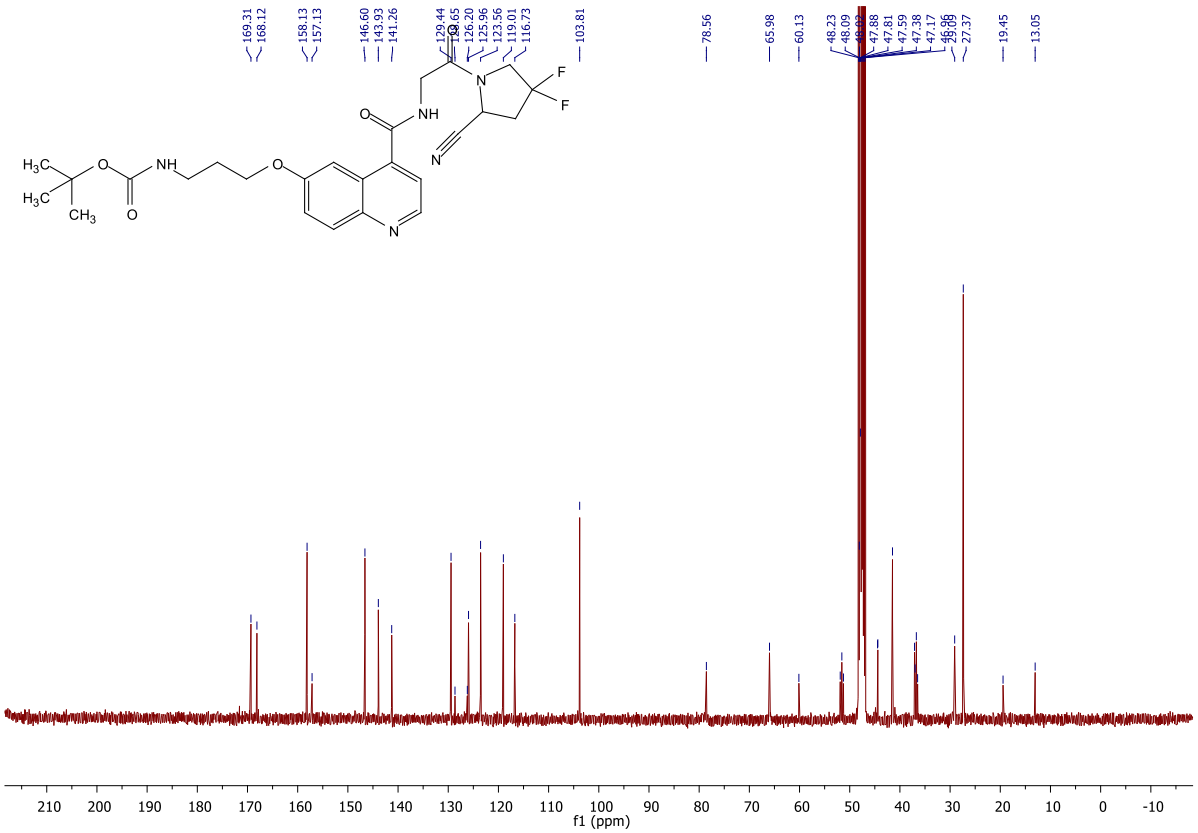

^{19}F NMR of compound 12

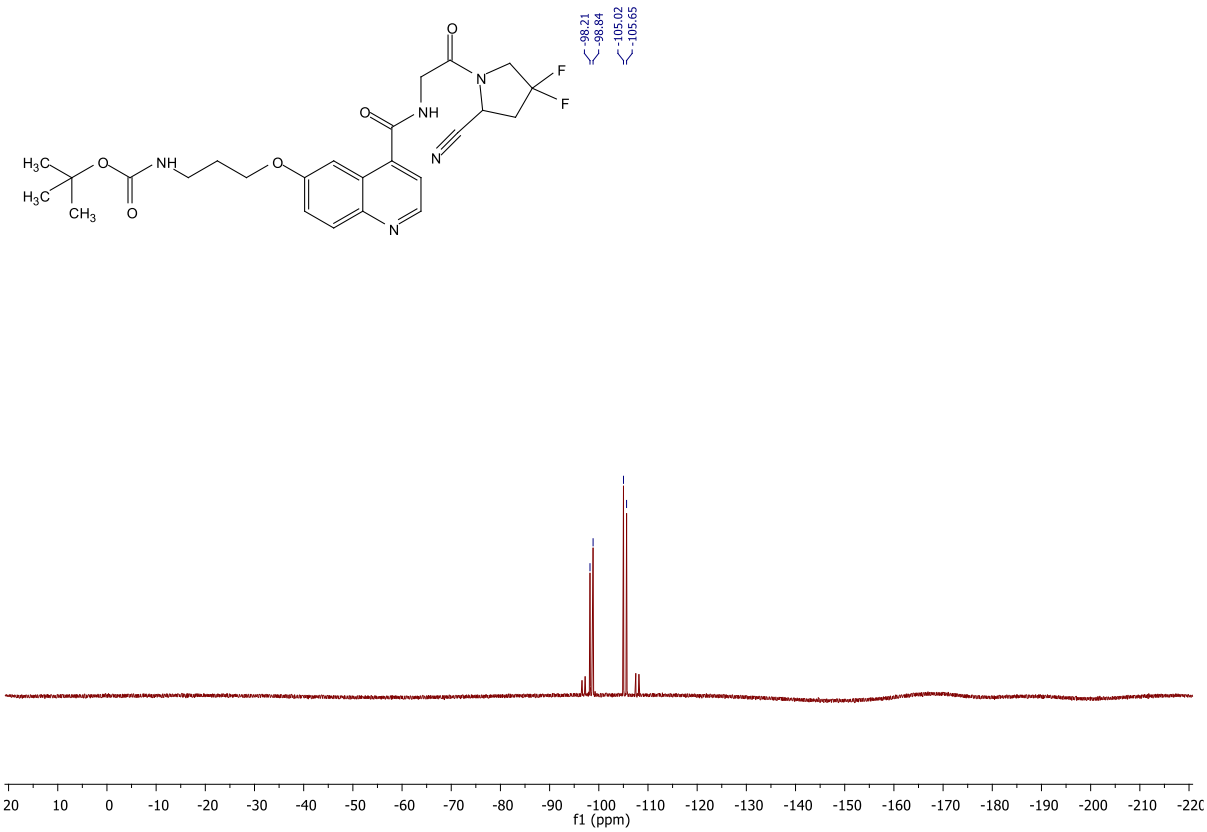

^{1}H NMR of compound 13

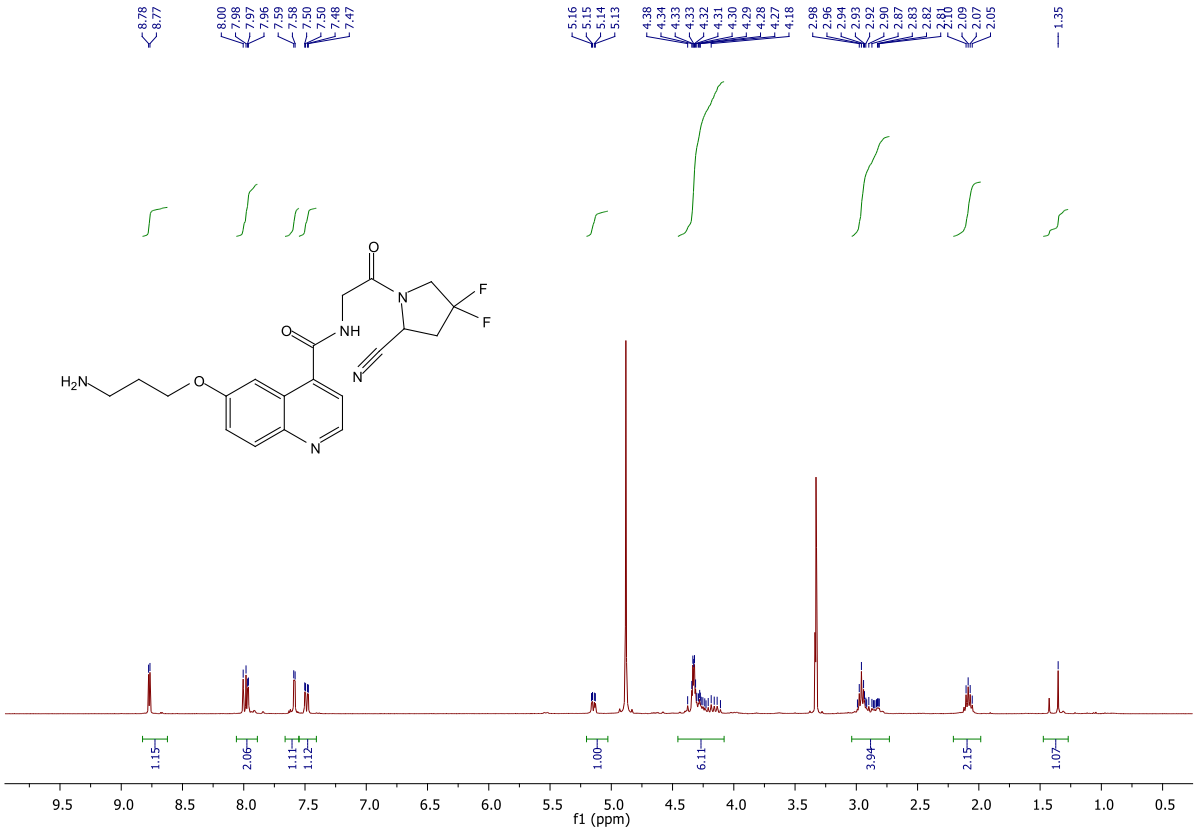

^{13}C NMR of compound 13

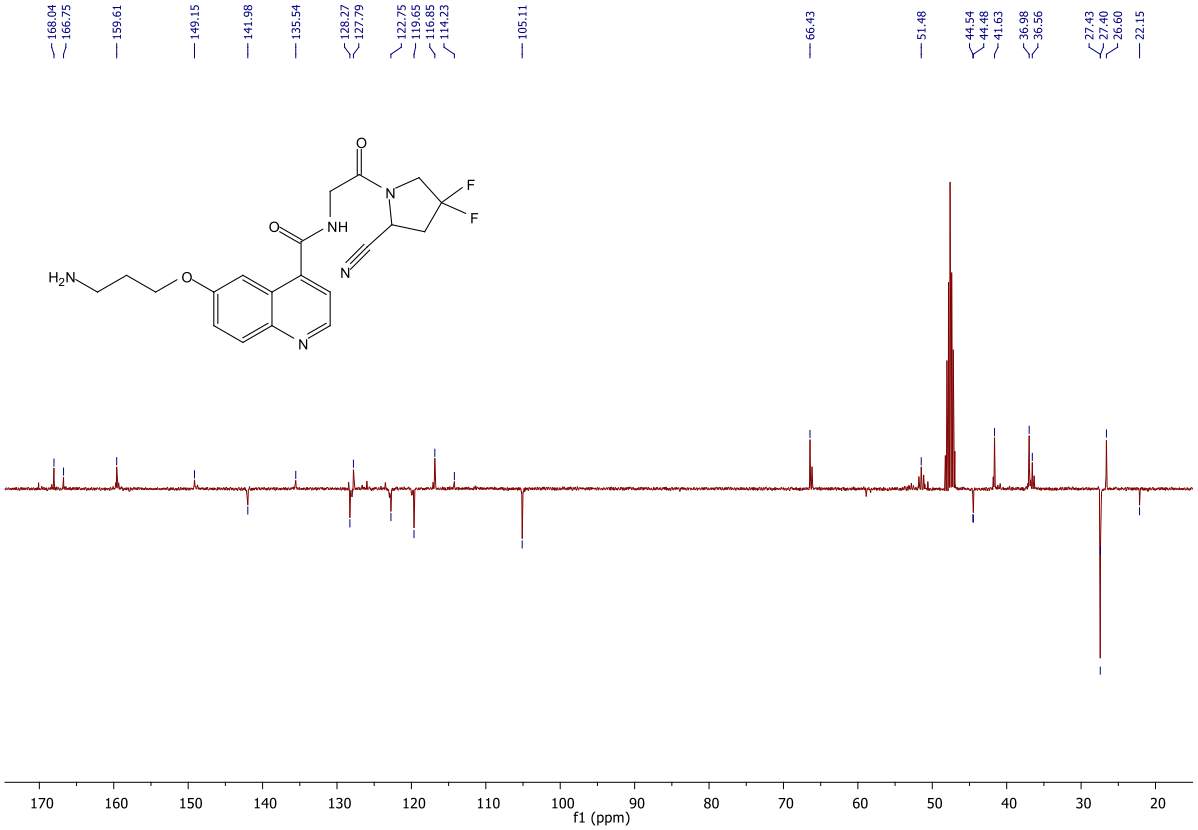

^{19}F NMR of compound 13

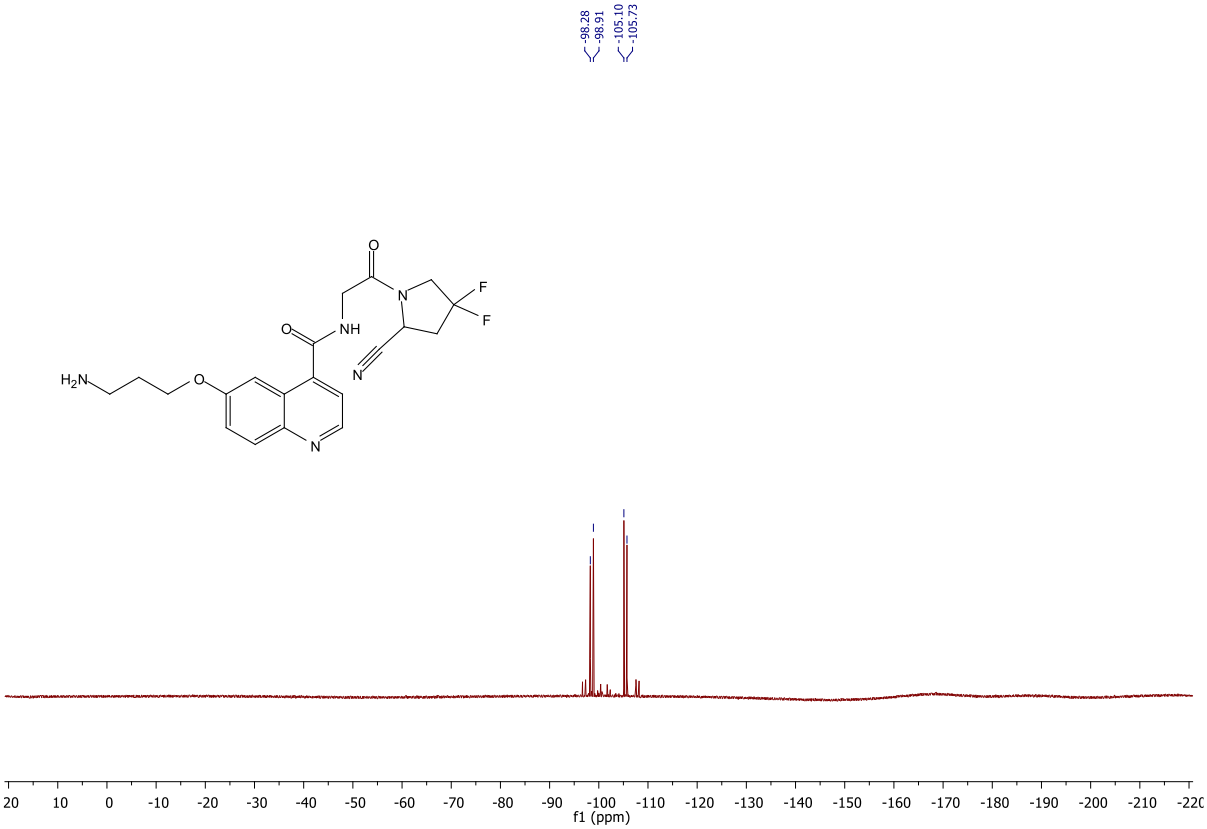

^{1}H NMR of Aza-FAPI

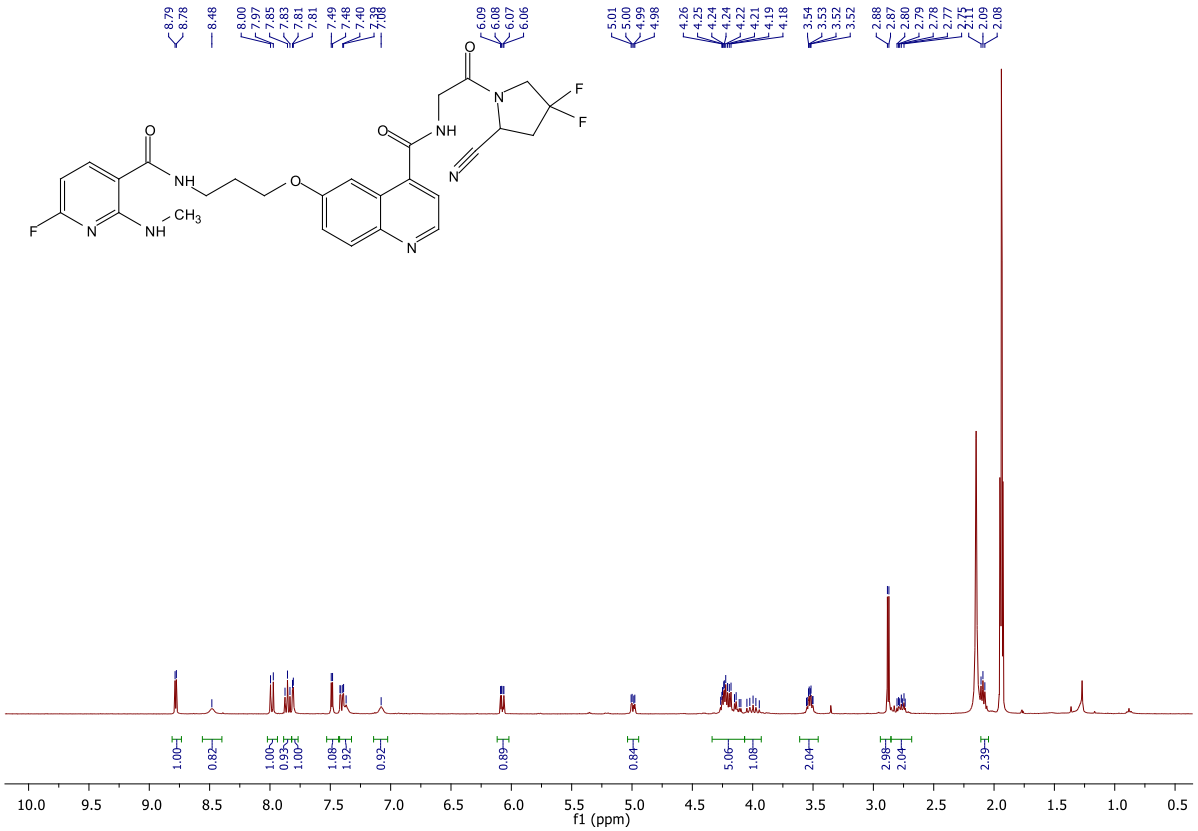

^{13}C NMR of Aza-FAPI

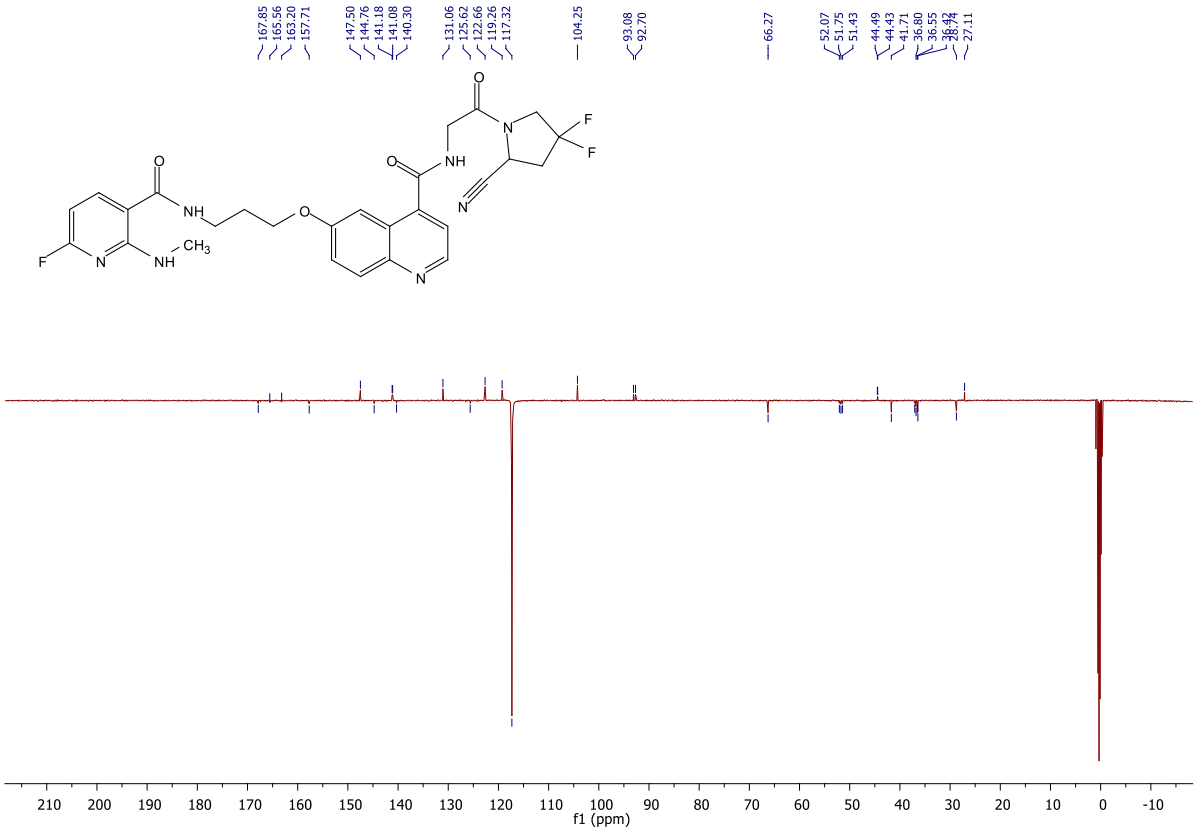

2 Radiochemistry

2.1 General conditions

[^{18}F]Fluoride ([^{18}F]F$^-$) was produced via the ^{18}O(p,n)^{18}F nuclear reaction by bombardment of enriched [^{18}O]H_2O with 16.5 MeV protons using a BC1710 cyclotron (The Japan Steel Works Ltd., Shinagawa, Japan) at the INM-5 (Forschungszentrum Jülich). All radiosyntheses were carried out in 5 mL Wheaton V-Vials equipped with PTFE-coated wing stir bars. Anhydrous solvents (DMI, PC, *n*BuOH and MeOH, dried over molecular sieves) were purchased from Sigma-Aldrich (Steinheim, Germany). Anion exchange resins (Sep-Pak Accell Plus QMA carbonate plus light cartridges 40 mg sorbent per cartridge) were obtained from Waters GmbH (Eschborn, Germany).

Processing of [^{18}F]F$^-$

Aqueous [^{18}F]F$^-$ was loaded (from the female side) onto a QMA cartridge (preconditioned with 1 mL H_2O) and the cartridge was washed (from the male side) with anhydrous MeOH (1 mL) to remove residual H_2O and dried (from the female side) with air (2×10 mL). [^{18}F]F$^-$ was eluted

(from the female to the male side) with a solution of Et_4NOTf in *n*BuOH (400 µL) directly into a solution of precursor and copper mediator.

High-Performance Liquid Chromatography (HPLC)

Analytical radio-HPLC was performed on a HPLC system (Knauer Wissenschaftliche Geräte GmbH, Berlin, Germany) with Azura P 6.1L pump and Azura UVD 2.1S UV/Vis detector. For monitoring absorbance at 254 nm and radioactivity, the UV/Vis detector was coupled in series with a Berthold NaI detector, giving a time of delay of 0.1–0.3 min between the corresponding responses, depending on the flow rate. For determination of radiochemical conversions (RCCs), the reaction mixtures were diluted with H_2O (2 mL) or 20% MeCN (2 mL) and analyzed by radio-HPLC with a post-column injection of the reaction mixture. The RCCs were then calculated by comparison of the peak areas of the radiolabeled product and the post-column injection, respectively.[https://doi.org/10.1016/j.jchromb.2023.123847]

2.2 Preparation of 6-[^{18}F]F-FAPI from boronic acid precursor

[^{18}F]F$^-$ was loaded onto a QMA carbonate cartridge and eluted with Et_4NOTf (1 mg, 3.6 µmol) in *n*BuOH (400 µL) as described above directly into a solution of **$$** and copper(II) complex (10 µmol of each) in DMI (800 µL). The reaction mixture was heated at 110 °C for 10 min. RCCs were determined by radio-HPLC as described above. The radiosyntheses were carried out in triplicate.

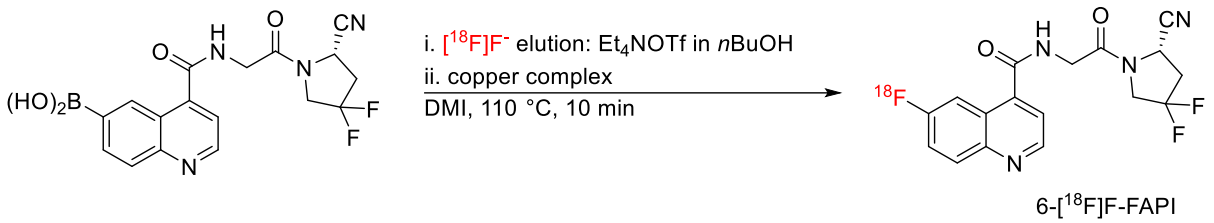

Table S1: RCCs of 6-[^{18}F]F-FAPI from radiosyntheses with copper(II) complexes.

Entry	Copper(II) complex	RCC [%]
1	$Cu(4\text{-}PhPy)_4(ClO_4)_2$	15±1
2	$Cu(3,4\text{-}Me_2Py)_4(ClO_4)_2$	17±3

2.3 Determination of carrier amount and molar activity of 6-[^{18}F]F-FAPI

An aliquot of the tracer solutions (20 µL) were analyzed by analytical HPLC as described in the main article. The carrier amount was determined from the peak area and the molar activity

was calculated according to a calibration curves (Figure S1 and S2), which were obtained using different concentrations of 6-[^{18}F]F-FAPI and [^{18}F]AFA-FAPI (Table S2 and S3).

$$A_M = \frac{A\ \left[\frac{GBq}{mL}\right]}{c\ \left[\frac{\mu mol}{mL}\right]}$$

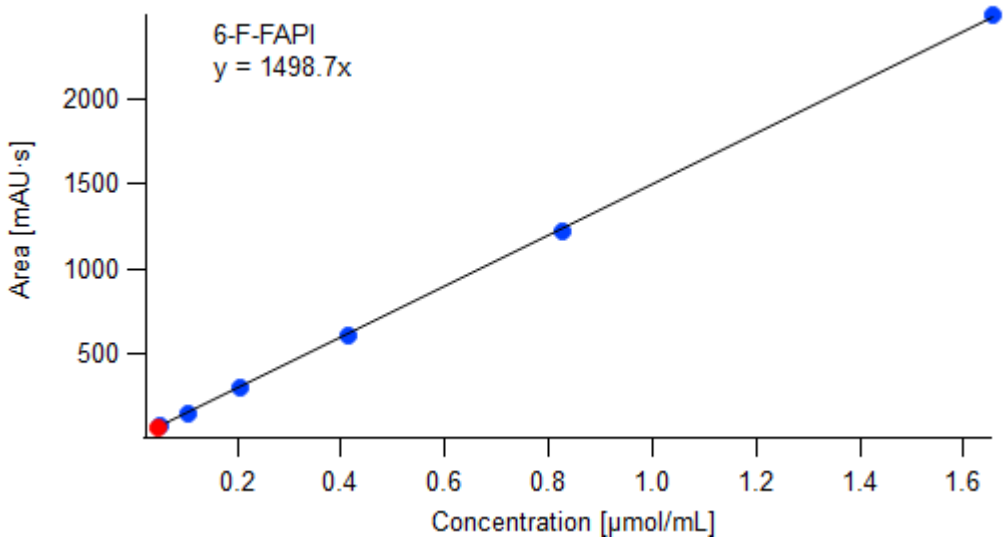

Figure 1: Calibration curve of 6-F-FAPI for calculation of the molar activity of 6-[^{18}F]F-FAPI. Raw data are shown in Table 1.

Table S2: Calibration data (measured at 254 nm) for determination of molar activity of 6-[^{18}F]F-FAPI.

Concentration [µmol/mL]	**Amount [µg]**	**Peak area [mAU·min]**
1.66	600	2491.8
0.828	300	1225.8
0.414	150	610.9
0.207	75.0	309.5
0.104	37.5	153.7
0.0518	18.8	85.4
Measured sample:		71.035
Volume [mL]		0.5
Activity [MBq]		663
Carrier amount (µg)		17.2
Carrier concentration [µmol/mL]		$47.4 \cdot 10^{-3}$
Molar activity [GBq/µmol]		28

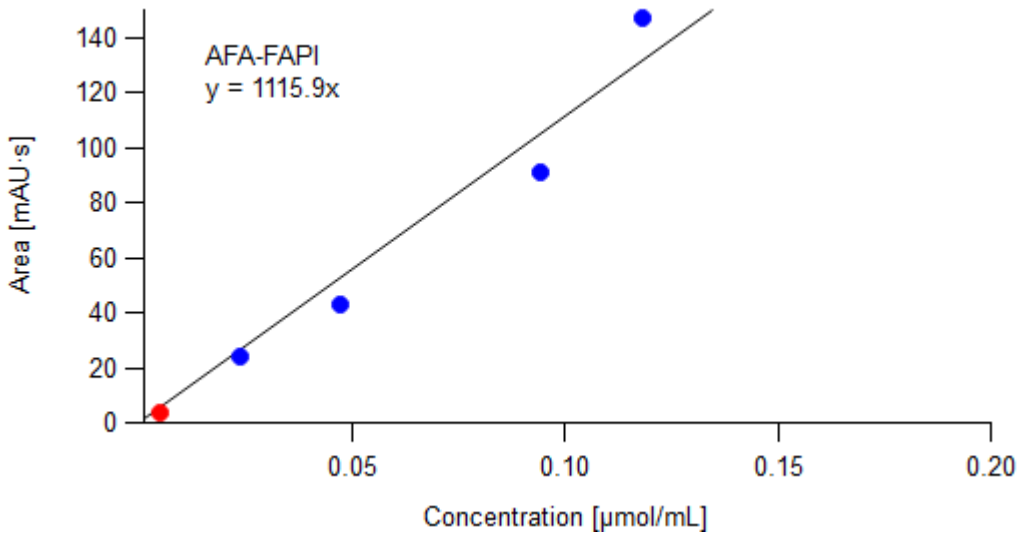

Figure 2: Calibration curve of AFA-FAPI for calculation of the molar activity of [^{18}F]AFF-FAPI. Raw data are shown in Table 2.

Table S3: Calibration data (measured at 254 nm) for determination of molar activity of [^{18}F]AFA-FAPI.

Concentration [µmol/mL]	**Amount [µg]**	**Peak area [mAU·min]**
0.188	100	147
0.0941	50.0	91.2
0.0470	25.0	42.9
0.0235	12.5	23.7
Measured sample:		3.687
Volume [mL]		1.0
Activity [MBq]		842
Carrier amount (µg)		2.62
Carrier concentration [µmol/mL]		$4.92 \cdot 10^{-3}$
Molar activity [GBq/µmol]		171

2.4 HPLC chromatograms

Preparative HPLC chromatogram and quality control of 6-[^{18}F]F-FAPI

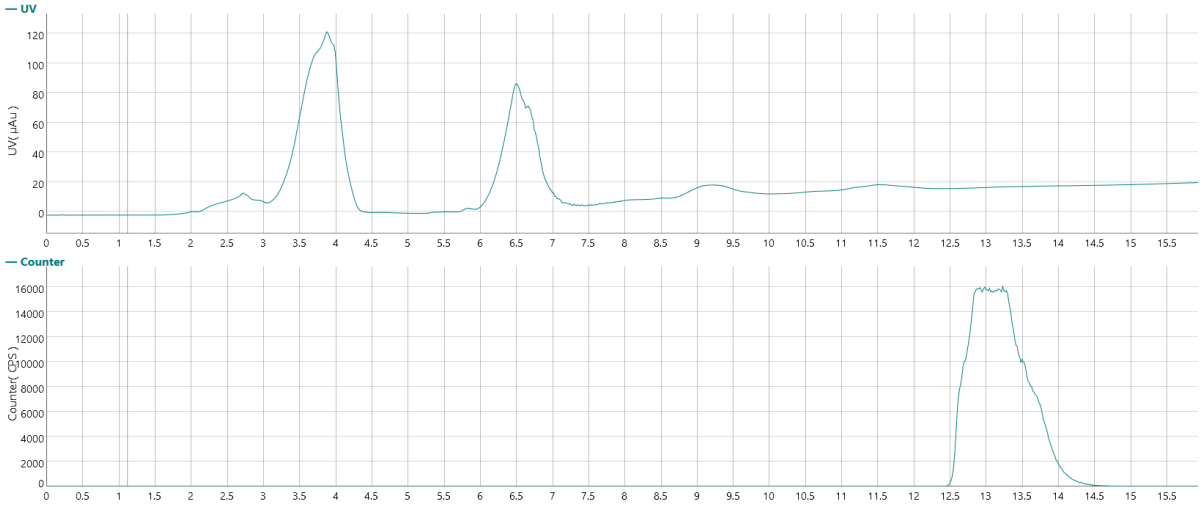

Figure S3: Purification of 6-[^{18}F]F-FAPI by preparative HPLC (top: UV trace, λ=254 nm; bottom: radioactivity trace).

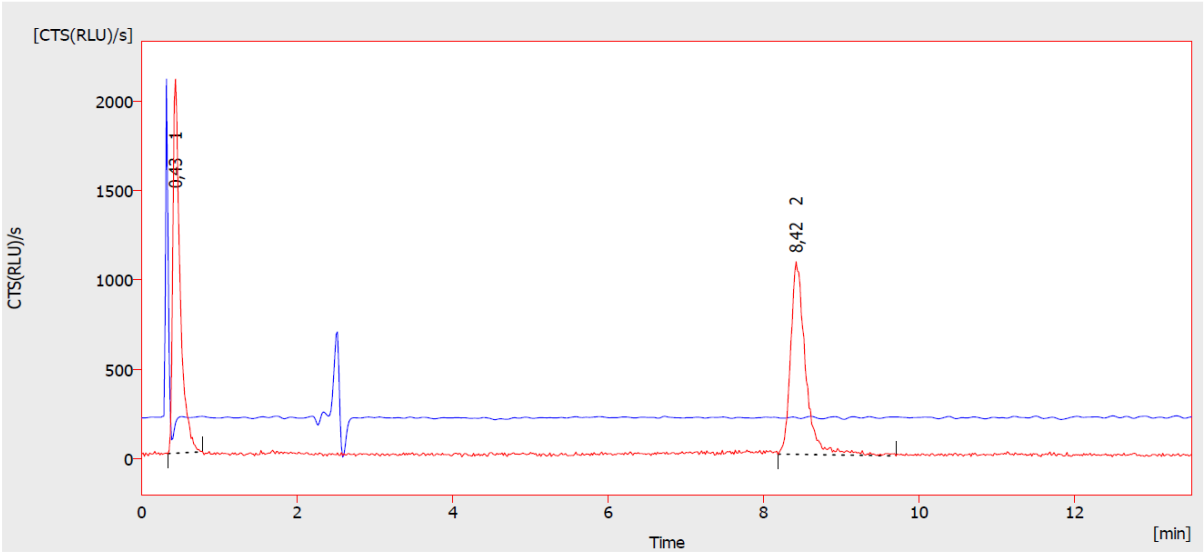

Result Table (Uncal - Data\alc-enhanced_324_28_10_2021_[4 DMI]_[18F]FAPI_liefersynthese_radio_purity - HERM)

	Reten. Time [min]	Area [CTS(RLU)/s.s]	Height [CTS(RLU)/s]	Area [%]
1	0,433	13557,000	2093,778	48,3
2	8,417	14515,500	1078,385	51,7
	Total	28072,500	3172,162	100,0

Figure S4: HPLC traces of purified 6-[^{18}F]F-FAPI for quality control. Blue trace: UV channel, λ=254 nm; red trace: radioactivity channel

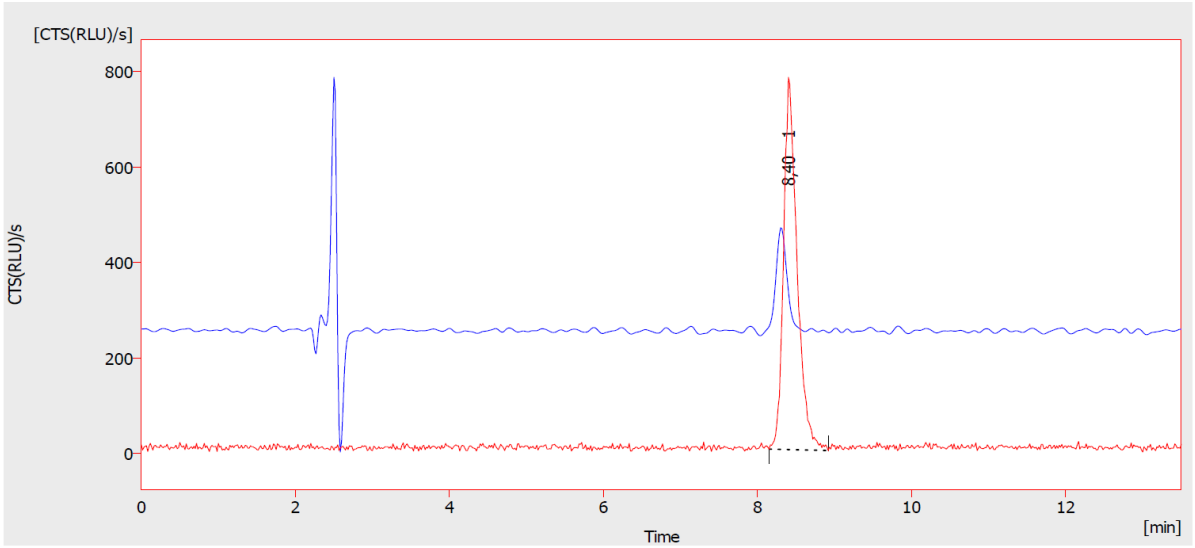

Result Table (Uncal - Data\alc-enhanced_325_28_10_2021_[4 DMI]_[18F]FAPI_liefersynthese_spiked - HERM)

	Reten. Time [min]	Area [CTS(RLU)/s.s]	Height [CTS(RLU)/s]	Area [%]
1	8,400	9540,000	779,978	100,0
	Total	9540,000	779,978	100,0

Figure S5: HPLC traces of purified 6-[^{18}F]F-FAPI spiked with an authentic sample of 6-F-FAPI. Blue trace: UV channel, λ=254 nm; red trace: radioactivity channel.

Preparative HPLC chromatogram and quality control of [^{18}F]AFA-FAPI

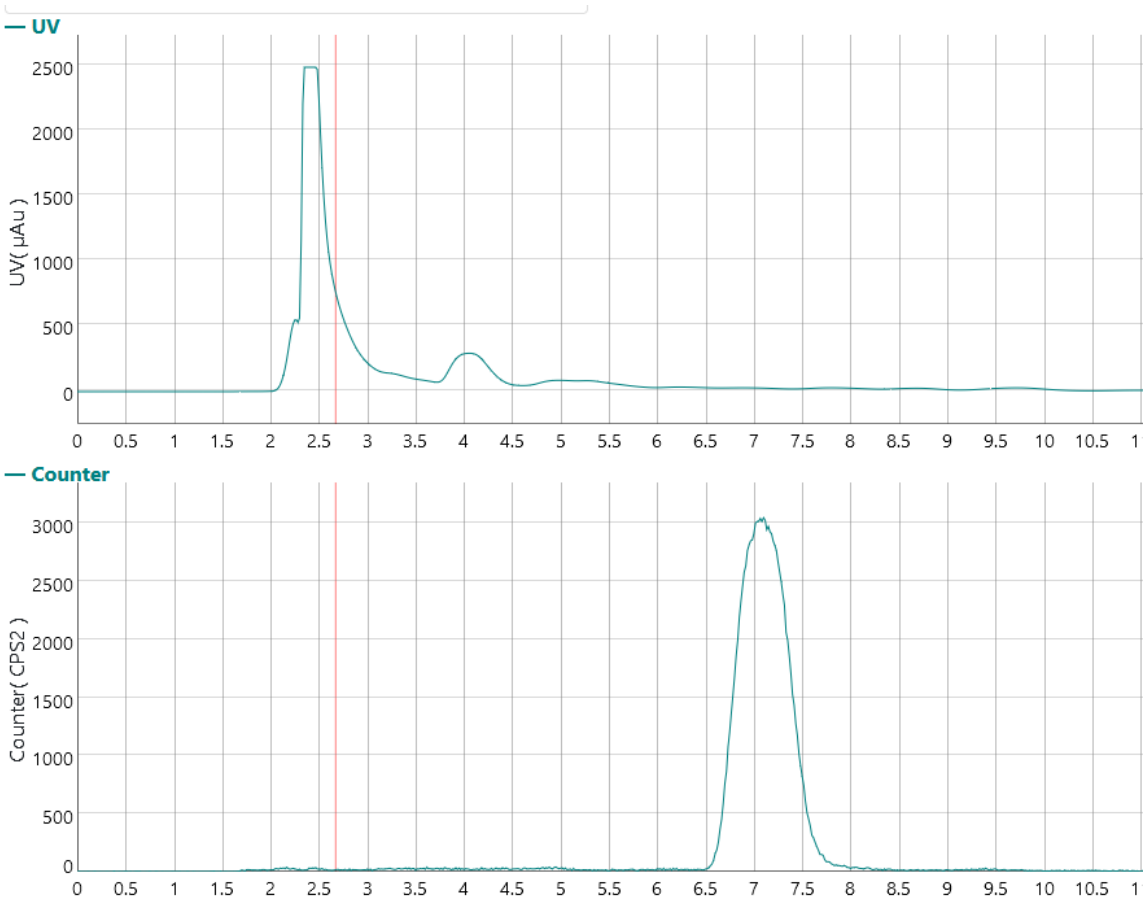

Figure S3: Purification of [^{18}F]AFA-FAPI by preparative HPLC (top: UV trace, λ=254 nm; bottom: radioactivity trace).

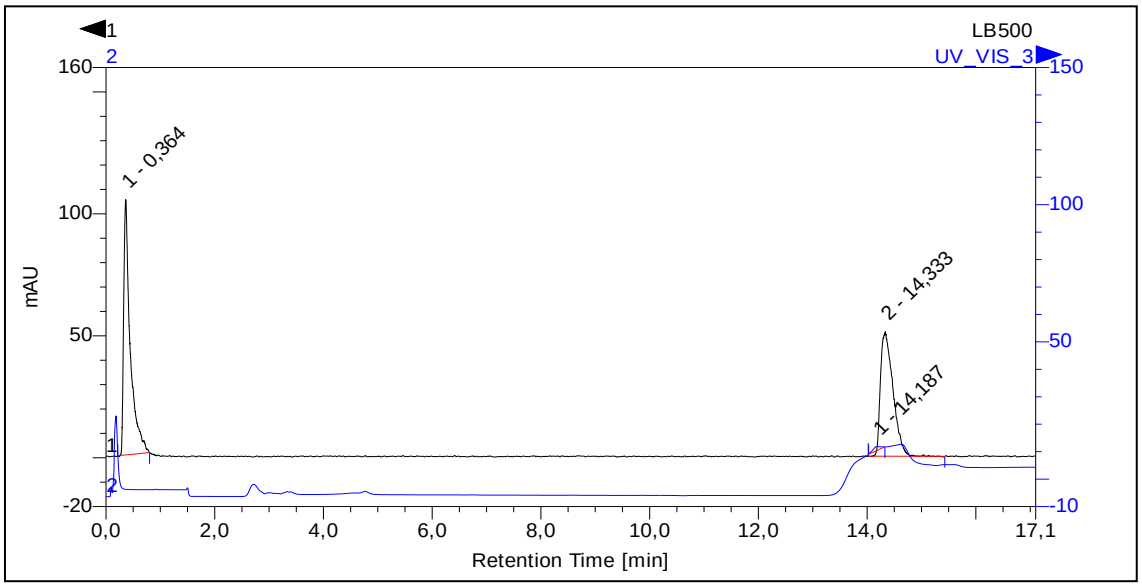

Figure S4: HPLC traces of purified [^{18}F]AFA-FAPI for quality control. Blue trace: UV channel, λ=254 nm; black trace: radioactivity channel

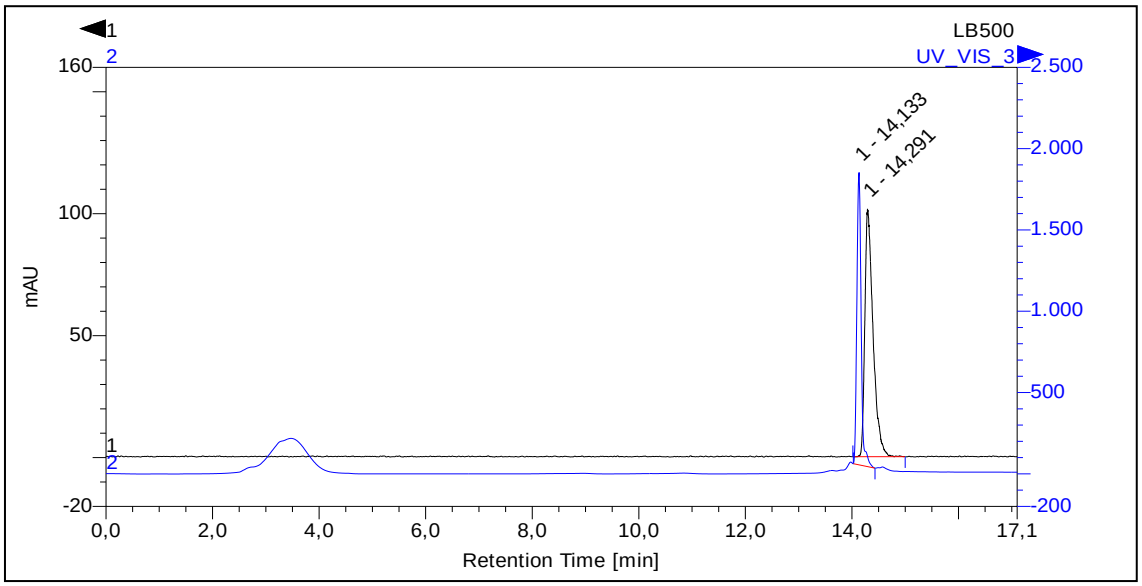

Figure S5: HPLC traces of purified [^{18}F]AFA-FAPI spiked with an authentic sample of 6-F-FAPI. Blue trace: UV channel, λ=254 nm; black trace: radioactivity channel.

8. Erklärung nach §7, Abs. 8 der prüfungsordnung

Hiermit versichere ich an Eides statt, dass ich die vorliegende Dissertation selbstständig und ohne die Benutzung anderer als der angegebenen Hilfsmittel und Literatur angefertigt habe. Alle Stellen, die wörtlich oder sinngemäß aus veröffentlichten und nicht veröffentlichten Werken dem Wortlaut oder dem Sinn nach entnommen wurden, sind als solche kenntlich gemacht. Ich versichere an Eides statt, dass diese Dissertation noch keiner anderen Fakultät oder Universität zur Prüfung vorgelegen hat; dass sie - abgesehen von unten angegebenen Teilpublikationen und eingebundenen Artikeln und Manuskripten - noch nicht veröffentlicht worden ist sowie, dass ich eine Veröffentlichung der Dissertation vor Abschluss der Promotion nicht ohne Genehmigung des Promotionsausschusses vornehmen werde. Die Bestimmungen dieser Ordnung sind mir bekannt. Darüber hinaus erkläre ich hiermit, dass ich die Ordnung zur Sicherung guter wissenschaftlicher Praxis und zum Umgang mit wissenschaftlichem Fehlverhalten der Universität zu Köln gelesen und sie bei der Durchführung der Dissertation zugrundeliegenden Arbeiten und der schriftlich verfassten Dissertation beachtet habe und verpflichte mich hiermit, die dort genannten Vorgaben bei allen wissenschaftlichen Tätigkeiten zu beachten und umzusetzen. Ich versichere, dass die eingereichte elektronische Fassung der eingereichten Druckfassung vollständig entspricht.

Köln, 05.02.2024

B. Gröner

Benedikt Gröner